University of Strathclyde

Department of mechanical and aerospace Engineering

Erosion-corrosion mapping of carbon steel in oil/water slurries

BY

Ghaith .H. Abdulrahman

The thesis presented for the degree of
Doctor of Philosophy

Glasgow, UK
2011

Declaration

The work in this thesis is based on experimental and it was carried out in the department of mechanical engineering of the University of Strathclyde, under the supervision of Professor Margaret Stack during the period from 2008 to 2011. Some of this thesis has been published as listed below;

Journal publication

1- M. Stack, G. Abdulrahman , Mapping erosion-corrosion of carbon steel in oil exploration conditions: Some new approaches to characterizing mechanisms and Synergies, Tribology International, 43 (7) (2010) 1268-1277.

2- M.M.Stack and G. H. Abdulrahman, Mapping erosion-corrosion of carbon steel in oil-water solutions as a function of velocity and potential: some new approaches,Wear (submitted)

Conference publication

1- G.H. Abdulrahman and M.M. Stack, Erosion-corrosion maps for carbon steel in crude oil/water slurries: impact angle and applied potential effects , 11th Mediterannean Petroleum Conference and Exhibition, Tripoli, Libya, 23-25 February 2010 pp1-10

2- M. M. Stack and G. H. Abdulrahman,A study of effect of erosion-corrosion on carbon steel in oil-water slurries as a function of impact angle and potential, Materials Challenges for Oil & Gas in the 21st Century, Tripoli, Libya, 27-29 September 2011 (submitted)

Erosion-corrosion mapping of carbon steel in oil/water slurries

Ghaith .H. Abdulrahman

Submitted for the degree of
Doctor of Philosophy
2011

Abstract

In this study, the combined effects of erosion and corrosion on carbon steel were investigated in crude oil/water slurries. The results have been used to construct erosion-corrosion mechanism and wastage maps to show the transitions between the erosion-corrosion regimes as functions of the effect of impact angles, applied potentials and impact velocities at different particle sizes and at room temperature. In addition, the effects of synergism-additive, wastage and erosion-corrosion mechanisms were superimposed on the maps.

For carbon steel in a water environment, the corrosion current density was greater than that in crude oil, which indicates that the corrosion contribution was greater than in crude oil. The oil film played the main role in protecting the surface of the specimen in the crude oil environment, while an oxide film played the main role in protecting the surface of the specimen in the reservoir water environment.

The results indicate that the corrosion contribution was increased with an increase in the percentage of reservoir water. There was good evidence that the corrosion rate (Kc) was increased with an increase in potential as the potential was swept from negative to positive values. However, in the crude oil environment there was little enhancement of the corrosion contribution (Kc).

There was little enhancement of increased erosion contribution (Ke) with an increase in potential in all test environments due to corrosion enhanced erosion. On the other hand, the total volume loss erosion-corrosion (Kec) was increased with an increase in the impact velocities in all test environments. The total volume loss erosion-corrosion (Kec) was significantly greater in the water environment compared to the other test environments.

The effect of erosion contribution was greater than the effect of corrosion contribution in the crude oil environment with particle sizes 600-710μm (90% compared to 10%). The effect of erosion contribution (Ke) on the specimen was similar to the effect of corrosion contribution (Kc) in the water environment with particle sizes 600-710μm. Possible reasons for such behaviour are attributed to the diffusion of oxygen in the various solutions as evidenced by the polarization data.

The objective and the Layout of this study

This study aims to predict and assess the effect of electrochemical erosion–corrosion on material which is used in oil field production. Moreover, maps have been produced to demonstrate material performance in different environments and test conditions to understand the complex interactions between erosion and corrosion processes of carbon steel (X52) in the oil/water slurries (the chemical composition of this crude oil is shown in table 2.5).

The effect of parameters on erosion–corrosion, such as impact angles and velocities, was also assessed. After each test, the results were used to produce maps to show the erosion–corrosion degrading mechanisms based on the experimental results. The extent of synergism was superimposed on the maps as a function of impact velocities, impact angles and applied potentials in three environments, crude oil, water reservoir and oil/20% water environments. From the findings of this study it can be predicted and the mass loss of material limited. The various chapter of this thesis are explained as follows;

1-The introduction and literature survey for some studies are described in chapter-1.

2-Experimental work and calibration test for the test rig are explained in chapter-2

3-The erosion-corrosion behaviour for carbon steel is illustrated within;

A- Chapter-3 by discussing the results for tests at different particle sizes and five constant applied potentials (-400,-200, 0,200 and 400mV) as function of impact velocities.

B- Chapter-4 by discussing the results for tests at different particle sizes and three constant impact velocities (2.5, 3.5, and 4.5 m s^{-1}) as function of impact angles. Moreover, the morphology of the eroded specimens was evaluated by using scanning electron microscopy (SEM).

C- Chapter-5 by discussing the results for tests at different particle size and six constant impact angles (15°, 30°, 45°, 60°, 75° and 90°) as function of impact applied potentials.

4-General discussion, conclusion (chapter -6) summaries the work, presents the main results obtained and proposes the future work.

ACKNOWLEDGEMENTS

Firstly I would like to thank God, and then I would like to express my deepest appreciation and gratitude to my supervisor Professor Margaret Stack who played the main role in all aspects of my research study. Her encouragement, patience, understanding and support enabled me to complete such a difficult task. I would like to thank Dr Shehab Abdelrahman for his support during my study in the Department of Mechanical Engineering.

DEDICATION

I would like to dedicate this work to the best person in my whole life, my mother, who has spent her whole life for me and my brothers. She is forever in my mind and I have never forgotten her. I would like also to dedicate this work to my brothers Salah and Masalah who are encouragement and supported me to achieve this academic accomplishment, my wife, my son Mohamed and my daughters, Amal, Fatama and Sarah, who provided me continued support during my study.

TABLE OF CONTENTS

Page

Declaration……..i
Abstract……..ii
The objective and the Layout of this study ……..iv
Acknowledgements ……..vi
Dedication ……...vii
Table of contents……viii
List of figures……..xiii
List of table……...xxvi

CHAPTER- 1

1.1**.** Introduction……1
1.2. Literature review……3
1.2.1. Erosion theory……..3
1.2.2. Corrosion ……3
1.2.2.1. Electrochemical parts ……....3
1.2.2.1.1. Anodic …….. 5
1.2.2.1.2. Cathode……..5
1.2.2.1.3. Electrolyte……..6
1.2.2.1.4. Conductivity ……..6
1.2.3. pH ……7
1.2.4. Dissolving of gases ……....8
1.2.4.1. Carbon dioxide……..8
1.2.4.2**.** Dissolved Oxygen ……9
1.2.5. Effect of temperature……..10
1.2.6. The influence of particle impact, shape, size on the erosion of materials……. 11
1.2.7. Effect of impact velocity……14
1.2.8. Erosion-corrosion in aqueous environment……15
1.2.9. General introduction of interaction between erosion and corrosion…… 16
1.2.9.1. The additive effect ……...……...17
1.2.9.2. The synergistic effect …….....19
1.2.10. Impact angle……20
1.3. Summary..... 22

CHAPTER -2 (Calibration test and experimental Methodology)

2.0. Calibration test and experimental Methodology……...23
2.1. Introduction……...23
2.2**.** Calibration test……..23
2.2.1. L-distance with variation of impact velocity and slurry particle concentration.23
2.2.2. d/D ratio with variation of impact velocity and slurry particle concentration...26
2. 3. Experimental Methodology...…….. 30
2.3.1 Structure of erosion test rig…….30

2. 3.2. The function of ejector……31
2.3.3 The electrochemical process……..31
2.4. Erosion-corrosion test…… 33
2.4.1. Materials …….....37
2.4.2. Slurry …….....38
2.5. Summary……..40

CHAPTER- 3 (Results and Discussion)
3.0. Introducation……41
3.1. Effect of impact angle, impact velocity for particle size
600-710µm on erosion-corrosion maps…..……..42
3.1.1. General……...42
3.1.2. The condition of test……..42
3.1.3. Polarization curves for particle sizes 600-710µm ……42
3.1.4. Volume loss for particle sizes 600-710µm ……51
3.1.4.1. Mass loss in water reservoir……51
3.1.4.2. Mass loss at crude oil environment…….52
3.1.4.3. Mass loss at oil /20% water environment……53

3.2. Effect of impact angle, impact velocity for particle size
150-30µm on erosion-corrosion maps…..……....85
3.2.1. The condition of test……..85
3.2.2. Polarization curves…….....85
3.2.3. Volume loss for particle sizes 150-300µm ……...90
3.2.3.1. Mass loss in water reservoir……90
3.2.3.2. Mass loss at crude oil environment…….....90
3.2.3.3. Mass loss at oil/20% water…….90
3.3. Discussion……...110
3.3.1. Polarization curves ..……110
3.3.2. Mass loss……..111
3.3.2. Erosion –Corrosion maps…….112
3.3.3.1. Erosion–corrosion mechanism maps…….112
3.3.3.2. Erosion–corrosion wastage maps……...114
3.3.3.3. Erosion–corrosion additive-synergism maps……115
3.4. Summary…….117

CHAPTER- 4 (Results and Discussion)

4.0. Introduction……....……190

4.1. Effect of impact angle and electrochemical potential on erosion-corrosion maps
for particle sizes 600-710µm and various impact velocities....……..……191
4.1.1. General……191
4.1.2. The procedure of testing……..191
4.1.3. Polarization curves for particles sizes 600-710µm …… 191
4.1.3.1. At impact velocity of 2.5 m s^{-1} ……192
4.1.3.2. At impact velocity of 3.5 m s^{-1} ……192
4.1.3.3. At impact velocity of 4.5 m s^{-1}……192
4.1.4. Mass loss for particles sizes 600-710µm ……197
4.1.5. SEM for particles sizes 600-710µm ……216

4.2. Effect of impact angle and potential on erosion- corrosion maps in three environments for particle sizes150-30µm ……..……..220
4.2.1. The procedure of testing……..220
4.2.2. Polarization curves for particles sizes 150-300µm …… 220
4.2.3. Mass loss for particles sizes 150-300µm.……....225
4.2.4. SEM for particles sizes 150-300µm ……..……..240
Discussion…….....246
4.3.1. Polarization curves……..246
4.3.2. Volume loss……247
4.3.3. SEM……247
4.3.2. Erosion –Corrosion maps.....248
4.3.4.1. Erosion-corrosion mechanism maps……248
4.3.4.2. Erosion-corrosion wastage maps……249
4.3.4.3. Erosion-corrosion synergistic-additive maps……..250
4.4. Summary……251

CHAPTER -5 (Results and Discussion)

5.0. Introduction……...……....298

5.1. Effect of applied potential, impact velocity for particle sizes 600-710µm on erosion-corrosion of carbon steel maps…….……299
5.1.1. General…… 299
5.1.2. Materials and procedure of erosion-corrosion test……..299
5.1.3. Polarization curves for particle sizes 600-710µm ..……...299
5.1.3.1. At impact angles of 15°, 90° and velocity 2.5 m s^{-1}…….299
5.1.3.2. At impact angles of 15°, 90° and velocity 3.5 m s^{-1}…….300
5.1.3.3. At impact angles of 15°, 90° and velocity 4.5 m s^{-1}…….300
5.1.4. Volume loss for particle sizes 600-710µm …….304
5.1.4.1. Mass loss in water reservoir……..304
5.1.4.2. Mass loss at crude oil environment……...305
5.1.4.3. Mass loss at oil/20% water……...305

5.2. Effect of applied potential, impact velocity for particle size 150-30µm on erosion-corrosion maps…….……..334
5.2.1. The condition of test……334
5.2.2. Polarization curves for particle sizes 150-300µm……334
5.2.2.1. At impact angles of 15°, 90° and velocity 2.5 m s^{-1}…….334
5.2.2.2. At impact angles of 15°, 90° and velocity 3.5 m s^{-1}…….335
5.2.2.3. At impact angles of 15°, 90° and velocity 4.5 m s^{-1}…….335
5.2.3. Volume loss for particle sizes 150-300µm……..339
5.2.3.1. Mass loss in water reservoir……..339
5.2.3.2. Mass loss at crude oil environment……...340
5.2.3.3. Mass loss at oil/20% water……...340
5.3. Discussion……...359
5.3.1. Polarization curves……...359
5.3.2. Erosion-corrosion mass loss……..360
5.3.2. Erosion –Corrosion maps…….361
5.3.3.1. Erosion-corrosion mechanism maps…….361

5.3.3.2. Erosion–corrosion wastage maps……..363
5.3.3.3. Erosion–corrosion additive-synergistic maps……...364
5.4. Summary…….365

Chapter – 6

6.1. General Discussion...……...447
6.1.1. Polarization curves…… 447
6.1.2. Erosion-corrosion mass loss…… 448
6.1.2. Erosion–corrosion maps...……450
6.1.3.1. Erosion-corrosion mechanism maps……... 450
6.1.3.2. Erosion-corrosion wastage maps……. 452
6.1.3.3. Erosion-corrosion additive-synergism maps…… 453
6.1.3. Mechanism description of test material……... 454
6.2. Conclusion…….. 458
6.3 Future work…….461
Bibliography…….....462

LIST OF FIGURES

Chapter-1 Page

Fig. 1.1: ESP destroyed by erosion–corrosion. 4

Fig. 1.2: Erosion-corrosion of carbon steel tubing. 4

Fig. 1.3: Erosion-corrosion of a joint. 4

Fig. 1.4: corrosion cell. 6

Fig. 1.5: Steel corrosion rate curve of variation related to hydrogen ion concentration in the electrolyte. 7

Fig. 1.6: Pourbaix diagram for iron in water 8

Fig.1.7: Concept of erosion-corrosion regimes 11

Fif.1.8: The effect of particle size on different materials 13

Fig. 1.9: Mass loss rate with sand size variation 14

Chapter-2

Fig. 2.1: Impact velocity vs. L-distance. 24

Fig. 2.2: Schematic diagram of the ejector. 25

Fig. 2.3: Slurry particle concentration vs. L-distance. 25

Fig. 2.4: Impact velocity as a function of d/D. 26

Fig. 2.5: Variation of slurry particle concentration as a function of d/D. 26

Fig. 2.6: Variation of slurry particle concentration as a function of impact velocity 26

Fig. 2.7: Schematic diagram of erosion-corrosion test rig 35

Fig.2.8: Electrochemical connection in the slurry erosion test. 35

Fig.2.9: Electrochemical interface with three electrodes ACM (Gillac). 36

Fig. 2.10: corrosion current vs. time during potentiostat test. 36

Fig. 2.11: Optical microscopy of aluminum oxide used in the erosion-corrosion test rig :(a) 600-710µm (b) 150-300µm. 38

Chapter-3

Fig.3.1: Polarization curves for carbon steel at various impact velocities, at impact angle 15° and particle size $600-710\mu m$ in (a) water (b) crude oil (c) oil /20% water. 45

Fig.3.2: Polarization curves for carbon steel at various impact velocities, at impact angle 30° and particle size $600-710\mu m$ in (a) water (b) crude oil (c) oil /20% water. 46

Fig.3.3: Polarization curves for carbon steel at various impact velocities, at impact angle 45° and particle size $600 - 710 \mu m$ in (a) water (b) crude oil (c) oil /20% water. 47

Fig.3.4: Polarization curves for carbon steel at various impact velocities, at impact angle 60° and particle size $600 - 710 \mu m$ in (a) water (b) crude oil (c) oil /20% water 48

Fig.3.5: Polarization curves for carbon steel at various impact velocities, at impact angle 75° and particle size $600 - 710 \mu m$ in (a) water (b) crude oil (c) oil /20% water. 49

Fig.3.6: Polarization curves for carbon steel at various impact velocities, at impact angle 90° and particle size $600 - 710 \mu m$ in (a) water (b) crude oil (c) oil /20% water. 50

Fig.3.7: Volume loss as function of impact velocities for carbon steel in water at -400 mV and particle size $600 - 710 \mu m$ (a) 15° (b) 30° (c) 45°(d) 60° (e) 75° (f) 90° 70

Fig.3.8: Volume loss as function of impact velocities for carbon steel in crude oil at -400 mV and particle size $600 - 710 \mu m$ (a) 15° (b) 30° (c) 45°(d) 60° (e) 75° (f) 90°. 71

Fig.3.9: Volume loss as function of impact velocities for carbon steel in oil /20% water at -400 mV and particle size $600 - 710 \mu m$ (a) 15° (b) 30° (c) 45°(d) 60° (e) 75° (f) 90° 72

Fig.3.10: Volume loss as function of impact velocities for carbon steel in water at -200 mV and particle size $600 - 710 \mu m$ (a) 15° (b) 30° (c) 45°(d) 60° (e) 75° (f) 90°. 73

Fig.3.11: Volume loss as function of impact velocities for carbon steel in crude oil at - 200 mV and particle size $600 - 710 \mu m$ (a) 15° (b) 30° (c) 45°(d) 60° (e) 75° (f) 90 74

Fig.3.12: Volume loss as function of impact velocities for carbon steel in oil /20% water at -200 mV and particle size $600 - 710 \mu m$ (a) 15° (b) 30° (c) 45°(d) 60° (e) 75° (f) 90°. 75

Fig.3.13: Volume loss as function of impact velocities for carbon steel in water at 0 mV and particle size $600 - 710 \mu m$ (a) 15° (b) 30° (c) 45°(d) 60° (e) 75° (f) 90°. 76

Fig.3.14: Volume loss as function of impact velocities for carbon steel in crude oil at 0 mV and particle size $600 - 710 \mu m$ (a) 15° (b) 30° (c) 45°(d) 60° (e) 75° (f) 90°. 77

Fig.3.15: Volume loss as function of impact velocities for carbon steel in oil /20% water at 0 mV and particle size $600 - 710 \mu m$ (a) 15° (b) 30° (c) 45°(d) 60° (e) 75° (f) 90°. 78

Fig.3.16: Volume loss as function of impact velocities for carbon steel in water at 200 mV and particle size $600 - 710 \mu m$ (a) 15° (b) 30° (c) 45°(d) 60° (e) 75° (f) 90°. 79

Fig.3.17: Volume loss as function of impact velocities for carbon steel in crude oil at 200 mV and particle size $600 - 710 \mu m$ (a) 15° (b) 30° (c) 45°(d) 60° (e) 75° (f) 90°. 80

Fig.3.18: Volume loss as function of impact velocities for carbon steel in oil /20% water at 200 mV and particle size $600 - 710 \mu m$ (a) 15° (b) 30° (c) 45°(d) 60° (e) 75° (f) 90°. 81

Fig.3.19: Volume loss as function of impact velocities for carbon steel in water at 400 mV and particle size $600 - 710 \mu m$ (a) 15° (b) 30° (c) 45°(d) 60° (e) 75° (f) 90°. 82

Fig.3.20: Volume loss as function of impact velocities for carbon steel in crude oil at 400 mV and particle size $600 - 710 \mu m$ (a) 15° (b) 30° (c) 45°(d) 60° (e) 75° (f) 90°. 83

Fig.3.21: Volume loss as function of impact velocities for carbon steel in oil /20% water at 400 mV and particle size $600 - 710 \mu m$ (a) 15° (b) 30° (c) 45°(d) 60° (e) 75° (f) 90°. 84

Fig.3.22: Polarization curves for carbon steel at various impact velocities, particle size $150 - 300 \mu m$ and impact angle 15° in (a) water (b) crude oil (c) oil /20% water. 87

Fig. 3.23: Polarization curves for carbon steel at various impact velocities, particle size $150 - 300 \mu m$ and impact angle 45° in (a) water (b) crude oil (c) oil /20% water. 88

Fig.3.24: Polarization curves for carbon steel at various impact velocities, particle size $150 - 300 \mu m$ and impact angle 90° in (a) water (b) crude oil (c) oil /20% water. 89

Fig.3.25: Volume loss as function of impact velocities for carbon steel in water at -400 mV and particle size $150 - 300 \mu m$ (a) 15° (b) 45° (c) 90°. 101

Fig.3.26: Volume loss as function of impact velocities for carbon steel in crude oil at -400 mV and particle size $150 - 300 \mu m$ (a) 15° (b) 45° (c) 90°. 102

Fig.3.27: Volume loss as function of impact velocities for carbon steel in oil /20% water at -400 mV and particle size $150 - 300 \mu m$ (a) 15° (b) 45° (c) 90°. 103

Fig.3.28: Volume loss as function of impact velocities for carbon steel in water at 0 mV and particle size $150 - 300 \mu m$ (a) 15° (b) 45° (c) 90°. 104

Fig.3.29: Volume loss as function of impact velocities for carbon steel in crude oil at 0 mV and particle size $150 - 300 \mu m$ (a) 15° (b) 45° (c) 90°. 105

Fig.3.30: Volume loss as function of impact velocities for carbon steel in oil /20% water at 0 mV and particle size $150 - 300 \mu m$ (a) 15° (b) 45° (c) 90°. 106

Fig.3.31: Volume loss as function of impact velocities for carbon steel in water at 400 mV and particle size $150 - 300 \mu m$ (a) 15° (b) 45° (c) 90. 107

Fig.3.32: Volume loss as function of impact velocities for carbon steel in crude oil at 400 mV and particle size $150 – 300\mu m$ (a) 15° (b) 45° (c) 90. 108

Fig.3.33: Volume loss as function of impact velocities for carbon steel in oil /20% water at 400 mV and particle size $150 – 300\mu m$ (a) 15° (b) 45° (c) 90. 109

Fig.3.34: Erosion-corrosion mechanism maps for carbon steel at -400 mV and particle size $600 – 710\mu m$ in (a) water (b) crude oil (c) oil /20% water. 118

Fig.3.35: Erosion-corrosion mechanism maps for carbon steel at -200 mV and particle size $600 – 710\mu m$ in (a) water (b) crude oil (c) oil /20% water. 119

Fig.3.36: Erosion-corrosion mechanism maps for carbon steel at 0 mV and particle size $600 – 710\mu m$ in (a) water (b) crude oil (c) oil /20% water. 120

Fig.3.37: Erosion-corrosion mechanism maps for carbon steel at 200 mV and particle size $600 – 710\mu m$ in (a) water (b) crude oil (c) oil /20% water. 121

Fig.3.38: Erosion-corrosion mechanism maps for carbon steel at -400 mV and particle size $150 – 300\mu m$ in (a) water (b) crude oil (c) oil /20% water. 122

Fig.3.39: Erosion-corrosion mechanism maps for carbon steel at 0 mV and particle size $150 – 300\mu m$ in (a) water (b) crude oil (c) oil /20% water. 123

Fig.3.40: Erosion-corrosion mechanism maps for carbon steel at 400 mV and particle size $150 – 300\mu m$ in (a) water (b) crude oil (c) oil /20% water. 124

Fig.3.41: Erosion-corrosion mechanism maps for carbon steel at 400 mV and particle size $600 – 710\mu m$ in (a) water (b) crude oil (c) oil /20% water. 125

Fig.3.42: Erosion-corrosion wastage maps for carbon steel at -400 mV and particle size $600 – 710\mu m$ in (a) water (b) crude oil (c) oil /20% water. 126

Fig.3.43: Erosion-corrosion wastage maps for carbon steel at -200 mV and particle size $600 – 710\mu m$ in (a) water (b) crude oil (c) oil /20% water. 127

Fig.3.44: Erosion-corrosion wastage maps for carbon steel at 0 mV and particle size $600 – 710\mu m$ in (a) water (b) crude oil (c) oil /20% water. 128

Fig.3.45: Erosion-corrosion wastage maps for carbon steel at 200 mV and particle size $600 – 710\mu m$ in (a) water (b) crude oil (c) oil /20% water. 129

Fig. 3.46: Erosion-corrosion wastage maps for carbon steel at 400 mV and particle size $600 – 710\mu m$ in (a) water (b) crude oil (c) oil /20% water. 130

Fig.3.47: Erosion-corrosion wastage maps for carbon steel at -400 mV and particle size

150 – 300μm in (a) water (b) crude oil (c) oil /20% water. 131

Fig.3.48: Erosion-corrosion wastage maps for carbon steel at 0 mV and particle size 150 – 300μm in (a) water (b) crude oil (c) oil /20% water 132

Fig.3.49: Erosion-corrosion wastage maps for carbon steel at 400 mV and particle size 150 – 300μm in (a) water (b) crude oil (c) oil /20% water. 133

Fig.3.50: Erosion-corrosion additive-synergism maps for carbon steel at -400 mV and particle size 600 – 710μm in (a) water (b) crude oil (c) oil /20% water 134

Fig.3.51: Erosion-corrosion additive-synergism maps for carbon steel at -200 mV and particle size 600 – 710μm in (a) water (b) crude oil (c) oil /20% water. 135

Fig.3.52: Erosion-corrosion additive-synergism maps for carbon steel at 0 mV and particle size 600 – 710μm in (a) water (b) crude oil (c) oil /20% water. 136

Fig.3.53: Erosion-corrosion additive-synergism maps for carbon steel at 200 mV and particle size 600 – 710μm in (a) water (b) crude oil (c) oil /20% water. 137

Fig.3.54: Erosion-corrosion additive-synergism maps for carbon steel at 400 mV and particle size 600 – 710μm in (a) water (b) crude oil (c) oil /20% water. 138

Fig.3.55: Erosion-corrosion additive-synergism maps for carbon steel at -400 mV and particle size 150 – 300μm in (a) water (b) crude oil (c) oil /20% water 139

Fig.3.56: Erosion-corrosion additive-synergism maps for carbon steel at 0 mV and particle size 150 – 300μm in (a) water (b) crude oil (c) oil /20% water. 140

Fig.3.57: Erosion-corrosion additive-synergism maps for carbon steel at 400 mV and particle size 150 – 300μm in (a) water (b) crude oil (c) oil /20% water. 141

Chapter-4

Fig.4.1: Polarization curves for carbon steel at various impact velocities, at various impact angles, 2.5 m s^{-1}velocity and particle size $600 - 710 \mu m$ in (a) water (b) crude oil (c) oil /20% water. 194

Fig.4.2: Polarization curves for carbon steel at various impact velocities, at various impact angles, 3.5 m s^{-1}velocity and particle size $600 - 710 \mu m$ in (a) water (b) crude oil (c) oil /20% water. 195

Fig .4.3: Polarization curves for carbon steel at various impact velocities, at various impacts angles, 4.5 m s^{-1}velocity and particle size $600 - 710 \mu m$ in (a) water (b) crude oil (c) oil /20% water. 196

Fig.4.4: Volume loss as function of impact angles for carbon steel in water at 2.5 m s^{-1} impact velocity and particle size $600 - 710 \mu m$ (a) -400mV (b) -200mV (c) 0mV (d) 200mV (e) 400mV 207

Fig.4.5: Volume loss as function of impact angles for carbon steel in crude oil at 2.5 m s^{-1} and particle size $600 - 710 \mu m$ (a) -400mV (b) -200mV (c) 0mV (d) 200mV (e) 400mV 208

Fig.4.6: Volume loss as function of impact angles for carbon steel in oil /20% water at 2.5 m s^{-1} and particle size $600 - 710 \mu m$ (a) -400mV (b) -200mV (c) 0mV (d) 200mV (e) 400mV 209

Fig.4.7: Volume loss as function of impact angles for carbon steel in water at 3.5 m s^{-1} and particle size $600 - 710 \mu m$ (a) -400mV (b) -200mV (c) 0mV (d) 200mV (e)-400mV. 210

Fig.4.8: Volume loss as function of impact angles for carbon steel in crude oil at 3.5 m s^{-1} and particle size $600 - 710 \mu m$ (a) -400mV (b) -200mV (c) 0mV (d) 200mV (e)-400mV 211

Fig.4.9: Volume loss as function of impact angles for carbon steel in oil /20% water at 3.5 m s^{-1} and particle size $600 - 710 \mu m$ (a) -400mV (b) -200mV (c) 0mV (d) 200mV (e)-400mV 212

Fig.4.10: Volume loss as function of impact angles for carbon steel in water at 4.5 m s^{-1} and particle size $600 - 710 \mu m$ (a) -400mV (b) -200mV (c) 0mV (d) 200mV (e) 400mV 213

Fig.4.11: Volume loss as function of impact angles for carbon steel in crude oil at 4.5 m s^{-1} and particle size $600 - 710 \mu m$ (a) -400mV (b) -200mV (c) 0mV (d) 200mV (e) 400mV 214

Fig.4.12: Volume loss as function of impact angles for carbon steel in oil /20% water at 4.5 m s^{-1} and particle size $600 - 710 \mu m$ (a) -400mV (b) -200mV (c) 0mV (d) 200mV (e) 400mV 215

Fig.4.13: Scanning electron micrographs of eroded carbon steel test specimen at 2.5 m s^{-1}, impact angle 15° and particle size $600 - 710\mu m$ (a) in water (b) in crude oil (c) in oil /20% water. 217

Fig. 4.14: Scanning electron micrographs of eroded carbon steel test specimen at 3.5 m s^{-1}, impact angle 45° and particle size $600 - 710\mu m$ (a) in water (b) in crude oil (c) in oil / 20% water. 218

Fig.4.15: Scanning electron micrographs of eroded carbon steel test specimen at 4.5 m s^{-1}, impact angle 90° and particle size $600 - 710\mu m$ (a)in water (b) in crude oil (c)in oil /20% water. 219

Fig.4.16: Polarization curves for carbon steel at various impact velocities, at various impact angles, 2.5 m s^{-1}velocity and particle size $150 - 300\mu m$ in (a) water (b) crude oil (c) oil /20% water. 222

Fig.4.17: Polarization curves for carbon steel at various impact velocities, at various impact angles, 3.5 m s^{-1}velocity and particle size $150 - 300\mu m$ in (a) water (b) crude oil (c) oil /20% water. 223

Fig.4.18: Polarization curves for carbon steel at various impact velocities, at various impacts angles, 4.5 m s^{-1}velocity and particle size $150 - 300\mu m$ in (a) water (b) crude oil (c) oil /20% water. 224

Fig.4.19: Volume loss as function of impact angles for carbon steel in water at 2.5 m s^{-1} impact velocity and particle size $150 - 300\mu m$ (a) -400mV (b) 0mV (c) 400mV 231

Fig.4.20: Volume loss as function of impact angles for carbon steel in crude oil at 2.5 m s^{-1}impact velocity and particle size $150 - 300\mu m$ (a) -400mV (b) 0mV (c) 400mV 232

Fig.4.21: Volume loss as function of impact angles for carbon steel in oil /20% water at 2.5 m s^{-1}impact velocity and particle size $150 - 300\mu m$ (a) -400mV (b) 0mV (c) 400mV 233

Fig.4.22: Volume loss as function of impact angles for carbon steel in water at 3.5 m s^{-1}impact velocity and particle size $150 - 300\mu m$ (a) -400mV (b) 0mV (c) 400mV 234

Fig.4.23: Volume loss as function of impact angles for carbon steel in crude oil at 3.5 m s^{-1} impact velocity and particle size $150 - 300\mu m$ (a) -400mV (b) 0mV(c) 400mV 235

Fig.4.24: Volume loss as function of impact angles for carbon steel in oil /20% water at 3.5 m s^{-1}impact velocity and particle size $150 - 300\mu m$ (a) -400mV (b) 0mV(c) 400mV 236

Fig.4.25: Volume loss as function of impact angles for carbon steel in water at 4.5 m s^{-1} impact velocity and particle size $150 - 300\mu m$ (a) -400mV (b) 0mV (c) 400mV. 237

Fig.4.26: Volume loss as function of impact angles for carbon steel in crude oil at 4.5 m s^{-1}impact velocity and particle size $150 - 300\mu m$ (a) -400mV (b) 0mV (c) 400mV 238

Fig.4.27: Volume loss as function of impact angles for carbon steel in oil /20% water at 4.5 m s^{-1}impact velocity and particle size $150 - 300\mu m$ (a) -400mV (b) 0mV (c) 400mV 239

Fig.4.28: Scanning electron micrographs of eroded carbon steel test specimen at 2.5 m s^{-1}, impact angle 15° and $150 - 300\mu m$: (a)in water (b) in crude oil (c) in oil /20% water. 241

Fig. 4.29: Scanning electron micrographs of eroded carbon steel test specimen at 3.5 m s^{-1}, impact angle 45° and $150 - 300\mu m$ in water (b) in crude oil (c) in oil /20% water. 242

Fig.4.30: Scanning electron micrographs of eroded carbon steel test specimen at 4.5 m s^{-1}, impact angle 90° and $150 - 300\mu m$ (a) in water (b) analysis of the spectrum-1 (c) analysis of the spectrum-2 (d) analysis of the spectrum-3 243

Fig.4.31: Scanning electron micrographs of eroded carbon steel test specimen at 4.5 m s^{-1}, impact angle 90° and $150 - 300\mu m$ (a) in crude oil (b) analysis of the spectrum-1 (c) analysis of the spectrum-2 (d) analysis of the spectrum-3 244

Fig.4.32: Scanning electron micrographs of eroded carbon steel test specimen at 4.5 m s^{-1}, impact angle 90° and $150 - 300\mu m$ in oil /20% water (b) analysis of the spectrum-1 (c) analysis of the spectrum-2(d) analysis of the spectrum-3 245

Fig.4.33: Erosion-corrosion mechanism maps for carbon steel at 2.5 m s^{-1} and particle size $600 - 710\mu m$ in (a) water (b) crude oil (c) oil /20% water. 252

Fig.4.34: Erosion-corrosion mechanism maps for carbon steel at 3.5 m $s^{-1}$and particle size $600 - 710\mu m$ in (a) water (b) crude oil (c) oil /20% water. 253

Fig.4.35: Erosion-corrosion mechanism maps for carbon steel at 4.5 m $s^{-1}$and particle size $600 - 710\mu m$ in (a) water (b) crude oil (c) oil /20% water. 254

Fig.4.36: Erosion-corrosion mechanism maps for carbon steel at 2.5 m $s^{-1}$and particle size $150 - 300\mu m$ in (a) water (b) crude oil (c) oil /20% water. 255

Fig.4.37: Erosion-corrosion mechanism maps for carbon steel at 3.5 m $s^{-1}$and particle size $150 - 300\mu m$ in (a) water (b) crude oil (c) oil /20% water. 256

Fig.4.38: Erosion-corrosion mechanism maps for carbon steel at 4.5 m $s^{-1}$and particle size $150 - 300\mu m$ in (a) water (b) crude oil (c) oil /20% water. 257

Fig.4.39: Erosion-corrosion wastage maps for carbon steel at 2.5 m s^{-1} and particle size $600 - 710\mu m$ in (a) water (b) crude oil (c) oil /20% water. 258

Fig.4.40: Erosion-corrosion wastage maps for carbon steel at 3.5 m s^{-1} and particle size $600 - 710\mu m$ in (a) water (b) crude oil (c) oil /20% water. 259

Fig.4.41: Erosion-corrosion wastage maps for carbon steel at 4.5 m s^{-1} and particle size $600 - 710\mu m$ in (a) water (b) crude oil (c) oil /20% water. 260

Fig.4.42: Erosion-corrosion wastage maps for carbon steel at 2.5 m $s^{-1}$and particle size $150 - 300\mu m$ in(a) water (b) crude oil (c) oil /20% water. 261

Fig.4.43: Erosion-corrosion wastage maps for carbon steel at 3.5 m $s^{-1}$and particle size $150 - 300\mu m$ in(a) water (b) crude oil (c) oil /20% water. 262

Fig.4.44: Erosion-corrosion wastage maps for carbon steel at 4.5 m $s^{-1}$and particle size $150 - 300\mu m$ in(a) water (b) crude oil (c) oil /20% water. 263

Fig.4.45: Erosion-corrosion additive-synergism maps for carbon steel at 2.5 m s^{-1} and particle size $600 - 710\mu m$ in(a) water (b) crude oil (c) oil /20% water. 264

Fig.4.46: Erosion-corrosion additive-synergism maps for carbon steel at 3.5 m s^{-1} and particle size $600 - 710\mu m$ in(a) water (b) crude oil (c) oil /20% water. 265

Fig.4.47: Erosion-corrosion additive-synergism maps for carbon steel at 4.5 m s^{-1} and particle size $600 - 710\mu m$ in(a) water (b) crude oil (c) oil /20% water. 266

Fig.4.48: Erosion-corrosion additive-synergism maps for carbon steel at 2.5m $s^{-1}$and particle size $150 - 300\mu m$ in (a) water (b) crude oil (c) oil /20% water. 267

Fig.4.49: Erosion-corrosion additive-synergism maps for carbon steel at 3.5m $s^{-1}$and particle size $150 - 300\mu m$ in (a) water (b) crude oil (c) oil /20% water. 268

Fig.4.50: Erosion-corrosion additive-synergism maps for carbon steel at 4.5m $s^{-1}$and particle size $150 - 300\mu m$ in (a) water (b) crude oil (c) oil /20% water. 269

Chapter-5

Fig.5.1: Polarization curves for carbon steel in three environments contain particle size $600 - 710\mu m$ and at 2.5 m s^{-1}: (a) 15° (b) 90°. 301

Fig.5.2: Polarization curves for carbon steel in three environments contain particle size $600 - 710\mu m$ and at 3.5 m s^{-1}: (a) 15° (b) 90°. 302

Fig.5.3: Polarization curves for carbon steel in three environments contain particle size $600-710\mu m$ and at 4.5 m s^{-1}: (a) 15° (b) 90°. 303
Fig.5.4: Volume loss as function of potentials for carbon steel in water at 2.5 m $s^{-1}$and particle size $600-710\mu m$ (a) 15° (b) 30° (c) 45°(d) 60° (e) 75° (f) 90°. 325

Fig.5.5: Volume loss as function of potentials for carbon steel in crude oil at 2.5 m $s^{-1}$and particle size $600-710\mu m$ (a) 15° (b) 30° (c) 45°(d) 60° (e) 75° (f) 90° . 326

Fig.5.6: Volume loss as function of potentials for carbon steel in oil /20% water at 2.5 m $s^{-1}$and particle size $600-710\mu m$ (a) 15° (b) 30° (c) 45°(d) 60° (e) 75° (f) 90° . 327

Fig.5.7: Volume loss as function of potentials for carbon steel in water at 3.5 m $s^{-1}$and particle size $600-710\mu m$ (a) 15° (b) 30° (c) 45°(d) 60° (e) 75° (f) 90° . 328

Fig.5.8: Volume loss as function of potentials for carbon steel in crude oil at 3.5 m $s^{-1}$and particle size $600-710\mu m$ (a) 15° (b) 30° (c) 45°(d) 60° (e) 75° (f) 90° . 329

Fig.5.9: Volume loss as function of potentials for carbon steel in oil /20% water , 3.5 m $s^{-1}$and particle size $600-710\mu m$ (a) 15° (b) 30° (c) 45°(d) 60° (e) 75° (f) 90°. 330

Fig.5.10: Volume loss as function of potentials for carbon steel in water at 4.5 m $s^{-1}$and particle size $600-710\mu m$ (a) 15° (b) 30° (c) 45°(d) 60° (e) 75° (f) 90° . 331

Fig.5.11: Volume loss as function of potentials for carbon steel in crude oil 4.5 m $s^{-1}$and particle size $600-710\mu m$ (a) 15° (b) 30° (c) 45°(d) 60° (e) 75° (f) 90° . 332

Fig.5.12: Volume loss as function of potentials for carbon steel in oil /20% water4.5 m $s^{-1}$and particle size $600-710\mu m$ (a) 15° (b) 30° (c) 45°(d) 60° (e) 75° (f) 90° . 333

Fig.5.13: Polarization curves for carbon steel in three environments contain particle size 150-300μm and at 2.5 m s^{-1}: (a) 15° (b) 90° 336

Fig.5.14: Polarization curves for carbon steel in three environments contain particle size 150-300μm and at 3.5 m s^{-1}: (a) 15° (b) 90° 337

Fig.5.15: Polarization curves for carbon steel in three environments contain particle size 150-300μm and at 4.5 m s^{-1}: (a) 15° (b) 90° 338

Fig.5.16: Volume loss as function of potentials for carbon steel in water at 2.5 m s^{-1} and particle size $150-300\mu m$ (a) 15° (b) 45° (c) 90°. 350

Fig.5.17: Volume loss as function of potentials for carbon steel in crude oil at 2.5 m s^{-1} and particle size $150-300\mu m$ (a) 15° (b) 45° (c) 90°. 351

Fig.5.18: Volume loss as function of potentials for carbon steel in oil /20% water at 2.5 m s^{-1} and particle size $150-300\mu m$ (a) 15° (b) 45° (c) 90° 352

Fig.5.19: Volume loss as function of potentials for carbon steel in water at 3.5 m s^{-1} and particle size $150 - 300 \mu m$ (a) 15° (b) 45° (c) 90° . 353

Fig.5.20: Volume loss as function of potentials for carbon steel in crude oil at 3.5 m s^{-1} and particle size $150 - 300 \mu m$ (a) 15° (b) 45° (c) 90° . 354

Fig.5.21: Volume loss as function of potentials for carbon steel in oil /20% water at 3.5 m s^{-1} and particle size $150 - 300 \mu m$ (a) 15° (b) 45° (c) 90° . 355

Fig.5.22: Volume loss as function of potentials for carbon steel in water at 4.5 m s^{-1} and particle size $150 - 300 \mu m$ (a) 15° (b) 45° (c) 90° . 356

Fig.5.23: Volume loss as function of potentials for carbon steel in crude oil at 4.5 m s^{-1} and particle size $150 - 300 \mu m$ (a) 15° (b) 45° (c) 90° . 357

Fig.5.24: Volume loss as function of potentials for carbon steel in oil /20% water at 4.5 m s^{-1} and particle size $150 - 300 \mu m$ (a) 15° (b) 45° (c) 90° . 358

Fig.5.25: Erosion-corrosion mechanism maps for carbon steel at constant impact angle 15° and particle size $600 - 710 \mu m$ in (a) water (b) crude oil (c) oil /20% water. 366

Fig.5.26: Erosion-corrosion mechanism maps for carbon steel at constant impact angle 30° and particle size $600 - 710 \mu m$ in (a) water (b) crude oil (c) oil /20% water. 367

Fig.5.27: Erosion-corrosion mechanism maps for carbon steel at constant impact angle 45° and particle size $600 - 710 \mu m$ in (a) water (b) crude oil (c) oil /20% water. 368

Fig.5.28: Erosion-corrosion mechanism maps for carbon steel at impact angle 60°and particle size $600 - 710 \mu m$ in (a) water (b) crude oil (c) oil /20% water. 369

Fig.5.29: Erosion-corrosion mechanism maps for carbon steel at constant impact angle 75° and particle size $600 - 710 \mu m$ in (a) water (b) crude oil (c) oil /20% water. 370

Fig.5.30: Erosion-corrosion mechanism maps for carbon steel at impact angle 90° and particle size $600 - 710 \mu m$ in (a) water (b) crude oil (c) oil /20% water. 371

Fig.5.31: Erosion-corrosion mechanism maps for carbon steel at constant impact angle 15° and particle size $150 - 300 \mu m$ in (a) water (b) crude oil (c) oil /20% water. 372

Fig.5.32: Erosion-corrosion mechanism maps for carbon steel at constant impact angle 45° and particle size $150 - 300 \mu m$ in (a) water (b) crude oil (c) oil /20% water. 373

Fig.5.33: Erosion-corrosion mechanism maps for carbon steel at constant impact angle 90° and particle size $150 - 300 \mu m$ in (a) water (b) crude oil (c) oil /20% water. 374

Fig.5.34: Erosion-corrosion wastage maps for carbon steel at constant impact angle 15° and particle size $600 - 710\mu m$ in (a) water (b) crude oil (c) oil /20% water. 375

Fig.5.35: Erosion-corrosion wastage maps for carbon steel at constant impact angle 30° and particle size $600 - 710\mu m$ in (a) water (b) crude oil (c) oil /20% water. 376

Fig.5.36: Erosion-corrosion wastage maps for carbon steel at constant impact angle 45° and particle size $600 - 710\mu m$ in (a) water (b) crude oil (c) oil /20% water 377

Fig.5.37: Erosion-corrosion wastage maps for carbon steel at constant impact angle 60° and particle size $600 - 710\mu m$ in (a) water (b) crude oil (c) oil /20% water. 378

Fig.5.38: Erosion-corrosion wastage maps for carbon steel at constant impact angle75° and particle size $600 - 710\mu m$ in (a) water (b) crude oil (c) oil /20% water. 379

Fig.5.39: Erosion-corrosion wastage maps for carbon steel at constant impact angle 90° and particle size $600 - 710\mu m$ in (a) water (b) crude oil (c) oil /20% water. 380

Fig.5.40: Erosion-corrosion wastage maps for carbon steel at constant impact angle 15° and particle size $150 - 300\mu m$ in (a) water (b) crude oil (c) oil /20% water. 381

Fig.5.41: Erosion-corrosion wastage maps for carbon steel at constant impact angle 45° and particle size $150 - 300\mu m$ in (a) water (b) crude oil (c) oil /20% water. 382

Fig.5.42: Erosion-corrosion wastage maps for carbon steel at constant impact angle 90° and particle size $150 - 300\mu m$ in (a) water (b) crude oil (c) oil /20% water. 383

Fig.5.43: Erosion-corrosion additive-synergism maps for carbon steel at constant impact angle 15° and particle size $600 - 710\mu m$ in (a) water (b) crude oil (c) oil /20% water.
384

Fig.5.44: Erosion-corrosion additive-synergism maps for carbon steel at constant impact angle 30° and particle size $600 - 710\mu m$ in (a) water (b) crude oil (c) oil /20% water.
385

Fig.5.45: Erosion-corrosion additive-synergism maps for carbon steel at constant impact angle 45° and particle size $600 - 710\mu m$ in (a) water (b) crude oil (c) oil /20% water.
386

Fig.5.46: Erosion-corrosion additive-synergism maps for carbon steel at constant impact angle 60° and particle size $600 - 710\mu m$ in (a) water (b) crude oil (c) oil /20% water
387

Fig.5.47: Erosion-corrosion additive-synergism maps for carbon steel at constant impact angle 75° and particle size $600 - 710\mu m$ in (a) water (b) crude oil (c) oil /20% water.
388

Fig.5.48: Erosion-corrosion additive-synergism maps for carbon steel at constant impact angle 90° and particle size $600 - 710\mu m$ in (a) water (b) crude oil (c) oil /20% water.
389

Fig.5.49: Erosion-corrosion additive-synergism maps for carbon steel at constant impact angle 15° and particle size $150 - 300\mu m$ in (a) water (b) crude oil (c) oil /20% water. 390

Fig.5.50: Erosion-corrosion additive-synergism maps for carbon steel at impact angle 45° and particle size $150 - 300\mu m$ in (a) water (b) crude oil (c) oil /20% water. 391

Fig.5.51: Erosion-corrosion additive-synergism maps for carbon steel at impact angle 90° and particle size $150 - 300\mu m$ in (a) water (b) crude oil (c) oil /20% water. 392

Chapter-6

Fig.6.1: Volume loss as function of impact angle for carbon steel at 200 mV and 2.5 m s^{-1} impact velocity in (a) water(b) crude oil (c) oil/ 20% water 455

Fig.6.2: Volume loss as function of impact angle for carbon steel with large particles sized 600-710µm at 200 mV and 4.5 m s^{-1} impact velocity in (a) water(b) crude oil (c) oil/ 20% water 455

Fig.6. 3: Schematic diagram showing changing in mechanism of erosion-corrosion for carbon steel with large particles sized 600-710µm at impact angle 15° and 2.5 m s^{-1} impact velocity in (a) water (b) crude oil (c) oil/20% water 455

Fig.6. 4: Schematic diagram showing changing in mechanism of erosion-corrosion for carbon steel with large particles sized 600-710µm at impact angle 45° and 2.5 m s^{-1} impact velocity in (a) water (b) crude oil (c) oil/20% water 456

Fig.6. 5: Schematic diagram showing changing in mechanism of erosion-corrosion for carbon steel with large particles sized 600-710µm at impact angle 90° and 2.5 m s^{-1} impact velocity in (a) water (b) crude oil (c) oil/20% water 456

Fig.6. 6: Schematic diagram showing changing in mechanism of erosion-corrosion for carbon steel with large particles sized 600-710µm at impact angle 15° and 4.5 m s^{-1} impact velocity in (a) water (b) crude oil (c) oil/20% water 457

Fig.6. 7: Schematic diagram showing changing in mechanism of erosion-corrosion for carbon steel with large particles sized 600-710µm at impact angle 45° and 4.5 m s^{-1} impact velocity in (a) water (b) crude oil (c) oil/20% water 457

Fig.6. 8: Schematic diagram showing changing in mechanism of erosion-corrosion for carbon steel with large particles sized 600-710µm at impact angle 90° and 4.5 m s^{-1} impact velocity in (a) water (b) crude oil (c) oil/20% water 457

LIST OF Tables

Page

Chapter-1

Table.1.1: Some of the factors affecting slurry erosion rates. 18

Chapter-2

Table.2.1: Calibration results of collect L-distance with variation of impact velocities. 27

Table.2.2: Calibration results of collect velocities by d/D ratio with variation of impact velocities. 28

Table.2.3: Calibration results of d/D ratio with variation of impact velocities. 29

Table.2.4: Chemical composition of carbon steel(X52) %. 37

Table.2.5: The chemical composition of crude oil. 39

Chapter-3

Tables.3.1: Volume loss as function of velocities for carbon steel at various impact angles in water at -400mV and particle size $600 - 710 \mu m$ (a) 15° (b) 30° (c) 45° (d) 60° (e) 75° (f) 90° 55

Tables.3.2: Volume loss as function of velocities for carbon steel at various impact angles in water at -200mV and particle size $600 - 710 \mu m$ (a) 15° (b) 30° (c) 45° (d) 60° (e) 75° (f) 90° 56

Tables.3.3: Volume loss as function of velocities for carbon steel at various impact angles in water at 0mV and particle size $600 - 710 \mu m$ (a) 15° (b) 30° (c) 45° (d) 60° (e) 75° (f) 90° 57

Tables.3.4: Volume loss as function of velocities for carbon steel at various impact angles in water at 200mV and particle size $600 - 710 \mu m$ (a) 15° (b) 30° (c) 45°(d) 60° (e) 75° (f) 90° 58

Tables.3.5: Volume loss as function of velocities for carbon steel at various impact angles in water at 400mV and particle size $600 - 710\mu m$ (a) 15° (b) 30° (c) 45° (d) 60° (e) 75° (f) 90° 59

Tables.3.6: Volume loss as function of velocities for carbon steel at various impact angles in crude oil at -400mV and particle size $600 - 710\mu m$ (a) 15° (b) 30° (c) 45°(d) 60° (e) 75° (f) 90° 60

Tables.3.7: Volume loss as function of velocities for carbon steel at various impact angles in crude oil at -200mV and particle size $600 - 710\mu m$ (a) 15° (b) 30° (c) 45° (d) 60° (e) 75° (f) 90° 61

Tables.3.8: Volume loss as function of velocities for carbon steel at various impact angles in crude oil at 0mV and particle size $600 - 710\mu m$ (a) 15° (b) 30° (c) 45° (d) 60° (e) 75° (f) 90° 62

Tables.3.9: Volume loss as function of velocities for carbon steel at various impact angles in crude oil at 200mV and particle size $600 - 710\mu m$ (a) 15° (b) 30° (c) 45°(d) 60° (e) 75° (f) 90° 63

Tables.3.10: Volume loss as function of velocities for carbon steel at various impact angles in crude oil at 400mV and particle size $600 - 710\mu m$ (a) 15° (b) 30° (c) 45° (d) 60° (e) 75° (f) 90. 64

Tables.3.11: Volume loss as function of velocities for carbon steel at various impact angles in oil /20% water at -400mV and particle size $600 - 710\mu m$ (a) 15° (b) 30° (c) 45° (d) 60° (e) 75° (f) 90°. 65

Tables.3.12: Volume loss as function of velocities for carbon steel at various impact angles in oil /20% water at -200mV and particle size $600 - 710\mu m$ (a) 15° (b) 30° (c) 45° (d) 60° (e) 75° (f) 90° 66

Tables.3.13: Volume loss as function of velocities for carbon steel at various impact angles in oil /20% water at 0mV and particle size $600 - 710\mu m$ (a) 15° (b) 30° (c) 45° (d) 60° (e) 75° (f) 90° 67

Tables.3.14: Volume loss as function of velocities for carbon steel at various impact angles in oil /20% water at 200mV and particle size $600 - 710\mu m$ (a) 15° (b) 30° (c) 45°(d) 60° (e) 75° (f) 90° 68

Tables.3.15: Volume loss as function of velocities for carbon steel at various impact angles in oil /20% water at 400mV and particle size $600 - 710\mu m$ (a) 15° (b) 30° (c) 45°(d) 60° (e) 75° (f) 90° 69

Tables.3.16: Volume loss as function of velocities for carbon steel at various impact angles in water at -400mV and particle size $150 - 300\mu m$ (a) 15° (b) 45° (c) 90°. 92

Tables.3.17: Volume loss as function of velocities for carbon steel at various impact angles in water at 0mV and particle size $150 - 300\mu m$ (a) 15° (b) 45° (c) 90°. 93

Tables.3.18:Volume loss as function of velocities for carbon steel at various impact angles in water at 400mV and particle size $150 - 300\mu m$ (a) 15° (b) 45° (c) 90°. 94

Tables.3.19: Volume loss as function of velocities for carbon steel at various impact angles in crude oil at -400mV and particle size $150 - 300\mu m$ (a) 15° (b) 45° (c) 90°. 95

Tables.3.20: Volume loss as function of velocities for carbon steel at various impact angles in crude oil at 0mV and particle size $150 - 300\mu m$ (a) 15° (b) 45° (c) 90°. 96

Tables.3.21: Volume loss as function of velocities for carbon steel at various impact angles in crude oil at 400mV and particle size $150 - 300\mu m$, (a) 15° (b) 45° (c) 90°. 97

Tables.3.22: Volume loss as function of velocities for carbon steel at various impact angles in oil /20% water at -400mV and particle size $150 - 300\mu m$, (a) 15° (b) 45° (c) 90°. 98

Tables.3.23: Volume loss as function of velocities for carbon steel at various impact angles in oil /20% water at 0mV and particle size $150 - 300\mu m$, (a) 15° (b) 45° (c) 90°. 99

Tables.3.24: Volume loss as function of velocities for carbon steel at various impact angles in oil /20% water at 400mV and particle size $150 - 300\mu m$, (a) 15° (b) 45° (c) 90°. 100

Tables.3.25: Erosion-corrosion mechanism maps for carbon steel in water at -400 mV and particle size $600 - 710\mu m$ (a) 15° (b) 30° (c) 45°(d) 60° (e) 75° (f) 90° 142

Tables.3.26: Erosion-corrosion mechanism maps for carbon steel in water at -200mV and particle size $600 - 710\mu m$ (a) 15° (b) 30° (c) 45° (d) 60° (e) 75° (f) 90° 143

Tables.3.27: for Erosion-corrosion mechanism maps for carbon steel in water at 0mV and particle size $600 - 710\mu m$ (a) 15° (b) 30° (c) 45°(d) 60° (e) 75° (f) 90 144

Tables.3.28: Erosion-corrosion mechanism maps for carbon steel in water at 200mV and particle size $600 - 710\mu m$ (a) 15° (b) 30° (c) 45° (d) 60° (e) 75° (f) 90° 145

Tables.3.29: Erosion-corrosion mechanism maps for carbon steel in water at 400mV and particle size $600 - 710\mu m$ (a) 15° (b) 30° (c) 45° (d) 60° (e) 75° (f) 90° 146

Tables.3.30: Erosion-corrosion mechanism maps for carbon steel in crude oil at -400mV and particle size $600 - 710\mu m$ (a) 15° (b) 30° (c) 45°(d) 60° (e) 75° (f) 90° 147

Tables.3.31: for Erosion-corrosion mechanism maps for carbon steel in crude oil at -200mV and particle size $600 - 710\mu m$ (a) 15° (b) 30° (c) 45° (d) 60° (e) 75° (f) 90° 148

Tables.3.32: Erosion-corrosion mechanism maps for carbon steel in crude oil at 0mV and particle size $600 - 710\mu m$ (a) 15° (b) 30° (c) 45°(d) 60° (e) 75° (f) 90° 149

Tables.3.33: Erosion-corrosion mechanism maps for carbon steel in crude oil at 200mV and particle size $600 - 710\mu m$ (a) 15° (b) 30° (c) 45° (d) 60° (e) 75° (f) 90° 150

Tables.3.34: Erosion-corrosion mechanism maps for carbon steel in crude oil at 400mV and particle size $600 - 710\mu m$ (a) 15° (b) 30° (c) 45° (d) 60° (e) 75° (f) 90° 151

Tables.3.35: Erosion-corrosion mechanism maps for carbon steel in oil /20% water at -400mV and particle size $600 - 710\mu m$ (a) 15° (b) 30° (c) 45° (d) 60° (e) 75° (f) 90° 152

Tables.3.36: Erosion-corrosion mechanism maps for carbon steel in oil /20% water at -200mV and particle size $600 - 710\mu m$ (a) 15° (b) 30° (c) 45°(d) 60° (e) 75° (f) 90° 153

Tables.3.37: Erosion-corrosion mechanism maps for carbon steel in oil /20% water at 0mV and particle size $600 - 710\mu m$ (a) 15° (b) 30° (c) 45° (d) 60° (e) 75° (f) 90° 154

Tables.3.38: Erosion-corrosion mechanism maps for carbon steel in oil /20% water at 200 mV and particle size $600 - 710\mu m$ (a) 15° (b) 30° (c) 45°(d) 60° (e) 75° (f) 90° 155

Tables.3.39: Erosion-corrosion mechanism maps for carbon steel in oil /20% water at 400mV and particle size $600 - 710\mu m$ (a) 15° (b) 30° (c) 45°(d) 60° (e) 75° (f) 90° 156

Tables.3.40: Erosion-corrosion mechanism maps for carbon steel in water at -400 mV and particle size $150 - 300\mu m$ (a) 15° (b) 45° (c) 90°. 157

Tables.3.41: Erosion-corrosion mechanism maps for carbon steel in water at 0mV and particle size $150 - 300\mu m$ (a) 15° (b) 45° (c) 90°. 158

Tables.3.42: Erosion-corrosion mechanism maps for carbon steel in water at 400mV and particle size $150 - 300\mu m$ (a) 15° (b) 45° (c) 90°. 159

Tables.3.43: Erosion-corrosion mechanism maps for carbon steel in crude oil at -400mV and particle size $150 - 300\mu m$ (a) 15° (b) 45° (c) 90° 160

Tables.3.44: Erosion-corrosion mechanism maps for carbon steel in crude oil at 0mV and particle size $150 - 300\mu m$ (a) 15° (b) 45° (c) 90°. 161

Tables.3.45: Erosion-corrosion mechanism maps for carbon steel in crude oil at 400mV and particle size $150 - 300\mu m$ (a) 15° (b) 45° (c) 90°. 162

Tables.3.46: Erosion-corrosion mechanism maps for carbon steel in oil /20% water at -400mV and particle size $150 - 300\mu m$ (a) 15° (b) 45° (c) 90° 163

Tables.3.47: Erosion-corrosion mechanism maps for carbon steel in oil /20% water at 0mV and particle size $150 - 300\mu m$ (a) 15° (b) 45° (c) 90° 164

Tables.3.48: Erosion-corrosion mechanism maps for carbon steel in oil /20% water at 400mV and particle size $150 - 300\mu m$ (a) 15° (b) 45° (c) 90° 165

Tables.3.49: Erosion-corrosion additive -synergism maps for carbon steel in water at -400mV and particle size $600 - 710\mu m$ (a) 15° (b) 30° (c) 45° (d) 60° (e) 75° (f) 90° 166

Tables.3.50:Erosion-corrosion additive -synergism maps for carbon steel in water at -200mV and particle size $600 - 710\mu m$ (a) 15° (b) 30° (c) 45° (d) 60° (e) 75° (f) 90° 167

Tables.3.51: Erosion-corrosion additive -synergism maps for carbon steel in water at 0mV and particle size $600 - 710\mu m$ (a) 15° (b) 30° (c) 45°(d) 60° (e) 75° (f) 90° 168

Tables.3.52: Erosion-corrosion additive -synergism maps for carbon steel in water at 200mV and particle size $600 - 710\mu m$ (a) 15° (b) 30° (c) 45°(d) 60° (e) 75° (f) 90° 169

Tables.3.53: Erosion-corrosion additive -synergism maps for carbon steel in water at 400mV and particle size $600 - 710\mu m$ (a) 15° (b) 30° (c) 45° (d) 60° (e) 75° (f) 90° 170

Tables.3.54: Erosion-corrosion additive -synergism maps for carbon steel in crude oil at -400mV and particle size $600 - 710\mu m$ (a) 15° (b) 30° (c) 45° (d) 60° (e) 75° (f) 90° 171

Tables.3.55: Erosion-corrosion additive -synergism maps for carbon steel in crude oil at -200mV and particle size $600 - 710\mu m$ (a) 15° (b) 30° (c) 45° (d) 60° (e) 75° (f) 90° 172

Tables.3.56: Erosion-corrosion additive -synergism maps for carbon steel in crude oil at 0mV and particle size $600-710\mu m$ (a) 15° (b) 30° (c) 45°(d) 60° (e) 75° (f) 90° 173

Tables.3.57: Erosion-corrosion additive -synergism maps for carbon steel in crude oil at 200mV and particle size $600-710\mu m$ (a) 15° (b) 30° (c) 45° (d) 60° (e) 75° (f) 90° 174

Tables.3.58: Erosion-corrosion additive -synergism maps for carbon steel in crude oil at 400mV and particle size $600-710\mu m$ (a) 15° (b) 30° (c) 45° (d) 60° (e) 75° (f) 90° 175

Tables.3.59:Erosion-corrosion additive -synergism maps for carbon steel in oil /20% water at -400mV and particle size $600-710\mu m$ (a) 15° (b) 30° (c) 45° (d) 60° (e) 75° (f) 90° 176

Tables.3.60: Erosion-corrosion additive -synergism maps for carbon steel in oil /20% water at -200mV and particle size $600-710\mu m$ (a) 15° (b) 30° (c) 45° (d) 60° (e) 75° (f) 90° 177

Tables.3.61:Erosion-corrosion additive -synergism maps for carbon steel in oil /20% water at 0mV and particle size $600-710\mu m$ (a) 15° (b) 30° (c) 45°(d) 60° (e) 75° (f) 90° 178

Tables.3.62: Erosion-corrosion additive -synergism maps for carbon steel in oil /20% water at 200mV and particle size $600-710\mu m$ (a) 15° (b) 30° (c) 45°(d) 60° (e) 75° (f) 90° 179

Tables.3.63: Erosion-corrosion additive -synergism maps for carbon steel in oil /20% water at 400mV and particle size $600-710\mu m$ (a) 15° (b) 30° (c) 45°(d) 60° (e) 75° (f) 90° 180

Tables.3.64: Erosion-corrosion additive -synergism maps for carbon steel in water at -400mV and particle size $150-300\mu m$ (a) 15° (b) 45° (c) 90°. 181

Tables.3.65: Erosion-corrosion additive -synergism maps for carbon steel in water at 0 mV and particle size $150-300\mu m$ (a) 15° (b) 45° (c) 90°. 182

Tables.3.66: Erosion-corrosion additive -synergism maps for carbon steel in water at 400mV and particle size $150-300\mu m$ (a) 15° (b) 45° (c) 90°. 183

Tables.3.67: Erosion-corrosion additive -synergism maps for carbon steel in oil at -400mV and particle size $150-300\mu m$ (a) 15° (b) 45° (c) 90°. 184

Tables.3.68: Erosion-corrosion additive -synergism maps for carbon steel in oil at 0mV and particle size $150-300\mu m$ (a) 15° (b) 45° (c) 90°. 185

Tables.3.69: Erosion-corrosion additive -synergism maps for carbon steel in oil at 400mV and particle size $150-300\mu m$ (a) 15° (b) 45° (c) 90°. 186

Tables.3.70: Erosion-corrosion additive -synergism maps for carbon steel in oil /20% water at -400mV and particle size $150 - 300\mu m$ (a) 15° (b) 45° (c) 90°. 187

Tables.3.71: Erosion-corrosion additive -synergism maps for carbon steel in oil /20% water at 0mV and particle size $150 - 300\mu m$ (a) 15° (b) 45° (c) 90°. 188

Tables.3.72: Erosion-corrosion additive -synergism maps for carbon steel in oil /20% water at 400mV and particle size $150 - 300\mu m$ (a) 15° (b) 45° (c) 90°. 189

Chapter-4

Tables.4.1: Mass loss as function of impact angles for carbon steel at various potentials in reservoir water at 2.5 m s^{-1} and particle size $600 - 710\mu m$ (a) -400mV (b) -200mV (c) 0mV (d) 200mV (e) 400mV 198

Tables.4.2:Mass loss as function of impact angles for carbon steel at various potentials in crude oil at 2.5 m s^{-1} and particle size $600 - 710\mu m$ (a) -400mV (b) -200mV (c) 0mV(d) 200mV (e) 400mV 199

Tables.4.3: Mass loss as function of impact angles for carbon steel at various potentials in oil /20% water at 2.5 m s^{-1} and particle size $600 - 710\mu m$ (a) -400mV(b) -200mV (c) 0mV(d) 200mV (e) 400mV. 200

Tables.4.4: Mass loss as function of impact angles for carbon steel at various potentials in water at 3.5 m s^{-1} and particle size $600 - 710\mu m$ (a) -400mV (b) -200mV (c) 0mV (d) 200mV (e) 400mV. 201

Tables.4.5: Mass losses as function of impact angles for carbon steel at various potentials in crude oil at 3.5 m s^{-1} and particle size $600 - 710\mu m$ (a) -400mV (b) -200mV (c) 0mV (d) 200mV (e) 400mV 202

Tables.4.6: Mass loss as function of impact angles for carbon steel at various potentials in oil /20% water at 3.5 m s^{-1} and particle size $600 - 710\mu m$ (a) -400mV (b) -200mV (c) 0mV (d) 200mV (e) 400mV 203

Tables.4.7: Mass loss as function of impact angles for carbon steel at various potentials in water at 4.5 m s^{-1} and particle size $600 - 710\mu m$ (a) -400mV (b) -200mV (c) 0mV(d) 200mV (e) 400mV 204

Table.4.8: Mass loss as function of impact angles for carbon steel at various potentials in crude oil at 4.5 m s^{-1} and particle size $600 - 710\mu m$ (a) -400mV (b) -200mV (c) 0mV(d) 200mV (e) 400mV 205

Table.4.9:Mass loss as function of impact angles for carbon steel at various potentials in oil /20% water at 4.5 m s^{-1} and particle size $600 - 710\mu m$ (a) -400mV (b) -200mV (c) 0mV(d) 200mV (e) 400mV 206

Tables .4.10:Volume loss as function of impact angles for carbon steel at various potentials in water at 2.5 m s^{-1} and particle size $150-300\mu m$ (a) -400mV (b) 0mV (c) 400mV. 226

Tables.4.11:Volume loss as function of impact angles for carbon steel at various potentials in crude oil at 2.5 m s^{-1} and particle size $150-300\mu m$ (a) -400mV (b) 0mV (c) 400mV. 226

Tables.4.12:Volume loss as function of impact angles for carbon steel at various potentials in oil /20% water at 2.5 m s^{-1} impact velocity and particle size $150-300\mu m$ (a) -400mV (b) 0mV (c) 400mV. 227

Table.4.13: Volume loss as function of impact angles for carbon steel at various potentials in water at3.5 m s^{-1}impact velocity and particle size $150-300\mu m$ (a) -400mV(b) 0mV (c) 400mV. 227

Tables.4.14: Volume loss as function of impact angles for carbon steel at various potentials in crude oil at 3.5 m s^{-1}impact velocity and particle size $150-300\mu m$ (a) -400mV (b) 0mV (c) 400mV. 228

Tables.4.15: Volume loss as function of impact angles for carbon steel at various potentials in oil /20% water at 3.5 m s^{-1} impact velocity and particle size $150-300\mu m$ (a) - 400mV (b) 0mV (c) 400mV 228

Tables.4.16: Volume loss as function of impact angles for carbon steel at various potentials in water at4.5 m s^{-1}impact velocity and particle size $150-300\mu m$ (a) -400mV (b) 0mV (c) 400mV 229

Table.4.17: Volume loss as function of impact angles for carbon steel at various potentials in crude oil 4.5 m s^{-1}impact velocity and particle size $150-300\mu m$ (a) -400mV (b) 0mV(c) 400mV 229

Table.4.18: Volume loss as function of impact angles for carbon steel at various potentials in oil /20% water at 4.5 m s^{-1}impact velocity and particle size $150-300\mu m$ (a) - 400mV (b) 0mV (c) 400mV 230

Tables.4.19: Erosion-corrosion mechanism maps for carbon steel in water at 2.5 m s−1 and particle size $600-710\mu m$ (a) -400mV (b) -200mV (c) 0mV (d) 200mV (e) 400mV 270

Tables.4.20: Erosion-corrosion mechanism maps for carbon steel in crude oil at 2.5 m s^{-1} and particle size 600-710 μ m (a) -400mV (b) -200mV (c) 0mV (d) 200mV (e) 400mV 271

Tables.4.21: Erosion-corrosion mechanism maps for carbon steel in oil /20% water at 2.5 m s−1 and particle size 600-710 μ m(a) -400mV (b) -200mV (c) 0mV(d) 200mV (e) 400mV 272

Tables.4.22: Erosion-corrosion mechanism maps for carbon steel in water at 3.5 m s−1 and particle size 600-710 μ m (a) -400mV (b) -200mV (c) 0mV (d) 200mV (e) 400mV 273

Tables.4.23: Erosion-corrosion mechanism maps for carbon steel in crude oil at 3.5 m s−1 and particle size 600-710 μ m(a) -400mV (b) -200mV (c) 0mV (d) 200mV (e) 400mV 274

Tables.4.24: Erosion-corrosion mechanism maps for carbon steel in oil /20% water at 3.5 m s−1 and particle size 600-710 μ m (a) -400mV (b) -200mV (c) 0mV(d) 200mV (e) 400mV 275

Tables.4.25: Erosion-corrosion mechanism maps for carbon steel in water at 4.5 m s−1 and particle size 600-710 μ m (a) -400mV (b) -200mV (c) 0mV(d) 200mV (e) 400mV 276

Tables.4.26: Erosion-corrosion mechanism maps for carbon steel in crude oil at 4.5 m s−1 and particle size 600-710 μ m (a) -400mV (b) -200mV (c) 0mV(d) 200mV (e) 400mV 277

Tables.4.27: Erosion-corrosion mechanism maps for carbon steel in oil /20% water at 4.5 m s−1 and particle size 600-710 μ m (a) -400mV (b) -200mV (c) 0mV(d) 200mV (e) 400mV 278

Tables.4.28: Erosion-corrosion mechanism maps for carbon steel in water at 2.5 m s−1 and particle size $150 - 300 \mu m$ (a) - 400mV (b) 0mV (c) 400mV 279

Tables.4.29: Erosion-corrosion mechanism maps for carbon steel in crude oil at 2.5 m s^{-1} and particle size $150 - 300 \mu m$ (a) - 400mV (b) 0mV (c) 400mV 279

Tables.4.30: Erosion-corrosion mechanism maps for carbon steel in oil /20% water at 2.5 m s−1 and particle size $150 - 300 \mu m$ (a) - 400mV (b) 0mV (c) 400mV 280

Tables.4.31: Erosion-corrosion mechanism maps for carbon steel in water at 3.5 m s^{-1} and particle size $150 - 300 \mu m$ (a) - 400mV (b) 0mV (c) 400mV 280

Tables.4.32:Erosion-corrosion mechanism maps for carbon steel in crude oil at 3.5 m s^{-1} and particle size $150 - 300 \mu m$ (a) - 400mV (b) 0mV (c) 400mV 281

Tables.4.33: Erosion-corrosion mechanism maps for carbon steel in oil /20% water at 3.5 m s−1 and particle size $150 - 300 \mu m$ (a) - 400mV (b) 0mV (c) 400mV 281

Tables.4.34: Erosion-corrosion mechanism maps for carbon steel in water at 4.5 m s^{-1} and particle size $150 - 300\mu m$ (a) - 400mV (b) 0mV (c) 400mV 282

Tables.4.35:Erosion-corrosion mechanism maps for carbon steel in crude oil at 4.5 m s^{-1} and particle size $150 - 300\mu m$ (a) - 400mV (b) 0mV (c) 400mV 282

Tables.4.36: Erosion-corrosion mechanism maps for carbon steel in oil /20% water at 4.5 m s−1 and particle size $150 - 300\mu m$ (a) - 400mV (b) 0mV (c) 400mV 283

Tables.4.37: Erosion-corrosion additive -synergism maps for carbon steel in water at 2.5 m $s^{-1}$and particle size $600 - 710\mu m$ (a) -400mV (b) -200mV (c) 0mV (d) 200mV (e) 400mV 284

Tables.4.38: Erosion-corrosion additive -synergism maps for carbon steel in crude oil at 2.5 m $s^{-1}$and particle size $600 - 710\mu m$ (a) -400mV (b) -200mV (c) 0mV (d) 200mV (e) 400mV 285

Tables.4.39: Erosion-corrosion additive -synergism maps for carbon steel in oil /20% water at 2.5 m $s^{-1}$and particle size $600 - 710\mu m$ (a) -400mV (b) -200mV (c) 0mV (d) 200mV (e) 400mV 286

Tables.4.40: Erosion-corrosion additive -synergism maps for carbon steel in water at 3.5 m $s^{-1}$and particle size $600 - 710\mu m$ (a) -400mV (b) -200mV (c) 0mV (d) 200mV (e) 400mV 287

Tables.4.41: Erosion-corrosion additive -synergism maps for carbon steel in crude oil at 3.5 m $s^{-1}$and particle size $600 - 710\mu m$ (a) -400mV (b) -200mV (c) 0mV (d) 200mV (e) 400mV 288

Tables.4.42: Erosion-corrosion additive -synergism maps for carbon steel in oil /20% water at 3.5 m $s^{-1}$and particle size $600 - 710\mu m$ (a) -400mV (b) -200mV (c) 0mV (d) 200mV (e) 400mV 289

Tables.4.43:Erosion-corrosion additive -synergism maps for carbon steel in water at 4.5 m $s^{-1}$and particle size $600 - 710\mu m$ (a) -400mV (b) -200mV (c) 0mV(d) 200mV (e) 400mV 290

Tables .4.44: Erosion-corrosion additive -synergism maps for carbon steel in crude oil at 4.5 m $s^{-1}$and particle size $600 - 710\mu m$ (a) -400mV (b) -200mV (c) 0mV(d) 200mV (e) 400mV 291

Tables.4.45: Erosion-corrosion additive -synergism maps for carbon steel in oil /20% water at 4.5 m $s^{-1}$and particle size $600 - 710\mu m$ (a) -400mV (b) -200mV (c) 0mV (d) 200mV (e) 400mV 292

Tables.4.46:Erosion-corrosion additive -synergism maps for carbon steel in water at 2.5 m s^{-1} and particle size $150 - 300\mu m$ (a) - 400mV (b) 0mV(c) 400mV 293

Tables.4.47: Erosion-corrosion additive -synergism maps for carbon steel in crude oil at 2.5 m s^{-1} and particle size 150 – 300μm (a) - 400mV (b) 0mV(c) 400mV 293

Tables.4.48: Erosion-corrosion additive -synergism maps for carbon steel in oil /20% water at 2.5 m s^{-1} and particle size 150 – 300μm (a) - 400mV (b) 0mV
(c) 400mV 294

Tables.4.49: Erosion-corrosion additive -synergism maps for carbon steel in water at 3.5 m s^{-1} and particle size 150 – 300μm (a) - 400mV (b) 0mV
(c) 400mV 294

Tables.4.50: Erosion-corrosion additive -synergism maps for carbon steel X52 in crude oil at 3.5 m s^{-1} and particle size 150 – 300μm (a) - 400mV (b) 0mV
(c) 400mV 295

Tables.4.51: Erosion-corrosion additive -synergism maps for carbon steel in oil /20% water at 3.5 m s^{-1} and particle size 150 – 300μm (a) - 400mV (b) 0mV
(c) 400mV 295

Tables.4.52: Erosion-corrosion additive -synergism maps for carbon steel in water at 4.5 m s^{-1} and particle size 150 – 300μm (a) - 400mV (b) 0mV
(c) 400mV 296

Tables.4.53:Erosion-corrosion additive -synergism maps for carbon steel in crude oil at 4.5 m s^{-1} and particle size 150 – 300μm (a) - 400mV (b) 0mV
(c) 400mV 296

Tables.4.54: Erosion-corrosion additive -synergism maps for carbon steel in oil /20% water at 4.5 m s^{-1} and particle size 150 – 300μm (a) - 400mV (b) 0mV
(c) 400mV 297

Chapter-5

Tables.5.1 Volume loss as function of potentials for carbon steel in water at 2.5 m $s^{-1}$and particle size 600 – 710μm (a) 15° (b) 30° (c) 45° 307

Tables.5.2: Volume loss as function of potentials for carbon steel in water at 2.5 m $s^{-1}$and particle size 600 – 710μm (a) 60° (b) 75° (c) 90° 308

Tables.5.3: Volume loss as function of potentials for carbon steel in crude oil at 2.5 m $s^{-1}$and particle size 600 – 710μm (a) 15° (b) 30° (c) 45° 309

Tables.5.4: Volume loss as function of potentials for carbon steel in crude oil at 2.5 m $s^{-1}$and particle size 600 – 710μm (a) 60° (b) 75° (c) 90° 310

Tables.5.5: Volume loss as function of potentials for carbon steel in oil /20% water at 2.5 m $s^{-1}$and particle size 600 – 710μm (a) 15° (b) 30° (c) 45° 311

Tables.5.6: Volume loss as function of potentials for carbon steel in oil /20% water at 2.5 m $s^{-1}$and particle size $600 - 710\mu m$ (a) 60° (b) 75° (c) 90° 312

Tables.5.7: Volume loss as function of potentials for carbon steel in water at 3.5 m $s^{-1}$and particle size $600 - 710\mu m$ (a) 15° (b) 30° (c) 45°. 313

Tables.5.8: Volume loss as function of potentials for carbon steel in water at 3.5 m $s^{-1}$and particle size $600 - 710\mu m$ (a) 60° (b) 75° (c) 90° 314

Tables.5.9: Volume loss as function of potentials for carbon steel in crude oil at 3.5 m $s^{-1}$and particle size $600 - 710\mu m$ (a) 15° (b) 30° (c) 45° 315

Tables.5.10:Volume loss as function of potentials for carbon steel in crude oil at 3.5 m $s^{-1}$and particle size $600 - 710\mu m$ (a) 60° (b) 75° (c) 90° 316

Tables.5.11: Volume loss as function of potentials for carbon steel in oil /20% water at 3.5 m $s^{-1}$and particle size $600 - 710\mu m$ (a) 15° (b) 30° (c) 45° 317

Tables.5.12: Volume loss as function of potentials for carbon steel in oil /20% water at 3.5 m $s^{-1}$and particle size $600 - 710\mu m$ (a) 60° (b) 75° (c) 90° 318

Tables.5.13: Volume loss as function of potentials for carbon steel in water at 4.5 m $s^{-1}$and particle size $600 - 710\mu m$ (a) 15° (b) 30° (c) 45° 319

Tables.5.14: Volume loss as function of potentials for carbon steel in water at 4.5 m $s^{-1}$and particle size $600 - 710\mu m$ (a) 60° (b) 75° (c) 90° 320

Tables.5.15: Volume loss as function of potentials for carbon steel in crude oil at 4.5 m $s^{-1}$and particle size $600 - 710\mu m$ (a) 15° (b) 30° (c) 45° 321

Tables.5.16: Volume loss as function of potentials for carbon steel in crude oil at 4.5 m $s^{-1}$and particle size $600 - 710\mu m$ (a) 60° (b) 75° (c) 90° 322

Tables.5.17: Volume loss as function of potentials for carbon steel in oil /20% water at 4.5 m $s^{-1}$and particle size $600 - 710\mu m$ (a) 15° (b) 30° (c) 45° 323

Tables.5.18: Volume loss as function of potentials for carbon steel in oil /20% water at 4.5 m $s^{-1}$and particle size $600 - 710\mu m$ (a) 60° (b) 75° (c) 90° 324

Tables.5.19: Volume loss as function of potentials for carbon steel in water at 2.5 m s^{-1} and particle size $150 - 300\mu m$ (a) 15° (b) 45° (c) 90° 341

Tables.5.20: Volume loss as function of potentials for carbon steel in water at 3.5 m s^{-1} and particle size $150 - 300\mu m$ (a) 15° (b) 45° (c) 90° 342

Tables.5.21: Volume loss as function of potentials for carbon steel in water at 4.5 m s^{-1} and particle size $150 - 300\mu m$ (a) 15° (b) 45° (c) 90° 343

Tables.5.22: Volume loss as function of potentials for carbon steel in crude oil at 2.5 m s^{-1} and particle size $150 - 300\mu m$ (a) 15° (b) 45° (c) 90° 344

Tables.5.23: Volume loss as function of potentials for carbon steel in crude oil at 3.5 m s^{-1} and particle size $150 - 300\mu m$ (a) 15° (b) 45° (c) 90° 345

Tables.5.24: Volume loss as function of potentials for carbon steel in crude oil at 4.5 m s^{-1} and particle size $150 - 300\mu m$ (a) 15° (b) 45° (c) 90° 346

Tables.5.25: Volume loss as function of potentials for carbon steel in oil /20% water at 2.5 m s^{-1} and particle size $150 - 300\mu m$ (a) 15° (b) 45° (c) 90° 347

Tables.5.26: Volume loss as function of potentials for carbon steel in oil /20% water at 3.5 m s^{-1} and particle size $150 - 300\mu m$ (a) 15° (b) 45° (c) 90° 348

Tables.5.27: Volume loss as function of potentials for carbon steel in oil /20% water 4.5 m s^{-1} and particle size $150 - 300\mu m$ (a) 15° (b) 45° (c) 90° 349

Tables.5. 28: Erosion-corrosion mechanism maps for carbon steel in water at 2.5 m s^{-1} and particle size $600 - 710\mu m$ (a) 15° (b) 30° (c) 45° 393

Tables.5. 29: Erosion-corrosion mechanism maps for carbon steel in water at 2.5 m s^{-1} and particle size $600 - 710\mu m$ (a) 60° (b) 75° (c) 90° 394

Tables.5. 30: Erosion-corrosion mechanism maps for carbon steel in crude oil at 2.5 m s^{-1} and particle size $600 - 710\mu m$ (a) 15° (b) 30° (c) 45° 395

Tables.5. 31: Erosion-corrosion mechanism maps for carbon steel in crude oil at 2.5 m s^{-1} and particle size $600 - 710\mu m$ (a) 60° (b) 75° (c) 90° 396

Tables.5.32: Erosion-corrosion mechanism maps for carbon steel in oil /20% water at 2.5 m s^{-1} and particle size $600 - 710\mu m$ (a) 15° (b) 30° (c) 45° 397

Tables.5.33:Erosion-corrosion mechanism maps for carbon steel in at 2.5 m s^{-1} and particle size $600 - 710\mu m$ (a) 60° (b) 75° (c) 90° 398

Tables.5. 34: Erosion-corrosion mechanism maps for carbon steel in water at 3.5 m s^{-1} and particle size $600 - 710\mu m$ (a) 15° (b) 30° (c) 45° 399

Tables.5. 35: Erosion-corrosion mechanism maps for carbon steel in water at 3.5 m s^{-1} and particle size $600 - 710\mu m$ (a) 60° (b) 75° (c) 90° 400

Tables.5. 36: Erosion-corrosion mechanism maps for carbon steel crude oil at 3.5 m s^{-1} and particle size $600 - 710\mu m$ (a) 15° (b) 30° (c) 45° 401

Tables.5.37: Erosion-corrosion mechanism maps for carbon steel in crude oil at 3.5 m s^{-1} and particle size $600 - 710 \mu m$ (a)60° (b) 75° (c) 90° 402

Tables.5. 38: Erosion-corrosion mechanism maps for carbon steel in oil /20% water at 3.5 m s^{-1} and particle size $600 - 710 \mu m$ (a) 15° (b) 30° (c) 45° 403

Tables.5. 39: Erosion-corrosion mechanism maps for carbon steel in oil /20% water at 3.5 m s^{-1} and particle size $600 - 710 \mu m$ (a) 60° (b) 75° (c) 90° 404

Tables.5. 40: Erosion-corrosion mechanism maps for carbon steel in water at 4.5 m s^{-1} and particle size $600 - 710 \mu m$ (a) 15° (b) 30° (c) 45° 405

Tables.5. 41: Erosion-corrosion mechanism maps for carbon steel in water at 4.5 m s^{-1} and particle size $600 - 710 \mu m$ (a) 60° (b) 75° (c) 90° 406

Tables.5. 42: Erosion-corrosion mechanism maps for carbon steel in crude oil at 4.5 m s^{-1} and particle size $600 - 710 \mu m$ (a) 15° (b) 30° (c) 45° 407

Tables.5. 43: Erosion-corrosion mechanism maps for carbon steel in crude oil at 4.5 m s^{-1} and particle size $600 - 710 \mu m$ (a) 60° (b) 75° (c) 90° 408

Tables.5. 44: Erosion-corrosion mechanism maps for carbon steel in oil /20% water at 4.5 m s^{-1} and particle size $600 - 710 \mu m$ (a) 15° (b) 30° (c) 45° 409

Tables.5. 45: Erosion-corrosion mechanism maps for carbon steel in oil /20% water at 4.5 m s^{-1} and particle size $600 - 710 \mu m$ (a) 60° (b) 75° (c) 90° 410

Tables.5. 46:Erosion-corrosion mechanism maps for carbon steel in water at 2.5 m s^{-1} and particle size $150 - 300 \mu m$ (a) 15° (b) 45° (c) 90°. 411

Tables.5. 47: Erosion-corrosion mechanism maps for carbon steel in water at 3.5 m s^{-1} and particle size $150 - 300 \mu m$ (a) 15° (b) 45° (c) 90°. 412

Tables.5. 48: Erosion-corrosion mechanism maps for carbon steel in water at 4.5 m s^{-1} and particle size $150 - 300 \mu m$ (a) 15° (b) 45° (c) 90°. 413

Tables.5. 49: Erosion-corrosion mechanism maps for carbon steel in crude oil at 2.5 m s^{-1} and particle size $150 - 300 \mu m$ (a) 15° (b) 45° (c) 90°. 414

Tables.5. 50: Erosion-corrosion mechanism maps for carbon steel in crude oil at 3.5 m s^{-1} and particle size $150 - 300 \mu m$ (a) 15° (b) 45° (c) 90°. 415

Tables.5. 51: Erosion-corrosion mechanism maps for carbon steel in crude oil at 4.5 m s^{-1} and particle size $150 - 300 \mu m$ (a) 15° (b) 45° (c) 90°. 416

Tables.5.52: Erosion-corrosion mechanism maps for carbon steel in oil /20% water at 2.5 m s^{-1} and particle size $150 - 300 \mu m$ (a) 15° (b) 45° (c) 90°. 417

Tables.5. 53: Erosion-corrosion mechanism maps for carbon steel in oil /20% water at 3.5 m s^{-1} and particle size $150 - 300 \mu m$ (a) 15° (b) 45° (c) 90°. 418

Tables.5. 54: Erosion-corrosion mechanism maps for carbon steel in oil /20% water at 4.5 m s^{-1} and particle size $150 - 300 \mu m$ (a) 15° (b) 45° (c) 90°. 419

Tables.5. 55: Erosion-corrosion additive -synergism maps for carbon steel in water at 2.5 m s^{-1} and particle size $600 - 710 \mu m$ (a) 15° (b) 30° (c) 45° 420

Tables.5. 56: Erosion-corrosion additive -synergism maps for carbon steel in water at 2.5 m s^{-1} and particle size $600 - 710 \mu m$ (a) 60° (b) 75° (c) 90° 421

Tables.5. 57: Erosion-corrosion additive -Synergism maps for carbon steel in water at 3.5 m s^{-1} and particle size $600 - 710 \mu m$ (a) 15° (b) 30° (c) 45° 422

Tables.5. 58: Erosion-corrosion additive -synergism maps for carbon steel in water at 3.5 m s^{-1} and particle size $600 - 710 \mu m$ (a) 60° (b) 75° (c) 90° 423

Tables.5. 59: Erosion-corrosion additive -synergism maps for carbon steel in water at 4.5 m s^{-1} and particle size $600 - 710 \mu m$ (a) 15° (b) 30° (c) 45° 424

Tables.5. 60: Erosion-corrosion additive -synergism maps for carbon steel in water at 4.5 m s^{-1} and particle size $600 - 710 \mu m$ (a) 60° (b) 75° (c) 90° 425

Tables.5. 61: Erosion-corrosion additive -Synergism maps for carbon steel in crude oil at 2.5 m s^{-1} and particle size $600 - 710 \mu m$ (a) 15° (b) 30° (c) 45° 426

Tables.5. 62: Erosion-corrosion additive -Synergism maps for carbon steel in crude oil at 2.5 m s^{-1} and particle size $600 - 710 \mu m$ (a) 60° (b) 75° (c) 90° 427

Tables.5. 63: Erosion-corrosion additive -Synergism maps for carbon steel in crude oil at 3.5 m s^{-1} and particle size $600 - 710 \mu m$ (a) 15° (b) 30° (c) 45° 428

Tables.5. 64: Erosion-corrosion additive -Synergism maps for carbon steel in crude oil at 3.5 m s^{-1} and particle size $600 - 710 \mu m$ (a) 60° (b) 75° (c) 90° 429

Tables.5. 65: Erosion-corrosion additive -Synergism maps for carbon steel in crude oil at 4.5 m s^{-1} and particle size $600 - 710 \mu m$ (a) 15° (b) 30° (c) 45° 430

Tables.5. 66:Erosion-corrosion additive -Synergism maps for carbon steel in crude oil at 4.5 m s^{-1} and particle size $600 - 710 \mu m$ (a) 60° (b) 75° (c) 90° 431

Tables.5. 67: Erosion-corrosion additive -synergism maps for carbon steel in oil /20% water at 2.5 m s^{-1} and particle size $600 - 710 \mu m$ (a) 15° (b) 30° (c) 45° 432

Tables.5. 68: Erosion-corrosion additive -synergism maps for carbon steel in oil /20% water at 2.5 m s^{-1} and particle size $600 - 710 \mu m$ (a)60° (b) 75° (c) 90°
433

Tables.5. 69: Erosion-corrosion additive -synergism maps for carbon steel in oil /20% water at 3.5 m s^{-1} and particle size $600 - 710 \mu m$ (a) 15° (b) 30° (c) 45°
434

Tables.5.70: Erosion-corrosion additive -synergism maps for carbon steel in oil /20% water at 3.5 m s^{-1} and particle size $600 - 710 \mu m$ (a) 60° (b) 75° (c) 90°
435

Tables.5. 71:Erosion-corrosion additive -synergism maps for carbon steel in oil /20% water at 4.5 m s^{-1} and particle size $600 - 710 \mu m$ (a) 15° (b) 30° (c) 45°
436

Tables.5. 72: Erosion-corrosion additive -synergism maps for carbon steel in oil /20% water at 4.5 m s^{-1} and particle size $600 - 710 \mu m$ (a) 60° (b) 75° (c) 90° 437

Tables.5.73: Erosion-corrosion additive -synergism maps for carbon steel in water at 2.5 m s^{-1} and particle size $150 - 300 \mu m$ (a) 15° (b) 45° (c) 90°. 438

Tables.5. 74: Erosion-corrosion additive -Synergism maps for carbon steel in water at 3.5 m s^{-1} and particle size $150 - 300 \mu m$ (a) 15° (b) 45° (c) 90°. 439

Tables.5. 75: Erosion-corrosion additive -synergism maps for carbon steel in water at 4.5 m s^{-1} and particle size $150 - 300 \mu m$ (a) 15° (b) 45° (c) 90°. 440

Tables.5. 76: Erosion-corrosion additive -synergism maps for carbon steel in crude oil at 2.5 m s^{-1} and particle size $150 - 300 \mu m$ (a) 15° (b) 45° (c) 90°. 441

Tables.5. 77: Erosion-corrosion additive -Synergism maps for carbon steel in crude oil at 3.5 m s^{-1} and particle size $150 - 300 \mu m$ (a) 15° (b) 45° (c) 90°. 442

Tables.5.78:Erosion-corrosion additive -Synergism maps for carbon steel in crude oil at 4.5 m s^{-1} and particle size $150 - 300 \mu m$ (a) 15° (b) 45° (c) 90°. 443

Tables.5. 79: Erosion-corrosion additive -synergism maps for carbon steel in oil /20% water at 2.5 m s^{-1} and particle size $150 - 300 \mu m$ (a) 15° (b) 45° (c) 90°. 444

Tables.5. 80: Erosion-corrosion additive -Synergism maps for carbon steel in oil /20% water at 3.5 m s^{-1} and particle size $150 - 300 \mu m$ (a) 15° (b) 45° (c) 90°. 445

Tables.5. 81: Erosion-corrosion additive -synergism maps for carbon steel in oil /20% water at 4.5 m s^{-1} and particle size $150 - 300 \mu m$ (a) 15° (b) 45° (c) 90°. 446

Chapter 1

LITERATURE REVIEW

1.1. Introduction

Corrosion is defined as the material degradation process that usually occurs due to chemical or electrochemical action, while erosion is defined as a mechanical wear process, such as solid particle impact [1-2]. If these two processes exist jointly, in a crude oil environment they cause erosion–corrosion.

The combined effects of erosion-corrosion can be considerably higher than the sum of the effects of the processes performed separately [2, 6 and 34]. Moreover, as proposed by many investigators [2, 6, 20 and36], this interface effect is due to the enhancement of corrosion by erosion or enhancement of erosion by corrosion. In such cases the combined effect may be low, particular for erosion at elevated temperature where the presence of ductile oxide may impede erosion.

The system in downhole oil wells is such that the sand is produced along with corrosive liquids and gases [1]. Material loss in these types of environments is more complex due to the combined effects of erosion and corrosion. Therefore, erosion–corrosion due to particle impact is an increasingly major problem in oil production.

There are a few studies in which synergism has been quantified, with the majority of works being carried out using jet impingement apparatus or rotating cylinder electrode systems [10-11]. The severity of erosion–corrosion in oil production depends on a range of factors in down hole oil wells, such as sand concentration, particle size, reservoir pressure, temperature, and H_2S (sour corrosion) and CO_2 (sweet corrosion) concentration, which cause mechanical and chemical damage to the ESP (electrical submersible pump), subsequently causing economic losses due to maintenance, leaks and exchanging of parts, leading to a decreased production rate [2 and 11].

Erosion-corrosion, being a complex process, causes major difficulties in terms of the ability to predict the rate of material loss. These processes are believed to be dependent on the erosive particle parameters such as size, shape, impact velocity at impact angle and the flow rate, the material parameters such as microstructure, hardness and the strength of adherence of the passivation layer of corrosion products, and the environment parameters such as temperature and pressure [16 -17].

The effects of these parameters when applied to oil and gas production activities have not been fully understood in the past due to not being able to determine the relationship between environmental parameters and the erosion-corrosion of material during design. Therefore, this project aims to investigate and assess the erosion–corrosion behaviour in slurry impingement containing crude oil with aluminium oxide (Al_2O_3) as an erodent particle at room room temperature. The carbon steel (X52) was tested as this is used in the majority of oil production piping (downstream and upstream). In addition, the investigation will involve impact velocities at ranges 2.5, 3.5, and 4.5 $m\,s^{-1}$, impact angles of 15°, 30°, 45°, 60°, 75° and 90° at various electrochemical applied potentials, and two different particle sizes. The results after test will be used to construct erosion-corrosion maps shown mechanism, wastage rate and an interaction between erosion-corrosion synergism-additive behaviour.

1.2. Literature review

Erosion-corrosion occurs in down stream and up stream in oil wells during the life of production and shut down of oil wells as shown in Figs.1.1, 1.2, and 1.3. Erosion-corrosion can be controlled by inhibited pumping into the downhole oil well, controlling velocities by decreasing the flow rate, and selecting suitable material to make tubing [1]. Corrosion in oil production is usually electrochemical due to current flow, which produces a chemical reaction whereby it loses and gains electrons [2].

1.2.1. Erosion theory

Erosion is a process whereby material is removed from the surface of a target material through the effect of impact particles. This theory of explaining the erosion of ductile material was developed in the 1960s by Finnie et al. [3] to describe the mechanism of material removal through solid particle erosion.

1.2.2. Corrosion

In case, where the corrosion occurs on metal at a high temperature it is termed dry corrosion, and in an aqueous environment it is termed aqueous corrosion. In an aqueous environment, corrosion is an electrochemical process whereby any reaction will contain two partial reactions: oxidation or anodic partial reaction and reduction or cathodic partial reaction [4].

1.2.2.1. Electrochemical parts

- Cathodes
- Anodic
- An electrical connection in between the anode and cathode allowing the flow of electrons
- A conducting environment for ionic movement (electrolyte)

Fig. 1.1: ESP destroyed by erosion–corrosion.

Fig. 1.2: Erosion-corrosion of carbon steel tubing.

Fig. 1.3: Erosion-corrosion of a joint.

1.2.2.1.1. Anodic

The anode is that part of a metal surface that is corroded. It is the position at which metal dissolves or goes into solution. When metal dissolves the metal atoms lose electrons and go into a solution as ion. Since atoms contain number of electrons, protons, the loss of electrons leaves an excess of positive charge and the resulting ions are positively charged [4]. The chemical reaction for iron is:

$Fe \longrightarrow Fe^{2+} + 2e^-$ 1.1

Iron atom $\longrightarrow$ iron ion (ferrous) +electron

This loss of electrons is called oxidation. The iron ion goes into a solution and two electrons are left behind in the metal.

1.2.2.1.2. Cathode

The cathode is that part of the metal surface which does not dissolve; however, it is the site of another chemical reaction which is necessary to the corrosion process. The electrons left behind by the solution of iron at the anode travel through the metal to the cathode surface area, where they are consumed by the reaction with an oxidizing factor presence in the water. This consumption of electrons is called a reduction reaction [4-5]. The typical reaction is:

$2H^+ + 2e^- \longrightarrow H_2$ 1.2

Hydrogen + electron $\longrightarrow$ hydrogen gas

If oxygen is presence, two other reactions are also possible:

$O_2 + 4H^+ + 4e^- \longrightarrow 2H_2O$ 1.3

(Acid solution)

$O_2 + 2H_2O + 4e^- \longrightarrow 4OH^-$ 1.4

(Alkaline solutions)

Therefore, the reaction at the anodic area produces electrons and the reaction at the cathode area consumes electrons. This is the necessary feature of an electrochemical reaction; electrons are generated by a chemical reaction at one point and then travel to another point where they are used up by another reaction [4].

Electrical current flow is actually the passage of electrons from one point to another point. The theory says that electrical current flows in the opposite direction to that which electrons move. Therefore, as electrons flow from the anode area to the cathode area, electrical current flows in the opposite direction: from the cathode to the anode area (all these currents flow within the metal). Thus, the metallic path between the anode and cathode should be a conductor of electricity [4-5].

1.2.2.1.3. Electrolyte

The metal surface (both the anode and the cathode) should be covered with an electrically conductive solution. Such a solution is called an electrolyte. Pure water is a poor electrolyte, although electrical conductivity increases rapidly with the addition of dissolved salts. The electrolyte conducts current from the anode to the cathode. The current then flows back to the anode through the metal, completing the circuit.

This combination of anode, cathode and electrolyte is called a corrosion cell as in Fig. 1.4 [5].

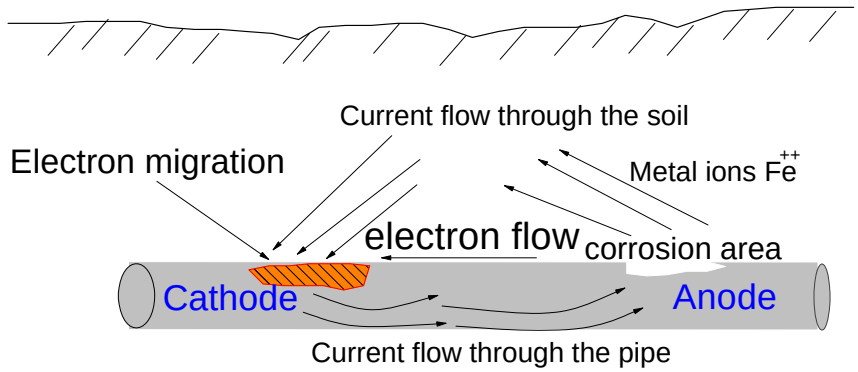

Fig. 1.4: corrosion cell.

1.2.2.1.4. Conductivity

The metal surface should be covered by an electrically conductive solution (or electrolyte) to carry electrical current from the cathode to the anode of the corrosion cell. Therefore, the more conductive the electrolyte, the easier current can flow. The less conductive the electrolyte, the greater the resistance to current flow and the slower the reaction. It is important to understand that the quantity of metal which dissolves is directly proportional to the amount of current that flows between the anode and the cathode [4-5]. For example, distilled water is not very conductive and is not very corrosive. In contrast, salt water is very conductive and can be very

corrosive, as in reservoir water. Moreover, the presence of dissolved gases, which cause a low pH electrolyte, may make a low conductivity electrolyte very corrosive. In an oilfield, if crude oil mixes with water the conductivity becomes more difficult to define. A mixture of salty, highly conductive water in oil may not be highly corrosive if the water is emulsified in oil, but if the water is produced as free water then a very corrosive condition may exist [4], as can be seen that in the next results.

1.2.3. pH

The pH of water is usually expressed as a number between 0 and 14. The midpoint of the pH scale is seven; a solution with this pH is neutral. A number below seven indicates acidity while above seven indicates alkalinity. Hydrogen ions [H+] make a solution acidic. Hydroxyl ions [OH-] make a solution basic or alkaline and push the pH upward [4-5]. The corrosion rate of steel usually increases as the pH of the environment decreases (becomes more acidic), although particularly high pH solutions can also be corrosive.The general difference of the corrosion rate of steel based on pH is shown in Fig 1.5. The actual difference of the corrosion rate with pH is obviously dependent on the composition of the environment or electrolyte. Moreover, in many oilfields, water protective scales such as iron hydroxides or carbonate scales may form on the steel surface and prevent or slow down further corrosion attack [2].In addiation; Pourbaix [7] constructed the relation between potential (E) and pH in digrams for several metals. The Pourbaix diagram is a graphical illustration of the possible corrosion phases at equilibrium for Iron/H_2O system at any operation temperature Fig1.6.

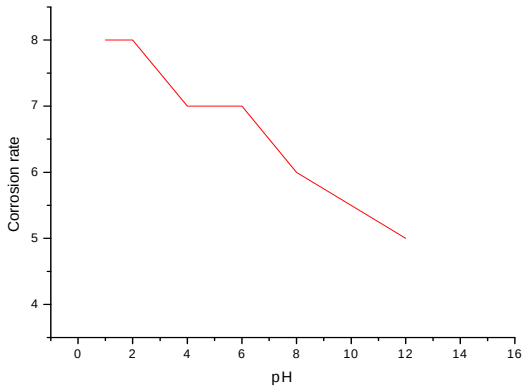

Fig. 1.5: Steel corrosion rate curve of variation related to hydrogen ion concentration in the electrolyte [4].

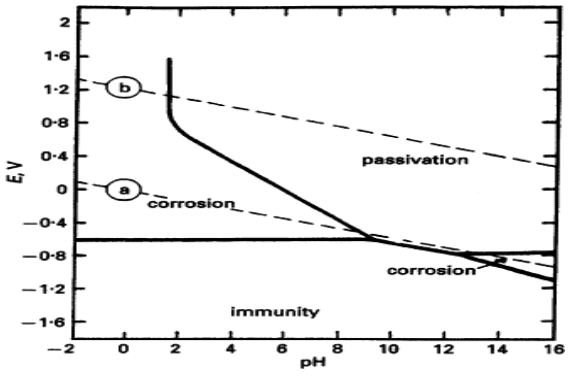

Fig. 1.6: Pourbaix diagram for iron in water [7]

1.2.4. Dissolving of gases

The corrosion of carbon steel is more difficult in downhole oil wells and it might occur at all stages of production, from down hole to the surface of the oil well, due to dissolution of gases [5]. Oxygen, carbon dioxide, and hydrogen sulphide dissolve in water and increase its corrosivity. In fact, dissolved gases are the main cause of most corrosion problems in gas and oil fields.

1.2.4.1. Carbon dioxide

When CO_2 dissolves in water it forms carbonic acid, decreases the pH of the water, and increases its corrosivity. It is not as corrosive as oxygen but it results in pitting [8-9]. Therefore,CO_2 corrosion leads to the formation of a corrosion product on the surface of metal, iron carbonate ($FeCO_3$), that when precipitated can form a protective coating depending on several environmental conditions, such as iron concentration, pH of solution, temperature in the solution [4-5]. Moreover, CO_2 corrosion is an electrochemical process with an overall reaction mechanism as follows:

$CO_2 + H_2O \longrightarrow H_2CO_3$ 1.5

Carbon dioxide + water $\longrightarrow$ carbon acid

$Fe + H_2CO_3 \longrightarrow FeCO_3 + H_2$ 1.6

Iron + carbon acid $\longrightarrow$ Iron carbonate (corrosion product) + hydrogen

Cui and Yang [8] investigated the influence of CO_2 on carbon steel. They found that corrosion due to carbon dioxide causes the failure of pipelines, which is a very serious problem in the production of oil. Similarly, Hamzah and Stephenson [1] investigated the influence of CO_2 on carbon steel. They found that the use of CO_2 increases the

rate of metal loss. Moreover, Yu and Pang [9] investigated the influence of carbon dioxide on carbon steel. They found that the damage on the surface of pipeline could be due to the carbon dioxide corrosion rate, particularly localized corrosion, since that damage can remove or prevent the scale from depositing on the surface of a pipe.

1.2.4.2. Dissolved oxygen

The solubility of oxygen in oil is a function of velocity and temperature. Oxygen corrosion occurs by the following reactions:

Anode reaction: $Fe \longrightarrow Fe + 2\,e^-$ 1.7

$Fe^{+2} + 2OH^- \longrightarrow Fe(OH)_2$ 1.8

Cathode reaction: $O_2 + 2H_2O + 2\,e^- \longrightarrow 2OH^-$ 1.9

Oxygen accelerates corrosion under most circumstances. It does this because it is a strong (provides a high electrochemical potential) and fast oxidizing factor in cathodic reactions at the cathode, and it allows the corrosion reaction to carry on at a rate limited primarily by the rate at which oxygen can diffuse to the cathode [4-5]. Moreover, oxygen usually causes pitting on the metal. If there is sufficient oxygen in the fluid, the oxidation may occur very rapidly before the Fe ions have a chance to diffuse away from the metal surface. In this case, $Fe(OH)_2$ can form on the metal surface and become protective. However, if sufficient chloride ions are presence, they interfere with the formation of a protective film and corrosion rates continue to increase with oxygen concentration [4-5]. Even a very small oxygen concentration can cause damage on the surface of metal. A strongly oxidizing environment will drastically increase corrosivity resulting from other dissolved gases, such as hydrogen sulphide or CO_2, by changing protective scales to be nonproductive and providing a higher potential to reduce resistances in the electrochemical cell, causing an increase in the corrosion rate [4-5].DU Cui-wei et al. [12] investigated the effect of oxygen concentration on carbon steel in simulated soil solution and found that with decrease of oxygen concentrations, the polarization resistance was increased and the corrosion current density decreased.

1.2.5. Effect of temperature

Hamzah [1] investigated the effect of temperature on carbon steel in oil environment and found that with an increase in temperature there was also an increase in the erosion-corrosion rate; the increase in temperature increases the corrosion scale on the surface. G.A. Zhang et al. [13] investigated the effect of temperature on carbon steel in oil/water emulsion and found that with an increase in temperature there was also decreases the solubility of oxygen in the solution and anodic current density of steel increases with the increase in temperature.

However, DU Cui-wei et al. [12] investigated the effect of temperature on carbon steel in simulated soil solution and found that with increase of temperature, the corrosion rate greatly decreased due to passivation due to low solubility of oxygen.

In another environment (air), Stack et al. [14] found that for high temperature erosion-corrosion, the weight loss could be visualised, as shown in Fig. 1.7. It can be seen that four regimes - erosion dominated, erosion-corrosion dominated, and corrosion - dominated in regime -3, and corrosion dominated in regime-4. They are supposed to be established depending on the behaviour of weight loss versus temperature in which the test is carried out. At T_1, the rate of corrosion may be very low and thus the weight loss due to erosion is predominant and an erosion dominated regime results.

As temperature is increased between T_1 and T_2, the weight loss rate increases to a maximum value, then the rate of scale growth begins to influence the rate of material loss; then an erosion-corrosion dominated regime is taking place. Between temperature T_2 and T_3, the rate of material loss begins to slow down to a lower value. However, the rate of scale growth increases such that the weight loss is influenced by the rate of corrosion. Thus, this regime is called corrosion dominated (regime-3). Above T_3, there is no more obvious weight loss, but the rate of scale growth is at its maximum and the properties of the layer are hard to particle erosion; thus, it is corrosion dominated (regime-4).

In a study of the effect of temperature on material, Levy [15] found that at low temperature, very low wastage is due to mechanical erosion at very low velocity. The corrosion rate can be increased by increasing temperature at a low pH when layer films do not form, while at a higher pH with increasing temperature the corrosion rate is decreased due to protective film formation [16 and17]. It can be concluded from these previous investigations that the effect of temperature on materials can indicate an increase in erosion-corrosion, but with different percentages of mass loss dependant on the sort of metal and the environment.

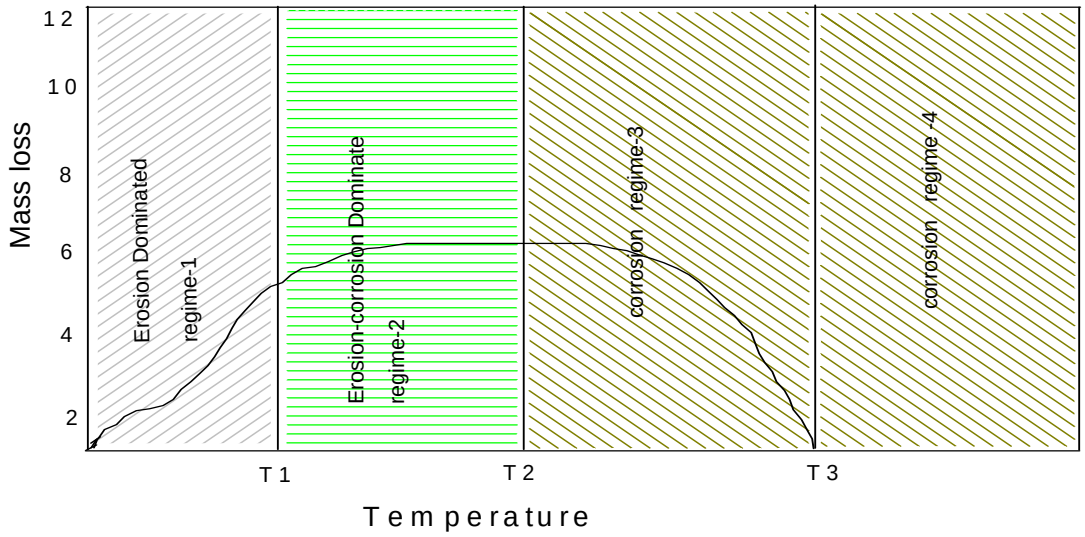

Fig. 1.7: Concept of erosion-corrosion regimes [14].

1.2.6. The influence of particle impact, shape, and size on the erosion of materials

The presence of sand in the oil produced provides many challenges to the oil industry. Material degradation due to the mechanical action of sand particles is known as erosion [1-2]. If there are even small amounts of entrained particle, it can cause a great damage to ESP (electrical submersible pump) in a downhole oil well and erosion of tubing at high velocities. Cheng and Tang [11] investigated the influence of sand on erosion-corrosion, finding that the addition of sand in oil–water emulsion can increase the mass loss of material.

Stack et al. [20 and 34] also investigated the effect of sand, finding that with an increase in sand concentration, weight loss increases. Rajahram et al.[17] investigated the influence of particle on erosion-corrosion by using a slurry pot erosion tester, finding that the sand particles accelerate the steel corrosion by breaking the oxide film layer on the surface of steel and thus exposing the surface to the corrosion and damaging the surface which indicated to the formation of oxide difficult.

In general, the erosion rate increases with an increase in particle size, hardness and angularity of the impacting angle [37]. However, these parameters are interdependent in the erosion process. Hard particles of a rounded shape may cause less erosion than relatively sharp particles [28, 32 and 36]. Stachowiak et al. [41] have investigated the effect of particle shape. Fig. 1.8 was derived from erosion tests on different materials, including graphite, steel, glass, and ceramics, by impingement of Sic erodent particle at an impact velocity of 152 m s^{-1}.

Fig 1.8 shows that the erosion peak shifts depending on the erodent particle size for both ductile and brittle materials. Moreover, it can be observed from Fig 1.8 that with an increase in erodent size, the erosion mechanism changes from “ductile” to “brittle”. In addition, it can also be observed from Fig. 1.8 that the shape of the material also changes with a change in erodent particle size [41]. In the majority of past studies, it can be observed that erosion rate increases with an increase in the particle size up to 100 μm .

Particle size has the main influence on the mechanism of erosion for materials. Erosion by solid particle impacts on a brittle substrate is caused by the formation and intersection of cracking. The types of crack that form on the erodent surface are dependent on the erosive particle shape and size. Lawn and Wilshaw [77], and Swan and Hagan [42] have reported that the impact of large round particles, greater than 200 μm in size, causes cracking, while small particles cause plastic deformation of the surface of the specimen.

The effect of particle size on the erosion rate of materials generally increases with an increase in erodent particle size. The effect of particle hardness becomes clearer when the high hard particle impacts on the surface of the specimen, such as erosion of mild steel by alumina particles [58].

Rajahram et al. [16] have investigated the effect of various particle sizes on erosion-corrosion for stainless steel (SS316L) and carbon steel (AISI 1020) in a slurry pot erosion tester. Fig. 1.9 shows that the variation of mass loss at different particle sizes. It can be observed from Fig. 1.9 that the medium sand size (150-300µm) produced the highest volume loss rate followed by coarse sand (300-600µm) with the lowest rates seen for investigation with fine sand (90-150µm) conditions.

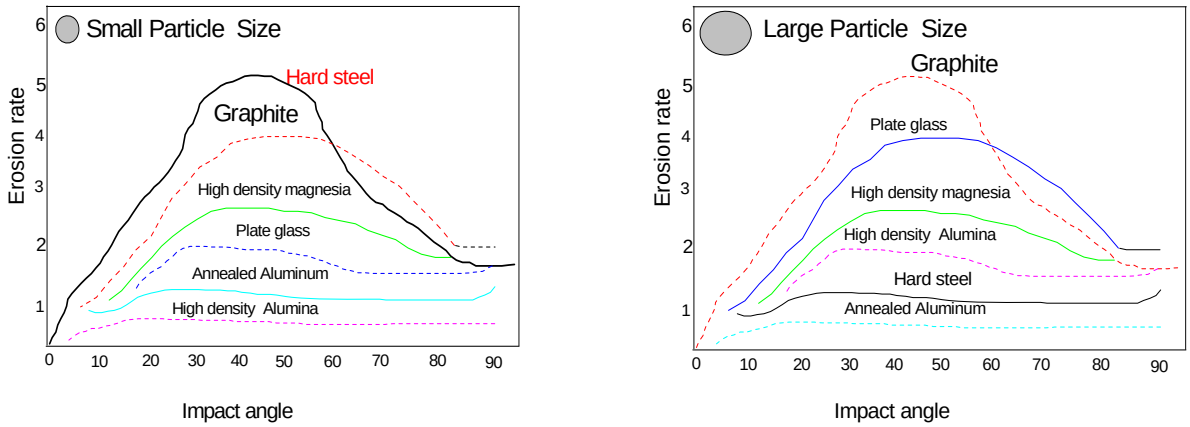

Fig. 1.8: The effect of particle size on different materials [41].

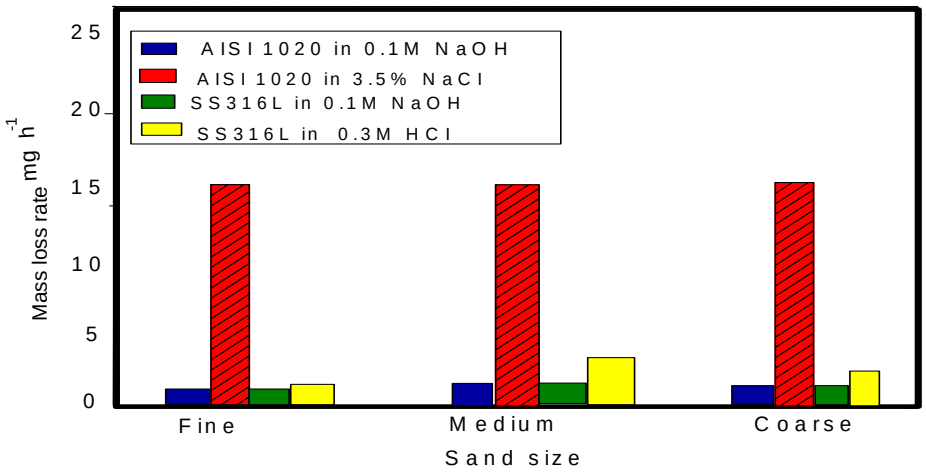

Fig. 1.9: Mass loss rate with sand size variation (7m s^{-1}, 1% sand concentration) [16].

1.2.7. Effect of impact velocity

Velocity is a very important issue in the effect of erosion–corrosion. It often has a strong influence on the mechanisms of corrosive reactions and erosion is effected at high values, particularly when the electrolyte contains solids (slurry) [34]. Velocity increases the erosion rate and many researchers have investigated the relation between the erosion rate of materials and velocities. They have found that erosion is increased with an increase in impact velocity through power law relationship [1and 6].

Stack et al. [2, 6 and 36] investigated the effect of velocity on erosion-corrosion in further studies and found that increased velocity causes a change in the rate of passivation and repassivation leading to corrosion currents increasing and then corrosion contribution will be increased due to removing the passive layer.

Hamzah and Stephenson [1] also investigated the influence of velocity on erosion-corrosion in another study. Their results show that at 25°C there is an increase erosion rate with an increase in impact velocity. Stack et al. [88, 97] studied the effect of velocity on the erosion-corrosion of mild steel. They found that the effect of impact velocity on erosion-corrosion is dependent on many factors, including temperature, alloy corrosion resistance and impact angles.

Stack et al. [56] also investigated the influence of velocity on mild steel in water environment contains on Al_2O_3 particles of size between 500–710 μm with a buffer solution of $Na_2CO_3 + NaHCO_3$. Their results show that erosion increased the corrosion rate when the velocity was increased.This was attributed to the removal of the oxide film from the metal surface by the particles impact. The change in erosion rate produced by a change in velocity is expressed using the relationship:

Erosion rate $\alpha \quad V^n$

where n is the velocity exponent, usually between 2 and 3. The velocity exponent n is always about 2.5 for ductile materials.

1.2.8. Erosion-corrosion in an aqueous environment

In an aqueous environment the main challenge is to understand the erosion–corrosion mechanisms resulting from the complex interaction between erosion and corrosion. The joint action of erosion and corrosion leads to synergistic effects, which are due to the effect of erosion on corrosion and the effect of corrosion on erosion [1].

It has been proposed by many researchers [10-14]that impinging particles remove deposits or the protective film on the surface of metal, resulting in continuous exposure of a clean the surface of metal to the corrosive environment, thus leading to a higher corrosion rate due to erosion enhanced corrosion (corrosion due to erosion)[17-20].

On the other hand, erosion due to corrosion (corrosion enhanced erosion) by increasing the surface of the specimen results in more roughness and reduces the surface hardness of the specimen by dissolution of the specimen surface [19 and 74]. Materials generally depend on the formation of a protective passive film (passivity layer) which protects the surface of the metal against any attack [1 and 2]. However, the oxide film is usually damaged by shear or normal stress [18-20]. The effect of erosion on the surface of metal can be prevented permanently by a protective film.

Stack et al. [34] also investigated the influence of erosion on corrosion, corrosion on erosion by water slurries in erosion test rig and have found that erosion affects corrosion by removal of surface deposits, increasing local turbulence, and corrosion affects erosion by roughening the surface of the specimen. Postlethwait and Rajahram [16 and 51] have reported that the effect of corrosion is that it roughens the surface of the metal, which in turn increases the erosion rate.

1.2.9. General introduction of interaction between erosion and corrosion

The interaction between erosion and corrosion depends on many process parameters, and one process might enhance another [34 and 36]. When the erosion enhances the corrosion process it is termed the additive effect ΔK_c, and when corrosion enhances the erosion process it is called the synergistic effect ΔK_e [34, 36 and 56]. Moreover, a new effect has recently been observed called the antagonistic effect in which corrosion products impedes the erosion process [95-97]. This effect has been observed to occur at elevated temperature, where formation of passive film or sulphide layers may protect the target surface. In slurry erosion, antagonistic phenomena may occur, which is indicative of the negative synergistic effect $-\Delta K_e$ [34 and 36].

The additive and synergistic effects have been used by Stack et al. [2, 6, 19 and 20] for construction of erosion-corrosion maps for various material and environments.
On the other hand, according to Stack et al. [19-20,34and 36], the total wastage rate of erosion–corrosion (Kec) can be described and construction maps by the following equation:

$$K_{ec} = K_{eo} + K_{co} + \Delta K_e + \Delta K_c \qquad 1.10$$

where keo is the rate of pure erosion in absence of any corrosion, kco is the rate pure corrosion in the absence of erosion, and ΔK_c is the erosion enhanced corrosion, ΔK_e is the corrosion enhanced erosion [2,6,34and 36]. Consequently, the total rate of erosion-corrosion contribution can be given in the following expression:

$$K_{ec} = K_e + K_c \qquad 1.12$$

$$K_e = K_{eo} + \Delta K_e \qquad 1.13$$

$$K_c = K_{co} + \Delta K_c \qquad 1.14$$

1.2.9.1. The additive effect

The additive effect enhances the corrosion rate through an erosion process (corrosion due to erosion). It can be noted that many investigators do not distinguish between the additive and synergistic effects. The mechanism of the additive effect of erosion enhanced corrosion is observed to be dependent on the specific corrosive condition, such as active,dissolution, passivaion, or mass transfer [2- 6, 20 and 34]. Moreover, erosion parameters such as slurry velocity, concentration, etc., play the main role in the mechanism.

Postlethwaite et al. [51] reported that in the erosion-corrosion of a carbon steel pipeline transporting particle, iron, limestone and coal slurries, at concentrations and velocity, the corrosion rate was increased by the presence of solid particles and the effect was dependent upon the solid concentration and the slurry velocity. Postlethwaite et al. [109] also reported that in the erosion–corrosion of a pipeline carrying slurry at an impact velocity ranging between 2 m s^{-1} and 6 m s^{-1}, the overall wastage was dominated by corrosion and the process was under oxygen mass transfer corrosion control. It was suggested that the prevention of erosion-corrosion wastage of such a pipeline requires control of the effect of corrosion rather than erosion.

Stack et al. [79] observed that the additive effect and the synergistic effect by using a rotating cylinder electrode apparatus. They found that the additive and the synergistic effects occur in erosion-corrosion depending on erosion parameters such as slurry velocity and corrosion parameters such as potential parameters, and that they can occur in both active and passive conditions. The corrosion rate in a passive condition is very low due to the formation of a protective oxide film on the surface of the specimen, which indicates a decrease in the current density and then a decrease in the corrosion rate. Therefore, the interaction between erosion and corrosion will be very high in passive conditions if the particles are able to remove the oxide film.

In fact, many investigators [2, 6, and 36] have concentrated on researching passive conditions and they agree that under passivation conditions, erosion enhanced corrosion can occur when particles remove completely or partially the protective passive film. If the film is removed, then the corrosion rate is enhanced by mass transfer. Rajahram et al. [16] suggest another probable mechanism of erosion enhanced corrosion. They suggest that surface roughening of specimen during particle impact causing enhanced mass loss effects and increased corrosion.

Hodgkiess et al. [53] observed that for the erosion-corrosion of three materials - C-Mn steel, austenitic steel and a duplex stainless steel - by liquid impact, the passive film on stainless steel was not destroyed and was able to protect the surface of the specimen against particle impact, whereas the passive film on C-Mn steel was completely destroyed. In addition, it was observed that when the same material was exposed to slurry erosion conditions, with an increase in concentration, then the passive film on the surface of stainless steel was destroyed due to an increase in impact particle concentration and velocity. It can be concluded from the above review that erosion accelerated corrosion by removing the passive film. Hence, increase in the current density is indicative occurs of an increase in the corrosion rate. The mechanism of these effects is dependent on the erosion parameters shown in table 1.1.

Table 1.1: Some of the factors affecting slurry erosion rates (6).

Fluid	**Materiel**	**Particles**
Temperature	Ductility–brittleness	Size, size range
pH	Target–particle velocity	Shape–angularity
Potential	Melting point	Angle of impact
Viscosity	Metallographic structure	Density
Density	Residual stress levels	Velocity
Surface activity–lubricity	hardness	hardness
Boundary layer properties		

1.2.9.2. The synergistic effect

Compared to the additive effect of erosion accelerated corrosion, little effort has been made to support the evidence that corrosion can accelerate the erosion rate (erosion due to corrosion). Rajahram et al. [16] observed erosion due to corrosion in an erosion-corrosion study of carbon steel. It was proposed that the corrosion attacks the grain boundaries resulting in grain loosening, which can increase the erosion rate (synergistic effect). In addition, the increment in the erosion rate was observed to be very sensitive to the impact angle of the solid particle.

Zhang et al. [144] suggested the mechanism of erosion enhancement by corrosion. It was observed that the dissolution of the high energy regime of the sample, such as grain boundaries, inclusion boundary, and defect, leads to mass loss of materials from the metal surface by erosive action. In addition, Oka et al. [44] reported that the synergistic effect could either be positive or negative depending on the relative magnitude of the erosion and corrosion process. The positive synergistic effect happens when the erosion rate due to corrosion (corrosion enhanced erosion) by roughness surface of metal(ΔKe) and the negative effect occur when corrosion impedes the erosion rate by creating the passive film on the surface of the specimen ($-\Delta Ke$).

Stack et al [58 and 88] was also reported that the synergistic effect depends on the slurry velocity and impact angle. It was suggested that the positive synergistic can occur due to dissolution of the hardened layer of the target surface and roughening of the surface of the specimen, while the negative effect (antagonistic) occurs due to occlusion of hydroxide on the specimen, which in turn inhibits the plastic deformation of the surface and results in a decrease in the erosion rate.

Li et al. [35] also observed the antagonistic and synergistic effects of erosion accelerated corrosion in their study on erosion–corrosion of aluminium in aqueous slurry by 600- 850 μm silica sand particles. They found that the effect was positive in acetic acid slurry and negative in Na_2CO_3 slurry. On the other hand, Postlethwaite et al. [50] observed in their experimentation that although acetic acid is less corrosive compared to sodium carbonate, it has a much greater effect on the subsequent erosion rate.

Rajahram et al. [16] suggest another probable mechanism of corrosion enhanced erosion. They suggest that the particle impacts the passive film and damages it. Surface dissolution leads to the removal of the work hardened layer and increases in the surface roughness. The particle is able to penetrate deeper into the surface of specimen resulting in increasing the value of the synergism ΔKe. They suggest another probable mechanism of antagonism i.e. it occurs due to increased work hardening of specimen due to corrosion mechanism. Stack et al. [34] also observed that the synergistic effect can be positive or negative. They termed the negative synergistic effect or the 'antagonistic' effect, which generally occurs in the erosion-corrosion process at elevated temperature, which indicates an increase in the passive film.

It can be concluded from the above review that the positive synergistic effect of corrosion enhanced erosion occurs when corrosion attacks the grain boundaries resulting in grain loosening [16]. On the other hand, the 'antagonistic' effect, which generally occurs in the erosion-corrosion process when the passive film is reducing erosion [1- 4].

1.2.10. Impact angle

Impact angle is an important parameter in erosive wear. In general, impact angle is defined as the angle between the surface of the specimen and the flow direction of the slurry [10 and 11]. The impact angle is thought to have two effects on the oxide film of the metal: shear stress effect and normal stress effect. Shear stress is increased by decreasing the impact angle below 50° with enhanced erosion-corrosion by thinning or removing the oxide film formed on the surface of the steel. Normal stress is increased by increasing the impact angle more than 50° with damage to the surface film and generation of pores in the metal [11].

However, at zero impact angles the erosion rate of both ductile and brittle materials is negligible because the erodent particle slips over the surface of the specimen [11]. Cheng et al. [11] investigated the influence of impact angle on erosion-corrosion by using erosion test rig containing oil/water slurries, finding that the erosion rate of ductile material peaks at an intermediate impact angle of about 30°-50°, whereas the erosion rate of brittle materials peaks at close to 90°.

On the other hand, in the water slurry, the effect of the impact angle on the erosion rate is dissimilar to that observed for erosion in oil environment [2 and 6]. Clark et al. [45] reported that for ductile material erosion by hard ceramic particles in aqueous slurry, the erosion rate peaks at intermediate angles between 20° and 40°. In addition, Stack et al [58] reported that in the case of aqueous slurry conditions, the anodic current density increases slightly at high shear stress and at high normal stress 90°.

Tian et al. [10] also have investigated the influence of slurry impact angle on erosion-corrosion, finding that the effect of slurry impact angle on erosion-corrosion of steel is more complex and depends on the magnitude and synergism of shear stress and normal stress applied to the surface of the specimen, which will enhance the steel erosion–corrosion by degrading the surface oxide film and damaging the surface of steel.

The rate of mass losses due to the effect of impact angle are also dependent on the sort of material [2].With ductile materials, high value of erosion loss occurs at below a 50° angle, while for brittle materials the mass loss occurs at an impact angle of 90°, which is named normal incidence [10-11]. Burstein et al. [26] observed that there was a maximum of erosion–corrosion rate at impact angles ranging from 40° to 50° for 304L stainless steel in silica sand/water slurry.

1.3. Summary

It can be concluded that all aspects of the erosion–corrosion effect on steel in sea water have been covered by previous researchers. However, few researchers have studied the effect of erosion–corrosion on carbon steel in oil/water slurries. In fact, in their experiments researchers have only used chemical compositions of crude oil and not natural crude oil, which may have resulted in inaccurate results. Therefore, this thesis has studied the effect of erosion–corrosion on carbon steel in natural crude oil high gravity (API 52) with different parameters, such as six impact angles, three impact velocities, five potentials, and two different particles sizes.

Chapter 2

Calibration test and experimental Methodology

2.0. Calibration test and experimental Methodology

2.1 Introduction

A calibration test is very important stage before beginning any experimental work because it ensures that the slurry impingement erosion test rig is working accurately [99]. Moreover, it is very important to investigate the effect of adjusting the ejector parts on the output of the rig, such as impact velocity and slurry particle concentration.

2.2. Calibration test

The ejector is an important part of erosion test rig Fig. 2.2. The ejector plays the main role in the erosion test rig because the ejector has a great affect on erosion-corrosion parameters such as impact velocity and slurry particle concentration [99]. The relationship between the difference in slurry particle concentration and impact velocity with L- distance and d/D, which is the inlet nozzle diameter divided by the outlet nozzle diameter, were presented in the calibration test.

2.2.1. L-distance with variation of impact velocity and slurry concentration

In table 2.1 it can be seen that the calibration test has been carried out at different impact velocities and L-distances. Moreover, the performance of the test rig has been assessed to chart the impact velocity as a function of L-distance. In Fig. 2.1 it can be seen that the variation of impact velocities with the L-distance at different distances. Moreover, it can be seen that the velocity is changed by the cross section area of the outlet nozzle, as in equation 2.1. The velocity begins to increase with an increase in the L-distance. The variation of L-distance changes the vacuum action power or the suction effect for particles from nozzle 2, as shown in Fig. 2.2.

$$Q = A*V \qquad 2.1$$

Where:

Q = flow rate of slurry (the amount of slurry per sec time)

A = the cross section area of the nozzle (outlet nozzle)

V = impact velocity or velocity of slurry

So, from 2.1 the impact velocity can be determined by:

$$V = Q/A \qquad 2.2$$

The position effect of L-distance on the slurry particle concentration is very important to control the slurry concentration rate [99], as shown in Fig.2.3. It can be seen that there was an increase in concentration at the negative points (with decrease in the L-distance) then it is decreased in slurry particle concentration with an increase in the L-distance. Moreover, the results show that the position of the driving nozzle, or L-distance, has a great effect on the slurry particle concentration at all positions [99]. It can also be seen that slurry particle concentration increases when L-distance is less then 0, while it decreases when L-distance is more than -1.5 mm as showing in Fig.2.3 and that consistent with Zu et al [99].

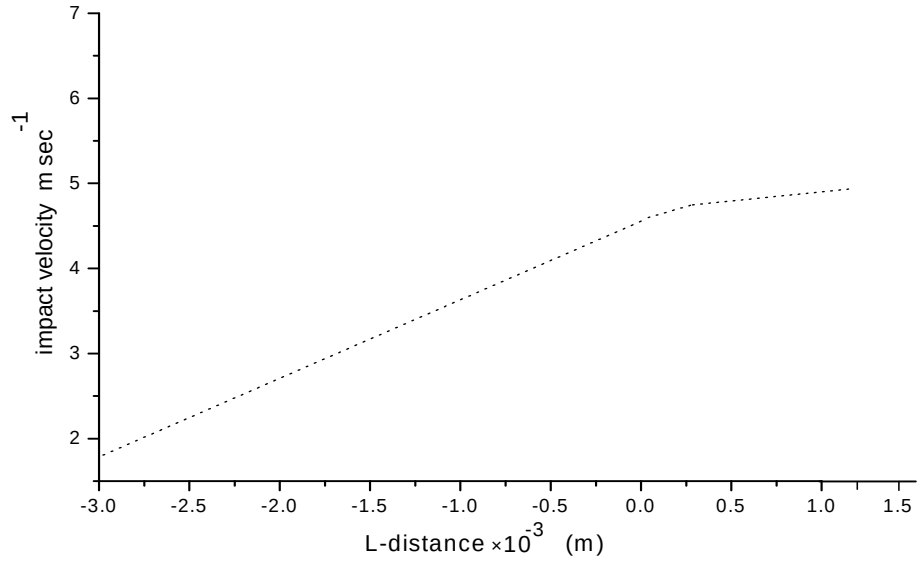

Fig. 2.1: Impact velocity vs. L-distance.

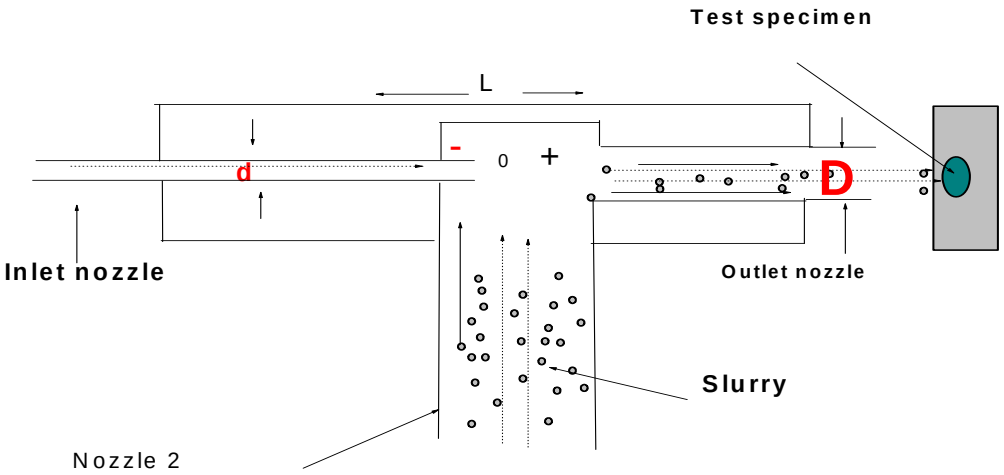

Fig. 2.2: Schematic diagram of the ejector.

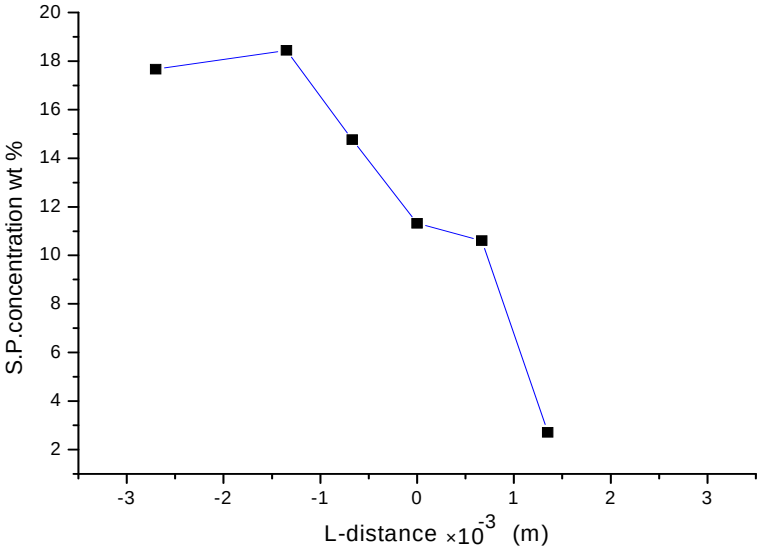

Fig. 2.3: Slurry particle concentration vs. L-distance.

2.2.2 d/D ratio with variation of impact velocity and slurry particle concentration.

The effect of the variation of d/D ratio (inlet nozzle diameter/outlet diameter nozzle) on impact velocity has been investigated and is shown in Fig. 2.4 and tables 2.2. It can be seen that the impact velocity increases with an increase of d/D ratio at every position. Moreover, the increase in the d/D ratio in such cases is attributed to a decrease in the outlet nozzle diameter (D). The d/D ratio effects on variation of the slurry particle concentration have been investigated and are shown in Fig. 2.5. It can be seen that the slurry particle concentration decreases with an increase in d/D ratio.From Fig. 2.6 it is clear that the slurry particle concentration decreases with an increase in impact velocity.

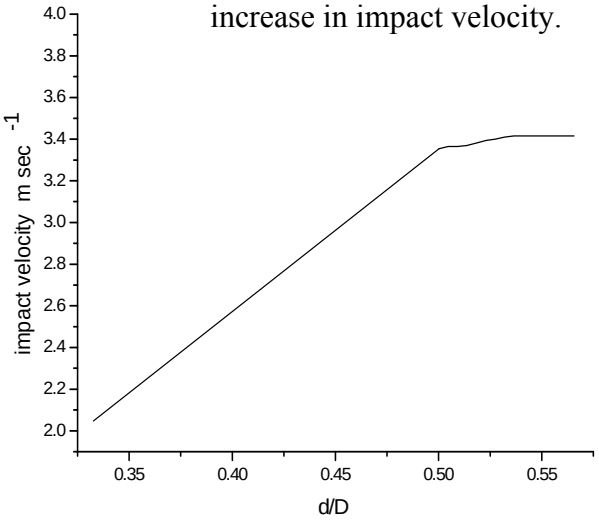

Fig. 2.4: Impact velocity as a function of d/D.

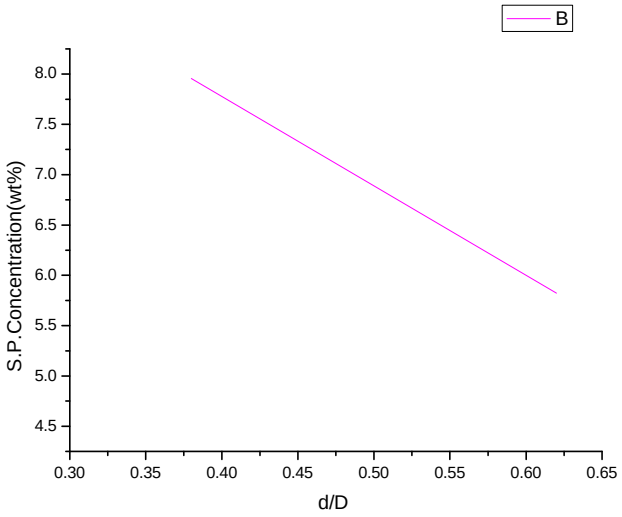

Fig. 2.5: Variation of slurry particle concentration as a function of d/D

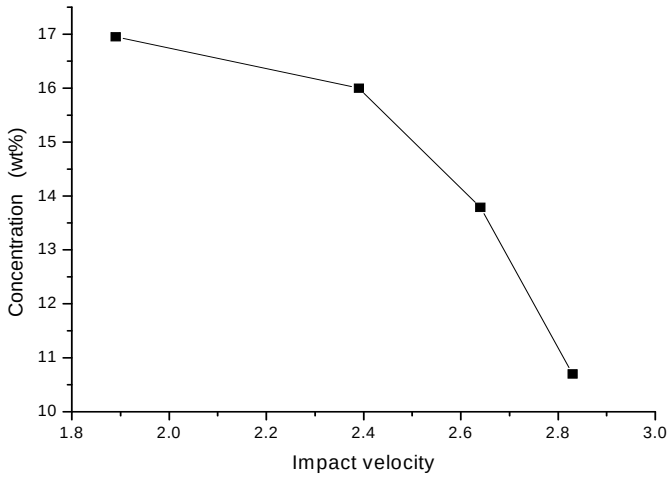

Fig. 2.6: Variation of slurry particle concentration as a function ofimpact velocity

Table 2.1 Calibration results of collected L-distance with variation of impact velocities.

Parameters	Unit	1	2	3	4	5	6
V_t	m^3	3.00E-04	3.80E-04	4.20E-04	4.50E-04	4.20E-04	4.35E-04
m_s	kg	4.60E-02	6.00E-02	5.50E-02	4.60E-02	4.07E-02	1.20E-02
ρ_s	kg/m^3	2.60E+03	2.60E+03	2.60E+03	2.60E+03	2.60E+03	2.60E+03
d	m	1.90E-03	1.90E-03	1.90E-03	1.90E-03	1.90E-03	1.90E-03
D	m	4.50E-03	4.50E-03	4.50E-03	4.50E-03	4.50E-03	4.50E-03
D_2	m	6.30E-03	6.30E-03	6.30E-03	6.30E-03	6.30E-03	6.30E-03
L	m	-2.7E-03	-1.35E-03	-0.67E-04	0	0.67 E-04	1.35 E-03
d/D		0.42	0.42	0.42	0.42	0.42	0.42
A	m^2	1.6E-05	1.59E-05	1.5904E-05	1.59E-05	1.59E-05	1.5904E-05
V	m/s	1.89	2.39	2.64	2.83	2.64	2.74
Vf	1/100 vol. %	0.059	0.061	0.050	0.04	0.037	0.010
c	wt. %	16. 95	16.29	13.79	10.73	10.09	2.67

where V_t is the total mass (slurry), m_s is the mass of the particle, ρ_s is the density of the particle, d is the diameter of the inlet nozzle, D is the diameter of the outlet nozzle, D_2 is the diameter of the nozzle 2, L is the distance, A is the area of outlet nozzle, V is the impact velocity, Vf is the frication = sand volume/ total mass and c is the concentration of the particle in the solution.

Table 2.2 Calibration results of collected velocities by d/D ratio with variation of impact velocities.

Parameters	Unit	1	2	3
V_t	m^3	5.35E-04	4.95E-04	7.00E-04
m_s	kg	2.40E-02	2.30E-02	4.96E-02
ρ_s	kg/m^3	2.60E+03	2.60E+03	2.60E+03
d	m	1.90E-03	2.50E-03	2.50E-03
D	m	5.50E-03	4.50E-03	5.50E-03
D_2	m	6.30E-03	6.30E-03	6.30E-03
L	m	-1.35E-03	-1.35E-03	-1.35E-03
d/D		0.346	0.556	0.456
A	m^2	2.38E-05	1.59E-05	2.38E-05
V	m/s	2.25	3.11	2.95

Table 2.3 Calibration results of d/D ratio with variation of impact velocities.

Parameters	Unit	1	2	3	4	5
V_t	m^3	7.20E-04	6.20E-04	3.80E-04	3.90E-04	5.70E-04
m_s	kg	9.99E-03	4.24E-02	9.83E-02	2.33E-02	2.33E-02
ρ_s	kg/m^3	2.60E+03	2.60E+03	2.60E+03	2.60E+03	2.60E+03
d	m	3.10E-03	3.10E-03	2.50E-03	2.50E-03	3.00E-03
D	m	4.50E-03	5.50E-03	6.00E-03	4.50E-03	4.50E-03
D_2	m	6.30E-03	6.30E-03	6.30E-03	6.30E-03	6.30E-03
L	m	-1.35E-03	-1.35E-03	-1.35E-03	-1.35E-03	-1.35E-03
d/D		0.69	0.56	0.42	0.56	0.67
A	m^2	1.59E-05	2.38E-05	2.83E-05	1.59E-05	1.59E-05
V	m/s	4.53	2.61	1.34	2.45	3.58

2. 3. Experiments methodology

2.3.1. Structure of erosion test rig

The slurry impingement erosion test rig is based on Zu's design [99], with some extra alterations added to the design so as to control temperatures, as in Fig. 2.7. The test rig can work at different impact angles, from 0°-90°. The impact velocities of the rig range from 1 to 7 m s^{-1}. Moreover, it can be used with different sized particles can be used as erodent particles.

The pump circulates fluid with variable speeds, and there is a motor to adjust the flow rate and the pressure of the flow to the chamber via the bypass valve. The rig contains a great plastic chamber with a dimension of 350 *200 *250 mm. It is made of Perspex sheets that can resist over 70°C. The test rig is divided into two main parts or chambers, the slurry part and the solution part, which are separated by a Perspex sheet containing a longitudinal slot with a material filter element to prevent escape of the erodent particles from chamber (1) to chamber (2).

The electrolyte is transported from the pump at high pressure during the out pass of the pump to the ejector. Moreover, most bypass valves are connected to the delivery pipeline and bottom slurry chamber. Part of the delivered solution passes directly to the slurry chamber causing stirrer action, and the other amount of the delivered solution can pass to the ejector when the bypass valve is partly closed. In addition, the bypass valve can control the flow rate of the fluid passed to the ejector by using the pump speed control. The slurry usually goes from the exit nozzle of the ejector with a certain concentration and impact velocity subjected to the test specimen that is fixed on the test specimen holder. The fluid which enters the pump is filtered. The filtration of the electrolyte is carried out in all stages to prevent damage of the pump.

The fluid passes in a closed loop from the pump and after that it impacts the specimen. The bypass is driven into the slurry chamber to create a stirrer action for the solution and erodent particles are conducted instead of the stirrer. The slurry is created in the ejector and impacts the test specimen through the outlet nozzle (see Fig. 2.2). The specimen angles are controlled by a holder on its axis. The dimensions of the test specimen are 25 mm length, 10 mm width, and 4 mm thickness. The tests were controlled at different angles from 15° to 90°.

2.3.2. The function of the ejector

The ejector is the main part of the test rig as it is used to control all erosion parameters as setting the ratio of the inlet nozzle to the outlet nozzle diameter (d/D), and the L-distance, as shown in Fig. 2.2, has an effect on the impact velocity and slurry particle concentration. The ejector is made from Perspex material to avoid any electrochemical interaction, and all material used in manufacturing the nozzle is nylon. The ejector contains three threaded nozzles, the inlet for the solution (without particle), the inlet for solid particles, and the last is the outlet for slurry which the solution and erodent particles (slurry) as in Figure.2.2. The inlet nozzle of the fluid without erodent with a variable bore of diameters from 1.5 to 4.5 mm and distance L. Moreover, the inlet is used to control the solid particles concentration with solution because of the vacuum action, which occurs in the T-section. The outlet nozzles have different diameters in the experimental work, from 1.5 mm to 6 mm according to the required impact velocity, as can be seen in tables 2.2 and 2.3.

2.3.3 The electrochemical process

In the oil field, the electrochemical method is used to assess erosion-corrosion rates of equipments and therefore predict the lifetime of material in oil field. Moreover, the electrochemical method lets the oilfield engineer to design, maintenance and replacement of that equipments were damaged by erosion corrosion. The benefit of using electrochemical methods in the oilfield is that information is real time, recording the corrosion reaction as erosion -corrosion occurs in the equipment [17].

Experiments were preformed in potentiostatic under fixed applied potential and potentiodynamic (polarization behaviour) conditions.Polarization curves were recorded at the required velocity and impact angle from -800 to 800mV.

Potentiostatic tests have been conducted to plot the corrosion current vs time under constant applied potential, Fig.2.10.The average corrosion current can be substituted in Faraday's Law to calculate the corrosion contribution.The corrosion rate can be calculated as an electrochemical process and was studied by measuring the changes that occurred in metal with time and current. Corrosion rates (Kc and Kco) could be controlled by passing anodic or cathode currents into the metal. When electrons are passed into the metal and reach the metal that points to the electrolyte interface (a cathode current), the anodic reaction will be reduced while the cathode reaction rate increases. If the anode is small then rapid of through thickness will occur, but if the anode area is large then only a small losses in the cross section will occur [4].

In the case of chemical environments, it is sometimes possible to achieve anodic protection, passing a current which takes electrons out of the metal and raising its potential. However, in a good situation it will be followed by the formation of a protective passive surface film on the surface of the specimen. Moreover, the electrochemical interface is very important to study the corrosion performance of the materials. The electrochemical method has been done by using three electrodes through an ACM (Gillac) potentiostat, as shown in Fig. 2.8. The saturated calomel electrode (SCE) as reference electrode (RE) and a Graphite bar is used as an auxiliary electrode (AE), while a working electrode (WR) is connected to the test specimens.

2.4. Test procedure

Erosion–corrosion of carbon steel was investigated by using an impinging jet apparatus, as shown in Fig. 2.7. The total value of erosion–corrosion was determined by weight loss measurement. The samples were weighed before and after each test. The test samples were set at various impact velocities, 2.5 m $s^{-1,}$ 3.5 m s^{-1} and 4.5 m s^{-1}, with different impact angles, such as 15°, 30°, 45°, 60°**,** 75° and 90° degrees to the impinging jet. The erosion–corrosion test continued for 30 minutes for each test sample. Erosion–corrosion was performed at applied potentials of -400,-200, 0, 200 and 400 mV for half an hour using a computer controlled ACM potentiostatic (GILLAC) (see Fig. 2.9). The experimental error was within ±5% based on the experiments repeated

The corrosion rate can be measured by determining the current density flowing between the two electrodes and the diffusion of species to and from the electrode surface. The corrosion rate is a measure of the quantity of material corroded on the surface of the specimen in a given period of time. It is often limited by the speed of ion transportation to and from the electrodes. Therefore, current density is an important factor when using corrosion rates to determine the life of equipments in a corrosive environment. The corrosion rate can be calculated by using the Faraday's Law as follows:

$$Kc = M\, i\, t \,/\, (n\, F) \qquad 2.3$$

where M is the atomic weight of the metal (55.85), n is the number of valence electrons transferred by each metal atom in the corrosion process (between 2-3), and F is the Faraday's constant (F = 26.8055 A.H/mol), t is the time (h) and i is current density/area (A/ $cm^{2)}$.From the corrosion rate can be calculated Δkc, which is corrosion due to erosion, using the following equation:

$$Kc = Kco + \Delta Kc \qquad 2.4$$

Kco is pure corrosion without erosion (no particle) can be calculated from Faraday's Law as in equation 2.3.

On the other hand, Kec is total erosion-corrosion mass loss was determined by mass loss measurement (using Mettler college 150 balance with an accuracy ±0.1mg and Ke is the erosion contribution can be determined by the following equation:

$$Ke=Kec-Kc \qquad 2.5$$

Δke is erosion due to corrosion can be determined by the following equation:

$$\Delta Ke = Ke-Keo \qquad 2.6$$

Keo is pure erosion and can be found from the weight balance at -500mV.

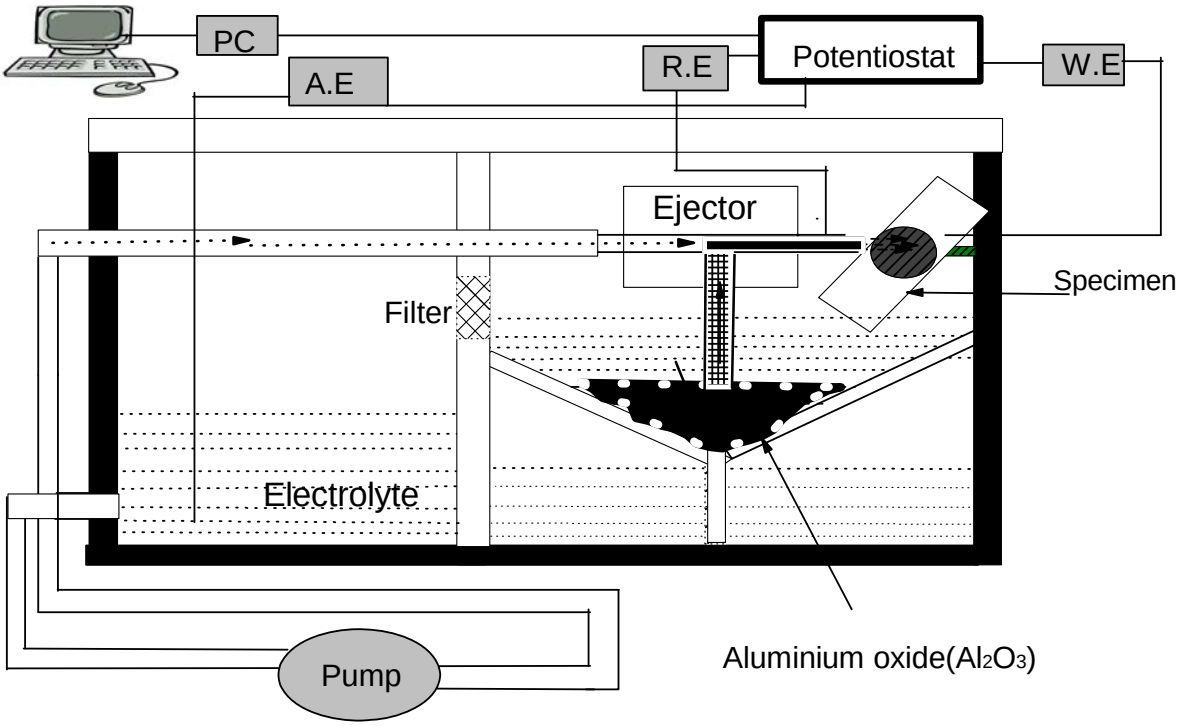

Fig. 2.7: Schematic diagram of erosion-corrosion test rig

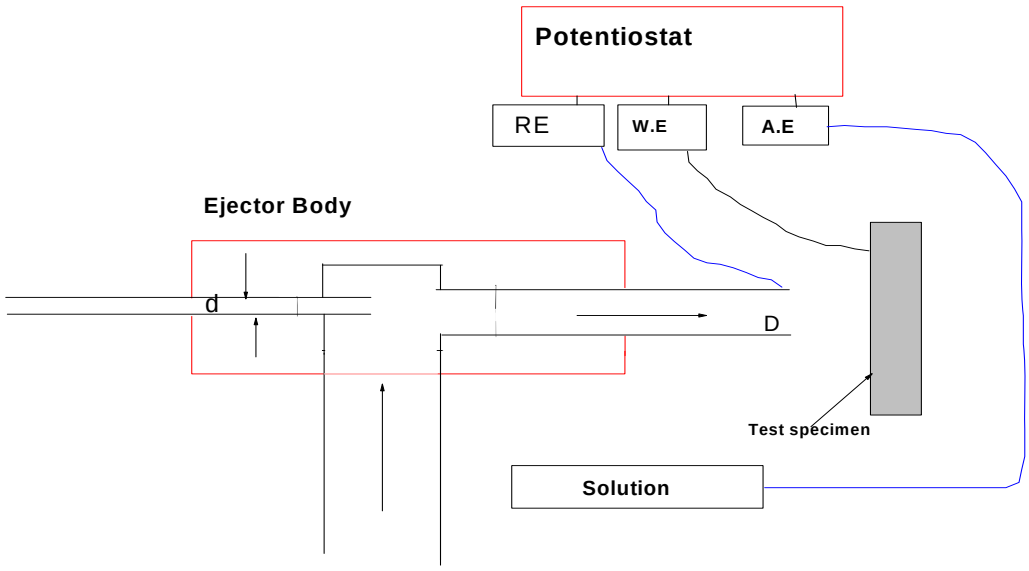

Fig. 2.8: Electrochemical connection in the slurry erosion test [36].

Fig. 2.9: Electrochemical interface with three electrodes ACM (Gillac).

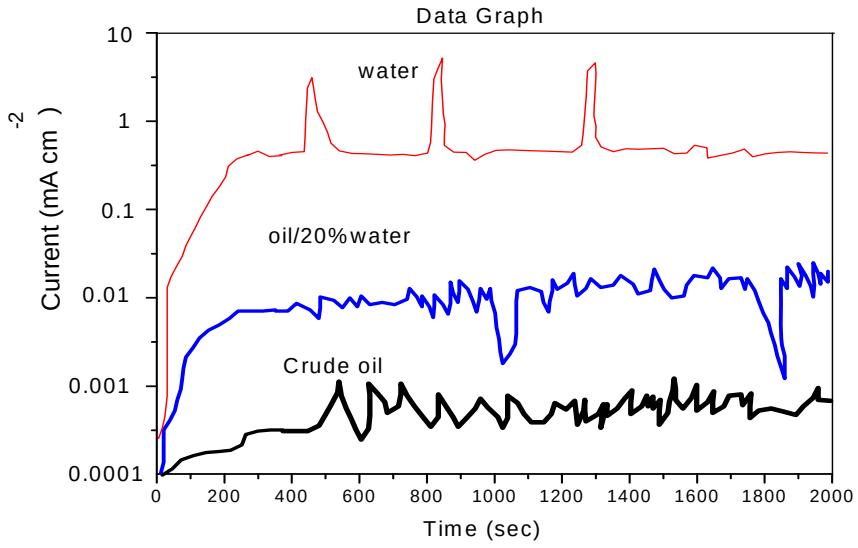

Fig. 2.10: corrosion current vs time during potentiostat test.

2.4.1. Materials

The target material for the erosion-corrosion tests was carbon steel (X52). The chemical composition of the carbon steel is given in table 2.4. All specimens were in the shape of flat sheets of 25×10 mm with a thickness of about 4 mm. At the end of the test the specimens were removed and cleaned with distilled water and acetone to remove any slurry or debris. Each test was repeated three times and the average results were taken. Specimens were examined using a scanning electron microscope (SEM) prior to and after testing to investigate the microstructure and mechanism of the specimens due to damage.

Table 2.4: Chemical composition of carbon steel (wt %)

C	0.18
Mn	1.6
Si	0.55
P	0.025
S	0.008
Cr	0.250
Ni	0.300
Cu	0.350
Fe	96.7.

2.4.2. Slurry

All experiments were performed using angular aluminium oxide (Al_2O_3) particles with a particle diameter range of 150-300µm and 600-710µm as erodent (Figs. 2.11(a) and (b)). The particles were used for 9 working hours after this time, then replaced with new particles to avoid any erosion effect due to the degradation of the impacting particles during the erosion-corrosion test (20 wt % particles to 80% solution). The erosion–corrosion test of carbon steel was performed in three environments. The water reservoir was a buffer solution of $Na2CO_3$ + $NaHCO_3$, with a pH value of 8.25, while in pure crude oil the pH was 5 (the chemical composition of crude oil is shown in table 2.5) and in the oil/20% water environment the pH was 8. All experiments were performed at room temperature.

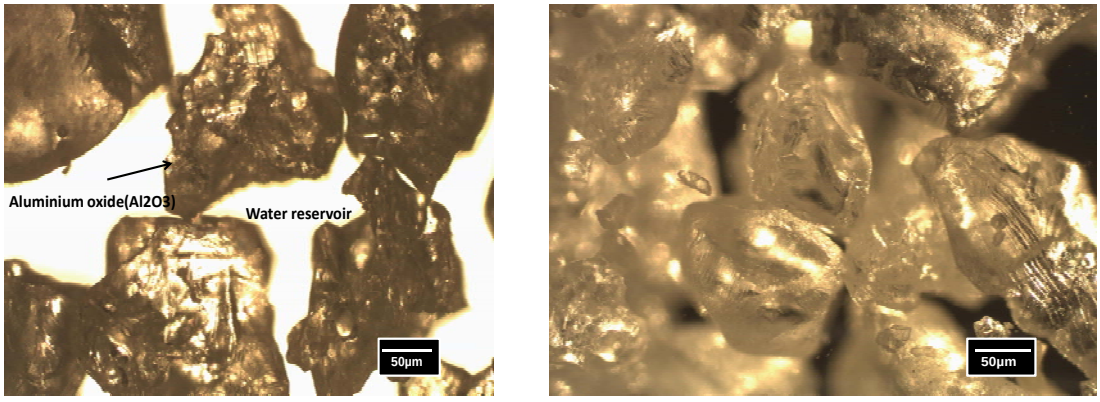

(a) (b)

Fig. 2.11: Optical microscopy of aluminium oxide used in the erosion-corrosion test rig :(a) 600-710µm (b) 150-300µm.

Table.2.5: The chemical composition of crude oil

Test	Result
Colour	Brown
A.P.I gravity at 60F	52.9
Specific gravity at 60 F	0.7674
Density g/ml	0.7670
Total sulphur % wt	0.0167
Total nitrogen %wt	0.08
Pour point F	+25
Viscosity at 77 F	1.750
Manganese (PPM wt)	0.11
Calcium (PPM wt)	33.31
Sodium (PPM wt)	04.26
Potassium (PPM wt)	01.07
Conradson carbon % wt	0.11
Asphaltenes %wt	0.07
Hydrogen sulfide % wt	0.0007
Sediment and water % VOL	0.05
Salt content (lbs/1000bbs)	5.2
Wax content % wt	3.82

2.5. Summary of calibration results

- The L-distance is inversely proportional to slurry particle concentration.
- The d/D ratio value is inversely proportional to slurry particle concentration.
- The L-distance is proportional to impact velocity.
- The d/D ratio value is proportional to impact velocity.

Chapter 3

Results and discussion

(Effect of impact angle, impact velocity for particle sizes 600-710µm and 150-300µm on erosion-corrosion maps)

3.0. Introduction

In this chapter the carbon steel in water, crude oil and combined environments with different particle sizes (600-710μm and 150-300μm) as erodent particles have been investigated at range of impact angles and impact velocities.The polarization curves have been investigated at constant of impact angle and at range of impact velocities for large particle sizes 600-710μm and a small particle sizes 150-300μm.The total mass loss rate due to erosion –corrosion and erosion contribution and corrosion contribution have been plotted as function of impact velocity at constant applied potentials for large particle sizes 600-710μm and a small particle sizes 150-300μm.
The results have been used to construct erosion-corrosion mechanism, wastage and additive –synergism maps as function of impact velocities and impact angles at range of constant applied potentials for particle sizes (600-710μm and 150-300μm).

3.1. Effect of impact angle, impact velocity for particle sizes 600-710µm on erosion-corrosion maps

3.1.1 General

The effect of impact angle and impact velocity on erosion-corrosion of carbon steel was investigated in a slurry erosion impingement test using a variety of environments (water, crude oil, and 20% water with crude oil); the electrolyte included aluminium oxide (Al_2O_3) 600-710µm. The volume loss was plotted as a function of impact angles and impact velocities at five constant applied potentials.

3.1.2. The Conditions of the test

The erosion–corrosion tests were undertaken using different environments (water, crude oil, and oil/20% water). The effect of impact velocities on erosion-corrosion were investigated at 2.5, 3.5 and 4.5 m s^{-1} with impact angles 15°, 30°, 45°, 60°, 75° and 90° at five constant applied potentials, -400, -200.0, 200 and 400mV.

3.1.3. Polarization curves for particle sizes 600-710µm

The polarization curves of the samples were investigated using a computer AC Gill potentiostat in different environments; water, crude oil, and crude oil / 20% water. The corrosion testing was conducted under potentiodynamic conditions, where samples were polarized at potentials 15°, 30°,45°, 60°,75° and 90°, and in different environments to observe the effect of corrosion attacks on material. The polarization curves for the carbon steel in three environments at various impact velocities and impact angles Figures 3.1-3.6. There was a clear difference between the effects of the environments on the carbon steel. The polarization curve tended to shift to higher current densities with higher velocities for all environments.

However, it was found that in crude oil and combined environments there was a lower current density than in the reservoir water environment, indicating a higher corrosion resistance compared to water. In the water environment at impact angle of 15°, there was a general increase in current density with increasing velocity from 2.5 to 4.5 ms^{-1} Fig. 3.1(a). Clear evidence of passivation was observed at low velocity 2.5ms^{-1}. The average free corrosion potential (Ecorr) was approximately -410 mV for all impact velocities, the average current density was between 0.20-1.17 mA c m^{-2} Fig. 3.1(a).

A similar pattern was observed for the carbon steel in the crude oil environment, with current density increasing with velocity Fig. 3.1-(b). However, in a crude oil environment (Fig. 3.1-(b)) it was observed that the average free corrosion potential (Ecorr) was higher than in the water environment. At an impact angle of 15° in the 20% water with crude oil environment, the average free corrosion potential (Ecorr) was roughly between -405 mV and -420 Fig. 3.1-(c). Moreover, there was an increase in the current value compared with in crude oil environment.

In the water environment at an impact angle of 30° Fig. 3.2-(a), the free corrosion potential (Ecorr) was similar to impact angle 15°.In addition, the current density was increased when the impact velocity increased. At an impact angle of 30° in the crude oil environment Fig. 3.2-(b), the free corrosion potential (Ecorr) was also similar to the corrosion potential (Ecorr) at impact angle 15°, between-400mVand-410mV. However, in the 20% water with crude oil environment at an impact angle of 30° Fig.3.2-(c), the corrosion potential (Ecorr) was around -415 mV approximately for all impact velocities.

At an impact angle of 45° in the water environment Fig.3.3-(a) , the corrosion potential (Ecorr) was approximately between -415mV and -425mV, and the current density was increased with velocity and impact angle from 30° to 45°, which was identified to increase the corrosion rate [10-11]. In the crude oil environment at an impact angle of 45° there was a small change in average corrosion potential (Ecorr), with an increase to approximately -405 mV. On the other hand, the average current density value for three impact velocities decreased very slowly at an impact angle of 45° Fig. 3.3-(b). In the crude oil/20% water environment at an impact angle of 45° the average corrosion potential (Ecorr) was roughly -420 mV Fig. 3.3-(c).

In the water environment, Fig. 3.4-(a), Fig. 3.5-(a) and Fig. 3.6-(a) at impact angles of 60°, 75° and 90° the current density increases with an increase in the velocity. However, the value of current at impact angle 75° was less than at previous impact angles. At impact angles of 60°, 75° and 90° in the crude oil environment, there was no indication of a shift in corrosion potential (Ecorr) Fig. 3.4-(b), Fig. 3.5-(b) and Fig. 3.6-(b).

In the 20% water with crude oil environment, there was an increase in current values due to an increased in impact velocity and the values of current density were increased at impact angle 90° compared with at impact angle 60° Fig. 3.4-(c), Fig. 3.5-(c) and Fig. 3.6-(c). It is clear that the results above for carbon steel in crude oil and combined environments indicate that the cathodic current densities increased as a function of impact velocity, and that this reaction was also reduced in the water conditions. However, it is interesting that the cathodic currents in oil (Figures 3.1(b)-3.6(b)) were significantly higher than the anodic currents and that this difference was not marked in the water environments (Figures 3.1(a)-3.6(a)) [10].

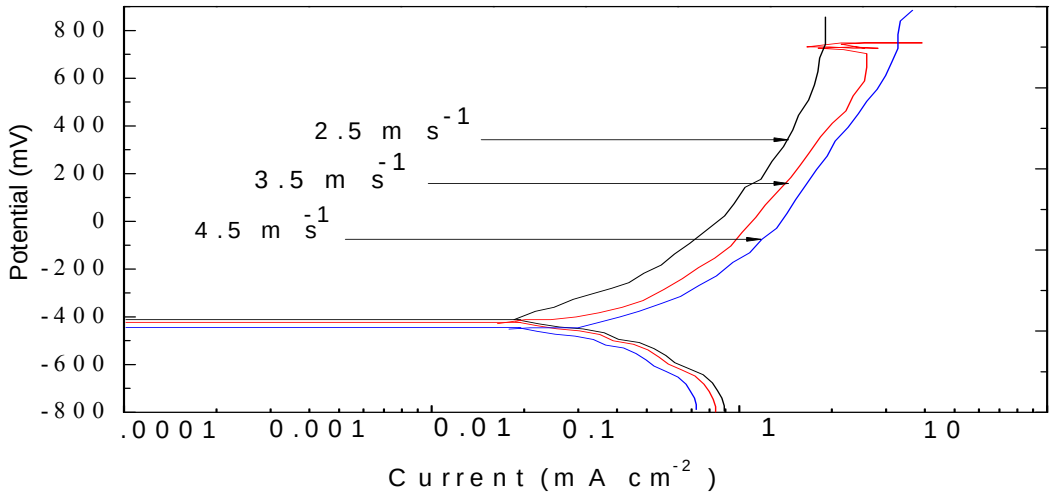

(a)

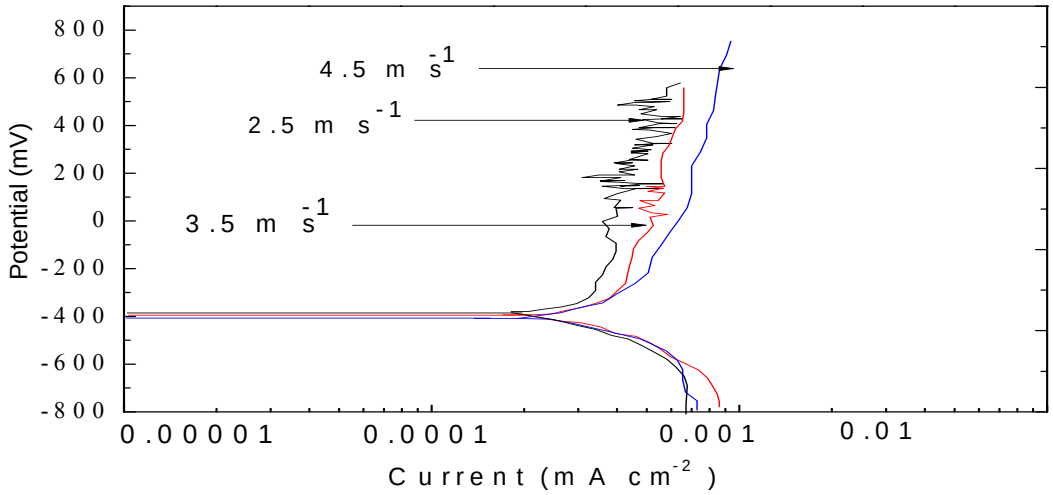

(b)

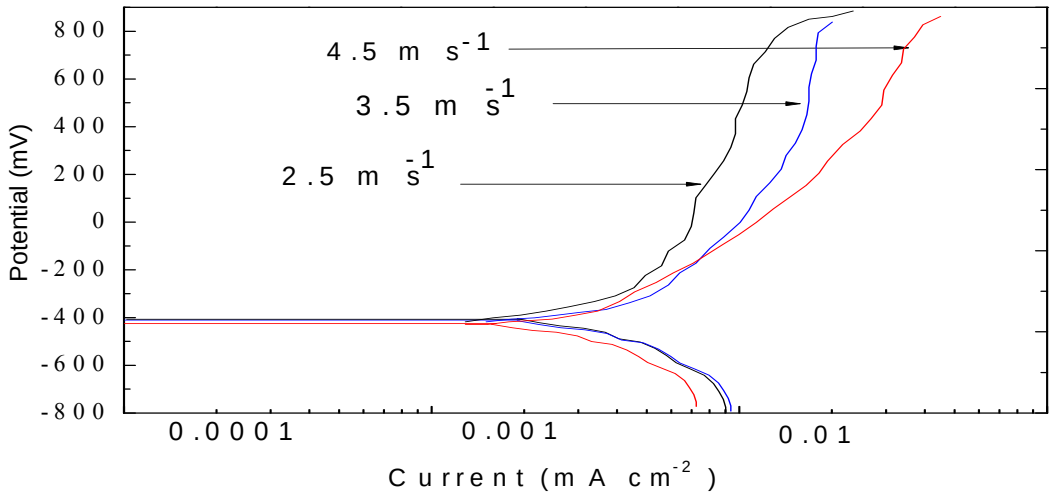

(c)

Fig.3.1: Polarization curves for carbon steel at various impact velocities, at impact angle 15° and particle size 600-710µm in (a) water (b) crude oil (c) oil /20% water.

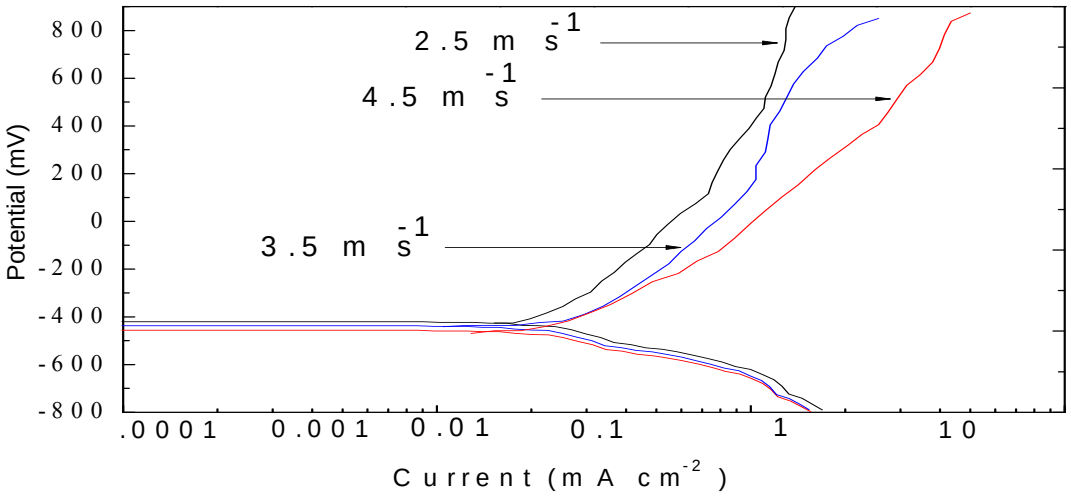

(a)

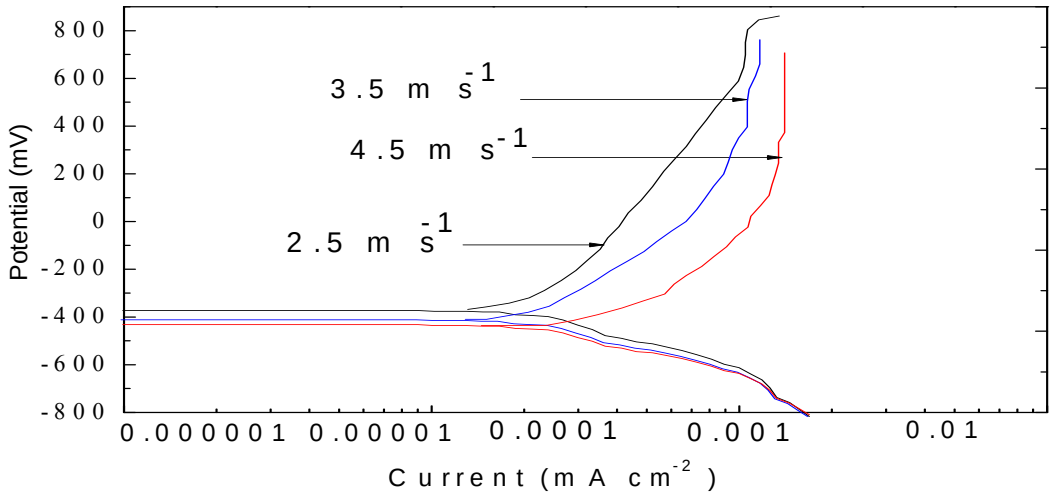

(b)

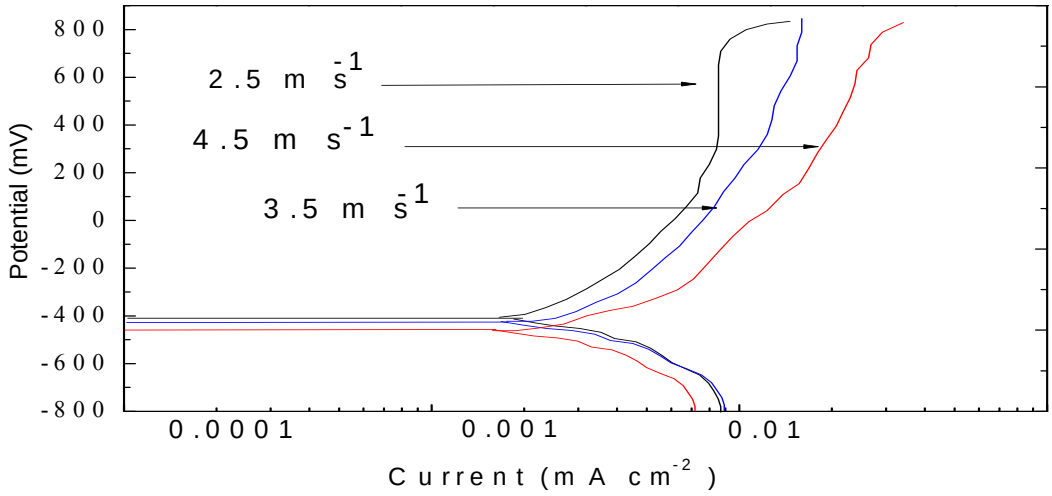

(c)

Fig.3.2: Polarization curves for carbon steel at various impact velocities, at impact angle 30° and particle size 600-710µm in (a) water (b) crude oil (c) oil /20% water.

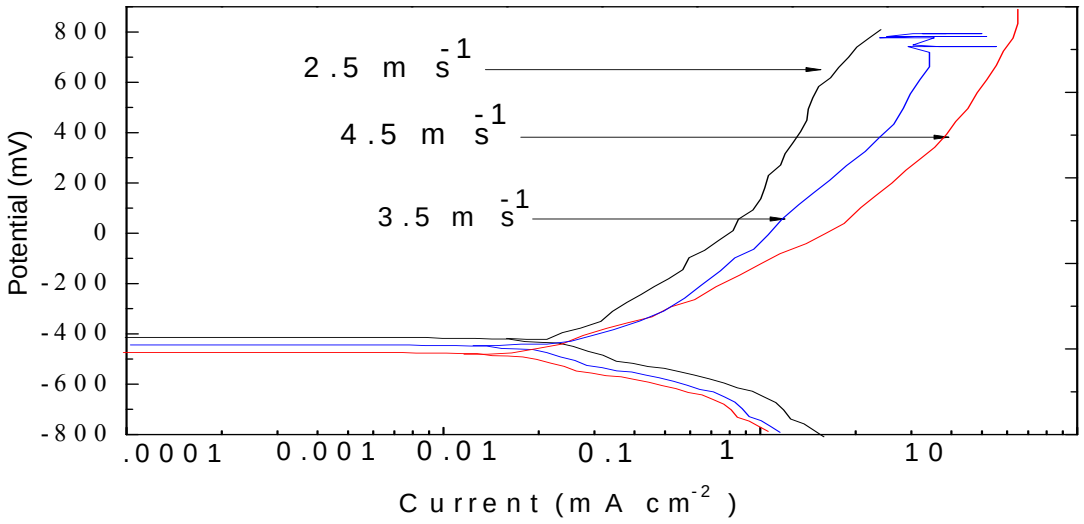

(a)

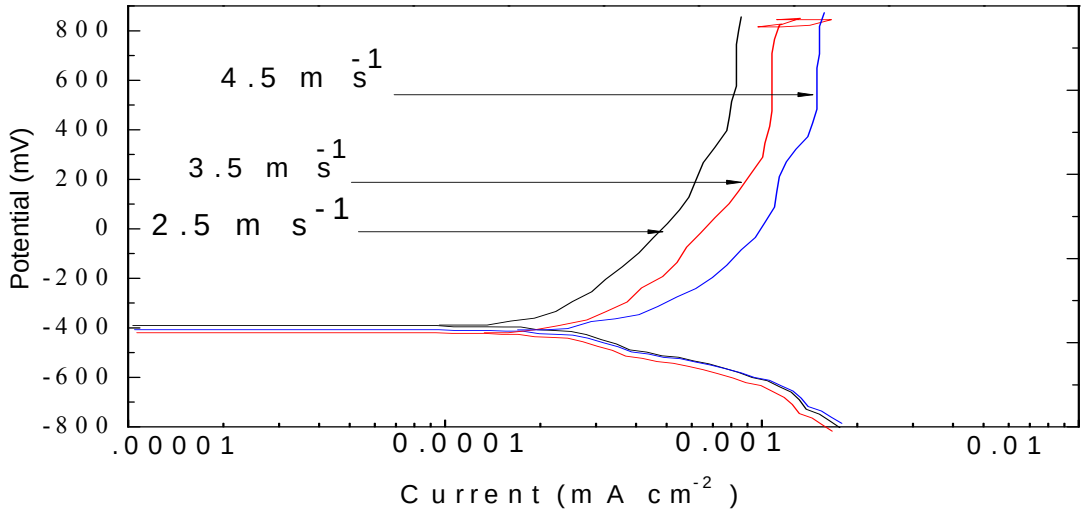

(b)

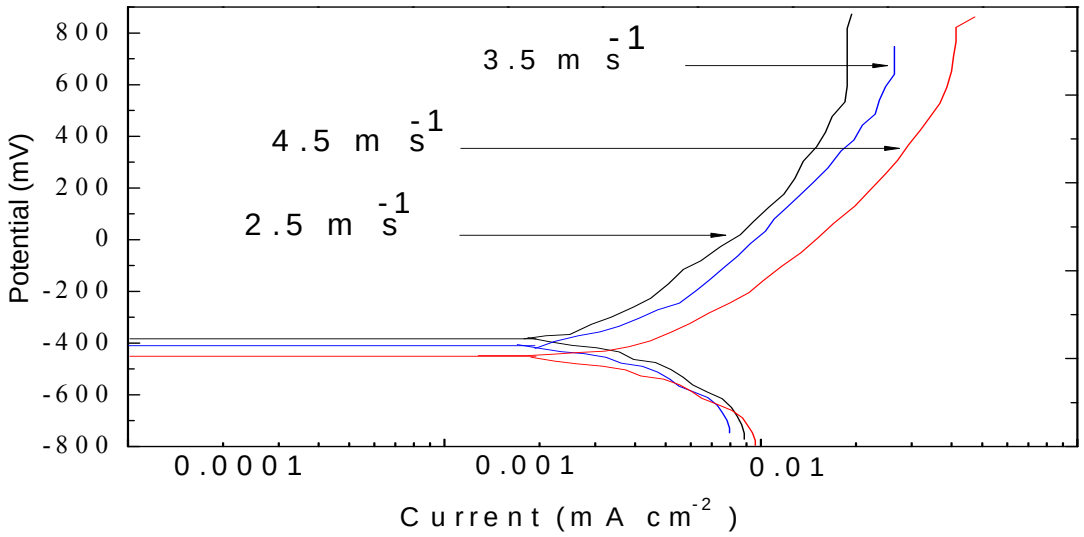

(c)

Fig.3.3: Polarization curves for carbon steel at various impact velocities, at impact angle 45° and particle size 600-710µm in (a) water (b) crude oil (c) oil /20% water.

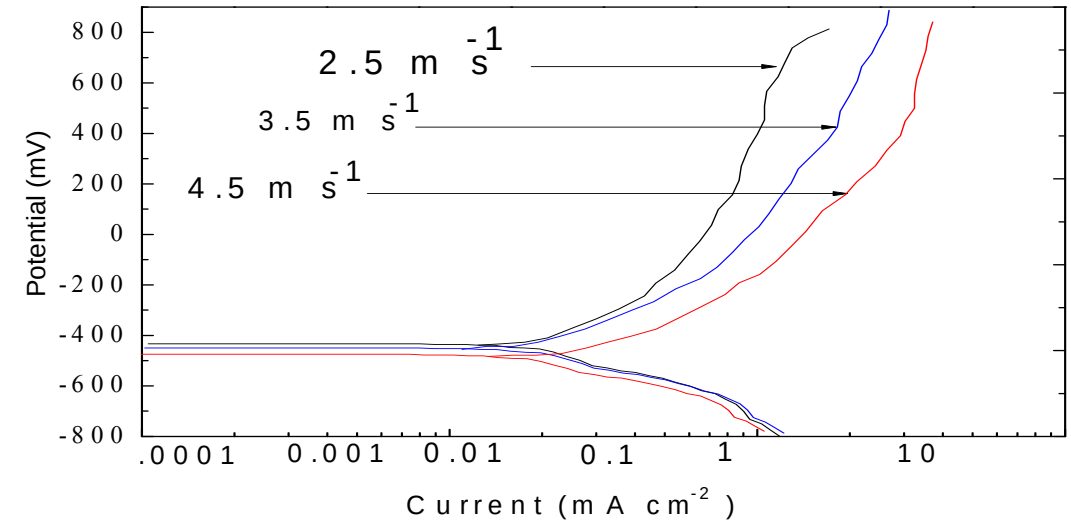

(a)

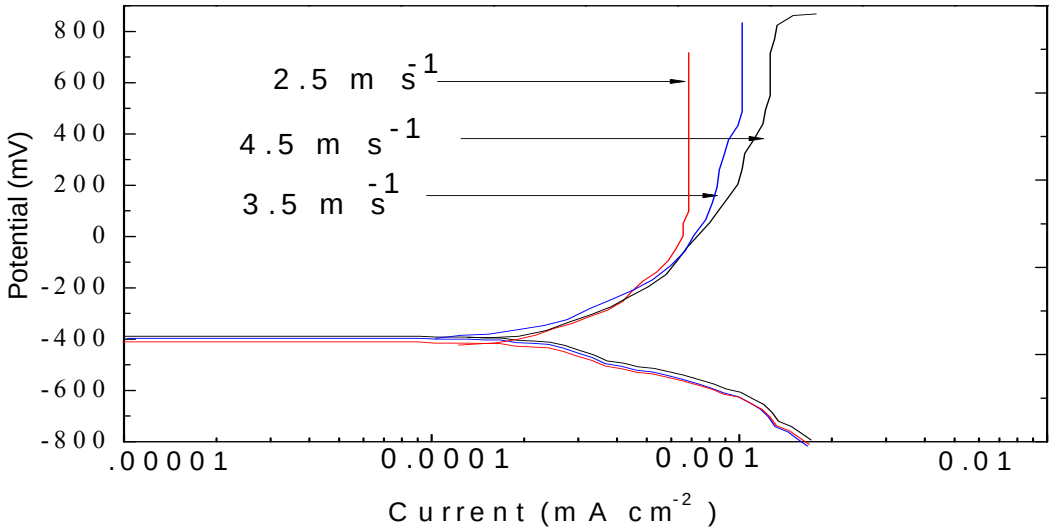

(b)

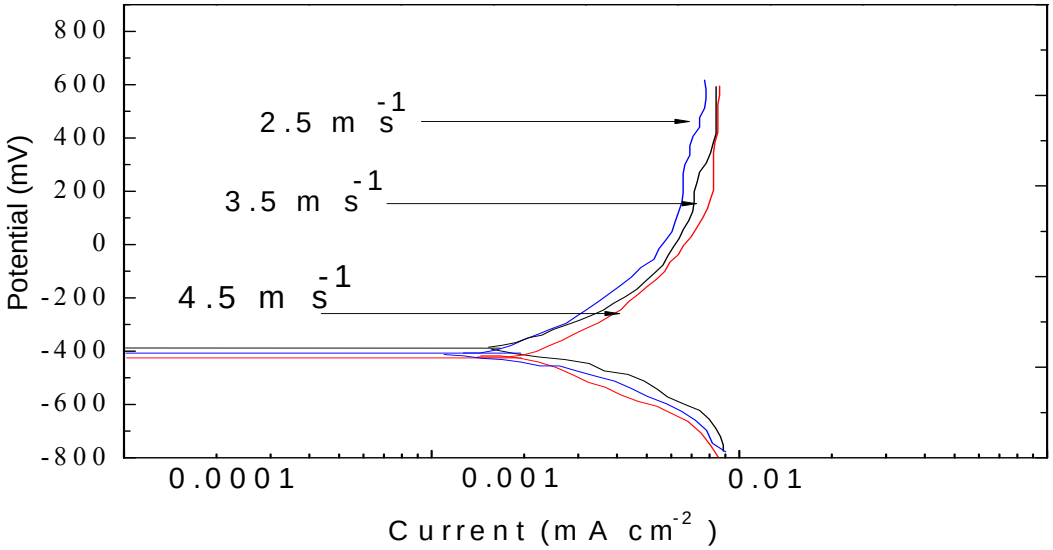

(c)

Fig.3.4: Polarization curves for carbon steel at various impact velocities, at impact angle 60° and particle size 600-710µm in (a) water (b) crude oil (c) oil /20% water.

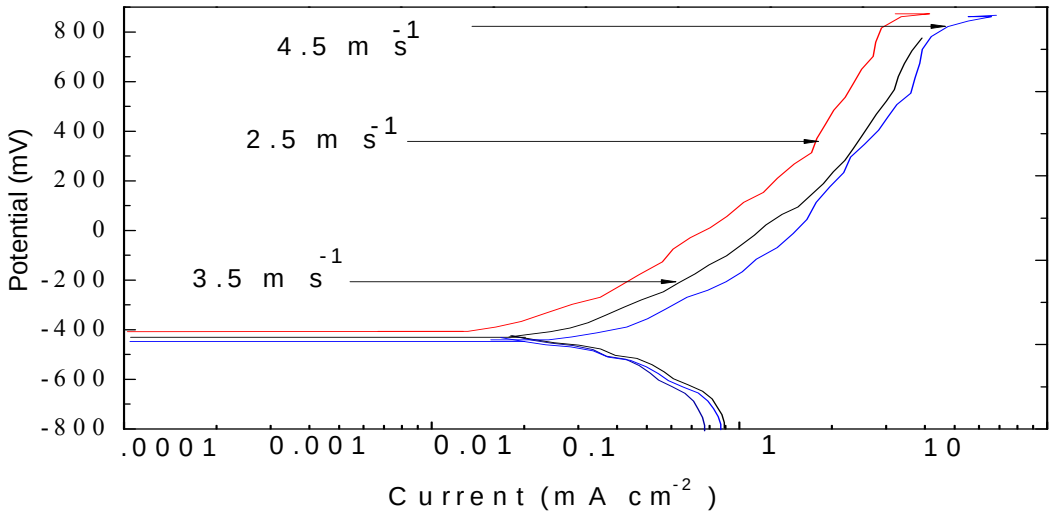

(a)

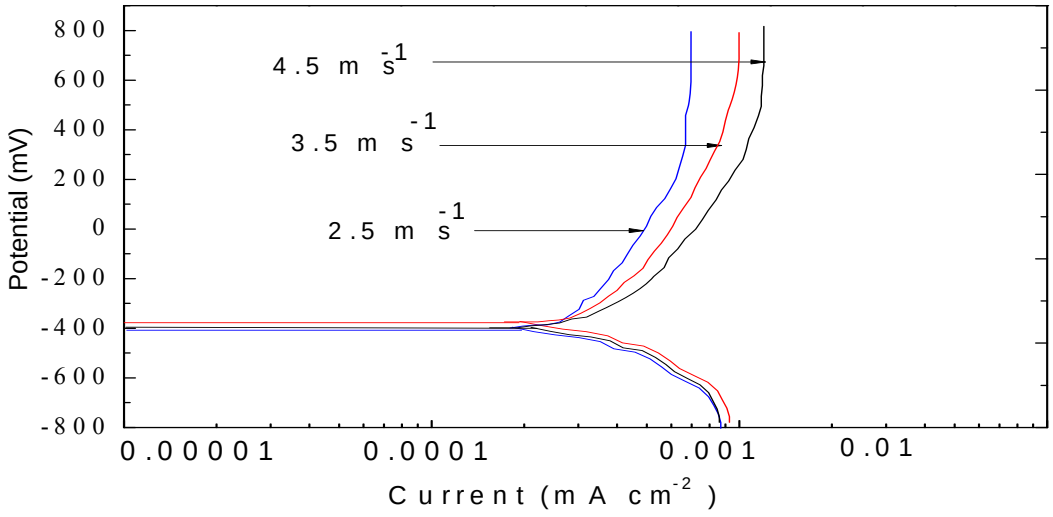

(b)

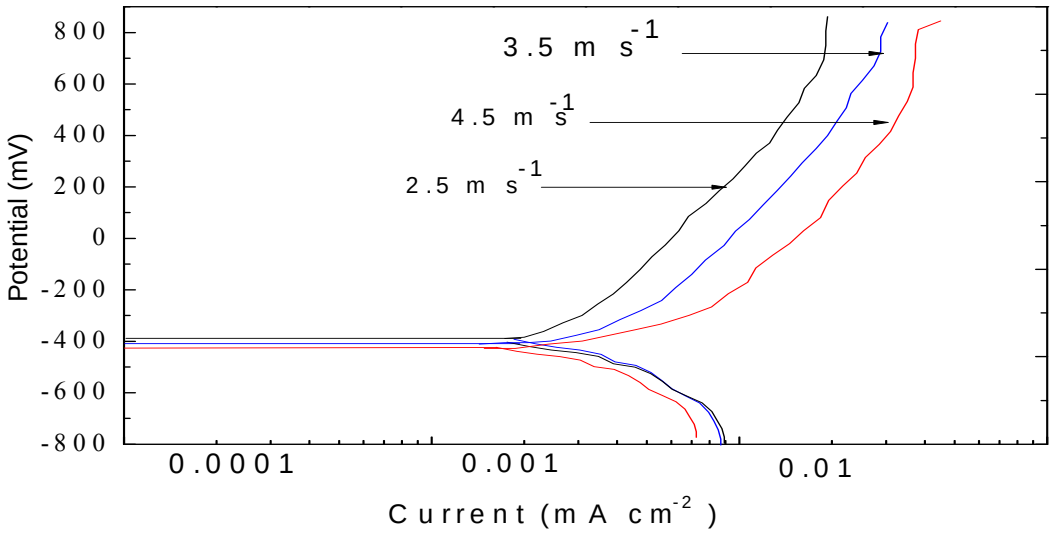

(c)

Fig.3.5: Polarization curves for carbon steel at various impact velocities, at impact angle 75° and particle size 600-710µm in (a) water (b) crude oil (c) oil /20% water.

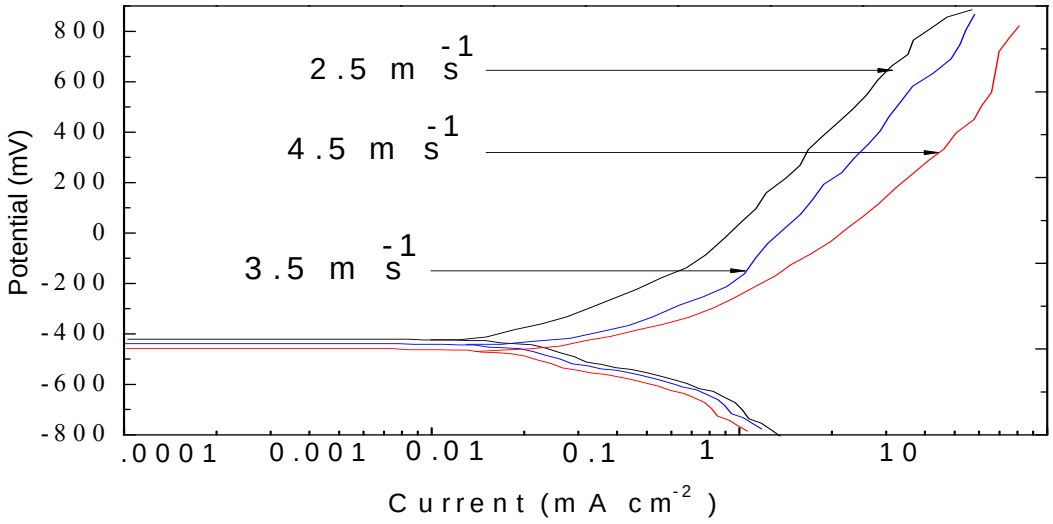

(a)

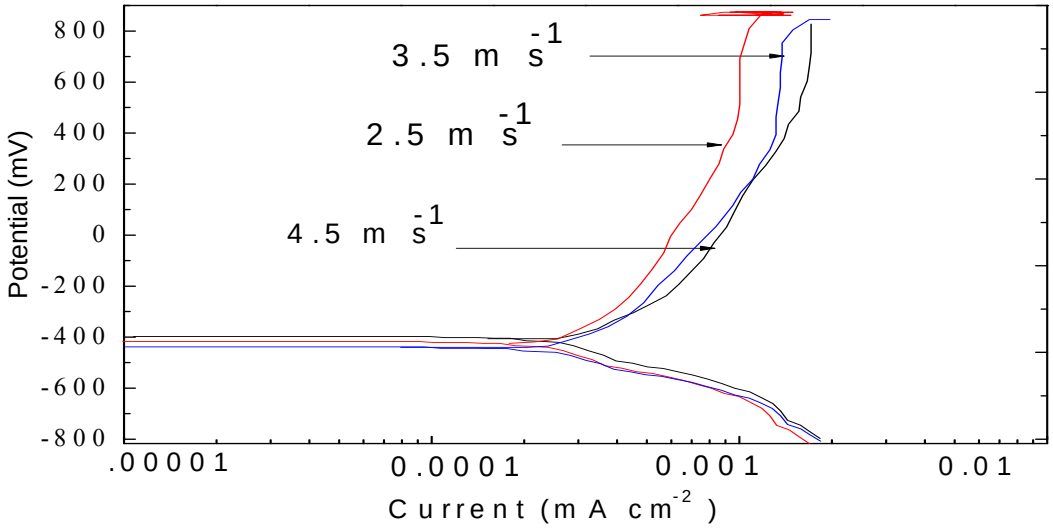

(b)

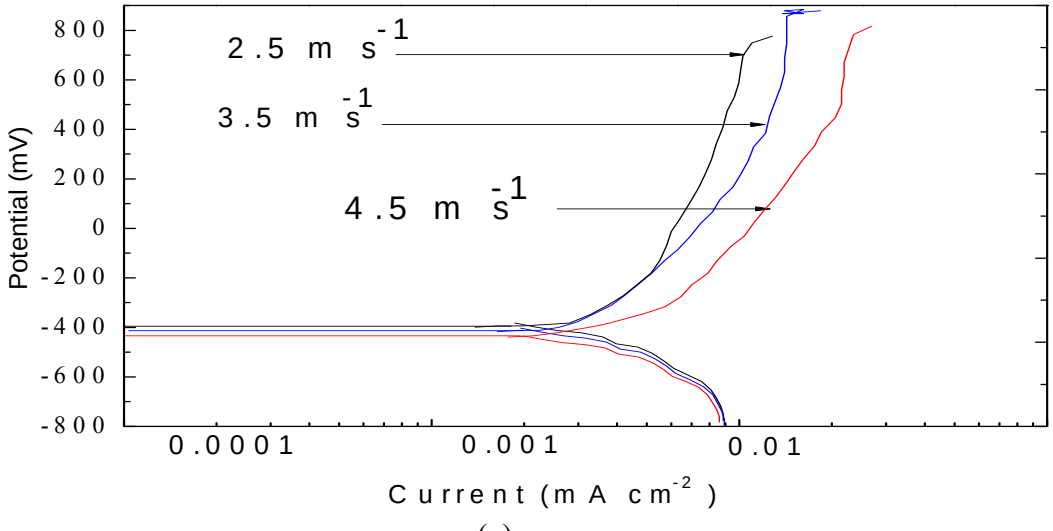

(c)

Fig.3.6: Polarization curves for carbon steel at various impact velocities, at impact angle 90° and particle size 600-710µm in (a) water (b) crude oil (c) oil /20% water.

3.1.4. Volume loss for particle sizes 600-710µm

The mass loss has been constructed as a function of impact velocity at impact angles and at constant potentials. The total erosion-corrosion Kec can be expressed from the calculation of the corrosion contribution Kc and the erosion contribution Ke [20-34 and 36]

$$Kec = Ke + Kc \quad 3.1$$

Kec is the interaction between the mechanical and electrochemical damage processes, erosion and corrosion can enhance each other.

$$Ke = Keo + \Delta Ke \quad 3.2$$

$$Kc = Kco + \Delta Kc \quad 3.3$$

where Keo is the pure erosion, Kco is the pure corrosion, ΔKc is the corrosion due to erosion, and ΔKe is the erosion due to corrosion. Tables 3.1-3.15 show the results of the calculations of volume loss for Ke, Kc and Kec for difference environments and impact velocities with various impact angles at various applied potentials.

3.1.4.1. Mass loss in water reservoir

With $NaHCO_3$ and Na_2CO_3 of pH 8.25 solutions, at an impact velocity of 2.5 m s^{-1}, the smallest effect of the corrosion rate was seen due to the protective oxide film on the surface of specimen. In addition, an increase in solution velocity from 3.5 m s^{-1} to 4.5 m s^{-1} increased the opportunity to remove such a protective film and therefore the corrosion rate was increased to twice that obtained at a low impact velocity of 2.5 m s^{-1}. The volume loss for carbon steel in the water environment at applied potential -400mV,it is interesting that the erosion-corrosion increases when impact angle is increased from 30^o to 60^o, with further increases at an impact angle of 90^o [10 -11].

Moreover, the value of corrosion contribution is greater than the value of erosion contribution at impact velocity 3.5 m s^{-1}. The erosion-corrosion peaks at the highest impact velocity 4.5 m s^{-1} and at impact angle 90^o about 9.47 mg cm^{-2} h^{-1} and the smallest value of erosion-corrosion is at 2.5 m s^{-1} and at an impact angle of 75^o about 3.89 mg cm^{-2} h^{-1}Figure 3.7. The total volume loss rate (kec) was in general increased with an increase in potential from -400mV to -200mV, impact velocity and high volume loss was at an impact velocity of 4.5 m s^{-1} and at an impact angle of 90^o about 10.31mg cm^{-2} h^{-1} Figure 3.10.It is interesting that the percentage of erosion contribution (Ke) was greater than the value of corrosion (Kc) contribution at some

impact velocities 2.5 m s^{-1} at some impact angles (15^o and30^o) Figures 3.10. (a) and(f). The total volume loss rate (kec) was raised with an increase in impact velocity, and volume loss was at its largest value at an impact velocity of 4.5 m s^{-1} and at an impact angle of 75^oabout 10.37mg cm $^{-2}$ h^{-1} Fig. 3.13.

In addition the mass loss was increased with an increase in the applied potential from 0mV to 200mV Fig. 3.16. Furthermore, the corrosion contribution (Kc) was increased with an increase in the applied potential which is consistent with the above polarization curves and the findings of many researchers [18] and [20]. The greatest value of erosion-corrosion was observed at an impact velocity of 4.5 m s^{-1} and at an impact angle of 45^o about 11.06mg cm $^{-2}$ h^{-1}. The volume loss kc (corrosion contribution) reached a peak value at potential 400 mV and at an impact angle of 75^o about 6.84mg cm $^{-2}$ h^{-1} Fig. 3.19. In addition the value of mass loss rate (Kec) was greatly increased with an increase in impact velocity as the mass loss was at its largest rate at an impact velocity of 4.5 m s^{-1}.

3.1.4.2. Mass loss in crude oil environment

The chemical composition of crude oil in ppm (mass) was (Ca: 33.26, Na: 4.26, K: 1.07, H_2S: 0.0007, pH 5 and API: 52). The specific gravity was 0.7674 and density was 767 g l^{-1}. At applied potential of -400 mV, there was a general decrease in corrosion contribution (Kc) and erosion contribution (ke) Fig. 3.8 compared with water environment. Moreover, it can be seen that the corrosion contribution was shifted to low value of mass loss and that it was consistent with the results of polarization curves. On the other hand, the percentage of total erosion-corrosion rate (Kec) was decreased compared with water environment; in fact, the percentage of erosion contribution (ke) representing the value of the total erosion-corrosion rate (Kec) due to the value of corrosion contribution (Kc) was very small.

At applied potentials of -200mV, the value of mass loss due to erosion contribution (Ke) was decreased in some cases (30^o and 75^o at an impact velocity of 3.5 m $s^{-1)}$ (Figures 3.11, (b) and (e)) compared with at -400mV. The total mass loss rate (Kec) in general increased with an increase in impact velocity and the highest volume of mass loss was at an impact velocity of 4.5 m s^{-1} and an impact angle of 90^o about 7.8 mg cm^{-2} h^{-1}. At potentials of 0 mV, the total mass loss was at its highest value at an impact velocity of 4.5 m s^{-1} and an impact angle of 15^o about 8 mg cm^{-2} h^{-1} Fig.3.14. In addition, there was a little increase in the value of erosion contribution with an increase in applied potential from -200mV to 0mV.

The total volume loss erosion-corrosion (Kec) increased with an increase in potentials, from 0mV to 200mV Fig.3.17.Furthermore, the corrosion contribution (Kc) was increased with increased applied potential, but the percentage of corrosion contribution was continuously small compared to the amount of erosion contribution. The volume loss Kc (corrosion contribution) reached its peak value at an applied potential of 400 mV Fig.3.20. In addition, the total volume loss rate (Kec) was increased with an increase in potential, and was at its highest value at an impact velocity of 4.5 m s^{-1}

3.1.4.3. Mass loss in oil /20% water environment

Generally, the mass loss in the crude oil /20% water environment at potential of -400mV, Fig.3.9, there was an increase in the corrosion contribution (Kc) compared with that recorded in crude oil environment consistent with the above polarization curves results and pervious investigators [2] and [11]. In contrast, the total volume loss of erosion–corrosion (Kec) generally increased and the highest volume loss was at an impact velocity of 4.5 m s^{-1} and an impact angle of 90^o about 8.6 mg cm^{-2} h^{-1} at potential of -200mV, Figure 3. 12.

It is clear that the total mass loss gradually increased with a reduction in the impact angle from 60^{o} to 30^{o} and an increase in impact velocities at applied potential 0mV (Fig. 3.15, a-f). In addition, the percentage of corrosion contribution was greater than the percentage of corrosion contribution compared at negative applied potential -200mV.

The percentage of corrosion contribution (Kc) increased with an increase in potential, from 0mV to 200mV. The total volume loss erosion-corrosion (Kec) was increased with an increase in the applied potential Fig. 3.18, which can be attributed to an increase in corrosion contribution (Kc). The corrosion contribution (Kc) reached a peak value with an applied potential of 400 mV, confirming the terms as the current density increases with an increase in potential Figs. 3.21.

Tables.3.1: Volume loss as function of velocities for carbon steel at various impact angles in water at -400mV and particle size 600-710µm (a) 15° (b) 30° (c) 45° (d) 60° (e) 75° (f) 90°

(a)

Velocities m s^{-1}	Ke(mg cm^{-2} h^{-1})	Kc(mg cm^{-2} h^{-1})	Kec(mg cm^{-2} h^{-1})
2.5	2.59	1.72	4.31
3.5	1.4	4.12	5.52
4.5	2.99	5.72	8.71

(b)

Velocities m s^{-1}	Ke(mg cm^{-2} h^{-1})	Kc(mg cm^{-2} h^{-1})	Kec(mg cm^{-2} h^{-1})
2.5	2.5	1.5	4
3.5	1.81	4.21	6.02
4.5	2.87	5.93	8.8

(c)

Velocities m s^{-1}	Ke(mg cm^{-2} h^{-1})	Kc(mg cm^{-2} h^{-1})	Kec(mg cm^{-2} h^{-1})
2.5	2.39	2.21	4.6
3.5	2.43	4.02	6.45
4.5	4.48	4.72	9.2

(d)

Velocities m s^{-1}	Ke(mg cm^{-2} h^{-1})	Kc(mg cm^{-2} h^{-1})	Kec(mg cm^{-2} h^{-1})
2.5	2.16	2.04	4.2
3.5	2.39	3.91	6.3
4.5	3.3	5.4	8.7

(e)

Velocities m s^{-1}	Ke(mg cm^{-2} h^{-1})	Kc(mg cm^{-2} h^{-1})	Kec(mg cm^{-2} h^{-1})
2.5	1.96	1.93	3.89
3.5	0.53	5.32	5.85
4.5	3	5.94	8.94

(f)

Velocities m s^{-1}	Ke(mg cm^{-2} h^{-1})	Kc(mg cm^{-2} h^{-1})	Kec(mg cm^{-2} h^{-1})
2.5	2.5	1.71	4.21
3.5	1.9	4.31	6.21
4.5	4.69	4.78	9.47

Tables.3.2: Volume loss as function of velocities for carbon steel at various impact angles in water at -200mV and particle size 600-710µm (a) 15° (b) 30° (c) 45° (d) 60° (e) 75° (f) 90°

(a)

Velocities m s^{-1}	Ke(mg cm^{-2} h^{-1})	Kc(mg cm^{-2} h^{-1})	Kec(mg cm^{-2} h^{-1})
2.5	2.45	1.78	4.23
3.5	1.77	4.21	5.98
4.5	2.39	5.84	8.23

(b)

Velocities m s^{-1}	Ke(mg cm^{-2} h^{-1})	Kc(mg cm^{-2} h^{-1})	Kec(mg cm^{-2} h^{-1})
2.5	2.59	1.72	4.31
3.5	2.11	3.91	6.02
4.5	4.88	4.12	9

(c)

Velocities m s^{-1}	Ke(mg cm^{-2} h^{-1})	Kc(mg cm^{-2} h^{-1})	Kec(mg cm^{-2} h^{-1})
2.5	2.17	2.43	4.6
3.5	1.89	5	6.89
4.5	4.17	5.85	10.02

(d)

Velocities m s^{-1}	Ke(mg cm^{-2} h^{-1})	Kc(mg cm^{-2} h^{-1})	Kec(mg cm^{-2} h^{-1})
2.5	1.89	2.12	4.01
3.5	2.2	4.25	6.45
4.5	4.65	5.67	10.32

(e)

Velocities m s^{-1}	Ke(mg cm^{-2} h^{-1})	Kc(mg cm^{-2} h^{-1})	Kec(mg cm^{-2} h^{-1})
2.5	1.57	2.24	3.81
3.5	1.59	4.61	6.2
4.5	3.45	5.89	9.34

(f)

Velocities m s^{-1}	Ke(mg cm^{-2} h^{-1})	Kc(mg cm^{-2} h^{-1})	Kec(mg cm^{-2} h^{-1})
2.5	1.9	2.21	4.11
3.5	1.97	4.38	6.35
4.5	5.48	4.83	10.31

Tables.3.3: Volume loss as function of velocities for carbon steel at various impact angles in water at 0mV and particle size 600-710µm (a) 15° (b) 30° (c) 45° (d) 60° (e) 75° (f) 90°

(a)

Velocities m s^{-1}	Ke(mg cm^{-2} h^{-1})	Kc(mg cm^{-2} h^{-1})	Kec(mg cm^{-2} h^{-1})
2.5	2.58	1.82	4.4
3.5	1.65	4.38	6.03
4.5	3.82	5.91	9.73

(b)

Velocities m s^{-1}	Ke(mg cm^{-2} h^{-1})	Kc(mg cm^{-2} h^{-1})	Kec(mg cm^{-2} h^{-1})
2.5	2.38	1.83	4.21
3.5	2.42	3.78	6.2
4.5	5.76	4.45	10.21

(c)

Velocities m s^{-1}	Ke(mg cm^{-2} h^{-1})	Kc(mg cm^{-2} h^{-1})	Kec(mg cm^{-2} h^{-1})
2.5	1.7	2.71	4.41
3.5	1.99	5.04	7.03
4.5	4.71	5.56	10.27

(d)

Velocities m s^{-1}	Ke(mg cm^{-2} h^{-1})	Kc(mg cm^{-2} h^{-1})	Kec(mg cm^{-2} h^{-1})
2.5	1.25	2.25	3.5
3.5	2.7	4.51	7.21
4.5	4.71	5.56	10.27

(e)

Velocities m s^{-1}	Ke(mg cm^{-2} h^{-1})	Kc(mg cm^{-2} h^{-1})	Kec(mg cm^{-2} h^{-1})
2.5	2.16	2.46	4.62
3.5	2.8	4.07	6.87
4.5	4.11	6.21	10.32

(f)

Velocities m s^{-1}	Ke(mg cm^{-2} h^{-1})	Kc(mg cm^{-2} h^{-1})	Kec(mg cm^{-2} h^{-1})
2.5	1.57	2.73	4.3
3.5	2.48	5	7.48
4.5	3.47	6.03	9.5

Tables.3.4: Volume loss as function of velocities for carbon steel at various impact angles in water at 200mV and particle size 600-710µm (a) 15° (b) 30° (c) 45°(d) 60° (e) 75° (f) 90°

(a)

Velocities m s^{-1}	Ke(mg cm^{-2} h^{-1})	Kc(mg cm^{-2} h^{-1})	Kec(mg cm^{-2} h^{-1})
2.5	2.43	1.95	4.38
3.5	1.73	4.48	6.21
4.5	4.76	5.24	10

(b)

Velocities m s^{-1}	Ke(mg cm^{-2} h^{-1})	Kc(mg cm^{-2} h^{-1})	Kec(mg cm^{-2} h^{-1})
2.5	2.56	1.94	4.5
3.5	3.4	4.1	7.5
4.5	5.51	4.81	10.32

(c)

Velocities m s^{-1}	Ke(mg cm^{-2} h^{-1})	Kc(mg cm^{-2} h^{-1})	Kec(mg cm^{-2} h^{-1})
2.5	2.58	2.03	4.61
3.5	3.88	4.12	8
4.5	5.74	5.32	11.06

(d)

Velocities m s^{-1}	Ke(mg cm^{-2} h^{-1})	Kc(mg cm^{-2} h^{-1})	Kec(mg cm^{-2} h^{-1})
2.5	1.5	2.71	4.21
3.5	2.83	5.01	7.84
4.5	4.88	5.87	10.75

(e)

Velocities m s^{-1}	Ke(mg cm^{-2} h^{-1})	Kc(mg cm^{-2} h^{-1})	Kec(mg cm^{-2} h^{-1})
2.5	2.26	1.34	3.6
3.5	2.8	4.5	7.3
4.5	4.52	6	10.52

(f)

Velocities m s^{-1}	Ke(mg cm^{-2} h^{-1})	Kc(mg cm^{-2} h^{-1})	Kec(mg cm^{-2} h^{-1})
2.5	1.22	2.78	4
3.5	2.5	5.52	8.02
4.5	4.19	6.13	10.32

Tables.3.5: Volume loss as function of velocities for carbon steel at various impact angles in water at 400mV and particle size 600-710µm (a) 15° (b) 30° (c) 45° (d) 60° (e) 75° (f) 90°

(a)

Velocities m s^{-1}	Ke(mg cm^{-2} h^{-1})	Kc(mg cm^{-2} h^{-1})	Kec(mg cm^{-2} h^{-1})
2.5	2.44	1.97	4.41
3.5	3.49	4.51	8
4.5	5.25	5.2	10.45

(b)

Velocities m s^{-1}	Ke(mg cm^{-2} h^{-1})	Kc(mg cm^{-2} h^{-1})	Kec(mg cm^{-2} h^{-1})
2.5	2.16	2.07	4.23
3.5	3.57	4.23	7.8
4.5	5.62	4.9	10.52

(c)

Velocities m s^{-1}	Ke(mg cm^{-2} h^{-1})	Kc(mg cm^{-2} h^{-1})	Kec(mg cm^{-2} h^{-1})
2.5	2.84	2.16	5
3.5	3.89	4.32	8.21
4.5	6.11	5.73	11.84

(d)

Velocities m s^{-1}	Ke(mg cm^{-2} h^{-1})	Kc(mg cm^{-2} h^{-1})	Kec(mg cm^{-2} h^{-1})
2.5	2.57	1.93	4.5
3.5	2.79	5.21	8
4.5	6.05	5.07	11.12

(e)

Velocities m s^{-1}	Ke(mg cm^{-2} h^{-1})	Kc(mg cm^{-2} h^{-1})	Kec(mg cm^{-2} h^{-1})
2.5	0.71	2.74	3.45
3.5	2.99	4.85	7.84
4.5	3.16	6.84	10

(f)

Velocities m s^{-1}	Ke(mg cm^{-2} h^{-1})	Kc(mg cm^{-2} h^{-1})	Kec(mg cm^{-2} h^{-1})
2.5	1.48	2.53	4.01
3.5	2.11	5.81	7.92
4.5	4.29	6.73	11.02

Tables.3.6: Volume loss as function of velocities for carbon steel at various impact angles in crude oil at -400mV and particle size 600-710µm (a) 15° (b) 30° (c) 45°(d) 60° (e) 75° (f) 90°

(a)

Velocities m s^{-1}	Ke(mg cm^{-2} h^{-1})	Kc(mg cm^{-2} h^{-1})	Kec(mg cm^{-2} h^{-1})
2.5	2.5	2.11E-02	2.5
3.5	4.6	1.89E-02	4.58
4.5	7.5	2.88E-02	7.5

(b)

Velocities m s^{-1}	Ke(mg cm^{-2} h^{-1})	Kc(mg cm^{-2} h^{-1})	Kec(mg cm^{-2} h^{-1})
2.5	1.9	1.22E-02	2
3.5	3.9	2.62E-02	4
4.5	6.2	3.28E-02	6.21

(c)

Velocities m s^{-1}	Ke(mg cm^{-2} h^{-1})	Kc(mg cm^{-2} h^{-1})	Kec(mg cm^{-2} h^{-1})
2.5	2	1.02E-02	2.01
3.5	4.48	2.00E-02	4.5
4.5	7.1	2.52E-02	7.12

(d)

Velocities m s^{-1}	Ke(mg cm^{-2} h^{-1})	Kc(mg cm^{-2} h^{-1})	Kec(mg cm^{-2} h^{-1})
2.5	2.1	1.85E-02	2.1
3.5	4.2	2.43E-02	4.21
4.5	6.7	3.19E-02	6.7

(e)

Velocities m s^{-1}	Ke(mg cm^{-2} h^{-1})	Kc(mg cm^{-2} h^{-1})	Kec(mg cm^{-2} h^{-1})
2.5	2.1	2.02E-02	2.12
3.5	4.7	1.92E-02	4.71
4.5	6.96	3.03E-02	7

(f)

Velocities m s^{-1}	Ke(mg cm^{-2} h^{-1})	Kc(mg cm^{-2} h^{-1})	Kec(mg cm^{-2} h^{-1})
2.5	2.1	1.81E-02	2.11
3.5	4.8	2.62E-02	4.78
4.5	7.1	4.12E-02	7.18

Tables.3.7: Volume loss as function of velocities for carbon steel at various impact angles in crude oil at -200mV and particle size 600-710µm (a) 15° (b) 30° (c) 45° (d) 60° (e) 75° (f) 90°

(a)

Velocities m s^{-1}	Ke(mg cm^{-2} h^{-1})	Kc(mg cm^{-2} h^{-1})	Kec(mg cm^{-2} h^{-1})
2.5	2.6	1.63E-02	2.6
3.5	5.1	2.09E-02	5.12
4.5	7.2	3.78E-02	7.28

(b)

Velocities m s^{-1}	Ke(mg cm^{-2} h^{-1})	Kc(mg cm^{-2} h^{-1})	Kec(mg cm^{-2} h^{-1})
2.5	2.4	1.65E-02	2.4
3.5	4.2	3.02E-02	4.2
4.5	6.9	3.41E-02	7

(c)

Velocities m s^{-1}	Ke(mg cm^{-2} h^{-1})	Kc(mg cm^{-2} h^{-1})	Kec(mg cm^{-2} h^{-1})
2.5	2.7	1.47E-02	2.7
3.5	4.6	2.21E-02	4.6
4.5	6.9	2.98E-02	7.02

(d)

Velocities m s^{-1}	Ke(mg cm^{-2} h^{-1})	Kc(mg cm^{-2} h^{-1})	Kec(mg cm^{-2} h^{-1})
2.5	2.8	1.93E-02	2.8
3.5	4.7	2.53E-02	4.7
4.5	6.8	4.19E-02	6.87

(e)

Velocities m s^{-1}	Ke(mg cm^{-2} h^{-1})	Kc(mg cm^{-2} h^{-1})	Kec(mg cm^{-2} h^{-1})
2.5	3.1	2.12E-02	3.16
3.5	4.8	2.02E-02	4.85
4.5	7.0	3.48E-02	7.05

(f)

Velocities m s^{-1}	Ke(mg cm^{-2} h^{-1})	Kc(mg cm^{-2} h^{-1})	Kec(mg cm^{-2} h^{-1})
2.5	3.1	1.97E-02	3.15
3.5	4.9	2.74E-02	5
4.5	7.8	3.99E-02	7.8

Tables.3.8: Volume loss as function of velocities for carbon steel at various impact angles in crude oil at 0mV and particle size 600-710µm (a) 15° (b) 30° (c) 45° (d) 60° (e) 75° (f) 90°

(a)

Velocities m s^{-1}	Ke(mg cm^{-2} h^{-1})	Kc(mg cm^{-2} h^{-1})	Kec(mg cm^{-2} h^{-1})
2.5	3.4	1.85E-02	3.401
3.5	5.1	2.59E-02	5.1
4.5	7.95	4.28E-02	8

(b)

Velocities m s^{-1}	Ke(mg cm^{-2} h^{-1})	Kc(mg cm^{-2} h^{-1})	Kec(mg cm^{-2} h^{-1})
2.5	3.10	1.71E-02	3.12
3.5	4.5	2.70E-02	4.5
4.5	7.4	4.01E-02	7.48

(c)

Velocities m s^{-1}	Ke(mg cm^{-2} h^{-1})	Kc(mg cm^{-2} h^{-1})	Kec(mg cm^{-2} h^{-1})
2.5	3.1	1.39E-02	3.14
3.5	4.98	1.81E-02	5
4.5	7.42	3.08E-02	7.45

(d)

Velocities m s^{-1}	Ke(mg cm^{-2} h^{-1})	Kc(mg cm^{-2} h^{-1})	Kec(mg cm^{-2} h^{-1})
2.5	3.4	1.90E-02	3.4
3.5	4.9	2.61E-02	4.9
4.5	6.96	3.89E-02	7

(e)

Velocities m s^{-1}	Ke(mg cm^{-2} h^{-1})	Kc(mg cm^{-2} h^{-1})	Kec(mg cm^{-2} h^{-1})
2.5	3.2	1.98E-02	3.26
3.5	4.8	2.76E-02	4.87
4.5	6.7	3.88E-02	6.7

(f)

Velocities m s^{-1}	Ke(mg cm^{-2} h^{-1})	Kc(mg cm^{-2} h^{-1})	Kec(mg cm^{-2} h^{-1})
2.5	3.38	2.00E-02	3.4
3.5	5.18	2.91E-02	5.21
4.5	7.40	4.56E-02	7.45

Tables.3.9: Volume loss as function of velocities for carbon steel at various impact angles in crude oil at 200mV and particle size 600-710µm (a) 15° (b) 30° (c) 45°(d) 60° (e) 75° (f) 90°

(a)

Velocities m s^{-1}	Ke(mg cm^{-2} h^{-1})	Kc(mg cm^{-2} h^{-1})	Kec(mg cm^{-2} h^{-1})
2.5	3.76	1.94E-02	3.78
3.5	5.57	2.61E-02	5.6
4.5	8.43	4.50E-02	8.47

(b)

Velocities m s^{-1}	Ke(mg cm^{-2} h^{-1})	Kc(mg cm^{-2} h^{-1})	Kec(mg cm^{-2} h^{-1})
2.5	3.5	1.49E-02	3.5
3.5	5.2	2.78E-02	5.2
4.5	7.9	3.91E-02	7.98

(c)

Velocities m s^{-1}	Ke(mg cm^{-2} h^{-1})	Kc(mg cm^{-2} h^{-1})	Kec(mg cm^{-2} h^{-1})
2.5	3.5	1.51E-02	3.56
3.5	5.85	1.92E-02	5.87
4.5	7.7	3.58E-02	7.78

(d)

Velocities m s^{-1}	Ke(mg cm^{-2} h^{-1})	Kc(mg cm^{-2} h^{-1})	Kec(mg cm^{-2} h^{-1})
2.5	3.1	2.00E-02	3.12
3.5	4.98	1.99E-02	5
4.5	7.1	4.09E-02	7.14

(e)

Velocities m s^{-1}	Ke(mg cm^{-2} h^{-1})	Kc(mg cm^{-2} h^{-1})	Kec(mg cm^{-2} h^{-1})
2.5	3.6	2.33E-02	3.6
3.5	5.1	3.76E-02	5.13
4.5	6.96	3.78E-02	7

(f)

Velocities m s^{-1}	Ke(mg cm^{-2} h^{-1})	Kc(mg cm^{-2} h^{-1})	Kec(mg cm^{-2} h^{-1})
2.5	3.97	2.42E-02	4
3.5	5.75	3.01E-02	5.78
4.5	7.95	4.78E-02	8

Tables.3.10: Volume loss as function of velocities for carbon steel at various impact angles in crude oil at 400mV and particle size 600-710µm (a) 15° (b) 30° (c) 45° (d) 60° (e) 75° (f) 90°

(a)

Velocities m s^{-1}	Ke(mg cm^{-2} h^{-1})	Kc(mg cm^{-2} h^{-1})	Kec(mg cm^{-2} h^{-1})
2.5	3.8	2.14E-02	3.78
3.5	6.97	2.58E-02	7
4.5	8.1	4.78E-02	8.12

(b)

Velocities m s^{-1}	Ke(mg cm^{-2} h^{-1})	Kc(mg cm^{-2} h^{-1})	Kec(mg cm^{-2} h^{-1})
2.5	3.5	1.52E-02	3.5
3.5	6.4	3.08E-02	6.4
4.5	7.96	4.51E-02	8

(c)

Velocities m s^{-1}	Ke(mg cm^{-2} h^{-1})	Kc(mg cm^{-2} h^{-1})	Kec(mg cm^{-2} h^{-1})
2.5	3.5	1.48E-02	3.56
3.5	6.18	2.02E-02	6.2
4.5	8.41	4.00E-02	8.45

(d)

Velocities m s^{-1}	Ke(mg cm^{-2} h^{-1})	Kc(mg cm^{-2} h^{-1})	Kec(mg cm^{-2} h^{-1})
2.5	3.09	2.31E-02	3.12
3.5	4.98	2.19E-02	5
4.5	8.05	5.19E-02	8.1

(e)

Velocities m s^{-1}	Ke(mg cm^{-2} h^{-1})	Kc(mg cm^{-2} h^{-1})	Kec(mg cm^{-2} h^{-1})
2.5	3.6	2.40E-02	3.6
3.5	5.97	2.96E-02	6
4.5	7.85	4.18E-02	7.89

(f)

Velocities m s^{-1}	Ke(mg cm^{-2} h^{-1})	Kc(mg cm^{-2} h^{-1})	Kec(mg cm^{-2} h^{-1})
2.5	3.98	2.65E-02	4
3.5	6.47	3.21E-02	6.5
4.5	8.18	5.18E-02	8.23

Tables.3.11: Volume loss as function of velocities for carbon steel at various impact angles in oil /20% water at -400mV and particle size 600-710µm (a) 15° (b) 30° (c) 45° (d) 60° (e) 75° (f) 90°

(a)

Velocities m s^{-1}	Ke(mg cm^{-2} h^{-1})	Kc(mg cm^{-2} h^{-1})	Kec(mg cm^{-2} h^{-1})
2.5	2.31	0.8	3.11
3.5	4.16	0.84	5
4.5	6.45	1.35	7.8

(b)

Velocities m s^{-1}	Ke(mg cm^{-2} h^{-1})	Kc(mg cm^{-2} h^{-1})	Kec(mg cm^{-2} h^{-1})
2.5	1.92	0.78	2.7
3.5	3.71	0.89	4.6
4.5	6.07	1.21	7.28

(c)

Velocities m s^{-1}	Ke(mg cm^{-2} h^{-1})	Kc(mg cm^{-2} h^{-1})	Kec(mg cm^{-2} h^{-1})
2.5	2.16	0.84	3
3.5	5.2	0.9	6.1
4.5	6.66	1.34	8

(d)

Velocities m s^{-1}	Ke(mg cm^{-2} h^{-1})	Kc(mg cm^{-2} h^{-1})	Kec(mg cm^{-2} h^{-1})
2.5	2.42	0.78	3.2
3.5	4.42	0.98	5.4
4.5	5.82	1.2	7.02

(e)

Velocities m s^{-1}	Ke(mg cm^{-2} h^{-1})	Kc(mg cm^{-2} h^{-1})	Kec(mg cm^{-2} h^{-1})
2.5	1.96	1	2.96
3.5	4.2	1	5.2
4.5	6.6	1.4	8

(f)

Velocities m s^{-1}	Ke(mg cm^{-2} h^{-1})	Kc(mg cm^{-2} h^{-1})	Kec(mg cm^{-2} h^{-1})
2.5	2.18	0.9	3.08
3.5	5	1.1	6.1
4.5	6.75	1.45	8.2

Tables.3.12: Volume loss as function of velocities for carbon steel at various impact angles in oil /20% water at -200mV and particle size 600-710µm (a) 15° (b) 30° (c) 45° (d) 60° (e) 75° (f) 90°

(a)

Velocities m s^{-1}	Ke(mg cm^{-2} h^{-1})	Kc(mg cm^{-2} h^{-1})	Kec(mg cm^{-2} h^{-1})
2.5	2.3	0.812	3.15
3.5	5.02	0.98	6
4.5	6.7	1.3	8

(b)

Velocities m s^{-1}	Ke(mg cm^{-2} h^{-1})	Kc(mg cm^{-2} h^{-1})	Kec(mg cm^{-2} h^{-1})
2.5	2.41	0.791	3.2
3.5	4.56	1	5.56
4.5	6.98	1.32	8.3

(c)

Velocities m s^{-1}	Ke(mg cm^{-2} h^{-1})	Kc(mg cm^{-2} h^{-1})	Kec(mg cm^{-2} h^{-1})
2.5	2.5	0.714	3.21
3.5	5.3	0.9	6.2
4.5	6.7	1.5	8.2

(d)

Velocities m s^{-1}	Ke(mg cm^{-2} h^{-1})	Kc(mg cm^{-2} h^{-1})	Kec(mg cm^{-2} h^{-1})
2.5	2.4	0.801	3.24
3.5	4.98	1.12	6.1
4.5	6.51	1.1	7.61

(e)

Velocities m s^{-1}	Ke(mg cm^{-2} h^{-1})	Kc(mg cm^{-2} h^{-1})	Kec(mg cm^{-2} h^{-1})
2.5	2.61	0.89	3.5
3.5	4.81	0.89	5.7
4.5	6.76	1.3	8.06

(f)

Velocities m s^{-1}	Ke(mg cm^{-2} h^{-1})	Kc(mg cm^{-2} h^{-1})	Kec(mg cm^{-2} h^{-1})
2.5	1.87	0.91	2.78
3.5	5.2	1	6.2
4.5	7.1	1.5	8.6

Tables.3.13: Volume loss as function of velocities for carbon steel at various impact angles in oil /20% water at 0mV and particle size 600-710µm (a) 15° (b) 30° (c) 45° (d) 60° (e) 75° (f) 90°

(a)

Velocities m s^{-1}	Ke(mg cm^{-2} h^{-1})	Kc(mg cm^{-2} h^{-1})	Kec(mg cm^{-2} h^{-1})
2.5	2.06	0.78	2.84
3.5	5.11	0.89	6
4.5	7.28	1.5	8.78

(b)

Velocities m s^{-1}	Ke(mg cm^{-2} h^{-1})	Kc(mg cm^{-2} h^{-1})	Kec(mg cm^{-2} h^{-1})
2.5	2.71	0.8	3.51
3.5	3.9	1.2	5.1
4.5	7.08	1.32	8.4

(c)

Velocities m s^{-1}	Ke(mg cm^{-2} h^{-1})	Kc(mg cm^{-2} h^{-1})	Kec(mg cm^{-2} h^{-1})
2.5	2.8	0.76	3.6
3.5	5.2	1	6.2
4.5	7.5	1.4	8.94

(d)

Velocities m s^{-1}	Ke(mg cm^{-2} h^{-1})	Kc(mg cm^{-2} h^{-1})	Kec(mg cm^{-2} h^{-1})
2.5	2.68	0.82	3.5
3.5	4.89	1.23	6.12
4.5	6.79	1.21	8

(e)

Velocities m s^{-1}	Ke(mg cm^{-2} h^{-1})	Kc(mg cm^{-2} h^{-1})	Kec(mg cm^{-2} h^{-1})
2.5	2.1	0.9	3
3.5	4.53	1	5.53
4.5	6.6	1.3	7.9

(f)

Velocities m s^{-1}	Ke(mg cm^{-2} h^{-1})	Kc(mg cm^{-2} h^{-1})	Kec(mg cm^{-2} h^{-1})
2.5	2.13	0.78	2.91
3.5	5.32	0.98	6.3
4.5	7.12	1.6	8.72

Tables.3.14: Volume loss as function of velocities for carbon steel at various impact angles in oil /20% water at 200mV and particle size 600-710µm (a) 15° (b) 30° (c) 45°(d) 60° (e) 75° (f) 90°

(a)

Velocities m s^{-1}	Ke(mg cm^{-2} h^{-1})	Kc(mg cm^{-2} h^{-1})	Kec(mg cm^{-2} h^{-1})
2.5	2.1	0.68	2.78
3.5	5.47	0.93	6.4
4.5	7.34	1.68	9.02

(b)

Velocities m s^{-1}	Ke(mg cm^{-2} h^{-1})	Kc(mg cm^{-2} h^{-1})	Kec(mg cm^{-2} h^{-1})
2.5	2.4	0.9	3.25
3.5	5.32	0.98	6.3
4.5	7.4	1.6	9

(c)

Velocities m s^{-1}	Ke(mg cm^{-2} h^{-1})	Kc(mg cm^{-2} h^{-1})	Kec(mg cm^{-2} h^{-1})
2.5	2.9	0.81	3.7
3.5	5.3	1.2	6.5
4.5	7.8	1.54	9.3

(d)

Velocities m s^{-1}	Ke(mg cm^{-2} h^{-1})	Kc(mg cm^{-2} h^{-1})	Kec(mg cm^{-2} h^{-1})
2.5	2.64	0.96	3.6
3.5	5.22	0.78	6
4.5	8.68	1.32	10

(e)

Velocities m s^{-1}	Ke(mg cm^{-2} h^{-1})	Kc(mg cm^{-2} h^{-1})	Kec(mg cm^{-2} h^{-1})
2.5	2.42	0.45	2.87
3.5	4.75	1.12	5.87
4.5	7.57	1.4	8.97

(f)

Velocities m s^{-1}	Ke(mg cm^{-2} h^{-1})	Kc(mg cm^{-2} h^{-1})	Kec(mg cm^{-2} h^{-1})
2.5	2.27	0.73	3
3.5	5.18	1.23	6.41
4.5	7.9	1.7	9.6

Tables.3.15: Volume loss as function of velocities for carbon steel at various impact angles in oil /20% water at 400mV and particle size 600-710µm (a) 15° (b) 30° (c) 45°(d) 60° (e) 75° (f) 90°

(a)

Velocities m s^{-1}	Ke(mg cm^{-2} h^{-1})	Kc(mg cm^{-2} h^{-1})	Kec(mg cm^{-2} h^{-1})
2.5	1.89	0.71	2.6
3.5	6.01	1.2	7.21
4.5	7.61	1.9	9.51

(b)

Velocities m s^{-1}	Ke(mg cm^{-2} h^{-1})	Kc(mg cm^{-2} h^{-1})	Kec(mg cm^{-2} h^{-1})
2.5	2.68	0.72	3.4
3.5	5.51	1	6.51
4.5	7.67	1.85	9.52

(c)

Velocities m s^{-1}	Ke(mg cm^{-2} h^{-1})	Kc(mg cm^{-2} h^{-1})	Kec(mg cm^{-2} h^{-1})
2.5	2.1	0.9	3
3.5	5.4	1.3	6.7
4.5	7.42	1.7	9.12

(d)

Velocities m s^{-1}	Ke(mg cm^{-2} h^{-1})	Kc(mg cm^{-2} h^{-1})	Kec(mg cm^{-2} h^{-1})
2.5	2.02	0.78	2.8
3.5	6.2	0.8	7
4.5	7.32	1.68	9

(e)

Velocities m s^{-1}	Ke(mg cm^{-2} h^{-1})	Kc(mg cm^{-2} h^{-1})	Kec(mg cm^{-2} h^{-1})
2.5	2.23	0.67	2.9
3.5	5.87	0.98	6.85
4.5	7.12	1.76	8.88

(f)

Velocities m s^{-1}	Ke(mg cm^{-2} h^{-1})	Kc(mg cm^{-2} h^{-1})	Kec(mg cm^{-2} h^{-1})
2.5	2.4	0.8	3.2
3.5	5.8	1.2	7
4.5	7.98	1.89	9.87

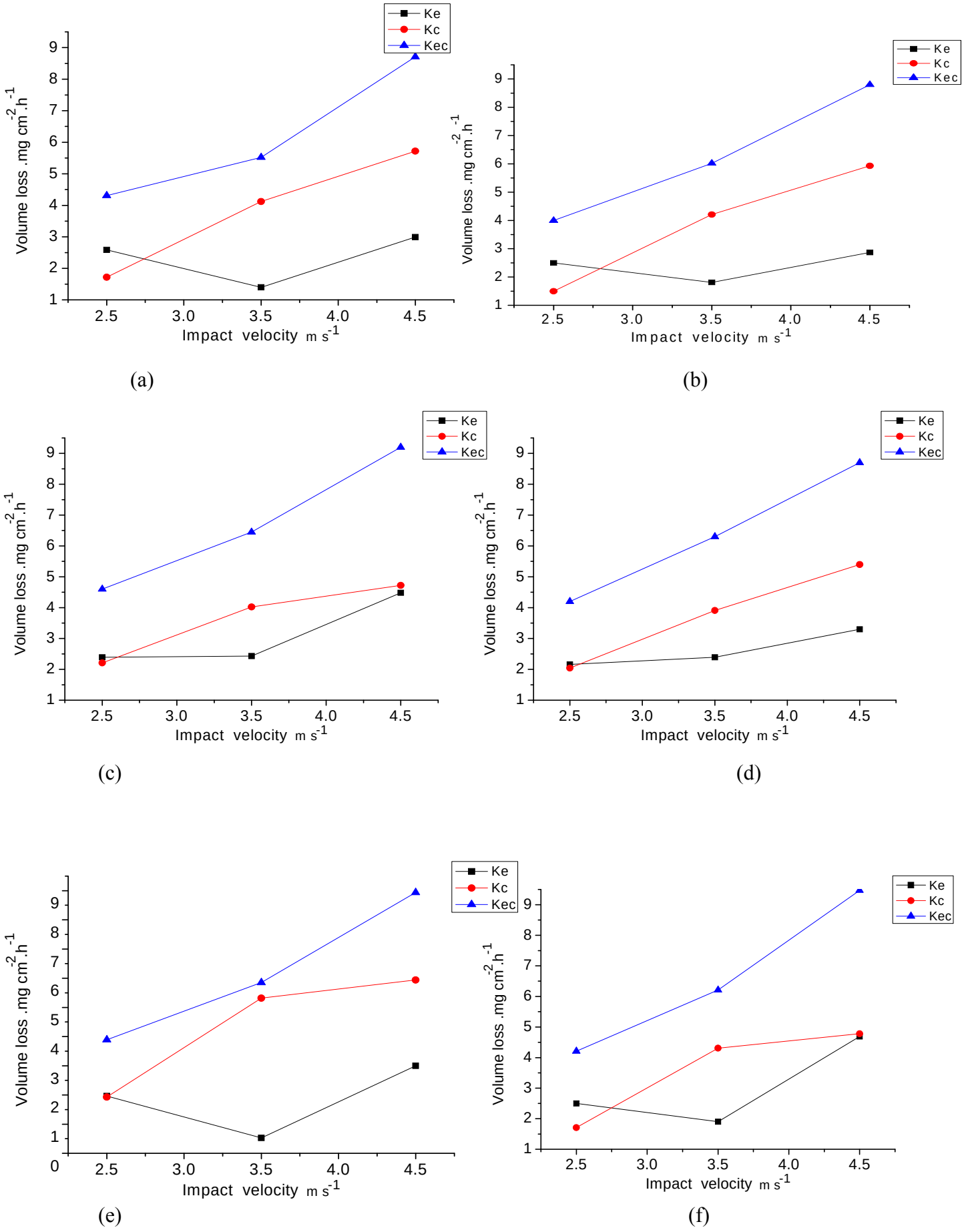

Fig.3.7 : Volume loss as function of impact velocities for carbon steel in water at -400 mV and particle size 600-710µm (a) 15° (b) 30° (c) 45°(d) 60° (e) 75° (f) 90° .

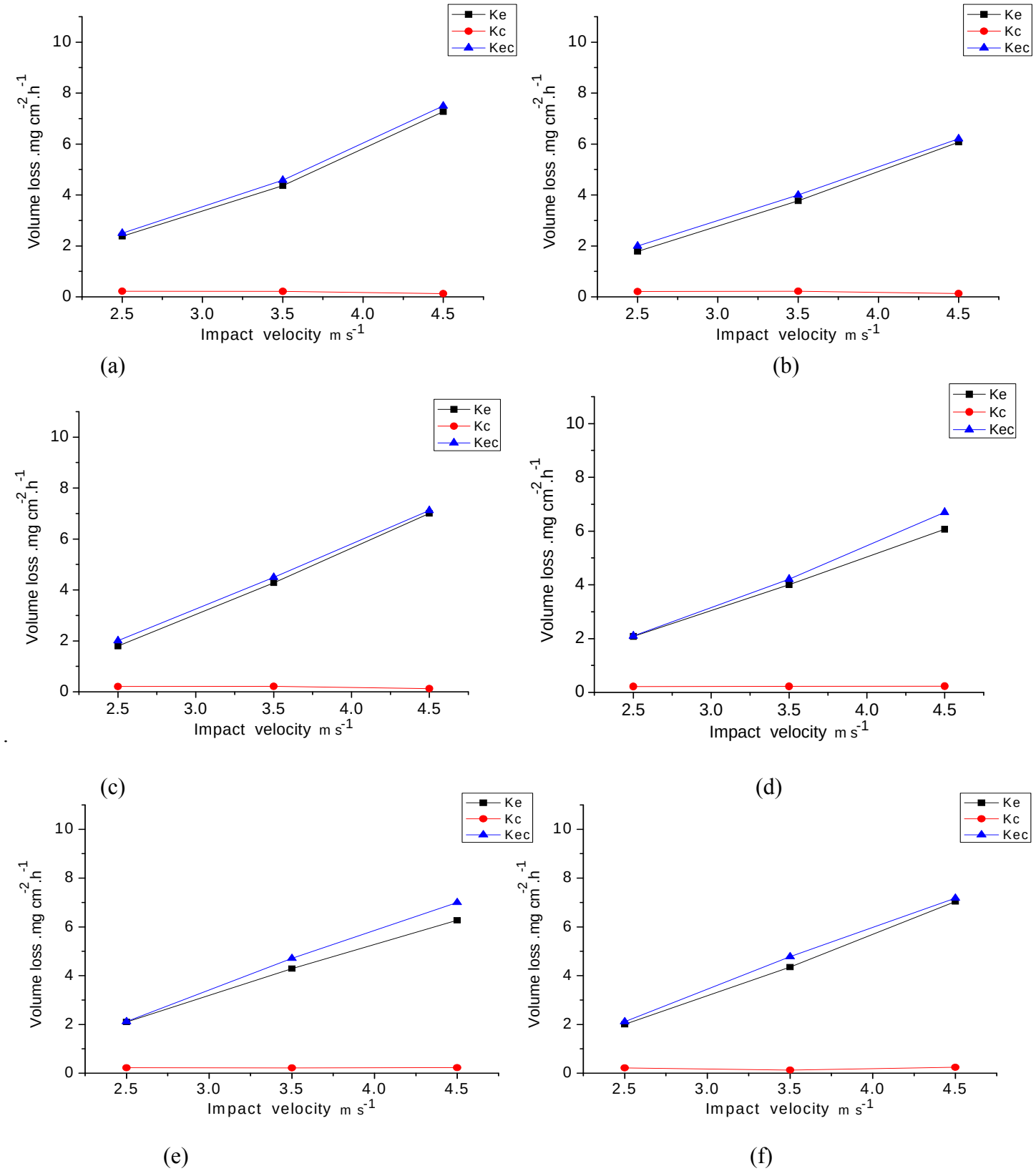

Fig.3.8 : Volume loss as function of impact velocities for carbon steel in crude oil at -400 mV and particle size 600-710µm (a) 15° (b) 30° (c) 45°(d) 60° (e) 75° (f) 90°.

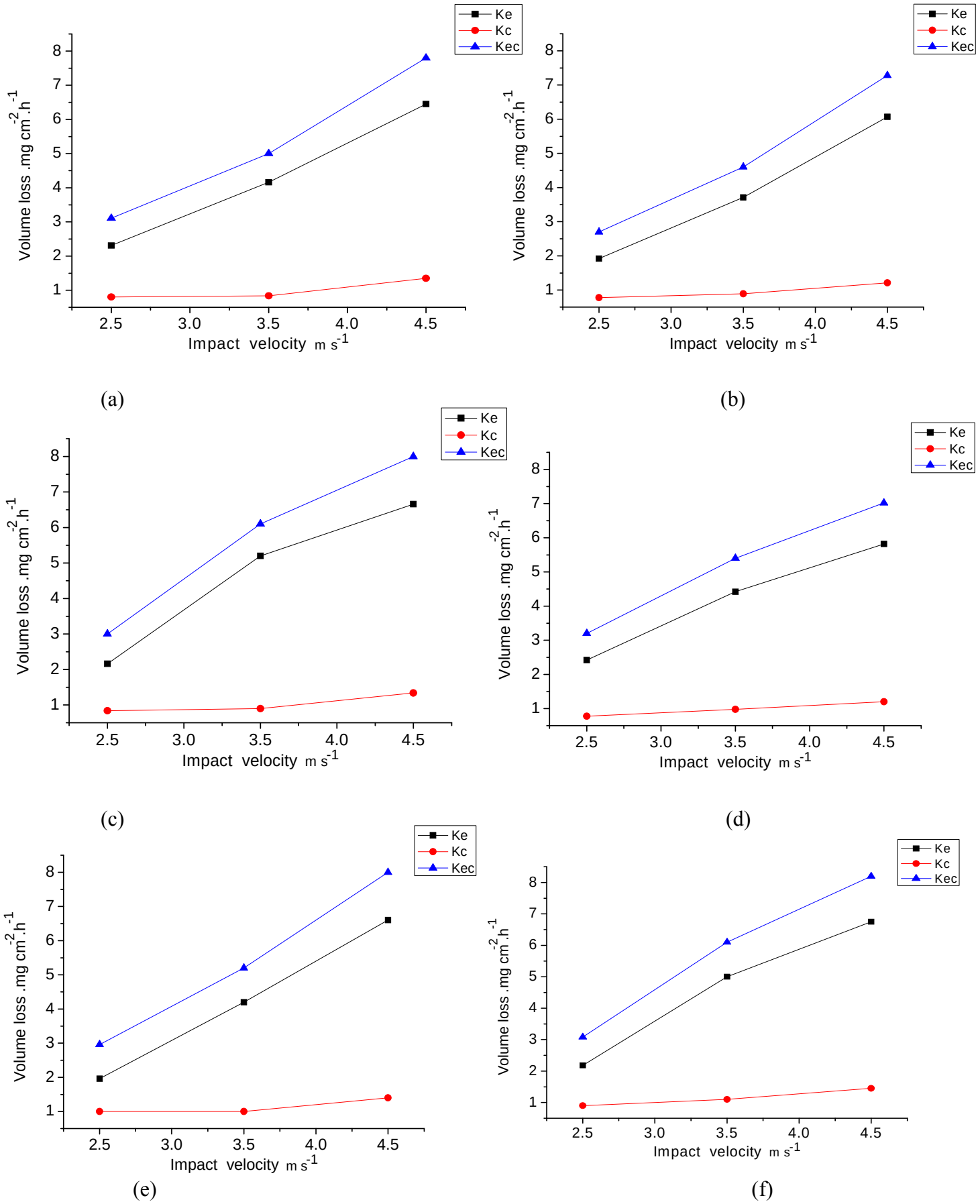

Fig.3.9: Volume loss as function of impact velocities for carbon steel in oil /20% water at -400 mV and particle size 600-710µm (a) 15° (b) 30° (c) 45°(d) 60° (e) 75° (f) 90°.

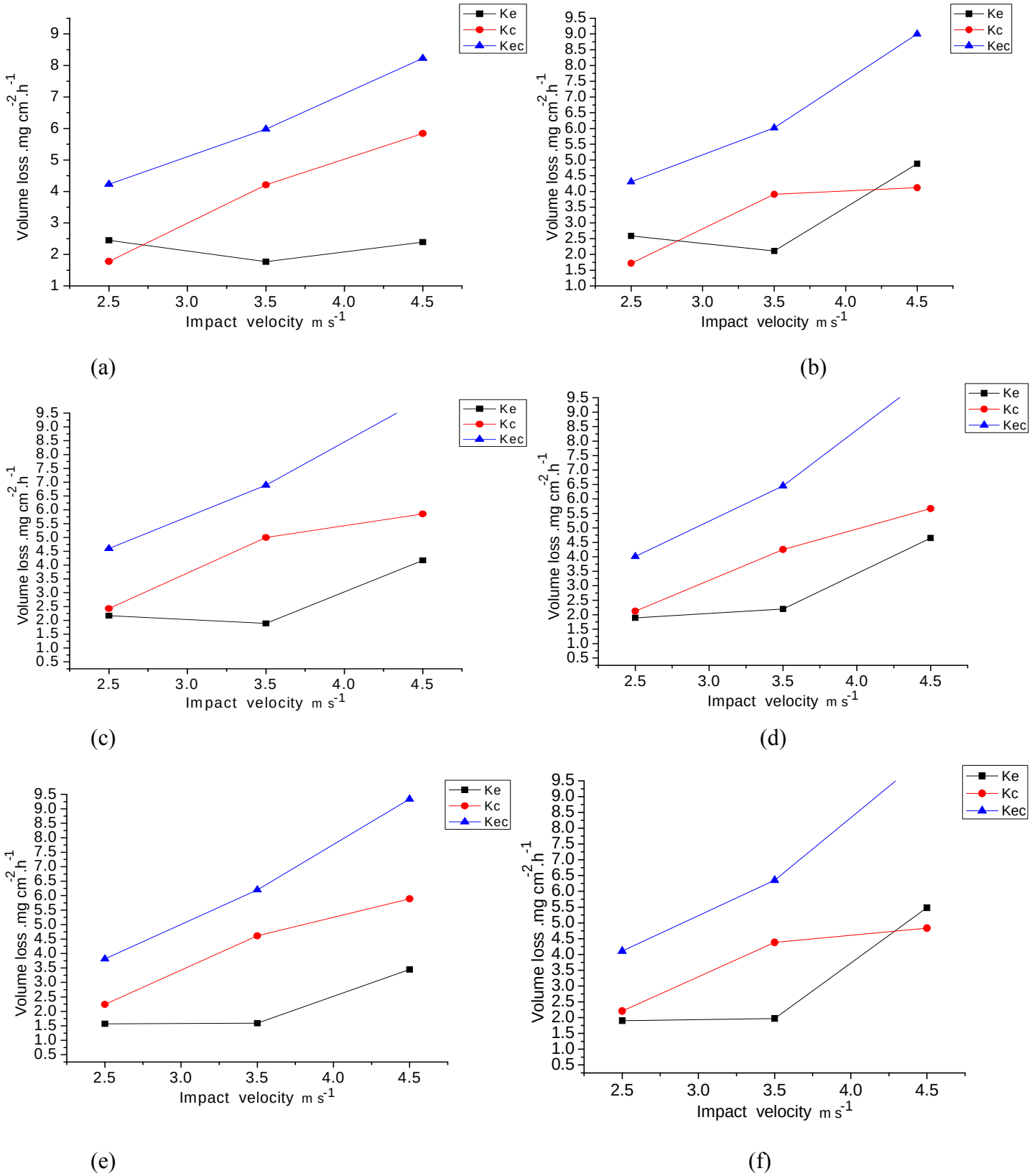

Fig.3.10: Volume loss as function of impact velocities for carbon steel in water at -200 mV and particle size 600-710µm (a) 15° (b) 30° (c) 45°(d) 60° (e) 75° (f) 90°.

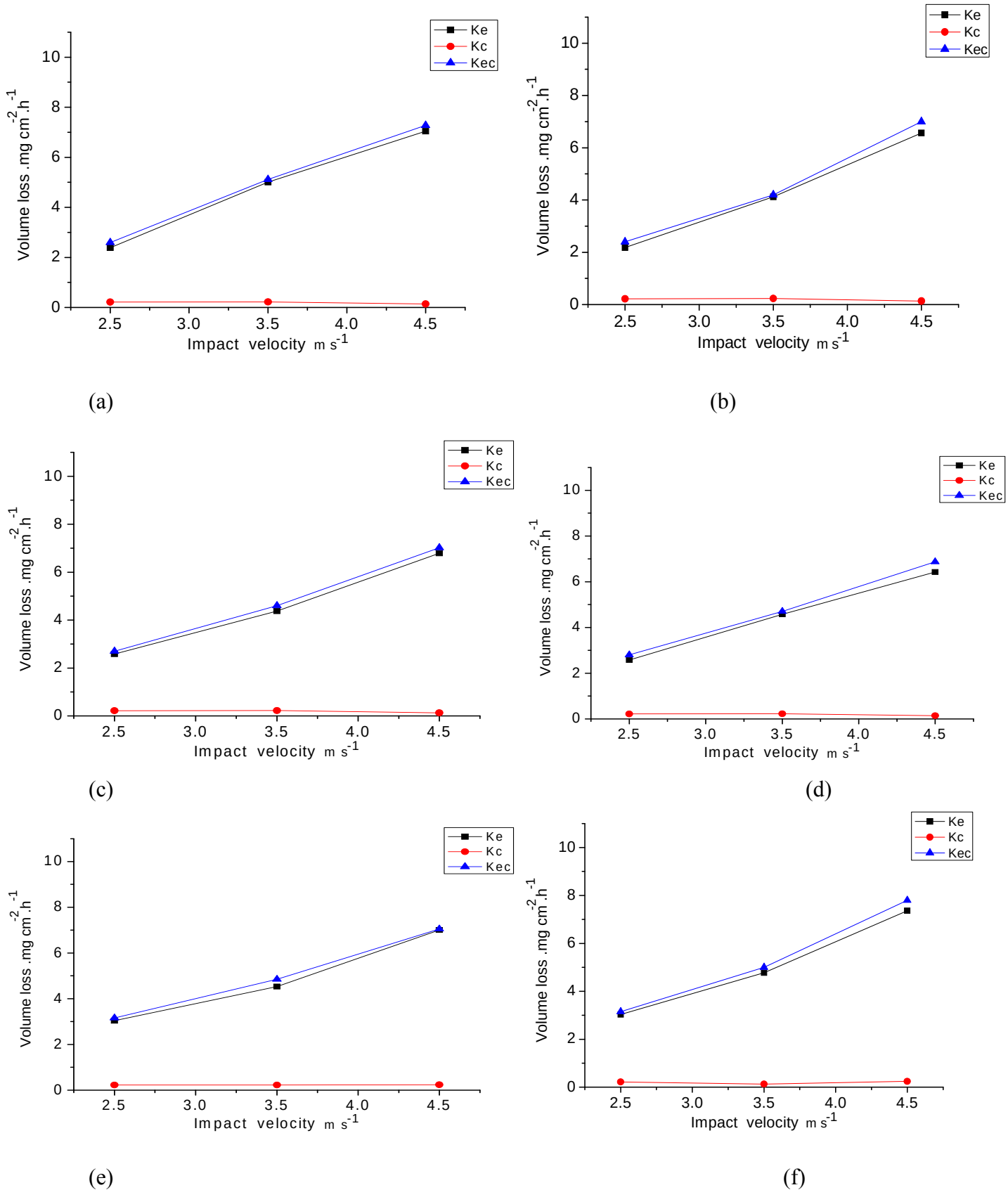

Fig.3.11: Volume loss as function of impact velocities for carbon steel in crude oil at -200 mV and particle size 600-710µm (a) 15° (b) 30° (c) 45°(d) 60° (e) 75° (f) 90°.

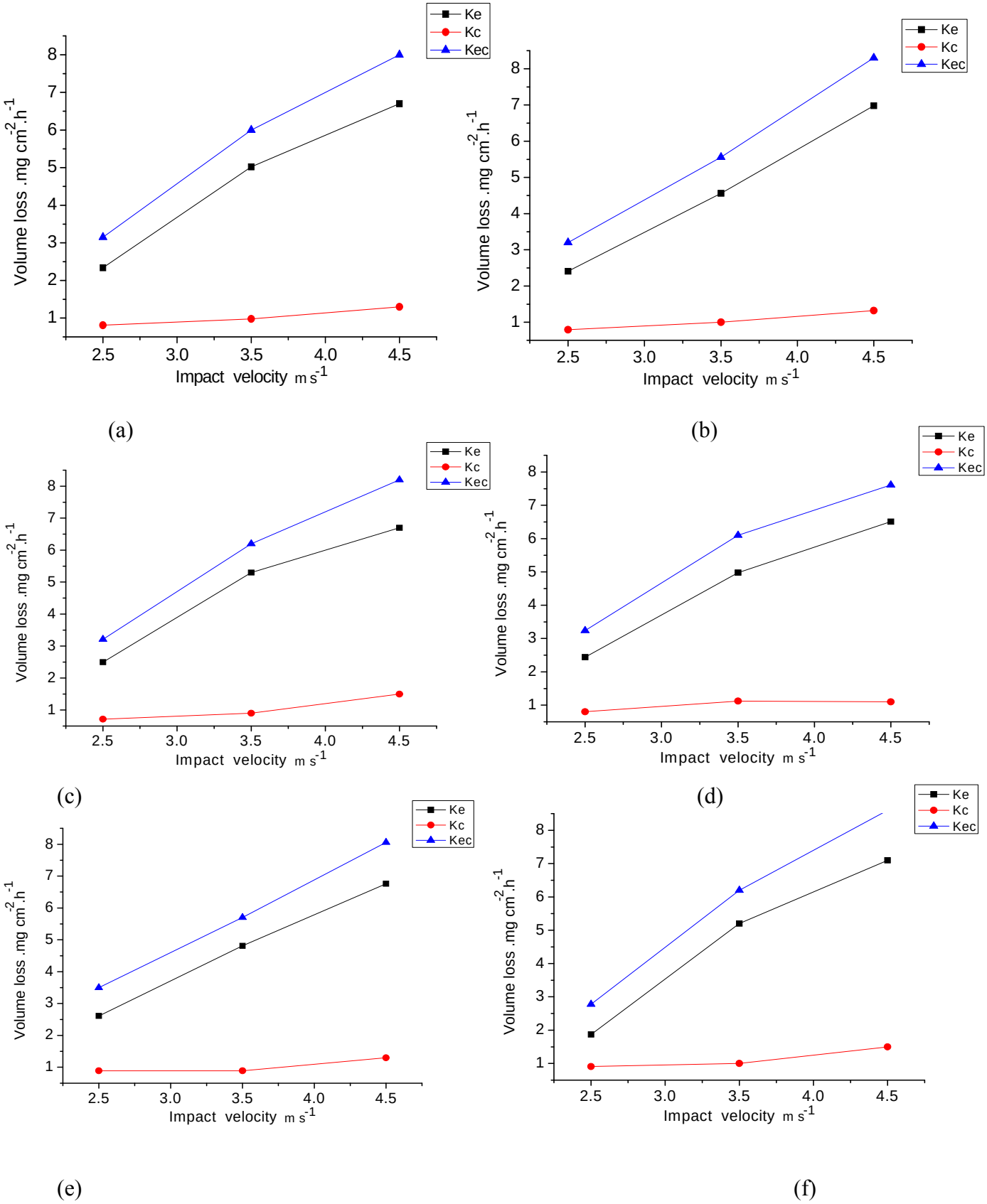

Fig.3.12: Volume loss as function of impact velocities for carbon steel in oil /20% water at -200 mV and particle size 600-710µm (a) 15° (b) 30° (c) 45°(d) 60° (e) 75° (f) 90°.

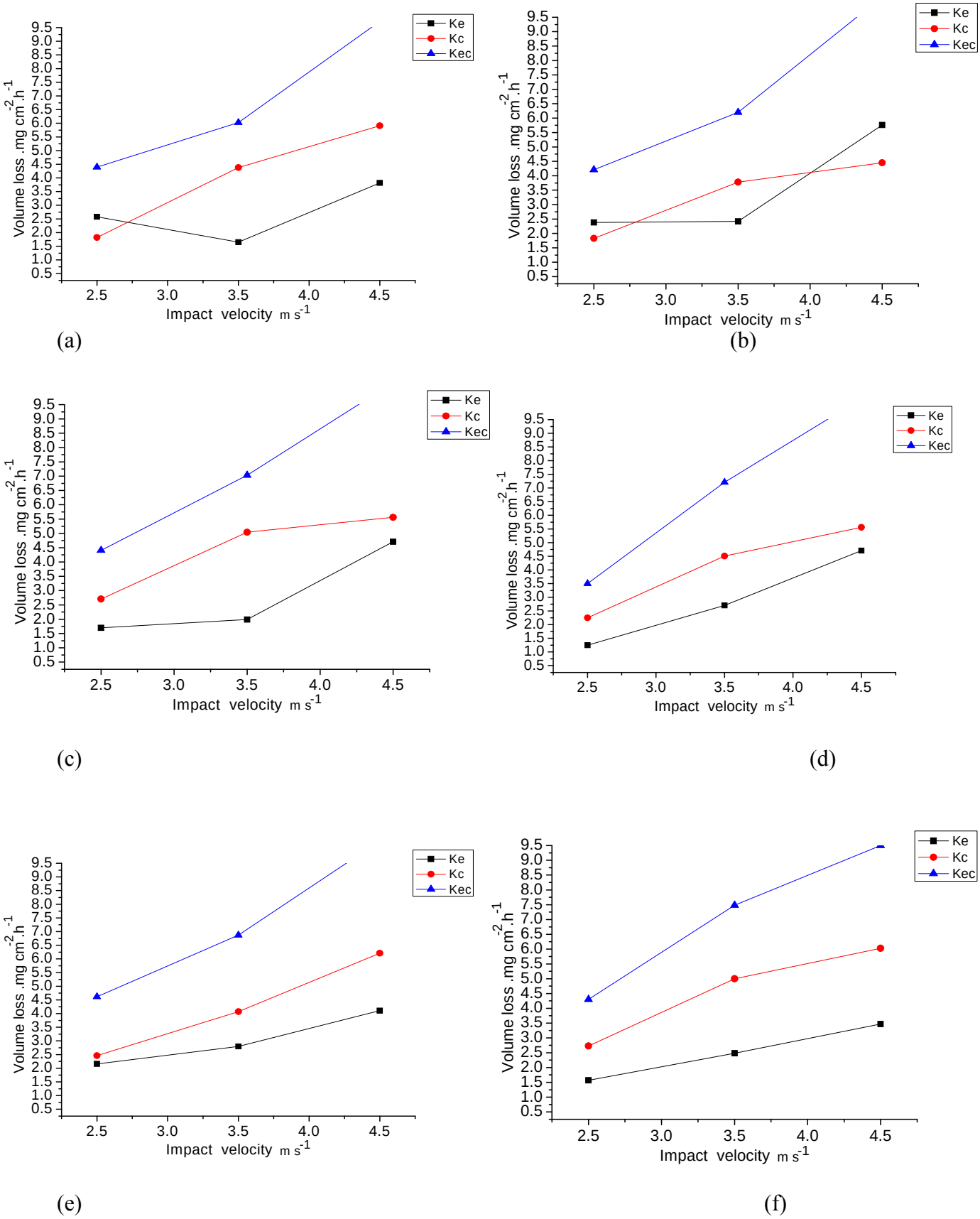

Fig.3.13: Volume loss as function of impact velocities for carbon steel in water at 0 mV and particle size 600-710µm (a) 15° (b) 30° (c) 45°(d) 60° (e) 75° (f) 90°.

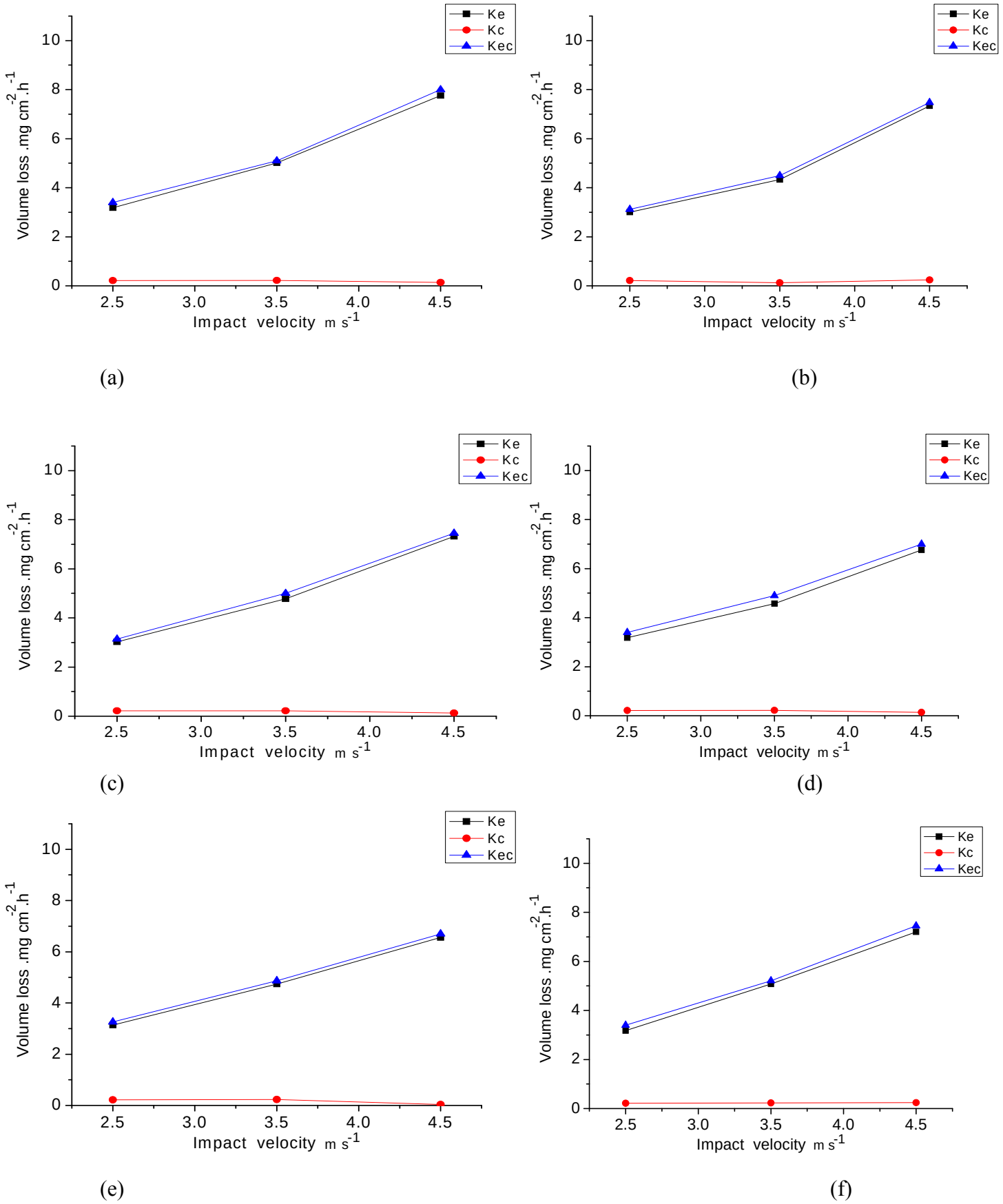

Fig.3.14: Volume loss as function of impact velocities for carbon steel in crude oil at 0 mV and particle size 600-710µm (a) 15° (b) 30° (c) 45°(d) 60° (e) 75° (f) 90°.

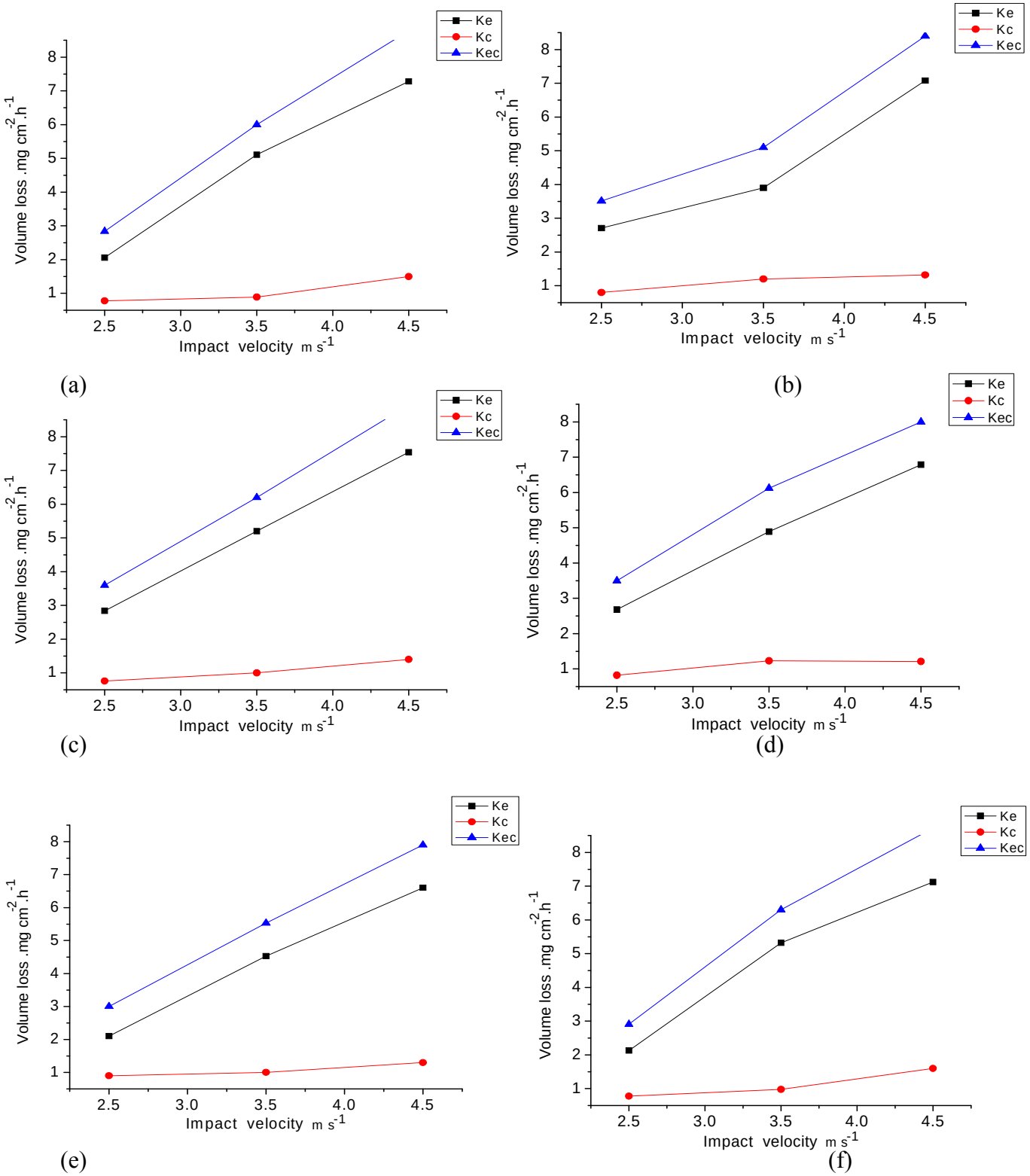

Fig.3.15: Volume loss as function of impact velocities for carbon steel in oil /20% water at 0 mV and particle size 600-710µm (a) 15° (b) 30° (c) 45°(d) 60° (e) 75° (f) 90°.

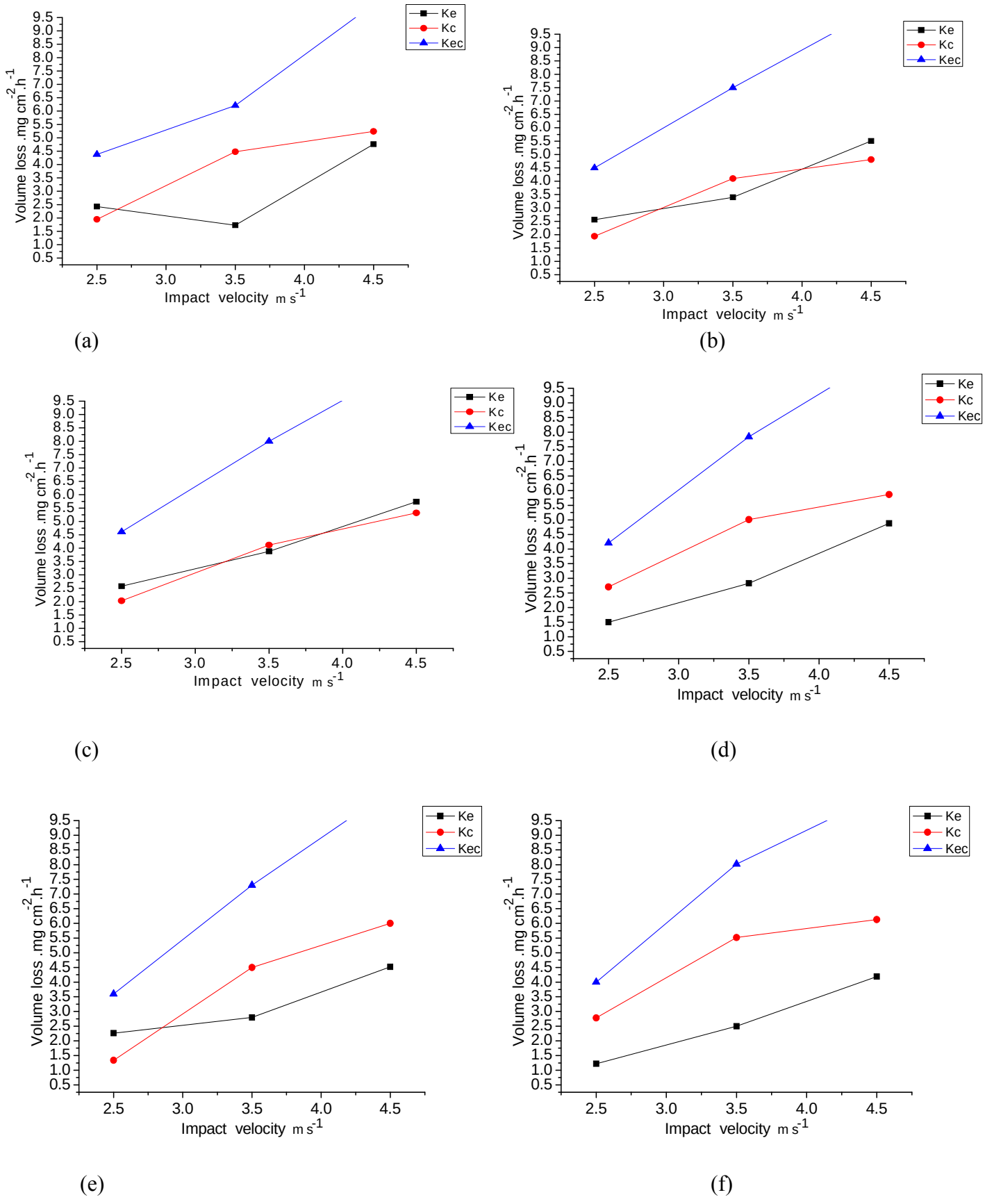

Fig.3.16: Volume loss as function of impact velocities for carbon steel in water at 200 mV and particle size 600-710µm (a) 15° (b) 30° (c) 45°(d) 60° (e) 75° (f) 90°.

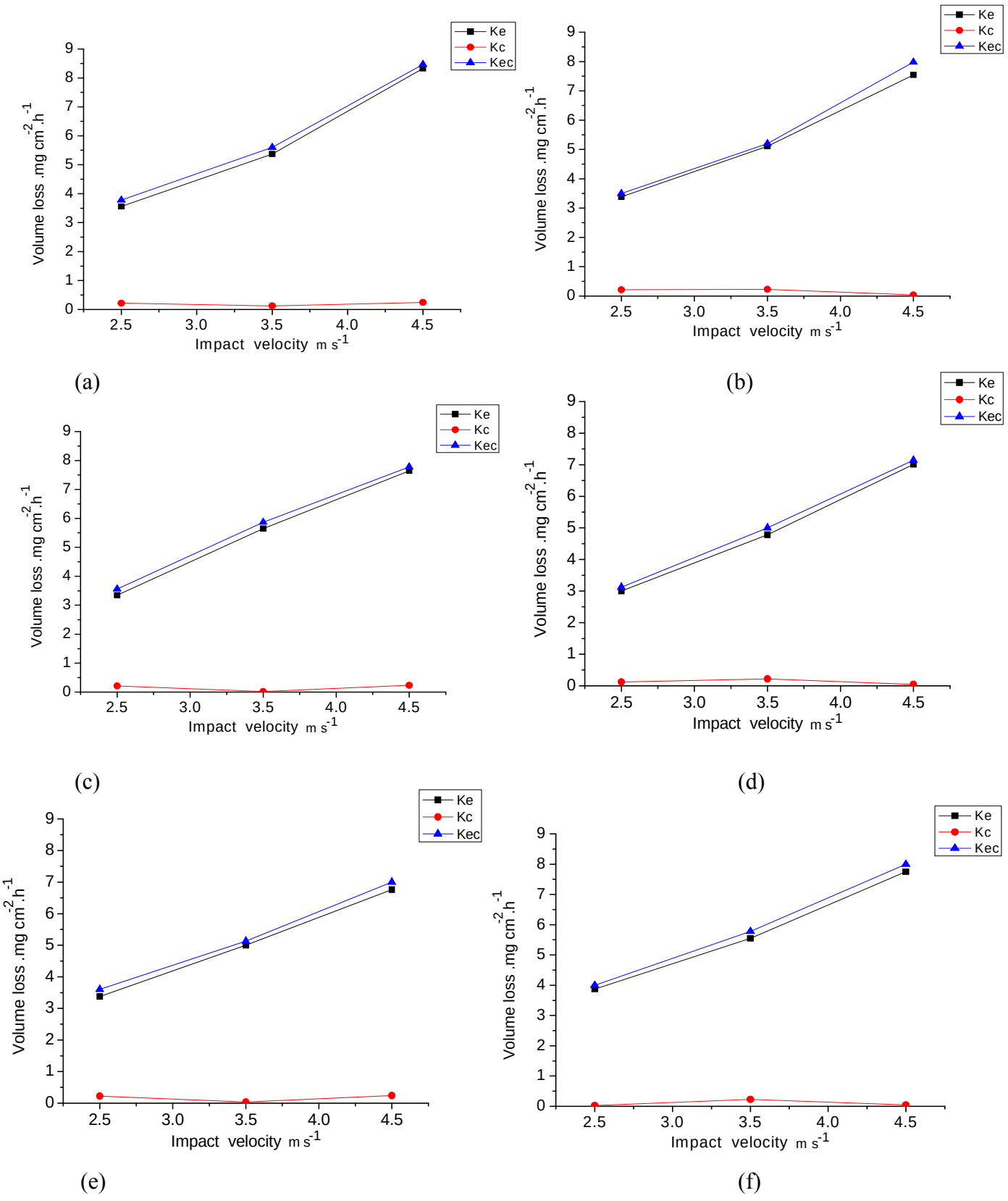

Fig.3.17: Volume loss as function of impact velocities for carbon steel in crude oil at 200 mV and particle size 600-710µm (a) 15° (b) 30° (c) 45°(d) 60° (e) 75° (f) 90°.

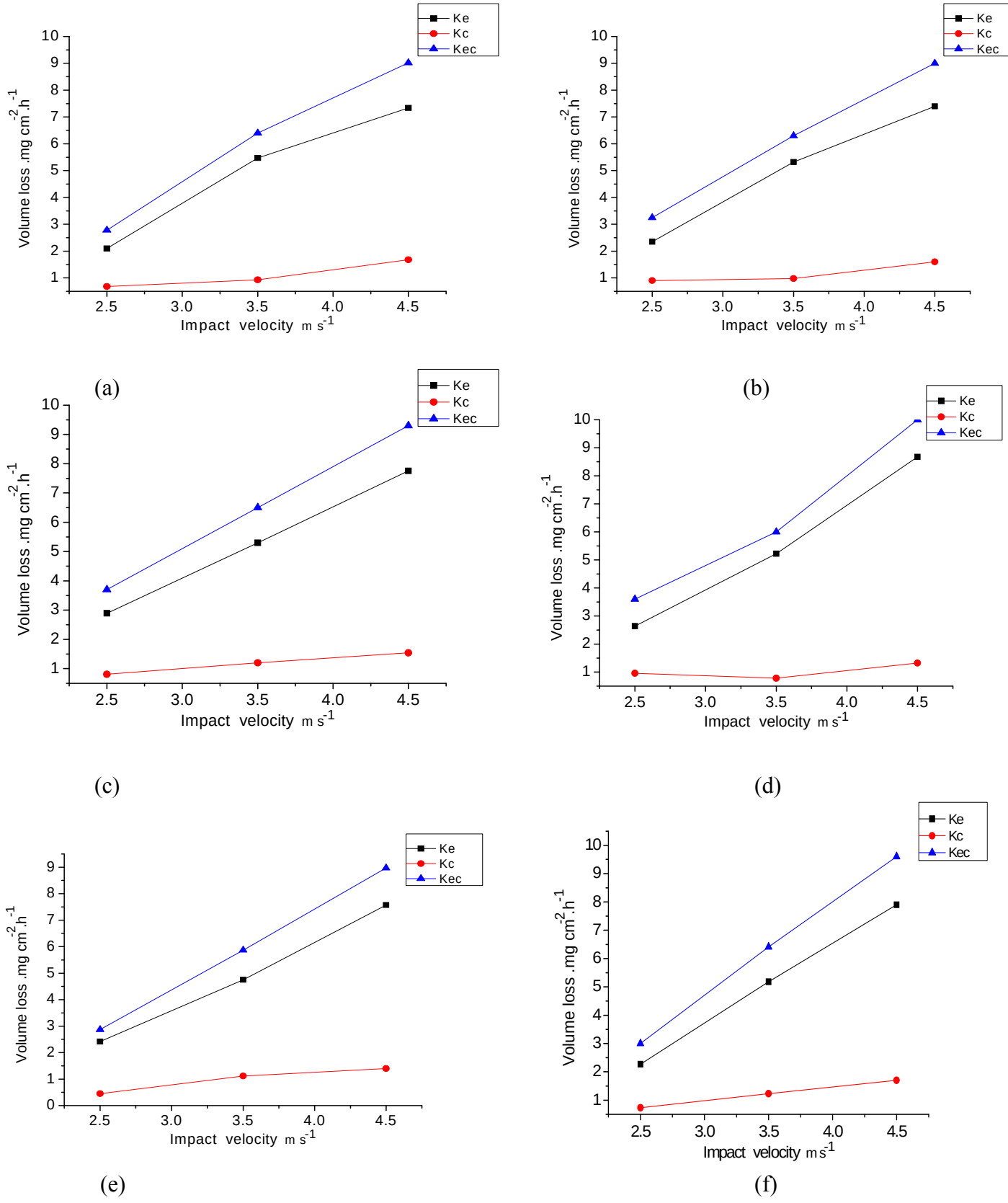

Fig.3.18: Volume loss as function of impact velocities for carbon steel in oil /20% water at 200 mV and particle size 600-710µm (a) 15° (b) 30° (c) 45°(d) 60° (e) 75° (f) 90°.

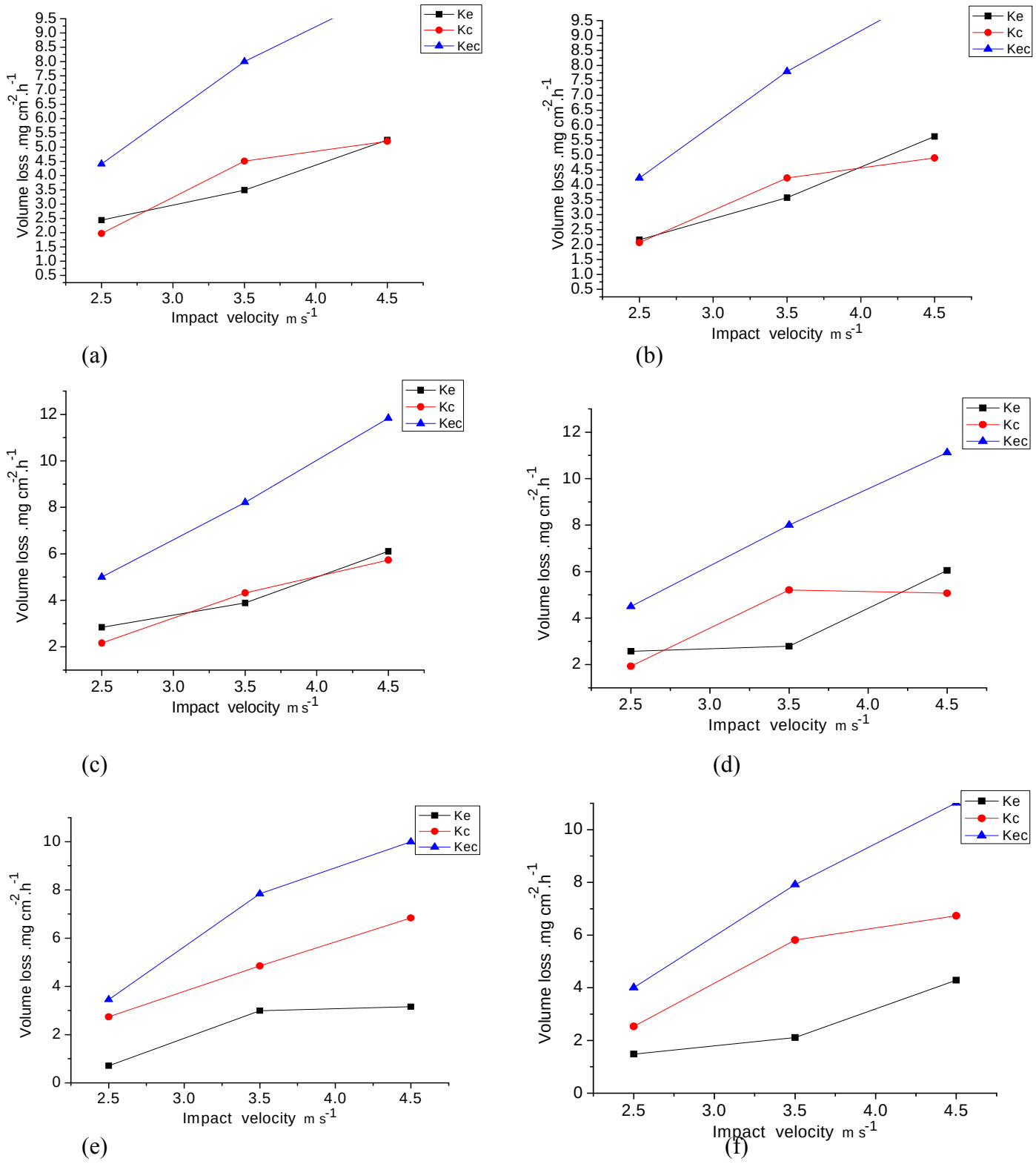

Fig.3.19: Volume loss as function of impact velocities for carbon steel in water at 400 mV and particle size 600-710µm (a) 15° (b) 30° (c) 45°(d) 60° (e) 75° (f) 90°.

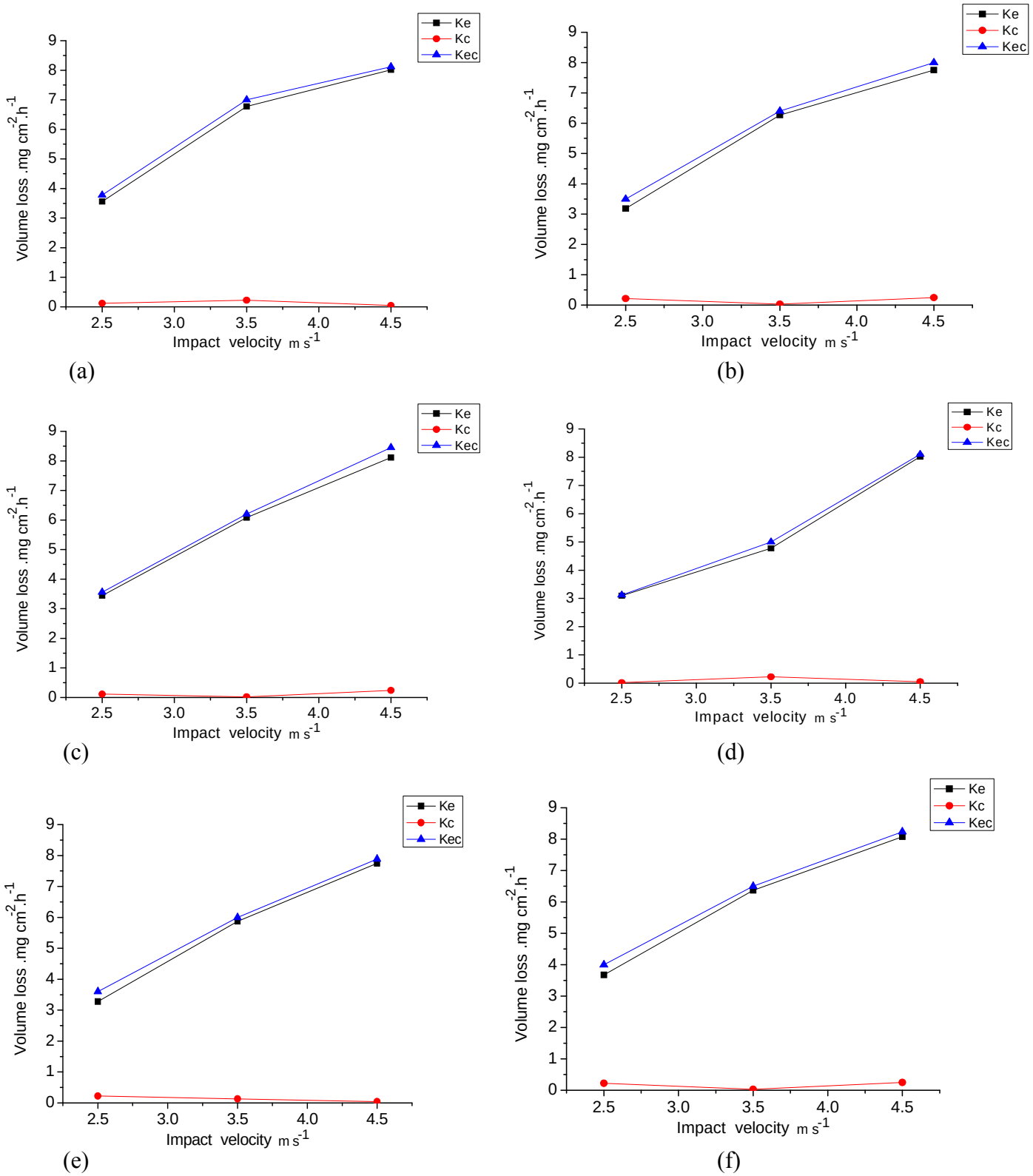

Fig.3.20: Volume loss as function of impact velocities for carbon steel in crude oil at 400 mV and particle size 600-710µm (a) 15° (b) 30° (c) 45°(d) 60° (e) 75° (f) 90°.

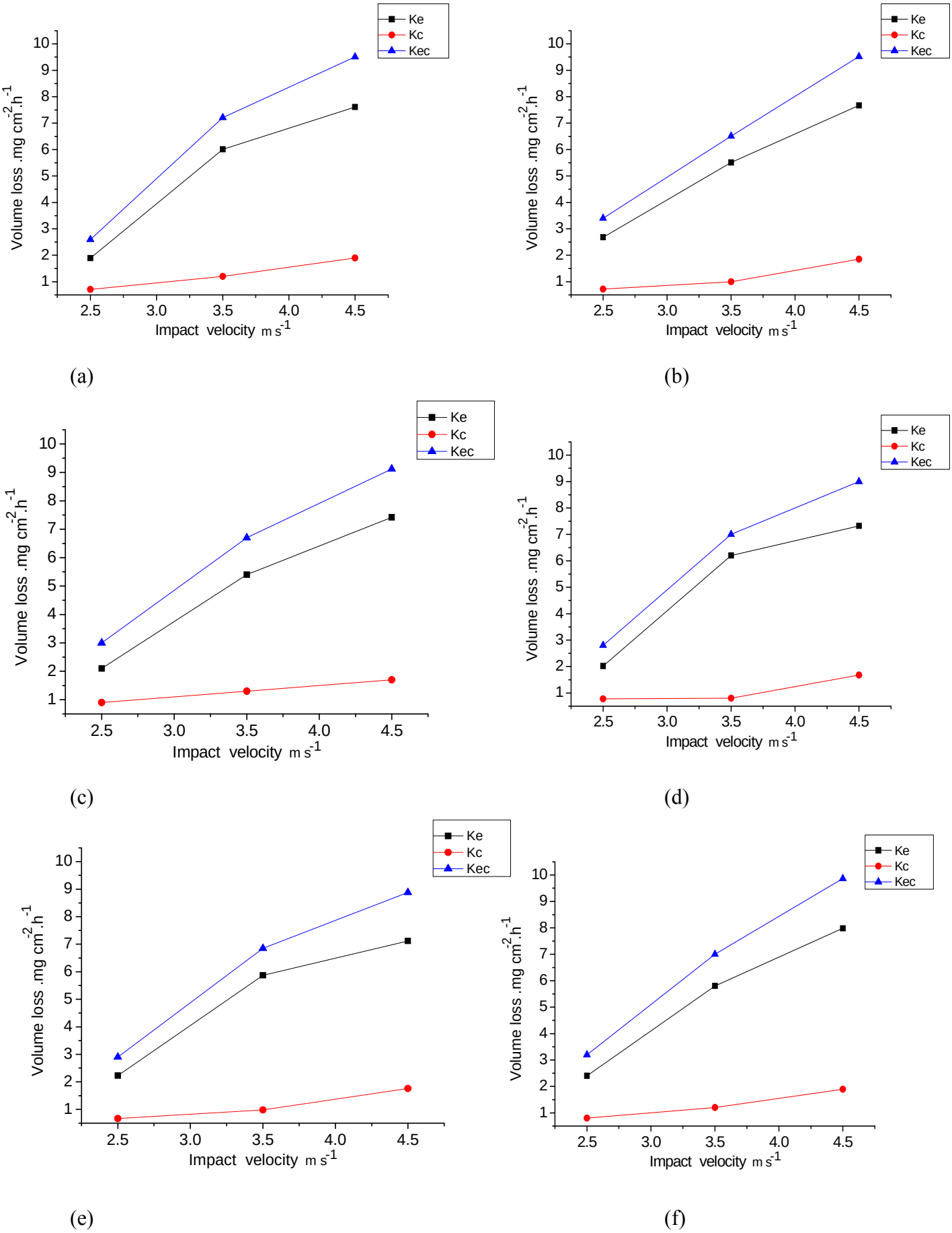

Fig.3.21: Volume loss as function of impact velocities for carbon steel in oil /20% water at 400 mV and particle size 600-710µm (a) 15° (b) 30° (c) 45°(d) 60° (e) 75° (f) 90°.

3.2. Effect of impact angle, impact velocity for particle size150-30µm on erosion-corrosion maps

3.2.1. Conditions of the test

The erosion–corrosion tests were carried out in different environments (i.e. water, crude oil, and oil/20% water). The effect of impact velocities on erosion-corrosion have been investigated at 2.5, 3.5 and 4.5 m s^{-1} with three impact angles 15°, 45° and 90°, and at three applied potentials, -400, 0 and 400 mV. The effect of erosion by aluminium oxide (Al_2O_3) in particle size range 150-300µm on the carbon steel has been investigated in the various environments.

3.2.2. Polarization curves for particle sizes 150-300µm

The polarization curves of the samples were investigated using a computer AC Gill potentiostat in the different environments. The corrosion testing was conducted under potentiodynamic conditions where samples were polarized at 15°, 45° and 90° in different environments to observe the corrosion behaviour of carbon steel. Figures 3.22-3.24 shows the polarization curves for carbon steel in the three environments with particle sizes 150-300µm and at various impact velocities. It was clear that there was a general increase in the anodic current density with decrease of particle sizes from 600-710µm to 150-300µm.

Polarization curves in Figures 3.22-3.24 (a) show that with corrosion in the water environment at 15°, 45° and 90° , there was a clear increase in current density with decrease in impact angle, from 90° and 45°, with an increase in impact velocity from 2.5 to 4.5 ms^{-1}. Thus, clear evidence of passivation was observed at low impact velocity and low impact angle of 15° Fig.3.22 (a).

For carbon steel in the crude oil environment at 15°, 45° and 90° there was a small increase in current density with an increase in impact angle from 15° to 90°, with an increase in impact velocity from 2.5- 4.5ms^{-1}. It was interesting that, the cathodic current density in oil was higher than the anodic current Figures 3.22-3.24 (b) that was not pronounced in the water environment. This will be addressing further in the discussion section. In the mixed environments and at 15°, 45° and 90° Figs 3.22-3.24 (c) the current density was greater than the value of the current density in crude oil environment.

In addition, it can be seen from the results that the value of free corrosion potential (Ecorr) for carbon steel in combined environments was higher than in the water environment, while the corrosion potential (Ecorr) for carbon steel in combined environment was lower than in crude oil environments. The value of current density for carbon steel in water was higher than in the combined environment, while current density for carbon steel in crude oil environments was lower than in combined environments.

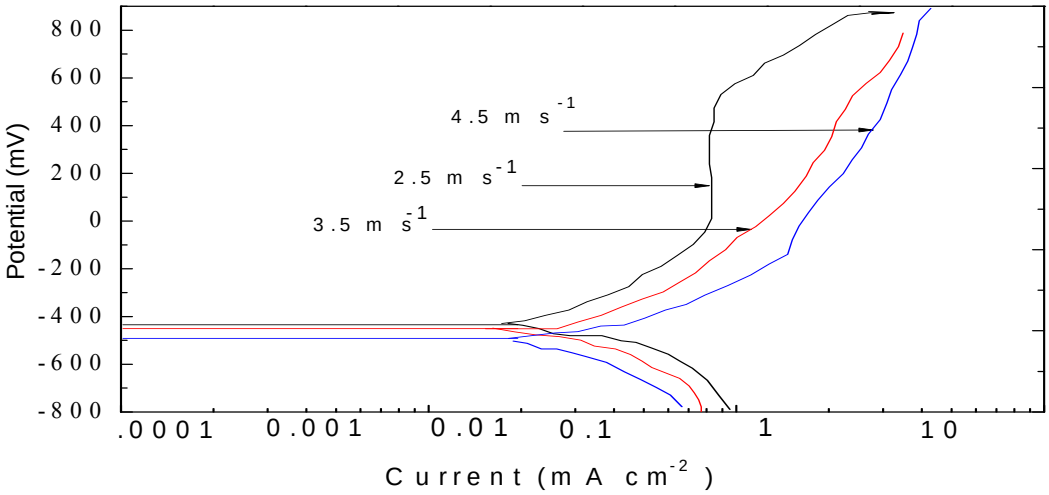

(a)

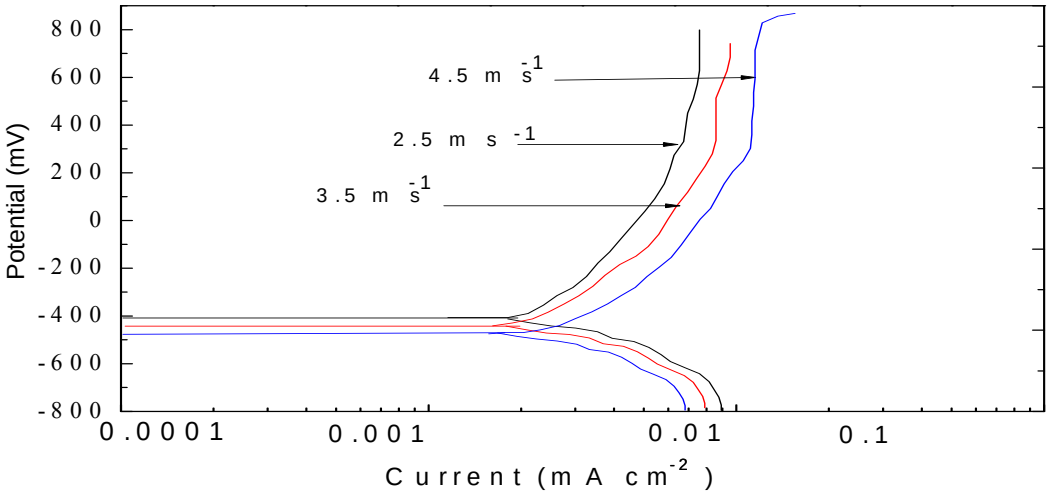

(b)

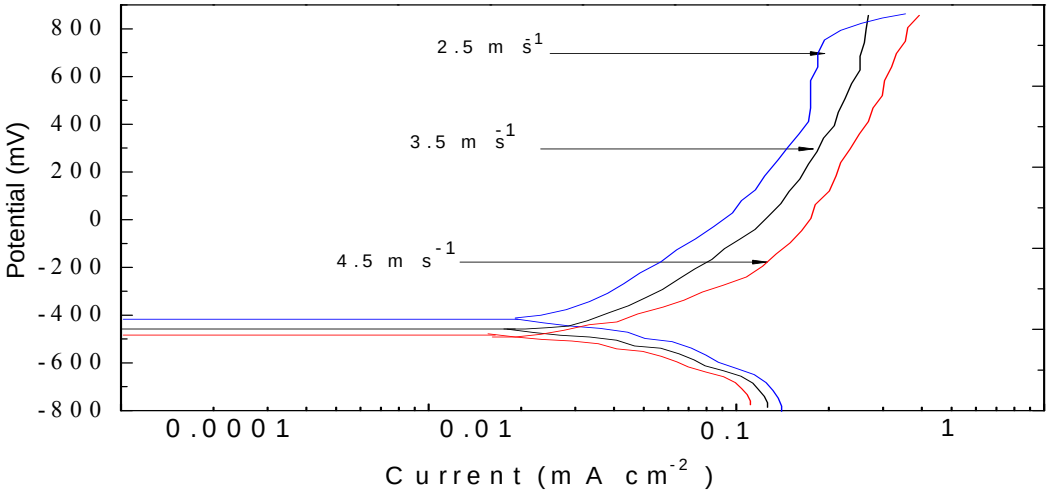

(c)

Fig.3.22: Polarization curves for carbon steel at various impact velocities, particle size 150-300µm and impact angle 15° in (a) water (b) crude oil (c) oil /20% water.

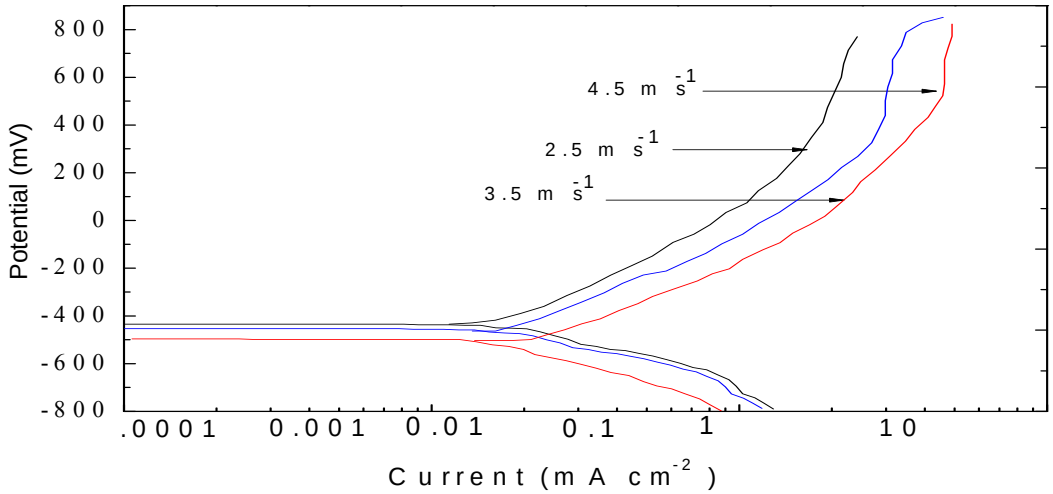

(a)

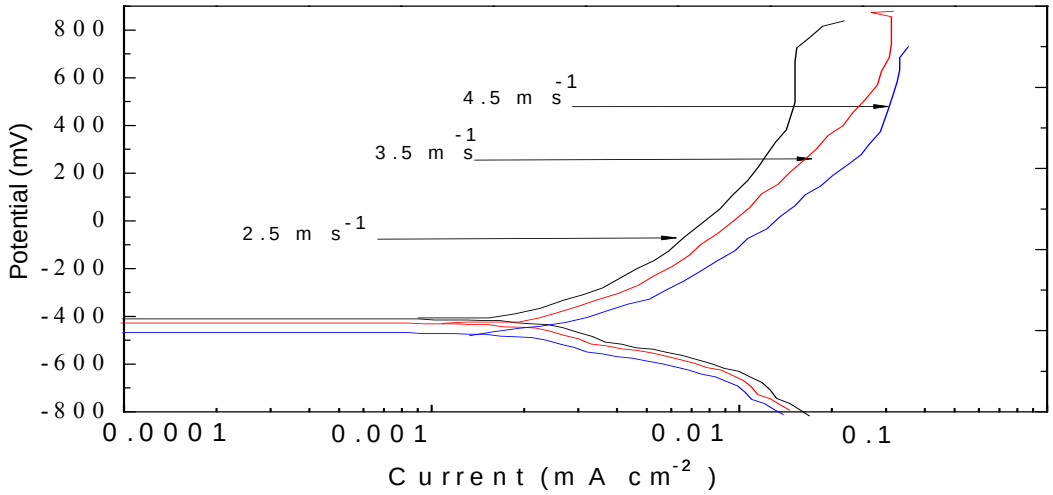

(b)

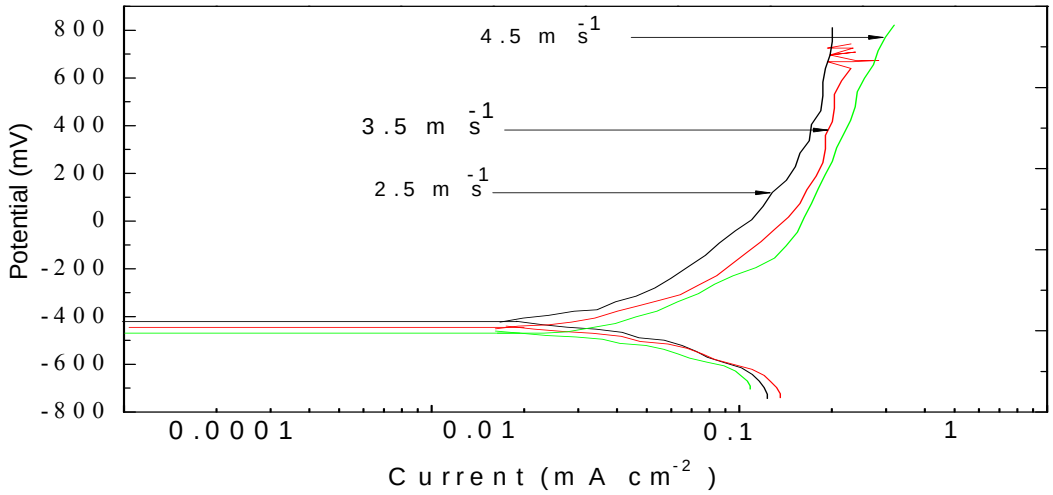

(c)

Fig. 3.23: Polarization curves for carbon steel at various impact velocities, particle size 150-300µm and impact angle 45° in (a) water (b) crude oil (c) oil /20% water.

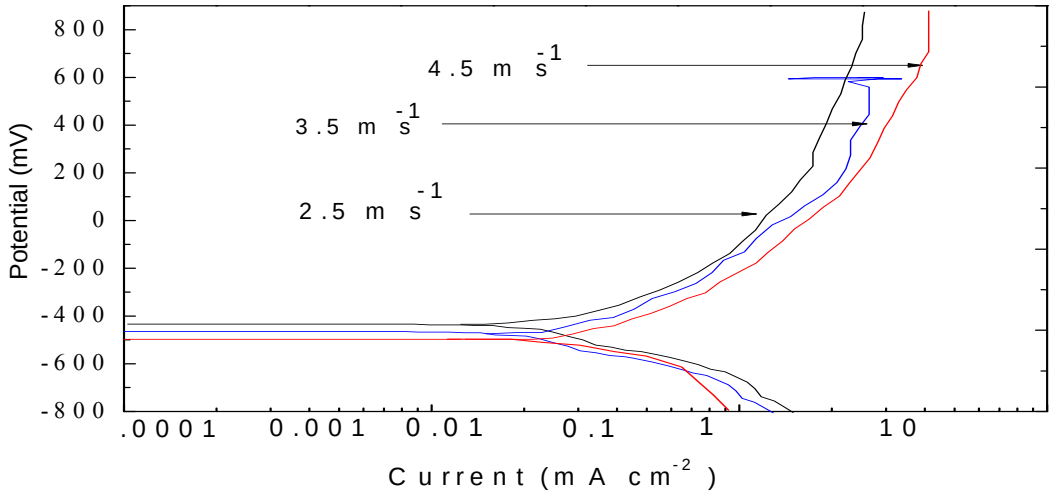

(a)

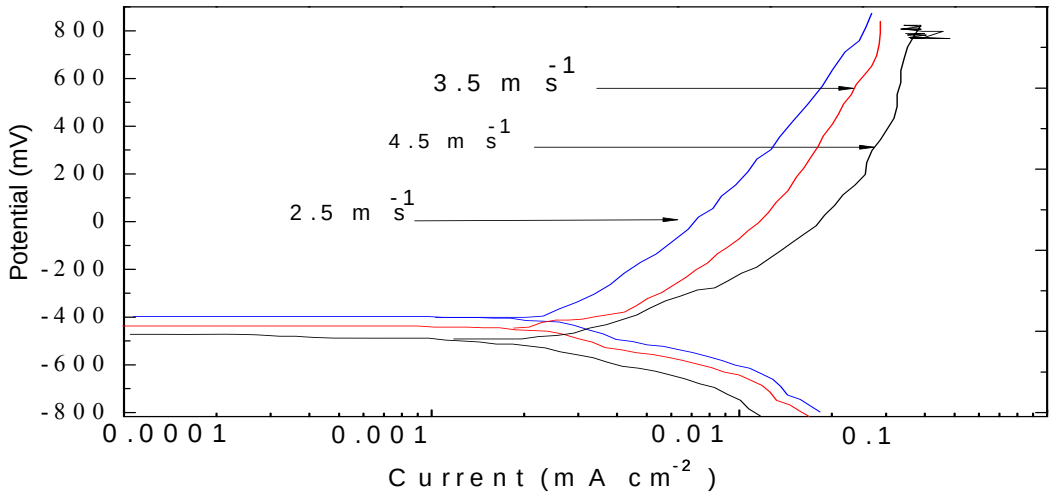

(b)

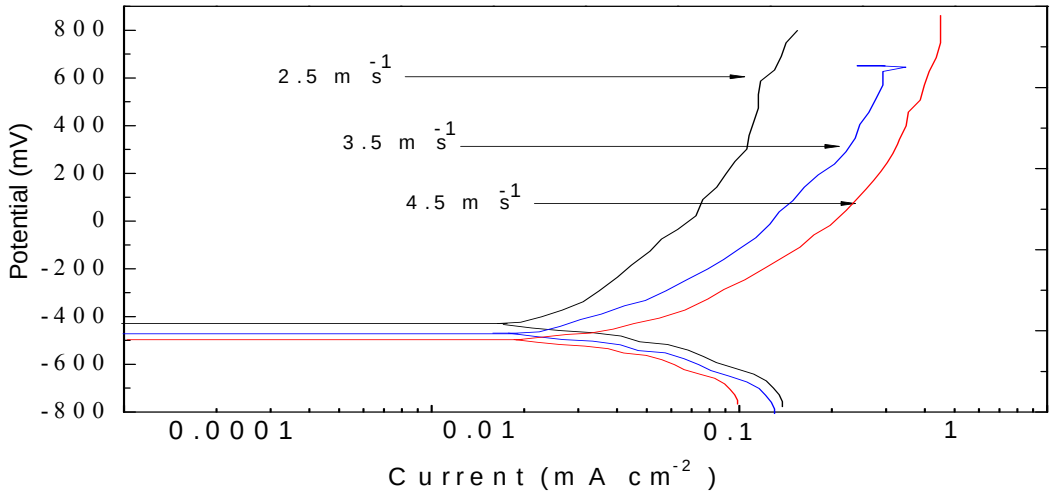

(c)

Fig.3.24: Polarization curves for carbon steel at various impact velocities, particle size 150-300µm and impact angle 90° in (a) water (b) crude oil (c) oil /20% water.

3.2.3. Volume loss for particle sizes 150-300µm

The mass loss charts have been constructed as a function of impact velocity with particle size 150-300µm and at three applied potentials in three environments. Tables 3.16-3.24 show the results of the calculations of volume loss for Ke, Kc and Kec for difference environments and impact velocities with various impact angles at various applied potentials.

3.2.3.1. Mass loss in water reservoir

For carbon steel in the water environment at -400mV,0 mV and 400mV Figures 3.25-3.28 and 3.31(a-c), there was a general increase in mass loss rate due to erosion-corrosion with a decrease in the impact angle from 90° to 45° and an increase in impact velocities from 2.5 to 4.5 m s^{-1}. The peak value of erosion contribution (Ke) was about 2.48 mg cm^{-2} h^{-1} at impact angle 45° and impact velocity 4.5 m s^{-1}, while the lowest value of erosion was 0.46 mg cm^{-2} h^{-1} at cathodic potential(-400mV). On the other hand, the greatest value of corrosion contribution (Kc) was 7 mg cm^{-2} h^{-1} at impact angle 90° and an applied potential of 400mV, which is consistent with the findings of previous research [20,34and 36]. The greatest value of erosion–corrosion (kec) was 8.78 mg cm^{-2} h^{-1} at impact angle 45° and velocity 4.5 m s^{-1}.

3.2.3.2. Mass loss in crude oil environment

It is interesting to see that the values of corrosion contribution Kc were small compared with the values of erosion contribution (Ke) at an applied potentials of -400 mV, 0mV and 400mV Figures 3.26, 3.29 and 3.32(a-c). Conversely, the peak value of erosion contribution was about 4.9 mg cm^{-2} h^{-1} at a high impact velocity of 4.5 m s^{-1} and an impact angle of 45°; while the peak value of corrosion contribution Kc was 1 mg cm^{-2} h^{-1} at 45° in anodic condition (400mV), which is consistent with [2, 6,34and36.]. This is also consistent with the results of the polarization curves.

3.2.3.3. Mass loss in oil/20% water

At applied potentials of -400 mV, 0mV and 400mV, the values of the corrosion contribution Kc increased compared with in the crude oil environment, and the peak value was about 4.55 mg cm^{-2} h^{-1} at impact angle 45°and velocity 4.5 m s^{-1} Figures 3.27, 3.30 and 3.33(a-c). Moreover, the value of corrosion contribution in the

combined environment was similar to the value of corrosion contribution (Kc) in the water environment and was greater than in crude oil environment. The peak value of erosion contribution (ke) in the combined environments was about 2.53 mg cm^{-2} h^{-1} at 45° and velocity 4.5 m s^{-1} at cathodic potential(-400mV). However, in the combined environment the values of erosion contribution were smaller than the values of corrosion contribution, as shown in tables 3.16-3.24.

By comparing between the mass loss for carbon steel in three environments containing small particles sizes150-300µm 3.25, 3.30 and 3.33 and large particles sizes 600-710µm Fig3.7-21., it can be observed that the value of total mass loss recorded for the small particles 150-300µm were lower that that recorded for large particle sizes 600-710µm.

Tables.3.16: Volume loss as function of velocities for carbon steel at various impact angles in water at -400mV and particle size 150-300µm (a) 15° (b) 45° (c) 90°.

(a)

Velocities m s^{-1}	Ke(mg cm^{-2} h^{-1})	Kc(mg cm^{-2} h^{-1})	Kec(mg cm^{-2} h^{-1})
2.5	1.5	2.5	4
3.5	1.22	3.98	5.2
4.5	2	5.5	7.5

(b)

Velocities m s^{-1}	Ke(mg cm^{-2} h^{-1})	Kc(mg cm^{-2} h^{-1})	Kec(mg cm^{-2} h^{-1})
2.5	1.59	2.6	4.19
3.5	1.51	4.2	5.71
4.5	2.3	5.5	7.8

(c)

Velocities m s^{-1}	Ke(mg cm^{-2} h^{-1})	Kc(mg cm^{-2} h^{-1})	Kec(mg cm^{-2} h^{-1})
2.5	1.14	2.4	3.54
3.5	1.1	4.5	5.6
4.5	1.6	5.7	7.3

Tables.3.17: Volume loss as function of velocities for carbon steel at various impact angles in water at 0mV and particle size 150-300μm (a) 15° (b) 45° (c) 90°.

(a)

Velocities m s^{-1}	Ke(mg cm^{-2} h^{-1})	Kc(mg cm^{-2} h^{-1})	Kec(mg cm^{-2} h^{-1})
2.5	0.47	3.74	4.21
3.5	1.5	4	5.5
4.5	1.01	6.2	7.21

(b)

Velocities m s^{-1}	Ke(mg cm^{-2} h^{-1})	Kc(mg cm^{-2} h^{-1})	Kec(mg cm^{-2} h^{-1})
2.5	0.7	3.8	4.5
3.5	1.05	5	6.05
4.5	2.11	5.89	8

(c)

Velocities m s^{-1}	Ke(mg cm^{-2} h^{-1})	Kc(mg cm^{-2} h^{-1})	Kec(mg cm^{-2} h^{-1})
2.5	0.46	3.84	4.3
3.5	0.6	4.81	5.41
4.5	0.65	6.4	7.05

Tables.3.18: Volume loss as function of velocities for carbon steel at various impact angles in water at 400mV and particle size 150-300µm (a) 15° (b) 45° (c) 90°.

(a)

Velocities m s^{-1}	Ke(mg cm^{-2} h^{-1})	Kc(mg cm^{-2} h^{-1})	Kec(mg cm^{-2} h^{-1})
2.5	0.46	3.84	4.3
3.5	2	4.2	6.2
4.5	0.95	6.5	7.45

(b)

Velocities m s^{-1}	Ke(mg cm^{-2} h^{-1})	Kc(mg cm^{-2} h^{-1})	Kec(mg cm^{-2} h^{-1})
2.5	1.51	3.9	5.41
3.5	2	5	7
4.5	2.48	6.3	8.78

(c)

Velocities m s^{-1}	Ke(mg cm^{-2} h^{-1})	Kc(mg cm^{-2} h^{-1})	Kec(mg cm^{-2} h^{-1})
2.5	0.5	3.9	4.4
3.5	0.6	5.4	6
4.5	1	7	8

Tables.3.19: Volume loss as function of velocities for carbon steel at various impact angles in crude oil at -400mV and particle size 150-300μm (a) 15° (b) 45° (c) 90°.

(a)

Velocities m s^{-1}	Ke(mg cm^{-2} h^{-1})	Kc(mg cm^{-2} h^{-1})	Kec(mg cm^{-2} h^{-1})
2.5	1.429	3.21E-01	1.75
3.5	3.05	4.00E-01	3.45
4.5	4.5	7.50E-01	5

(b)

Velocities m s^{-1}	Ke(mg cm^{-2} h^{-1})	Kc(mg cm^{-2} h^{-1})	Kec(mg cm^{-2} h^{-1})
2.5	1.7	3.42E-01	2
3.5	3.4	5.00E-01	3.9
4.5	4.62	8.00E-01	5.42

(c)

Velocities m s^{-1}	Ke(mg cm^{-2} h^{-1})	Kc(mg cm^{-2} h^{-1})	Kec(mg cm^{-2} h^{-1})
2.5	1.1	5.91E-01	1.65
3.5	2.7	5.41E-01	3.25
4.5	3.8	8.23E-01	4.65

Tables.3.20: Volume loss as function of velocities for carbon steel at various impact angles in crude oil at 0mV and particle size 150-300µm (a) 15° (b) 45° (c) 90°.

(a)

Velocities m s^{-1}	Ke(mg cm^{-2} h^{-1})	Kc(mg cm^{-2} h^{-1})	Kec(mg cm^{-2} h^{-1})
2.5	1.5	3.95E-01	1.85
3.5	3.2	5.32E-01	3.75
4.5	4.65	8.53E-01	5.5

(b)

Velocities m s^{-1}	Ke(mg cm^{-2} h^{-1})	Kc(mg cm^{-2} h^{-1})	Kec(mg cm^{-2} h^{-1})
2.5	1. 8	3.40E-01	2.11
3.5	3.4	4.40E-01	3.85
4.5	4.9	8.91E-01	5.75

(c)

Velocities m s^{-1}	Ke(mg cm^{-2} h^{-1})	Kc(mg cm^{-2} h^{-1})	Kec(mg cm^{-2} h^{-1})
2.5	1.44	4.10E-01	1.85
3.5	2.9	6.00E-01	3.5
4.5	4.3	8.68E-01	5.2

Tables.3.21: Volume loss as function of velocities for carbon steel at various impact angles in crude oil at 400mV and particle size 150-300µm , (a) 15° (b) 45° (c) 90°.

(a)

Velocities m s^{-1}	Ke(mg cm^{-2} h^{-1})	Kc(mg cm^{-2} h^{-1})	Kec(mg cm^{-2} h^{-1})
2.5	1.6	4.24E-01	1.98
3.5	3.2	6.12E-01	3.84
4.5	4.6	9.00E-01	5.45

(b)

Velocities m s^{-1}	Ke(mg cm^{-2} h^{-1})	Kc(mg cm^{-2} h^{-1})	Kec(mg cm^{-2} h^{-1})
2.5	1.95	3.57E-01	2.304
3.5	3.4	5.70E-01	4
4.5	4.9	1.00E+01	5.9

(c)

Velocities m s^{-1}	Ke(mg cm^{-2} h^{-1})	Kc(mg cm^{-2} h^{-1})	Kec(mg cm^{-2} h^{-1})
2.5	1.73	4.70E-01	2.2
3.5	3.17	6.30E-01	3.8
4.5	4.2	1.00E+01	5.4

Tables.3.22: Volume loss as function of velocities for carbon steel at various impact angles in oil /20% water at -400mV and particle size 150-300µm, (a) 15° (b) 45° (c) 90°.

(a)

Velocities m s^{-1}	Ke(mg cm^{-2} h^{-1})	Kc(mg cm^{-2} h^{-1})	Kec(mg cm^{-2} h^{-1})
2.5	1.2	1.11E+00	2.3
3.5	1.6	2.46E+00	4
4.5	2.53	3.37E+00	5.9

(b)

Velocities m s^{-1}	Ke(mg cm^{-2} h^{-1})	Kc(mg cm^{-2} h^{-1})	Kec(mg cm^{-2} h^{-1})
2.5	1.3	1.21E+00	2.5
3.5	1.3	2.95E+00	4.21
4.5	2.4	3.60E+00	6

(c)

Velocities m s^{-1}	Ke(mg cm^{-2} h^{-1})	Kc(mg cm^{-2} h^{-1})	Kec(mg cm^{-2} h^{-1})
2.5	1.4	1.03E+00	2.43
3.5	1.7	2.26E+00	3.98
4.5	2	3.52E+00	5.5

Tables.3.23: Volume loss as function of velocities for carbon steel at various impact angles in oil /20% water at 0mV and particle size 150-300µm, (a) 15° (b) 45° (c) 90°.

(a)

Velocities m s^{-1}	Ke(mg cm^{-2} h^{-1})	Kc(mg cm^{-2} h^{-1})	Kec(mg cm^{-2} h^{-1})
2.5	1.1	1.51E+00	2.6
3.5	1.3	2.97E+00	4.3
4.5	2.4	4.00E+00	6.4

(b)

Velocities m s^{-1}	Ke(mg cm^{-2} h^{-1})	Kc(mg cm^{-2} h^{-1})	Kec(mg cm^{-2} h^{-1})
2.5	0.9	1.75E+00	2.7
3.5	1.5	3.00E+00	4.46
4.5	2.1	4.45E+00	6.5

(c)

Velocities m s^{-1}	Ke(mg cm^{-2} h^{-1})	Kc(mg cm^{-2} h^{-1})	Kec(mg cm^{-2} h^{-1})
2.5	0.85	1.65E+00	2.5
3.5	1.15	2.85E+00	4
4.5	1.9	4.30E+00	6.2

Tables.3.24: Volume loss as function of velocities for carbon steel at various impact angles in oil /20% water at 400mV and particle size 150-300µm, (a) 15° (b) 45° (c) 90°.

(a)

Velocities m s^{-1}	Ke(mg cm^{-2} h^{-1})	Kc(mg cm^{-2} h^{-1})	Kec(mg cm^{-2} h^{-1})
2.5	0.98	1.77E+00	2.75
3.5	1.73	3.02E+00	4.75
4.5	2.42	4.23E+00	6.65

(b)

Velocities m s^{-1}	Ke(mg cm^{-2} h^{-1})	Kc(mg cm^{-2} h^{-1})	Kec(mg cm^{-2} h^{-1})
2.5	1.55	1.85E+00	3.4
3.5	1.5	3.32E+00	4.8
4.5	2.2	4.55E+00	6.78

(c)

Velocities m s^{-1}	Ke(mg cm^{-2} h^{-1})	Kc(mg cm^{-2} h^{-1})	Kec(mg cm^{-2} h^{-1})
2.5	0.82	1.83E+00	2.65
3.5	1.54	2.94E+00	4.51
4.5	2.1	4.42E+00	6.5

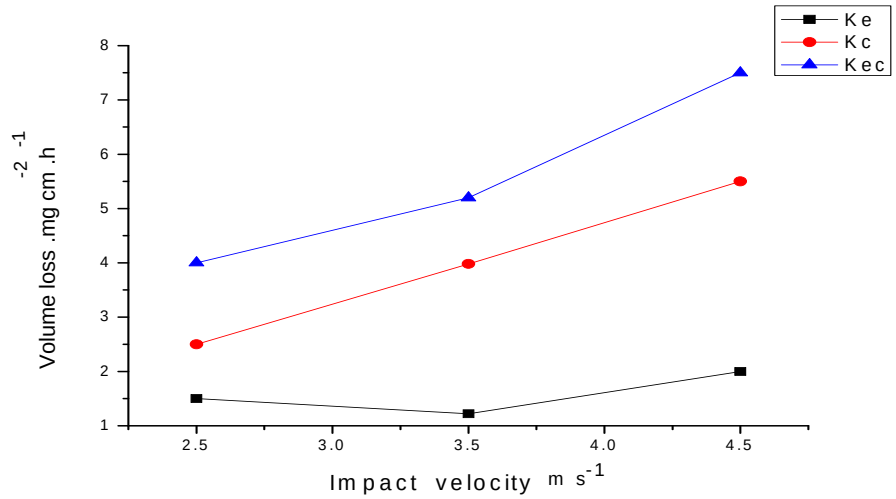

(a)

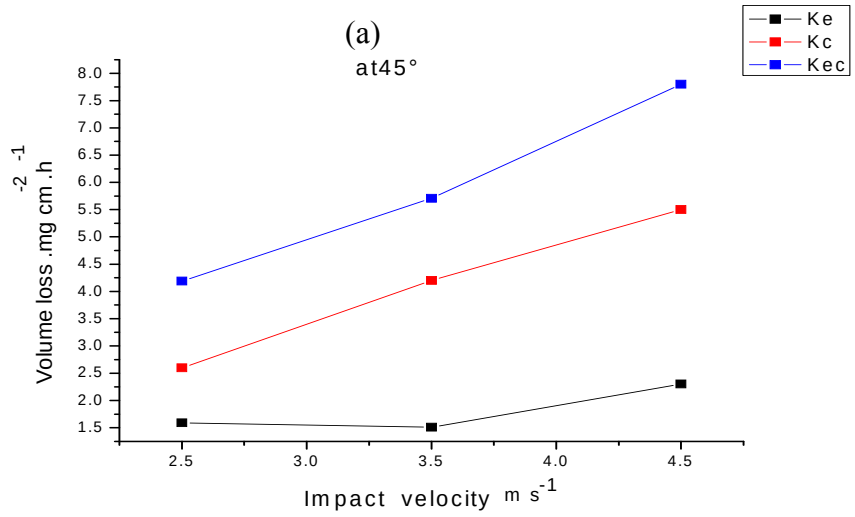

(b)

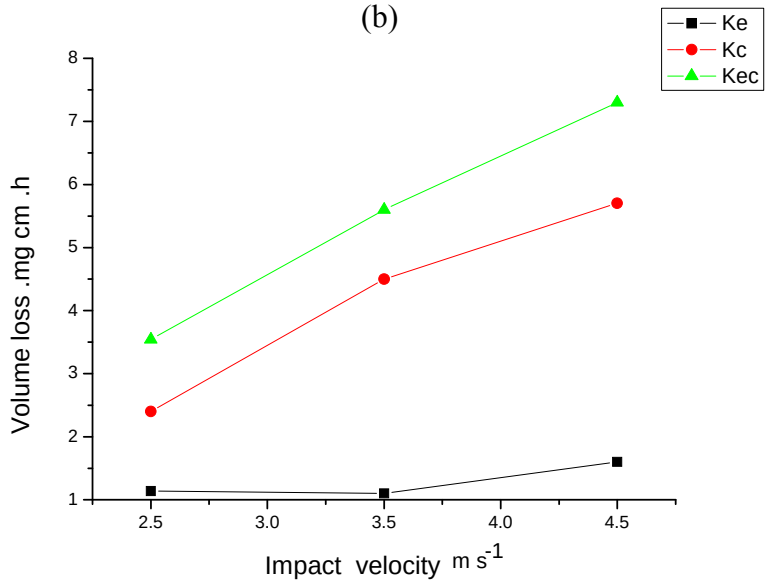

(c)

Fig.3.25 : Volume loss as function of impact velocities for carbon steel in water at -400 mV and particle size 150-300µm (a) 15° (b) 45° (c) 90°.

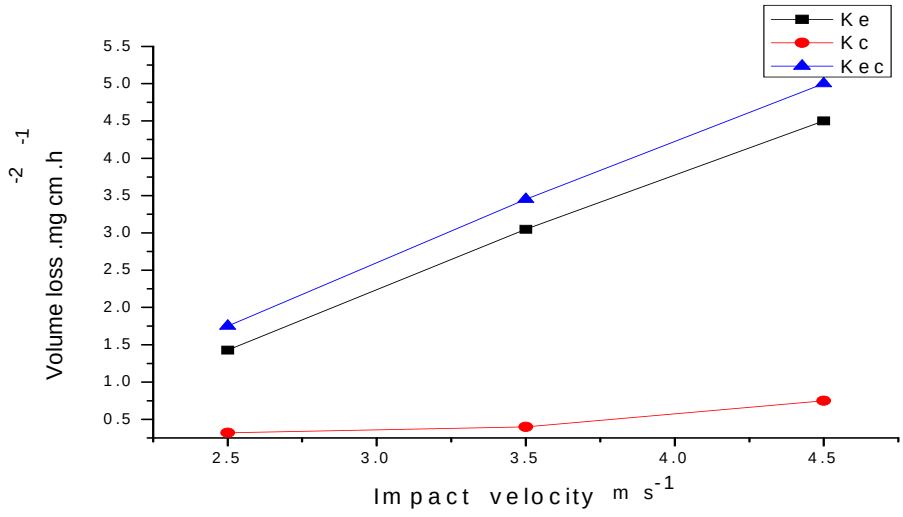

(a)

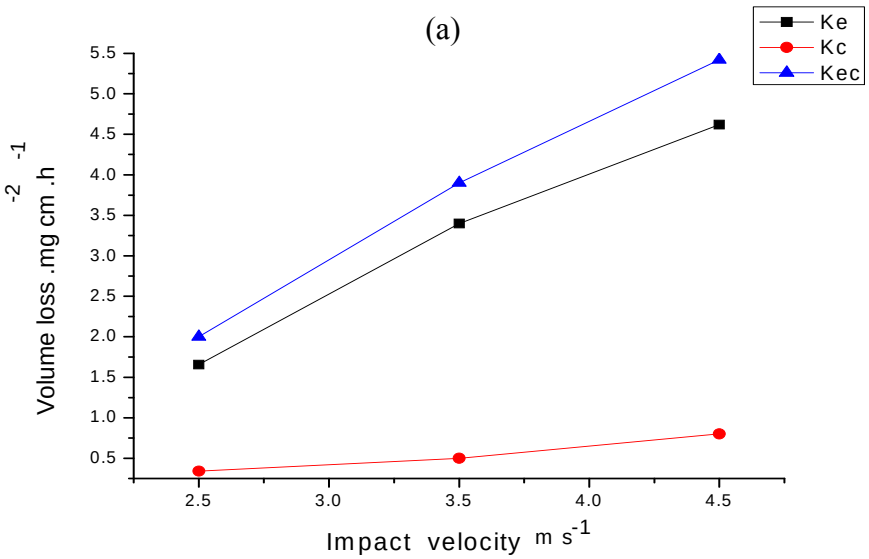

(b)

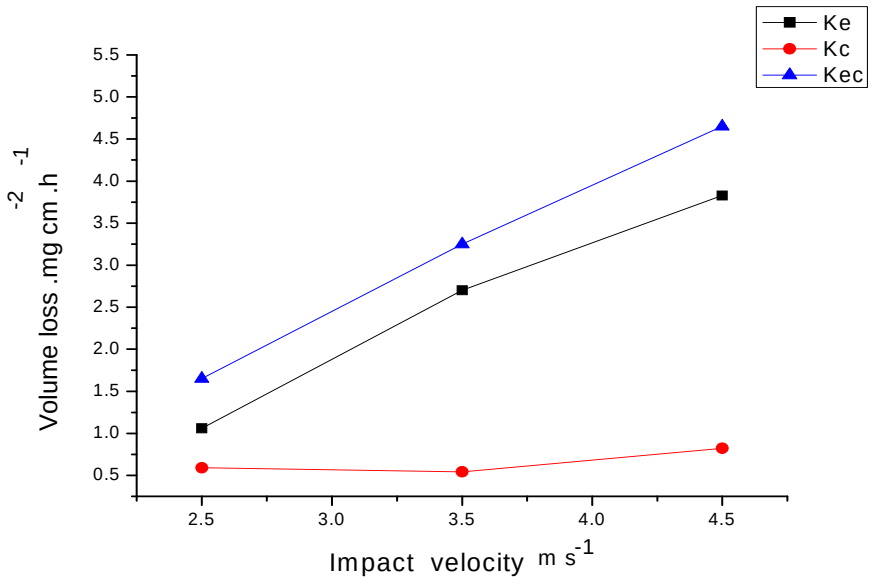

(c)

Fig.3.26: Volume loss as function of impact velocities for carbon steel in crude oil at -400 mV and particle size 150-300µm (a) 15° (b) 45° (c) 90°.

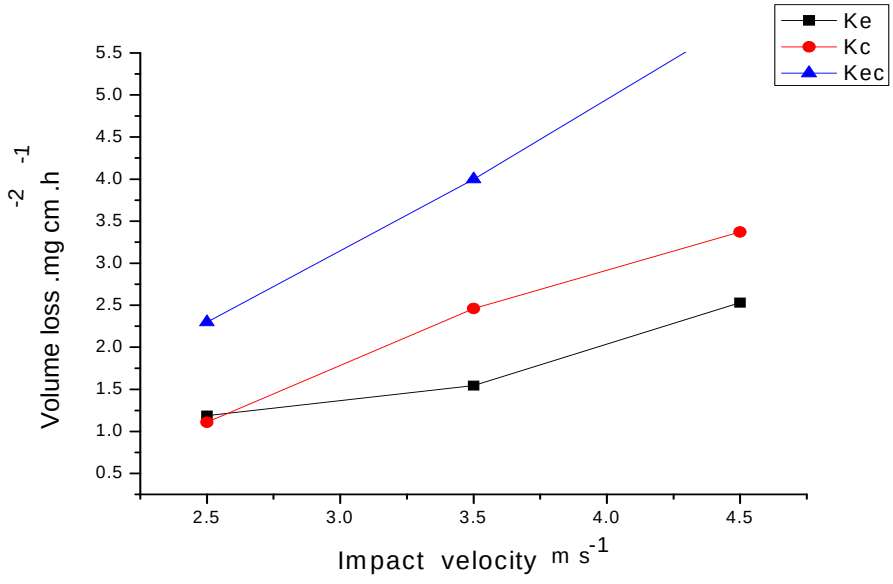

(a)

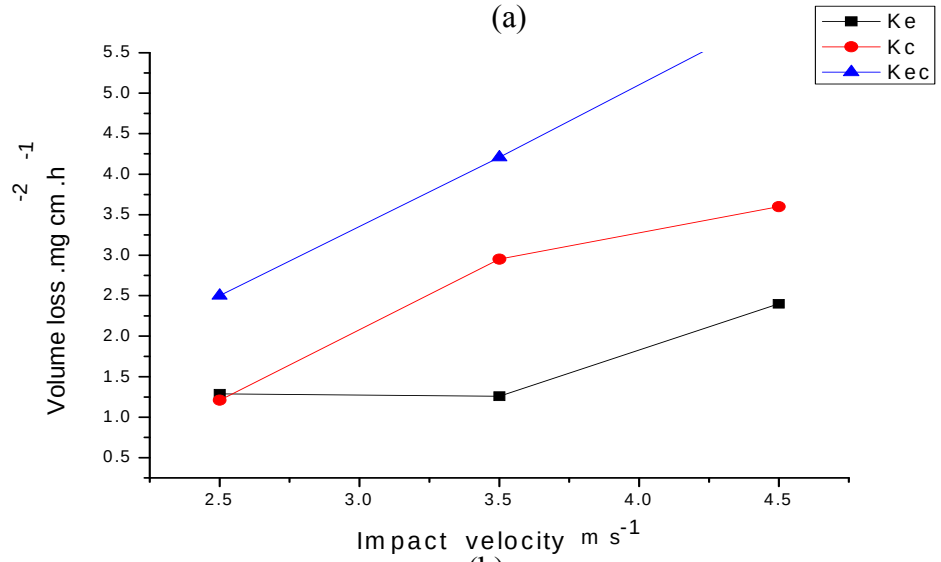

(b)

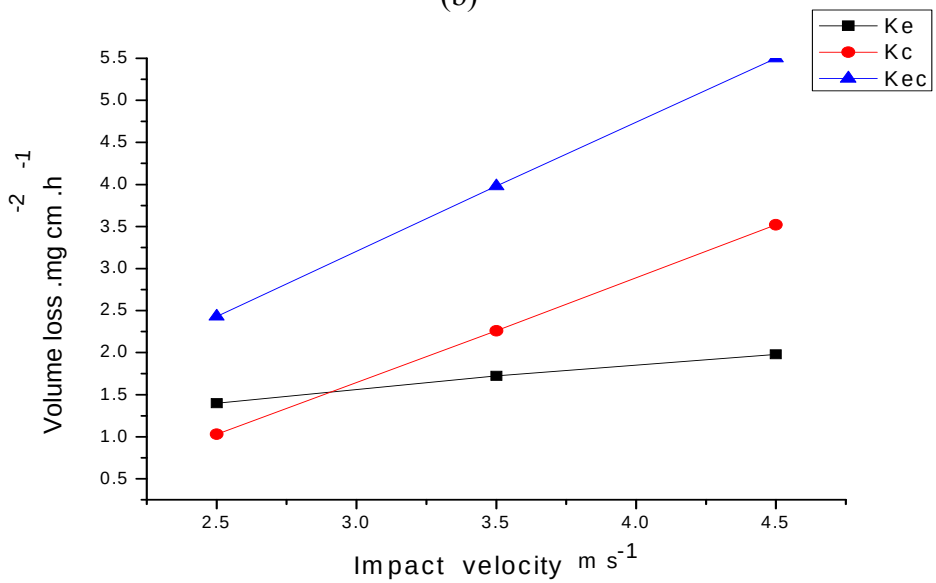

(c)

Fig.3.27: Volume loss as function of impact velocities for carbon steel in oil /20% water at -400 mV and particle size 150-300µm (a) 15° (b) 45° (c) 90°.

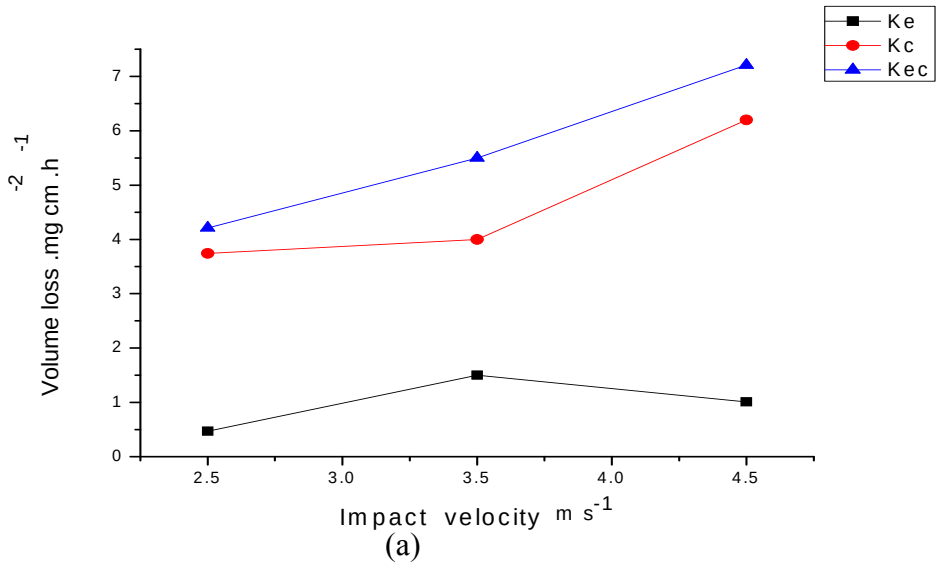

(a)

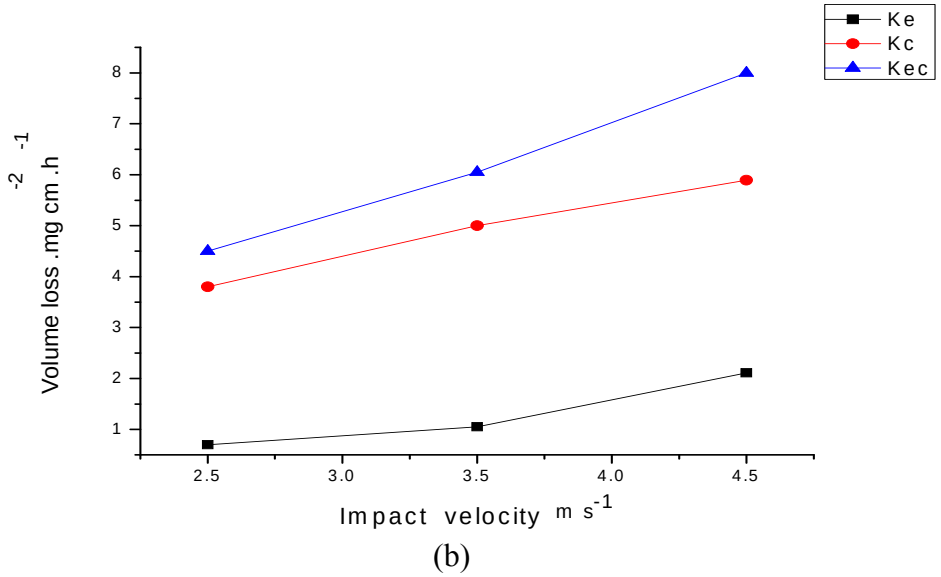

(b)

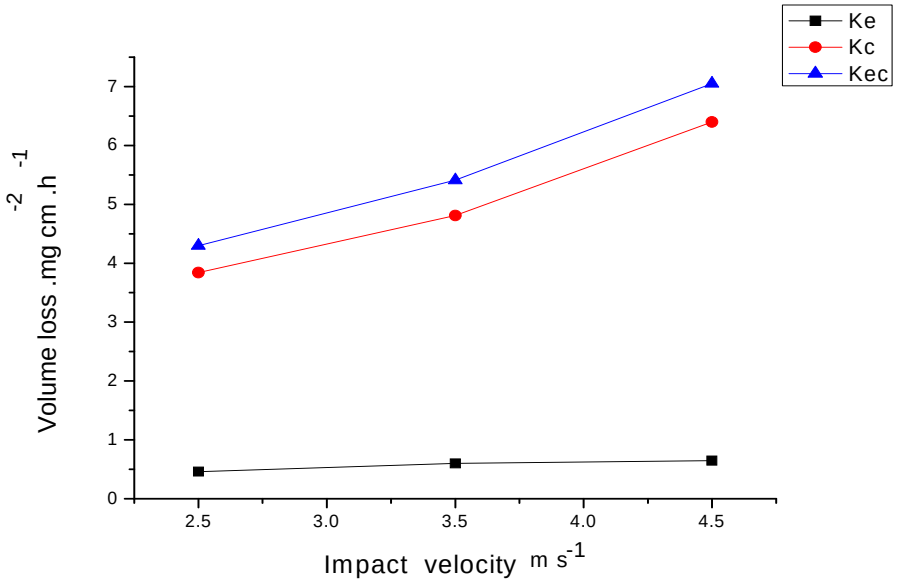

(c)

Fig.3.28 : Volume loss as function of impact velocities for carbon steel in water at 0 mV and particle size 150-300µm (a) 15° (b) 45° (c) 90°.

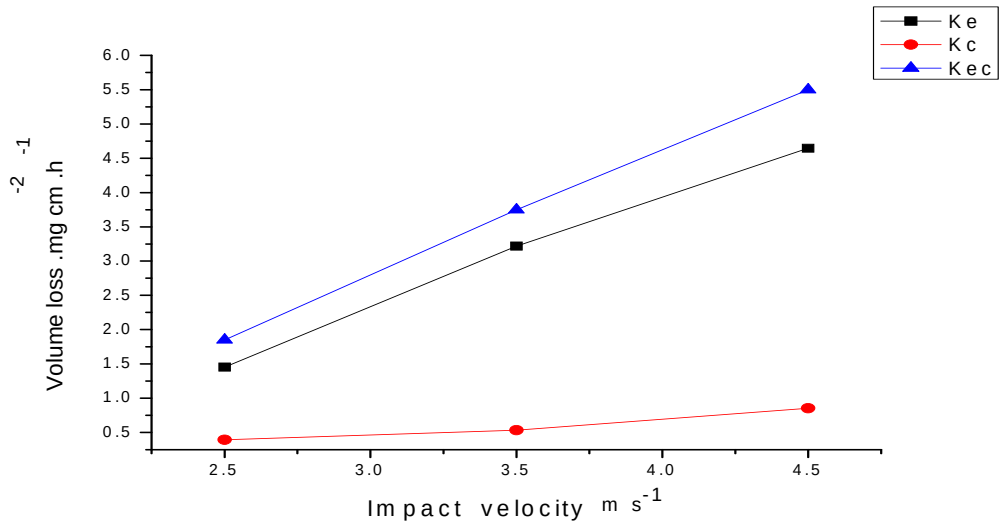

(a)

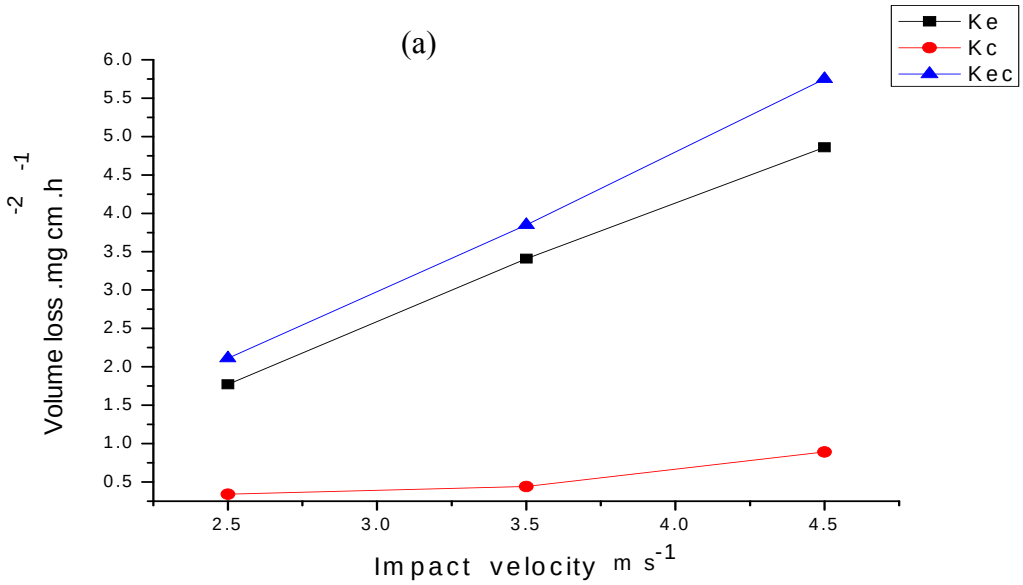

(b)

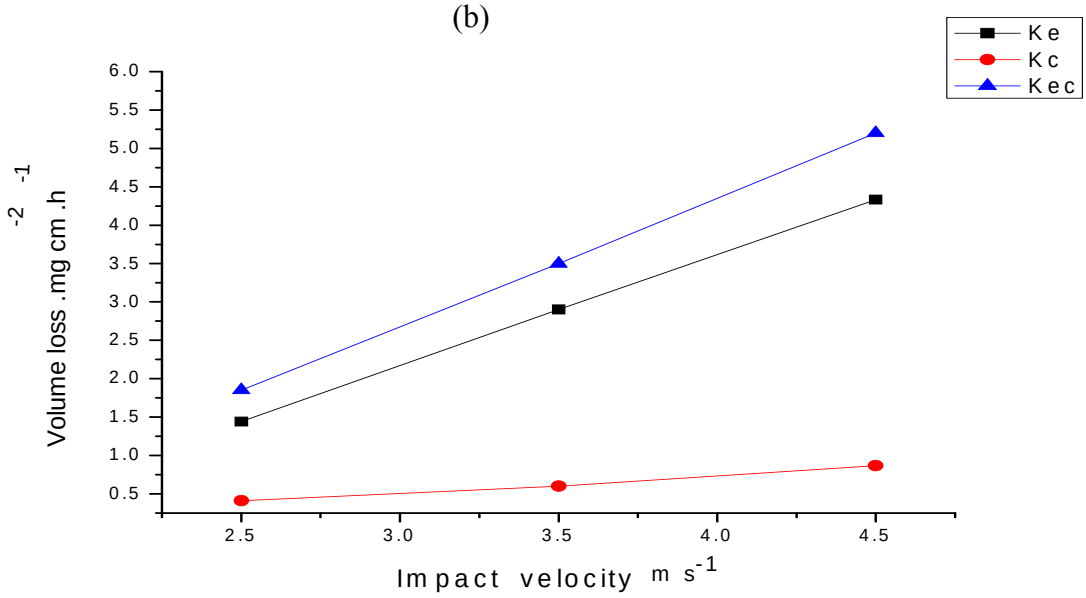

(c)

Fig.3.29: Volume loss as function of impact velocities for carbon steel in crude oil at 0 mV and particle size 150-300µm (a) 15° (b) 45° (c) 90°.

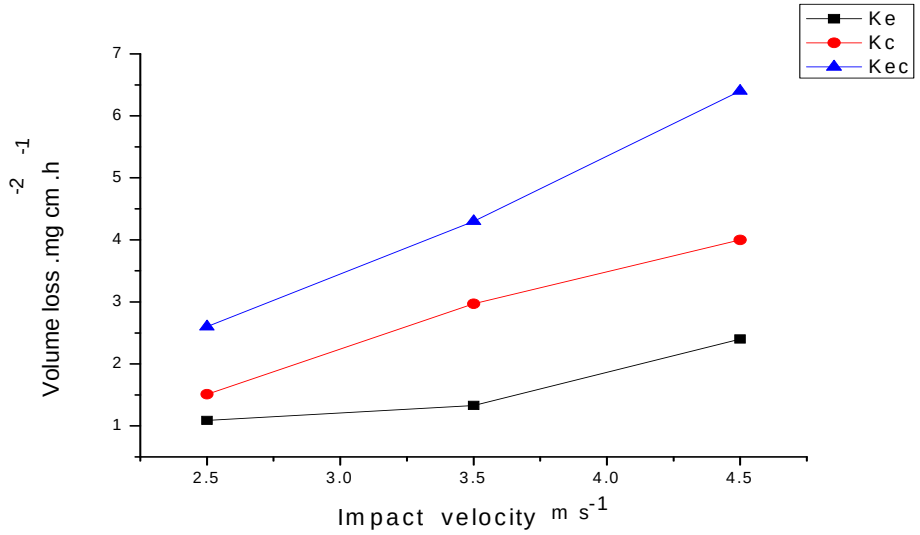

(a)

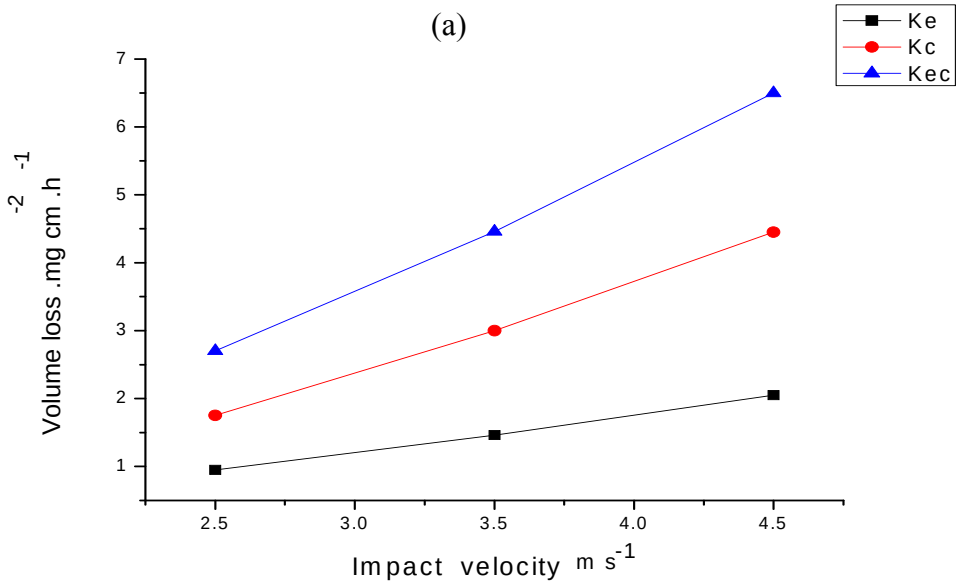

(b)

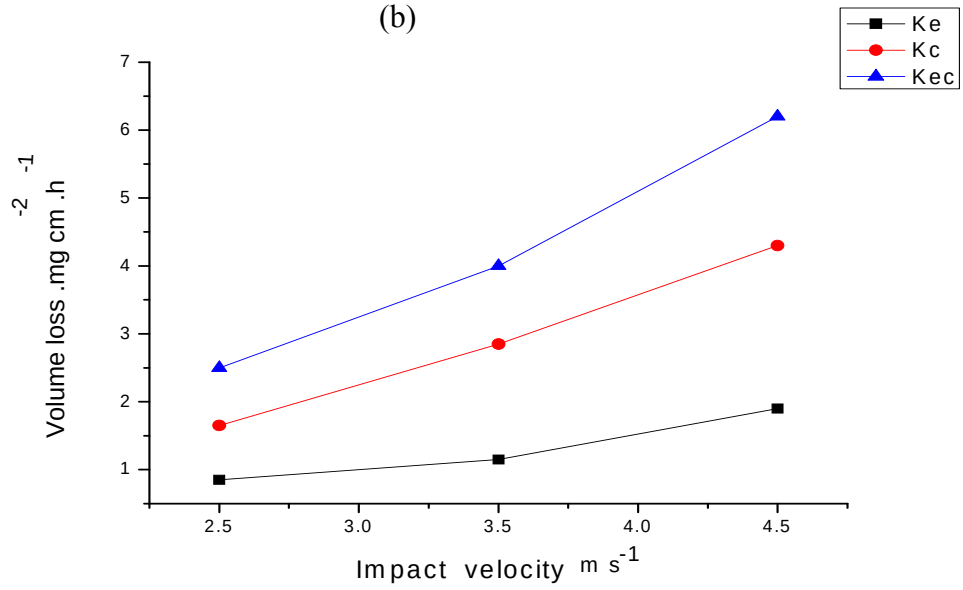

(c)

Fig.3.30 : Volume loss as function of impact velocities for carbon steel in oil /20% water at 0 mV and particle size 150-300µm (a) 15° (b) 45° (c) 90°.

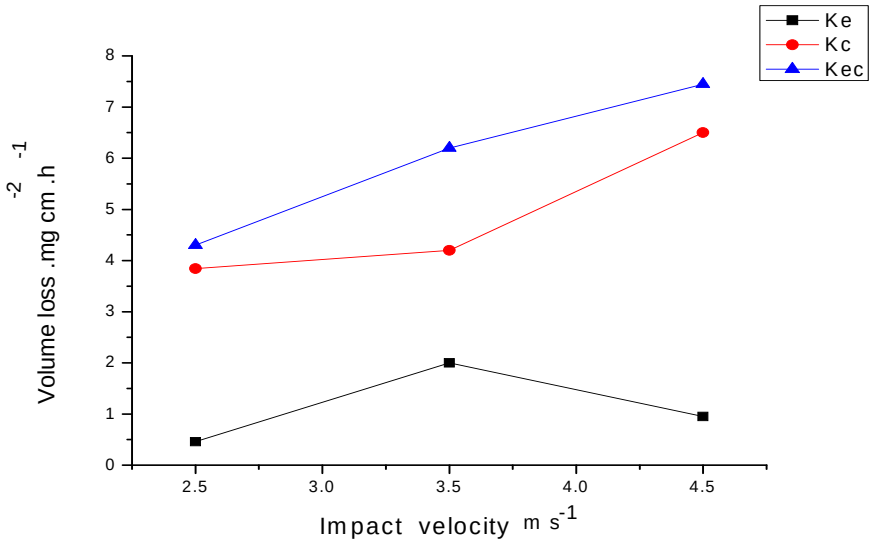

(a)

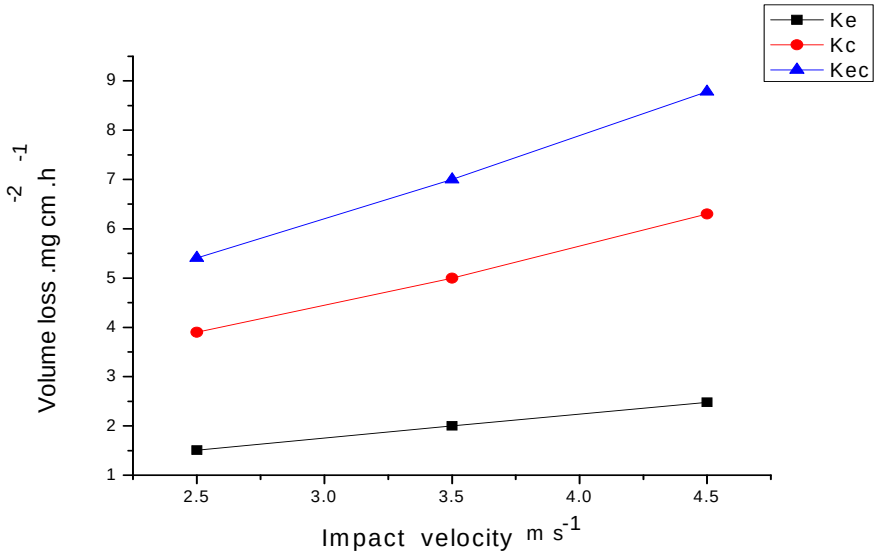

(b)

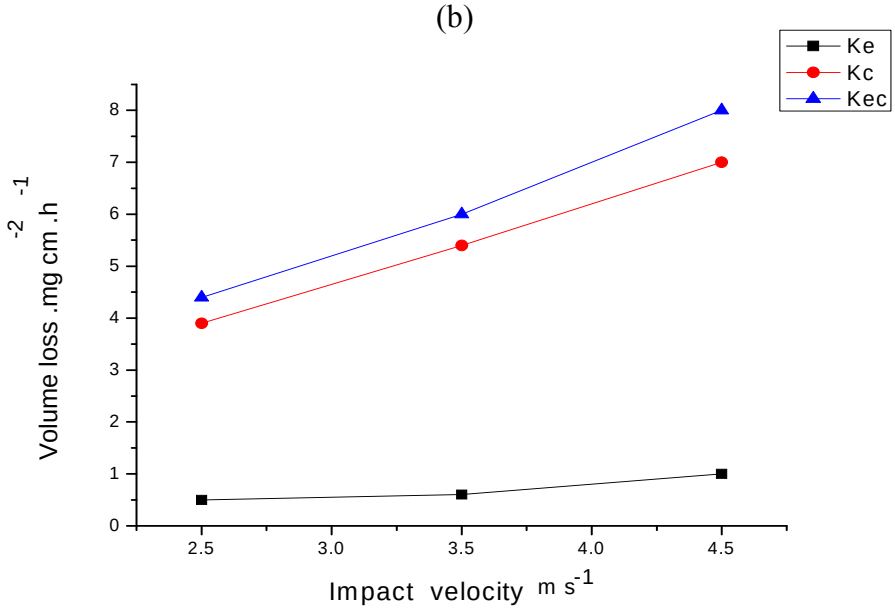

(c)

Fig.3.31: Volume loss as function of impact velocities for carbon steel in water at 400 mV and particle size 150-300µm (a) 15° (b) 45° (c) 90.

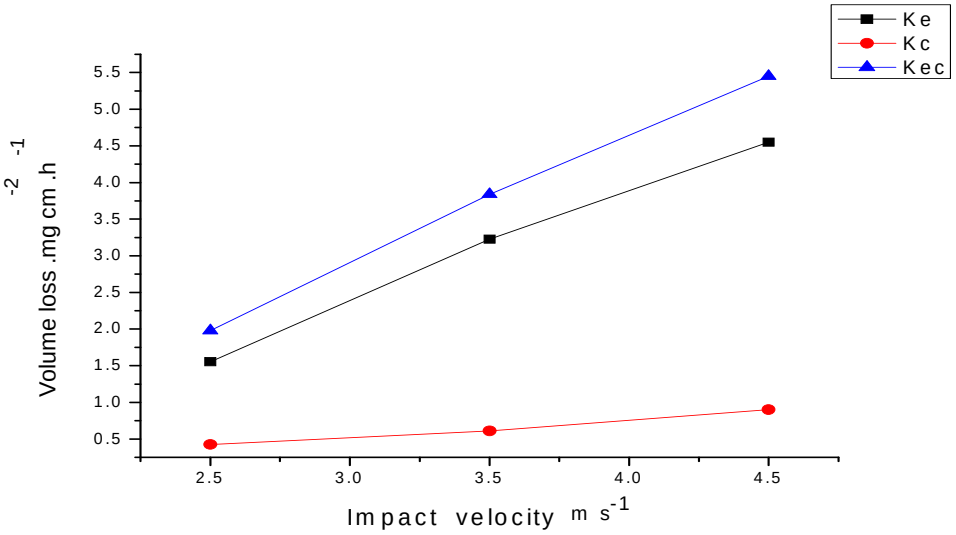

(a)

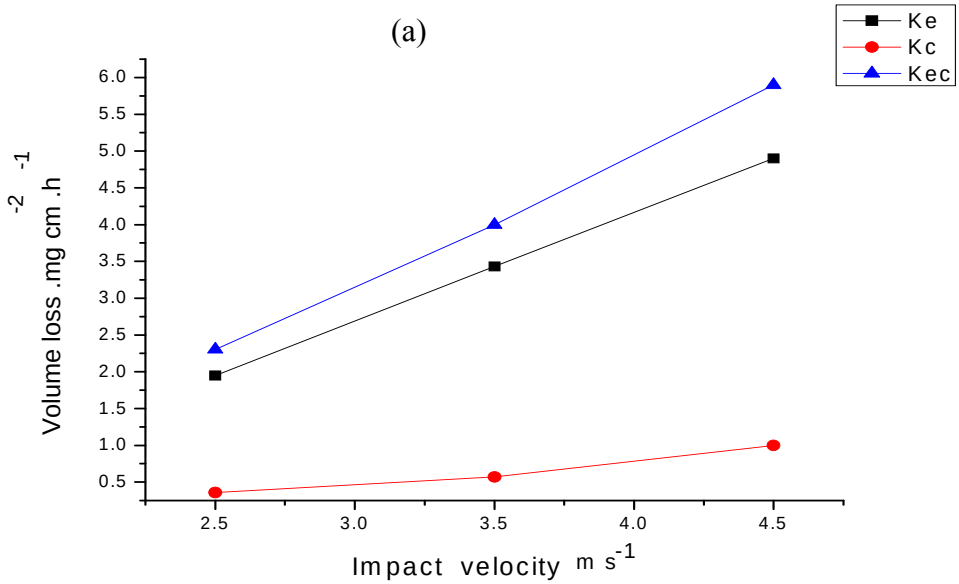

(b)

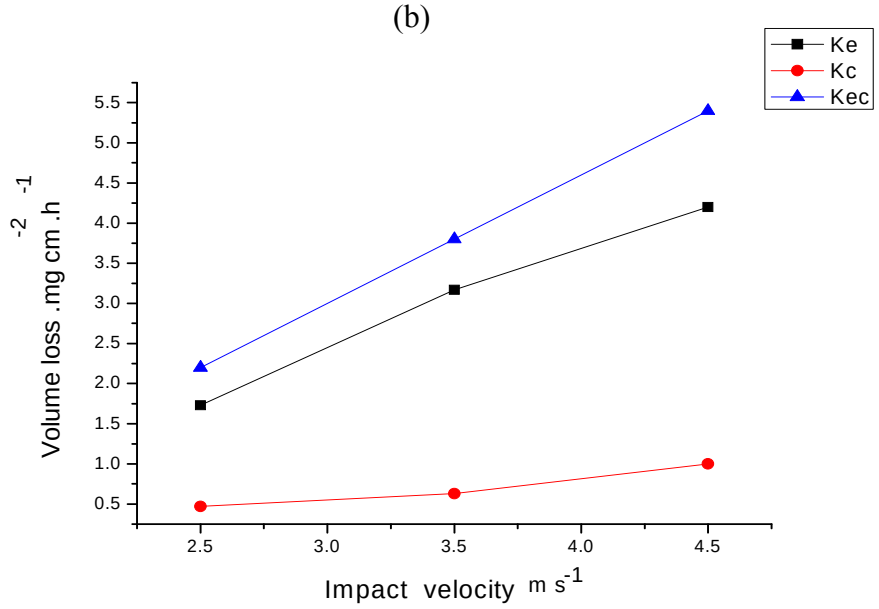

(c)

Fig.3.32: Volume loss as function of impact velocities for carbon steel in crude oil at 400 mV and particle size 150-300µm (a) 15° (b) 45° (c) 90.

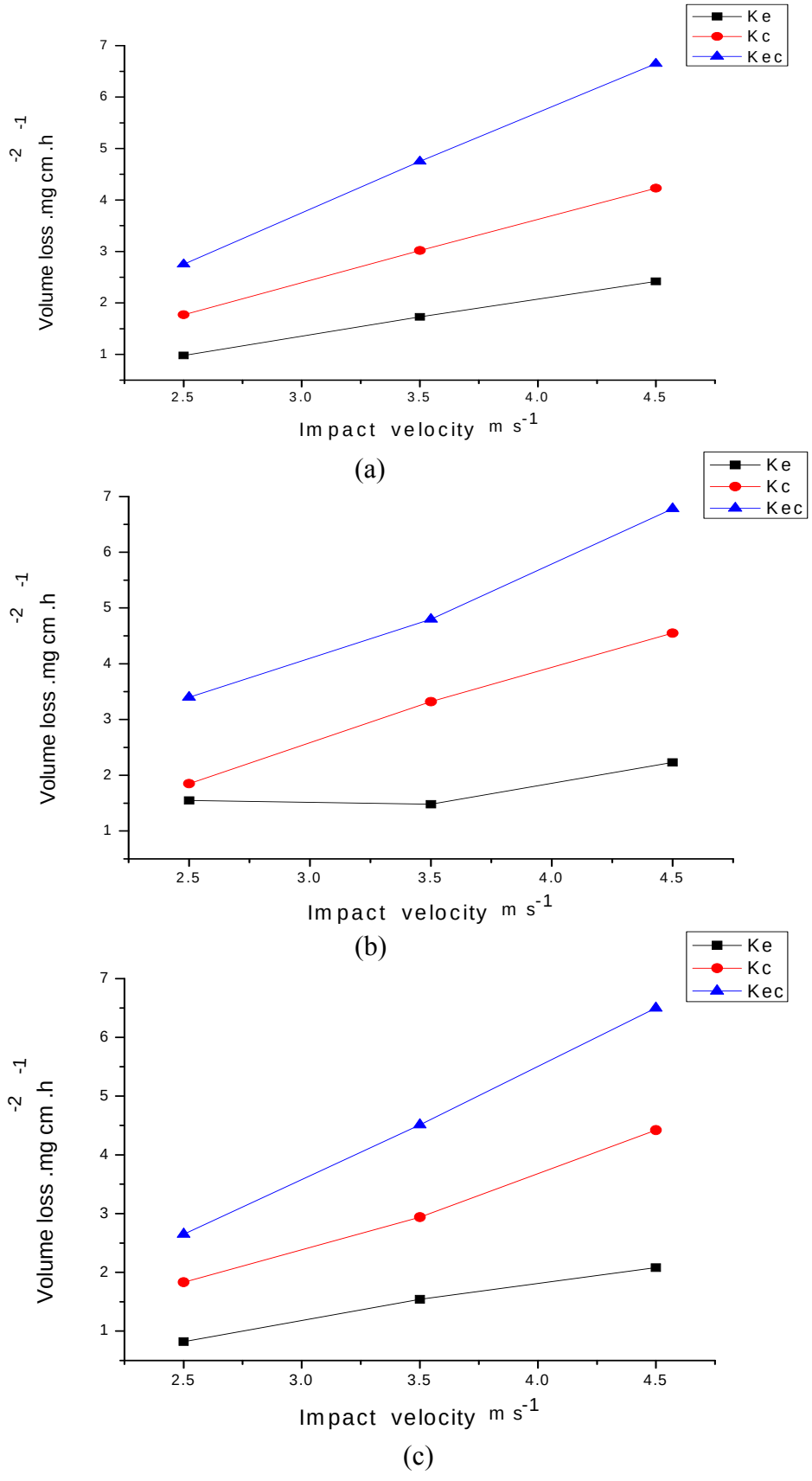

Fig.3.33: Volume loss as function of impact velocities for carbon steel in oil /20% water at 400 mV and particle size 150-300µm (a) 15° (b) 45° (c) 90.

3.3. Discussion

3.3.1. Polarization curves

In the water environment, the current densities increased with an increase in impact velocity (Figures 3.1-3.6(a), and Figures 3.22 -3.24(a)). This implies that an increase in velocity increases the corrosion rate of the carbon steel, which is consistent with the findings of Stack et al. [6, 34 and36]. This could be due to surface roughening and an increase in exposure area, leading to higher localized dissolution rates on the surface of the specimen.

On the other hand, in the crude oil environment and combined environment a similar pattern was observed, with an increase in velocity resulting in an increase in the overall current densities (Figures 3.1-6(b-c), and Figures 3.22-3.24(b-c)). However, the magnitude of such increases was not as high as in the reservoir water; probably due to the higher corrosion resistance of the oil film in the crude oil and combined environments compared to the reservoir water.

In the crude oil, it can be seen that increase in the cathode current density as oxygen has a higher solubility in crude oil than in water environment [2, 10 and 11]. This increase in cathodic current density is observed particularly in the crude oil environment (Figures 3.1-6(b-c), and Figures 3.22-3.24(b-c)). On the other hand, the anodic current density is reduced, which can be attributed to the higher resistance of current in the crude oil environment[2,10and11], and therefore passivation is considered less possible to occur. Hence, the oil film can have an important role in reducing erosion-corrosion (Kec) in crude oil and combined environments.

3.3.2. Mass loss

There is a general increase in total mass loss (kec) with an increase in potential for carbon steel in all three environments, perhaps indicating that corrosion played the main role in the degradation process (Figures 3.7-3.21, and Figures 3.25-3.33) [2,6and 36]. The total erosion–corrosion mass losses are much lower for carbon steel in the crude oil and combined environments compared with the reservoir water, which could be due to a decrease in the value of current density (Figures 3.7-3.21, and Figures 3.25-3.33). This is in spite of the fact that the polarization data indicate a general increase in current density with an increase in potential in the active regime (Figures 3.7-3.21, and Figures 3.25-3.33).

It is clear that there are general increase in the total mass loss with increase of particle sizes from 150-300µm to 600-710µm, however, the corrosion contribution value tended to increase with decrease in particle sizes from 600-710µm to150-300µm (Figures 3.7-3.21, and Figures 3.25-3.33).

3.3.3. Erosion–corrosion maps

3.3.3.1. Erosion–corrosion mechanism maps

The mechanism maps of carbon steel have been constructed to show transition boundary regimes between erosion-corrosion, corrosion-erosion, corrosion and erosion by terms of ratio Ke/ Kc [20, 34 and 36].

Ke/Kc < 0.1	Corrosion -dominated	3.4
1>Ke/Kc ≥0.1	Corrosion -erosion	3.5
10>Ke/Kc ≥1	Erosion- corrosion	3.6
Ke/Kc ≥10	Erosion-dominated	3.7

The corrosion process can be dissolution, passivation, transpassivation, or pitting [20,34and 36]. The erosion–corrosion mechanism map results (Figures 3.34-38, and Figures 3.39- 3.41), based on tables 3.25-3.39, and tables 3.40-3.48) at three impact velocities, six impact angles and particle sizes 600-710μm show that at an applied potentials, i.e. -400 and −200 mV. The dissolution-erosion regime dominated in reservoir water and erosion-dissolution regime for both reservoir water and the combined environments and except in crude oil the erosion regime dominates. However, the degree of corrosion appears to be higher for the carbon steel in reservoir water compared to in crude oil and mixed environments, which is consistent with the mass loss results.

The maps indicate, not surprisingly, that the amount of passivation is at a maximum in reservoir water (Figures 3.36-3.38(a), and Figures 3.39-3.41 (a)), where passivation-erosion dominates the majority of the area of the map with an increase in potentials. In the crude oil environment containing large particles sized 600-710μm (Figures 3.34-38(b)) erosion dominates. However, erosion-passivation comes to dominate all areas of the map in crude oil containing small particles sized 150-300μm (Figures 3.39-3.41(b)).

In the combined environment containing particles sized 600-710μm erosion-passivation dominates in anodic conditions (at 0, 200 and 400mV). However, in the combined environment containing small particles sized 150-300μm (Figs.3.40-41(c)) the passivation- erosion regime dominates in anodic conditions, which may be due to the lower ability of particles to remove the passive film.

It is interesting that increases in impact velocity and potentials increase the corrosion affected regimes (Figures 3.34-38(a) and (c)). The possible reason is that increase the impact velocity increases the oxygen in the environment then leading to increase the rate of oxidation [34 and 36].

3.3.3.2. Erosion–corrosion wastage maps

Erosion-corrosion wastage maps (Figs.3.42-49) have been generated to demonstrate the transition between wastage regimes, where low, medium and high regimes are less or equal to 6 mg cm^{-2} h^{-1}, between 6 and 50 mg cm^{-2} h^{-1}, and greater or equal to 50 mg cm^{-2} h^{-1}. Tables 3.1-3.24 show the results of the calculations for Kec for difference environments and impact velocities with various impact angles at various applied potentials.It is clear that the low wastage regime predominates at much lower potentials (cathodic condition) in the crude oil, combined environments (Figures 3.42-3.43 (b-c) comparing with that observed for the reservoir water. This could be due to the effect of corrosion contribution being small compared to at high potential (in anodic condition).

For carbon steel in the reservoir water (Figures 3.44, 3.46(a) and Figures 3.48, 3.49(a)) the medium wastage regime dominates at higher applied potentials, i.e. more than 0 mV. It is interesting that only at the high impact velocity and potential, transitions to medium wastage dominate for the carbon steel in all three environments with particle sizes 600-710μm (Figures 3.42-3.46). Clearly, the passive film has some effect in conditions of reducing the erosion-corrosion at high impact angles and at low impact velocities in water (Figures 3.47-3.49(a)). It is interesting that the low wastage regime dominate for the carbon steel in crude oil environment with particle sizes 150-300μm (Figures 3.47-3.49(b)).

3.3.3.3. Erosion–corrosion additive-synergism maps

Additive-synergism maps of erosion-corrosion have been constructed according to the following regimes [18,20and 34]:

$\Delta Ke/\Delta Kc < 0.1$	Additive	3.8
$1 > \Delta Ke/\Delta Kc \geq 0.1$	Additive-synergistic	3.9
$\Delta Ke/\Delta Kc > 1$	Synergistic	3.10

It can be seen in tables 3.49-3.72 that the values of $\Delta Ke/\Delta Kc$ ratio for the carbon steel in the various environments show the relationship between the boundaries as a function of impact angles and impact velocities at five applied potentials, namely -400, -200, 0, 200, and 400mV.

Erosion-corrosion additive-synergism maps can be defined depending on whether the erosion-corrosion is additive, synergistic or antagonistic. Additive behaviour is defined as a situation where the enhancement of corrosion due to erosion (Δkc) [2, 6 and 36]. Where corrosion may enhance the erosion ΔKe, this interaction is defined as synergistic behaviour [2 and 38]. On the other hand, where it inhibits erosion, i.e. where the film layer reduces erosion, then the reverse occurs and the mechanism is defined as antagonistic ($-\Delta Ke$) ([20,34 and 36]. Both synergistic and antagonistic behaviors are characteristics of erosion-corrosion processes [2, 38].

If the passive film forms on the surface in the exposure conditions and is effective in reducing erosion, i.e. $\Delta Ke/\Delta Kc > -1$, then synergistic should be replaced by antagonistic behavior [2,20and38]. In the reservoir water containing large particles sized 600-710µm (Fig. 3.52 (a)) indicates that the additive regime, where erosion enhances corrosion (corrosion due to erosion) - i.e. through removal and reformation of the passive film.

On other hand, in the reservoir water environment the antagonistic regimes occupy an area at a lower impact velocity at 30°and between 45°-75° impact angles implying that synergistic is replaced by antagonistic behavior (Fig. 3.52 (a)). In the crude oil containing small particles sized150-300µm the synergistic regime dominates Fig. 3.55(b). This is attributed to increase in the value of mass loss due to erosion. In the combined environment containing a small particle sized 150-300µm at an applied

potential of -400mV, the additive-synergistic regime dominates at high velocities (Fig. 3.55 (c)).

In the crude oil and oil /20%water environments containing large particles sized 600-710µm, the synergistic regime dominated where the film is removed by the effect of particle on the surface (Figures 3.50 (b-c)).The regimes of antagonism and synergism sit in different forms of conditions in the oil and oil /20%water slurries (Figures 3.50 (b-c)), possibly indicating different mechanisms of protecting the surfaces in such cases. At higher potentials(0,200 and 400mV), different regimes transitions are observed, with the level of additive behaviour being reduced in water containing large particles sized 600-710µm (Fig. 3.52 (a)) compared with at -200mV(Fig. 3.51 (a)).

On the other hand, in water containing small particles sized 150-300µm the level of additive behaviour is increased (Figures 3.56-57(a)) compared with large particles sized 600-710µm (Fig.3.50-3.52 (a)),which suggests that the value of corrosion contribution of carbon steel changes as particle size is decreased from 600-710µm to 150-300µm.

The regimes of antagonistic behaviour reduce and disappear on the maps in the crude oil and combined environments containing small particles sized 150-300µm (Figures 3.55-57(b-c)). The passivation chemistry may have a significant effect on the ability of the surface to provide protection against erosion-corrosion in such conditions. Also, the time interval between large particles size 600-710µm is greater than by a small particles 150-300µm.Hence, the passive film has longer time to repair itself after erosion for the large particle.

3.4. Summary

(i) The mass loss of carbon steel in the three environments containing particles sized 600-710µm and150-300µm have been investigated at constant applied potential.

(ii) The results indicate that an increase in particle size, applied potential, and impact velocity, and a decrease in impact angle from 90° to 30°, can have a significant effect on the mass removal of carbon steel in the three environments containing large particles sized 600-710µm.

(iii) The highest value of erosion contribution (ke) was at an impact angle of 45° for carbon steel in the three environments containing small particles sized 150-300µm.

(iv) Erosion-corrosion maps have been constructed showing the change in erosion-corrosion mechanisms, the rank of wastage, and the extent of additive-synergistic/antagonistic behaviour, based on the results at constant applied potential. .

(v) For carbon steel in the crude oil environment containing small particles sized 150-300µm showed that the erosion-passive regimes dominated the whole maps, while the erosion regime dominated in the crude oil environment containing large particles sized 600-710µm.

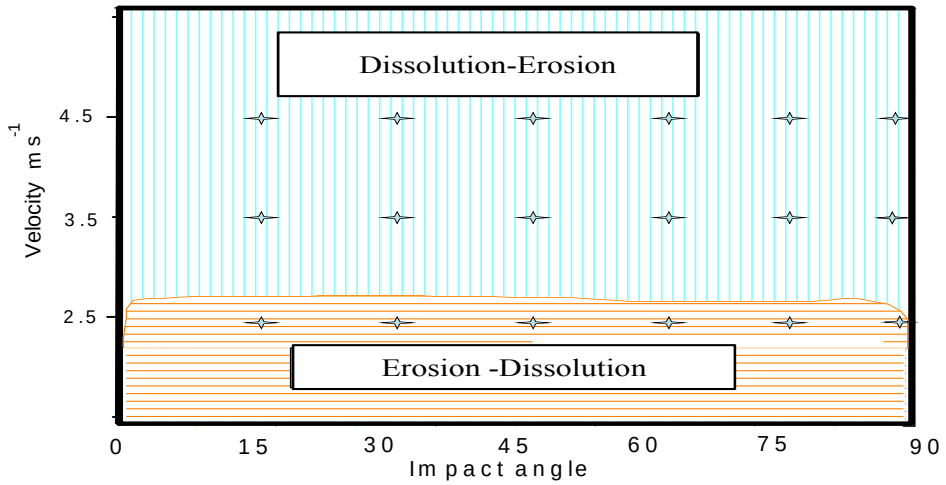

(a)

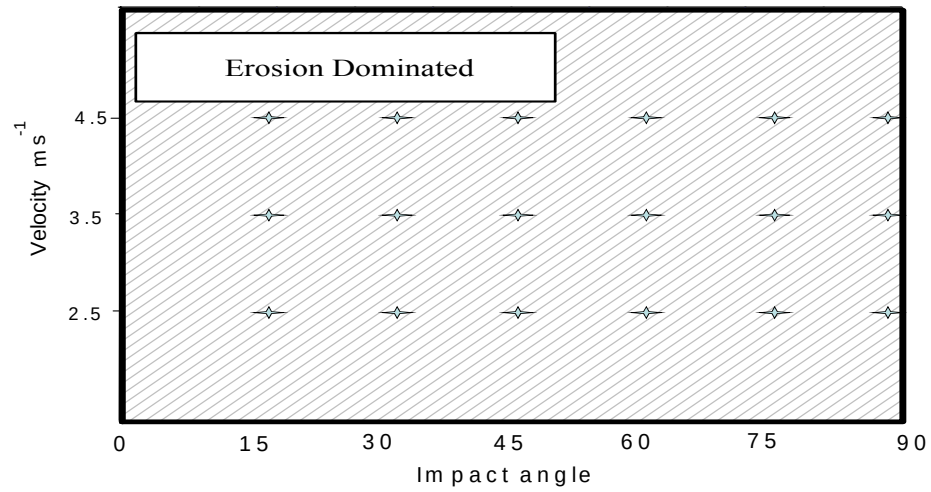

(b)

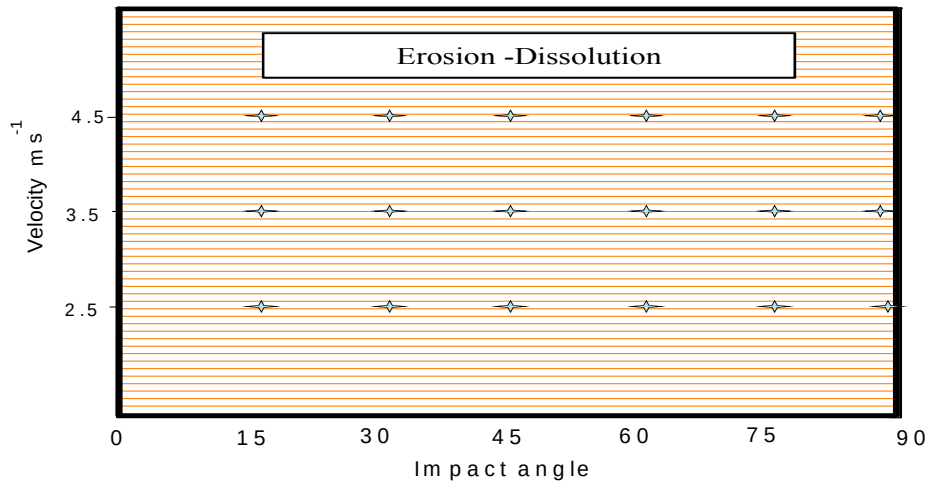

(c)

Fig.3.34: Erosion-corrosion mechanism maps for carbon steel at -400 mV and particle size 600-710µm in (a) water (b) crude oil (c) oil /20% water.

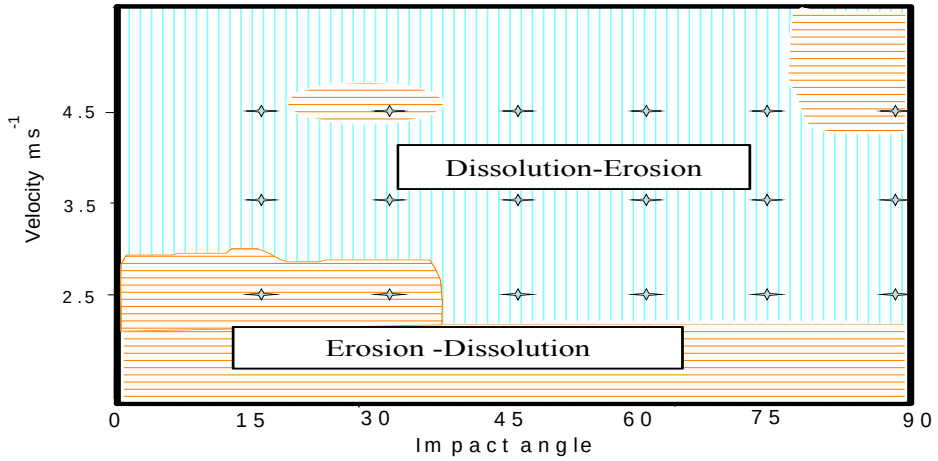

(a)

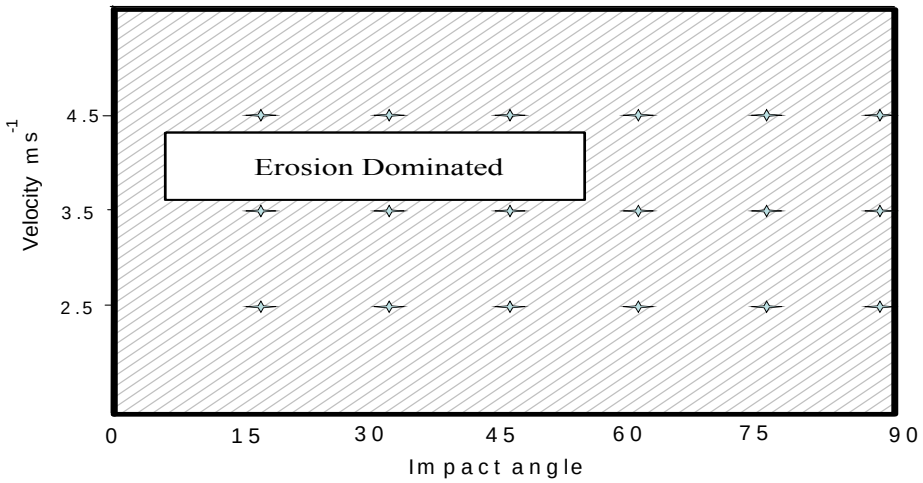

(c)

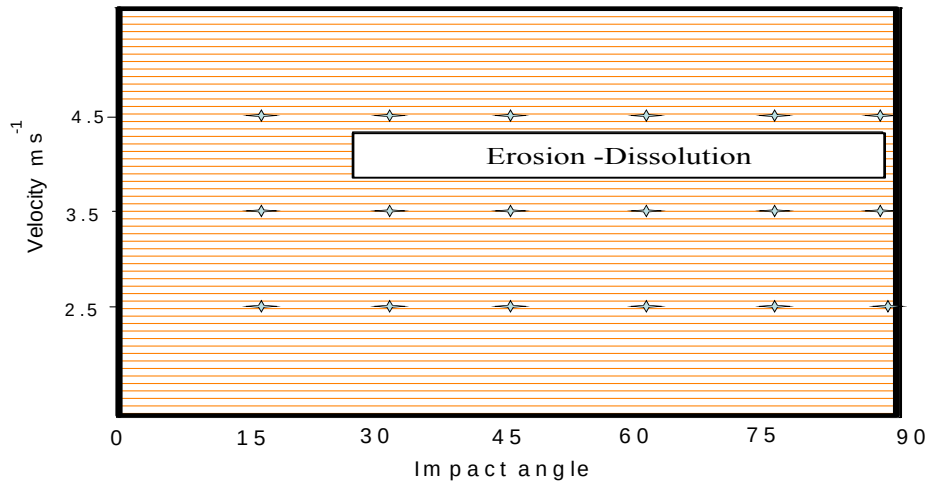

(c)

Fig.3.35: Erosion-corrosion mechanism maps for carbon steel at -200 mV and particle size 600-710µm in (a) water (b) crude oil (c) oil /20% water.

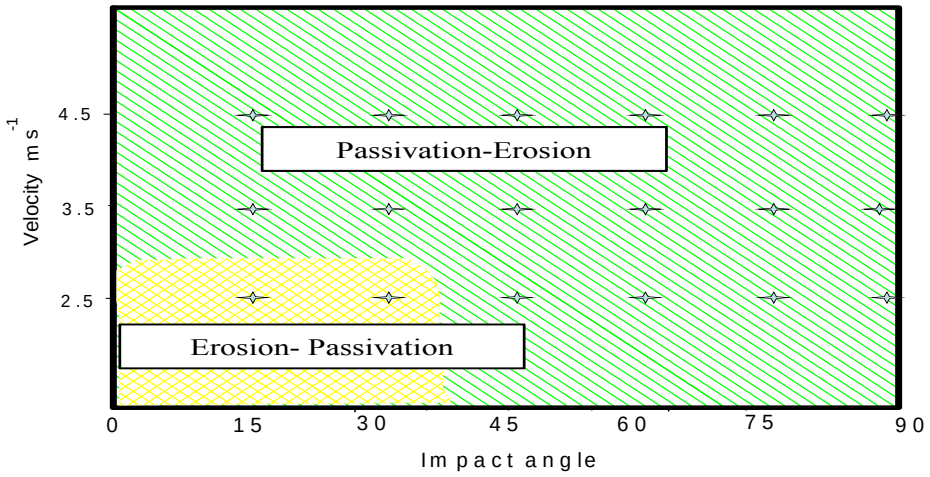

(a)

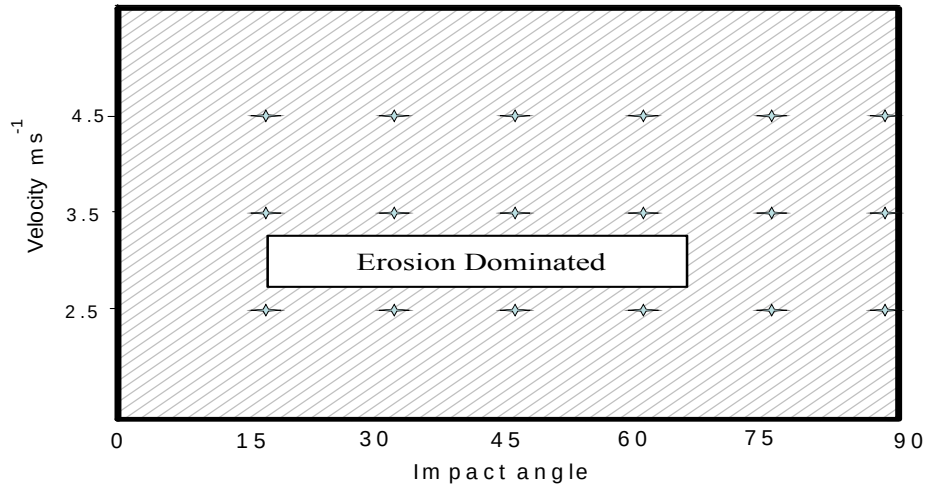

(b)

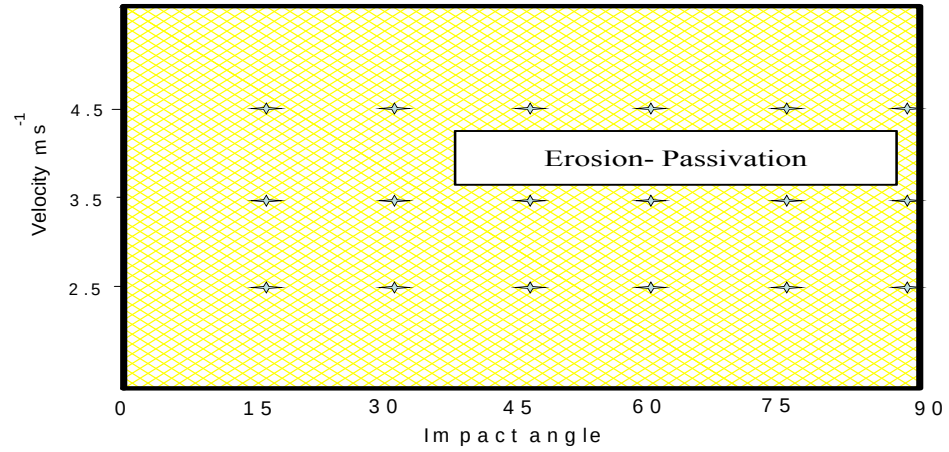

(c)

Fig.3.36: Erosion-corrosion mechanism maps for carbon steel at 0 mV and particle size 600-710µm in (a) water (b) crude oil (c) oil /20% water.

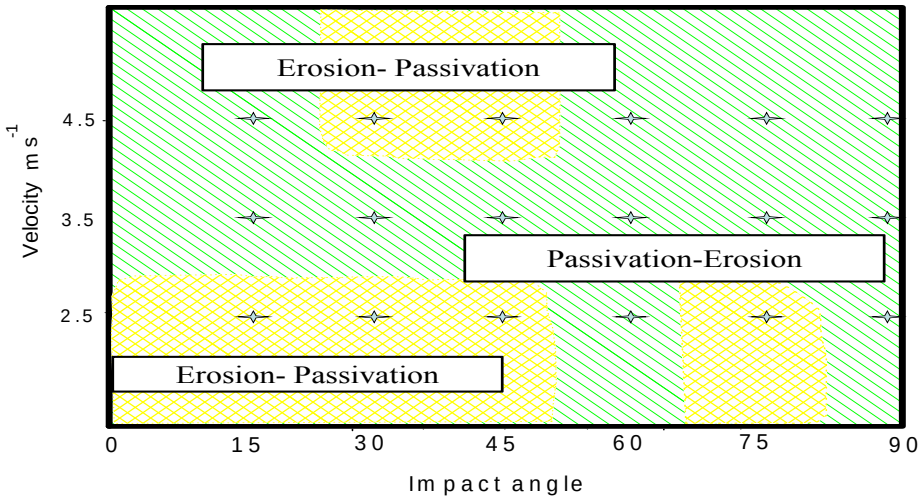

(a)

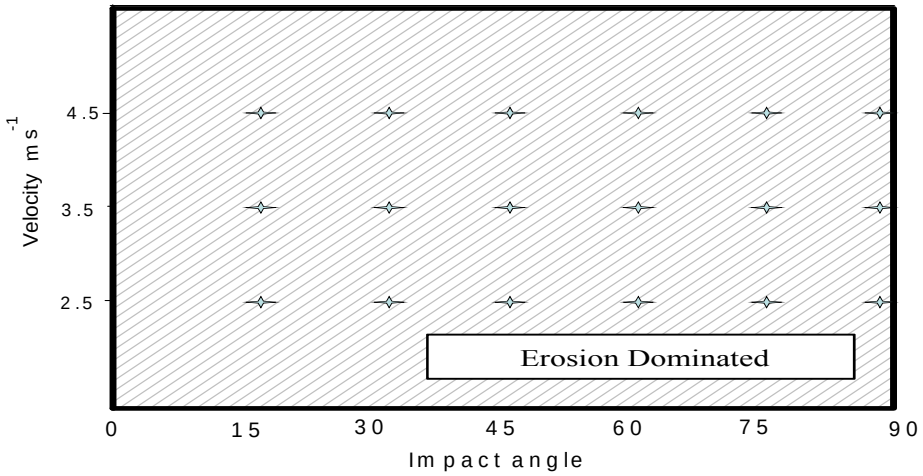

(b)

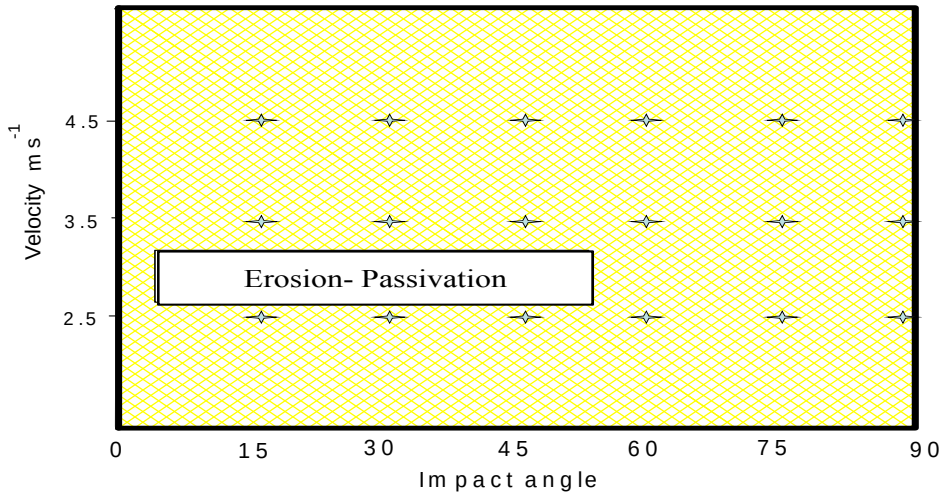

(c)

Fig.3.37: Erosion-corrosion mechanism maps for carbon steel at 200 mV and particle size 600-710µm in (a) water (b) crude oil (c) oil /20% water.

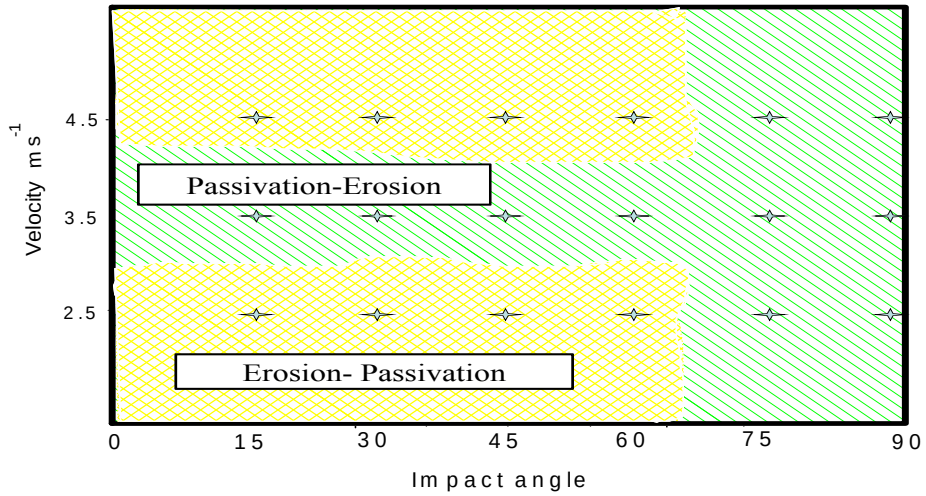

(a)

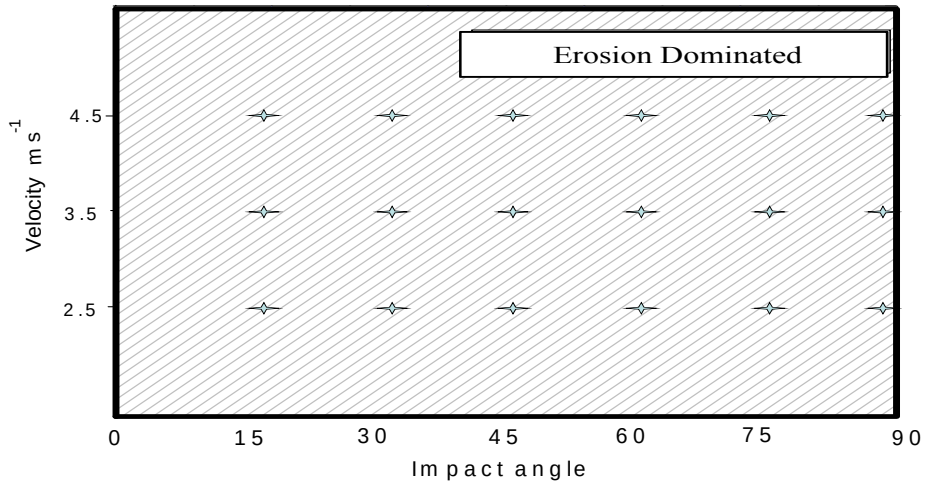

(b)

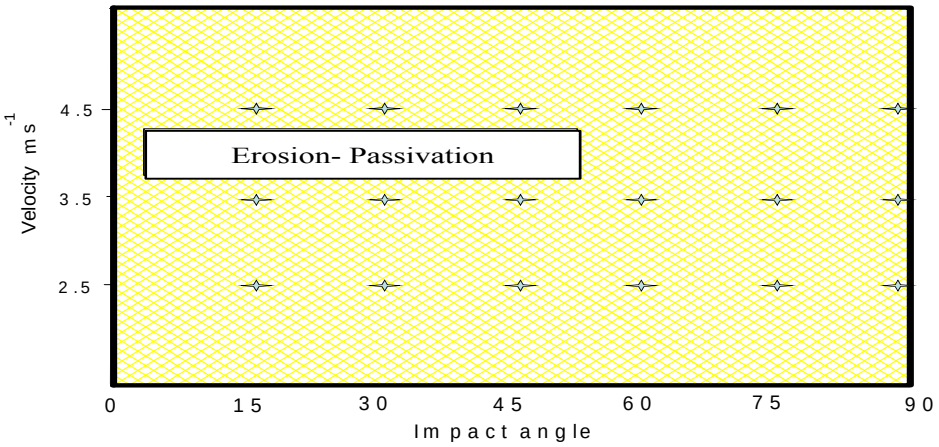

(c)

Fig.3.38: Erosion-corrosion mechanism maps for carbon steel at 400 mV and particle size 600-710µm in (a) water (b) crude oil (c) oil /20% water.

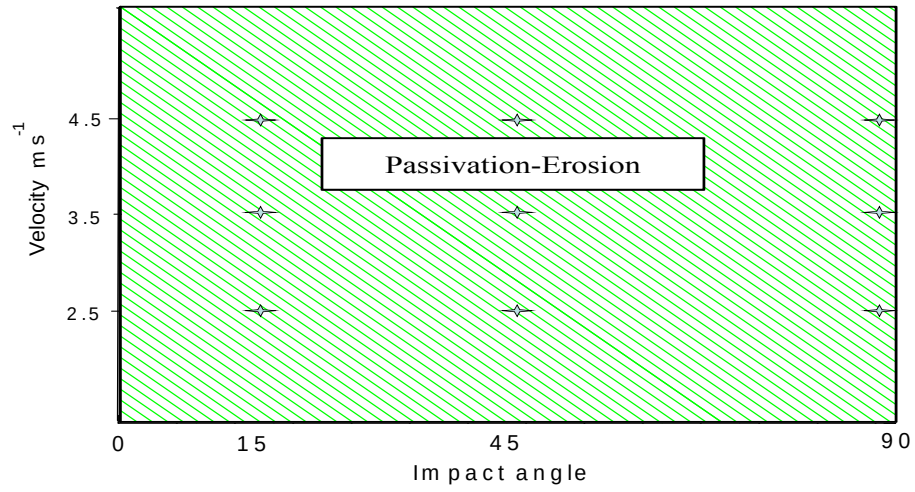

(a)

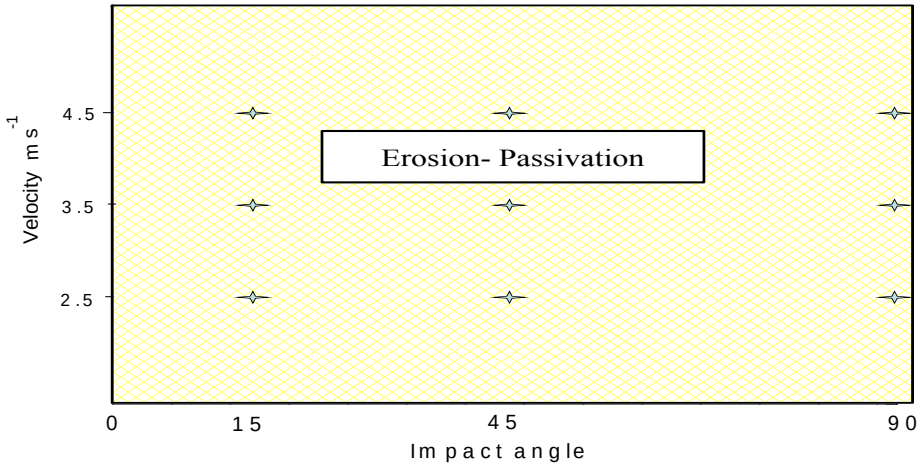

(b)

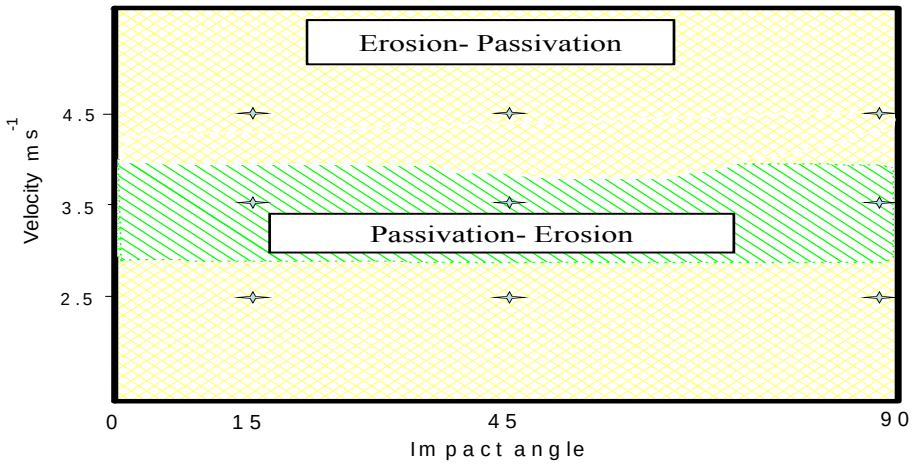

(c)

Fig.3.39: Erosion-corrosion mechanism maps for carbon steel at -400 mV and particle size 150-300µm in (a) water (b) crude oil (c) oil /20% water.

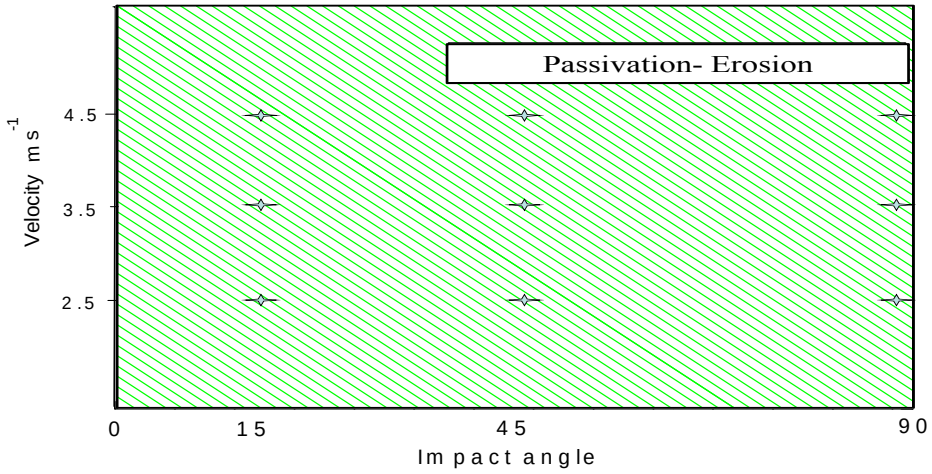

(a)

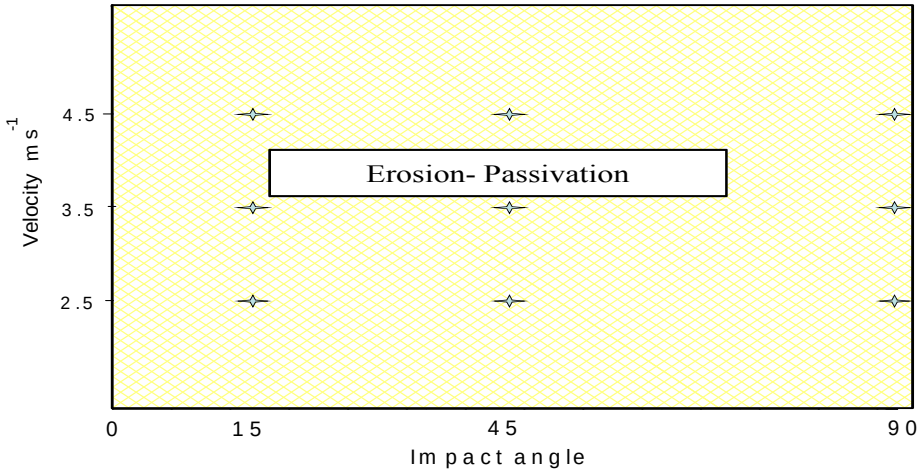

(b)

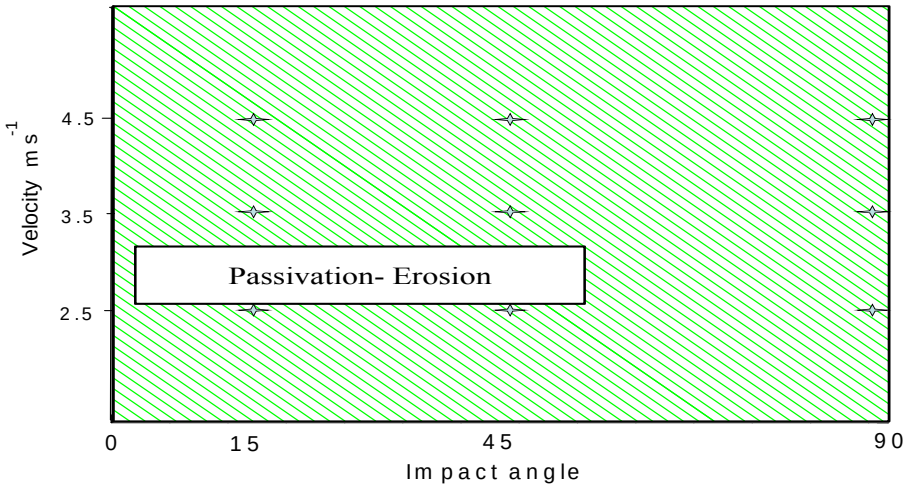

(c)

Fig.3.40: Erosion-corrosion mechanism maps for carbon steel at 0 mV and particle size 150-300μm in (a) water (b) crude oil (c) oil /20% water.

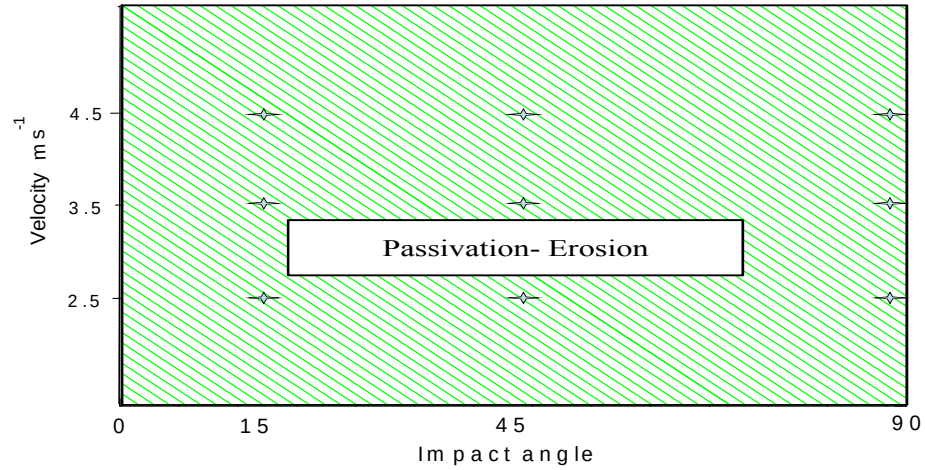

(a)

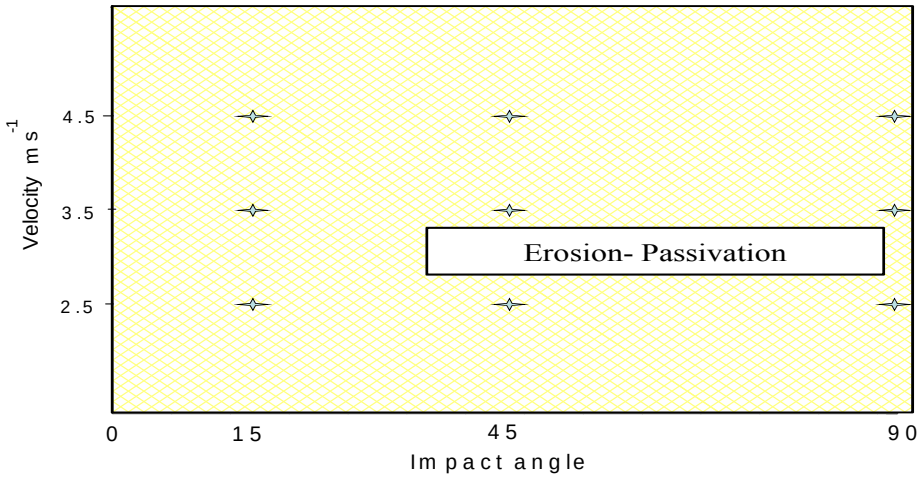

(b)

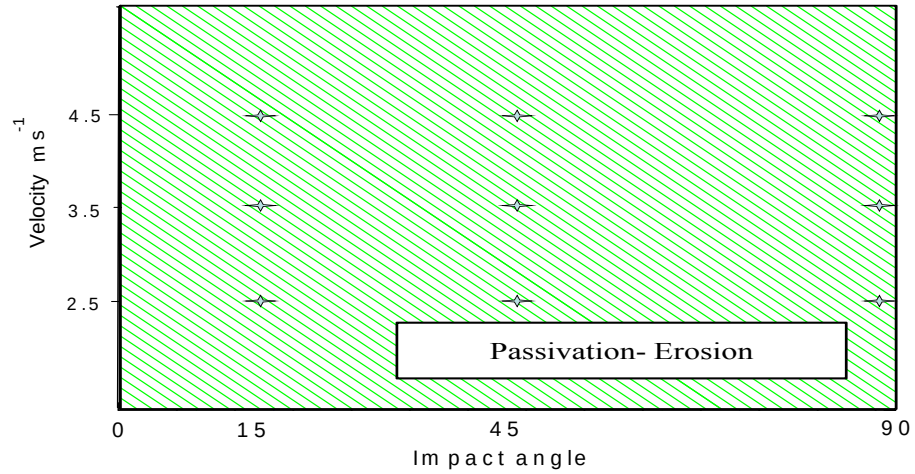

(c)

Fig.3.41: Erosion-corrosion mechanism maps for carbon steel at 400 mV and particle size 150-300μm in (a) water (b) crude oil (c) oil /20% water.

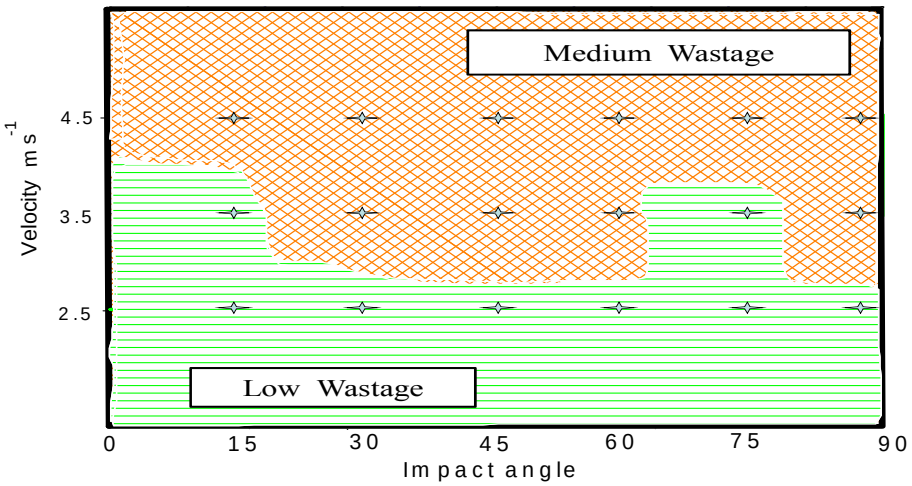

(a)

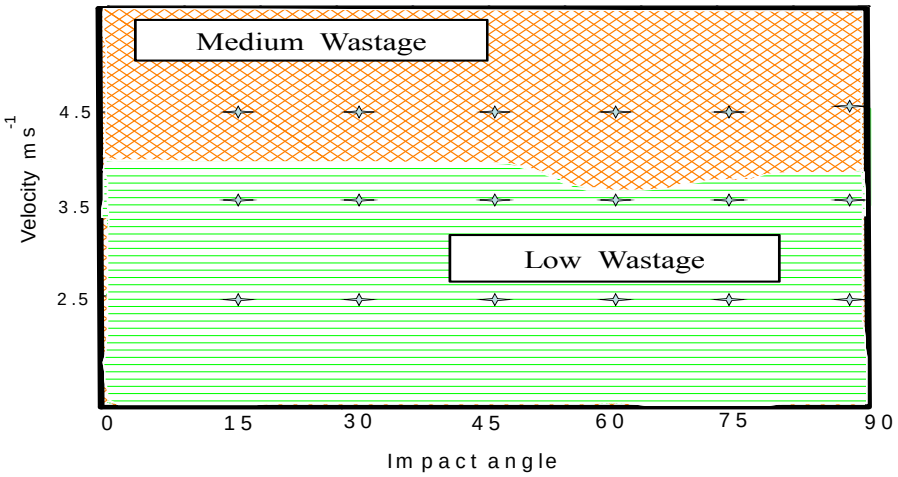

(b)

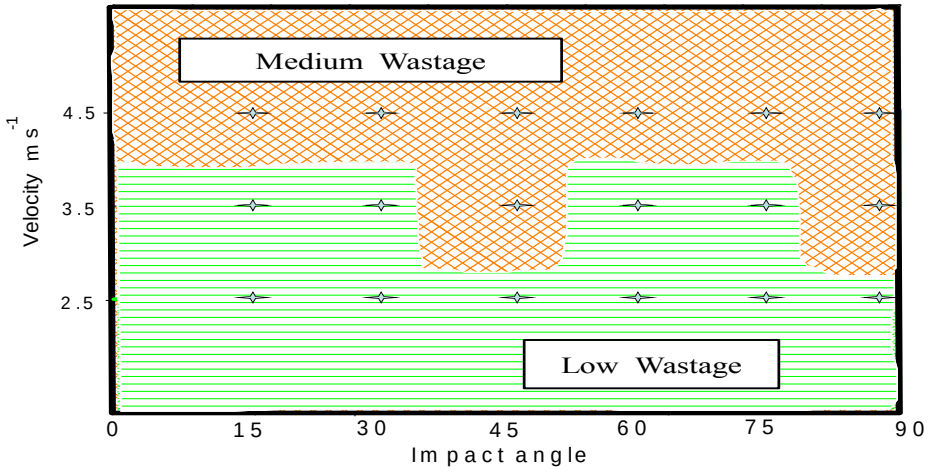

(c)

Fig.3.42: Erosion-corrosion wastage maps for carbon steel at -400 mV and particle size 600-710µm in (a) water (b) crude oil (c) oil /20% water.

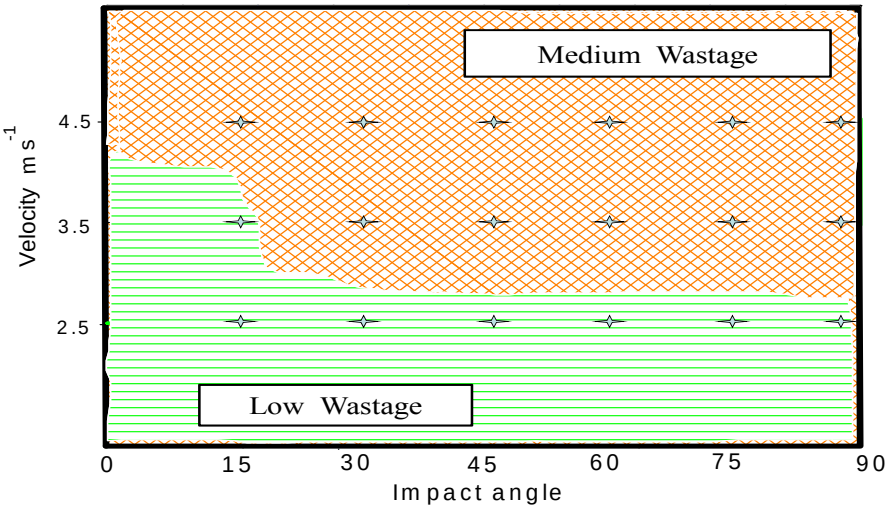

(a)

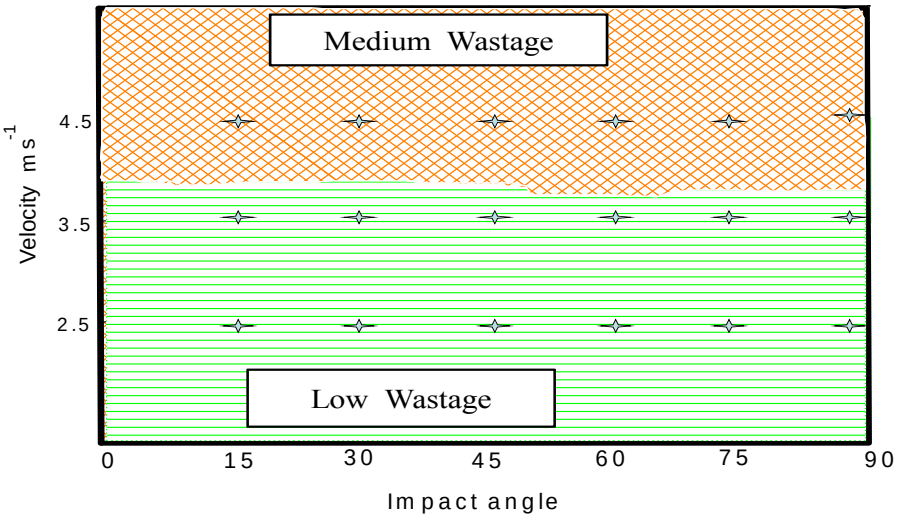

(b)

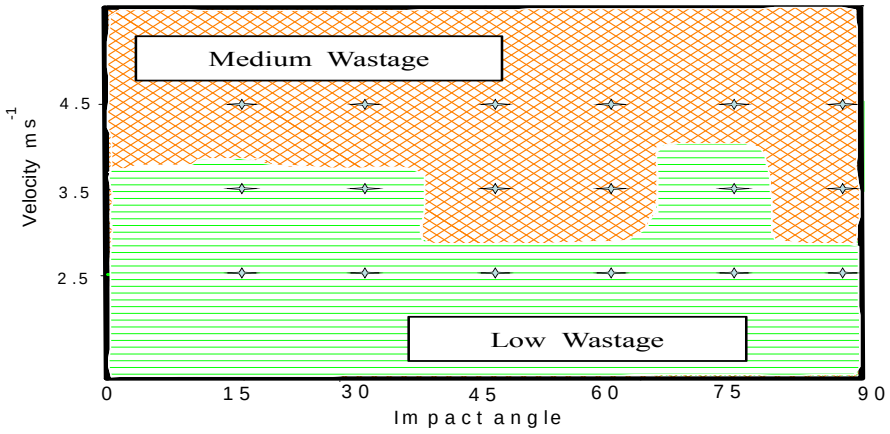

(c)

Fig.3.43: Erosion-corrosion wastage maps for carbon steel at -200 mV and particle size 600-710µm in (a) water (b) crude oil (c) oil /20% water.

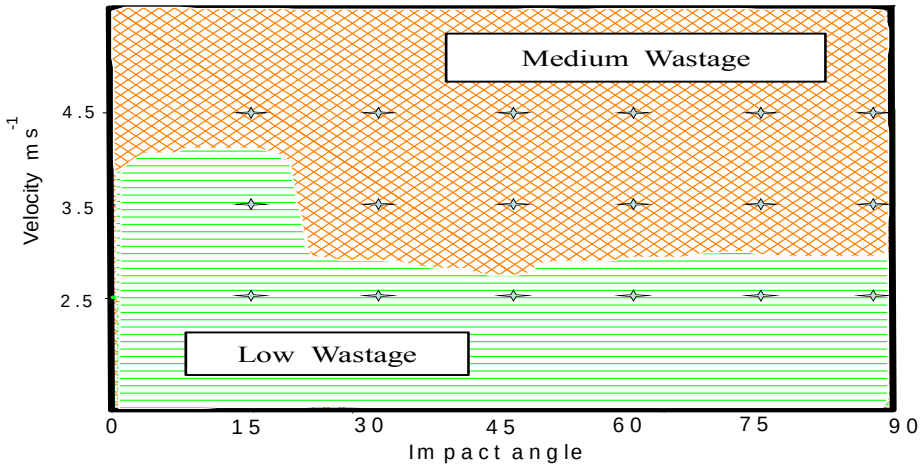

(a)

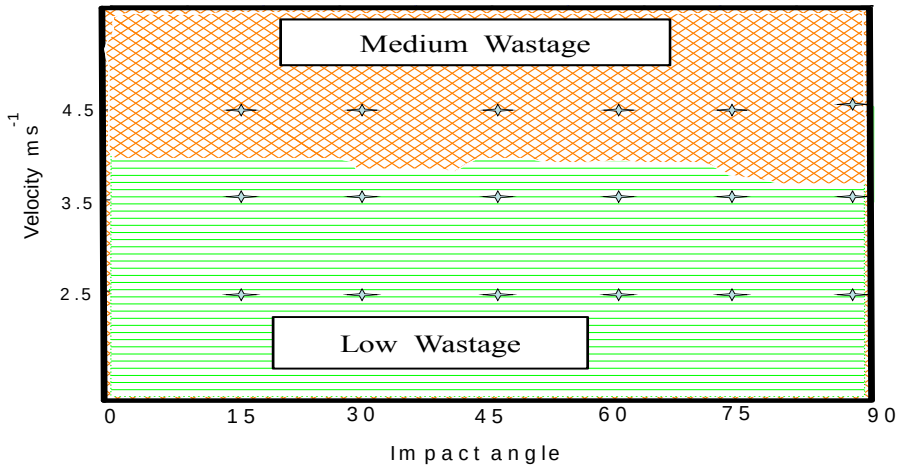

(b)

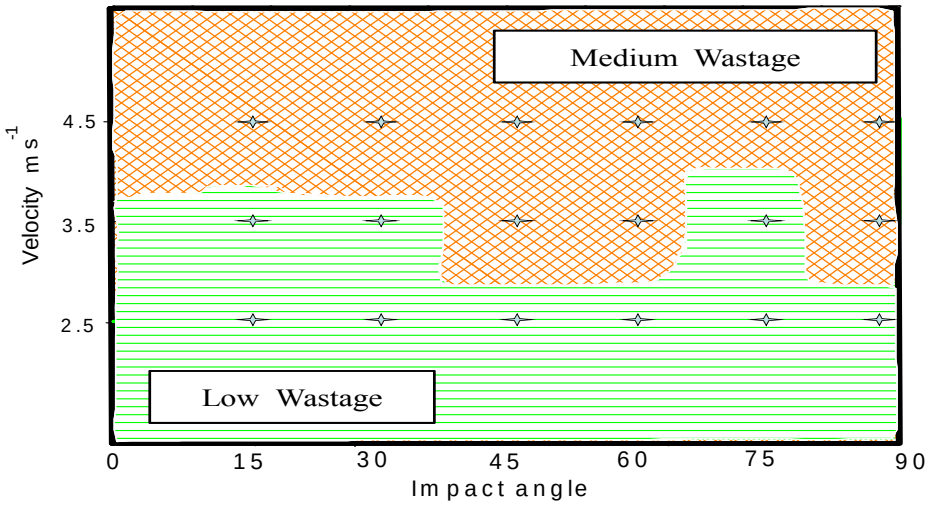

(c)

Fig.3.44: Erosion-corrosion wastage maps for carbon steel at 0 mV and particle size 600-710µm in (a) water (b) crude oil (c) oil /20% water.

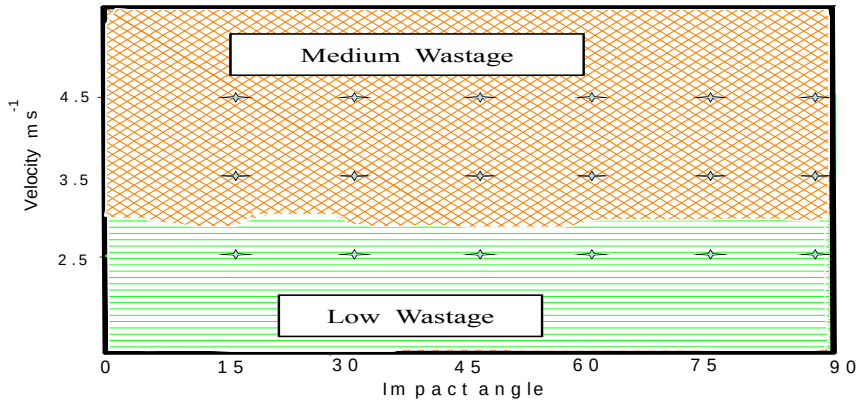

(a)

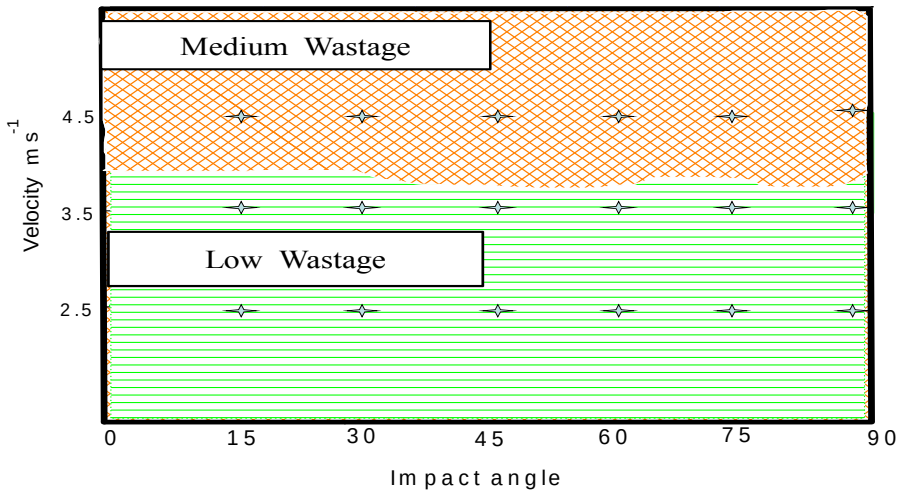

(b)

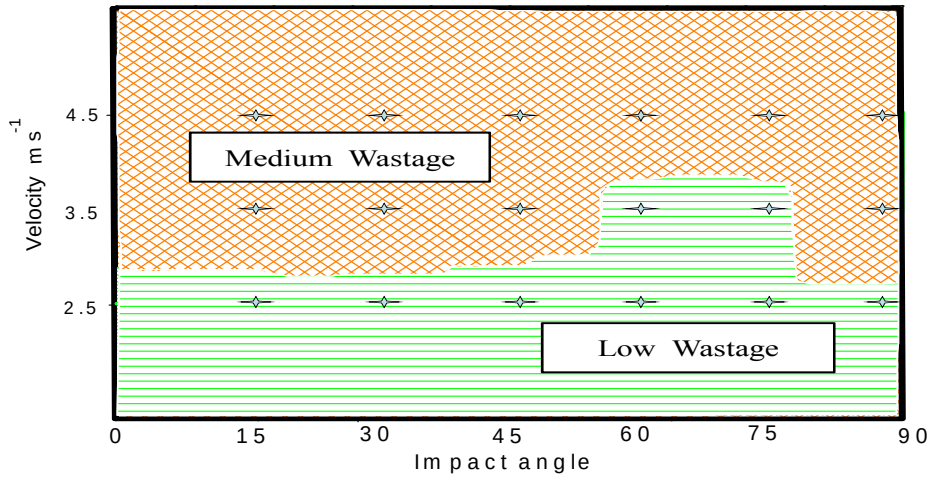

(c)

Fig.3.45: Erosion-corrosion wastage maps for carbon steel at 200 mV and particle size 600-710µm in (a) water (b) crude oil (c) oil /20% water.

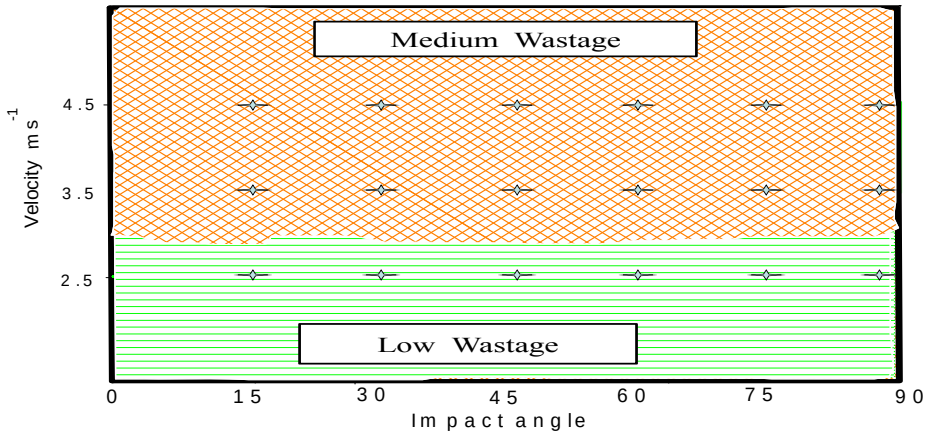

(a)

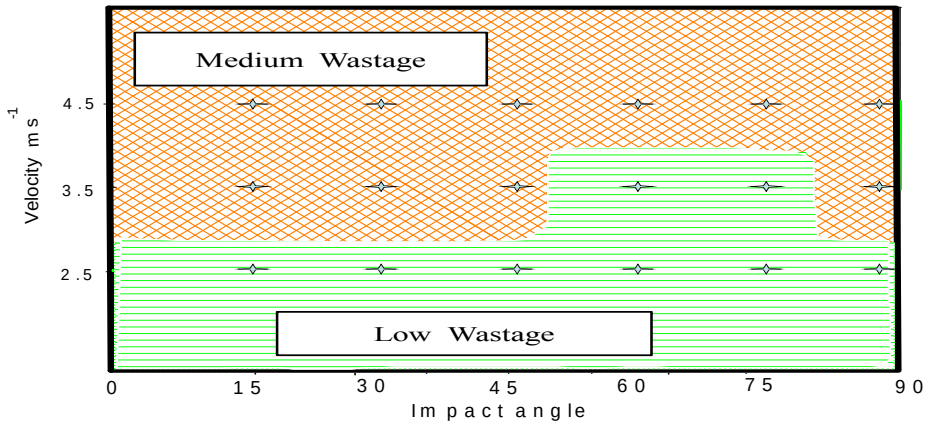

(b)

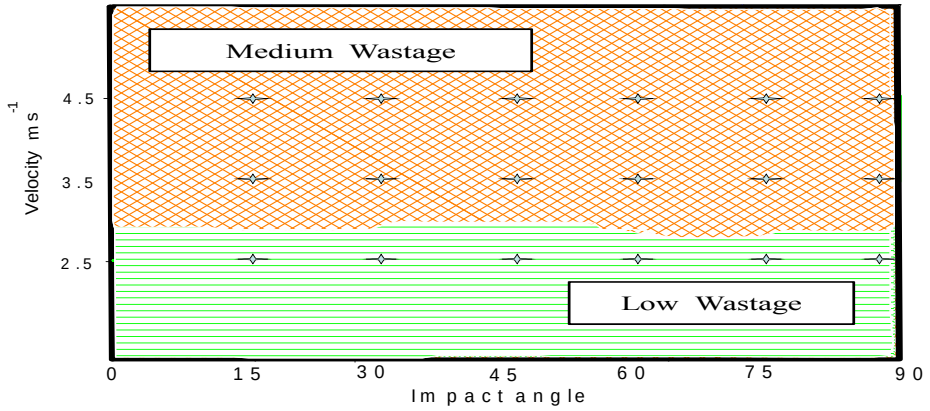

(c)

Fig. 3.46: Erosion-corrosion wastage maps for carbon steel at 400 mV and particle size 600-710µm in (a) water (b) crude oil (c) oil /20% water.

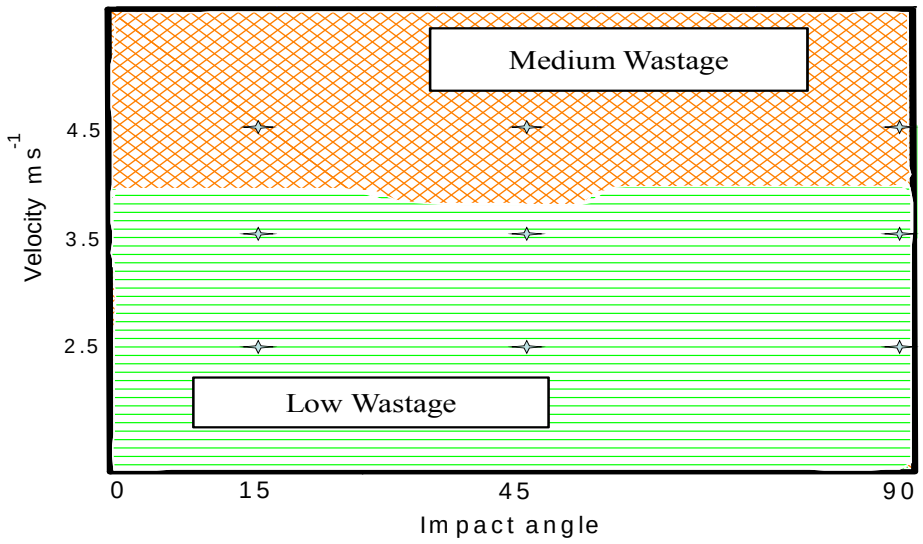

(a)

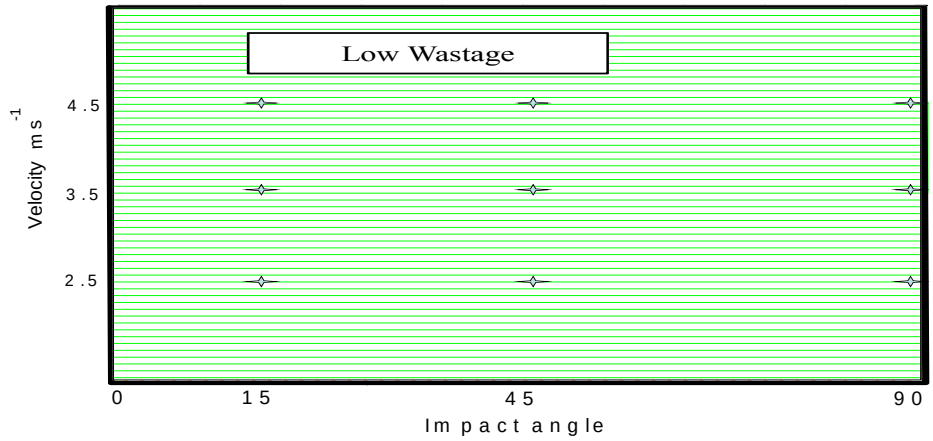

(b)

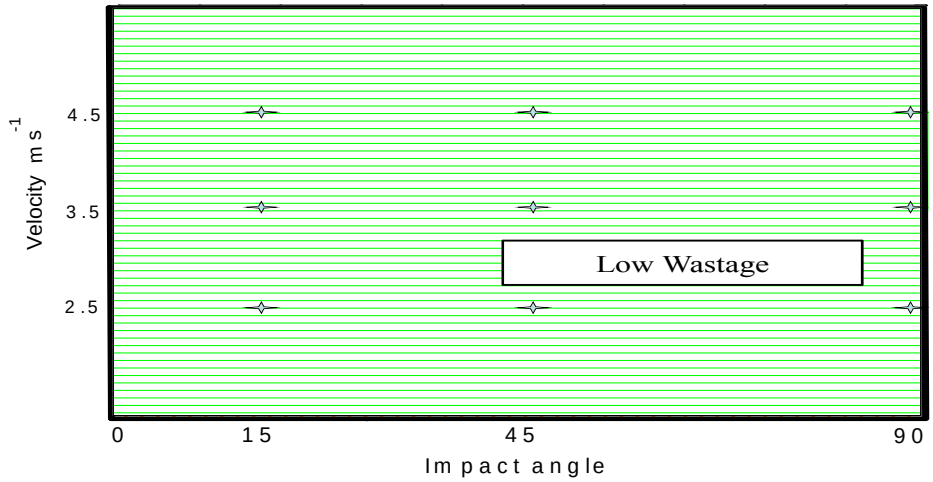

(c)

Fig.3.47: Erosion-corrosion wastage maps for carbon steel at -400 mV and particle size 150-300µm in (a) water (b) crude oil (c) oil /20% water.

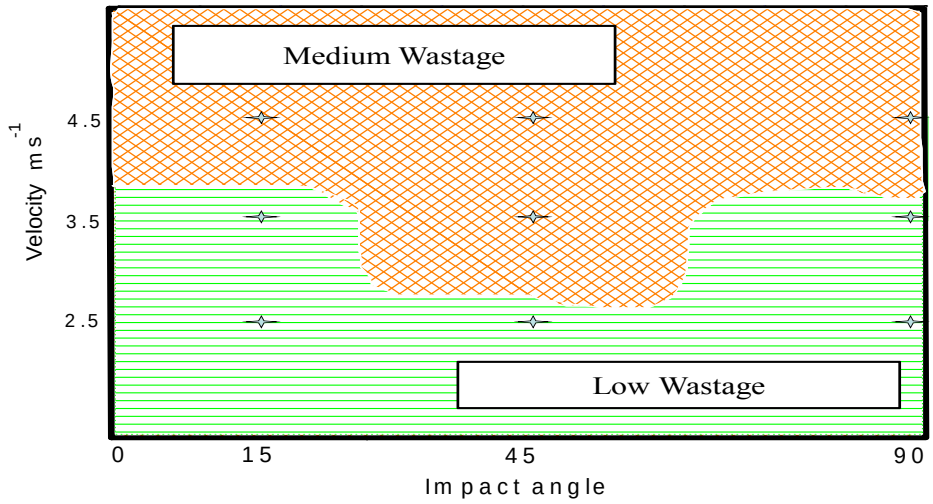

(a)

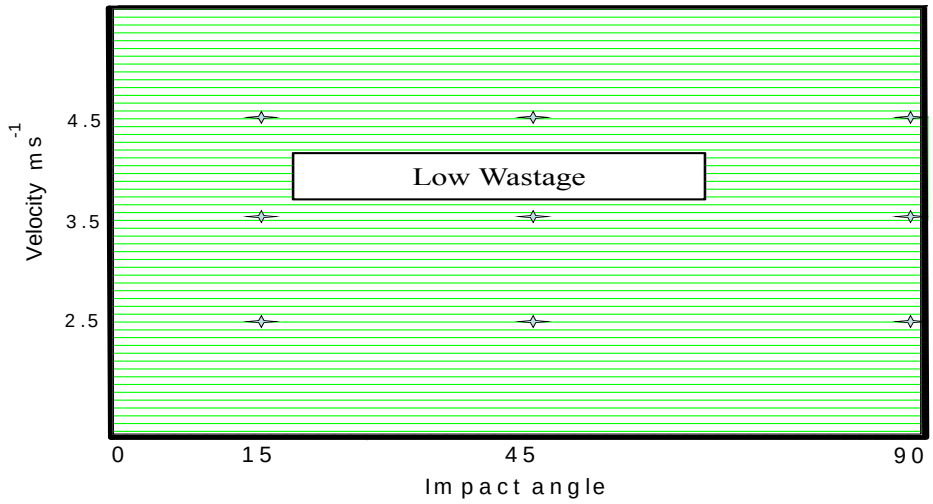

(b)

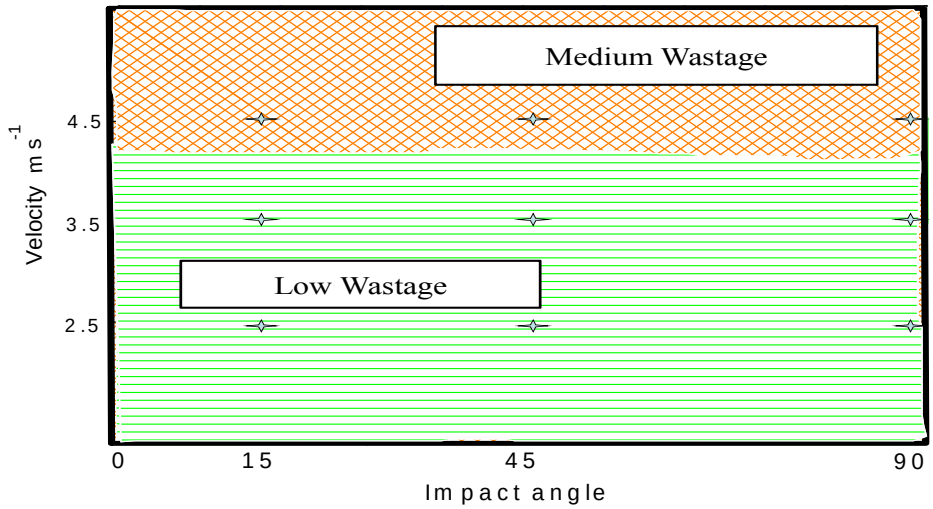

(c)

Fig.3.48: Erosion-corrosion wastage maps for carbon steel at 0 mV and particle size 150-300µm in (a) water (b) crude oil (c) oil /20% water.

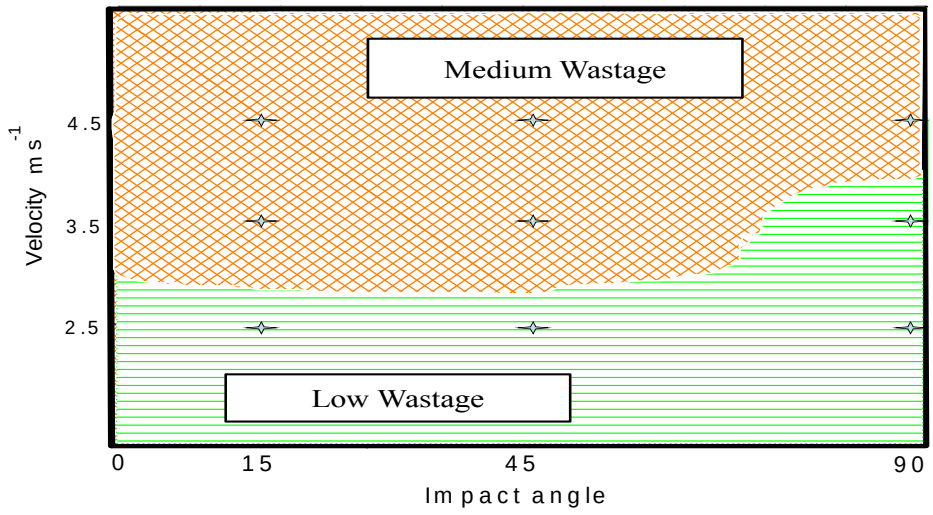

(a)

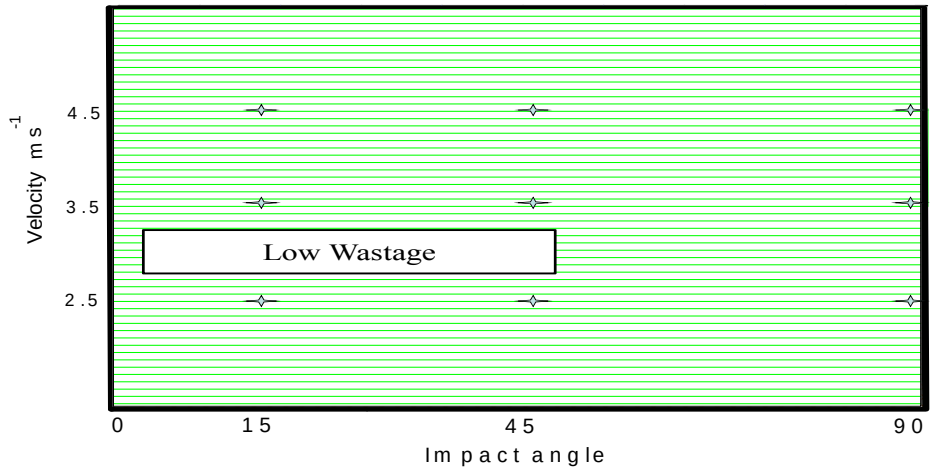

(b)

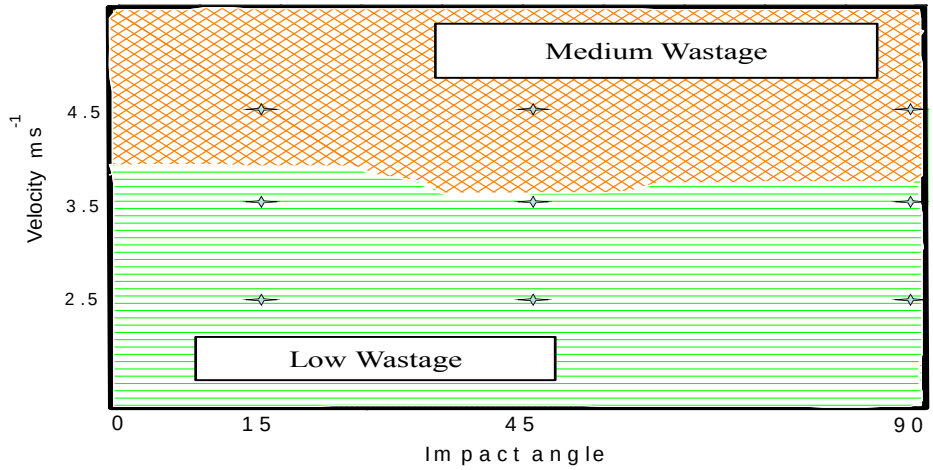

(c)

Fig.3.49: Erosion-corrosion wastage maps for carbon steel at 400 mV and particle size 150-300μm in (a) water (b) crude oil (c) oil /20% water.

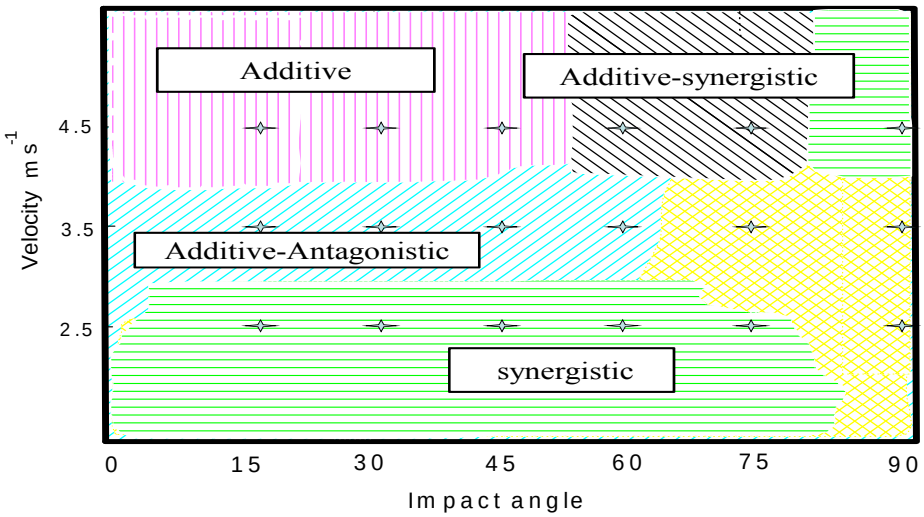

(a)

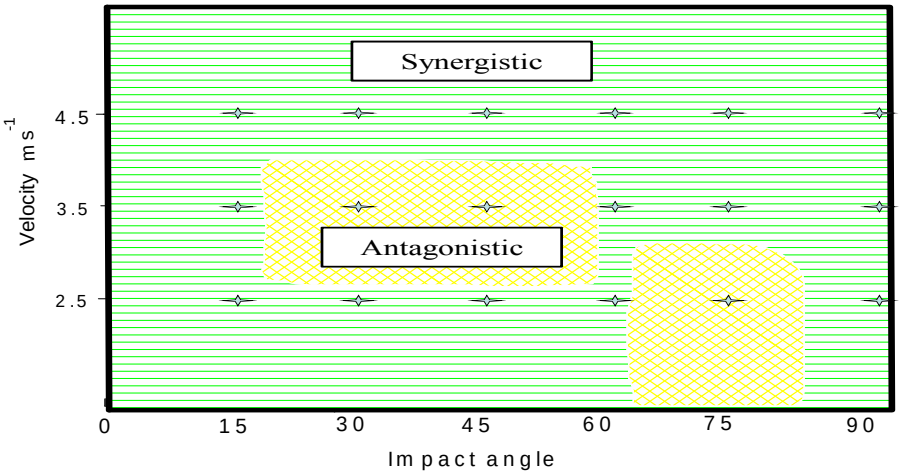

(b)

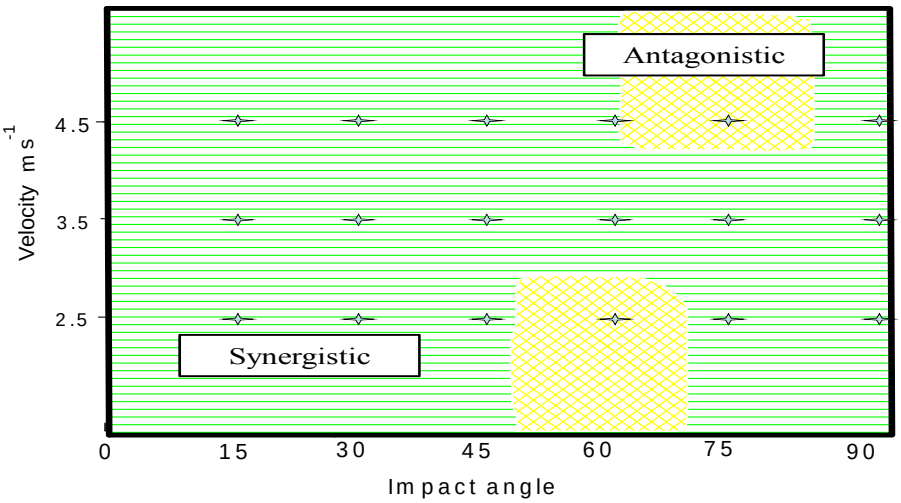

(c)

Fig.3.50: Erosion-corrosion additive-synergism maps for carbon steel at -400 mV and particle size 600-710µm in (a) water (b) crude oil (c) oil /20% water.

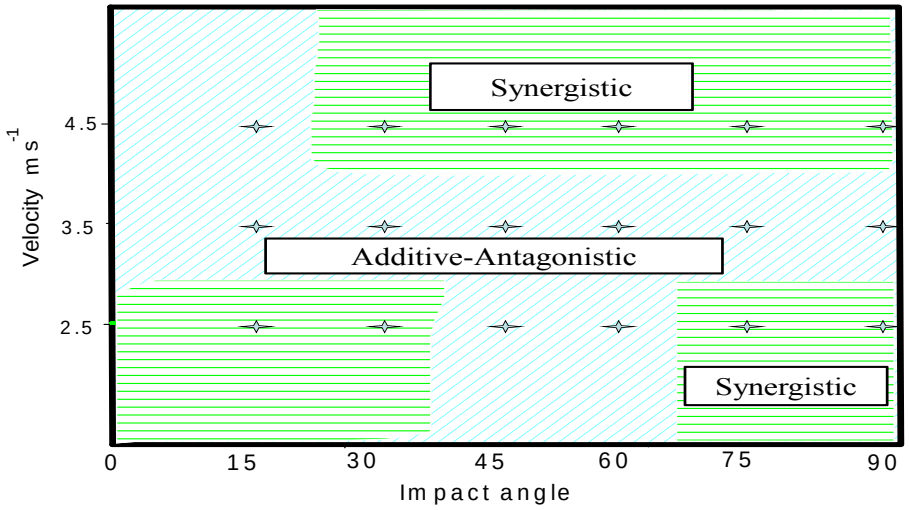

(a)

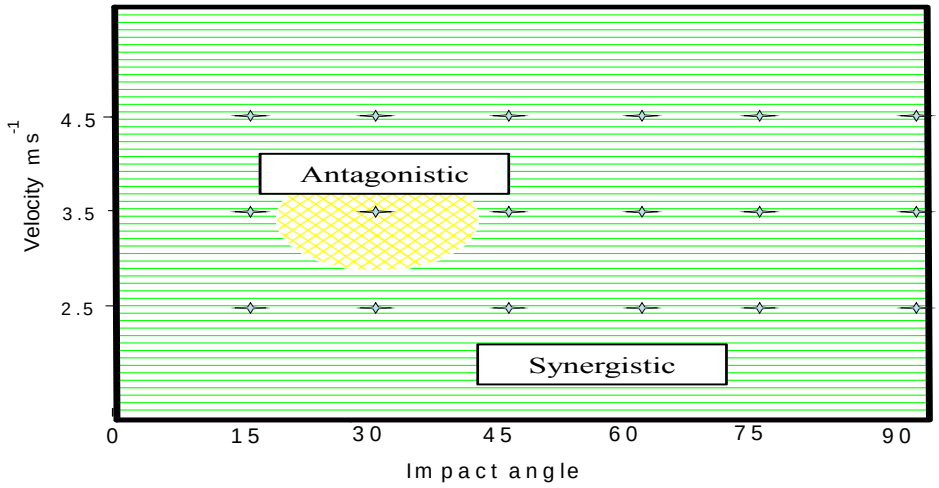

(b)

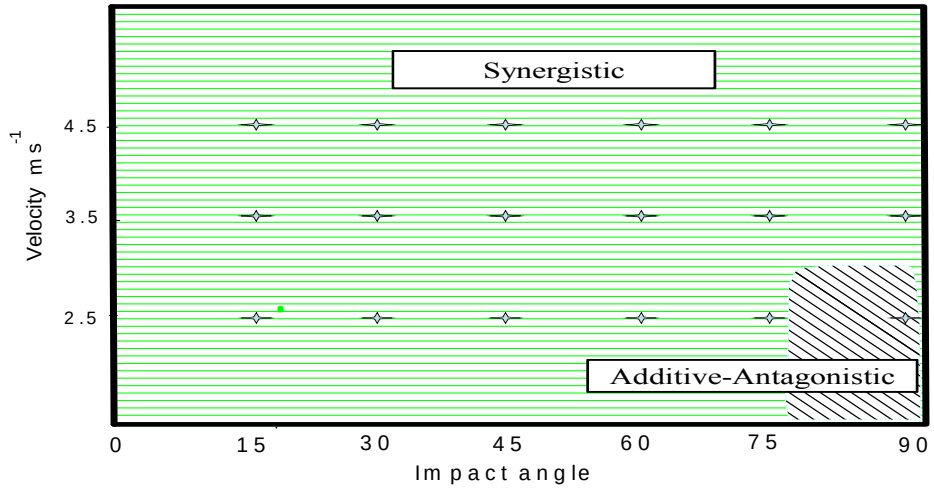

(c)

Fig.3.51: Erosion-corrosion additive-synergism maps for carbon steel at -200 mV and particle size 600-710µm in (a) water (b) crude oil (c) oil /20% water.

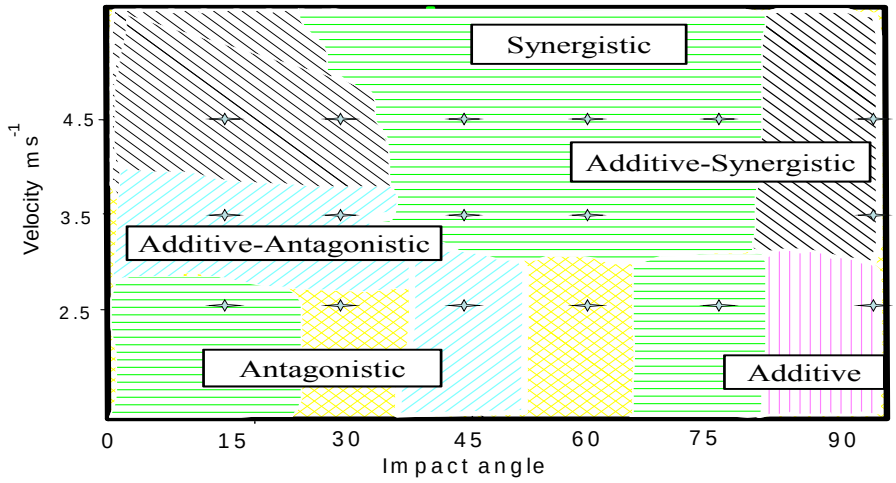

(a)

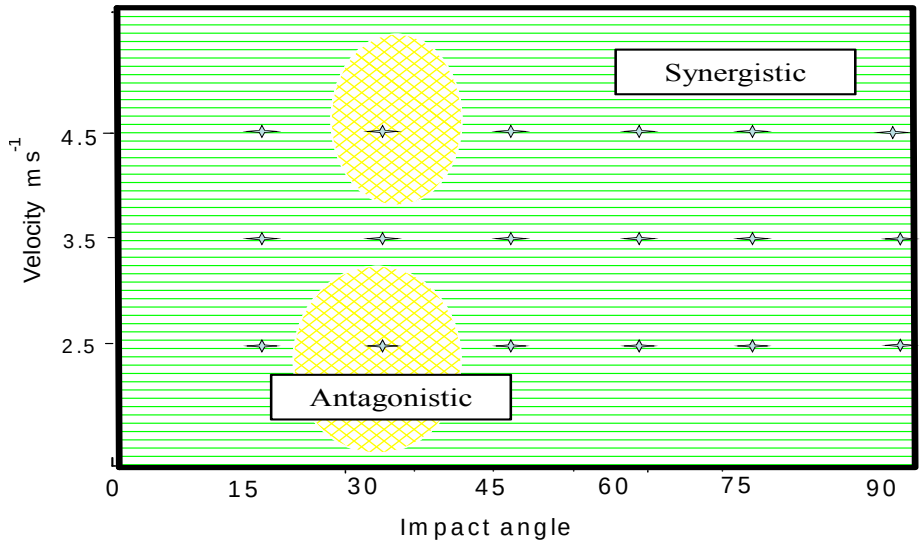

(b)

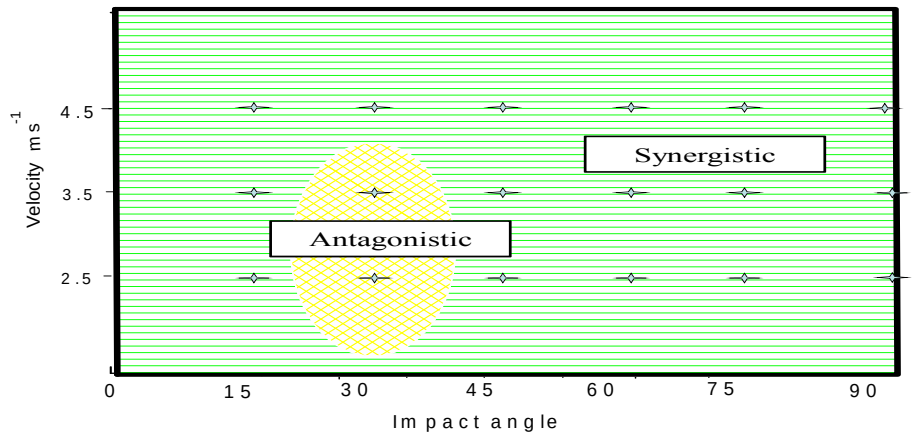

(c)

Fig.3.52: Erosion-corrosion additive-synergism maps for carbon steel at 0 mV and particle size 600-710µm in (a) water (b) crude oil (c) oil /20% water.

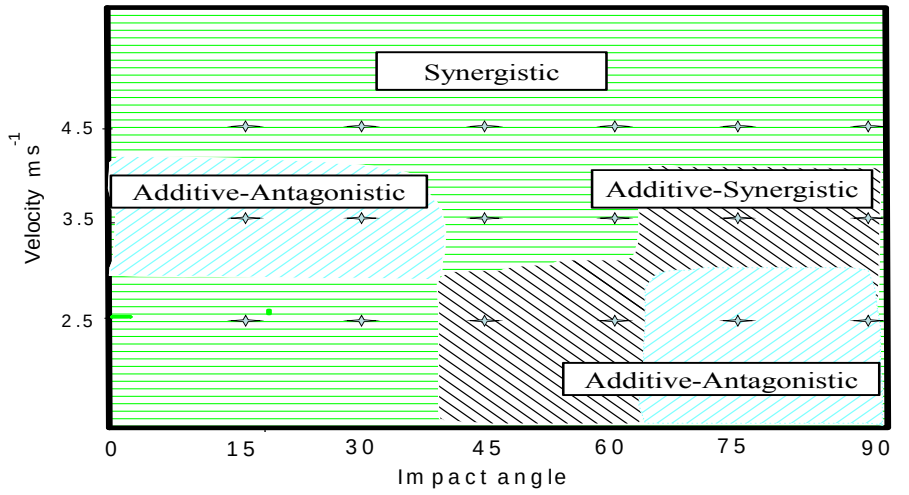

(a)

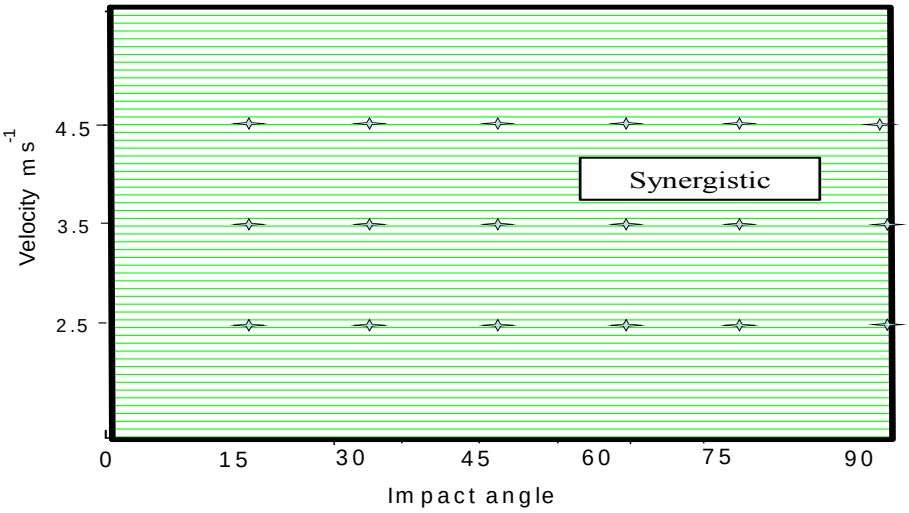

(b)

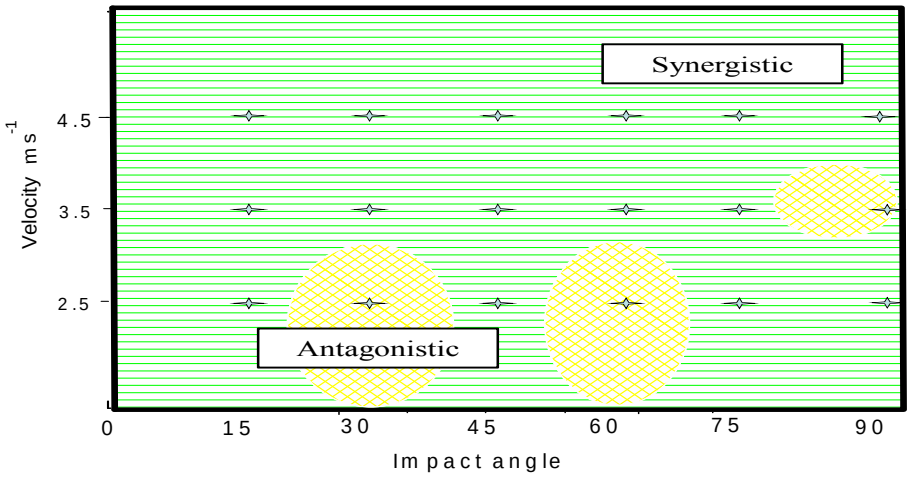

(c)

Fig.3.53: Erosion-corrosion additive-synergism maps for carbon steel at 200 mV and particle size 600-710µm in (a) water (b) crude oil (c) oil /20% water.

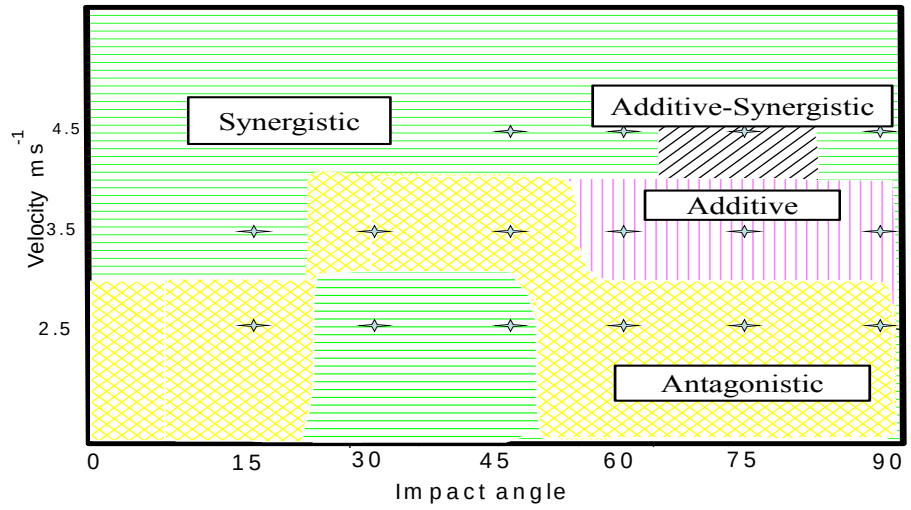

(a)

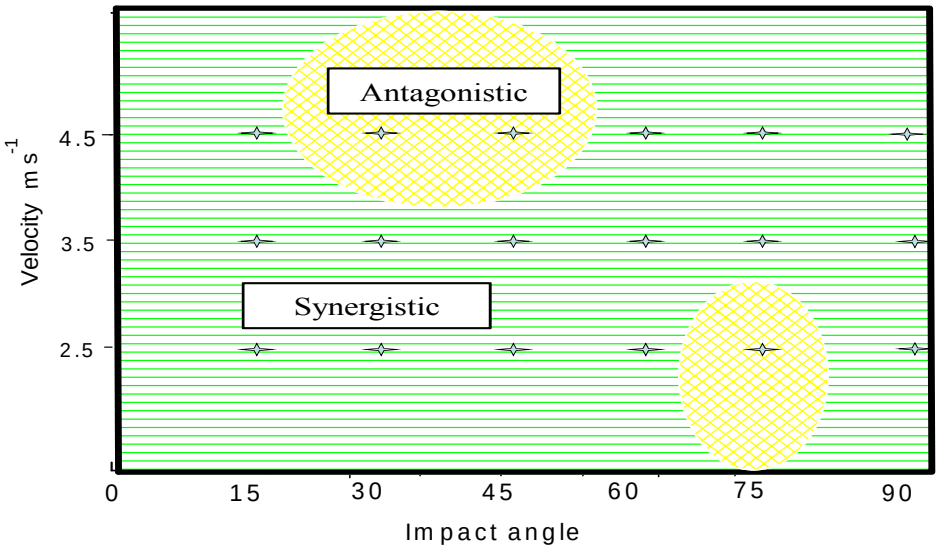

(b)

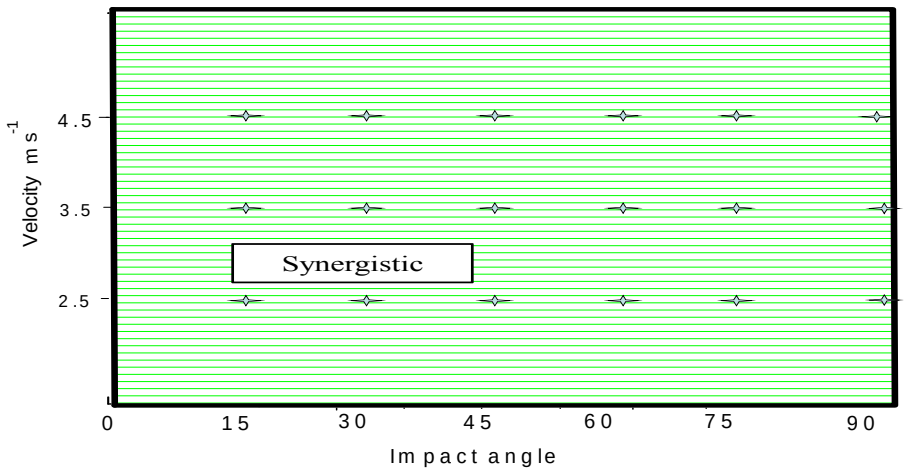

(c)

Fig.3.54: Erosion-corrosion additive-synergism maps for carbon steel at 400 mV and particle size 600-710µm in (a) water (b) crude oil (c) oil /20% water.

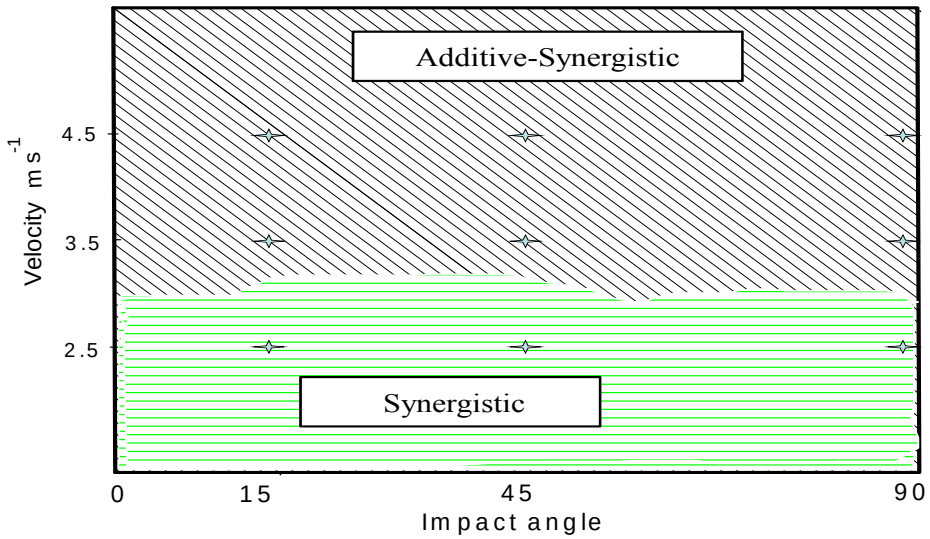

(a)

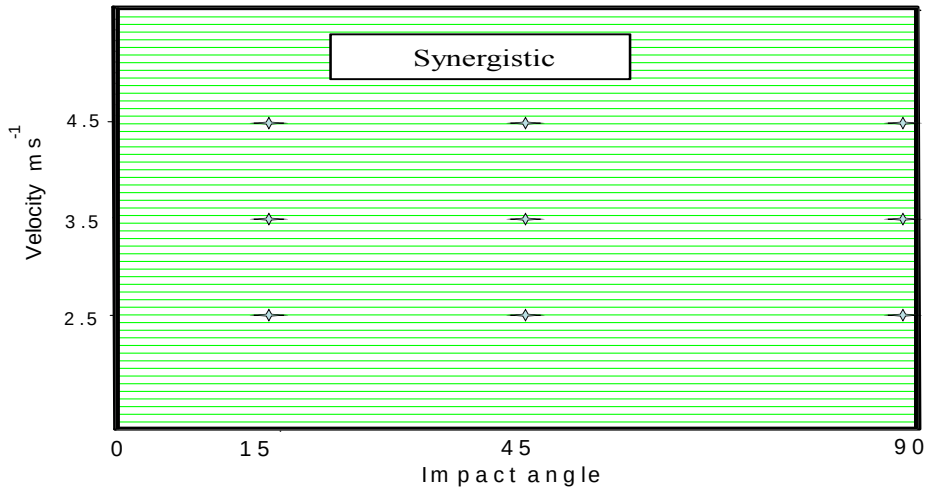

(b)

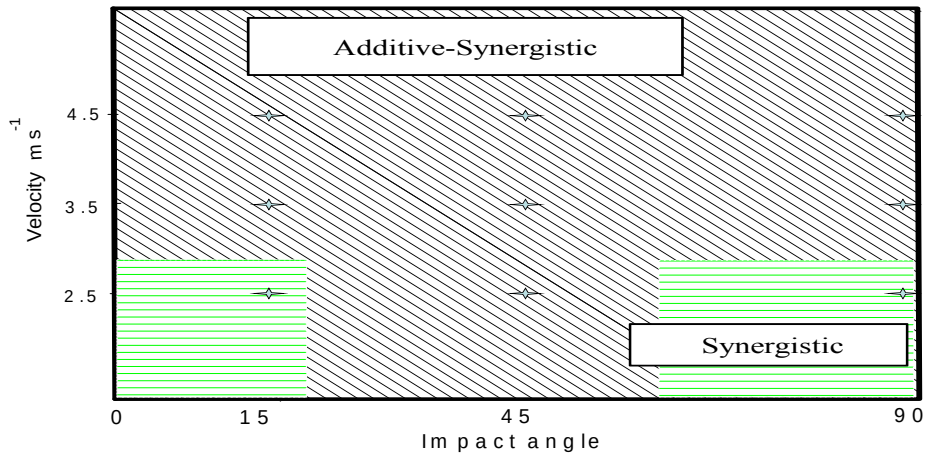

(c)

Fig.3.55: Erosion-corrosion additive-synergism maps for carbon steel at -400 mV and particle size 150-300µm in (a) water (b) crude oil (c) oil /20% water

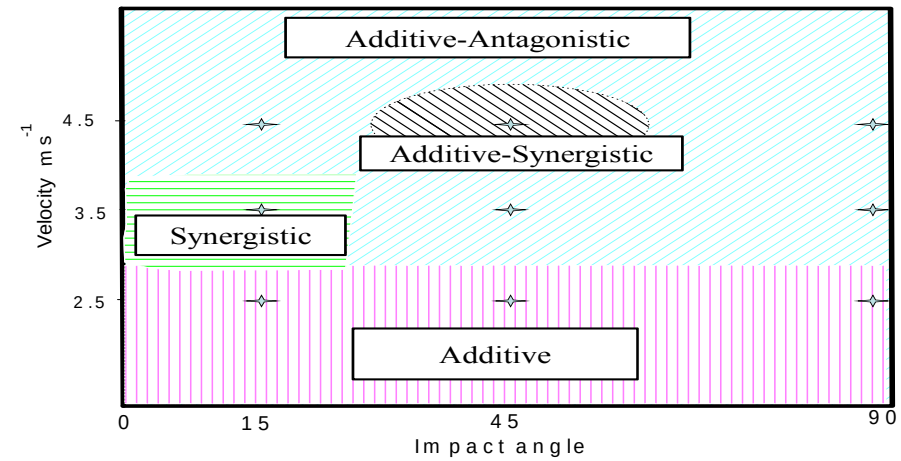

(a)

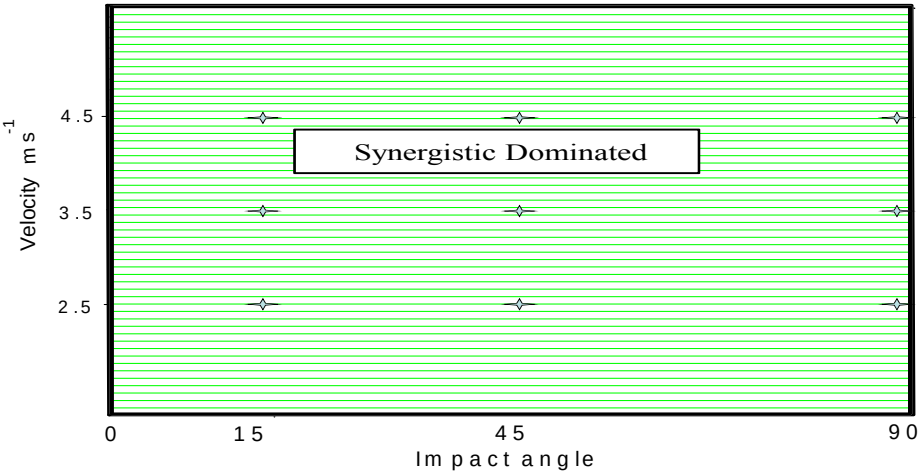

(b)

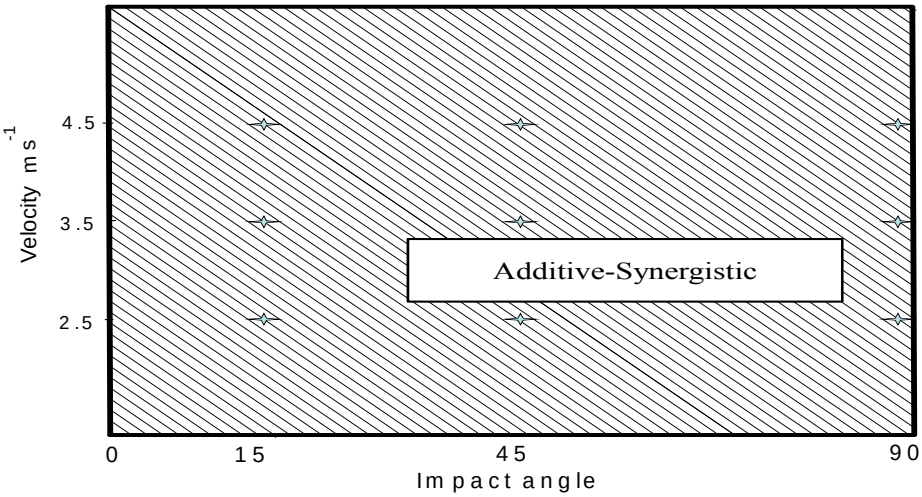

(c)

Fig.3.56: Erosion-corrosion additive-synergism maps for carbon steel at 0 mV and particle size 150-300µm in (a) water (b) crude oil (c) oil /20% water.

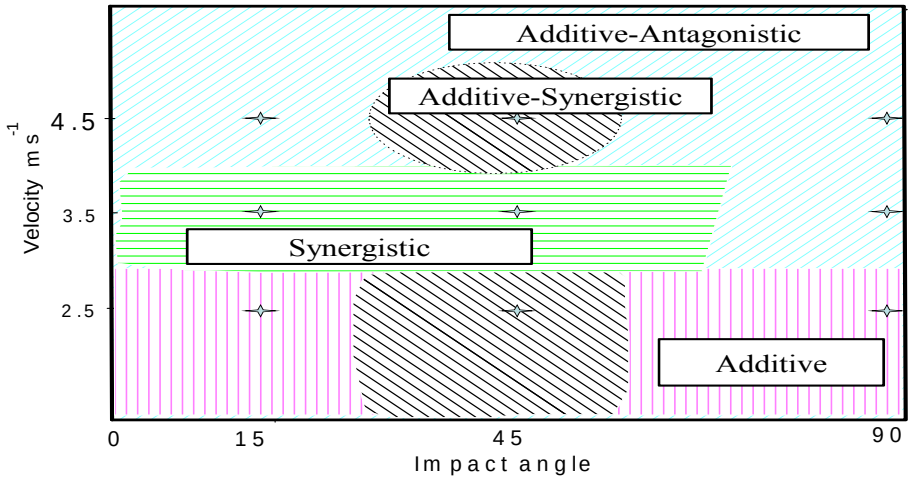

(a)

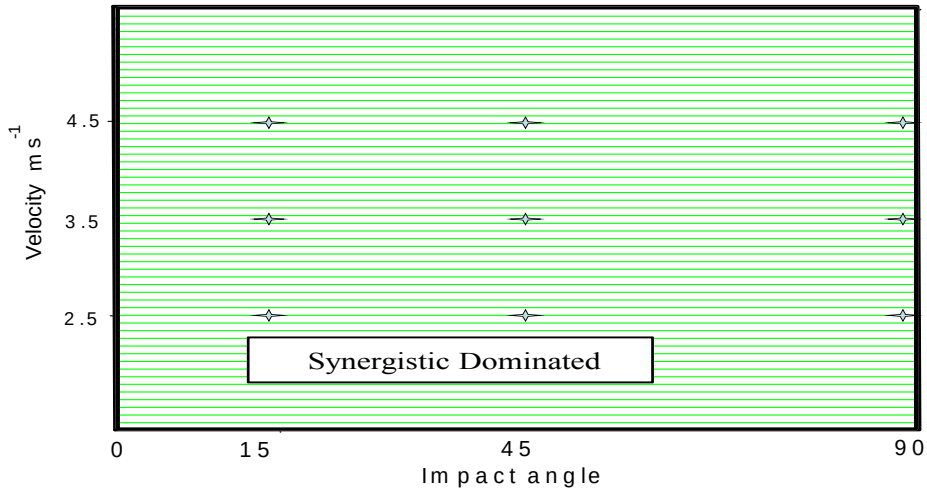

(b)

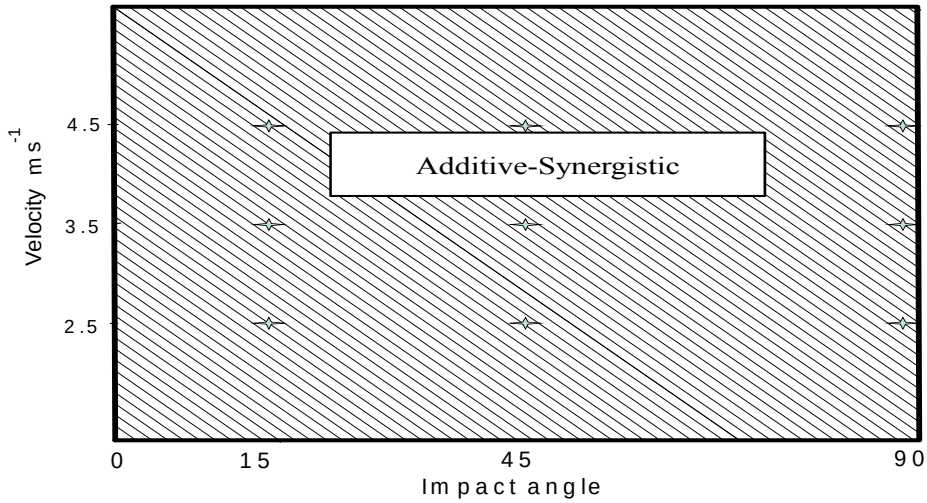

(c)

Fig.3.57: Erosion-corrosion additive-synergism maps for carbon steel at 400 mV and particle size 150-300µm in (a) water (b) crude oil (c) oil /20% water.

Tables.3.25: Erosion-corrosion mechanism maps for carbon steel in water at -400 mV and particle size 600-710µm (a) 15° (b) 30° (c) 45°(d) 60° (e) 75° (f) 90°

(a)

Velocities m s^{-1}	Ke(mg cm^{-2} h^{-1})	Kc(mg cm^{-2} h^{-1})	Ke/Kc
2.5	2.59	1.72	1.51
3.5	1.4	4.12	0.34
4.5	3	5.72	0.5

(b)

Velocities m s^{-1}	Ke(mg cm^{-2} h^{-1})	Kc(mg cm^{-2} h^{-1})	Ke/Kc
2.5	2.5	1.5	1.66
3.5	1.81	4.21	0.43
4.5	2.87	5.93	0.48

(c)

Velocities m s^{-1}	Ke(mg cm^{-2} h^{-1})	Kc(mg cm^{-2} h^{-1})	Ke/Kc
2.5	2.39	2.21	1.08
3.5	2.43	4.02	0.60
4.5	4.48	4.72	0.95

(d)

Velocities m s^{-1}	Ke(mg cm^{-2} h^{-1})	Kc(mg cm^{-2} h^{-1})	Ke/Kc
2.5	2.16	2.04	1.06
3.5	2.39	3.91	0.61
4.5	3.3	5.4	0.61

(e)

Velocities m s^{-1}	Ke(mg cm^{-2} h^{-1})	Kc(mg cm^{-2} h^{-1})	Ke/Kc
2.5	1.96	1.93	1.02
3.5	0.53	5.32	0.09
4.5	3	5.94	0.51

(f)

Velocities m s^{-1}	Ke(mg cm^{-2} h^{-1})	Kc(mg cm^{-2} h^{-1})	Ke/Kc
2.5	2.5	1.71	1.46
3.5	1.9	4.31	0.44
4.5	4.69	4.78	0.98

Tables.3.26: Erosion-corrosion mechanism maps for carbon steel in water at -200mV and particle size 600-710μm (a) 15° (b) 30° (c) 45° (d) 60° (e) 75° (f) 90°

(a)

Velocities m s^{-1}	Ke(mg cm^{-2} h^{-1})	Kc(mg cm^{-2} h^{-1})	Ke/Kc
2.5	2.45	1.78	1.38
3.5	1.77	4.21	0.42
4.5	2.39	5.84	0.41

(b)

Velocities m s^{-1}	Ke(mg cm^{-2} h^{-1})	Kc(mg cm^{-2} h^{-1})	Ke/Kc
2.5	2.59	1.72	1.51
3.5	2.11	3.91	0.54
4.5	4.88	4.12	1.18

(c)

Velocities m s^{-1}	Ke(mg cm^{-2} h^{-1})	Kc(mg cm^{-2} h^{-1})	Ke/Kc
2.5	2.17	2.43	0.89
3.5	1.89	5	0.38
4.5	4.17	5.85	0.71

(d)

Velocities m s^{-1}	Ke(mg cm^{-2} h^{-1})	Kc(mg cm^{-2} h^{-1})	Ke/Kc
2.5	1.89	2.1	0.89
3.5	2.2	4.3	0.5
4.5	4.65	5.7	0.82

(e)

Velocities m s^{-1}	Ke(mg cm^{-2} h^{-1})	Kc(mg cm^{-2} h^{-1})	Ke/Kc
2.5	1.57	2.24	0.70
3.5	1.59	4.61	0.34
4.5	3.45	5.89	0.59

(f)

Velocities m s^{-1}	Ke(mg cm^{-2} h^{-1})	Kc(mg cm^{-2} h^{-1})	Ke/Kc
2.5	1.9	2.21	0.86
3.5	1.97	4.38	0.45
4.5	5.48	4.83	1.13

Tables.3.27: for Erosion-corrosion mechanism maps for carbon steel in water at 0mV and particle size 600-710µm (a) 15° (b) 30° (c) 45°(d) 60° (e) 75° (f) 90°

(a)

Velocities m s^{-1}	Ke(mg cm^{-2} h^{-1})	Kc(mg cm^{-2} h^{-1})	Ke/Kc
2.5	2.58	1.82	1.42
3.5	1.65	4.38	0.38
4.5	3.82	5.91	0.65

(b)

Velocities m s^{-1}	Ke(mg cm^{-2} h^{-1})	Kc(mg cm^{-2} h^{-1})	Ke/Kc
2.5	2.38	1.83	1.30
3.5	2.42	3.78	0.64
4.5	5.76	4.45	1.29

(c)

Velocities m s^{-1}	Ke(mg cm^{-2} h^{-1})	Kc(mg cm^{-2} h^{-1})	Ke/Kc
2.5	1.7	2.71	0.63
3.5	1.99	5.04	0.39
4.5	4.71	5.56	0.85

(d)

Velocities m s^{-1}	Ke(mg cm^{-2} h^{-1})	Kc(mg cm^{-2} h^{-1})	Ke/Kc
2.5	1.25	2.25	0.56
3.5	2.7	4.51	0.59
4.5	4.71	5.56	0.85

(e)

Velocities m s^{-1}	Ke(mg cm^{-2} h^{-1})	Kc(mg cm^{-2} h^{-1})	Ke/Kc
2.5	2.16	2.46	0.88
3.5	2.8	4.07	0.69
4.5	4.11	6.21	0.66

(f)

Velocities m s^{-1}	Ke(mg cm^{-2} h^{-1})	Kc(mg cm^{-2} h^{-1})	Ke/Kc
2.5	1.57	2.7	0.58
3.5	2.48	5	0.50
4.5	3.47	6	0.58

Tables.3.28: Erosion-corrosion mechanism maps for carbon steel in water at 200mV and particle size 600-710µm (a) 15° (b) 30° (c) 45° (d) 60° (e) 75° (f) 90°

(a)

Velocities m s^{-1}	Ke(mg cm^{-2} h^{-1})	Kc(mg cm^{-2} h^{-1})	Ke/Kc
2.5	2.43	1.95	1.25
3.5	1.73	4.48	0.39
4.5	4.76	5.24	0.91

(b)

Velocities m s^{-1}	Ke(mg cm^{-2} h^{-1})	Kc(mg cm^{-2} h^{-1})	Ke/Kc
2.5	2.56	1.94	1.32
3.5	3.4	4.1	0.83
4.5	5.51	4.81	1.15

(c)

Velocities m s^{-1}	Ke(mg cm^{-2} h^{-1})	Kc(mg cm^{-2} h^{-1})	Ke/Kc
2.5	2.58	2.03	1.27
3.5	3.88	4.12	0.94
4.5	5.74	5.32	1.08

(d)

Velocities m s^{-1}	Ke(mg cm^{-2} h^{-1})	Kc(mg cm^{-2} h^{-1})	Ke/Kc
2.5	1.5	2.71	0.55
3.5	2.83	5.01	0.56
4.5	4.88	5.87	0.83

(e)

Velocities m s^{-1}	Ke(mg cm^{-2} h^{-1})	Kc(mg cm^{-2} h^{-1})	Ke/Kc
2.5	2.26	1.34	1.69
3.5	2.8	4.5	0.62
4.5	4.52	6	0.75

(f)

Velocities m s^{-1}	Ke(mg cm^{-2} h^{-1})	Kc(mg cm^{-2} h^{-1})	Ke/Kc
2.5	1.22	2.78	0.44
3.5	2.5	5.52	0.45
4.5	4.19	6.13	0.68

Tables.3.29: Erosion-corrosion mechanism maps for carbon steel in water at 400mV and particle size 600-710µm (a) 15° (b) 30° (c) 45° (d) 60° (e) 75° (f) 90°

(a)

Velocities m s^{-1}	Ke(mg cm^{-2} h^{-1})	Kc(mg cm^{-2} h^{-1})	Ke/Kc
2.5	2.44	1.97	1.24
3.5	3.49	4.51	0.77
4.5	5.25	5.2	1.01

(b)

Velocities m s^{-1}	Ke(mg cm^{-2} h^{-1})	Kc(mg cm^{-2} h^{-1})	Ke/Kc
2.5	2.16	2.07	1.04
3.5	3.57	4.23	0.84
4.5	5.62	4.9	1.15

(c)

Velocities m s^{-1}	Ke(mg cm^{-2} h^{-1})	Kc(mg cm^{-2} h^{-1})	Ke/Kc
2.5	2.84	2.16	1.31
3.5	3.89	4.32	0.90
4.5	6.11	5.73	1.07

(d)

Velocities m s^{-1}	Ke(mg cm^{-2} h^{-1})	Kc(mg cm^{-2} h^{-1})	Ke/Kc
2.5	2.57	1.93	1.33
3.5	2.79	5.21	0.54
4.5	6.05	5.07	1.19

(e)

Velocities m s^{-1}	Ke(mg cm^{-2} h^{-1})	Kc(mg cm^{-2} h^{-1})	Ke/Kc
2.5	0.71	2.74	0.26
3.5	2.99	4.85	0.62
4.5	3.16	6.84	0.46

(f)

Velocities m s^{-1}	Ke(mg cm^{-2} h^{-1})	Kc(mg cm^{-2} h^{-1})	Ke/Kc
2.5	1.48	2.53	0.58
3.5	2.11	5.81	0.36
4.5	4.29	6.73	0.64

Tables.3.30: Erosion-corrosion mechanism maps for carbon steel in crude oil at -400mV and particle size 600-710µm (a) 15° (b) 30° (c) 45°(d) 60° (e) 75° (f) 90°

(a)

Velocities m s^{-1}	Ke(mg cm^{-2} h^{-1})	Kc(mg cm^{-2} h^{-1})	Ke/Kc
2.5	2.5	2.11E-02	117.5
3.5	4.6	1.89E-02	241.3
4.5	7.5	2.88E-02	259.4

(b)

Velocities m s^{-1}	Ke(mg cm^{-2} h^{-1})	Kc(mg cm^{-2} h^{-1})	Ke/Kc
2.5	2	1.22E-02	162.9
3.5	4	2.62E-02	151.7
4.5	6.2	3.28E-02	188.3

(c)

Velocities m s^{-1}	Ke(mg cm^{-2} h^{-1})	Kc(mg cm^{-2} h^{-1})	Ke/Kc
2.5	2	1.02E-02	196.1
3.5	4.5	2.00E-02	224
4.5	7.1	2.52E-02	281.5

(d)

Velocities m s^{-1}	Ke(mg cm^{-2} h^{-1})	Kc(mg cm^{-2} h^{-1})	Ke/Kc
2.5	2.1	1.85E-02	112.5
3.5	4.2	2.43E-02	172.3
4.5	6.6681	3.19E-02	209.0

(e)

Velocities m s^{-1}	Ke(mg cm^{-2} h^{-1})	Kc(mg cm^{-2} h^{-1})	Ke/Kc
2.5	2.1	2.02E-02	104
3.5	4.7	1.92E-02	244.3
4.5	7	3.03E-02	230.0

(f)

Velocities m s^{-1}	Ke(mg cm^{-2} h^{-1})	Kc(mg cm^{-2} h^{-1})	Ke/Kc
2.5	2.1	1.81E-02	115.6
3.5	4.8	2.62E-02	181.4
4.5	7.1	4.12E-02	173.3

Tables.3.31: for Erosion-corrosion mechanism maps for carbon steel in crude oil at -200mV and particle size 600-710µm (a) 15° (b) 30° (c) 45° (d) 60° (e) 75° (f) 90°

(a)

Velocities m s^{-1}	Ke(mg cm^{-2} h^{-1})	Kc(mg cm^{-2} h^{-1})	Ke/Kc
2.5	2.6	1.63E-02	158.5
3.5	5.1	2.09E-02	244
4.5	7.2	3.78E-02	191.6

(b)

Velocities m s^{-1}	Ke(mg cm^{-2} h^{-1})	Kc(mg cm^{-2} h^{-1})	Ke/Kc
2.5	2.4	1.65E-02	144.5
3.5	4.2	3.02E-02	138.1
4.5	6.97	3.41E-02	204.3

(c)

Velocities m s^{-1}	Ke(mg cm^{-2} h^{-1})	Kc(mg cm^{-2} h^{-1})	Ke/Kc
2.5	2.7	1.47E-02	182.7
3.5	4.6	2.21E-02	207.1
4.5	7	2.98E-02	234.6

(d)

Velocities m s^{-1}	Ke(mg cm^{-2} h^{-1})	Kc(mg cm^{-2} h^{-1})	Ke/Kc
2.5	2.8	1.93E-02	144.1
3.5	4.7	2.53E-02	184.8
4.5	6.8	4.19E-02	163

(e)

Velocities m s^{-1}	Ke(mg cm^{-2} h^{-1})	Kc(mg cm^{-2} h^{-1})	Ke/Kc
2.5	3.14	2.12E-02	148.1
3.5	4.83	2.02E-02	239.1
4.5	7.02	3.48E-02	201.6

(f)

Velocities m s^{-1}	Ke(mg cm^{-2} h^{-1})	Kc(mg cm^{-2} h^{-1})	Ke/Kc
2.5	3.13	1.97E-02	158.9
3.5	4.97	2.74E-02	181.5
4.5	7.76	3.99E-02	194.5

Tables.3.32: Erosion-corrosion mechanism maps for carbon steel in crude oil at 0mV and particle size 600-710µm (a) 15° (b) 30° (c) 45°(d) 60° (e) 75° (f) 90°

(a)

Velocities m s^{-1}	Ke(mg cm^{-2} h^{-1})	Kc(mg cm^{-2} h^{-1})	Ke/Kc
2.5	3.38	1.85E-02	182.8
3.5	5.07	2.59E-02	195.9
4.5	7.96	4.28E-02	185.9

(b)

Velocities m s^{-1}	Ke(mg cm^{-2} h^{-1})	Kc(mg cm^{-2} h^{-1})	Ke/Kc
2.5	3.10	1.71E-02	181.5
3.5	4.47	2.70E-02	165.7
4.5	7.44	4.01E-02	185.5

(c)

Vlocities m s^{-1}	Ke(mg cm^{-2} h^{-1})	Kc(mg cm^{-2} h^{-1})	Ke/Kc
2.5	3.13	1.39E-02	224.9
3.5	4.98	1.81E-02	275.2
4.5	7.42	3.08E-02	240.9

(d)

Velocities m s^{-1}	Ke(mg cm^{-2} h^{-1})	Kc(mg cm^{-2} h^{-1})	Ke/Kc
2.5	3.38	1.90E-02	177.9
3.5	4.87	2.61E-02	186.7
4.5	6.96	3.89E-02	178.9

(e)

Velocities m s^{-1}	Ke(mg cm^{-2} h^{-1})	Kc(mg cm^{-2} h^{-1})	Ke/Kc
2.5	3.24	1.98E-02	163.6
3.5	4.84	2.76E-02	175.4
4.5	6.66	3.88E-02	171.7

(f)

Velocities m s^{-1}	Ke(mg cm^{-2} h^{-1})	Kc(mg cm^{-2} h^{-1})	Ke/Kc
2.5	3.38	2.00E-02	169
3.5	5.18	2.91E-02	178.0
4.5	7.40	4.56E-02	162.4

Tables.3.33: Erosion-corrosion mechanism maps for carbon steel in crude oil at 200mV and particle size 600-710µm (a) 15° (b) 30° (c) 45° (d) 60° (e) 75° (f) 90°

(a)

Velocities m s^{-1}	Ke(mg cm^{-2} h^{-1})	Kc(mg cm^{-2} h^{-1})	Ke/Kc
2.5	3.8	1.94E-02	193.8
3.5	5.6	2.61E-02	213.6
4.5	8.4	4.50E-02	187.2

(b)

Velocities m s^{-1}	Ke(mg cm^{-2} h^{-1})	Kc(mg cm^{-2} h^{-1})	Ke/Kc
2.5	3.49	1.49E-02	233.9
3.5	5.2	2.78E-02	186.1
4.5	7.9	3.91E-02	203.1

(c)

Velocities m s^{-1}	Ke(mg cm^{-2} h^{-1})	Kc(mg cm^{-2} h^{-1})	Ke/Kc
2.5	3.6	1.51E-02	234.8
3.5	5.9	1.92E-02	304.7
4.5	7.7	3.58E-02	216.3

(d)

Velocities m s^{-1}	Ke(mg cm^{-2} h^{-1})	Kc(mg cm^{-2} h^{-1})	Ke/Kc
2.5	3.1	2.00E-02	155
3.5	4.98	1.99E-02	250.3
4.5	7.1	4.09E-02	173.6

(e)

Velocities m s^{-1}	Ke(mg cm^{-2} h^{-1})	Kc(mg cm^{-2} h^{-1})	Ke/Kc
2.5	3.6	2.33E-02	153.5
3.5	5.1	3.76E-02	135.4
4.5	6.96	3.78E-02	184.2

(f)

Velocities m s^{-1}	Ke(mg cm^{-2} h^{-1})	Kc(mg cm^{-2} h^{-1})	Ke/Kc
2.5	3.98	2.42E-02	164.3
3.5	5.75	3.01E-02	191.0
4.5	7.95	4.78E-02	166.4

Tables.3.34: Erosion-corrosion mechanism maps for carbon steel in crude oil at 400mV and particle size 600-710µm (a) 15° (b) 30° (c) 45° (d) 60° (e) 75° (f) 90°

(a)

Velocities m s^{-1}	Ke(mg cm^{-2} h^{-1})	Kc(mg cm^{-2} h^{-1})	Ke/Kc
2.5	3.76	2.14E-02	175.6
3.5	6.97	2.58E-02	270.3
4.5	8.07	4.78E-02	168.9

(b)

Velocities m s^{-1}	Ke(mg cm^{-2} h^{-1})	Kc(mg cm^{-2} h^{-1})	Ke/Kc
2.5	3.49	1.52E-02	229.3
3.5	6.37	3.08E-02	206.8
4.5	7.96	4.51E-02	176.4

(c)

Velocities m s^{-1}	Ke(mg cm^{-2} h^{-1})	Kc(mg cm^{-2} h^{-1})	Ke/Kc
2.5	3.6	1.48E-02	239.5
3.5	6.2	2.02E-02	305.9
4.5	8.4	4.00E-02	210.3

(d)

Velocities m s^{-1}	Ke(mg cm^{-2} h^{-1})	Kc(mg cm^{-2} h^{-1})	Ke/Kc
2.5	3.1	2.31E-02	134.1
3.5	5	2.19E-02	227.3
4.5	8.0	5.19E-02	155.1

(e)

Velocities m s^{-1}	Ke(mg cm^{-2} h^{-1})	Kc(mg cm^{-2} h^{-1})	Ke/Kc
2.5	3.6	2.40E-02	149
3.5	5.97	2.96E-02	201.7
4.5	7.85	4.18E-02	187.8

(f)

Velocities m s^{-1}	Ke(mg cm^{-2} h^{-1})	Kc(mg cm^{-2} h^{-1})	Ke/Kc
2.5	4	2.65E-02	150
3.5	6.5	3.21E-02	201.5
4.5	8.2	5.18E-02	157.9

Tables.3.35: Erosion-corrosion mechanism maps for carbon steel in oil /20% water at -400mV and particle size 600-710µm (a) 15° (b) 30° (c) 45° (d) 60° (e) 75° (f) 90°

(a)

Velocities m s^{-1}	Ke(mg cm^{-2} h^{-1})	Kc(mg cm^{-2} h^{-1})	Ke/Kc
2.5	2.31	0.8	2.9
3.5	4.16	0.84	5
4.5	6.45	1.35	4.777778

(b)

Velocities m s^{-1}	Ke(mg cm^{-2} h^{-1})	Kc(mg cm^{-2} h^{-1})	Ke/Kc
2.5	1.92	0.78	2.5
3.5	3.71	0.89	4.2
4.5	6.07	1.21	5.0

(c)

Velocities m s^{-1}	Ke(mg cm^{-2} h^{-1})	Kc(mg cm^{-2} h^{-1})	Ke/Kc
2.5	2.16	0.84	2.6
3.5	5.2	0.9	5.8
4.5	6.66	1.34	5

(d)

Velocities m s^{-1}	Ke(mg cm^{-2} h^{-1})	Kc(mg cm^{-2} h^{-1})	Ke/Kc
2.5	2.42	0.78	3.1
3.5	4.42	0.98	4.5
4.5	5.82	1.2	4.9

(e)

Velocities m s^{-1}	Ke(mg cm^{-2} h^{-1})	Kc(mg cm^{-2} h^{-1})	Ke/Kc
2.5	1.96	1	1.96
3.5	4.2	1	4.2
4.5	6.6	1.4	4.7

(f)

Velocities m s^{-1}	Ke(mg cm^{-2} h^{-1})	Kc(mg cm^{-2} h^{-1})	Ke/Kc
2.5	2.18	0.9	2.4
3.5	5	1.1	4.5
4.5	6.75	1.45	4.7

Tables.3.36: Erosion-corrosion mechanism maps for carbon steel in oil /20% water at -200mV and particle size 600-710µm (a) 15° (b) 30° (c) 45°(d) 60° (e) 75° (f) 90°

(a)

Velocities m s^{-1}	Ke(mg cm^{-2} h^{-1})	Kc(mg cm^{-2} h^{-1})	Ke/Kc
2.5	2.3	0.8	2.9
3.5	5.02	0.98	5.1
4.5	6.7	1.3	5.2

(b)

Velocities m s^{-1}	Ke(mg cm^{-2} h^{-1})	Kc(mg cm^{-2} h^{-1})	Ke/Kc
2.5	2.409	0.8	3.0
3.5	4.56	1	4.6
4.5	6.98	1.32	5.29

(c)

Velocities m s^{-1}	Ke(mg cm^{-2} h^{-1})	Kc(mg cm^{-2} h^{-1})	Ke/Kc
2.5	2.5	0.714	3.5
3.5	5.3	0.9	5.9
4.5	6.7	1.5	4.5

(d)

Velocities m s^{-1}	Ke(mg cm^{-2} h^{-1})	Kc(mg cm^{-2} h^{-1})	Ke/Kc
2.5	2.4	0.8	3.0
3.5	4.98	1.12	4.4
4.5	6.51	1.1	5.9

(e)

Velocities m s^{-1}	Ke(mg cm^{-2} h^{-1})	Kc(mg cm^{-2} h^{-1})	Ke/Kc
2.5	2.61	0.89	2.9
3.5	4.81	0.89	5.4
4.5	6.76	1.3	5.2

(f)

Velocities m s^{-1}	Ke(mg cm^{-2} h^{-1})	Kc(mg cm^{-2} h^{-1})	Ke/Kc
2.5	1.87	0.91	2.1
3.5	5.2	1	5.2
4.5	7.1	1.5	4.7

Tables.3.37: Erosion-corrosion mechanism maps for carbon steel in oil /20% water at 0mV and particle size 600-710µm (a) 15° (b) 30° (c) 45° (d) 60° (e) 75° (f) 90°

(a)

Velocities m s^{-1}	Ke(mg cm^{-2} h^{-1})	Kc(mg cm^{-2} h^{-1})	Ke/Kc
2.5	2.06	0.78	2.6
3.5	5.11	0.89	5.7
4.5	7.28	1.5	4.9

(b)

Velocities m s^{-1}	Ke(mg cm^{-2} h^{-1})	Kc(mg cm^{-2} h^{-1})	Ke/Kc
2.5	2.71	0.8	3.4
3.5	3.9	1.2	3.3
4.5	7.08	1.32	5.4

(c)

Velocities m s^{-1}	Ke(mg cm^{-2} h^{-1})	Kc(mg cm^{-2} h^{-1})	Ke/Kc
2.5	2.84	0.76	3.7
3.5	5.2	1	5.2
4.5	7.54	1.4	5.4

(d)

Velocities m s^{-1}	Ke(mg cm^{-2} h^{-1})	Kc(mg cm^{-2} h^{-1})	Ke/Kc
2.5	2.68	0.82	3.3
3.5	4.89	1.23	3.9
4.5	6.79	1.21	5.6

(e)

Velocities m s^{-1}	Ke(mg cm^{-2} h^{-1})	Kc(mg cm^{-2} h^{-1})	Ke/Kc
2.5	2.1	0.9	2.3
3.5	4.53	1	4.5
4.5	6.6	1.3	5.1

(f)

Velocities m s^{-1}	Ke(mg cm^{-2} h^{-1})	Kc(mg cm^{-2} h^{-1})	Ke/Kc
2.5	2.13	0.78	2.7
3.5	5.32	0.98	5.4
4.5	7.12	1.6	4.45

Tables.3.38: Erosion-corrosion mechanism maps for carbon steel in oil /20% water at 200 mV and particle size 600-710µm (a) 15° (b) 30° (c) 45°(d) 60° (e) 75° (f) 90°

(a)

Velocities m s^{-1}	Ke(mg cm^{-2} h^{-1})	Kc(mg cm^{-2} h^{-1})	Ke/Kc
2.5	2.1	0.68	3.1
3.5	5.47	0.93	5.9
4.5	7.34	1.68	4.4

(b)

Velocities m s^{-1}	Ke(mg cm^{-2} h^{-1})	Kc(mg cm^{-2} h^{-1})	Ke/Kc
2.5	2.35	0.9	2.6
3.5	5.32	0.98	5.4
4.5	7.4	1.6	4.6

(c)

Velocities m s^{-1}	Ke(mg cm^{-2} h^{-1})	Kc(mg cm^{-2} h^{-1})	Ke/Kc
2.5	2.89	0.81	3.6
3.5	5.3	1.2	4.4
4.5	7.76	1.54	5.0

(d)

Velocities m s^{-1}	Ke(mg cm^{-2} h^{-1})	Kc(mg cm^{-2} h^{-1})	Ke/Kc
2.5	2.64	0.96	2.6
3.5	5.22	0.78	6.7
4.5	8.68	1.32	6.6

(e)

Velocities m s^{-1}	Ke(mg cm^{-2} h^{-1})	Kc(mg cm^{-2} h^{-1})	Ke/Kc
2.5	2.42	0.45	5.4
3.5	4.75	1.12	4.2
4.5	7.57	1.4	5.4

(f)

Velocities m s^{-1}	Ke(mg cm^{-2} h^{-1})	Kc(mg cm^{-2} h^{-1})	Ke/Kc
2.5	2.27	0.73	3.1
3.5	5.18	1.23	4.2
4.5	7.9	1.7	4.6

Tables.3.39: Erosion-corrosion mechanism maps for carbon steel in oil /20% water at 400mV and particle size 600-710µm (a) 15° (b) 30° (c) 45°(d) 60° (e) 75° (f) 90°

(a)

Velocities m s^{-1}	Ke(mg cm^{-2} h^{-1})	Kc(mg cm^{-2} h^{-1})	Ke/Kc
2.5	1.89	0.71	2.7
3.5	6.01	1.2	5.0
4.5	7.61	1.9	4.0

(b)

Velocities m s^{-1}	Ke(mg cm^{-2} h^{-1})	Kc(mg cm^{-2} h^{-1})	Ke/Kc
2.5	2.68	0.72	3.7
3.5	5.51	1	5.5
4.5	7.67	1.85	4.1

(c)

Velocities m s^{-1}	Ke(mg cm^{-2} h^{-1})	Kc(mg cm^{-2} h^{-1})	Ke/Kc
2.5	2.1	0.9	2.3
3.5	5.4	1.3	4.2
4.5	7.42	1.7	4.4

(d)

Velocities m s^{-1}	Ke(mg cm^{-2} h^{-1})	Kc(mg cm^{-2} h^{-1})	Ke/Kc
2.5	2.02	0.78	2.6
3.5	6.2	0.8	7.8
4.5	7.32	1.68	4.4

(e)

Velocities m s^{-1}	Ke(mg cm^{-2} h^{-1})	Kc(mg cm^{-2} h^{-1})	Ke/Kc
2.5	2.23	0.67	3.3
3.5	5.87	0.98	5.9
4.5	7.12	1.76	4.0

(f)

Velocities m s^{-1}	Ke(mg cm^{-2} h^{-1})	Kc(mg cm^{-2} h^{-1})	Ke/Kc
2.5	2.4	0.8	3
3.5	5.8	1.2	4.8
4.5	7.98	1.89	4.2

Tables.3.40: Erosion-corrosion mechanism maps for carbon steel in water at -400 mV and particle size 150-300μm (a) 15° (b) 45° (c) 90°.

(a)

Velocities m s^{-1}	Ke(mg cm^{-2} h^{-1})	Kc(mg cm^{-2} h^{-1})	Ke /Kc
2.5	1.5	2.5	0.6
3.5	1.22	3.98	0.31
4.5	2	5.5	0.36

(b)

Velocities m s^{-1}	Ke(mg cm^{-2} h^{-1})	Kc(mg cm^{-2} h^{-1})	Ke /Kc
2.5	1.59	2.6	0.61
3.5	1.51	4.2	0.36
4.5	2.3	5.5	0.42

(c)

Velocities m s^{-1}	Ke(mg cm^{-2} h^{-1})	Kc(mg cm^{-2} h^{-1})	Ke /Kc
2.5	1.14	2.4	0.48
3.5	1.1	4.5	0.24
4.5	1.6	5.7	0.29

Tables.3.41: Erosion-corrosion mechanism maps for carbon steel in water at 0mV and particle size 150-300μm (a) 15° (b) 45° (c) 90°.

(a)

Velocities m s^{-1}	Ke(mg cm^{-2} h^{-1})	Kc(mg cm^{-2} h^{-1})	Ke /Kc
2.5	0.47	3.74	0.13
3.5	1.5	4	0.38
4.5	1.01	6.2	0.16

(b)

Velocities m s^{-1}	Ke(mg cm^{-2} h^{-1})	Kc(mg cm^{-2} h^{-1})	Ke /Kc
2.5	0.7	3.8	0.18
3.5	1.05	5	0.21
4.5	2.11	5.89	0.36

(c)

Velocities m s^{-1}	Ke(mg cm^{-2} h^{-1})	Kc(mg cm^{-2} h^{-1})	Ke /Kc
2.5	0.46	3.84	0.12
3.5	0.6	4.81	0.12
4.5	0.65	6.4	0.10

Tables.3.42: Erosion-corrosion mechanism maps for carbon steel in water at 400mV and particle size 150-300μm (a) 15° (b) 45° (c) 90°.

(a)

Velocities m s^{-1}	Ke(mg cm^{-2} h^{-1})	Kc(mg cm^{-2} h^{-1})	Ke /Kc
2.5	0.46	3.84	0.12
3.5	2	4.2	0.48
4.5	0.95	6.5	0.15

(b)

Velocities m s^{-1}	Ke(mg cm^{-2} h^{-1})	Kc(mg cm^{-2} h^{-1})	Ke /Kc
2.5	1.51	3.9	0.39
3.5	2	5	0.4
4.5	2.48	6.3	0.39

(c)

Velocities m s^{-1}	Ke(mg cm^{-2} h^{-1})	Kc(mg cm^{-2} h^{-1})	Ke /Kc
2.5	0.5	3.9	0.13
3.5	0.6	5.4	0.11
4.5	1	7	0.14

Tables.3.43: Erosion-corrosion mechanism maps for carbon steel in crude oil at -400mV and particle size 150-300µm (a) 15° (b) 45° (c) 90°

(a)

Velocities m s^{-1}	Ke(mg cm^{-2} h^{-1})	Kc(mg cm^{-2} h^{-1})	Ke /Kc
2.5	1.4	3.21E-01	4.45
3.5	3.1	4.00E-01	7.63
4.5	4.5	7.50E-01	5.66

(b)

Velocities m s^{-1}	Ke(mg cm^{-2} h^{-1})	Kc(mg cm^{-2} h^{-1})	Ke /Kc
2.5	1.7	3.42E-01	4.85
3.5	3.4	5.00E-01	6.8
4.5	4.62	8.00E-01	5.77

(c)

Velocities m s^{-1}	Ke(mg cm^{-2} h^{-1})	Kc(mg cm^{-2} h^{-1})	Ke /Kc
2.5	1.1	5.91E-01	1.8
3.5	2.7	5.41E-01	5
4.5	3.8	8.23E-01	4.65

Tables.3.44: Erosion-corrosion mechanism maps for carbon steel in crude oil at 0mV and particle size 150-300μm (a) 15° (b) 45° (c) 90°.

(a)

Velocities m s^{-1}	Ke(mg cm^{-2} h^{-1})	Kc(mg cm^{-2} h^{-1})	Ke /Kc
2.5	1.5	3.95E-01	3.7
3.5	3.2	5.32E-01	6
4.5	4.7	8.53E-01	5.45

(b)

Velocities m s^{-1}	Ke(mg cm^{-2} h^{-1})	Kc(mg cm^{-2} h^{-1})	Ke /Kc
2.5	1.77	3.40E-01	5.20
3.5	3.41	4.40E-01	7.8
4.5	4.86	8.91E-01	5.45

(c)

Velocities m s^{-1}	Ke(mg cm^{-2} h^{-1})	Kc(mg cm^{-2} h^{-1})	Ke /Kc
2.5	1.44	4.10E-01	3.51
3.5	2.9	6.00E-01	4.83
4.5	4.3	8.68E-01	4.99

Tables.3.45: Erosion-corrosion mechanism maps for carbon steel in crude oil at 400mV and particle size 150-300µm (a) 15° (b) 45° (c) 90°.

(a)

Velocities m s^{-1}	Ke(mg cm^{-2} h^{-1})	Kc(mg cm^{-2} h^{-1})	Ke /Kc
2.5	1.6	4.24E-01	3.66
3.5	3.2	6.12E-01	5.27
4.5	4.6	9.00E-01	5.06

(b)

Velocities m s^{-1}	Ke(mg cm^{-2} h^{-1})	Kc(mg cm^{-2} h^{-1})	Ke /Kc
2.5	1.95	3.57E-01	5.45
3.5	3.43	5.70E-01	6
4.5	4.9	1.00E+01	4.9

(c)

Velocities m s^{-1}	Ke(mg cm^{-2} h^{-1})	Kc(mg cm^{-2} h^{-1})	Ke /Kc
2.5	1.73	4.70E-01	3.68
3.5	3.17	6.30E-01	5.03
4.5	4.2	1.00E+01	3.5

Tables.3.46: Erosion-corrosion mechanism maps for carbon steel in oil /20% water at -400mV and particle size 150-300µm (a) 15° (b) 45° (c) 90°

(a)

Velocities m s^{-1}	Ke(mg cm^{-2} h^{-1})	Kc(mg cm^{-2} h^{-1})	Ke /Kc
2.5	1.2	1.11E+00	1.07
3.5	1.6	2.46E+00	0.63
4.5	2.53	3.37E+00	0.75

(b)

Velocities m s^{-1}	Ke(mg cm^{-2} h^{-1})	Kc(mg cm^{-2} h^{-1})	Ke /Kc
2.5	1.3	1.21E+00	1.06
3.5	1.3	2.95E+00	0.43
4.5	2.4	3.60E+00	0.66

(c)

Velocities m s^{-1}	Ke(mg cm^{-2} h^{-1})	Kc(mg cm^{-2} h^{-1})	Ke /Kc
2.5	1.4	1.03E+00	1.36
3.5	1.7	2.26E+00	0.76
4.5	1.98	3.52E+00	0.56

Tables.3.47: Erosion-corrosion mechanism maps for carbon steel in oil /20% water at 0mV and particle size 150-300µm (a) 15° (b) 45° (c) 90°

(a)

Velocities m s^{-1}	Ke(mg cm^{-2} h^{-1})	Kc(mg cm^{-2} h^{-1})	Ke /Kc
2.5	1.1	1.51E+00	0.72
3.5	1.3	2.97E+00	0.45
4.5	2.4	4.00E+00	0.6

(b)

Velocities m s^{-1}	Ke(mg cm^{-2} h^{-1})	Kc(mg cm^{-2} h^{-1})	Ke /Kc
2.5	0.9	1.75E+00	0.54
3.5	1.46	3.00E+00	0.48
4.5	2.05	4.45E+00	0.46

(c)

Velocities m s^{-1}	Ke(mg cm^{-2} h^{-1})	Kc(mg cm^{-2} h^{-1})	Ke /Kc
2.5	0.8	1.65E+00	0.51
3.5	1.149	2.85E+00	0.40
4.5	1.9	4.30E+00	0.44

Tables.3.48: Erosion-corrosion mechanism maps for carbon steel in oil /20% water at 400mV and particle size 150-300µm (a) 15° (b) 45° (c) 90°

(a)

Velocities m s^{-1}	Ke(mg cm^{-2} h^{-1})	Kc(mg cm^{-2} h^{-1})	Ke /Kc
2.5	0.98	1.77E+00	0.55
3.5	1.7	3.02E+00	0.57
4.5	2.42	4.23E+00	0.57

(b)

Velocities m s^{-1}	Ke(mg cm^{-2} h^{-1})	Kc(mg cm^{-2} h^{-1})	Ke /Kc
2.5	1.6	1.85E+00	0.84
3.5	1.48	3.32E+00	0.45
4.5	2.23	4.55E+00	0.49

(c)

Velocities m s^{-1}	Ke(mg cm^{-2} h^{-1})	Kc(mg cm^{-2} h^{-1})	Ke /Kc
2.5	0.8	1.83E+00	0.45
3.5	1.54	2.94E+00	0.53
4.5	2.1	4.42E+00	0.47

Tables.3.49: Erosion-corrosion additive -synergism maps for carbon steel in water at -400mV and particle size600-710µm (a) 15° (b) 30° (c) 45° (d) 60° (e) 75° (f) 90°

(a)

Velocities m s^{-1}	Δke(mg cm^{-2} h^{-1})	Δkc(mg cm^{-2} h^{-1})	Δke/Δkc
2.5	0.9	-0.214	-4.16
3.5	-0.6	1.1	-0.55
4.5	-0.01	1.22	-0.01

(b)

Velocities m s^{-1}	Δke(mg cm^{-2} h^{-1})	Δkc(mg cm^{-2} h^{-1})	Δke/Δkc
2.5	0.9	-0.37	-2.43
3.5	-0.06	0.8	-0.08
4.5	-0.11	1.11	-0.10

(c)

Velocities m s^{-1}	Δke(mg cm^{-2} h^{-1})	Δkc(mg cm^{-2} h^{-1})	Δke/Δkc
2.5	-0.11	0.16	-0.7
3.5	-0.8	0.22	-3.5
4.5	0.6	-0.29	-2

(d)

Velocities m s^{-1}	Δke(mg cm^{-2} h^{-1})	Δkc(mg cm^{-2} h^{-1})	Δke/Δkc
2.5	0.8	0.03	25.33
3.5	0.6	0.5	1.2
4.5	0.2	0.59	0.34

(e)

Velocities m s^{-1}	Δke(mg cm^{-2} h^{-1})	Δkc(mg cm^{-2} h^{-1})	Δke/Δkc
2.5	0.86	-0.22	-3.91
3.5	-1.17	1.32	-0.89
4.5	0.7	0.71	0.99

(f)

Velocities m s^{-1}	Δke(mg cm^{-2} h^{-1})	Δkc(mg cm^{-2} h^{-1})	Δke/Δkc
2.5	0.9	-0.2	-4.5
3.5	-0.3	0.21	-1.43
4.5	1.8	-0.07	-25.57

Tables.3.50:Erosion-corrosion additive -synergism maps for carbon steel in water at -200mV and particle size 600-710µm (a) 15° (b) 30° (c) 45° (d) 60° (e) 75° (f) 90°

(a)

Velocities m s^{-1}	Δke(mg cm^{-2} h^{-1})	Δkc(mg cm^{-2} h^{-1})	Δke/Δkc
2.5	0.75	-0.14	-5.36
3.5	-0.23	0.73	-0.32
4.5	-0.61	1.23	-0.50

(b)

Velocities m s^{-1}	Δke(mg cm^{-2} h^{-1})	Δkc(mg cm^{-2} h^{-1})	Δke/Δkc
2.5	0.99	0.04	24.75
3.5	0.24	-0.29	-0.83
4.5	1.9	-0.81	-2.35

(c)

Velocities m s^{-1}	Δke(mg cm^{-2} h^{-1})	Δkc(mg cm^{-2} h^{-1})	Δke/Δkc
2.5	-0.33	0.53	-0.62
3.5	-1.31	0.99	-1.32
4.5	0.27	0.12	2.25

(d)

Velocities m s^{-1}	Δke(mg cm^{-2} h^{-1})	Δkc(mg cm^{-2} h^{-1})	Δke/Δkc
2.5	0.49	-0.18	-2.72
3.5	0.4	0.75	0.53
4.5	1.55	1.09	1.42

(e)

Velocities m s^{-1}	Δke(mg cm^{-2} h^{-1})	Δkc(mg cm^{-2} h^{-1})	Δke/Δkc
2.5	0.47	0.09	5.22
3.5	-0.11	0.51	-0.22
4.5	1.15	0.99	1.16

(f)

Velocities m s^{-1}	Δke(mg cm^{-2} h^{-1})	Δkc(mg cm^{-2} h^{-1})	Δke/Δkc
2.5	0.3	0.28	1.07
3.5	-0.23	0.48	-0.48
4.5	2.58	-0.54	-4.78

Tables.3.51: Erosion-corrosion additive -synergism maps for carbon steel in water at 0mV and particle size 600-710µm (a) 15° (b) 30° (c) 45°(d) 60° (e) 75° (f) 90°

(a)

Velocities m s^{-1}	Δke(mg cm^{-2} h^{-1})	Δkc(mg cm^{-2} h^{-1})	Δke/Δkc
2.5	0.88	-0.16	-5.5
3.5	-0.35	0.86	-0.41
4.5	0.82	1.1	0.75

(b)

Velocities m s^{-1}	Δke(mg cm^{-2} h^{-1})	Δkc(mg cm^{-2} h^{-1})	Δke/Δkc
2.5	0.78	-0.18	-4.33
3.5	0.55	0.17	3.24
4.5	2.78	-0.22	-12.64

(c)

Velocities m s^{-1}	Δke(mg cm^{-2} h^{-1})	Δkc(mg cm^{-2} h^{-1})	Δke/Δkc
2.5	-0.8	1.47	-0.54
3.5	-1.21	0.23	-5.26
4.5	1.61	0.25	6.44

(d)

Velocities m s^{-1}	Δke(mg cm^{-2} h^{-1})	Δkc(mg cm^{-2} h^{-1})	Δke/Δkc
2.5	-0.15	0.08	-1.875
3.5	0.9	0.82	1.09
4.5	1.61	0.25	6.44

(e)

Velocities m s^{-1}	Δke(mg cm^{-2} h^{-1})	Δkc(mg cm^{-2} h^{-1})	Δke/Δkc
2.5	1.06	-0.24	-4.42
3.5	1.1	-0.6	-1.83
4.5	1.81	1.24	1.46

(f)

Velocities m s^{-1}	Δke(mg cm^{-2} h^{-1})	Δkc(mg cm^{-2} h^{-1})	Δke/Δkc
2.5	-0.03	0.48	-0.06
3.5	0.28	0.99	0.28
4.5	0.57	0.83	0.67

Tables.3.52: Erosion-corrosion additive -synergism maps for carbon steel in water at 200mV and particle size600-710µm (a) 15° (b) 30° (c) 45°(d) 60° (e) 75° (f) 90°

(a)

Velocities m s^{-1}	Δke(mg cm^{-2} h^{-1})	Δkc(mg cm^{-2} h^{-1})	Δke/Δkc
2.5	0.73	-0.05	-14.6
3.5	-0.27	0.87	-0.31
4.5	1.76	0.26	6.769

(b)

Velocities m s^{-1}	Δke(mg cm^{-2} h^{-1})	Δkc(mg cm^{-2} h^{-1})	Δke/Δkc
2.5	0.96	-0.16	-6
3.5	1.53	0.6	2.55
4.5	2.53	-0.2	-12.65

(c)

Velocities m s^{-1}	Δke(mg cm^{-2} h^{-1})	Δkc(mg cm^{-2} h^{-1})	Δke/Δkc
2.5	0.08	0.08	1
3.5	0.68	0.02	34
4.5	1.84	0.28	6.57

(d)

Velocities m s^{-1}	Δke(mg cm^{-2} h^{-1})	Δkc(mg cm^{-2} h^{-1})	Δke/Δkc
2.5	0.1	0.63	0.15
3.5	1.03	0.41	2.51
4.5	1.78	0.39	4.56

(e)

Velocities m s^{-1}	Δke(mg cm^{-2} h^{-1})	Δkc(mg cm^{-2} h^{-1})	Δke/Δkc
2.5	1.16	-0.96	-1.20
3.5	1.1	0.7	1.57
4.5	2.22	1.04	2.13

(f)

Velocities m s^{-1}	Δke(mg cm^{-2} h^{-1})	Δkc(mg cm^{-2} h^{-1})	Δke/Δkc
2.5	-0.38	0.5	-0.76
3.5	0.3	1.61	0.186
4.5	1.29	0.63	2.05

Tables.3.53: Erosion-corrosion additive -synergism maps for carbon steel in water at 400mV and particle size 600-710µm (a) 15° (b) 30° (c) 45° (d) 60° (e) 75° (f) 90°

(a)

Velocities m s^{-1}	Δke(mg cm^{-2} h^{-1})	Δkc(mg cm^{-2} h^{-1})	Δke/Δkc
2.5	0.74	-0.07	-10.57
3.5	1.49	0.51	2.92
4.5	2.25	0.12	18.75

(b)

Velocities m s^{-1}	Δke(mg cm^{-2} h^{-1})	Δkc(mg cm^{-2} h^{-1})	Δke/Δkc
2.5	0.56	0.04	14
3.5	1.7	0.75	2.27
4.5	2.64	-0.12	-22

(c)

Velocities m s^{-1}	Δke(mg cm^{-2} h^{-1})	Δkc(mg cm^{-2} h^{-1})	Δke/Δkc
2.5	0.34	0.31	1.09
3.5	0.69	-0.49	-1.41
4.5	2.21	0.84	2.63

(d)

Velocities m s^{-1}	Δke(mg cm^{-2} h^{-1})	Δkc(mg cm^{-2} h^{-1})	Δke/Δkc
2.5	1.17	-0.47	-2.49
3.5	0.99	0.91	1.09
4.5	2.95	0.11	26.82

(e)

Velocities m s^{-1}	Δke(mg cm^{-2} h^{-1})	Δkc(mg cm^{-2} h^{-1})	Δke/Δkc
2.5	-0.39	0.32	-1.22
3.5	1.29	0.05	25.8
4.5	0.86	1.74	0.49

(f)

Velocities m s^{-1}	Δke(mg cm^{-2} h^{-1})	Δkc(mg cm^{-2} h^{-1})	Δke/Δkc
2.5	-0.12	0.1	-1.2
3.5	-0.09	1.49	-0.06
4.5	1.39	1.03	1.35

Tables.3.54: Erosion-corrosion additive -synergism maps for carbon steel in crude oil at -400mV and particle size600-710µm (a) 15° (b) 30° (c) 45° (d) 60° (e) 75° (f) 90°

(a)

Velocities m s^{-1}	Δke(mg cm^{-2} h^{-1})	Δkc(mg cm^{-2} h^{-1})	Δke/Δkc
2.5	0.5	1.10E-02	45.35
3.5	2.3	-2.60E-03	-869.7
4.5	3.87	1.00E-03	3871.2

(b)

Velocities m s^{-1}	Δke(mg cm^{-2} h^{-1})	Δkc(mg cm^{-2} h^{-1})	Δke/Δkc
2.5	0.8	1.00E-02	787.8
3.5	2.2	5.10E-03	426.
4.5	3.2	2.60E-03	1222

(c)

Velocities m s^{-1}	Δke(mg cm^{-2} h^{-1})	Δkc(mg cm^{-2} h^{-1})	Δke/Δkc
2.5	0.1	-4.00E-03	-24.95
3.5	2.1	2.00E-04	1040
4.5	4	-4.60E-03	-846.7

(d)

Velocities m s^{-1}	Δke(mg cm^{-2} h^{-1})	Δkc(mg cm^{-2} h^{-1})	Δke/Δkc
2.5	1.1	4.30E-03	251.5
3.5	2.2	-1.20E-03	-1821.42
4.5	3.8	-1.30E-03	-2898.5

(e)

Velocities m s^{-1}	Δke(mg cm^{-2} h^{-1})	Δkc(mg cm^{-2} h^{-1})	Δke/Δkc
2.5	1.1	4.00E-03	270
3.5	2.8	-1.00E-03	-2841
4.5	4.7	-1.50E-03	-3113

(f)

Velocities m s^{-1}	Δke(mg cm^{-2} h^{-1})	Δkc(mg cm^{-2} h^{-1})	Δke/Δkc
2.5	0.4	-1.70E-03	-231
3.5	2.7	4.70E-03	575
4.5	3.9	6.90E-03	571

Tables.3.55: Erosion-corrosion additive -synergism maps for carbon steel in crude oil at -200mV and particle size600-710μm (a) 15° (b) 30° (c) 45° (d) 60° (e) 75° (f) 90°

(a)

Velocities m s^{-1}	Δke(mg cm^{-2} h^{-1})	Δkc(mg cm^{-2} h^{-1})	Δke/Δkc
2.5	0.6	2.20E-03	274.4
3.5	2.8	-2.20E-03	-1272.3
4.5	3.6	5.00E-03	728.4

(b)

Velocities m s^{-1}	Δke(mg cm^{-2} h^{-1})	Δkc(mg cm^{-2} h^{-1})	Δke/Δkc
2.5	1.2	2.40E-03	493.1
3.5	2.4	4.10E-03	578
4.5	3.97	-5.00E-04	-7931.8

(c)

Velocities m s^{-1}	Δke(mg cm^{-2} h^{-1})	Δkc(mg cm^{-2} h^{-1})	Δke/Δkc
2.5	0.8	-5.00E-04	-1570.6
3.5	2.2	3.40E-03	640.6
4.5	3.8	-5.00E-04	-7580.4

(d)

Velocities m s^{-1}	Δke(mg cm^{-2} h^{-1})	Δkc(mg cm^{-2} h^{-1})	Δke/Δkc
2.5	1.8	5.20E-03	342.4
3.5	2.7	5.00E-04	5349.4
4.5	3.9	6.00E-04	6546.8

(e)

Velocities m s^{-1}	Δke(mg cm^{-2} h^{-1})	Δkc(mg cm^{-2} h^{-1})	Δke/Δkc
2.5	2.1	5.20E-03	407.5
3.5	2.98	-5.80E-03	-513.8
4.5	4.7	2.00E-04	23576

(f)

Velocities m s^{-1}	Δke(mg cm^{-2} h^{-1})	Δkc(mg cm^{-2} h^{-1})	Δke/Δkc
2.5	1.4	7.00E-04	2043.3
3.5	2.9	4.90E-03	596.5
4.5	4.6	7.40E-03	616.2

Tables.3.56: Erosion-corrosion additive -synergism maps for carbon steel in crude oil at 0mV and particle size 600-710µm (a) 15° (b) 30° (c) 45°(d) 60° (e) 75° (f) 90°

(a)

Velocities m s^{-1}	Δke(mg cm^{-2} h^{-1})	Δkc(mg cm^{-2} h^{-1})	Δke/Δkc
2.5	1.4	-6.00E-04	-2337.5
3.5	2.8	5.80E-03	478.3
4.5	4.4	1.80E-03	2420.7

(b)

Velocities m s^{-1}	Δke(mg cm^{-2} h^{-1})	Δkc(mg cm^{-2} h^{-1})	Δke/Δkc
2.5	1.9	2.00E-03	951.5
3.5	2.7	-2.00E-04	-13365
4.5	4.44	5.00E-03	887.98

(c)

Velocities m s^{-1}	Δke(mg cm^{-2} h^{-1})	Δkc(mg cm^{-2} h^{-1})	Δke/Δkc
2.5	1.2	-6.00E-04	-2043.5
3.5	2.58	-1.10E-03	-2347.18
4.5	4.22	-4.60E-03	-917.2

(d)

Velocities m s^{-1}	Δke(mg cm^{-2} h^{-1})	Δkc(mg cm^{-2} h^{-1})	Δke/Δkc
2.5	2.4	4.60E-03	517.6
3.5	2.87	1.00E-04	28739
4.5	4.06	-3.20E-03	-1269

(e)

Velocities m s^{-1}	Δke(mg cm^{-2} h^{-1})	Δkc(mg cm^{-2} h^{-1})	Δke/Δkc
2.5	2.2	4.60E-03	482.65
3.5	3	8.00E-04	3740.5
4.5	4.4	3.80E-03	1147.7

(f)

Velocities m s^{-1}	Δke(mg cm^{-2} h^{-1})	Δkc(mg cm^{-2} h^{-1})	Δke/Δkc
2.5	1.7	5.00E-04	3360
3.5	3.1	6.90E-03	453.8
4.5	4.2	1.04E-02	404.3

Tables.3.57: Erosion-corrosion additive -synergism maps for carbon steel in crude oil at 200mV and particle size 600-710µm (a) 15° (b) 30° (c) 45° (d) 60° (e) 75° (f) 90°

(a)

Velocities m s^{-1}	Δke(mg cm^{-2} h^{-1})	Δkc(mg cm^{-2} h^{-1})	Δke/Δkc
2.5	1.8	5.00E-04	3561.2
3.5	3.3	2.00E-03	1636.95
4.5	4.8	7.00E-03	689.3

(b)

Velocities m s^{-1}	Δke(mg cm^{-2} h^{-1})	Δkc(mg cm^{-2} h^{-1})	Δke/Δkc
2.5	2.3	-1.20E-03	-1904.25
3.5	3.37	-3.00E-04	-11240.7
4.5	4.9	-1.00E-03	-4940.9

(c)

Velocities m s^{-1}	Δke(mg cm^{-2} h^{-1})	Δkc(mg cm^{-2} h^{-1})	Δke/Δkc
2.5	1.6	-4.00E-04	-4112.3
3.5	3.5	-4.00E-04	-8627
4.5	4.5	-1.60E-03	-2840.12

(d)

Velocities m s^{-1}	Δke(mg cm^{-2} h^{-1})	Δkc(mg cm^{-2} h^{-1})	Δke/Δkc
2.5	2.1	5.80E-03	362.1
3.5	2.98	-5.90E-03	-505.1
4.5	4.2	-2.00E-04	-20995.5

(e)

Velocities m s^{-1}	Δke(mg cm^{-2} h^{-1})	Δkc(mg cm^{-2} h^{-1})	Δke/Δkc
2.5	2.6	7.10E-03	360.1
3.5	3.2	1.06E-02	305.9
4.5	4.7	-3.20E-03	-1456.9

(f)

Velocities m s^{-1}	Δke(mg cm^{-2} h^{-1})	Δkc(mg cm^{-2} h^{-1})	Δke/Δkc
2.5	2.3	5.20E-03	437.7
3.5	3.7	7.10E-03	521.1
4.5	4.8	9.10E-03	522.2

Tables.3.58: Erosion-corrosion additive -synergism maps for carbon steel in crude oil at 400mV and particle size 600-710µm (a) 15° (b) 30° (c) 45° (d) 60° (e) 75° (f) 90°

(a)

Velocities m s^{-1}	Δke(mg cm^{-2} h^{-1})	Δkc(mg cm^{-2} h^{-1})	Δke/Δkc
2.5	1.8	2.90E-03	613.3
3.5	4.7	5.00E-04	9348.4
4.5	4.5	-2.00E-04	-22361

(b)

Velocities m s^{-1}	Δke(mg cm^{-2} h^{-1})	Δkc(mg cm^{-2} h^{-1})	Δke/Δkc
2.5	2.3	-1.90E-03	-1202.53
3.5	4.6	1.60E-03	2855.75
4.5	5	4.00E-03	1238.7

(c)

Velocities m s^{-1}	Δke(mg cm^{-2} h^{-1})	Δkc(mg cm^{-2} h^{-1})	Δke/Δkc
2.5	1.7	-1.30E-03	-1265.54
3.5	3.8	5.00E-04	7559.6
4.5	5.2	8.00E-04	6512.5

(d)

Velocities m s^{-1}	Δke(mg cm^{-2} h^{-1})	Δkc(mg cm^{-2} h^{-1})	Δke/Δkc
2.5	2.1	-1.10E-03	-1906.3
3.5	2.98	-4.30E-03	-692.6
4.5	5.2	1.21E-02	425.5

(e)

Velocities m s^{-1}	Δke(mg cm^{-2} h^{-1})	Δkc(mg cm^{-2} h^{-1})	Δke/Δkc
2.5	2.556	6.80E-03	375.9
3.5	4.1204	1.80E-03	2289.1
4.5	5.5482	-2.00E-04	-27741

(f)

Velocities m s^{-1}	Δke(mg cm^{-2} h^{-1})	Δkc(mg cm^{-2} h^{-1})	Δke/Δkc
2.5	2.3	7.00E-03	324.8
3.5	4.4	7.80E-03	566.4
4.5	4.98	1.01E-02	492.9

Tables.3.59:Erosion-corrosion additive -synergism maps for carbon steel in oil /20% water at -400mV and particle size 600-710µm (a) 15° (b) 30° (c) 45° (d) 60° (e) 75° (f) 90°

(a)

Velocities m s^{-1}	Δke(mg cm^{-2} h^{-1})	Δkc(mg cm^{-2} h^{-1})	Δke/Δkc
2.5	0.33	-0.12	-2.75
3.5	1.86	-0.1	-26.6
4.5	2.85	-0.1	-57

(b)

Velocities m s^{-1}	Δke(mg cm^{-2} h^{-1})	Δkc(mg cm^{-2} h^{-1})	Δke/Δkc
2.5	0.72	0.22	3.3
3.5	1.91	0.21	9.1
4.5	3.07	-0.11	-27.90

(c)

Velocities m s^{-1}	Δke(mg cm^{-2} h^{-1})	Δkc(mg cm^{-2} h^{-1})	Δke/Δkc
2.5	0.26	0.22	1.18
3.5	2.8	0.15	18.67
4.5	3.46	0.14	24.71

(d)

Velocities m s^{-1}	Δke(mg cm^{-2} h^{-1})	Δkc(mg cm^{-2} h^{-1})	Δke/Δkc
2.5	1.42	-0.13	-10.92
3.5	2.42	0.33	7.33
4.5	2.92	-0.1	-29.2

(e)

Velocities m s^{-1}	Δke(mg cm^{-2} h^{-1})	Δkc(mg cm^{-2} h^{-1})	Δke/Δkc
2.5	0.94	0.43	2.19
3.5	2.35	0.3	7.83
4.5	4.3	-0.1	-53.75

(f)

Velocities m s^{-1}	Δke(mg cm^{-2} h^{-1})	Δkc(mg cm^{-2} h^{-1})	Δke/Δkc
2.5	0.5	0.2	2.09
3.5	2.95	0.3	9.22
4.5	3.55	0.3	14.2

Tables.3.60: Erosion-corrosion additive -synergism maps for carbon steel in oil /20% water at -200mV and particle size600-710µm (a) 15° (b) 30° (c) 45° (d) 60° (e) 75° (f) 90°

(a)

Velocities m s^{-1}	Δke(mg cm^{-2} h^{-1})	Δkc(mg cm^{-2} h^{-1})	Δke/Δkc
2.5	0.358	-0.04	-9.42
3.5	2.72	0.11	24.7
4.5	3.1	0.2	15.5

(b)

Velocities m s^{-1}	Δke(mg cm^{-2} h^{-1})	Δkc(mg cm^{-2} h^{-1})	Δke/Δkc
2.5	1.209	0.17	7.07
3.5	2.76	0.3	9.52
4.5	3.98	0.2	20.20

(c)

Velocities m s^{-1}	Δke(mg cm^{-2} h^{-1})	Δkc(mg cm^{-2} h^{-1})	Δke/Δkc
2.5	0.596	-0.03	-22.92
3.5	2.9	0.12	24.17
4.5	3.5	0.3	11.67

(d)

Velocities m s^{-1}	Δke(mg cm^{-2} h^{-1})	Δkc(mg cm^{-2} h^{-1})	Δke/Δkc
2.5	1.439	-0.1	-20.86
3.5	2.98	0.4	7.27
4.5	3.61	-0.2	-16.41

(e)

Velocities m s^{-1}	Δke(mg cm^{-2} h^{-1})	Δkc(mg cm^{-2} h^{-1})	Δke/Δkc
2.5	1.59	0.19	8.37
3.5	2.96	0.09	32.89
4.5	4.46	0.3	14.87

(f)

Velocities m s^{-1}	Δke(mg cm^{-2} h^{-1})	Δkc(mg cm^{-2} h^{-1})	Δke/Δkc
2.5	0.17	0.3	0.57
3.5	3.15	0.02	157.5
4.5	3.9	0.29	13.45

Tables.3.61:Erosion-corrosion additive -synergism maps for carbon steel in oil /20% water at 0mV and particle size 600-710µm (a) 15° (b) 30° (c) 45°(d) 60° (e) 75° (f) 90°

(a)

Velocities m s^{-1}	Δke(mg cm^{-2} h^{-1})	Δkc(mg cm^{-2} h^{-1})	Δke/Δkc
2.5	0.08	-0.1	-1
3.5	2.81	-0.03	-93.67
4.5	3.68	0.2	18.4

(b)

Velocities m s^{-1}	Δke(mg cm^{-2} h^{-1})	Δkc(mg cm^{-2} h^{-1})	Δke/Δkc
2.5	1.51	0.05	30.2
3.5	2.1	0.4	5.83
4.5	4.08	0.2	20.71

(c)

Velocities m s^{-1}	Δke(mg cm^{-2} h^{-1})	Δkc(mg cm^{-2} h^{-1})	Δke/Δkc
2.5	0.94	-0.04	-23.5
3.5	2.8	0.1	28
4.5	4.34	0.2	21.7

(d)

Velocities m s^{-1}	Δke(mg cm^{-2} h^{-1})	Δkc(mg cm^{-2} h^{-1})	Δke/Δkc
2.5	1.68	0.1	24
3.5	2.89	0.4	6.57
4.5	3.89	-0.11	-35.36

(e)

Velocities m s^{-1}	Δke(mg cm^{-2} h^{-1})	Δkc(mg cm^{-2} h^{-1})	Δke/Δkc
2.5	1.08	0.09	12
3.5	2.68	-0.23	-11.65
4.5	4.3	0.1	43

(f)

Velocities m s^{-1}	Δke(mg cm^{-2} h^{-1})	Δkc(mg cm^{-2} h^{-1})	Δke/Δkc
2.5	0.43	-0.02	-21.5
3.5	3.27	0.2	16.35
4.5	3.92	0.3	13.07

Tables.3.62: Erosion-corrosion additive -synergism maps for carbon steel in oil /20% water at 200mV and particle size 600-710µm (a) 15° (b) 30° (c) 45°(d) 60° (e) 75° (f) 90°

(a)

Velocities m s^{-1}	Δke(mg cm^{-2} h^{-1})	Δkc(mg cm^{-2} h^{-1})	Δke/Δkc
2.5	0.12	-0.03	-4
3.5	3.17	0.1	24.38
4.5	3.74	-0.02	-187

(b)

Velocities m s^{-1}	Δke(mg cm^{-2} h^{-1})	Δkc(mg cm^{-2} h^{-1})	Δke/Δkc
2.5	1.15	0.1	8.21
3.5	3.52	-0.2	-16
4.5	4.4	-0.1	-44

(c)

Velocities m s^{-1}	Δke(mg cm^{-2} h^{-1})	Δkc(mg cm^{-2} h^{-1})	Δke/Δkc
2.5	0.99	-0.1	-11
3.5	2.9	0.2	14.5
4.5	4.56	-0.1	-32.57

(d)

Velocities m s^{-1}	Δke(mg cm^{-2} h^{-1})	Δkc(mg cm^{-2} h^{-1})	Δke/Δkc
2.5	1.64	0.1	10.25
3.5	3.22	-0.1	-29.27
4.5	5.78	-0.4	-15.21

(e)

Velocities m s^{-1}	Δke(mg cm^{-2} h^{-1})	Δkc(mg cm^{-2} h^{-1})	Δke/Δkc
2.5	1.4	-0.2	-6.09
3.5	2.9	-0.1	-36.25
4.5	5.27	-0.1	-52.7

(f)

Velocities m s^{-1}	Δke(mg cm^{-2} h^{-1})	Δkc(mg cm^{-2} h^{-1})	Δke/Δkc
2.5	0.57	-0.1	-9.5
3.5	3.13	0.4	7.28
4.5	4.7	0.3	15.67

Tables.3.63: Erosion-corrosion additive -synergism maps for carbon steel in oil /20% water at 400mV and particle size 600-710µm (a) 15° (b) 30° (c) 45°(d) 60° (e) 75° (f) 90°

(a)

Velocities m s^{-1}	Δke(mg cm^{-2} h^{-1})	Δkc(mg cm^{-2} h^{-1})	Δke/Δkc
2.5	-0.09	-0.09	1
3.5	3.71	0.2	18.55
4.5	4.01	-0.1	-40.1

(b)

Vvelocities m s^{-1}	Δke(mg cm^{-2} h^{-1})	Δkc(mg cm^{-2} h^{-1})	Δke/Δkc
2.5	1.48	0.04	37
3.5	3.71	0.1	37.1
4.5	4.67	-0.13	-35.92

(c)

Velocities m s^{-1}	Δke(mg cm^{-2} h^{-1})	Δkc(mg cm^{-2} h^{-1})	Δke/Δkc
2.5	0.2	0.15	1.33
3.5	3	0.46	6.52
4.5	4.22	-0.08	-52.75

(d)

Velocities m s^{-1}	Δke(mg cm^{-2} h^{-1})	Δkc(mg cm^{-2} h^{-1})	Δke/Δkc
2.5	1.02	0.13	7.85
3.5	4.2	-0.1	-42
4.5	4.42	0.2	22.1

(e)

Velocities m s^{-1}	Δke(mg cm^{-2} h^{-1})	Δkc(mg cm^{-2} h^{-1})	Δke/Δkc
2.5	1.21	-0.03	-40.33
3.5	4.02	-0.16	-25.13
4.5	4.82	0.16	30.13

(f)

Velocities m s^{-1}	Δke(mg cm^{-2} h^{-1})	Δkc(mg cm^{-2} h^{-1})	Δke/Δkc
2.5	0.7	0.02	35
3.5	3.75	0.36	10.42
4.5	4.78	-0.11	-43.45

Tables.3.64: Erosion-corrosion additive -synergism maps for carbon steel in water at -400mV and particle size 150-300µm (a) 15° (b) 45° (c) 90°.

(a)

Velocities m s^{-1}	Δke(mg cm^{-2} h^{-1})	Δkc(mg cm^{-2} h^{-1})	Δke/Δkc
2.5	09	0.6	1.59
3.5	0.28	1	0.29
4.5	0.25	1	0.25

(b)

Velocities m s^{-1}	Δke(mg cm^{-2} h^{-1})	Δkc(mg cm^{-2} h^{-1})	Δke/Δkc
2.5	0.69	1	1.25
3.5	0.19	0.4	0.48
4.5	0.3	0.5	0.61

(c)

Velocities m s^{-1}	Δke(mg cm^{-2} h^{-1})	Δkc(mg cm^{-2} h^{-1})	Δke/Δkc
2.5	0.61	0.5	1.24
3.5	0.18	0.4	0.45
4.5	0.1	0.9	0.12

Tables.3.65: Erosion-corrosion additive -synergism maps for carbon steel in water at 0 mV and particle size 150-300μm (a) 15° (b) 45° (c) 90°.

(a)

Velocities m s^{-1}	Δke(mg cm^{-2} h^{-1})	Δkc(mg cm^{-2} h^{-1})	Δke/Δkc
2.5	-0.13	1.8	-0.08
3.5	0.5	0.5	1.17
4.5	-0.7	1.39	-0.53

(b)

Velocities m s^{-1}	Δke(mg cm^{-2} h^{-1})	Δkc(mg cm^{-2} h^{-1})	Δke/Δkc
2.5	-0.2	2.6	-0.08
3.5	-0.27	0.2	-1.43
4.5	0.11	0.5	0.22

(c)

Velocities m s^{-1}	Δke(mg cm^{-2} h^{-1})	Δkc(mg cm^{-2} h^{-1})	Δke/Δkc
2.5	-0.1	1.6	-0.04
3.5	-0.3	0.8	-0.4
4.5	-0.85	1.2	-0.71

Tables.3.66: Erosion-corrosion additive -synergism maps for carbon steel in water at 400mV and particle size 150-300μm (a) 15° (b) 45° (c) 90°.

(a)

Velocities m s^{-1}	Δke(mg cm^{-2} h^{-1})	Δkc(mg cm^{-2} h^{-1})	Δke/Δkc
2.5	-0.14	1.8	-0.08
3.5	1.1	0.2	5.3
4.5	-0.8	1.4	-0.56

(b)

Velocities m s^{-1}	Δke(mg cm^{-2} h^{-1})	Δkc(mg cm^{-2} h^{-1})	Δke/Δkc
2.5	0.61	2.1	0.3
3.5	0.68	0.19	3.6
4.5	0.48	1.41	0.34

(c)

Velocities m s^{-1}	Δke(mg cm^{-2} h^{-1})	Δkc(mg cm^{-2} h^{-1})	Δke/Δkc
2.5	-0.03	1.47	-0.02
3.5	-.32	1.08	-0.296
4.5	-0.5	1.3	-0.38

Tables.3.67: Erosion-corrosion additive -synergism maps for carbon steel in oil at -400mV and particle size 150-300µm (a) 15° (b) 45° (c) 90°.

(a)

Velocities m s^{-1}	Δke(mg cm^{-2} h^{-1})	Δkc(mg cm^{-2} h^{-1})	Δke/Δkc
2.5	0.919	0.22	4.18
3.5	2.27	0.185	12.27
4.5	2.85	0.5	6.04

(b)

Velocities m s^{-1}	Δke(mg cm^{-2} h^{-1})	Δkc(mg cm^{-2} h^{-1})	Δke/Δkc
2.5	0.91	0.2	4.54
3.5	2.6	0.3	8.47
4.5	2.92	0.5	5.82

(c)

Velocities m s^{-1}	Δke(mg cm^{-2} h^{-1})	Δkc(mg cm^{-2} h^{-1})	Δke/Δkc
2.5	0.7	0.4	4.54
3.5	1.95	0.33	5.98
4.5	2.83	0.5	5.89

Tables.3.68: Erosion-corrosion additive -synergism maps for carbon steel in oil at 0mV and particle size 150-300µm (a) 15° (b) 45° (c) 90°.

(a)

Velocities m s^{-1}	Δke(mg cm^{-2} h^{-1})	Δkc(mg cm^{-2} h^{-1})	Δke/Δkc
2.5	0.945	0.20	4.63
3.5	2.438	0.33	7.37
4.5	3.247	0.44	7.33

(b)

Velocities m s^{-1}	Δke(mg cm^{-2} h^{-1})	Δkc(mg cm^{-2} h^{-1})	Δke/Δkc
2.5	1.02	0.195	5.23
3.5	2.57	0.248	10.36
4.5	3.16	0.54	5.89

(c)

Velocities m s^{-1}	Δke(mg cm^{-2} h^{-1})	Δkc(mg cm^{-2} h^{-1})	Δke/Δkc
2.5	1.04	0.22	4.84
3.5	2.14	0.38	5.66
4.5	3.33	0.52	6.46

Tables.3.69: Erosion-corrosion additive -synergism maps for carbon steel in oil at 400mV and particle size 150-300μm (a) 15° (b) 45° (c) 90°.

(a)

Velocities m s^{-1}	Δke(mg cm^{-2} h^{-1})	Δkc(mg cm^{-2} h^{-1})	Δke/Δkc
2.5	1.1	0.24	4.38
3.5	2.45	0.36	6.82
4.5	3.15	0.42	7.5

(b)

Velocities m s^{-1}	Δke(mg cm^{-2} h^{-1})	Δkc(mg cm^{-2} h^{-1})	Δke/Δkc
2.5	1.2	0.24	4.4
3.5	2.6	0.4	7
4.5	3.2	0.608	5.23

(c)

Velocities m s^{-1}	Δke(mg cm^{-2} h^{-1})	Δkc(mg cm^{-2} h^{-1})	Δke/Δkc
2.5	1.33	0.28	4.84
3.5	2.41	0.4	6.23
4.5	3.2	0.78	4.09

Tables.3.70: Erosion-corrosion additive -synergism maps for carbon steel in oil /20% water at -400mV and particle size 150-300µm (a) 15° (b) 45° (c) 90°.

(a)

Velocities m s^{-1}	Δke(mg cm^{-2} h^{-1})	Δkc(mg cm^{-2} h^{-1})	Δke/Δkc
2.5	0.68	0.19	3.55
3.5	0.77	1.55	0.50
4.5	1.13	1.97	0.57

(b)

Velocities m s^{-1}	Δke(mg cm^{-2} h^{-1})	Δkc(mg cm^{-2} h^{-1})	Δke/Δkc
2.5	0.54	0.59	0.91
3.5	0.42	2.20	0.19
4.5	0.7	2.4	0.29

(c)

Velocities m s^{-1}	Δke(mg cm^{-2} h^{-1})	Δkc(mg cm^{-2} h^{-1})	Δke/Δkc
2.5	1	0.36	2.77
3.5	0.96	1.5	0.65
4.5	0.98	2.32	0.42

Tables.3.71: Erosion-corrosion additive -synergism maps for carbon steel in oil /20% water at 0mV and particle size 150-300μm (a) 15° (b) 45° (c) 90°.

(a)

Velocities m s^{-1}	Δke(mg cm^{-2} h^{-1})	Δkc(mg cm^{-2} h^{-1})	Δke/Δkc
2.5	0.58	0.65	0.89
3.5	0.55	2.1	0.27
4.5	1	2.7	0.37

(b)

Velocities m s^{-1}	Δke(mg cm^{-2} h^{-1})	Δkc(mg cm^{-2} h^{-1})	Δke/Δkc
2.5	0.2	0.95	0.21
3.5	0.62	2.1	0.295
4.5	0.35	3.25	0.11

(c)

Velocities m s^{-1}	Δke(mg cm^{-2} h^{-1})	Δkc(mg cm^{-2} h^{-1})	Δke/Δkc
2.5	0.45	0.85	0.53
3.5	0.4	2.1	0.19
4.5	0.9	3	0.3

Tables.3.72: Erosion-corrosion additive -synergism maps for carbon steel in oil /20% water at 400mV and particle size 150-300μm (a) 15° (b) 45° (c) 90°.

(a)

Velocities m s^{-1}	Δke(mg cm^{-2} h^{-1})	Δkc(mg cm^{-2} h^{-1})	Δke/Δkc
2.5	0.47	0.97	0.48
3.5	0.95	2.02	0.47
4.5	1.02	2.2	0.46

(b)

Velocities m s^{-1}	Δke(mg cm^{-2} h^{-1})	Δkc(mg cm^{-2} h^{-1})	Δke/Δkc
2.5	0.8	1.1	0.73
3.5	0.6	2.5	0.26
4.5	0.53	2.78	0.19

(c)

Velocities m s^{-1}	Δke(mg cm^{-2} h^{-1})	Δkc(mg cm^{-2} h^{-1})	Δke/Δkc
2.5	0.42	1.1	0.398
3.5	0.81	2.1	0.39
4.5	1.08	2.42	0.45

Chapter 4

Results and discussion

(Effect of impact angle and electrochemical potential on erosion-corrosion maps for particle sizes 600-710µm and 150-300µm)

4.0. Introduction

In this chapter the carbon steel have been investigated at range of impact angles and applied potentials in water, crude oil and combined environments with different particle sizes (600-710µm and 150-300µm) as erodent particles.The polarization curves have been investigated at constant of impact velocity and at range of impact angles for large particle sizes 600-710µm and a small particle sizes 150-300µm.The total mass loss rate due to erosion –corrosion and erosion contribution and corrosion contribution have been plotted as function of impact angle at range of potentials at constant impact velocity for large particle sizes 600-710µm and a small particle sizes 150-300µm.

The specimens after the test have investigated by SEM to show the effect of particle sizes on the specimens. The results have been used to establish erosion-corrosion mechanism, wastages and additive –synergism maps as function of applied potentials and impact angles at range of constant impact velocities for particle sizes (600-710µm and 150-300µm).

4.1. Effect of impact angle and electrochemical potential on erosion-corrosion maps for particle sizes 600-710µm and various impact velocities

4.1.1. General

Specimens of carbon steel were subjected to a variety of impact angles and applied potentials in three environments containing particles sized between 600-710µm**,** at three impact velocities, 2.5, 3.5 and 4.5 m s^{-1}. The results were used to create maps containing regimes as functions of the erosion–corrosion parameters. Moreover, the wastage regimes and synergism between erosion and corrosion were presented on erosion-corrosion maps. The aims of these maps were to demonstrate material performance in different environments and testing conditions.

4.1.2. The procedure of testing

The dimensions of the specimens were 25mm × 10mm × 4 mm. The area exposed to an impingement jet was 0.19cm^2, whilst the remaining area was covered by a coating in order to ensure that all corrosion measurements were related to the erosion-corrosion process only. Before each test the specimen was dipped in acetone, dried in a stream of hot air then weighed. Moreover, after each test the specimens were dried in stream and re-weighed, and every experiment was repeated at least 2 or 3 times. The average mass losses were reported in the results. The erosion-corrosion was assessed at a room temperature and at six impact angles and applied potentials under three impact velocities. The impact angles were varied at six values, 15°, 30°, 45°, 60°, 75° and 90°, and at three impact velocities, 2.5, 3.5 and 4.5m s^{-1}. Erosion-corrosion tests were achieved at potentials of -400, -200, 0, 200, 400 mV for 30 min.

4.1.3. Polarization curves for particles sizes 600-710µm

Figures 4.1-4.3 show the polarization curve of carbon steel at room temperature in environments containing particles sized between 600-710µm (water, crude oil and 20% water with crude oil) and at three constant impact velocities, 2.5, 3.5 and 4.5 m s^{-1}, under impact angles of 15°, 30°, 45°, 60°, 75° and 90°.

4.1.3.1. At impact velocity of 2.5 m s^{-1}

For carbon steel in the water environment there was general increase in the current density with an increase in impact angle from 30° to 45° Fig.4.1 (a). Conversely, in the crude oil environment Fig. 4.1 (b) the average free corrosion potential (Ecorr) was around -400mV approximately for all impact angles and there was a general decrease in the value of the current density at all impact angles compared with in water environment. In the 20% water with crude oil environment, the average corrosion potential (Ecorr) was between -410 and -415mV approximately for all impact angles and there was some evidence of an increase in current density at all impact angles (Fig. 4.1 (c)).

4.1.3.2. At impact velocity of 3.5 m s^{-1}

The average free corrosion potential for carbon steel in the water environment was -425mV approximately for all impact angles Fig. 4.2 (a). In addition, there was an increase in the anodic current with an increase in impact velocity from 2.5 to 3.5 m s^{-1} at all test conditions. In the crude oil environment (Fig. 4.2 (b)) the corrosion potential (Ecorr) was between -405 and -415 mV at all impact angles and the current density was increased gradually with an increase in impact velocities from 2.5 to 3.5 m s^{-1}.It is clear that, in the 20% water with crude oil environment(Fig. 4.2 (c), the average free corrosion potential for all impact angles was around -420mV approximately and there was a general increase in the current density compared with in crude oil environment.

4.1.3.3. At impact velocity of 4.5 m s^{-1}

In water environment there was an increase in the current density with an increase in impact velocity from 3.5 to 4.5 m s^{-1} at the all test conditions. The peak value of current density was 1.22 m A cm^{-2}, at impact angle75° while the lowest value of current density was about 1 m A cm^{-2} at impact angle 30°. However, in the crude oil environment (Fig. 4.3 (b)) the value of current density was increased slowly with increase in impact angle from 15° to 45°. It is interesting to see that the peak value of current density was 0.009 m A cm^{-2} at impact angle 15° while the lowest value of current density was about 0.002 m A cm^{-2} at impact angle 60°.

In the oil / 20% water environment Fig. 4.3(c), the anodic current density was increased with an increase in velocity from 3.5 m s^{-1} to 4.5 m s^{-1} and the value of current density was different at each impact angle. The peak value of current density was 0.32 m A cm^{-2} at 15° while the lowest value of current density was about 0.096 m A cm^{-2} at 60°.

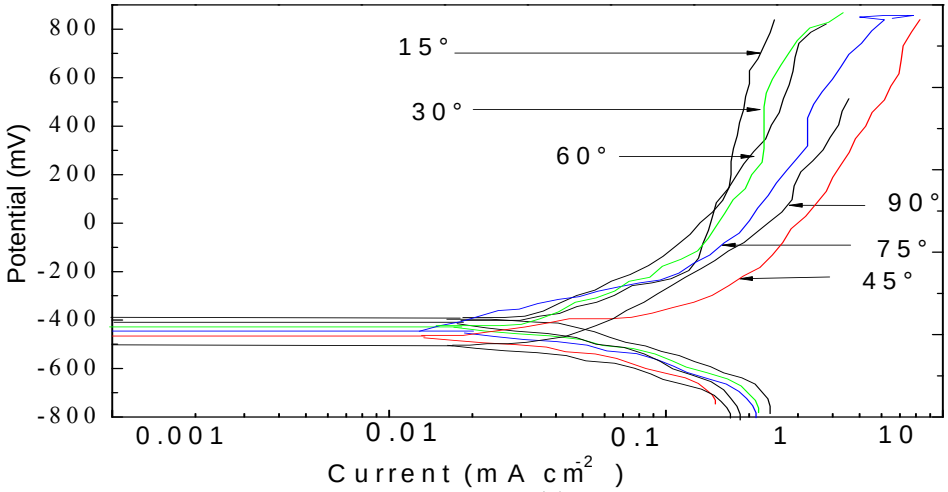

(a)

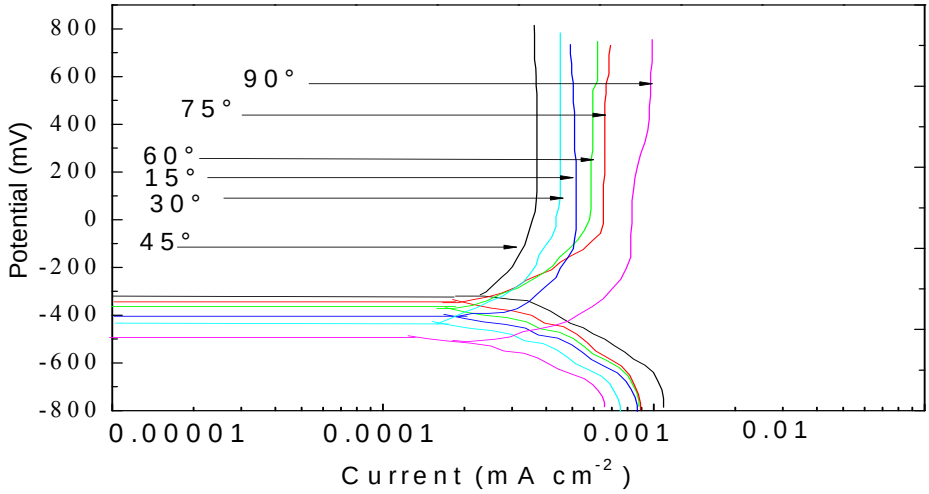

(b)

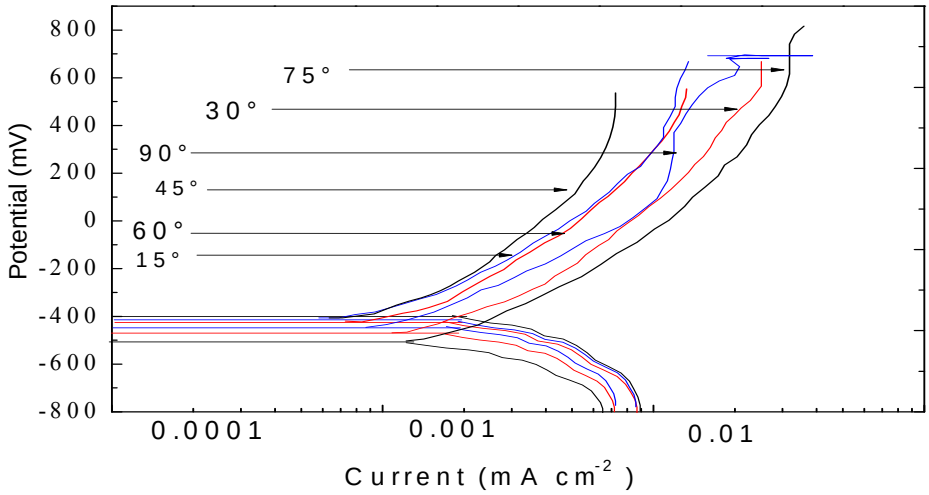

(c)

Fig.4.1: Polarization curves for carbon stee at various impact angles, 2.5 m s^{-1}velocity and particle size 600-710µm in (a) water (b) crude oil (c) oil /20% water.

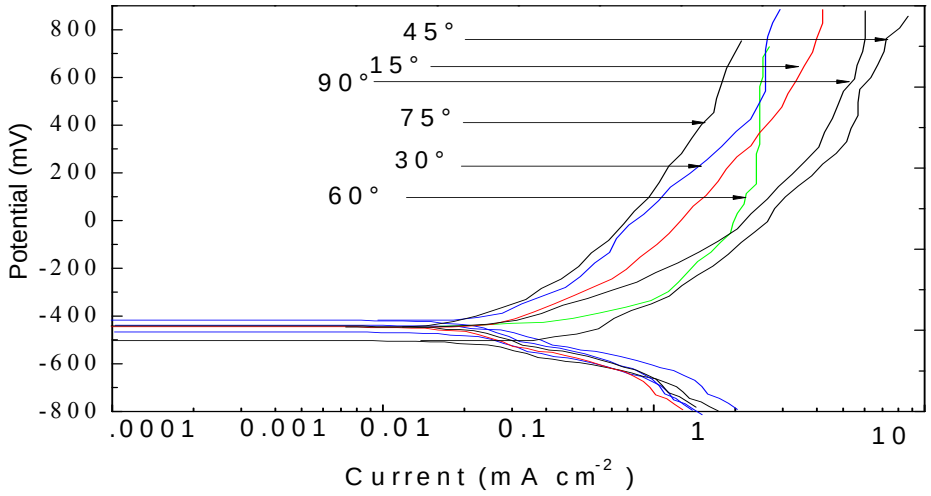

(a)

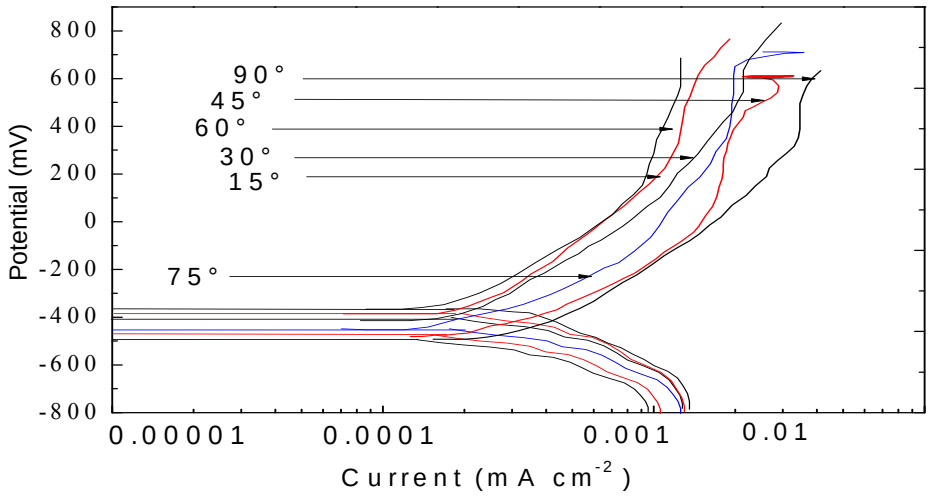

(b)

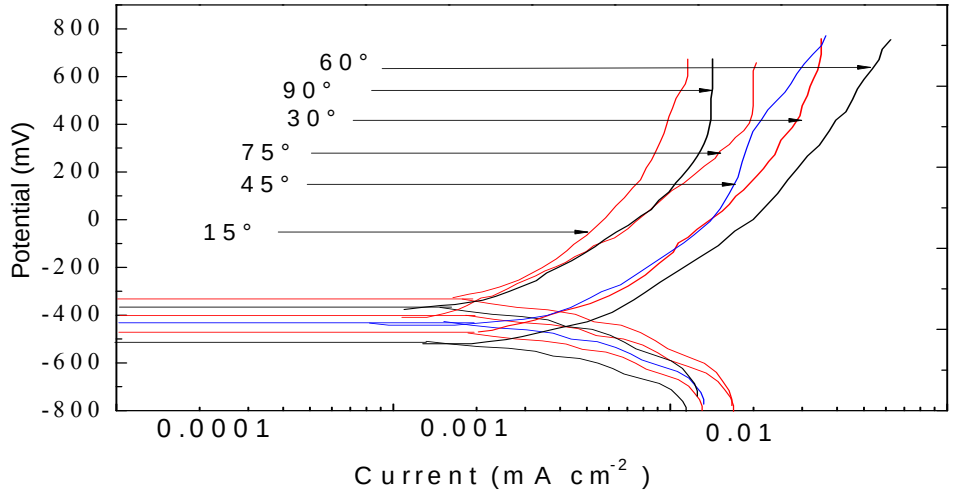

(c)

Fig.4.2: Polarization curves for carbon steel a various impact angles, 3.5 m s^{-1} velocity and particle size 600-710µm in (a) water (b) crude oil (c) oil /20% water.

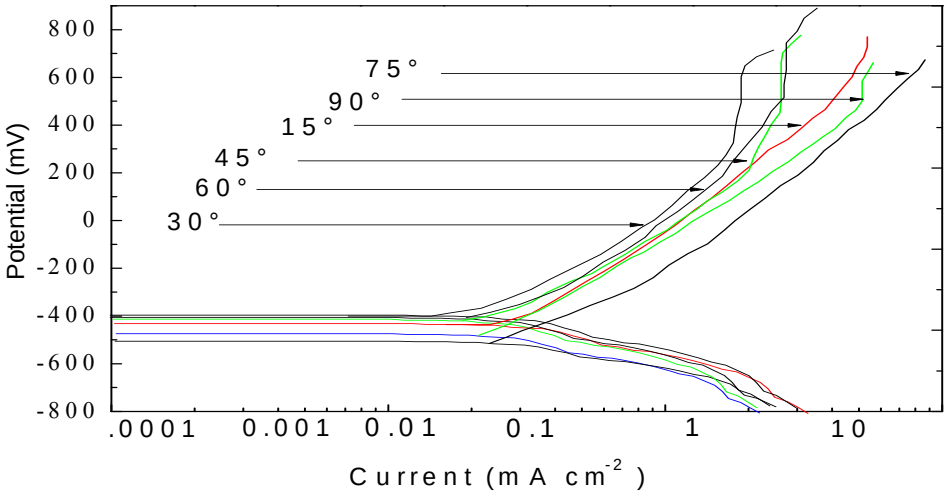

(a)

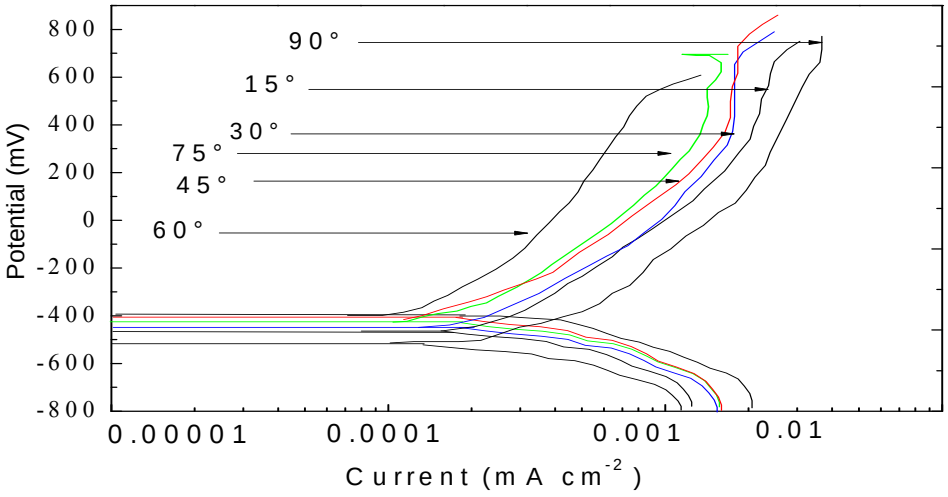

(b)

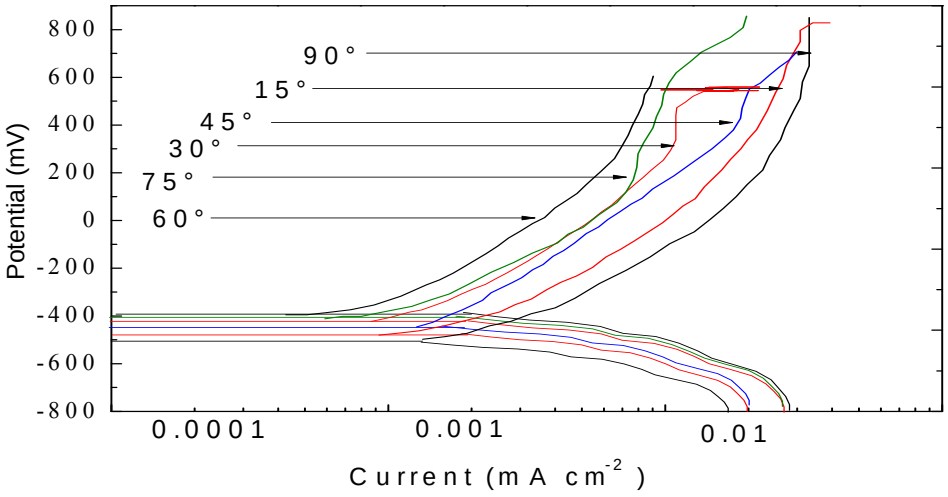

(c)

Fig .4.3: Polarization curves for carbon steel at various impact angles, 4.5 m s^{-1} velocity and particle size 600-710µm in (a) water (b) crude oil (c) oil /20% water.

4.1.4. Mass loss for particles sizes 600-710µm

The total volume loss Kec was recorded at three impact velocities, 2.5, 3.5 and 4.5m s^{-1}. Tables 4.1-4.9 show the results of calculations of the mass loss for Ke, Kc and kec in the environments and at different impact velocities with various impact angles and applied potentials. At a low impact velocity of 2.5 m s^{-1} and applied potential -400mV in the water environment, the value of erosion contribution (Ke) was greater than the value of corrosion contribution at all impact angles (Fig. 4.4 (a)).However, at higher impact velocities of 3.5 m s^{-1} and 4.5 m s^{-1}, the value of corrosion contribution (Kc) increased at higher applied potentials (anodic condition) (Figures 4.7 and 4.10 (c-e)).

Conversely, in crude oil environment the value of corrosion contribution Kc was very small compared with the value of erosion contribution (Ke) Figures 4.5-4.11.However, in mixed environments (oil/20%water) the value of corrosion (Kc)gradually increased with an increase in applied potential and impact velocity (Figures 4.6-4.12) compared with in crude oil. The value of the erosion contribution Ke remained greater than the values of corrosion contribution (Kc) in mixed environments. It is interesting that the total volume loss (Kec) was higher at the high potential of 400 mV and at the high velocity of 4.5 m s^{-1}, which is consistent with the results for small particle sizes150-300µm.

Tables.4.1: Mass loss as function of impact angles for carbon steel at various potentials in reservoir water at 2.5 m s^{-1} and particle size 600-710µm (a) -400mV (b) -200mV (c) 0mV (d) 200mV (e) 400mV

(a)

Impact angle	Ke(mg cm^{-2} h^{-1})	Kc(mg cm^{-2} h^{-1})	Kec(mg cm^{-2} h^{-1})
15°	2.59	1.72	4.31
30°	2.5	1.5	4
45°	2.39	2.21	4.6
60°	2.16	2.04	4.2
75°	1.96	1.93	3.89
90°	2.5	1.71	4.21

(b)

Impact angle	Ke(mg cm^{-2} h^{-1})	Kc(mg cm^{-2} h^{-1})	Kec(mg cm^{-2} h^{-1})
15°	2.45	1.78	4.23
30°	2.59	1.72	4.3
45°	2.17	2.43	4.6
60°	1.89	2.12	4
75°	1.57	2.24	3.8
90°	1.9	2.21	4.1

(c)

Impact angle	Ke(mg cm^{-2} h^{-1})	Kc(mg cm^{-2} h^{-1})	Kec(mg cm^{-2} h^{-1})
15°	2.58	1.82	4.4
30°	2.38	1.83	4.2
45°	1.7	2.71	4.4
60°	1.25	2.25	3.5
75°	2.16	2.46	4.6
90°	1.57	2.73	4.3

(d)

Impact angle	Ke(mg cm^{-2} h^{-1})	Kc(mg cm^{-2} h^{-1})	Kec(mg cm^{-2} h^{-1})
15°	2.43	1.95	4.38
30°	2.56	1.94	4.5
45°	2.58	2.03	4.6
60°	1.5	2.71	4.2
75°	2.26	1.34	3.6
90°	1.22	2.78	4

(e)

Impact angle	Ke(mg cm^{-2} h^{-1})	Kc(mg cm^{-2} h^{-1})	Kec(mg cm^{-2} h^{-1})
15°	2.44	1.97	4.41
30°	2.16	2.07	4.2
45°	3.16	2.16	5.3
60°	2.57	1.93	4.5
75°	0.71	2.74	3.5
90°	1.48	2.53	4

Tables.4.2: Mass loss as function of impact angles for carbon steel at various potentials in crude oil at 2.5 m s^{-1} and particle size 600-710µm (a) -400mV (b) -200mV (c) 0 mV(d) 200mV (e) 400mV

(a)

Impact angle	Ke(mg cm^{-2} h^{-1})	Kc(mg cm^{-2} h^{-1})	Kec(mg cm^{-2} h^{-1})
15°	2	2.11E-02	2.5
30°	2	1.22E-02	2
45°	2	1.02E-02	2.01
60°	2.1	1.85E-02	2.1
75°	2.1	2.02E-02	2.12
90°	2.1	1.81E-02	2.11

(b)

Impact angle	Ke(mg cm^{-2} h^{-1})	Kc(mg cm^{-2} h^{-1})	Kec(mg cm^{-2} h^{-1})
15°	2.584	1.63E-02	2.6
30°	2.4	1.65E-02	2.4
45°	2.7	1.47E-02	2.7
60°	2.8	1.93E-02	2.8
75°	3.14	2.12E-02	3.16
90°	3.13	1.97E-02	3.15

(c)

Impact angle	Ke(mg cm^{-2} h^{-1})	Kc(mg cm^{-2} h^{-1})	Kec(mg cm^{-2} h^{-1})
15°	3.38	1.85E-02	3.401
30°	3.10	1.71E-02	3.12
45°	3.13	1.39E-02	3.14
60°	3.38	1.90E-02	3.4
75°	3.24	1.98E-02	3.26
90°	3.38	2.00E-02	3.4

(d)

Impact angle	Ke(mg cm^{-2} h^{-1})	Kc(mg cm^{-2} h^{-1})	Kec(mg cm^{-2} h^{-1})
15°	3.761	1.94E-02	3.78
30°	3.485	1.49E-02	3.5
45°	3.545	1.51E-02	3.56
60°	3.1	2.00E-02	3.12
75°	3.58	2.33E-02	3.6
90°	3.98	2.42E-02	4

(e)

Impact angle	Ke(mg cm^{-2} h^{-1})	Kc(mg cm^{-2} h^{-1})	Kec(mg cm^{-2} h^{-1})
15°	4.29	2.14E-02	4.31
30°	3.52	1.52E-02	3.53
45°	4.16	1.48E-02	4.2
60°	3.98	2.31E-02	4
75°	3.69	2.40E-02	3.71
90°	4.08	2.65E-02	4.11

Tables.4.3: Mass loss as function of impact angles for carbon steel at various potentials in oil /20% water at 2.5 m s^{-1} and particle size 600-710µm (a) -400mV(b) -200mV (c) 0mV (d) 200mV (e) 400mV

(a)

Impact angle	Ke(mg cm^{-2} h^{-1})	Kc(mg cm^{-2} h^{-1})	Kec(mg cm^{-2} h^{-1})
15°	2.31	0.8	3.11
30°	1.92	0.8	2.7
45°	2.16	0.8	3
60°	2.42	0.78	3.2
75°	1.96	1	2.96
90°	2.18	0.9	3.08

(b)

Impact angle	Ke(mg cm^{-2} h^{-1})	Kc(mg cm^{-2} h^{-1})	Kec(mg cm^{-2} h^{-1})
15°	2.34	0.81	3.15
30°	2.41	0.79	3.2
45°	2.5	0.71	3.21
60°	2.44	0.8	3.24
75°	2.61	0.89	3.5
90°	1.87	0.91	2.78

(c)

Impact angle	Ke(mg cm^{-2} h^{-1})	Kc(mg cm^{-2} h^{-1})	Kec(mg cm^{-2} h^{-1})
15°	2.06	0.78	2.84
30°	2.7	0.8	3.51
45°	2.8	0.76	3.6
60°	2.68	0.82	3.5
75°	2.1	0.9	3
90°	2.13	0.78	2.91

(d)

Impact angle	Ke(mg cm^{-2} h^{-1})	Kc(mg cm^{-2} h^{-1})	Kec(mg cm^{-2} h^{-1})
15°	2.1	0.68	2.78
30°	2.35	0.9	3.25
45°	2.89	0.81	3.7
60°	2.64	0.96	3.6
75°	2.42	0.45	2.87
90°	2.27	0.73	3

(e)

Impact angle	Ke(mg cm^{-2} h^{-1})	Kc(mg cm^{-2} h^{-1})	Kec(mg cm^{-2} h^{-1})
15°	1.89	0.71	2.6
30°	2.68	0.72	3.4
45°	2.1	0.9	3
60°	2.02	0.78	2.8
75°	2.23	0.67	2.9
90°	2.4	0.8	3.2

Tables.4.4: Mass loss as function of impact angles for carbon steel at various potentials in water at 3.5 m s^{-1} and particle size 600-710µm (a) -400mV (b) -200mV (c) 0mV (d) 200mV (e) 400mV

(a)

Impact angle	Ke(mg cm^{-2} h^{-1})	Kc(mg cm^{-2} h^{-1})	Kec(mg cm^{-2} h^{-1})
15°	1.4	4.12	5.52
30°	1.81	4.21	6.02
45°	2.43	4.02	6.45
60°	2.39	3.91	6.3
75°	0.53	5.32	5.85
90°	1.9	4.31	6.21

(b)

Impact angle	Ke(mg cm^{-2} h^{-1})	Kc(mg cm^{-2} h^{-1})	Kec(mg cm^{-2} h^{-1})
15°	1.77	4.21	5.98
30°	2.11	3.91	6.02
45°	1.89	5	6.89
60°	2.2	4.25	6.45
75°	1.59	4.61	6.2
90°	1.97	4.38	6.35

(c)

Impact angle	Ke(mg cm^{-2} h^{-1})	Kc(mg cm^{-2} h^{-1})	Kec(mg cm^{-2} h^{-1})
15°	1.65	4.38	6.03
30°	2.42	3.78	6.2
45°	1.99	5.04	7.03
60°	2.7	4.51	7.21
75°	2.8	4.07	6.87
90°	2.48	5	7.48

(d)

Impact angle	Ke(mg cm^{-2} h^{-1})	Kc(mg cm^{-2} h^{-1})	Kec(mg cm^{-2} h^{-1})
15°	1.73	4.48	6.21
30°	3.4	4.1	7.5
45°	3.88	4.12	8
60°	2.83	5.01	7.84
75°	2.8	4.5	7.3
90°	2.5	5.52	8.02

(e)

Impact angle	Ke(mg cm^{-2} h^{-1})	Kc(mg cm^{-2} h^{-1})	Kec(mg cm^{-2} h^{-1})
15°	3.49	4.51	8
30°	3.57	4.23	7.8
45°	3.89	4.32	8.21
60°	2.79	5.21	8
75°	2.99	4.85	7.84
90°	2.11	5.81	7.92

Tables.4.5: Mass losses as function of impact angles for carbon steel at various potentials in crude oil at 3.5 m s^{-1} and particle size 600-710µm (a) -400mV (b) -200mV (c) 0mV (d) 200mV (e) 400mV

(a)

Impact angle	Ke(mg cm^{-2} h^{-1})	Kc(mg cm^{-2} h^{-1})	Kec(mg cm^{-2} h^{-1})
15°	4.6	1.89E-02	4.58
30°	3.98	2.62E-02	4
45°	4.48	2.00E-02	4.5
60°	4.19	2.43E-02	4.21
75°	4.69	1.92E-02	4.71
90°	4.75	2.62E-02	4.78

(b)

Impact angle	Ke(mg cm^{-2} h^{-1})	Kc(mg cm^{-2} h^{-1})	Kec(mg cm^{-2} h^{-1})
15°	5.1	2.09E-02	5.12
30°	4.17	3.02E-02	4.2
45°	4.58	2.21E-02	4.6
60°	4.68	2.53E-02	4.7
75°	4.83	2.02E-02	4.85
90°	4.97	2.74E-02	5

(c)

Impact angle	Ke(mg cm^{-2} h^{-1})	Kc(mg cm^{-2} h^{-1})	Kec(mg cm^{-2} h^{-1})
15°	5.1	2.59E-02	5.1
30°	4.47	2.70E-02	4.5
45°	4.98	1.81E-02	5
60°	4.87	2.61E-02	4.9
75°	4.84	2.76E-02	4.87
90°	5.18	2.91E-02	5.21

(d)

Impact angle	Ke(mg cm^{-2} h^{-1})	Kc(mg cm^{-2} h^{-1})	Kec(mg cm^{-2} h^{-1})
15°	5.57	2.61E-02	5.6
30°	5.17	2.78E-02	5.2
45°	5.85	1.92E-02	5.87
60°	4.98	1.99E-02	5
75°	5.09	3.76E-02	5.13
90°	5.75	3.01E-02	5.78

(e)

Impact angle	Ke(mg cm^{-2} h^{-1})	Kc(mg cm^{-2} h^{-1})	Kec(mg cm^{-2} h^{-1})
15°	6.97	2.58E-02	7
30°	6.37	3.08E-02	6.4
45°	6.18	2.02E-02	6.2
60°	4.98	2.19E-02	5
75°	5.97	2.96E-02	6
90°	6.47	3.21E-02	6.5

Tables.4.6: Mass loss as function of impact angles for carbon steel at various potentials in oil /20% water at 3.5 m s^{-1} and particle size 600-710µm (a) -400mV (b) -200mV (c) 0mV (d) 200mV (e) 400mV

(a)

Impact angle	Ke(mg cm^{-2} h^{-1})	Kc(mg cm^{-2} h^{-1})	Kec(mg cm^{-2} h^{-1})
15°	4.16	0.84	5
30°	3.71	0.89	4.6
45°	5.2	0.9	6.1
60°	4.42	0.98	5.4
75°	4.2	1	5.2
90°	5	1.1	6.1

(b)

Impact angle	Ke(mg cm^{-2} h^{-1})	Kc(mg cm^{-2} h^{-1})	Kec(mg cm^{-2} h^{-1})
15°	5.02	0.98	6
30°	4.56	1	5.56
45°	5.3	0.9	6.2
60°	4.98	1.12	6.1
75°	4.81	0.89	5.7
90°	5.2	1	6.2

(c)

Impact angle	Ke(mg cm^{-2} h^{-1})	Kc(mg cm^{-2} h^{-1})	Kec(mg cm^{-2} h^{-1})
15°	5.11	0.89	6
30°	3.9	1.2	5.1
45°	5.2	1	6.2
60°	4.89	1.23	6.12
75°	4.53	1	5.53
90°	5.32	0.98	6.3

(d)

Impact angle	Ke(mg cm^{-2} h^{-1})	Kc(mg cm^{-2} h^{-1})	Kec(mg cm^{-2} h^{-1})
15°	5.47	0.93	6.4
30°	5.32	0.98	6.3
45°	5.3	1.2	6.5
60°	5.22	0.78	6
75°	4.75	1.12	5.87
90°	5.18	1.23	6.41

(e)

Impact angle	Ke(mg cm^{-2} h^{-1})	Kc(mg cm^{-2} h^{-1})	Kec(mg cm^{-2} h^{-1})
15°	6.01	1.2	7.21
30°	5.51	1	6.51
45°	5.4	1.3	6.7
60°	6.2	0.8	7
75°	5.87	0.98	6.85
90°	5.8	1.2	7

Tables.4.7: Mass loss as function of impact angles for carbon steel at various potentials in water at 4.5 m s^{-1} and particle size 600-710µm (a) -400mV (b) -200mV (c) 0mV(d) 200mV (e) 400mV

(a)

Impact angle	Ke(mg cm^{-2} h^{-1})	Kc(mg cm^{-2} h^{-1})	Kec(mg cm^{-2} h^{-1})
15°	2.99	5.72	8.71
30°	2.87	5.93	8.8
45°	4.48	4.72	9.2
60°	3.3	5.4	8.7
75°	3	5.94	8.94
90°	4.69	4.78	9.47

(b)

Impact angle	Ke(mg cm^{-2} h^{-1})	Kc(mg cm^{-2} h^{-1})	Kec(mg cm^{-2} h^{-1})
15°	2.39	5.84	8.23
30°	4.88	4.12	9
45°	4.17	5.85	10.02
60°	4.65	5.67	10.32
75°	3.45	5.89	9.34
90°	5.48	4.83	10.31

(c)

Impact angle	Ke(mg cm^{-2} h^{-1})	Kc(mg cm^{-2} h^{-1})	Kec(mg cm^{-2} h^{-1})
15°	3.82	5.91	9.73
30°	5.76	4.45	10.21
45°	5.44	5.01	10.45
60°	4.71	5.56	10.27
75°	4.11	6.21	10.32
90°	3.47	6.03	9.5

(d)

Impact angle	Ke(mg cm^{-2} h^{-1})	Kc(mg cm^{-2} h^{-1})	Kec(mg cm^{-2} h^{-1})
15°	4.76	5.24	10
30°	5.51	4.81	10.32
45°	5.74	5.32	11.06
60°	4.88	5.87	10.75
75°	4.52	6	10.52
90°	4.19	6.13	10.32

(e)

Impact angle	Ke(mg cm^{-2} h^{-1})	Kc(mg cm^{-2} h^{-1})	Kec(mg cm^{-2} h^{-1})
15°	5.25	5.2	10.45
30°	5.62	4.9	10.52
45°	6.11	5.73	11.84
60°	6.05	5.07	11.12
75°	3.16	6.84	10
90°	4.29	6.73	11.02

Table.4.8: Mass loss as function of impact angles for carbon steel at various potentials in crude oil at 4.5 m s^{-1} and particle size 600-710µm (a) -400mV (b) -200mV (c) 0mV(d) 200mV (e) 400mV

(a)

Impact angle	Ke(mg cm^{-2} h^{-1})	Kc(mg cm^{-2} h^{-1})	Kec(mg cm^{-2} h^{-1})
15°	7.47	2.88E-02	7.5
30°	6.18	3.28E-02	6.21
45°	7.1	2.52E-02	7.12
60°	6.7	3.19E-02	6.7
75°	6.97	3.03E-02	7
90°	7.14	4.12E-02	7.18

(b)

Impact angle	Ke(mg cm^{-2} h^{-1})	Kc(mg cm^{-2} h^{-1})	Kec(mg cm^{-2} h^{-1})
15°	7.24	3.78E-02	7.28
30°	6.97	3.41E-02	7
45°	6.99	2.98E-02	7.02
60°	6.83	4.19E-02	6.87
75°	7.02	3.48E-02	7.05
90°	7.76	3.99E-02	7.8

(c)

Impact angle	Ke(mg cm^{-2} h^{-1})	Kc(mg cm^{-2} h^{-1})	Kec(mg cm^{-2} h^{-1})
15°	7.957	4.28E-02	8
30°	7.44	4.01E-02	7.48
45°	7.42	3.08E-02	7.45
60°	6.96	3.89E-02	7
75°	6.66	3.88E-02	6.7
90°	7.404	4.56E-02	7.45

(d)

Impact angle	Ke(mg cm^{-2} h^{-1})	Kc(mg cm^{-2} h^{-1})	Kec(mg cm^{-2} h^{-1})
15°	8.43	4.50E-02	8.47
30°	7.94	3.91E-02	7.98
45°	7.74	3.58E-02	7.78
60°	7.099	4.09E-02	7.14
75°	6.96	3.78E-02	7
90°	7.95	4.78E-02	8

(e)

Impact angle	Ke(mg cm^{-2} h^{-1})	Kc(mg cm^{-2} h^{-1})	Kec(mg cm^{-2} h^{-1})
15°	8.07	4.78E-02	8.12
30°	7.96	4.51E-02	8
45°	8.41	4.00E-02	8.45
60°	8.05	5.19E-02	8.1
75°	7.85	4.18E-02	7.89
90°	8.18	5.18E-02	8.23

Table.4.9:Mass loss as function of impact angles for carbon steel at various potentials in oil /20% water at 4.5 m s^{-1} and particle size 600-710µm (a) -400mV (b) -200mV (c) 0mV(d) 200mV (e) 400mV

(a)

Impact angle	Ke(mg cm^{-2} h^{-1})	Kc(mg cm^{-2} h^{-1})	Kec(mg cm^{-2} h^{-1})
15°	6.45	1.35	7.8
30°	6.07	1.21	7.28
45°	6.66	1.34	8
60°	5.82	1.2	7.02
75°	6.6	1.4	8
90°	6.75	1.45	8.2

(b)

Impact angle	Ke(mg cm^{-2} h^{-1})	Kc(mg cm^{-2} h^{-1})	Kec(mg cm^{-2} h^{-1})
15°	6.7	1.3	8
30°	6.98	1.32	8.3
45°	6.7	1.5	8.2
60°	6.51	1.1	7.61
75°	6.76	1.3	8.06
90°	7.1	1.5	8.6

(c)

Impact angle	Ke(mg cm^{-2} h^{-1})	Kc(mg cm^{-2} h^{-1})	Kec(mg cm^{-2} h^{-1})
15°	7.28	1.5	8.78
30°	7.08	1.32	8.4
45°	7.54	1.4	8.94
60°	6.79	1.21	8
75°	6.6	1.3	7.9
90°	7.12	1.6	8.72

(d)

Impact angle	Ke(mg cm^{-2} h^{-1})	Kc(mg cm^{-2} h^{-1})	Kec(mg cm^{-2} h^{-1})
15°	7.34	1.68	9.02
30°	7.4	1.6	9
45°	7.76	1.54	9.3
60°	8.68	1.32	10
75°	7.57	1.4	8.97
90°	7.9	1.7	9.6

(e)

Impact angle	Ke(mg cm^{-2} h^{-1})	Kc(mg cm^{-2} h^{-1})	Kec(mg cm^{-2} h^{-1})
15°	7.61	1.9	9.51
30°	7.67	1.85	9.52
45°	7.42	1.7	9.12
60°	7.32	1.68	9
75°	7.12	1.76	8.88
90°	7.98	1.89	9.87

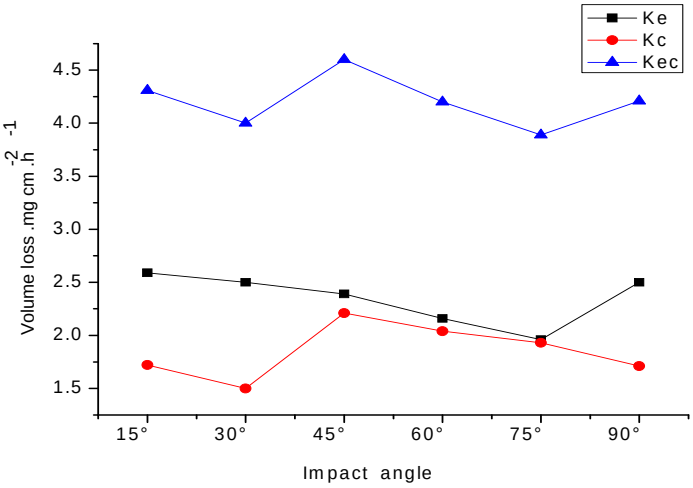

(a)

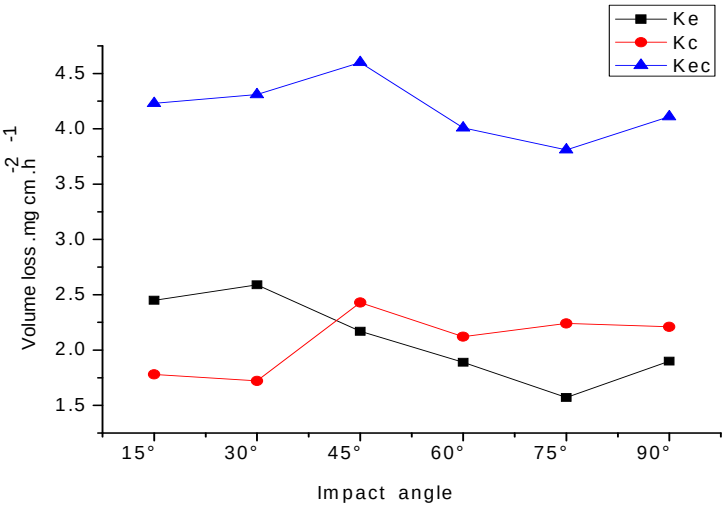

(b)

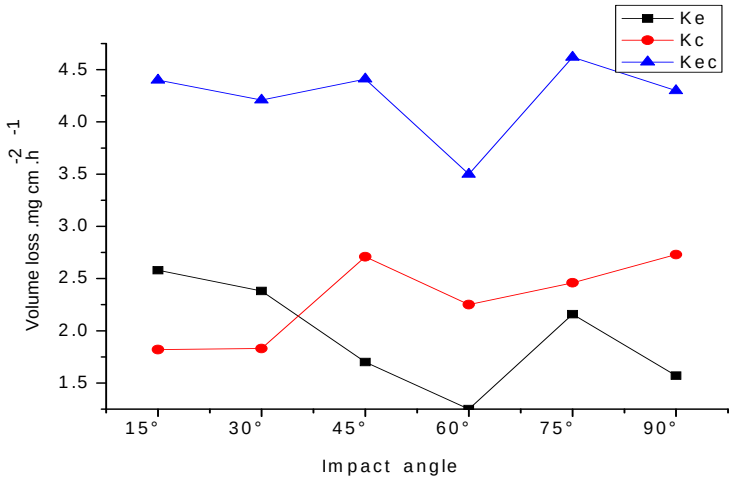

(c)

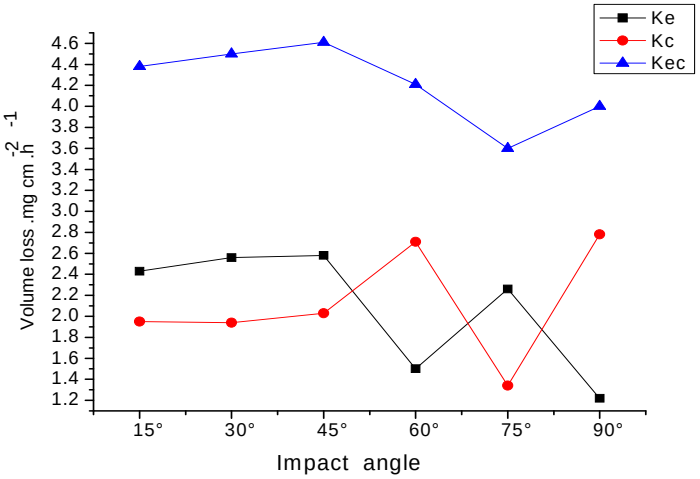

(d)

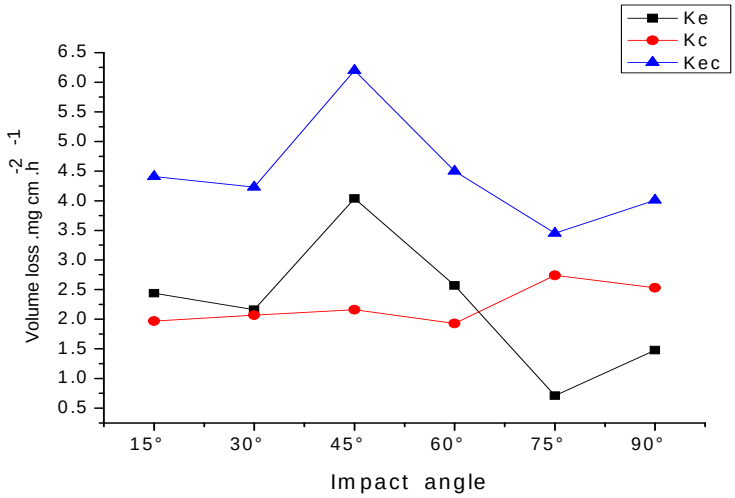

(e)

Fig.4.4: Volume loss as function of impact angles for carbon steel in water at 2.5 m s^{-1} impact velocity and particle size 600-710µm (a) -400mV (b) -200mV (c) 0mV (d) 200mV (e) 400mV

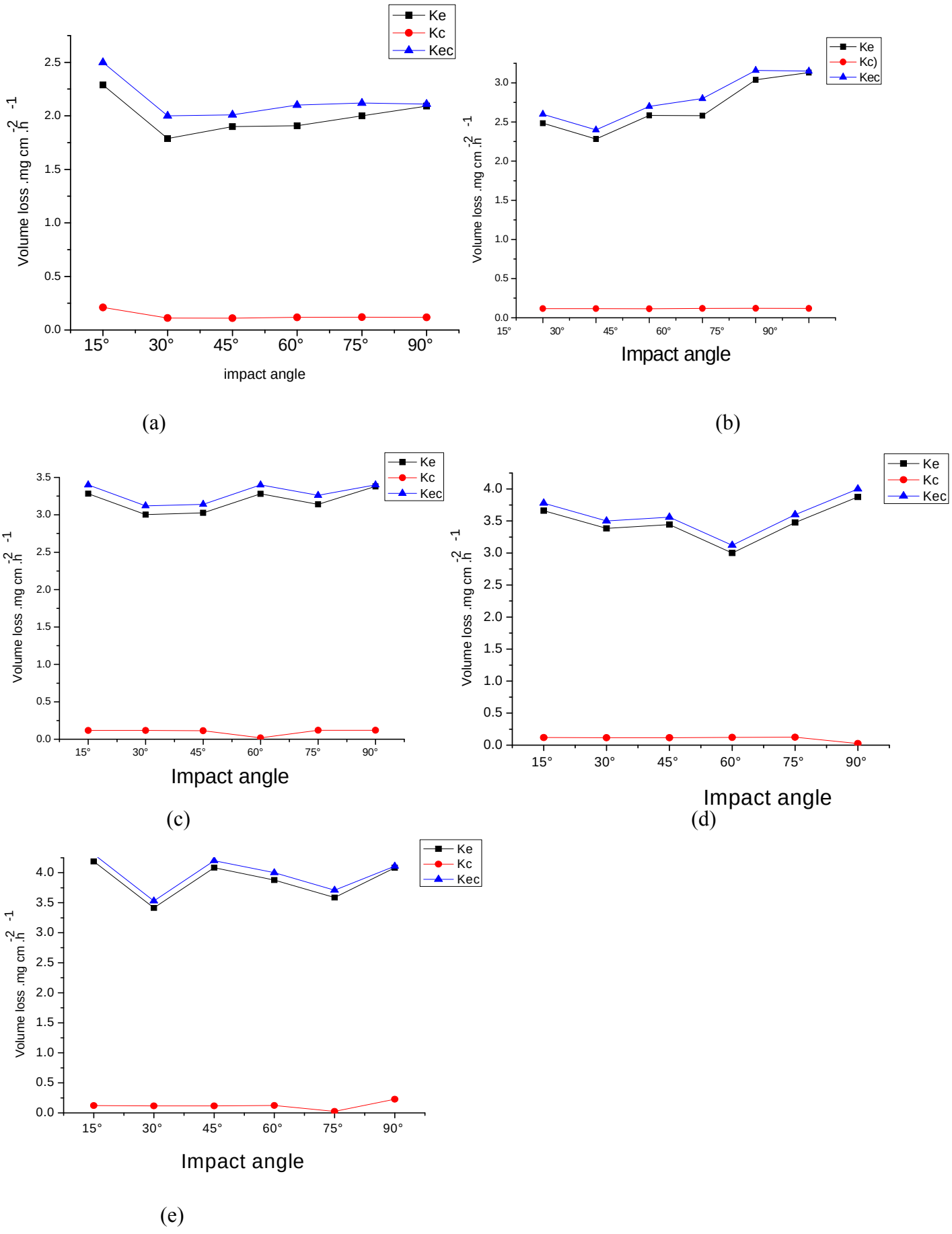

Fig.4.5: Volume loss as function of impact angles for carbon steel in crude oil at 2.5 m s^{-1} and particle size 600-710µm (a) -400mV (b) -200mV (c) 0mV (d) 200mV (e) 400mV

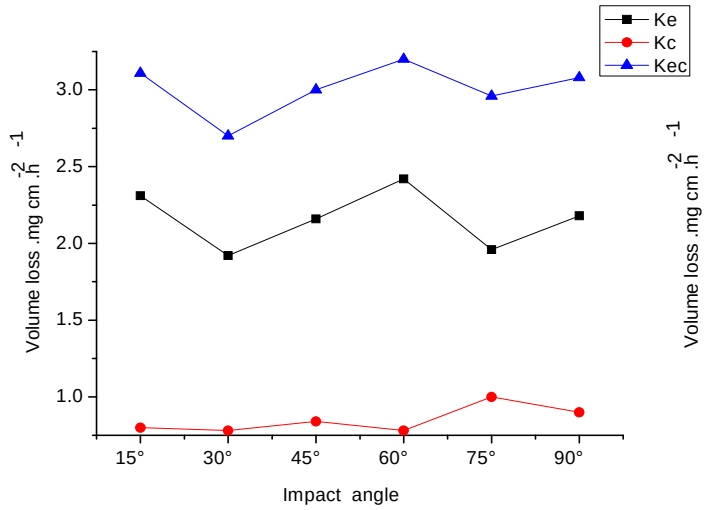

(a)

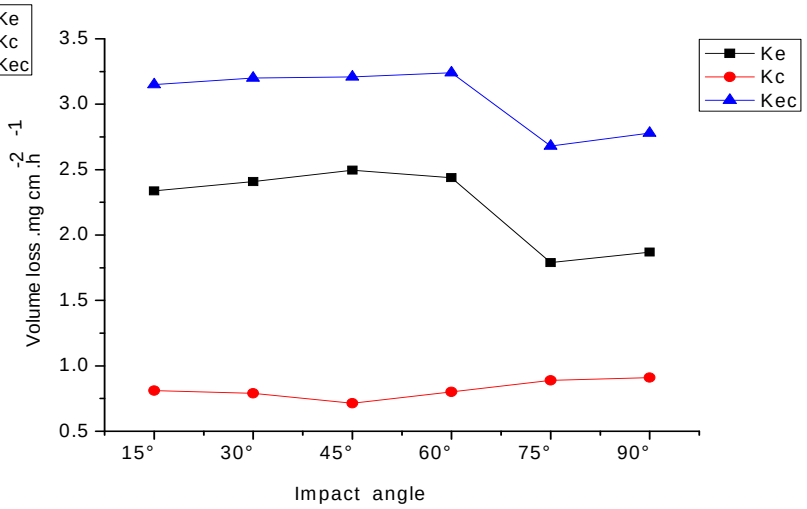

(b)

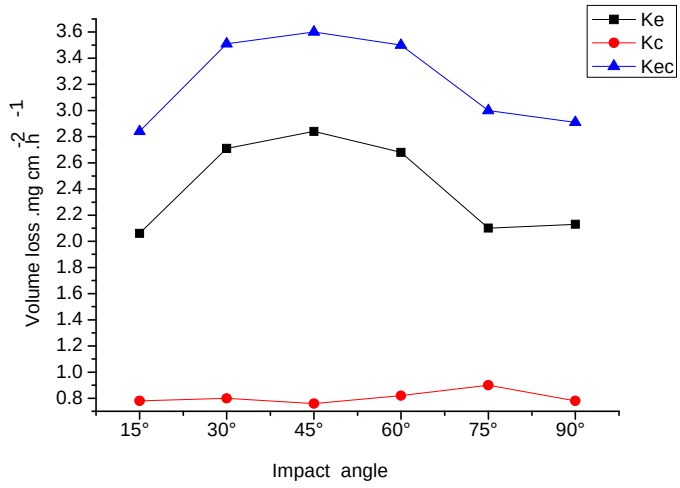

(c)

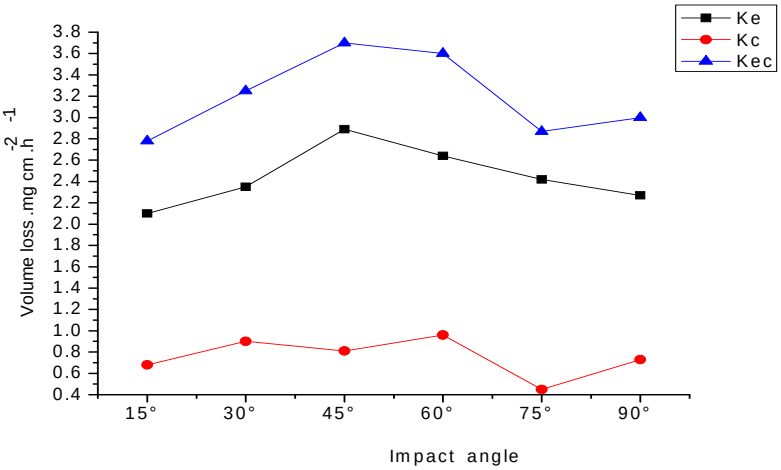

(d)

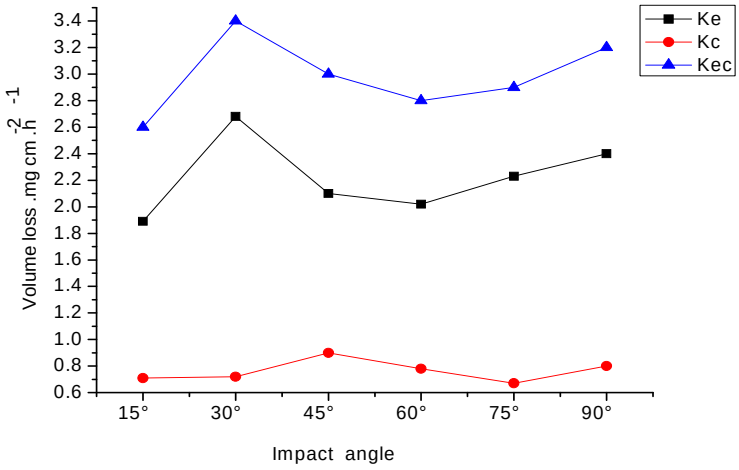

(e)

Fig.4.6: Volume loss as function of impact angles for carbon steel in oil /20% water at 2.5 m s^{-1} and particle size 600-710µm (a) -400mV (b) -200mV (c) 0mV (d) 200mV (e)400

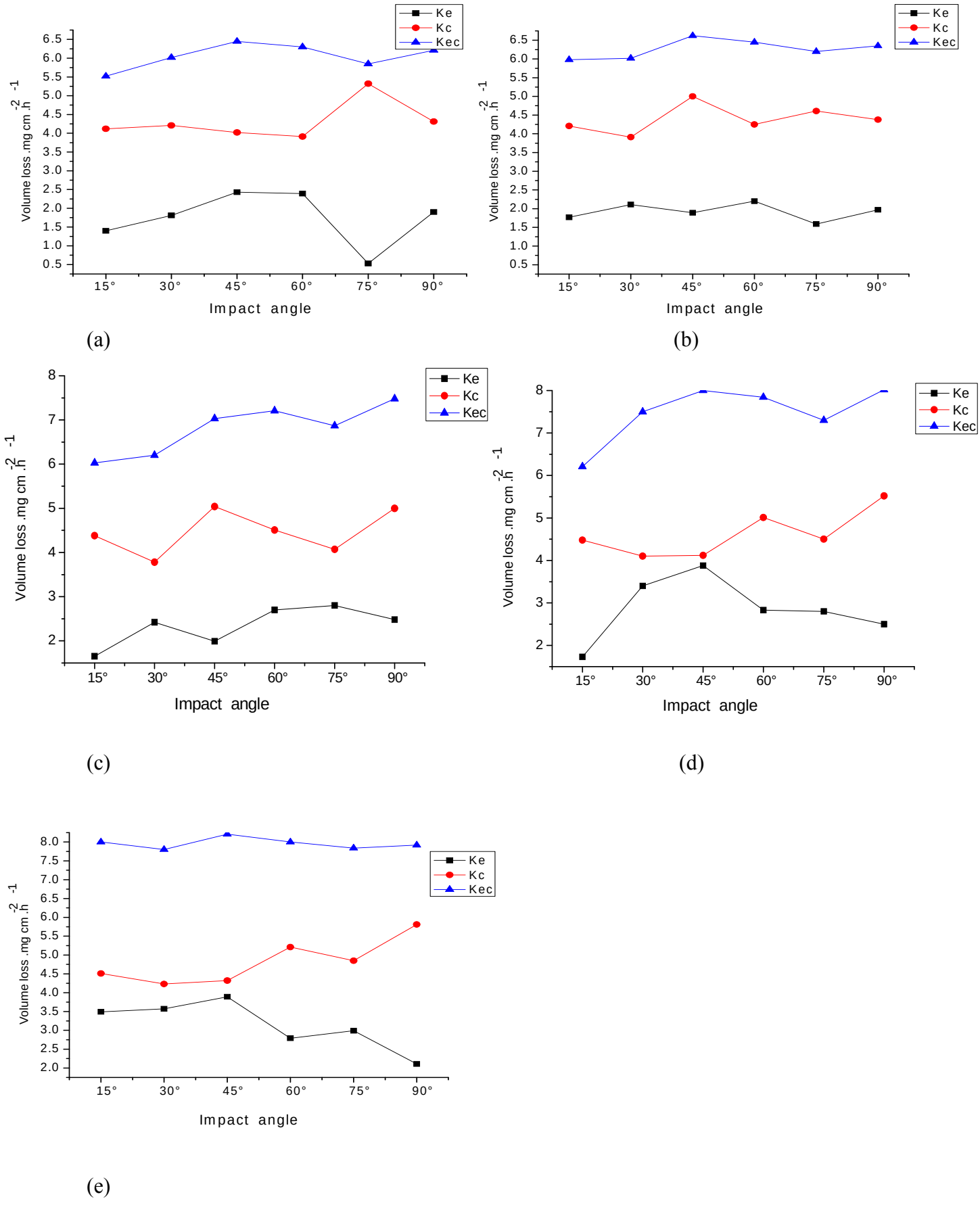

Fig.4.7: Volume loss as function of impact angles for carbon steel in water at 3.5 m s^{-1} and particle size 600-710µm (a) -400mV (b) -200mV (c) 0mV (d) 200mV (e)-400mV.

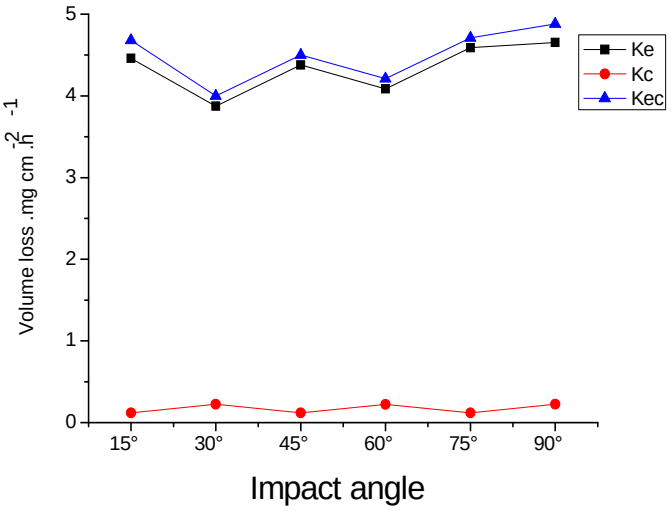

(a)

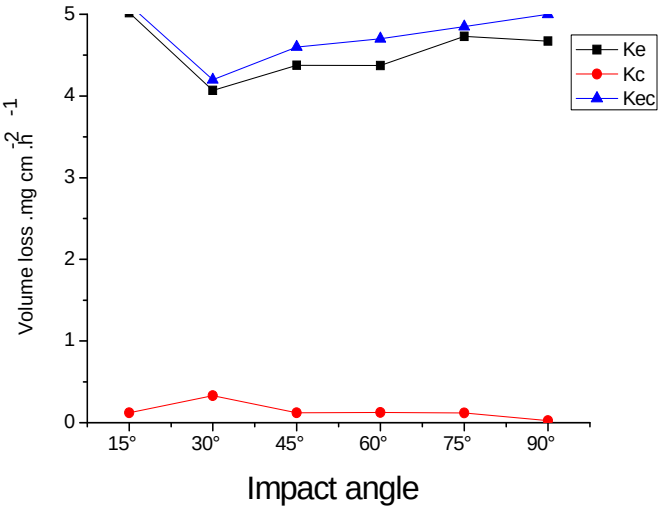

(b)

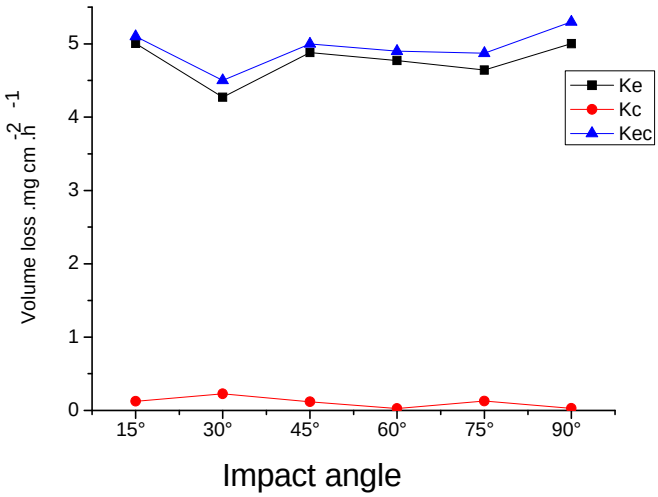

(c)

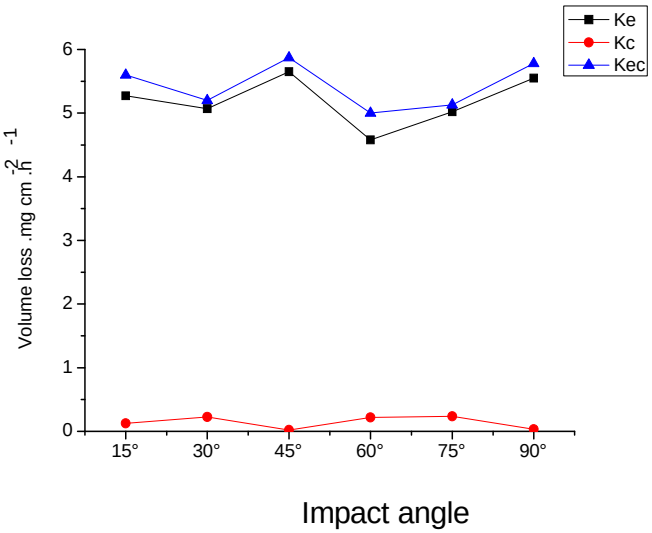

(d)

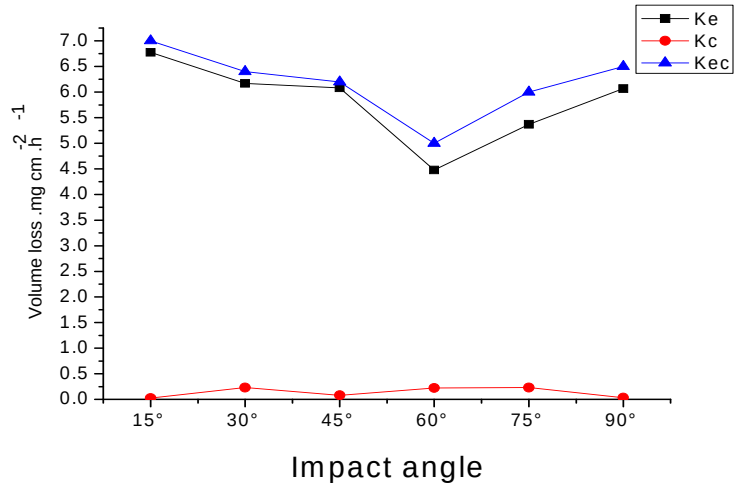

(e)

Fig.4.8: Volume loss as function of impact angles for carbon steel in crude oil at 3.5 m s^{-1} and particle size 600-710µm (a) -400mV (b) -200mV (c) 0mV (d) 200mV (e)-400mV

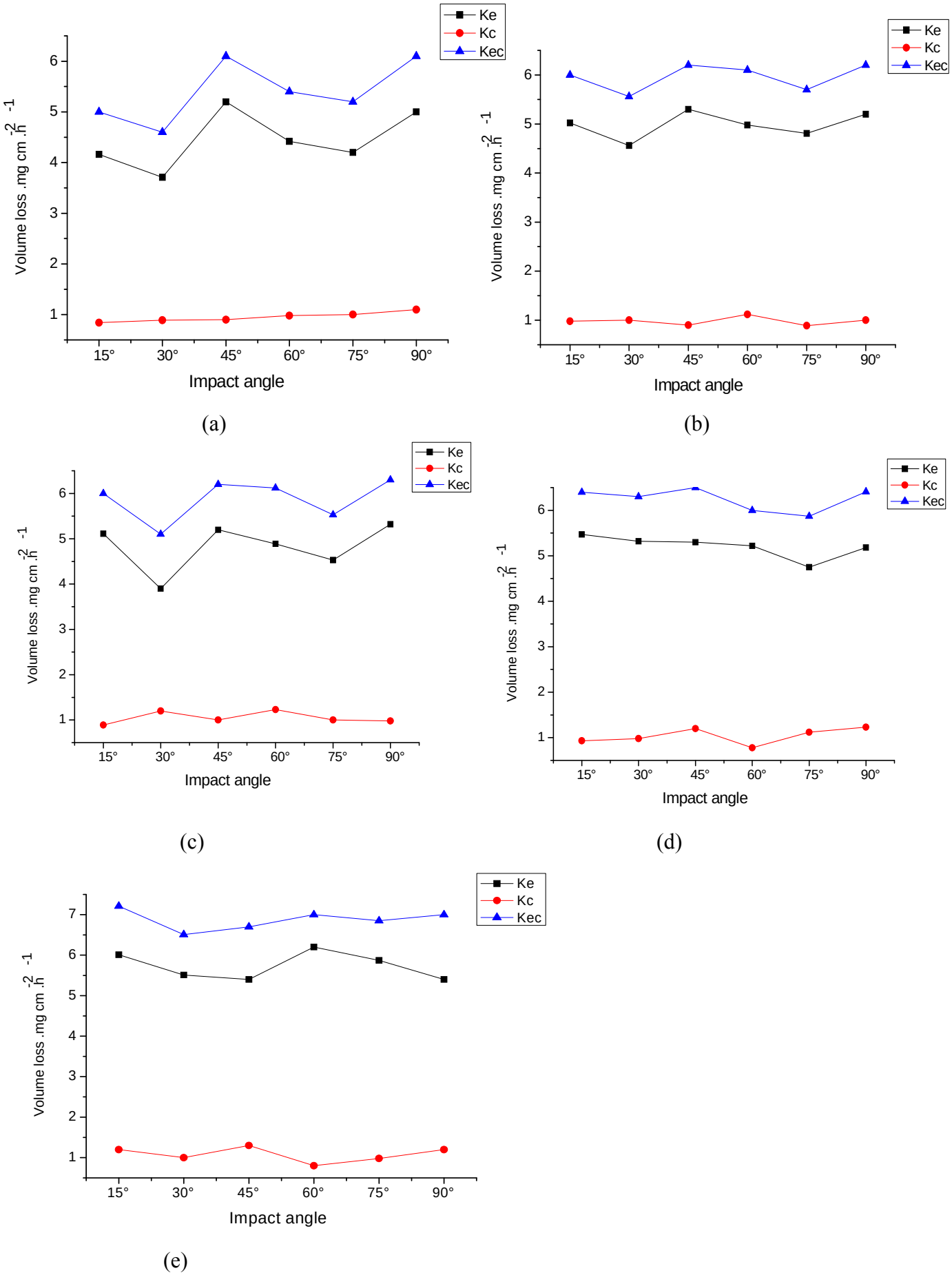

Fig.4.9: Volume loss as function of impact angles for carbon steel in oil /20% water at3.5 m s^{-1} and particle size 600-710µm (a) -400mV (b) -200mV (c) 0mV (d) 200mV (e)-400mV

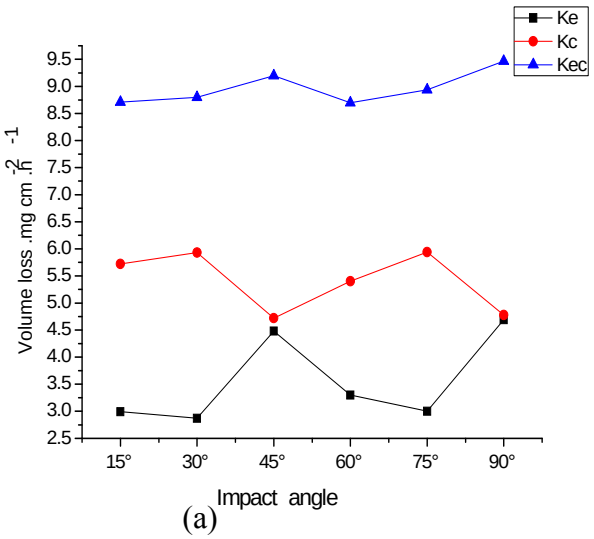

(a)

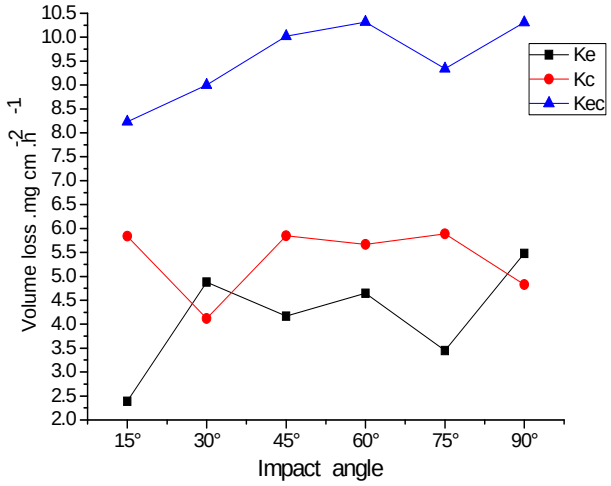

(b)

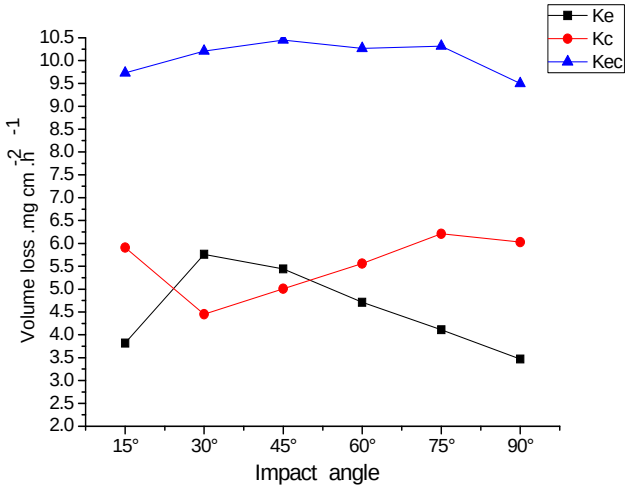

(c)

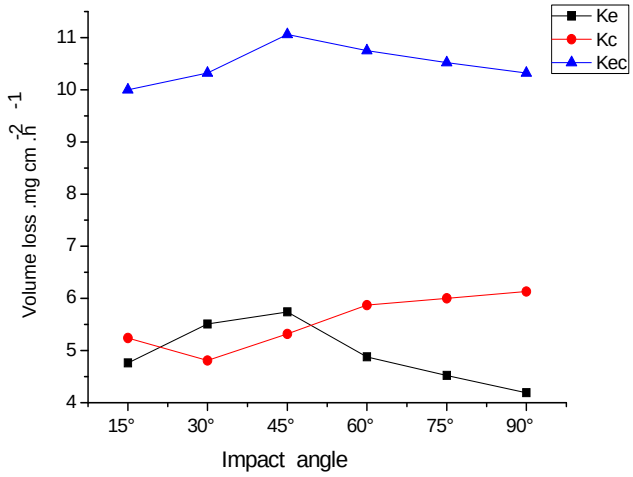

(d)

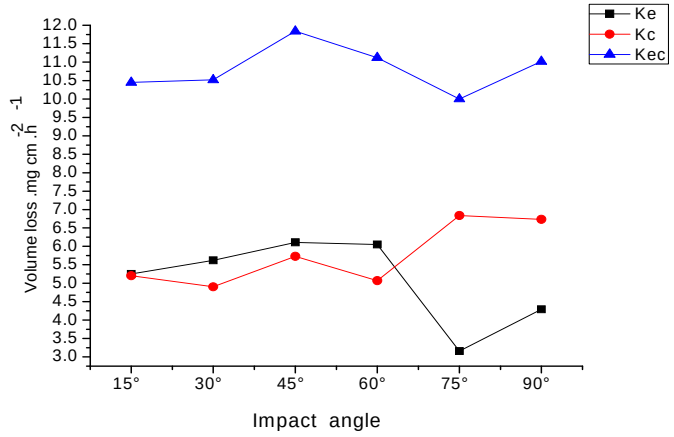

(e)

Fig.4.10: Volume loss as function of impact angles for carbon steel in water at 4.5 m s^{-1} and particle size 600-710µm (a) -400mV (b) -200mV (c) 0mV (d) 200mV (e) 400mV

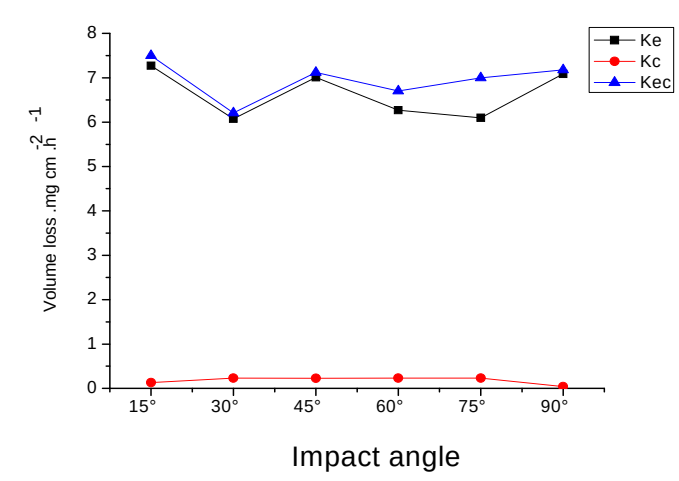

(a)

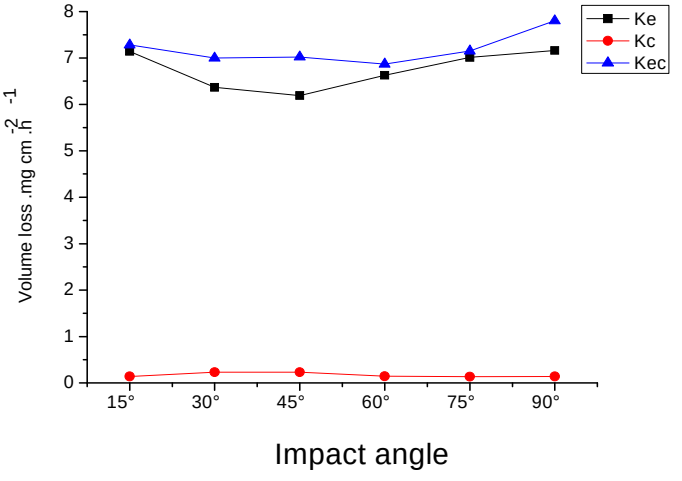

(b)

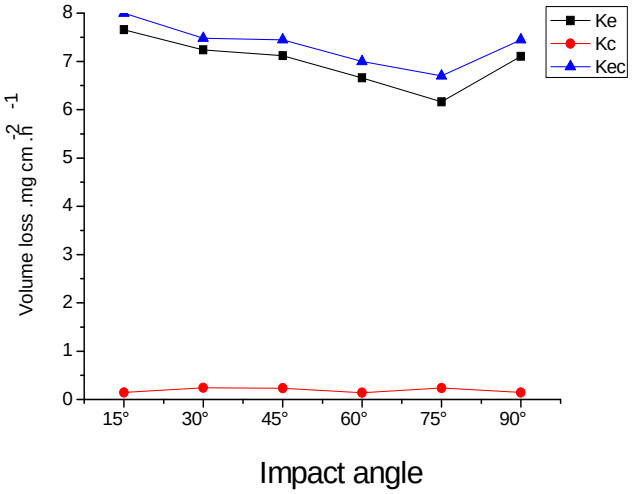

(c)

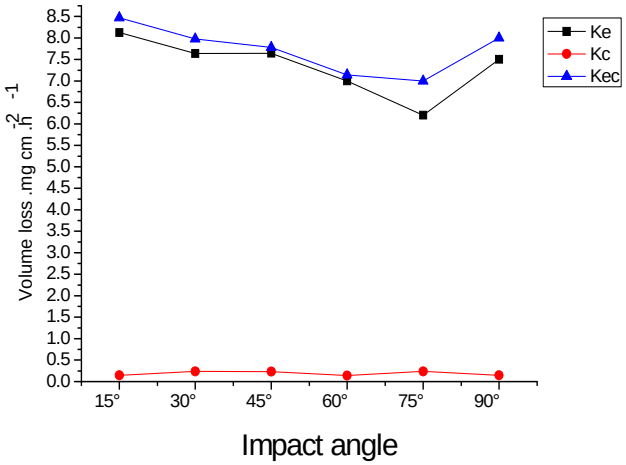

(d)

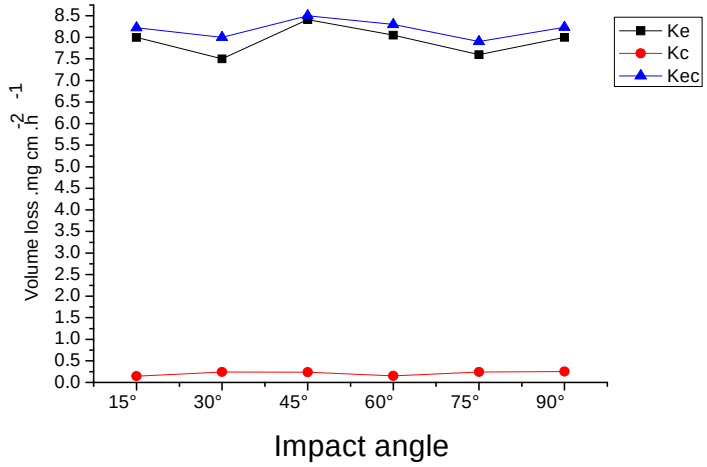

(e)

Fig.4.11: Volume loss as function of impact angles for carbon steel in crude oil at 4.5 m s^{-1} and particle size 600-710µm (a) -400mV (b) -200mV (c) 0mV (d) 200mV (e) 400mV

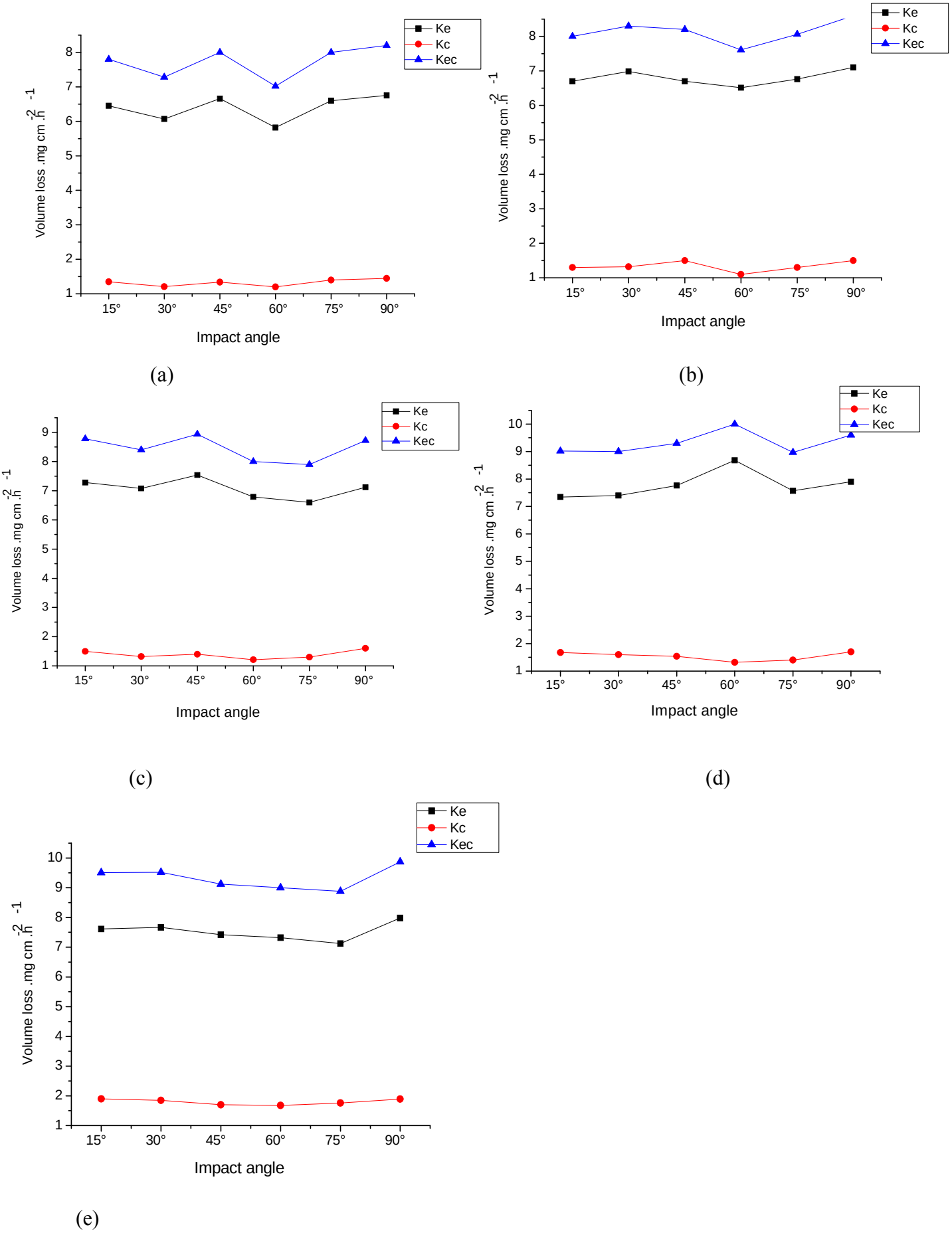

Fig.4.12: Volume loss as function of impact angles for carbon steel in oil /20% water at 4.5 m s^{-1} and particle size 600-710µm (a) -400mV (b) -200mV (c) 0mV (d) 200mV (e) 400mV .

4.1.5. SEM for particles sizes 600-710µm

Figures 4.13-4.15 shows that scanning electron micrographs of eroded carbon steel test specimen were affected by a change in impact velocity and impact angle in all three environments containing particles sized 600-710µm. It can be seen that the carbon steel showed plastic deformation on the surface which tended to rise with an increase in impact velocity due to the presence of shallow deformation on the surface of the specimen. The surface of the specimen in the water slurry environment was rough, while the surface of the specimen was less rough in the mixed environment (20% water with crude oil) Figures 4.13-(c) to 4.15-(c), the surface of the specimen was similar to smooth, without visible corrosion in the crude oil environment Figures 4.13-(b) to 4.15-(b).

The extent of ploughing increased with an increase in impact velocity and a decrease in impact angle. Fig. 4.14-(a) shows that there was good evidence of an oxide film on the surface of the specimen at applied potential 0 mV, resulting from an increase in the oxidation areas on the surface with an increase in applied potential. It can be concluded from the above it is clear that, material removal during erosion-corrosion was dependent on many factors that include properties and structure of target material, physical and chemical characteristics of erodent particles.

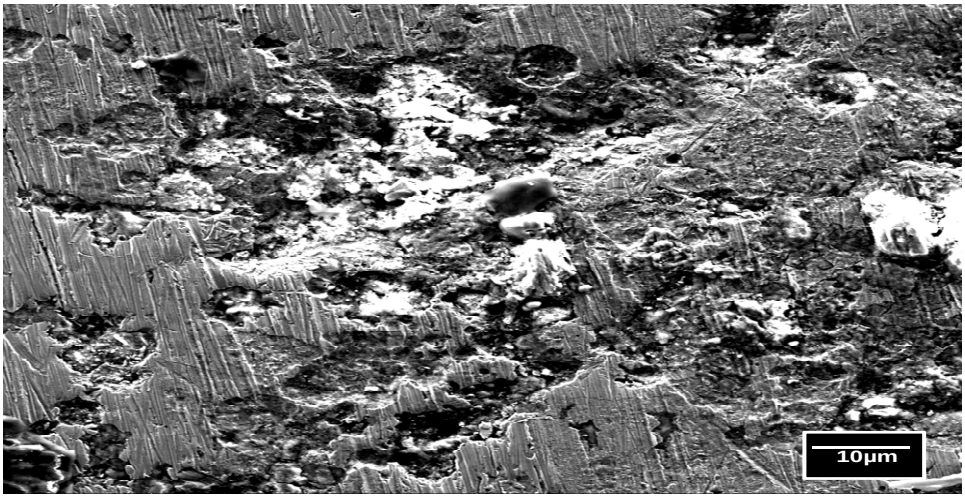

(a)

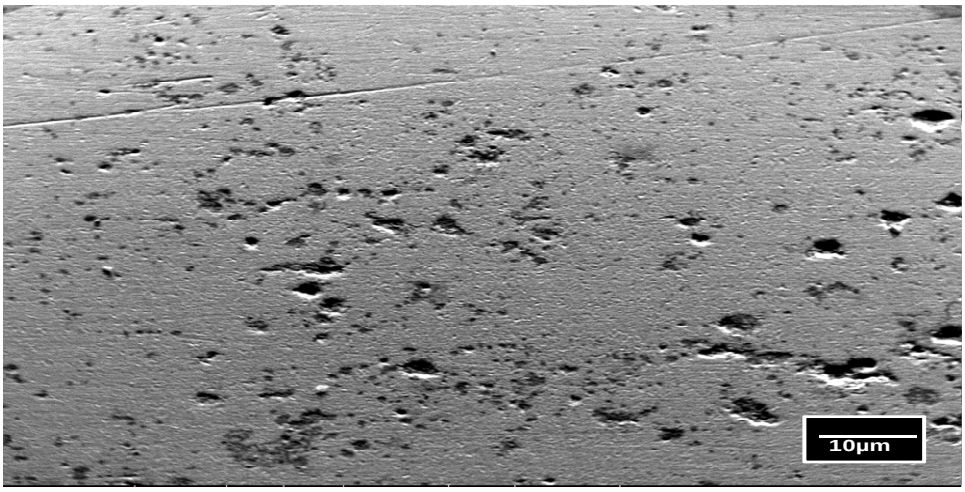

(b)

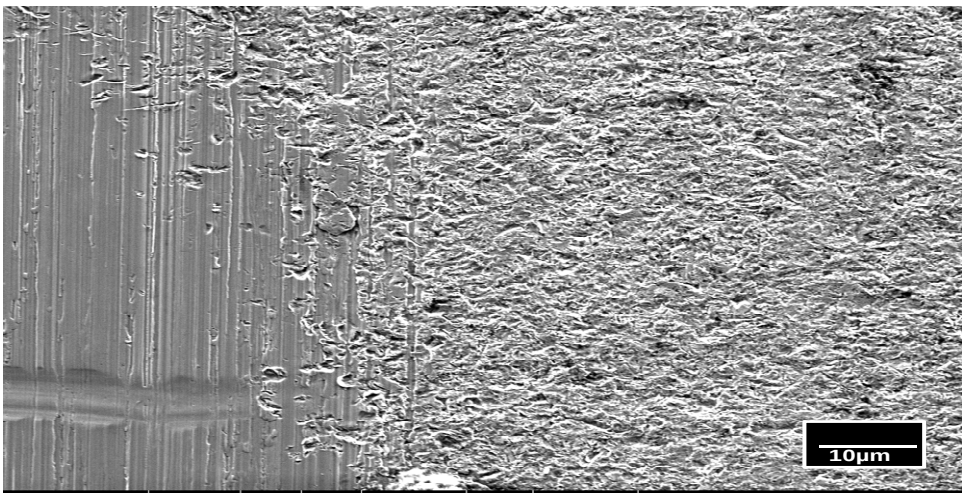

(c)

Fig.4.13: Scanning electron micrographs of eroded carbon steel test specimen at 2.5 m s^{-1},impact angle 15° and particle size 600-710µm (a)in water (b) in crude oil (c)in oil /20% water

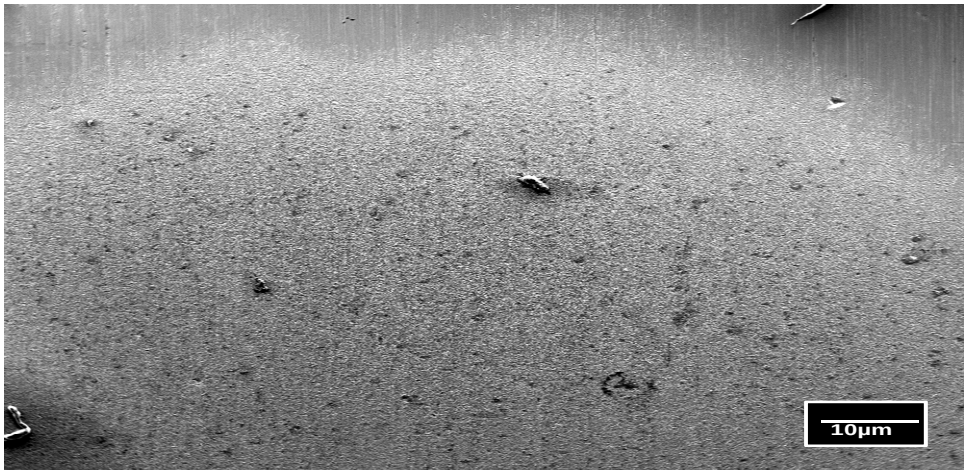

(a)

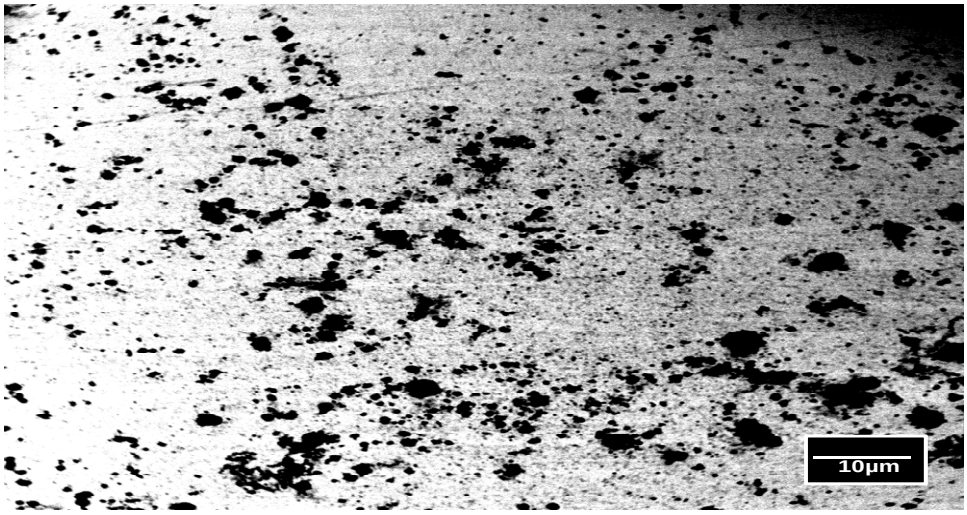

(b)

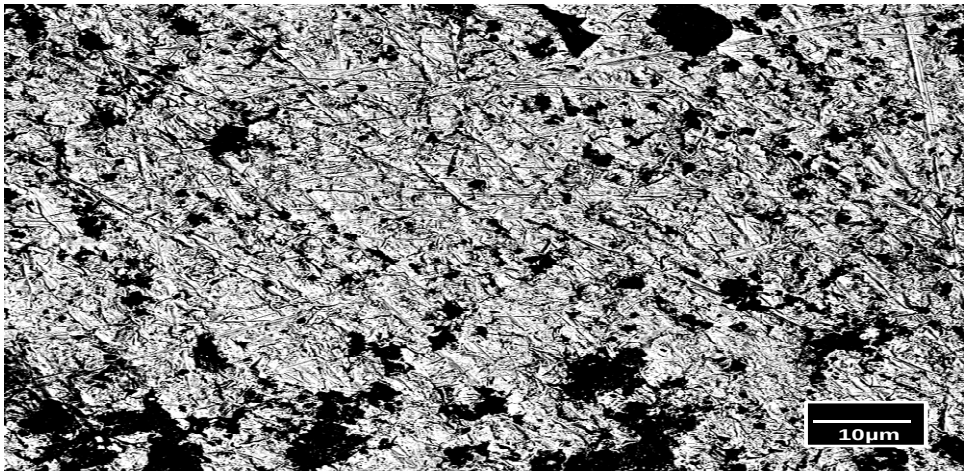

(c)

Fig. 4.14: Scanning electron micrographs of eroded carbon steel test specimen at 3.5 m s^{-1},impact angle 45° and particle size 600-710µm (a)in water (b) in crude oil (c)in oil /20% water.

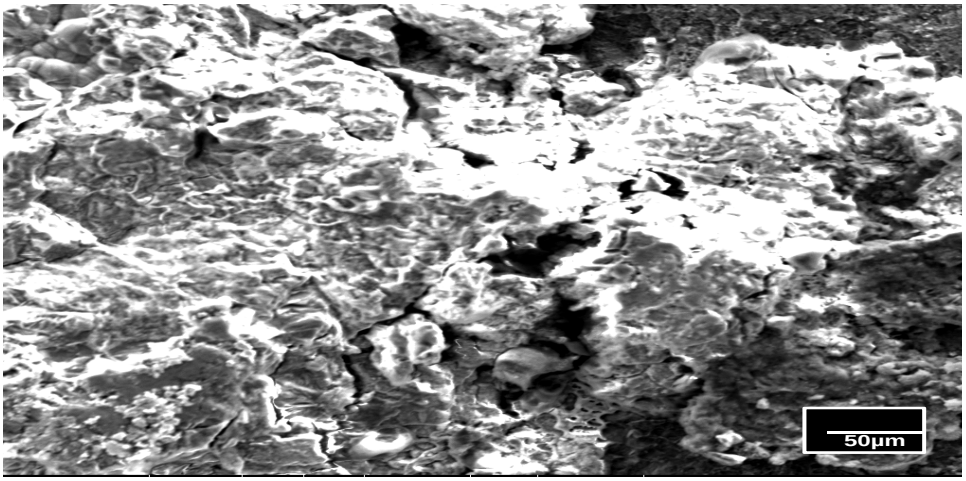

(a)

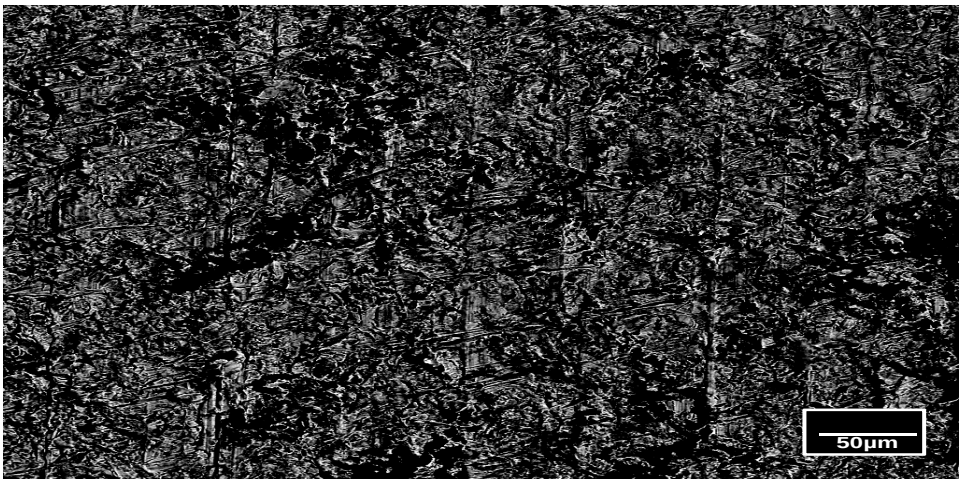

(b)

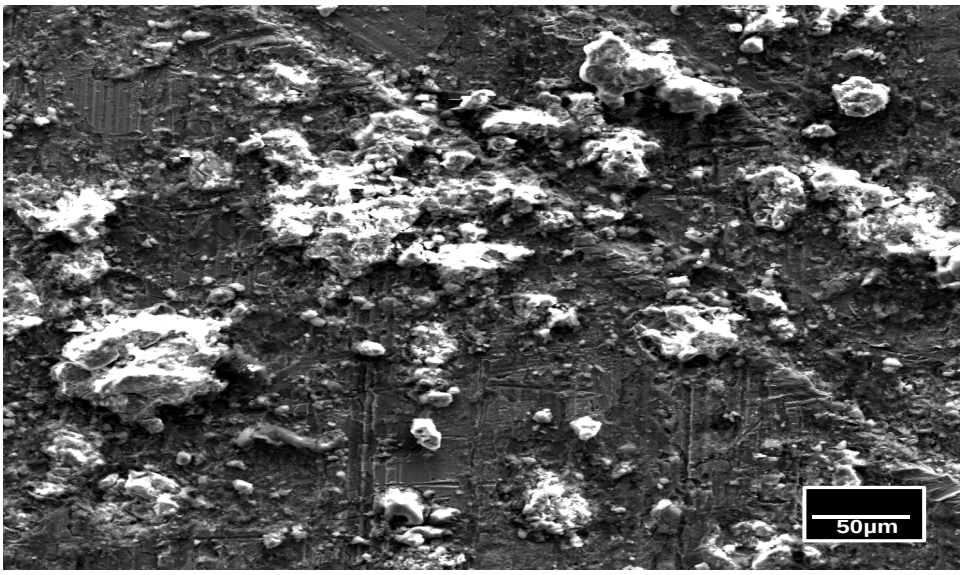

(c)

Fig.4.15: Scanning electron micrographs of eroded carbon steel test specimen at 4.5 m s^{-1}, impact angle 90° and particle size 600-710µm (a) in water (b) in crude oil (c) in oil /20% water.

4.2. Effect of impact angle and potential on erosion- corrosion maps in three environments for particle sizes150-30µm

4.2.1. The procedure of testing

The erosion-corrosion performances were assessed at room temperature and at three impact angles and three applied potentials under various impact velocities in three environments containing particles sized 150-300µm. The impact angles were varied at three values, 15°, 45° and 90°, and at three impact velocities, 2.5, 3.5 and 4.5m s^{-1}. The erosion-corrosion tests were achieved at three potentials, -400, 0 and 400 mV for half an hour.

4.2.2. Polarization curves for particles sizes 150-300µm

For carbon steel in the water environment at impact velocity of 2.5 m s^{-1} Fig. 4.16 (a), the highest value of current density was at impact angle 90°, which is consistent with the results of mass loss of Kc (table .4.10-4.18). In the crude oil environment, at impact velocity 2.5 m s^{-1} Fig. 4.16 (b), the average corrosion potential (Ecorr) was between-405mV and -415 mV approximately for all three impact angles and there was a general decrease in the current density compared with in water environment Fig. 4.16 (a). The peak value of the current density in crude oil was 0.050 mA.cm^{-2} at impact angle 90°. In oil/20% water environment at impact velocity 2.5 m s^{-1}Fig. 4.16 (c), the average free corrosion potential (Ecorr) was between -410mV and -420mV approximately and there was a general increase in the current density compared with that in the crude oil environment Fig. 4.16 (b).

At an impact velocity 3.5 m s^{-1} and in the carbon steel in water environment, there was an increase in the current density with an increase in impact velocity Fig. 4.17 (a).The highest value of corrosion was at an impact angle of 45°, which is consistent with the findings of previous work [2, 6 and 10]. For carbon steel in the water environment at impact velocity 4.5 m s^{-1}, there was an increase in the current density with an increase in impact velocity from 3.5 to 4.5 m s^{-1}.The peak value of corrosion contribution was at an impact angle of 90°. However, the lowest value of corrosion contribution was at an impact angle of 45°Fig. 4.18 (a).

In the crude oil and combined environments, the current density was gradually increased with an increase in impact velocity from 3.5 m $s^{-1}$to 4.5 m s^{-1}Fig. 4.17-18(b) and Fig. 4.17-18(c). By comparing between the polarization curves for small particles sizes150-300µm and large particle size 600-710µm for three environments, it was observed that the anodic current values recorded for small particle sizes were higher than those recorded for large particle sizes.

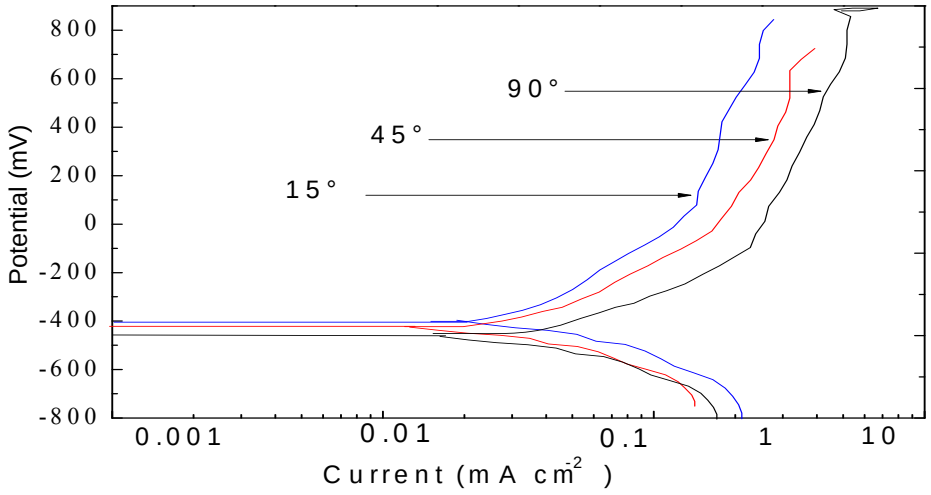

(a)

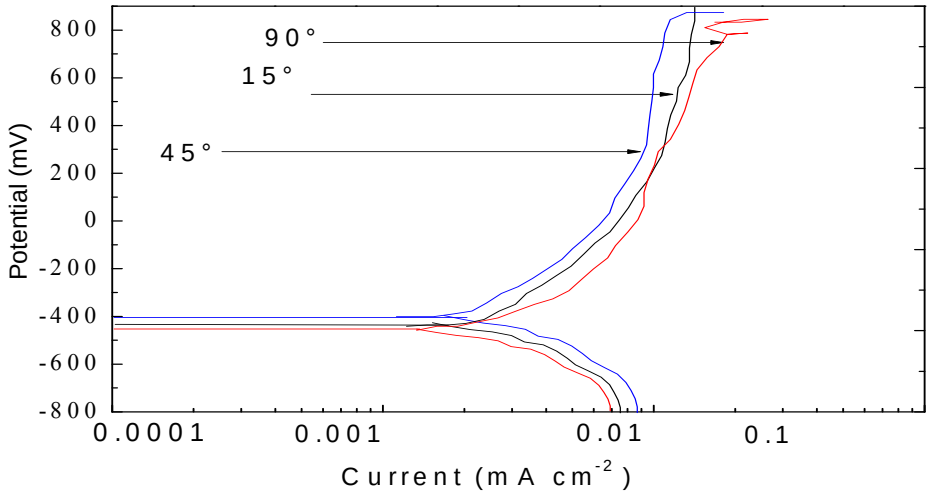

(b)

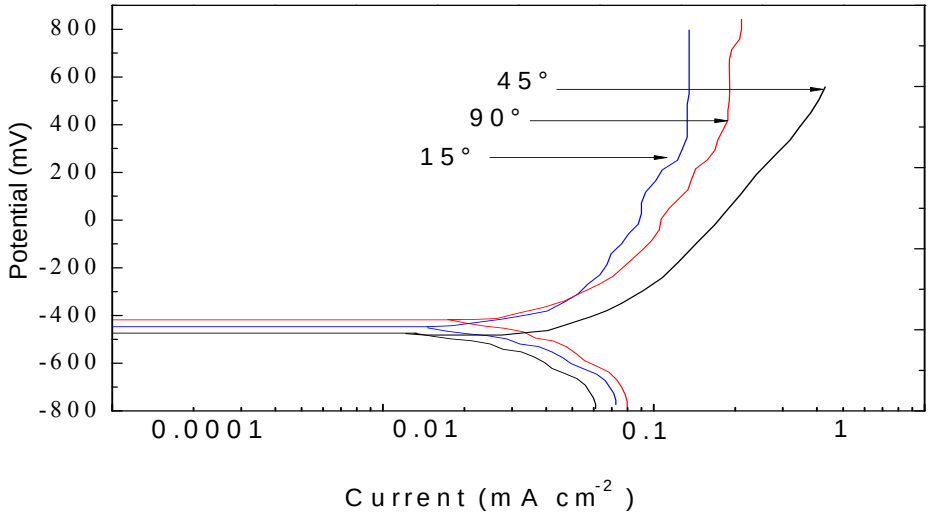

(c)

Fig.4.16: Polarization curves for carbon steel various impact angles, 2.5 m s^{-1} velocity and particle size 150-300µm in (a) water (b) crude oil (c) oil /20% water.

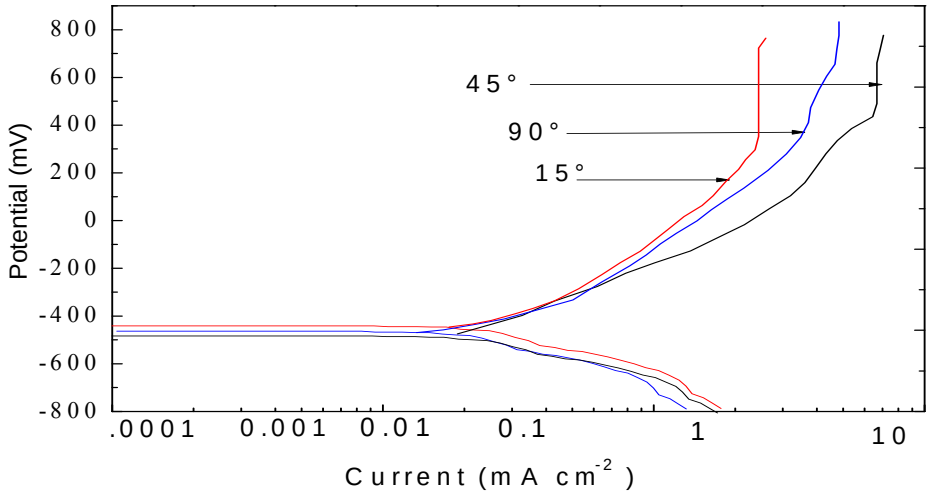

(a)

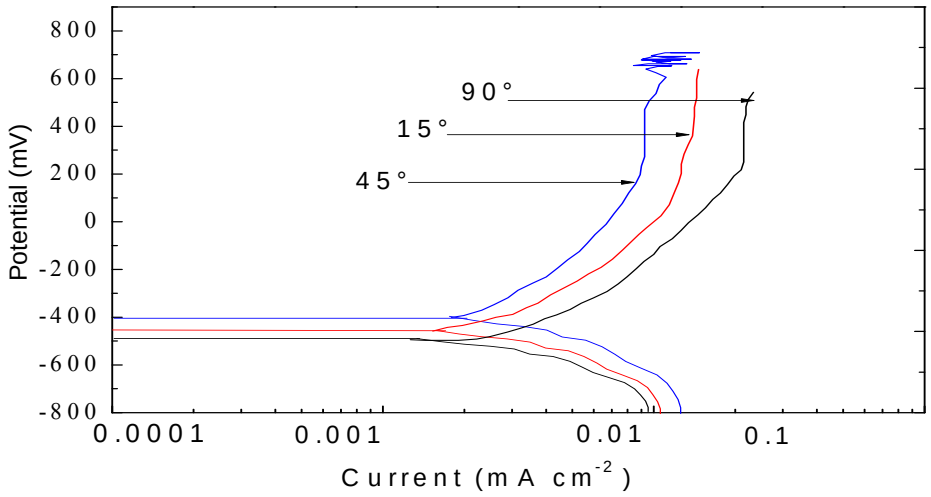

(b)

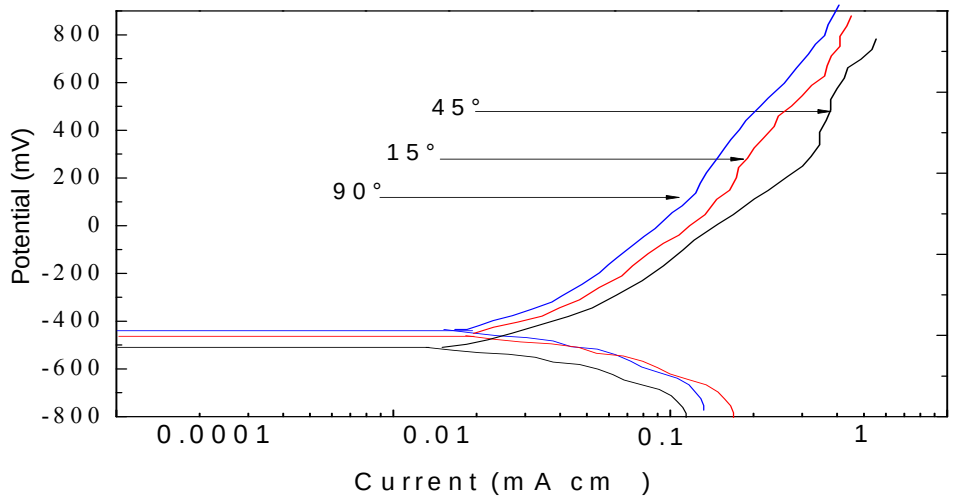

(c)

Fig.4.17: Polarization curves for carbon steel at various impact angles, 3.5 m s^{-1}velocity and particle size 150-300µm in (a) water (b) crude oil (c) oil /20% water.

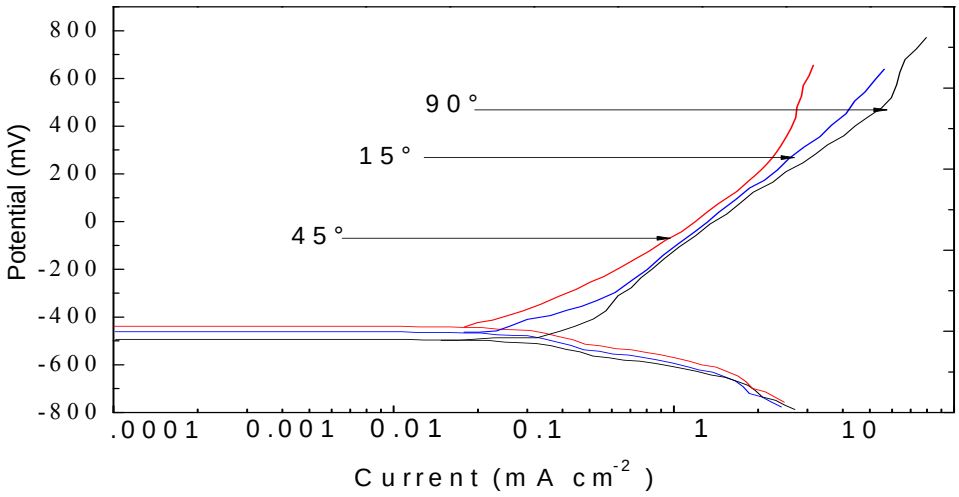

(a)

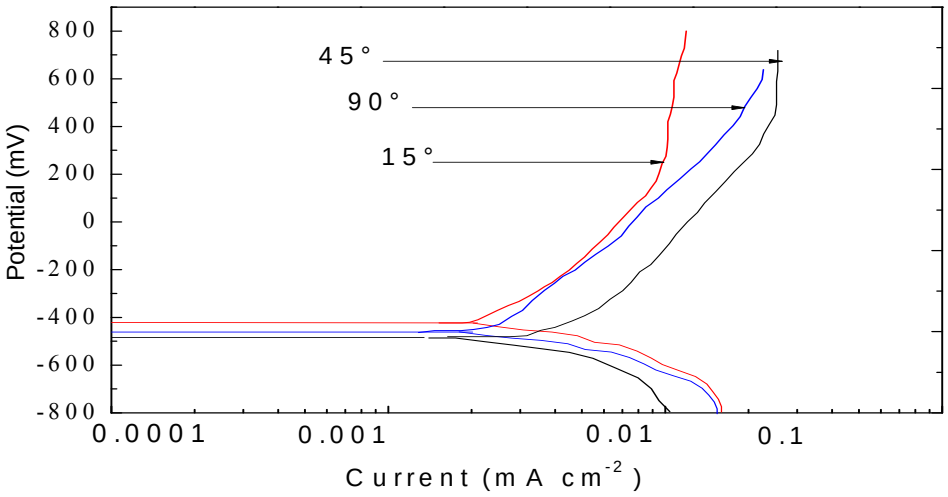

(b)

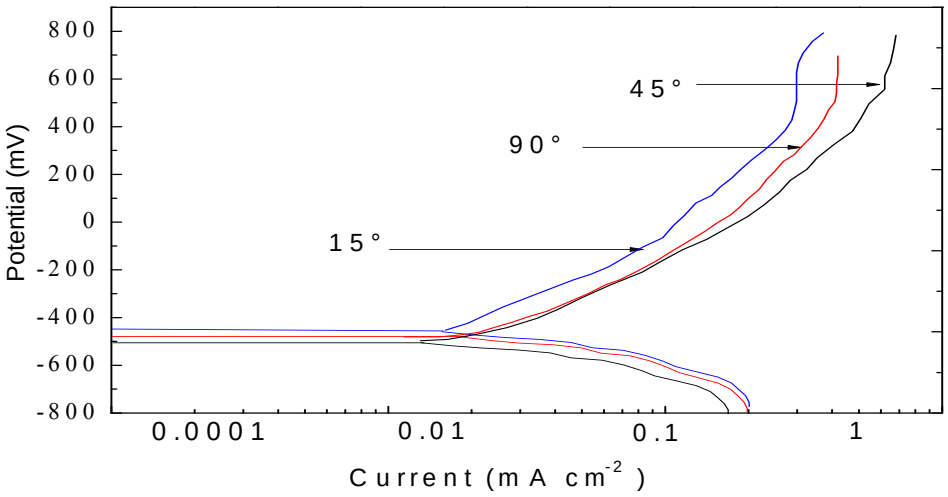

(c)

Fig.4.18: Polarization curves for carbon stee at various impact angles, 4.5 m s^{-1}velocity and particle size 150-300µm in (a) water (b) crude oil (c) oil /20% water.

4.2.3. Mass loss for particles sizes 150-30µm

Tables 4.10-4.18 show the results of calculation of volume loss for erosion contribution (Ke), corrosion contribution (Kc) and total erosion-corrosion (Kec) in the different environments and for different velocities with various impact angles and applied potentials. For carbon steel in the water environment at three impact velocities, it can be seen that the value of erosion contribution for small particles was decreased compared with the value of the erosion contribution for the largest particles sized 600-710µm. In addition, the value of corrosion contribution Kc was increased more than with large particles sized 600-710µm Figures 4.19, 4.22 and 4.25.

The higher value of erosion contribution (Ke) in the water environment containing particles sized 150-300µm was 2.48 mg cm^{-2} h^{-1} at an impact angle of 45° at 400mV, while, the high value of mass loss (Kec) and corrosion contribution (Kc) was 8.78mg cm^{-2} h^{-1} and 7 mg cm^{-2} h^{-1} at impact angles 45° and 90° at potential 400mV and at 4.5m s^{-1}. In addition, the low value of total mass loss in the water environment containing particles sized 150-300µm was 3.54 mg cm^{-2} h^{-1} at impact angles of 90° and -400 mV Figures 4.19, 4.22 and 4.25. For carbon steel in the crude oil environment at three impact velocities, the value of erosion contribution was decreased compared with the value of erosion contribution in the crude oil environment for the largest particles sized 600-710µm Figures 4.20, 4.23 and 4.26.

Moreover, the value of erosion remained greater than corrosion Kc, even with a change in particle size from a large particle to a small particle size Figures 4.20, 4.23 and 4.26. The highest value of total mass loss of carbon steel in the crude oil environment for particles sized150-300µm was 5.9 mg cm^{-2} h^{-1} at potential 400mV and impact angle 45°, while the low value of total mass loss (Kec) for carbon steel in the crude oil environment was 1.65 mg cm^{-2} h^{-1} at -400mV Figures 4.20, 4.23 and 4.26. In the oil/20%water environment containing particles sized150-300µm at three impact velocities Figures 4.21, 4.24 and 4.27, the value of erosion decreased compared with that in the crude oil/ 20% water containing particles sized600-710µm. The higher value of total mass loss kec was 6.78 mg cm^{-2} h^{-1} at potential 400mV and impact angle 45° Figure 4.27(c).

Tables .4.10:Volume loss as function of impact angles for carbon steel at various potentials in water at 2.5 m s^{-1} and particle size 150-300µm (a) -400mV (b) 0mV (c) 400mV.

(a)

Impact angle	Ke(mg cm^{-2} h^{-1})	Kc(mg cm^{-2} h^{-1})	Kec(mg cm^{-2} h^{-1})
15°	1.5	2.5	4
45°	1.59	2.6	4.19
90°	1.14	2.4	3.54

(b)

Impact angle	Ke(mg cm^{-2} h^{-1})	Kc(mg cm^{-2} h^{-1})	Kec(mg cm^{-2} h^{-1})
15°	0.47	3.74	4.21
45°	0.7	3.8	4.5
90°	0.46	3.84	4.3

(c)

Impact angle	Ke(mg cm^{-2} h^{-1})	Kc(mg cm^{-2} h^{-1})	Kec(mg cm^{-2} h^{-1})
15°	0.46	3.84	4.3
45°	1.51	3.9	5.41
90°	0.5	3.9	4.4

Tables.4.11:Volume loss as function of impact angles for carbon steel at various potentials in crude oil at 2.5 m s^{-1} and particle size 150-300µm (a) -400mV (b) 0mV (c) 400mV.

(a)

Impact angle	Ke(mg cm^{-2} h^{-1})	Kc(mg cm^{-2} h^{-1})	Kec(mg cm^{-2} h^{-1})
15°	1.43	3.21E-01	1.75
45°	1.66	3.42E-01	2
90°	1.06	5.91E-01	1.65

(b)

Impact angle	Ke(mg cm^{-2} h^{-1})	Kc(mg cm^{-2} h^{-1})	Kec(mg cm^{-2} h^{-1})
15°	1.46	3.95E-01	1.85
45°	1.77	3.40E-01	2.11
90°	1.44	4.10E-01	1.85

(c)

Impact angle	Ke(mg cm^{-2} h^{-1})	Kc(mg cm^{-2} h^{-1})	Kec(mg cm^{-2} h^{-1})
15°	1.556	4.24E-01	1.98
45°	1.95	3.57E-01	2.30
90°	1.73	4.70E-01	2.2

Tables.4.12:Volume loss as function of impact angles for carbon steel at various potentials in oil /20% water at 2.5 m s^{-1} impact velocity and particle size150-300µm (a) -400mV (b) 0mV (c) 400mV.

(a)

Impact angle	Ke(mg cm^{-2} h^{-1})	Kc(mg cm^{-2} h^{-1})	Kec(mg cm^{-2} h^{-1})
15°	1.19	1.11E+00	2.3
45°	1.29	1.21E+00	2.5
90°	1.4	1.03E+00	2.43

(b)

Impact angle	Ke(mg cm^{-2} h^{-1})	Kc(mg cm^{-2} h^{-1})	Kec(mg cm^{-2} h^{-1})
15°	1.1	1.51E+00	2.6
45°	0.95	1.75E+00	2.7
90°	0.85	1.65E+00	2.5

(c)

Impact angle	Ke(mg cm^{-2} h^{-1})	Kc(mg cm^{-2} h^{-1})	Kec(mg cm^{-2} h^{-1})
15°	0.98	1.77E+00	2.75
45°	1.55	1.85E+00	3.4
90°	0.82	1.83E+00	2.65

Table.4.13: Volume loss as function of impact angles for carbon steel at various potentials in water at 3.5 m s^{-1}impact velocity and particle size 150-300µm (a) -400mV(b) 0mV (c) 400mV.

(a)

Impact angle	Ke(mg cm^{-2} h^{-1})	Kc(mg cm^{-2} h^{-1})	Kec(mg cm^{-2} h^{-1})
15°	1.22	3.98	5.2
45°	1.51	4.2	5.71
90°	1.1	4.5	5.6

(b)

Impact angle	Ke(mg cm^{-2} h^{-1})	Kc(mg cm^{-2} h^{-1})	Kec(mg cm^{-2} h^{-1})
15°	1.5	4	5.5
45°	1.05	5	6.05
90°	0.6	4.81	5.41

(c)

Impact angle	Ke(mg cm^{-2} h^{-1})	Kc(mg cm^{-2} h^{-1})	Kec(mg cm^{-2} h^{-1})
15°	2	4.2	6.2
45°	2	5	7
90°	0.6	5.4	6

Tables.4.14: Volume loss as function of impact angles for carbon steel at various potentials in crude oil at 3.5 m s^{-1}impact velocity and particle size 150-300µm (a) -400mV(b) 0mV (c) 400mV.

(a)

Impact angle	Ke(mg cm^{-2} h^{-1})	Kc(mg cm^{-2} h^{-1})	Kec(mg cm^{-2} h^{-1})
15°	3.05	4.00E-01	3.45
45°	3.4	5.00E-01	3.9
90°	2.71	5.41E-01	3.25

(b)

Impact angle	Ke(mg cm^{-2} h^{-1})	Kc(mg cm^{-2} h^{-1})	Kec(mg cm^{-2} h^{-1})
15°	3.22	5.32E-01	3.75
45°	3.41	4.40E-01	3.85
90°	2.9	6.00E-01	3.5

(c)

Impact angle	Ke(mg cm^{-2} h^{-1})	Kc(mg cm^{-2} h^{-1})	Kec(mg cm^{-2} h^{-1})
15°	3.23	6.12E-01	3.84
45°	3.43	5.70E-01	4
90°	3.17	6.30E-01	3.8

Tables.4.15: Volume loss as function of impact angles for carbon steel at various potentials in oil /20% water at 3.5 m s^{-1} impact velocity and particle size 150-300µm (a) - 400mV (b) 0mV (c) 400mV

(a)

Impact angle	Ke(mg cm^{-2} h^{-1})	Kc(mg cm^{-2} h^{-1})	Kec(mg cm^{-2} h^{-1})
15°	1.55	2.46E+00	4
45°	1.26	2.95E+00	4.21
90°	1.73	2.26E+00	3.98

(b)

Impact angle	Ke(mg cm^{-2} h^{-1})	Kc(mg cm^{-2} h^{-1})	Kec(mg cm^{-2} h^{-1})
15°	1.33	2.97E+00	4.3
45°	1.46	3.00E+00	4.46
90°	1.15	2.85E+00	4

(c)

Impact angle	Ke(mg cm^{-2} h^{-1})	Kc(mg cm^{-2} h^{-1})	Kec(mg cm^{-2} h^{-1})
15°	1.73	3.02E+00	4.75
45°	1.48	3.32E+00	4.8
90°	1.57	2.94E+00	4.51

Tables.4.16: Volume loss as function of impact angles for carbon steel at various potentials in water at 4.5 m s^{-1}impact velocity and particle size 150-300µm
(a) - 400mV (b) 0mV (c) 400mV

(a)

Impact angle	Ke(mg cm^{-2} h^{-1})	Kc(mg cm^{-2} h^{-1})	Kec(mg cm^{-2} h^{-1})
15°	2	5.5	7.5
45°	2.3	5.5	7.8
90°	1.6	5.7	7.3

(b)

Impact angle	Ke(mg cm^{-2} h^{-1})	Kc(mg cm^{-2} h^{-1})	Kec(mg cm^{-2} h^{-1})
15°	1.01	6.2	7.21
45°	2.11	5.89	8
90°	0.65	6.4	7.05

(c)

Impact angle	Ke(mg cm^{-2} h^{-1})	Kc(mg cm^{-2} h^{-1})	Kec(mg cm^{-2} h^{-1})
15°	0.95	6.5	7.45
45°	2.48	6.3	8.78
90°	1	7	8

Table.4.17: Volume loss as function of impact angles for carbon steel at various potentials in crude oil 4.5 m s^{-1}impact velocity and particle size 150-300µm
(a) - 400mV (b) 0mV (c) 400mV

(a)

Impact angle	Ke(mg cm^{-2} h^{-1})	Kc(mg cm^{-2} h^{-1})	Kec(mg cm^{-2} h^{-1})
15°	4.25	7.50E-01	5
45°	4.62	8.00E-01	5.42
90°	3.83	8.23E-01	4.65

(b)

Impact angle	Ke(mg cm^{-2} h^{-1})	Kc(mg cm^{-2} h^{-1})	Kec(mg cm^{-2} h^{-1})
15°	4.65	8.53E-01	5.5
45°	4.86	8.91E-01	5.75
90°	4.33	8.68E-01	5.2

(c)

Impact angle	Ke(mg cm^{-2} h^{-1})	Kc(mg cm^{-2} h^{-1})	Kec(mg cm^{-2} h^{-1})
15°	4.55	9.00E-01	5.45
45°	4.9	1.00E+00	5.9
90°	4.2	1.20E+00	5.4

Table.4.18: Volume loss as function of impact angles for carbon steel at various potentials in oil /20% water at 4.5 m s^{-1}impact velocity and particle size 150-300µm (a) - 400mV (b) 0mV (c) 400mV

(a)

Impact angle	Ke(mg cm^{-2} h^{-1})	Kc(mg cm^{-2} h^{-1})	Kec(mg cm^{-2} h^{-1})
15°	2.53	3.37E+00	5.9
45°	2.4	3.60E+00	6
90°	1.98	3.52E+00	5.5

(b)

Impact angle	Ke(mg cm^{-2} h^{-1})	Kc(mg cm^{-2} h^{-1})	Kec(mg cm^{-2} h^{-1})
15°	2.4	4.00E+00	6.4
45°	2.05	4.45E+00	6.5
90°	1.9	4.30E+00	6.2

(c)

Impact angle	Ke(mg cm^{-2} h^{-1})	Kc(mg cm^{-2} h^{-1})	Kec(mg cm^{-2} h^{-1})
15°	2.42	4.23E+00	6.65
45°	2.23	4.55E+00	6.78
90°	2.08	4.42E+00	6.5

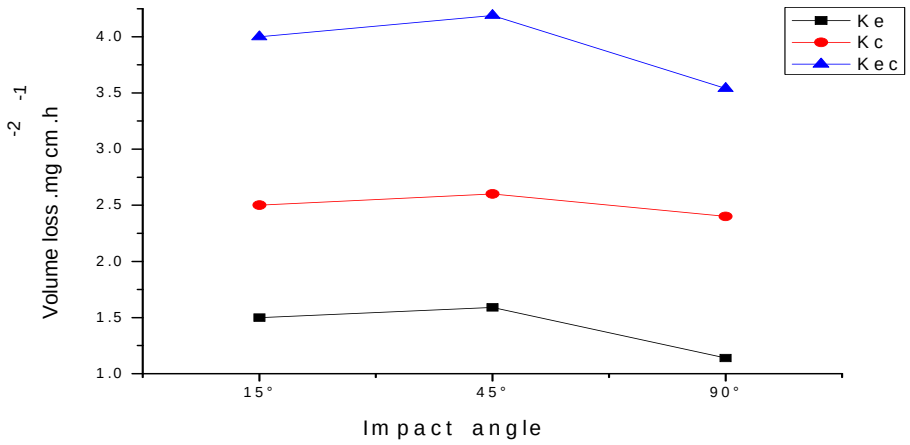

(a)

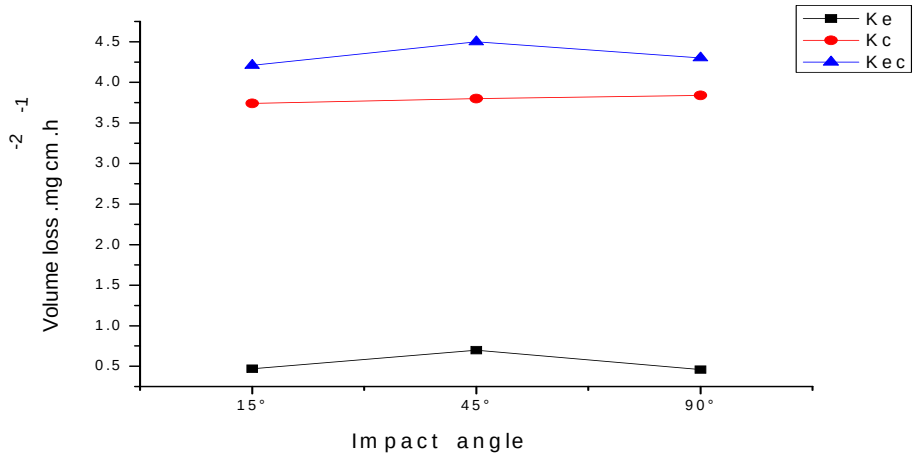

(b)

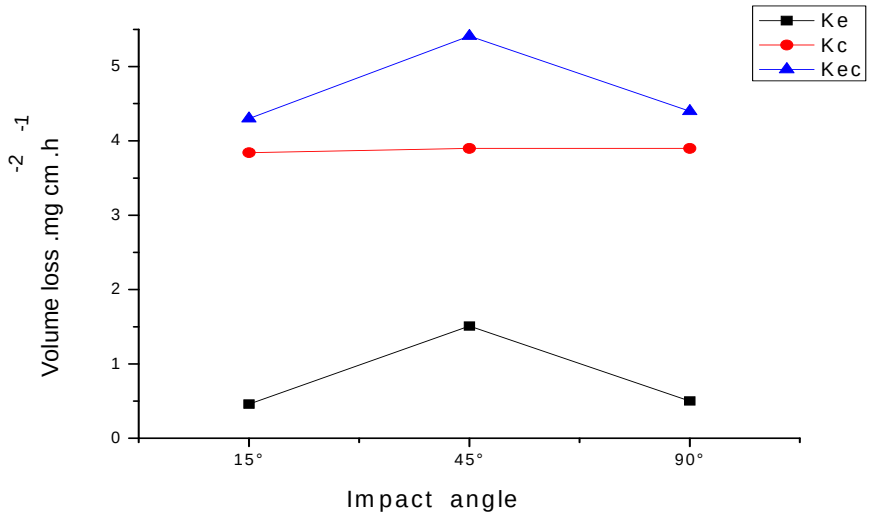

(c)

Fig.4.19: Volume loss as function of impact angles for carbon steel in water at 2.5 m s^{-1} impact velocity and particle size 150-300µm (a) -400mV (b) 0mV (c) 400mV

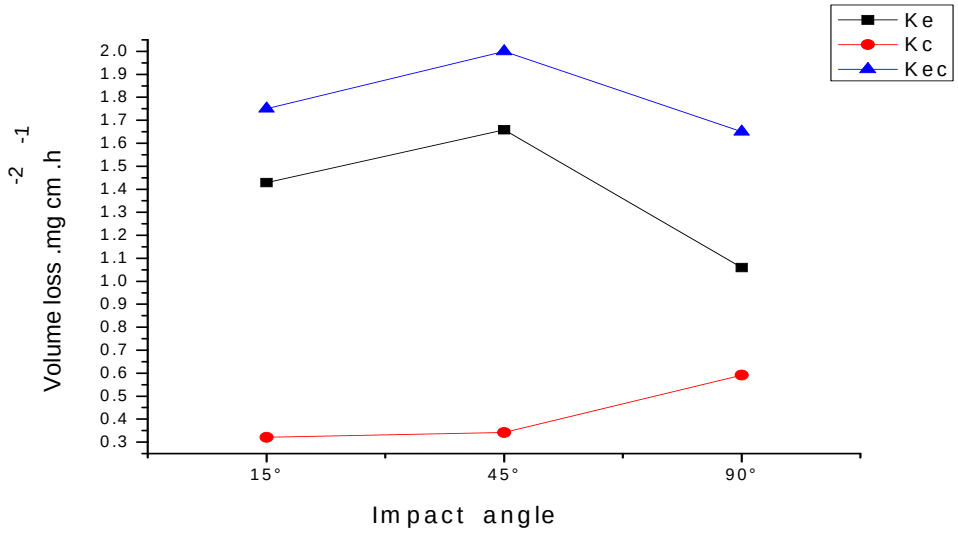

(a)

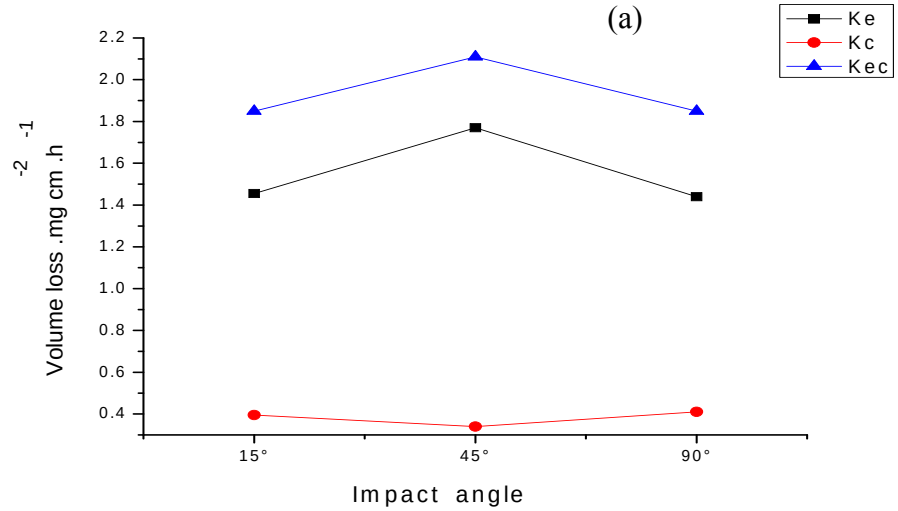

(b)

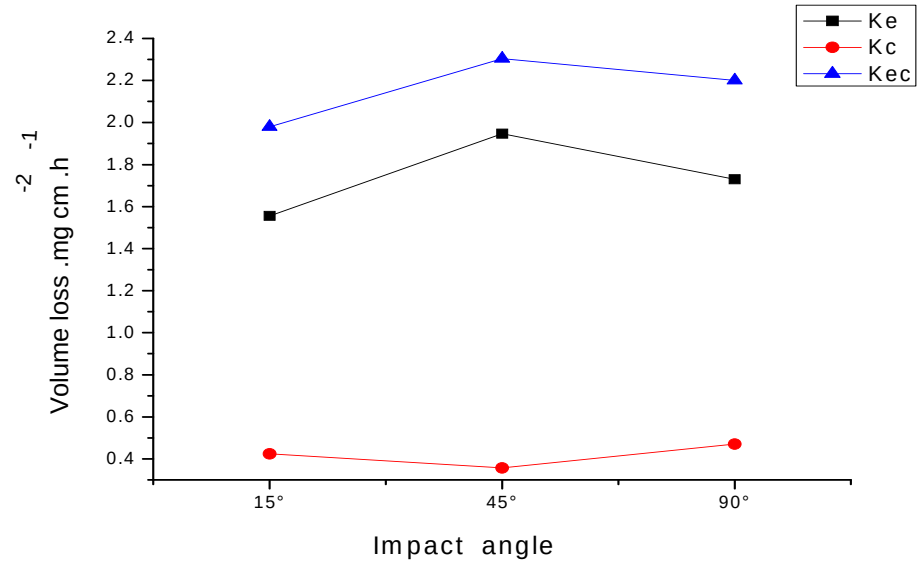

(c)

Fig.4.20: Volume loss as function of impact angles for carbon steel in crude oil at 2.5 m s^{-1}impact velocity and particle size 150-300µm (a) -400mV (b) 0mV (c) 400mV

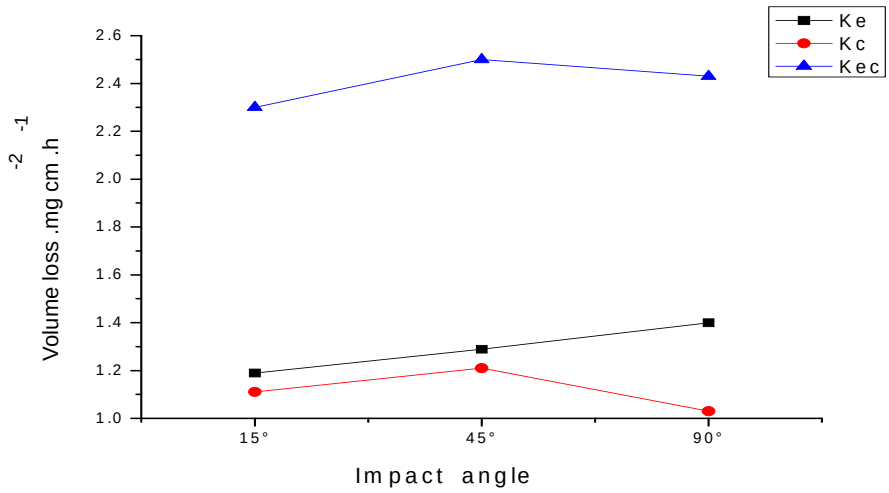

(a)

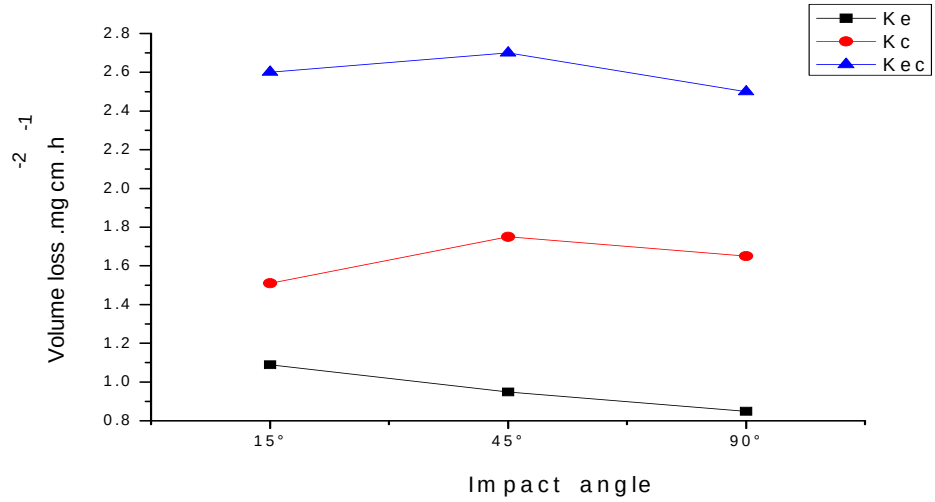

(b)

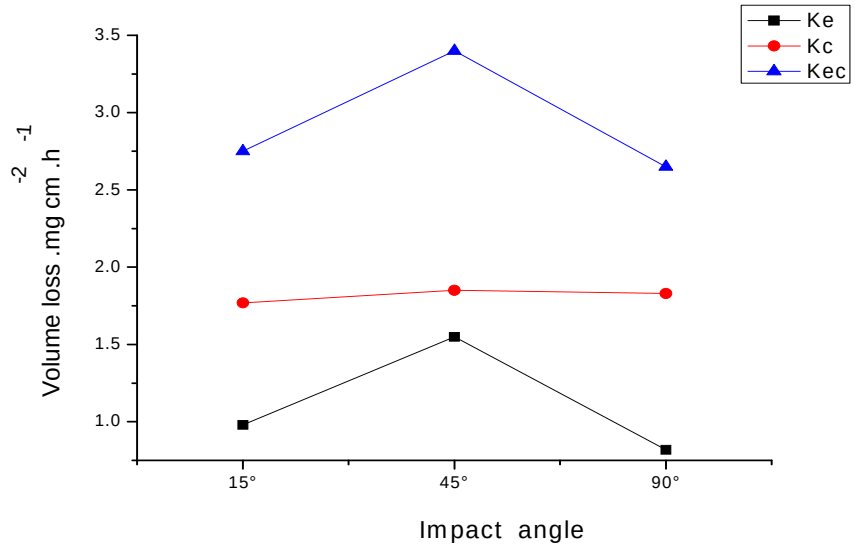

(c)

Fig.4.21: Volume loss as function of impact angles for carbon steel in oil /20% water at 2.5 m s^{-1}impact velocity and particle size 150-300µm (a) -400mV (b) 0mV (c) 400mV

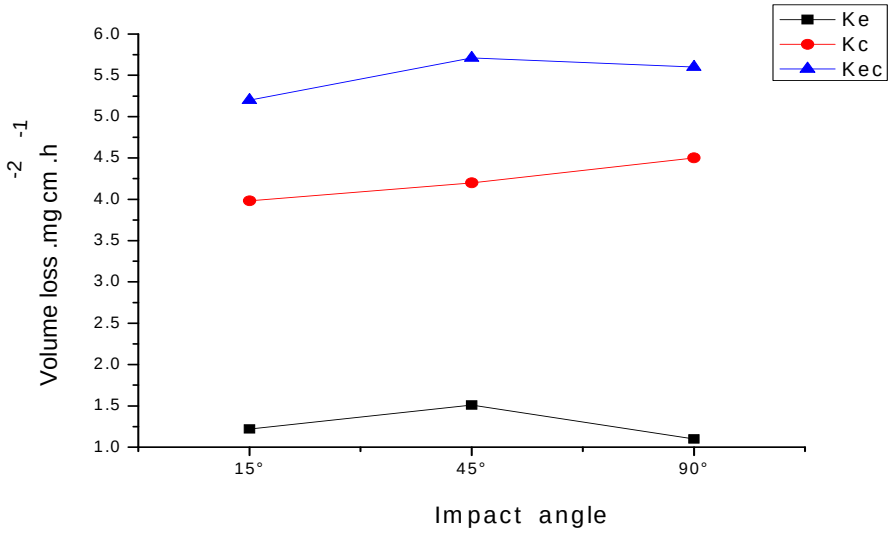

(a)

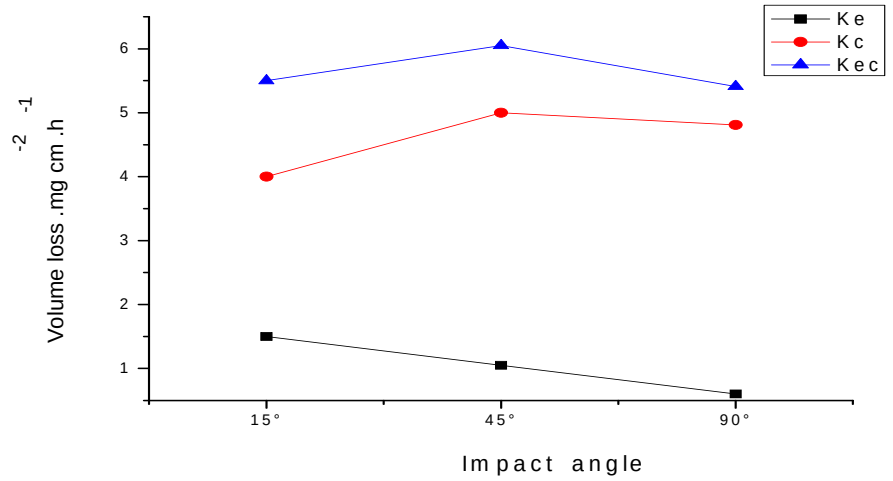

(b)

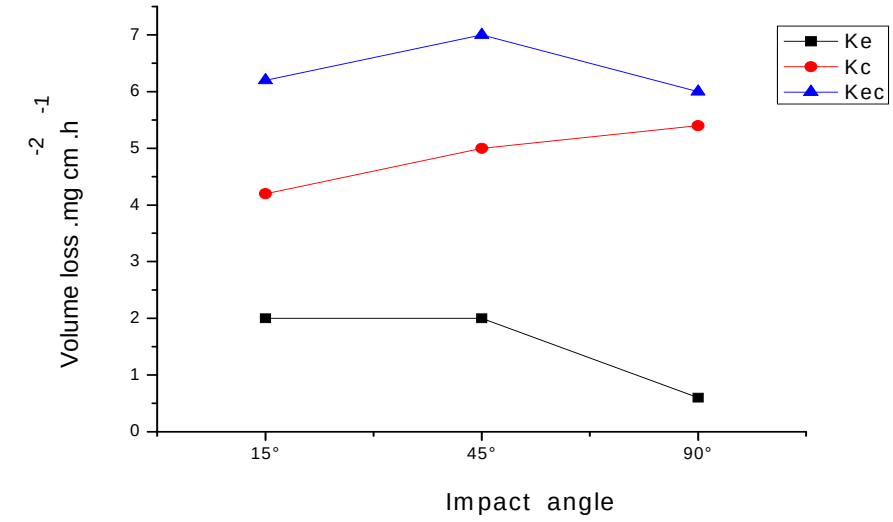

(c)

Fig.4.22: Volume loss as function of impact angles for carbon steel in water at 3.5 m s^{-1}impact velocity and particle size 150-300µm (a) -400mV (b) 0mV (c) 400mV

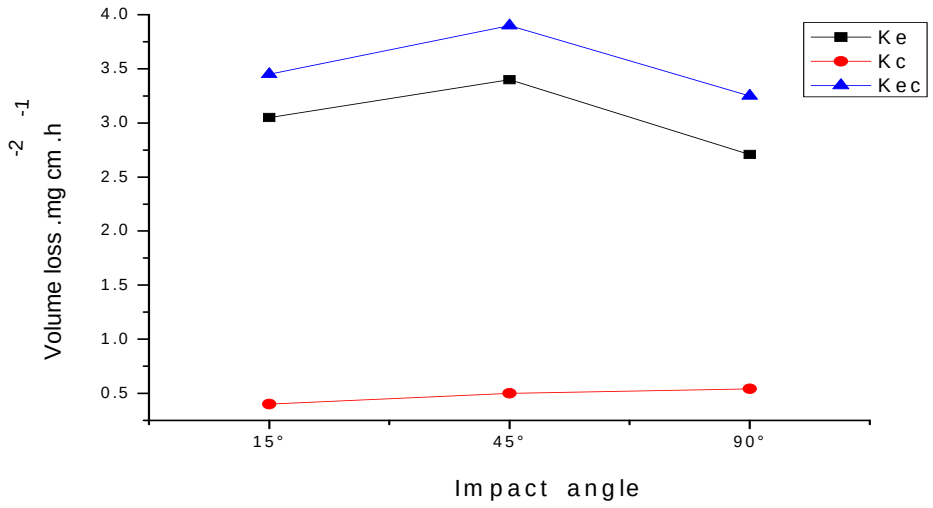

(a)

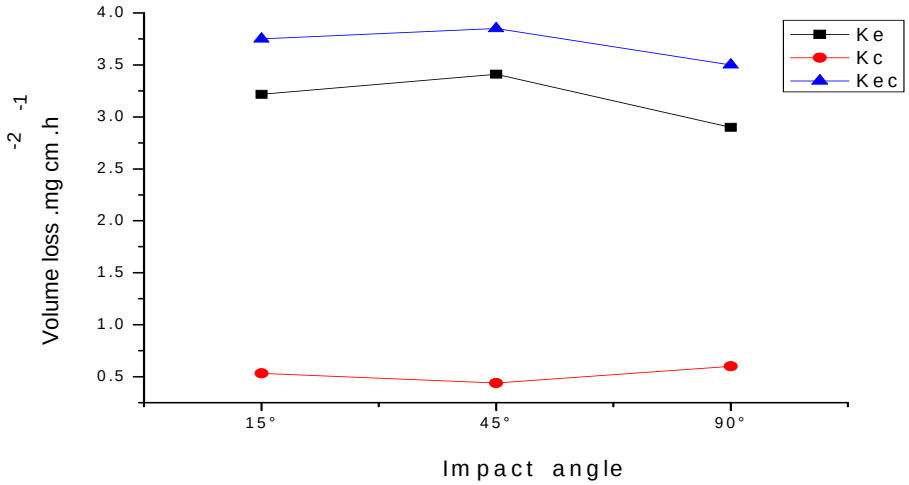

(b)

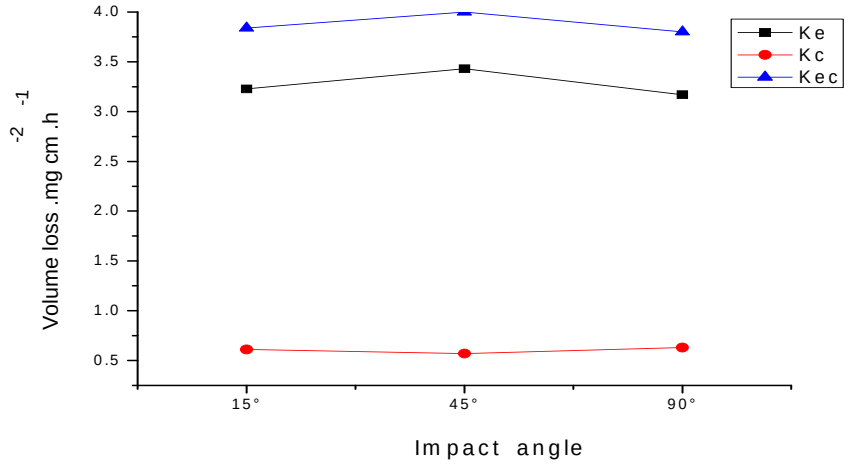

(c)

Fig.4.23: Volume loss as function of impact angles for carbon steel in crude oil at 3.5 m s^{-1} impact velocity and particle size 150-300µm (a) -400mV (b) 0mV(c) 400mV

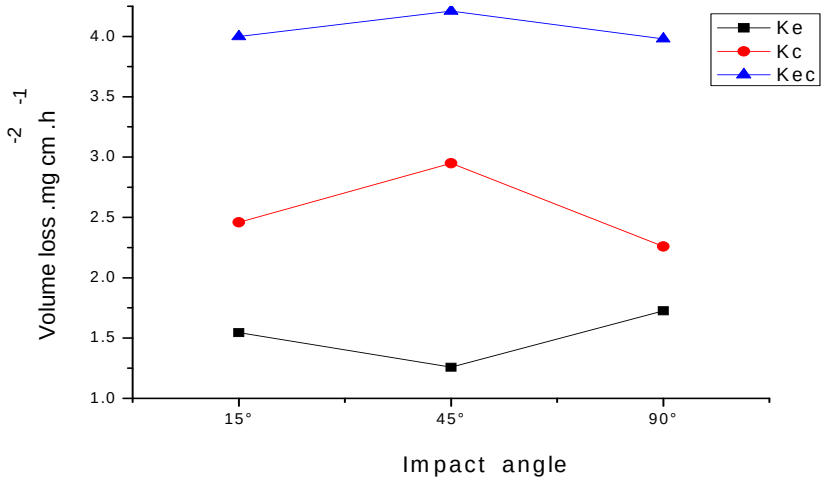

(a)

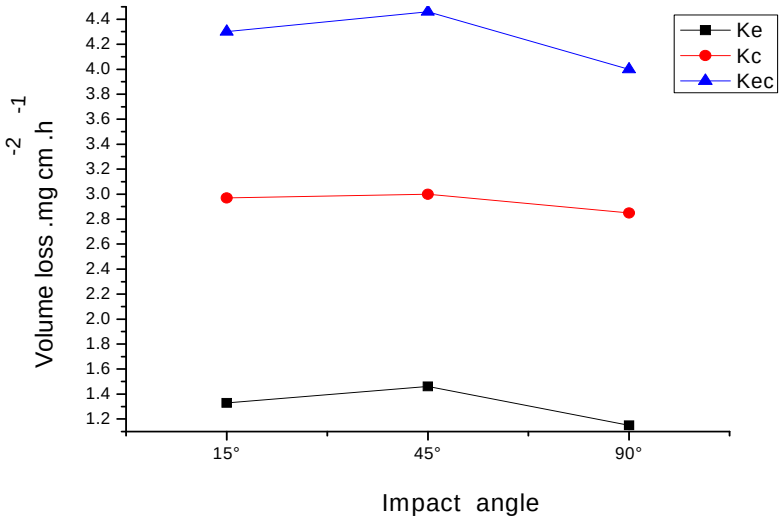

(b)

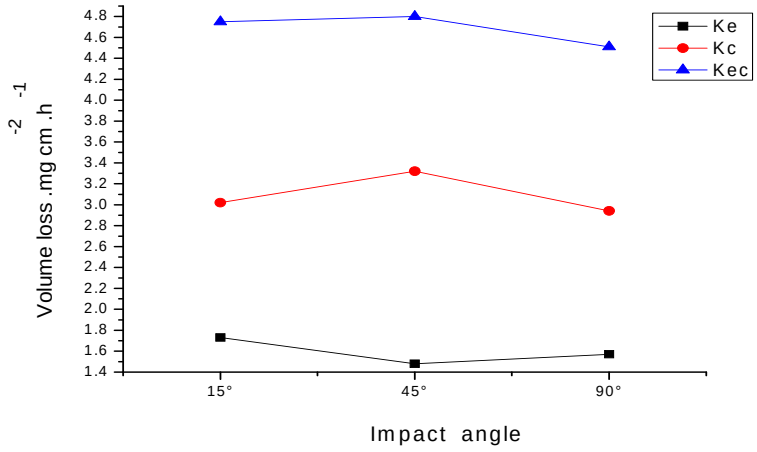

(c)

Fig.4.24: Volume loss as function of impact angles for carbon steel in oil /20% water at 3.5 m s^{-1}impact velocity and particle size 150-300µm (a) -400mV (b) 0mV(c) 400mV

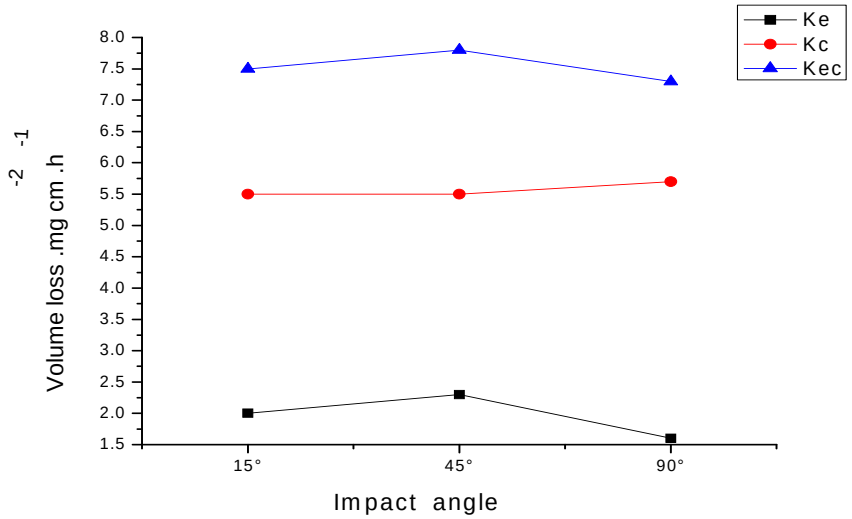

(a)

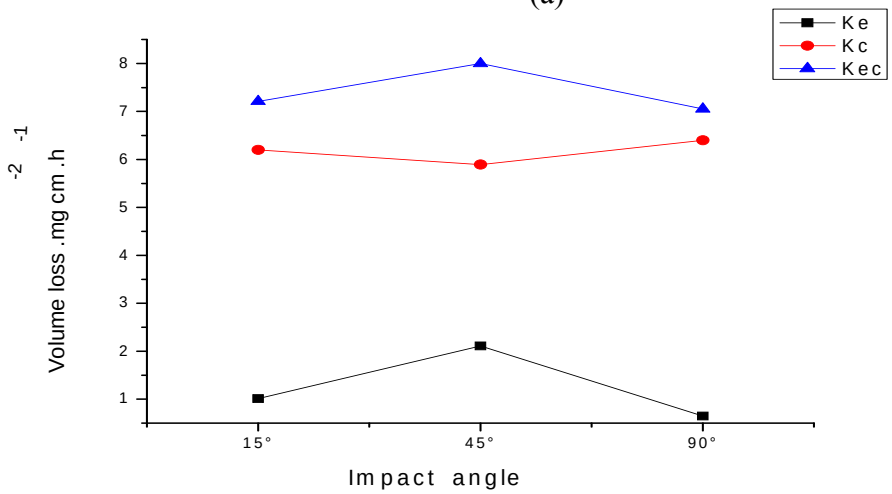

(b)

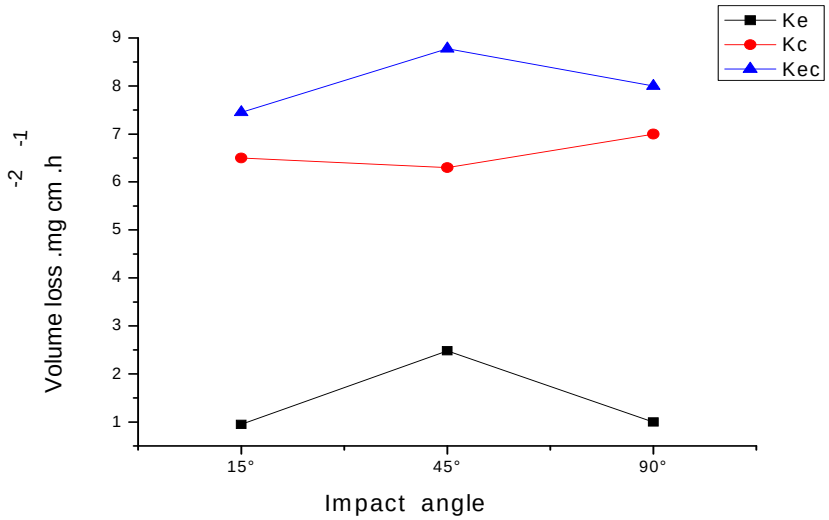

(c)

Fig.4.25: Volume loss as function of impact angles for carbon steel in water at 4.5 m s^{-1}impact velocity and particle size 150-300µm (a) -400mV (b) 0mV (c) 400mV

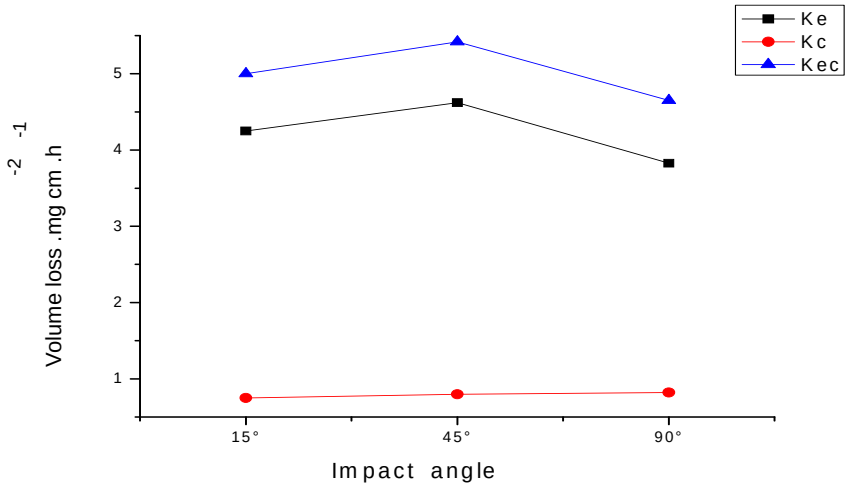

(a)

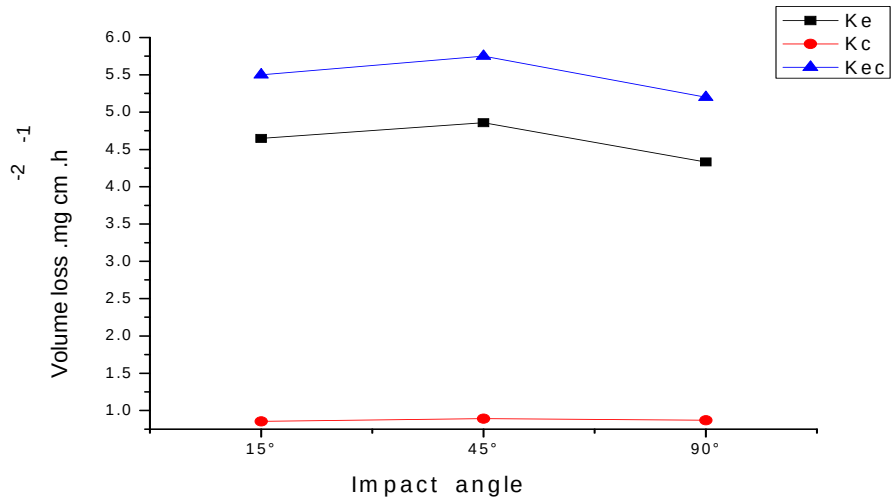

(b)

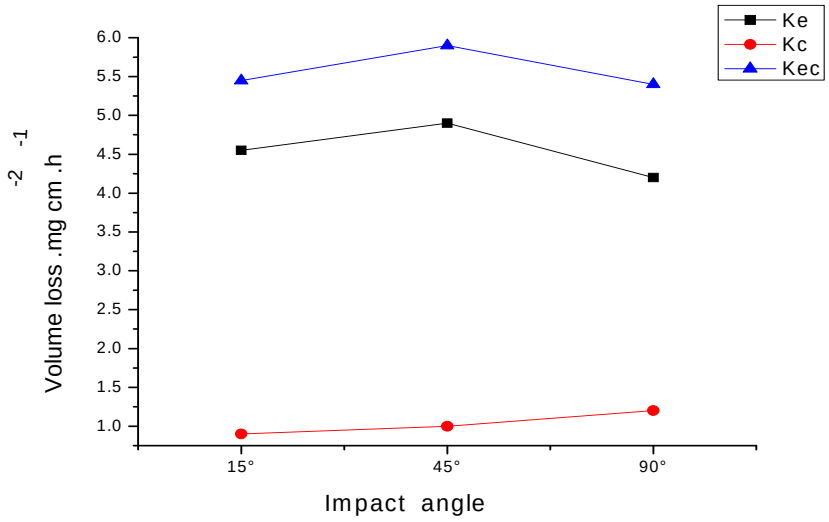

(c)

Fig.4.26: Volume loss as function of impact angles for carbon steel in crude oil at 4.5 m s^{-1}impact velocity and particle size 150-300µm (a) -400mV (b) 0mV (c) 400mV

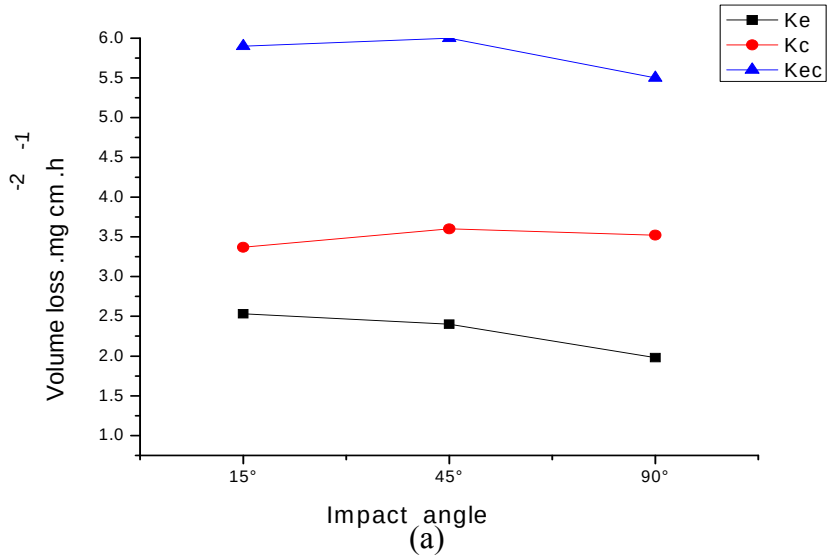

(a)

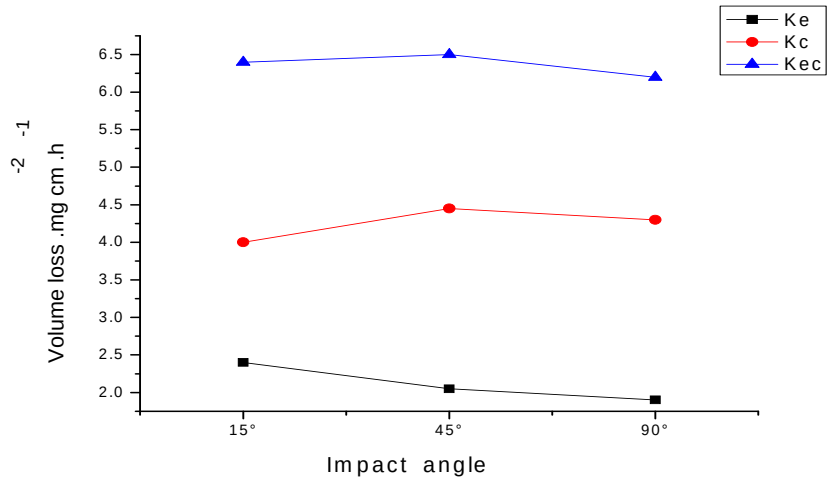

(b)

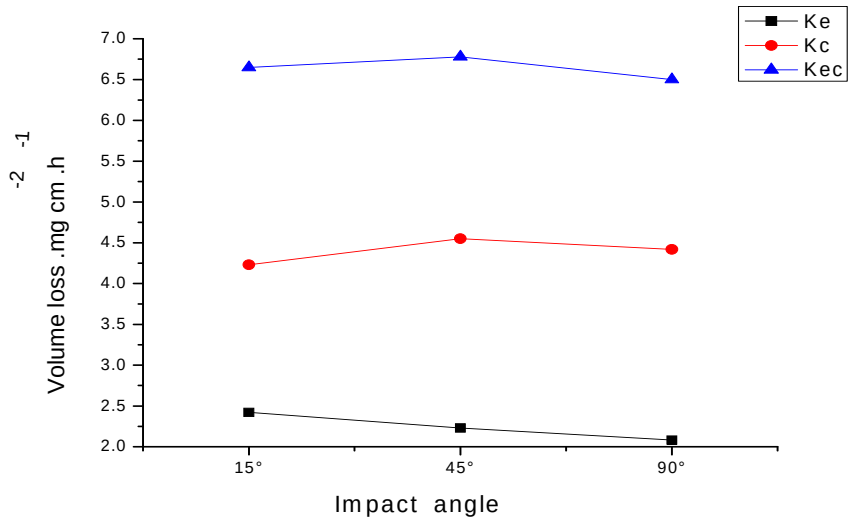

(c)

Fig.4.27: Volume loss as function of impact angles for carbon steel in oil /20% water at 4.5 m s^{-1}impact velocity and particle size 150-300µm (a) -400mV (b) 0mV (c) 400mV

4.2.4. SEM for particles sizes 150-30µm

Figures 4.28-4.32 show scanning electron micrographs of eroded carbon steel. The specimen was affected by a change in impact velocity and impact angle in all three environments containing particles sized150-300µm.

In the reservoir water environment Fig. 4.30-(a), it can be seen that there was good evidence of plastic deformation on the surface of the specimen by the impact of erodent particles at applied potential 400 mV. The displaced lips of passive film remains attached to the surface of specimen. Moreover, it can be seen from Figures 4.30. (b- d) that, the composition of spectrums 1, 2 and 3 indicates the presence of aluminium which is coming from the particle, while oxygen is coming from the environment.

For carbon steel in crude oil environment the mass loss tended to rise with an increase in the impact velocity, resulting in the presence of deformation on the surface of the specimen which could be due to the impact of particles as can be seen in Fig. 4.31-(a). The surface of the specimens in the three environments containing particles sized 150-300µm exhibits less damage compared with large impact particles sized 600-710µm. Moreover, analysis of the surface of the specimen indicated the presence of some elements of the chemical composition of crude oil such as sodium, potassium and sulphur (Figures 4.31(b-d)).

For carbon steel in the crude oil/20% water environments Fig 4.32(b-d) showed the chemical composition contain the sodium traces as consistent with experimental for crude oil. Other elements on the surface of the specimen indicate the chemical composition of carbon steel.

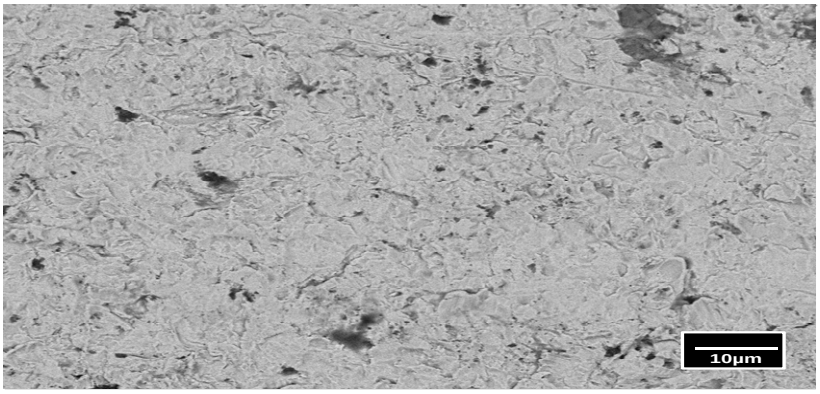

(a)

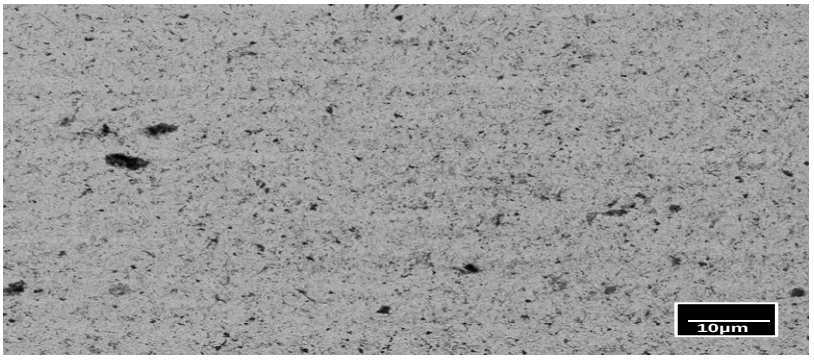

(b)

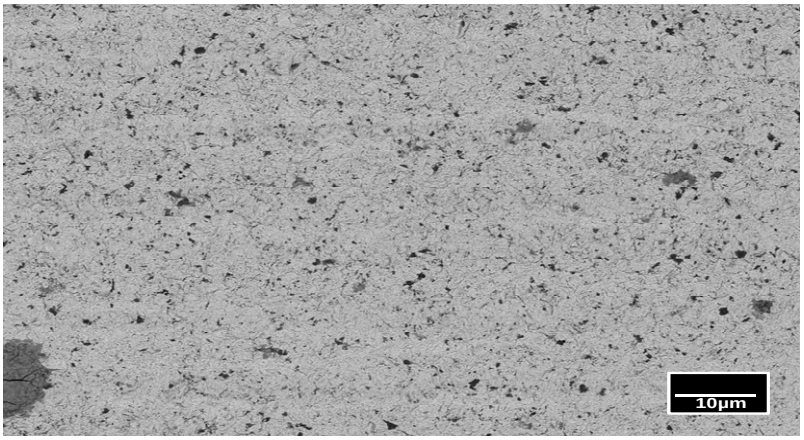

(c)

Fig.4.28: Scanning electron micrographs of eroded carbon steel test specimen at 2.5 m s^{-1}, impact angle 15° and 150-300µm in (a) water (b) crude oil (c) oil /20% water.

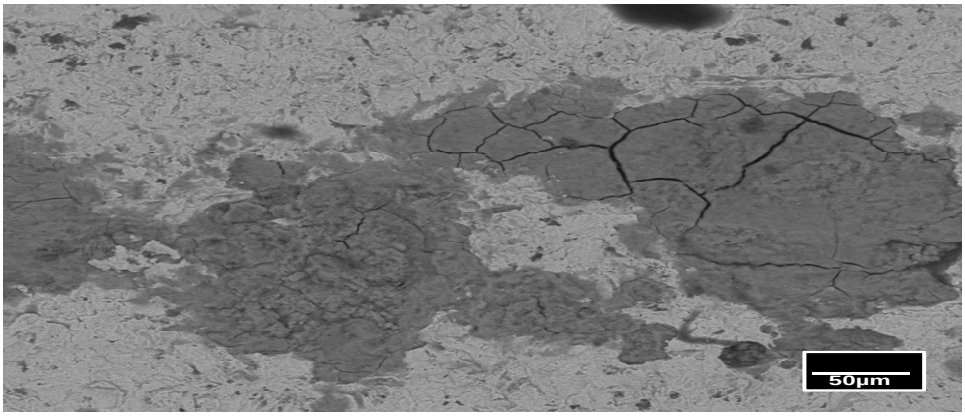

(a)

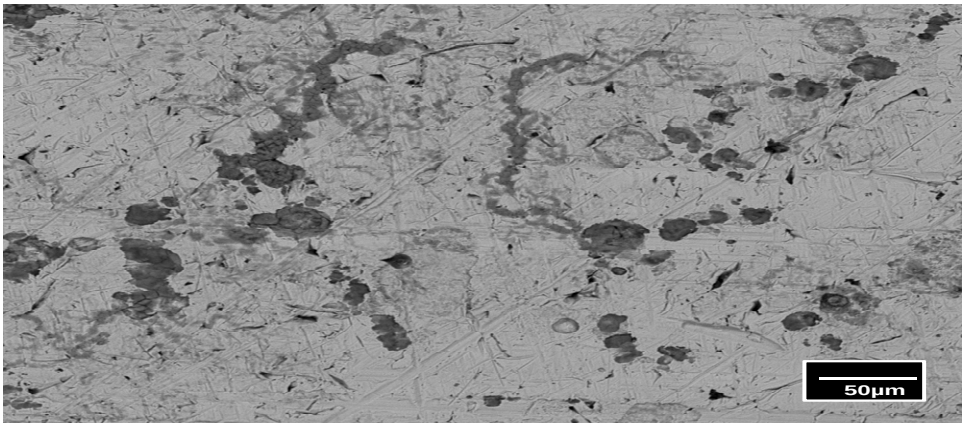

(b)

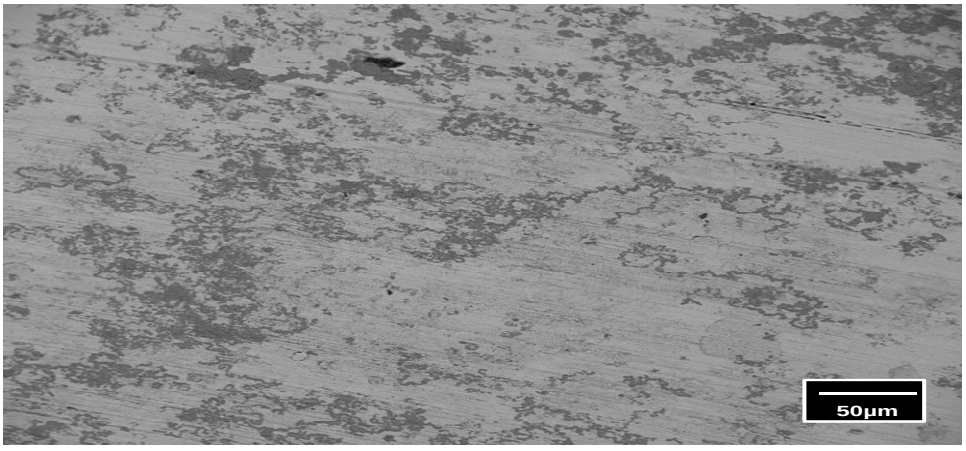

(c)

Fig. 4.29: Scanning electron micrographs of eroded carbon steel test specimen at 3.5 m s^{-1},impact angle 45° and 150-300µm in (a) water (b) crude oil (c) oil /20% water.

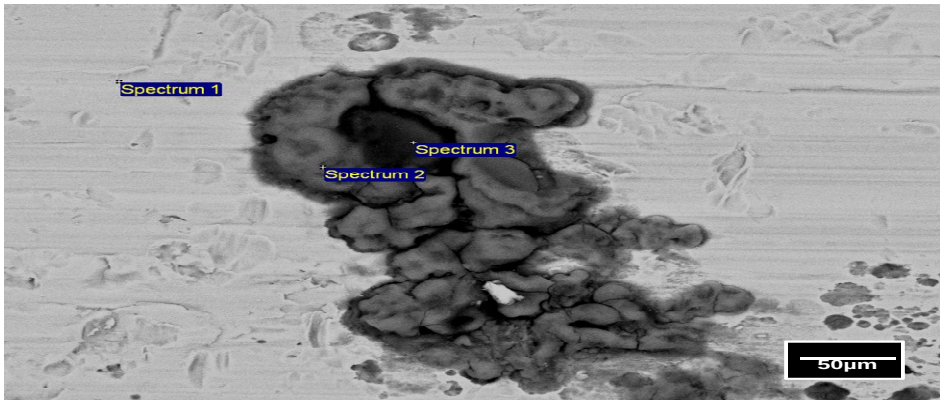

(a)

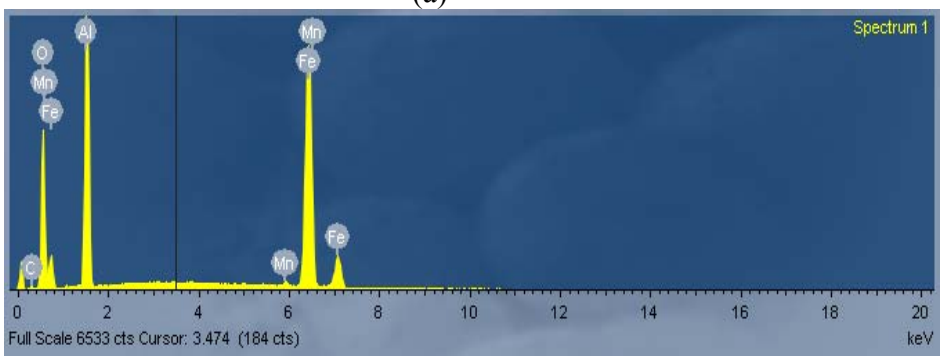

(b)

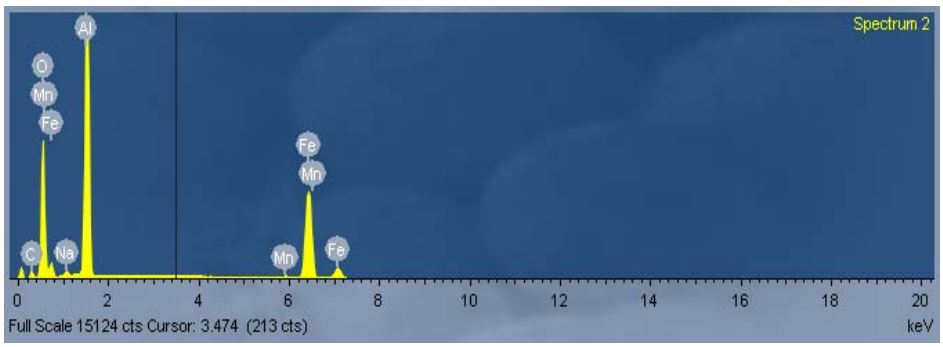

(c)

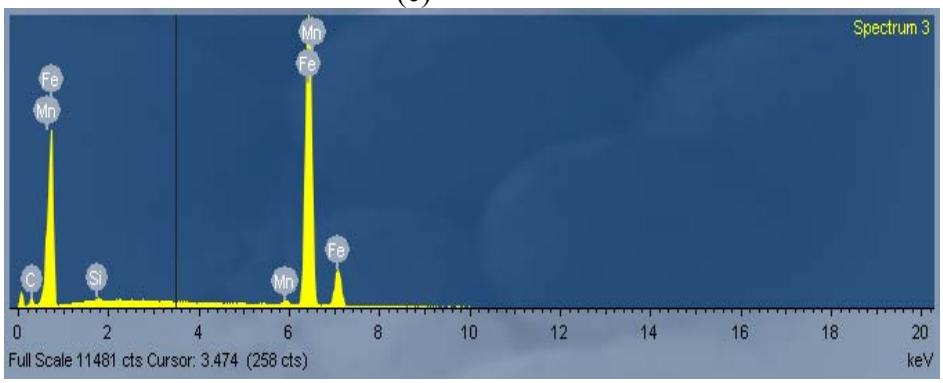

(d)

Fig.4.30: Scanning electron micrographs of eroded carbon steel test specimen at 4.5 m s^{-1}, impact angle 90° and 150-300µm (a) in water (b) analysis of the spectrum-1 (c) analysis of the spectrum-2 (d) analysis of the spectrum-3

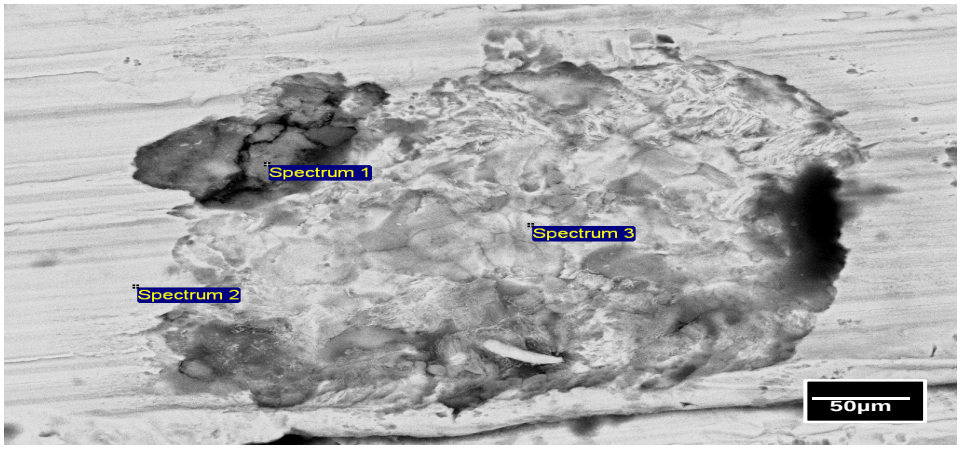

(a)

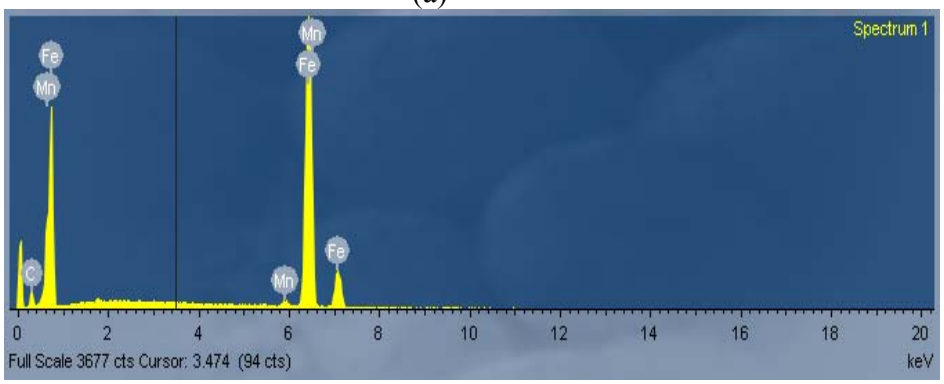

(b)

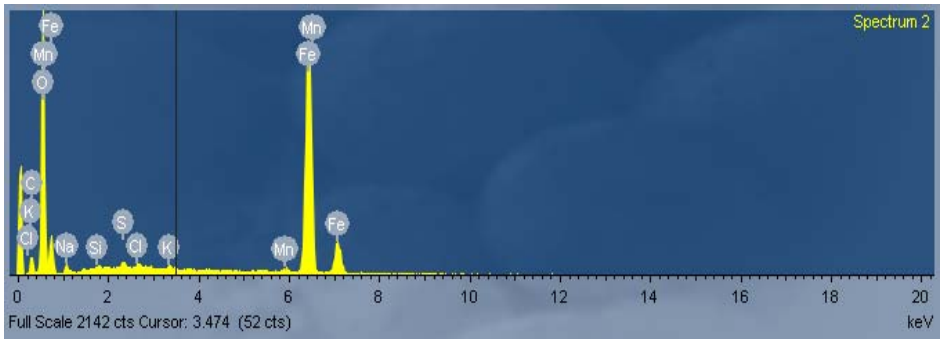

(c)

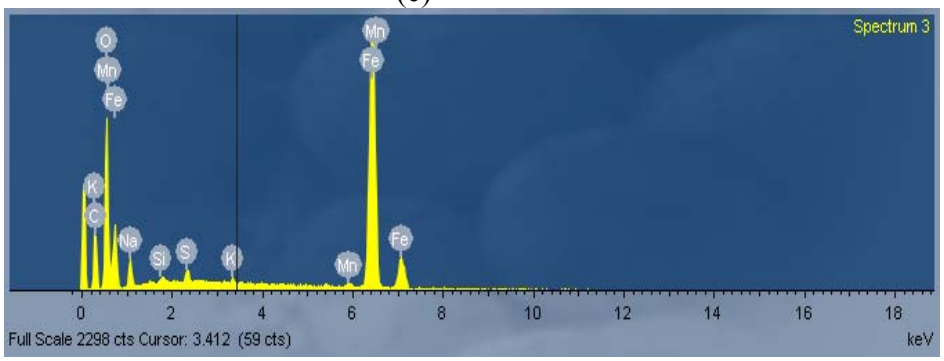

(d)

Fig.4.31: Scanning electron micrographs of eroded carbon steel test specimen at 4.5 m s^{-1}, impact angle 90° and 150-300µm (a) in crude oil (b) analysis of the spectrum-1 (c) analysis of the spectrum-2 (d) analysis of the spectrum-3

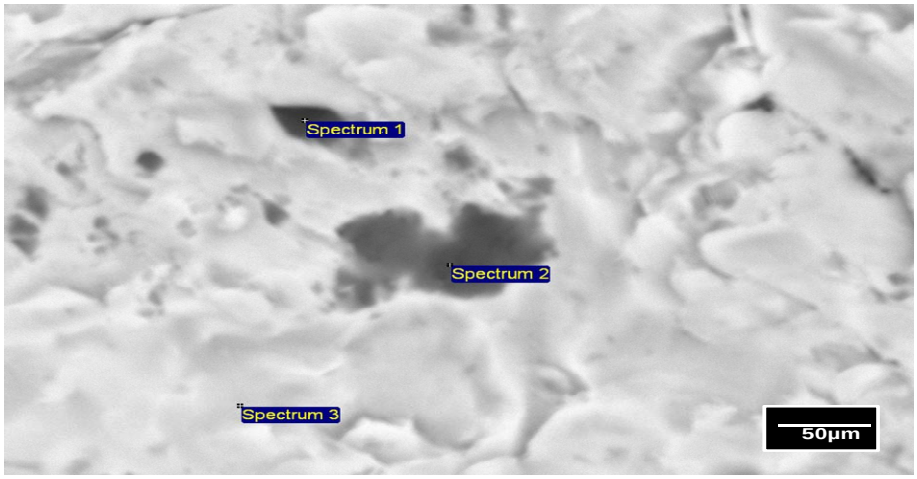

(a)

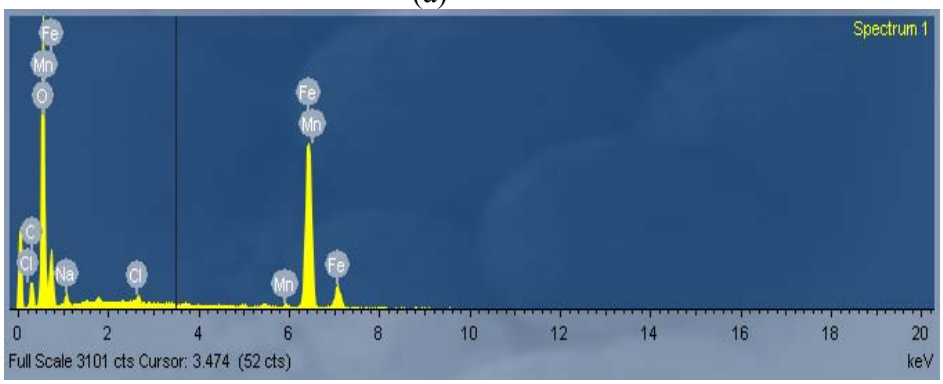

(b)

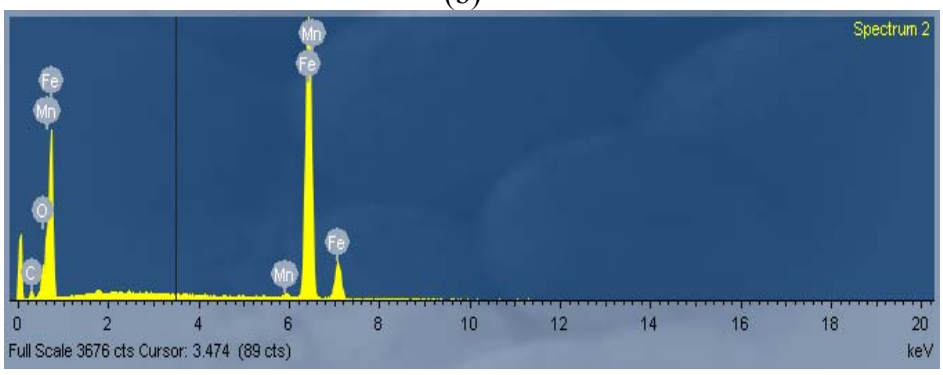

(c)

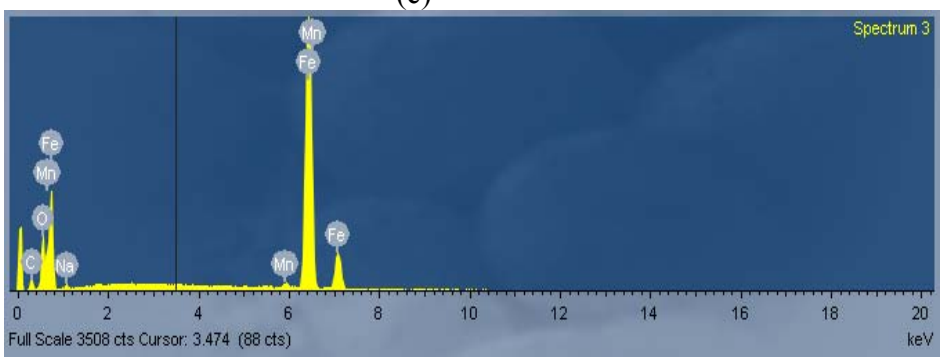

(d)

Fig.4.32: Scanning electron micrographs of eroded carbon steel test specimen at 4.5 m s^{-1}, impact angle 90° and 150-300µm in oil /20% water (b) analysis of the spectrum-1 (c) analysis of the spectrum-2(d) analysis of the spectrum-3

4.3. Discussion

4.3.1. Polarization curves

The results for carbon steel in the three environments containing two different particle sizes indicate that there is a significant reduction in the corrosion current density (Figures 4.1-4.3 (a-b) and Figures 4.16-4.18 (a-b)) when the experimental conditions are changed from water to crude oil and from a small particle size of 150-300μm to a larger particle size of 600-710μm. However, the results for carbon steel in oil/ 20%water slurry indicate current densities are in between those recorded in the two other environments (Figures 4.1-4.3(c) and Figures 4.16-4.18(c)).

This indicates that corrosion contribution is reduced significantly in crude oil environments and this can be attributed to a decrease in the diffusion of iron (Fe) ions in the crude oil environment due to the oil film on the surface of specimen [10] and [17]. In addition, the diffusion of oxygen is higher in crude oil than in reservoir water and this is the possibly the reason why the cathodic current densities are higher than the anodic current densities in the crude oil environment [2, 10 and 11] (Figures 4.1-4.3 (b) and Figures 4.16-4.18(b)). In the water environments containing particles sized 600-710μm ,a maximum corrosion current density is observed at an impact angle between 30^o and 60^o (Figure 4.1 (a)). This indicates that in reservoir water environment where formation of a corrosion product is built, impingement at low impacts angle tends to cause higher degradation rates, unlike that which is observed in the oil environment containing particles sized 600-710μm where the maximum recorded is at 75^o and 90^o (Figure 4.1 (b)).

On the other hand, in the water environments containing particles sized 150-300μm, a maximum corrosion current is observed at impact angles 45^o and 90^o (Figures 4.16-4.17 (a)). A similar situation to that is observed in the crude oil environment containing the same sized particles of 150-300μm, where the maximum recorded is at 45^o and 90^o (Figure 4.18 (b)).

4.3.2. Volume loss

In the water environment the effect of applied potentials at various impact angle and constant velocity shows good trends of the value of erosion contribution and corrosion contribution (Figures 4.4-4.10 and Figures 4.19-4.25). However, in the crude oil environment for carbon steel with two different particle sizes(150-300 μm and 600-710μm), there is a marginally higher mass loss (Kec) at 400 mV and at impact velocities of 2.5m s^{-1} and 4.5m s^{-1} (Fig. 4.5 (e) and Fig. 4.26(c)) compared to that observed at lower potentials -400 mV. In addition, the trends for the effect of impact angle indicate that the maximum mass loss (Kec) is at 90^{o} and 45^{o} Fig. 4.19- Fig. 4.26, consistent with the results on the polarization data, Figures 4.1-4.3(b) and Figures 4.16-4.18 (b). Clearly, the reduction in oil film reduces the erosion-corrosion resistance of the layer, whilst increasing the film formed on the surface increases the erosion resistance [6].

It can be concluded from these results that, the corrosion rate changes extensively in the reservoir water environment with an increase in impact velocity and applied potential due to removal of the passive film during slurry impact. Since the film growth increases directly with an increase in potential, increases in velocity result in higher current densities due to removal of the passive film [16-17].

4.3.3. SEM

For carbon steel in the three environments showed less damage due to the effect of a small impact particle size 150-300μm Figures 4.28-4.32 compared with the effect of a large impact particle sized 600-710μm(Fig.4.13-15) on the surface of the specimen. The effect of a small impact particle size on the surface of carbon steel in the water and combined environments resulted in less value of mass loss due to a decrease in the particle size compared with the previous large particle size, and it is interesting to see for a small particle size 150-300μm that the presence of the corrosion products on the surface of the specimen tended to increase with an increase in potential on the surface of the specimen at low impact velocity 2.5 m $s^{-1}$and impact angle 15° Figures 4.28-4.29(a and c).

4.3.4. Erosion–corrosion maps

4.3.4.1. Erosion-corrosion mechanism maps

The erosion-corrosion mechanism maps show different changes in the regimes as a function of impact angles and potentials. Tables 4.19-4.27 and 4.28-4.36 show the various Ke, Kc and Ke/Kc values. In the reservoir water environment containing particles sized 600-710µm at constant impact velocity of 2.5m s^{-1} Fig.4.33-(a), as can be seen, the passivation-erosion regime dominates at intermediate and high impact angles. However, at potentials lower than -300 mV in cathodic conditions the erosion-dissolution regime dominates. The erosion-passivation regime is dominated from intermediate to low impact angles and high potentials (i.e. at 400 mV).

However, in the reservoir water environment containing particles sized 150-300µm (Figures 4.36-4.38 (a)) at constant impact velocities of 2.5, 3.5 and 4.5m s^{-1} the passivation-erosion regime dominates the impact angle and potential range studies.This confirm the higher corrosion rate for the small particle.

For carbon steel in the crude oil environment containing particles sized 600-710µm at constant impact velocities of 2.5, 3.5 and 4.5m s^{-1} Figures 4.33-35(b), as can be seen, the total area of the map is dominated by erosion, indicating that there is very low value of corrosion contribution in such conditions, consistent with the results of mass loss (Figures 4.5-4.11). On the other hand, Figures 4.36-4.38(b) shows carbon steel in the crude oil environment containing small particles sized 150-300µm at constant impact velocities of 2.5,3.5 and 4.5m s^{-1}, the map is dominated by erosion-passivation regime, indicating that particle impact has small effect on the surface of specimen.

However, in the combined environments containing small particles sized 150-300µm, as shows in Figures 4.36-4.38 (c), the map is dominated by passivation–erosion at potentials greater than -400mV, which could be attributed to the passive film not being affected by the effect of small particles. On the other hand, erosion-passivation dominates at potentials lower than -400mV at impact velocity 2.5 m s^{-1} Figure 4.36(c).

4.3.4.2. Erosion-corrosion wastage maps

Tables 4.1- 4.9, 4.10-4.18 show the methodology for calculation of the values of boundaries (Kec) in three environments for particle sizes (150-300µm and 600-710µm). The maps (Figures 4.39(a-c) and Figures 4.42) indicate that low wastage regime is dominant for all three environments containing particles sized 600-710µm and 150-300µm at constant impact velocity 2.5 $m\,s^{-1}$, which could be due to low impact velocity (low oxygen solubility), indicating low mass loss due to oil and passivation film on the surface of specimen.

However, in the reservoir water, crude oil and combined environment containing particles sized 600-710µm at constant impact velocity 3.5 $m\,s^{-1}$ there is strong evidence of the presence of the medium wastage regime at high applied potentials due to removal of the passive and oil film by particles impact, indicating an increase in the erosion–corrosion mass loss (Fig. 4.40(a- c)).

However, for carbon steel in water containing small particles sized 150-300µm the medium wastage regime covers the area in the anodic condition and shifts to the low potential at an impact angle of 45° (Fig. 4.43 (a)) that indicated to the mass loss increased at an impact angle of 45° which is consistent with previous researchers[10] and [11].The medium wastage regime becomes dominant in all the maps in the reservoir water, combined environment containing particles sized 600-710µm and 150-300µm at constant impact velocity 4.5 $m\,s^{-1}$ and that can be attributed to an increase in mass loss due to impact velocity(Fig. 4.41(a & c) and Fig. 4.44(a & c)).

In the reservoir water and combined environment containing particles sized 600-710µm ,the low wastage is dominant at lower impact angle (i.e. 15° to 30°) (Fig. 4.40 (a) and(c), which could be due to the skidding of the particle on the surface of the specimen and decreasing the value of erosion contribution Ke.

4.3.4.3. Erosion-corrosion synergistic-additive maps

Tables 4.37-4.54 show the various ΔKe, ΔKc and Δke/Δke values. In three envionments the reservoir water, crude oil and oil/20%water environment containing particles sized 600-710μm and 150-300μm. The maps for the synergistic-additive contributions (Figures 4.45 (a-c) and Figures 4.48 (a-c)) show that the synergistic regimes are more dominant for the carbon steel in crude oil than for the reservoir water containing particles sized (150-300μm and 600-710μm) at impact velocity of 2.5 m s^{-1}. This greater percentage of synergistic behaviour in the crude oil environment could be due to the action of the particle impact on the surface of the specimen.

The synergistic regime observed at higher velocities 3.5 m s^{-1} and 4.5 m s^{-1} for carbon steel in the water and combined environments containing particles sized 600-710μm (Fig. 4.46 (a & c) and Fig. 4.47 (a & c)) may be attributed to increasing in the interaction between the erosion and corrosion due to increase of velocities. On the other hand, the antagonistic regime was also observed at higher impact velocity4.5 m s^{-1} in crude oil and combined environments containing particles sized 600-710μm (Figure47 (b-c)). This could be due to the impact of large particles on the surface of the specimen taking a long time between the first impact and the second impact, allowing oil film and passive film to form on the surface of the specimen.

4.4. Summary

(i) The volume loss of carbon steel in the three environments containing particles sized 600-710μm and150-300μm have been investigated at constant impact velocity

(ii) Polarization curves for erosion-corrosion of carbon steel in the three environments containing particles sized 600-710μm and 150-300μm have been produced at constant impact velocity.

(iii) The results on surface morphology indicate significantly more plastic deformation in the water environment compared to the crude oil environment.

(iv) Erosion-corrosion maps have been constructed based on the results showing the changes in erosion-corrosion mechanisms, the rank of wastage, and the extent of additive-synergistic/antagonistic behaviour at constant impact velocity.

(v) For carbon steel in the crude oil environment containing small particles sized 150-300μm showed that the low wastage regimes dominated the whole maps, while the medium wastage regime was presence in the crude oil environment containing large particles sized 600-710μm.

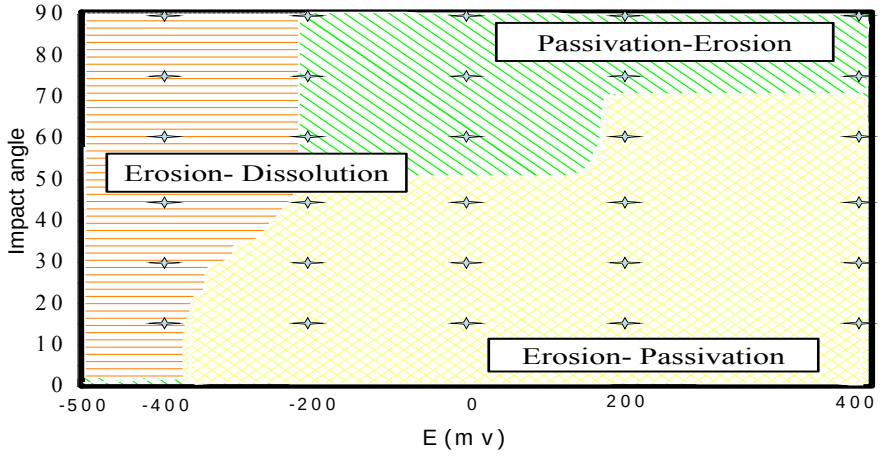

(a)

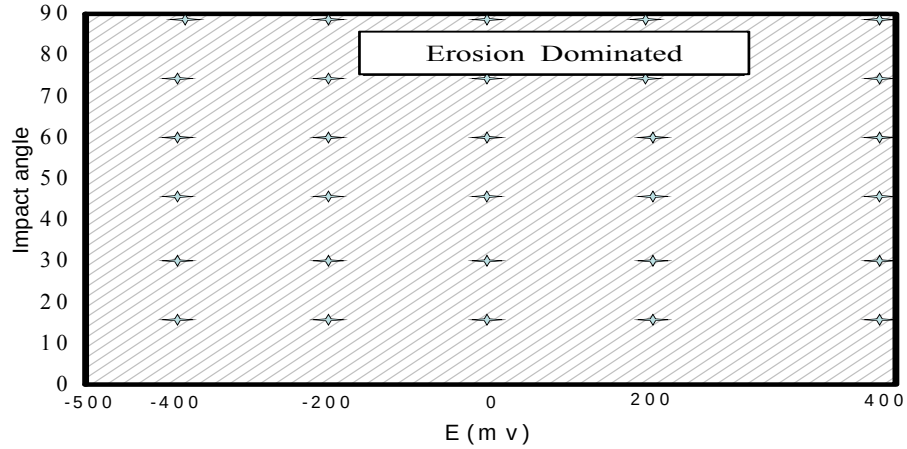

(b)

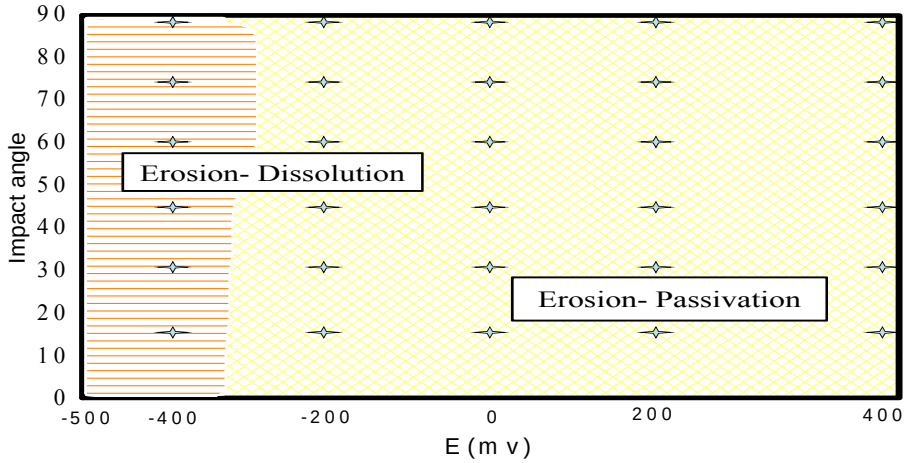

(c)

Fig.4.33: Erosion-corrosion mechanism maps for carbon steel at 2.5 m s^{-1} and particle size 600-710µm in (a) water (b) crude oil (c) oil /20% water.

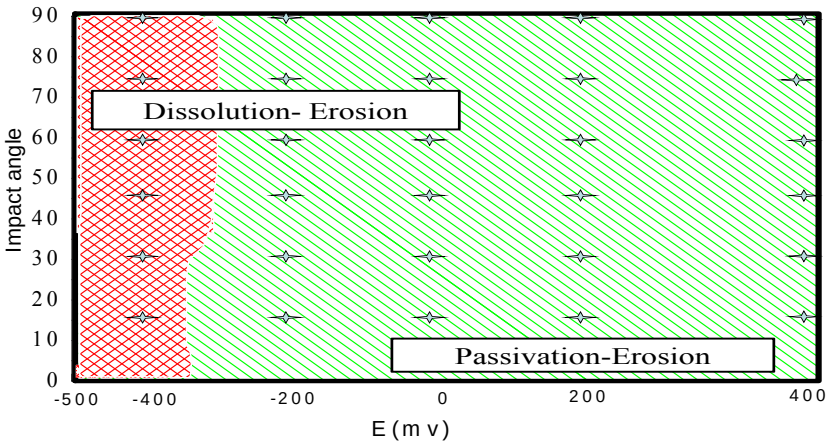

(a)

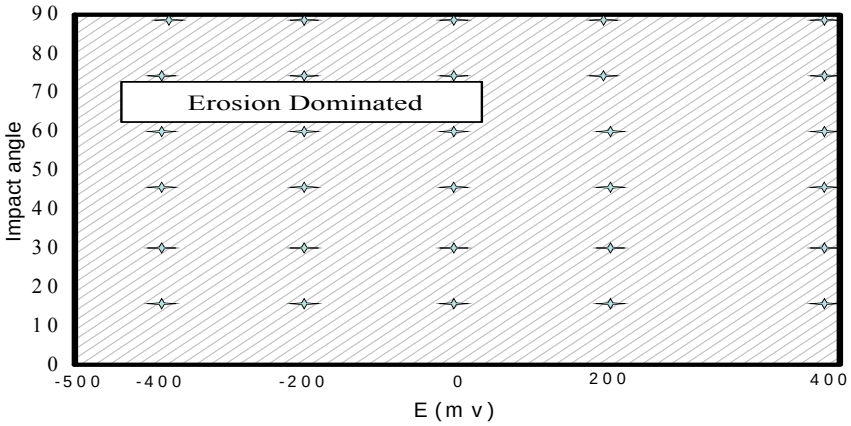

(b)

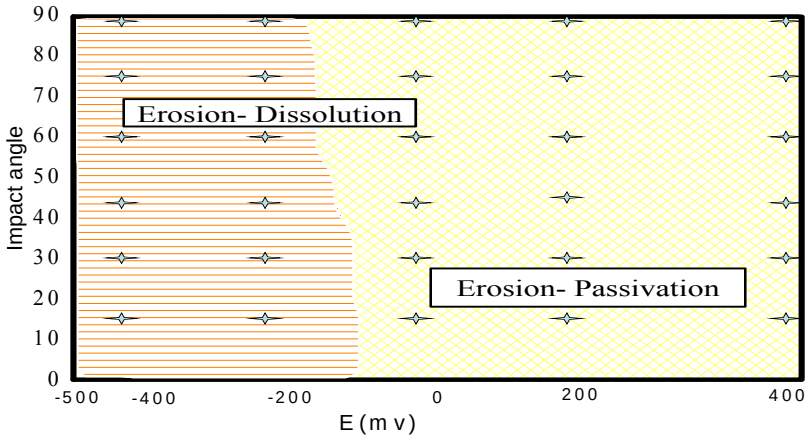

(c)

Fig.4.34: Erosion-corrosion mechanism maps for carbon steel at 3.5 m $s^{-1}$and particle size 600-710µm in (a) water (b) crude oil (c) oil /20% water.

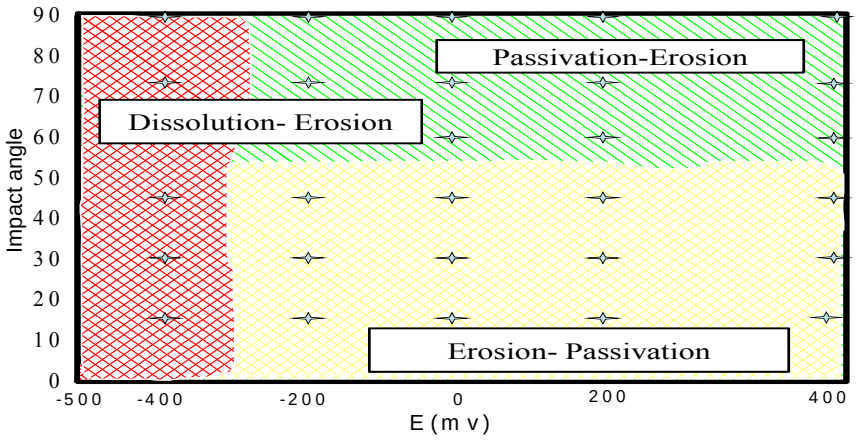

(a)

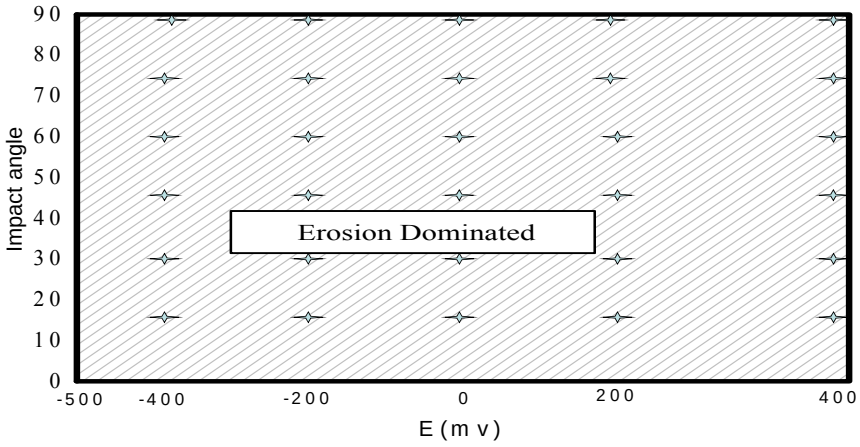

(b)

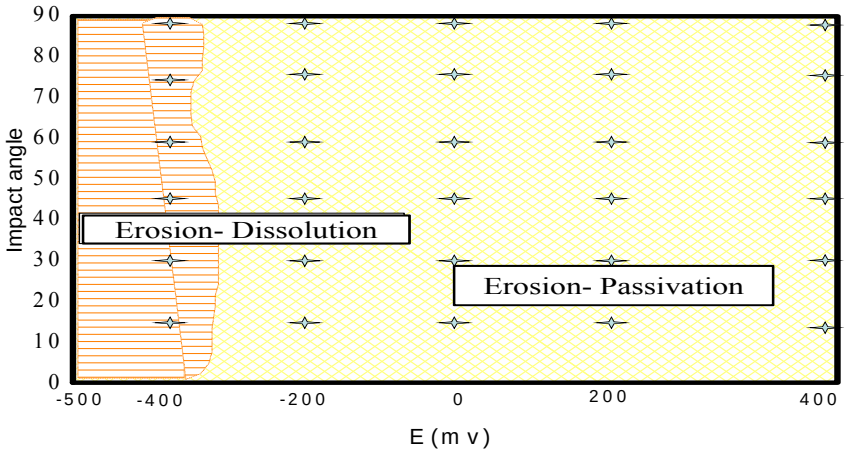

(c)

Fig.4.35: Erosion-corrosion mechanism maps for carbon steel at 4.5 m $s^{-1}$and particle size 600-710µm in (a) water (b) crude oil (c) oil /20% water.

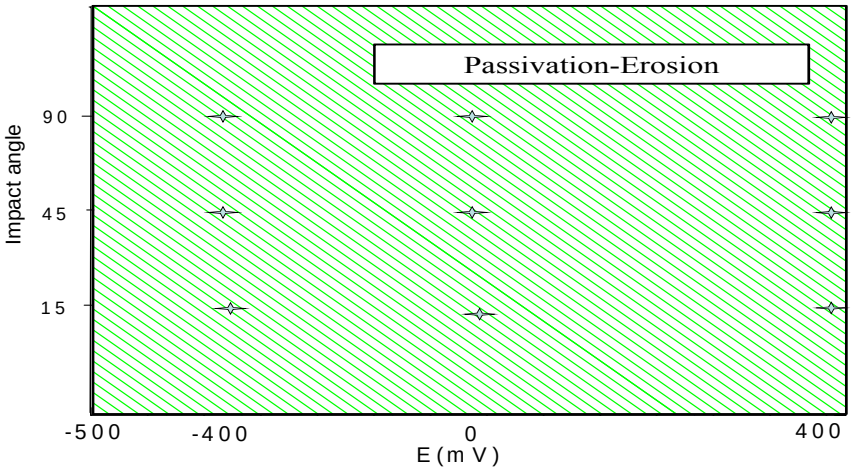

(a)

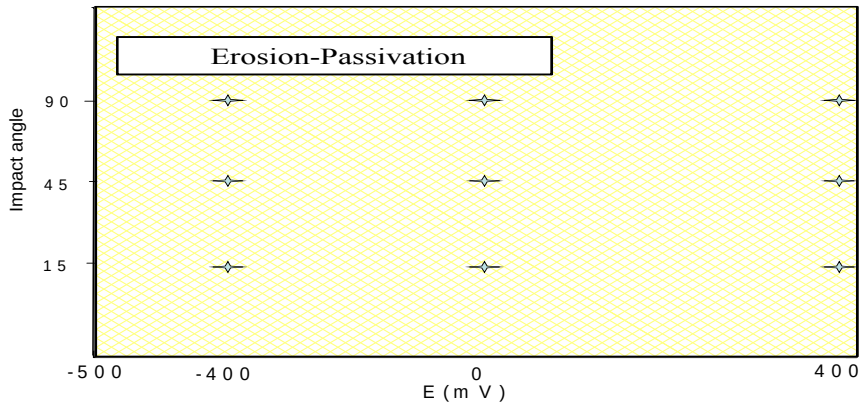

(b)

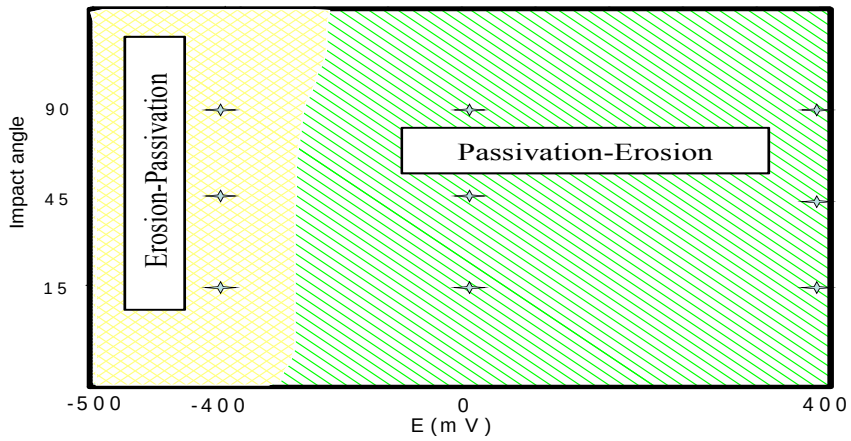

(c)

Fig.4.36: Erosion-corrosion mechanism maps for carbon steel at 2.5 m $s^{-1}$and particle size 150-300µm in (a) water (b) crude oil (c) oil /20% water.

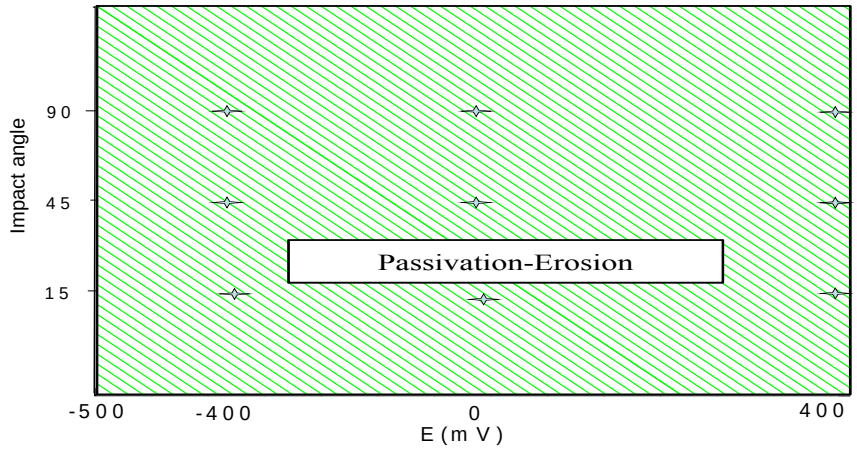

(a)

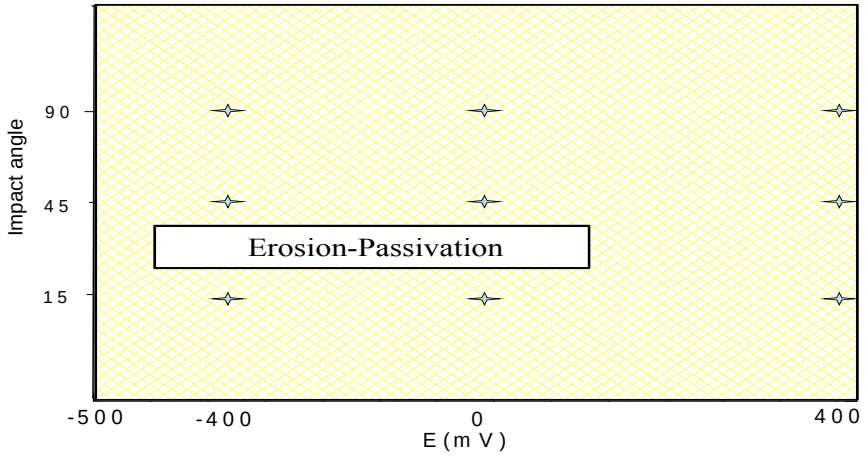

(b)

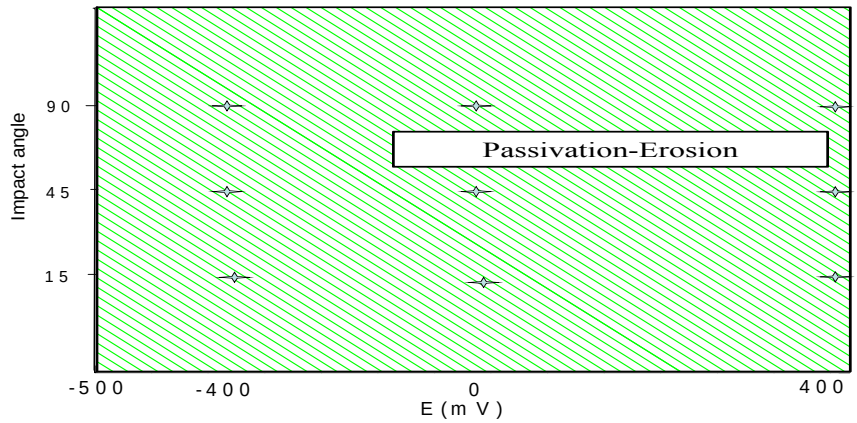

(c)

Fig.4.37: Erosion-corrosion mechanism maps for carbon steel at 3.5 m $s^{-1}$and particle size 150-300µm in (a) water (b) crude oil (c) oil /20% water.

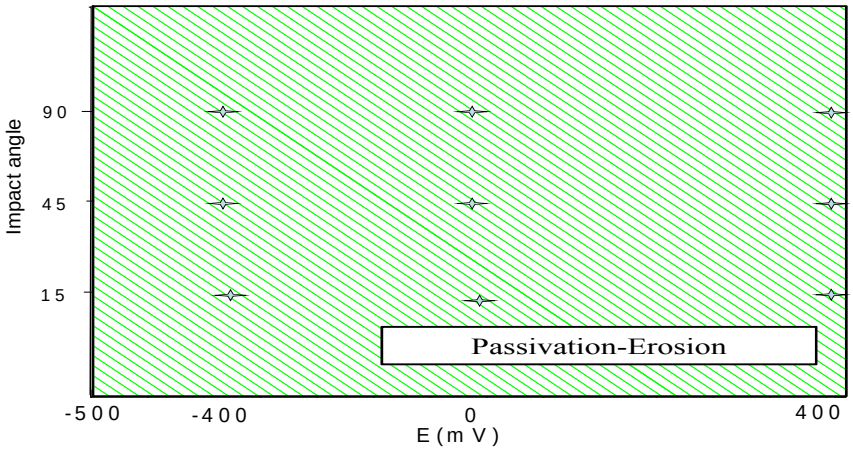

(a)

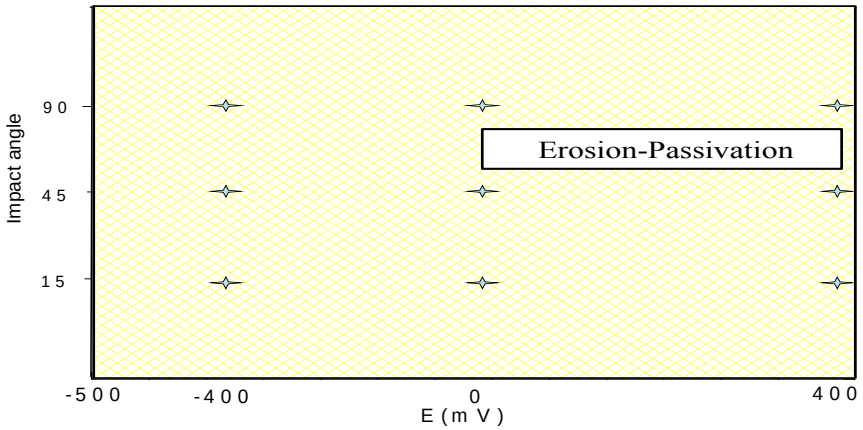

(b)

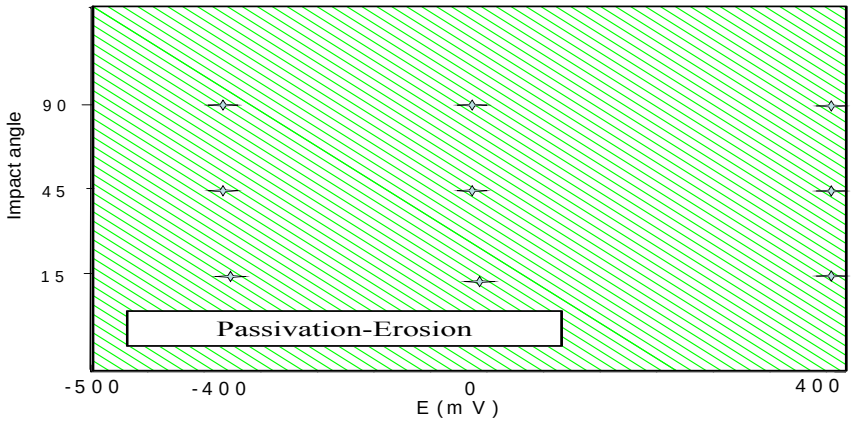

(c)

Fig.4.38: Erosion-corrosion mechanism maps for carbon steel at 4.5 m $s^{-1}$and particle size 150-300μm in (a) water (b) crude oil (c) oil /20% water.

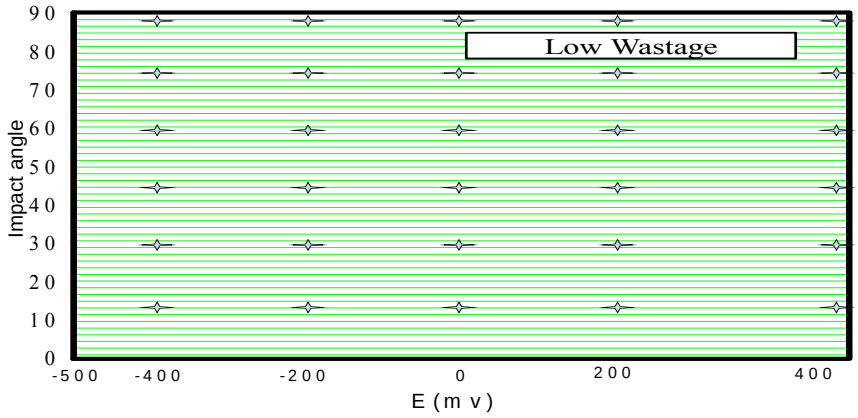

(a)

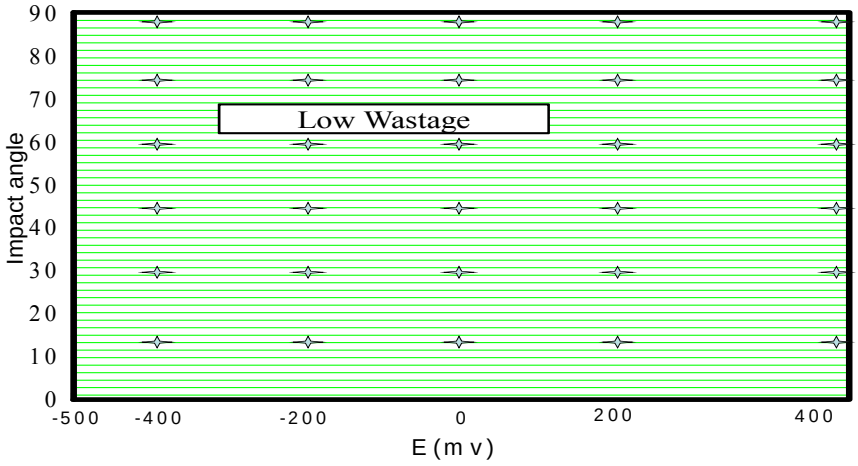

(b)

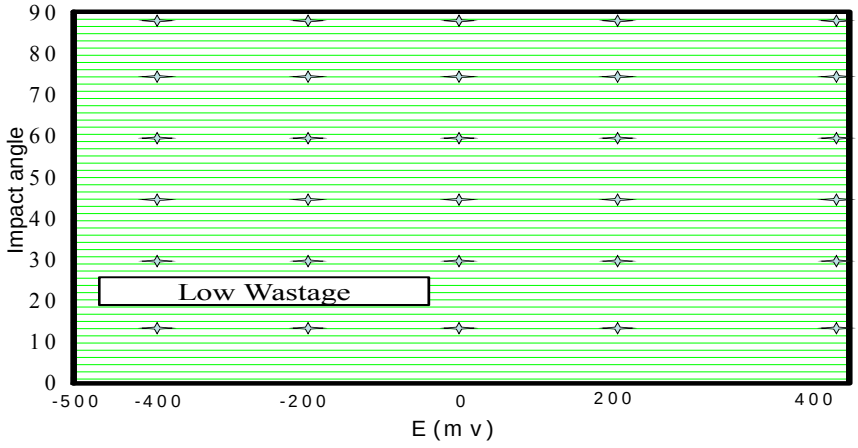

(c)

Fig.4.39: Erosion-corrosion wastage maps for carbon steel at 2.5 m s^{-1} and particle size 600-710µm in (a) water (b) crude oil (c) oil /20% water.

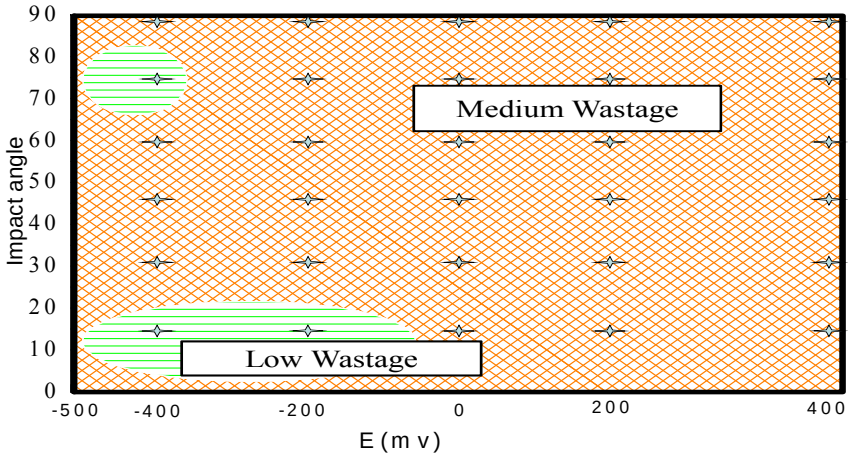

(a)

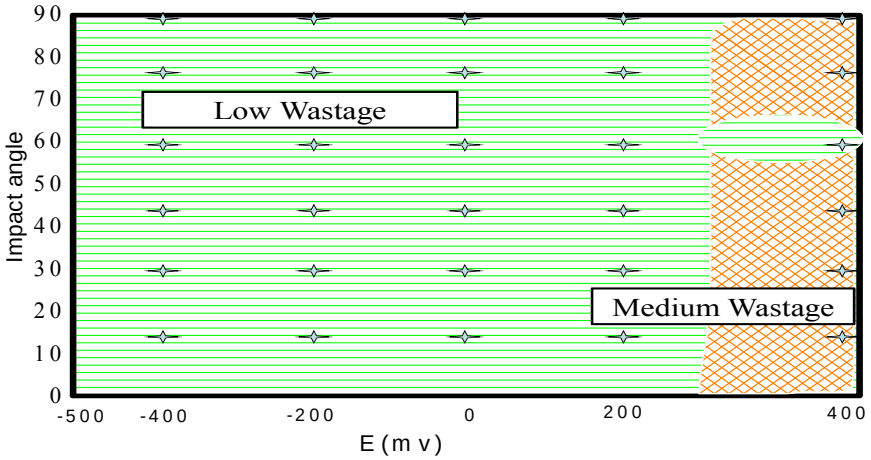

(b)

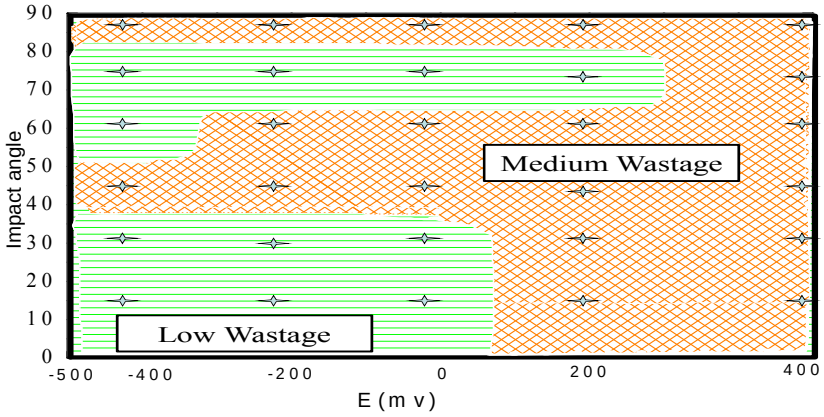

(c)

Fig.4.40: Erosion-corrosion wastage maps for carbon steel at 3.5 m s^{-1} and particle size 600-710µm in (a) water (b) crude oil (c) oil /20% water.

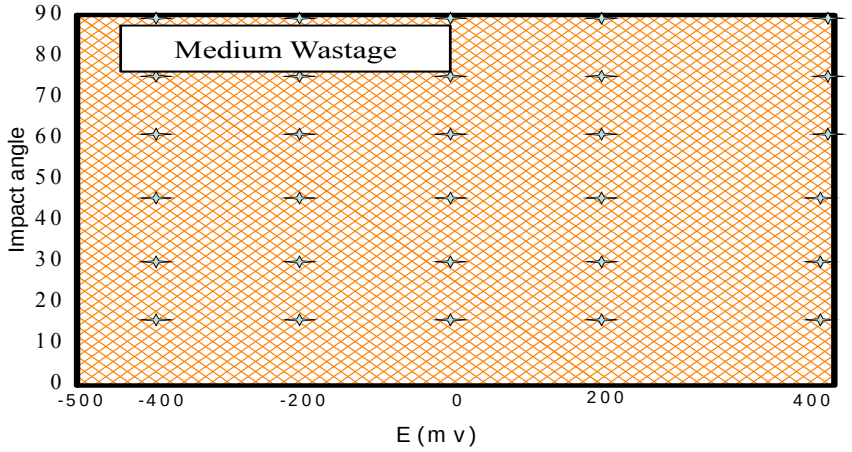

(a)

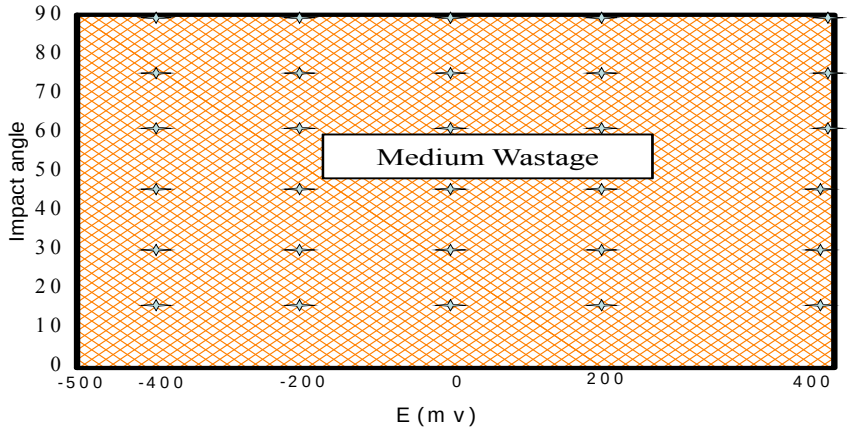

(b)

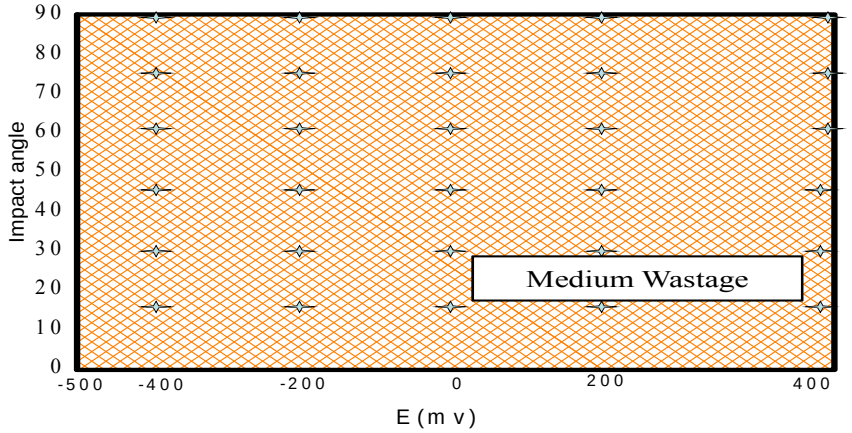

(c)

Fig.4.41: Erosion-corrosion wastage maps for carbon steel at 4.5 m s^{-1} and particle size 600-710µm in (a) water (b) crude oil (c) oil /20% water.

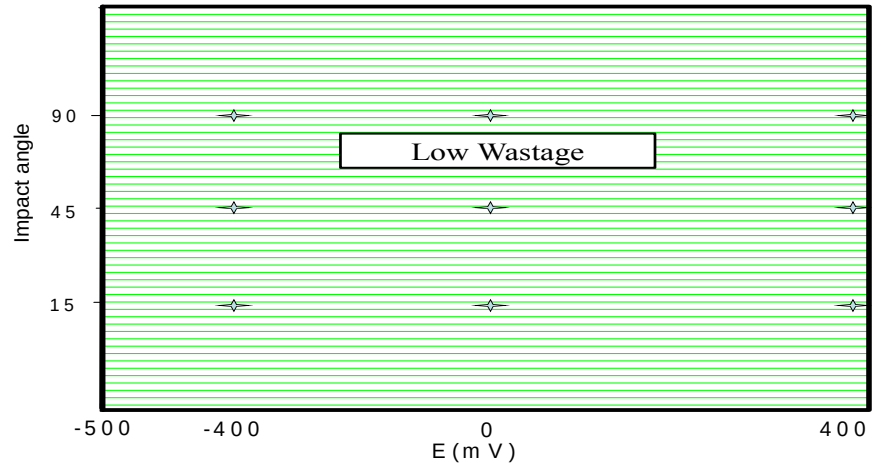

(a)

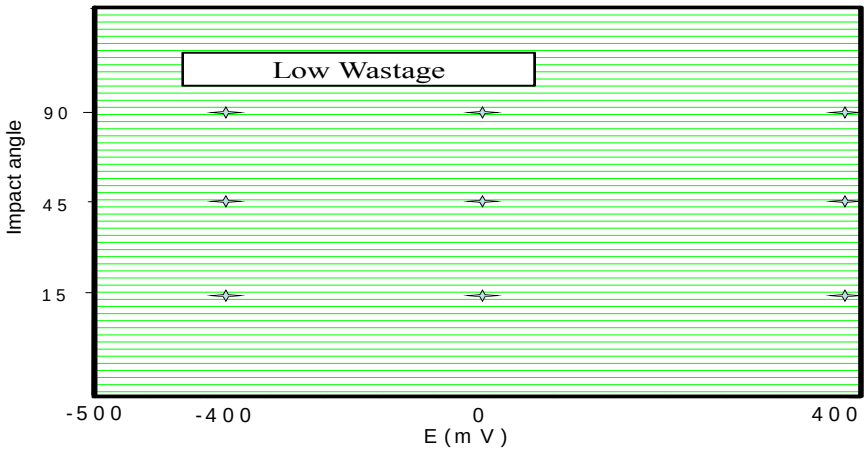

(b)

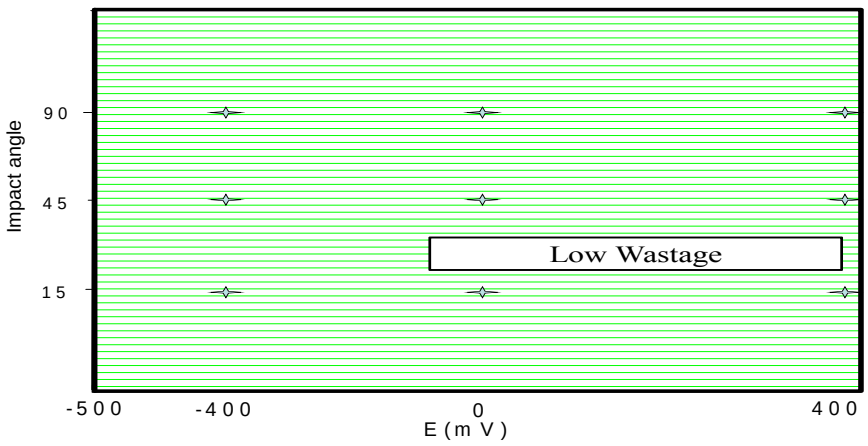

(c)

Fig.4.42: Erosion-corrosion wastage maps for carbon steel at 2.5 m $s^{-1}$and particle size 150-300µm in (a) water (b) crude oil (c) oil /20% water.

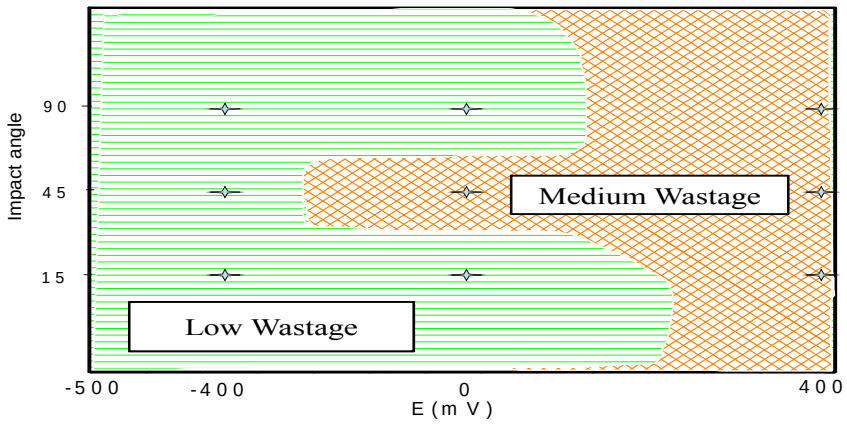

(a)

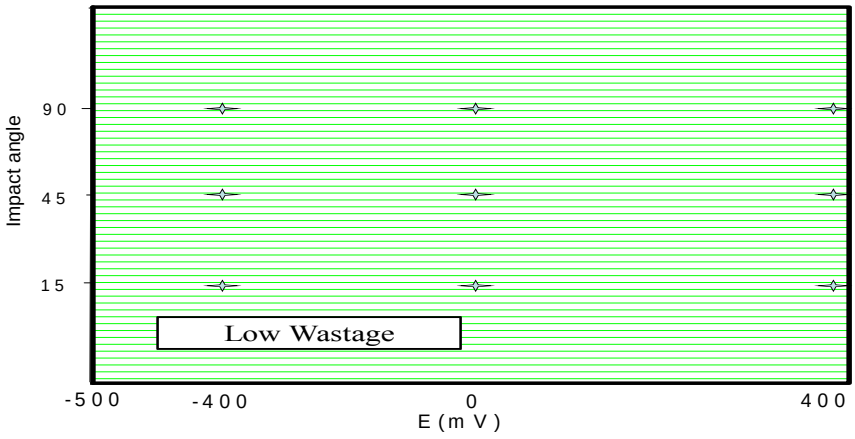

(b)

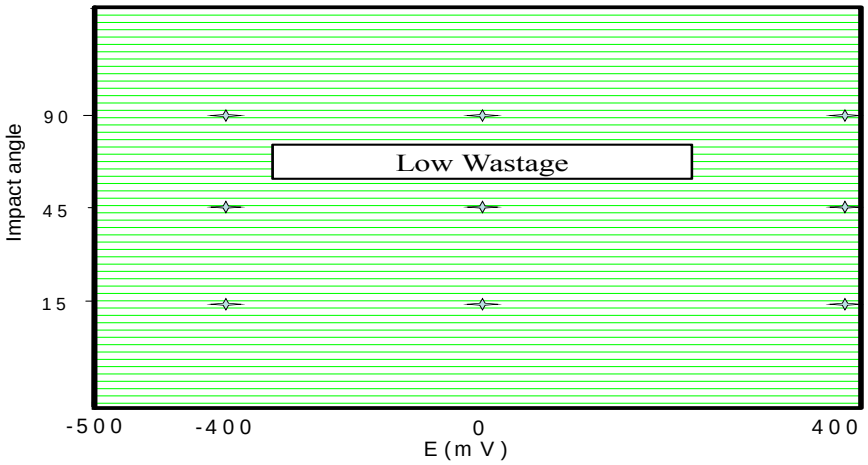

(c)

Fig.4.43: Erosion-corrosion wastage maps for carbon steel at 3.5 m $s^{-1}$and particle size 150-300μm in (a) water (b) crude oil (c) oil /20% water.

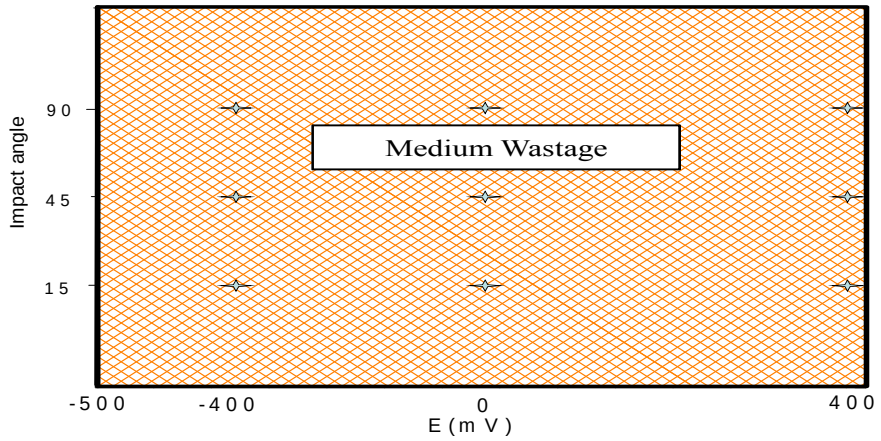

(a)

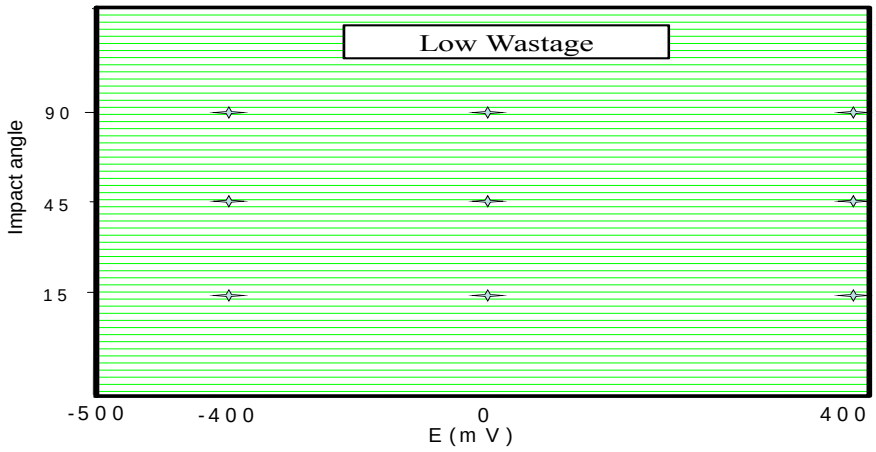

(b)

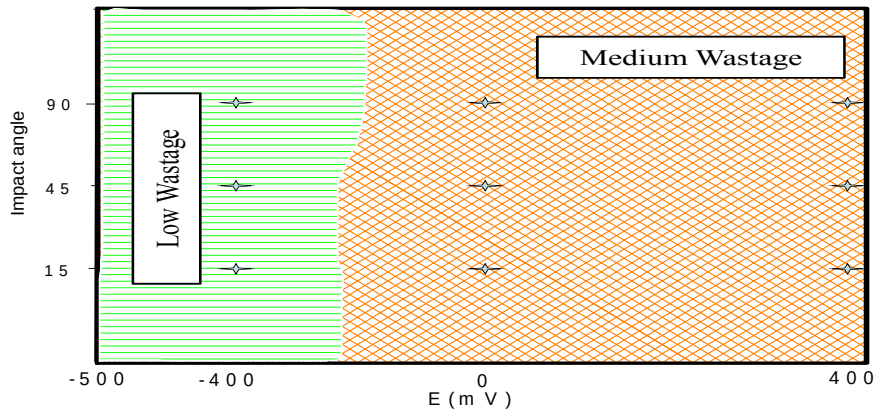

(c)

Fig.4.44: Erosion-corrosion wastage maps for carbon steel at 4.5 m $s^{-1}$and particle size 150-300µm in(a) water (b) crude oil (c) oil /20% water

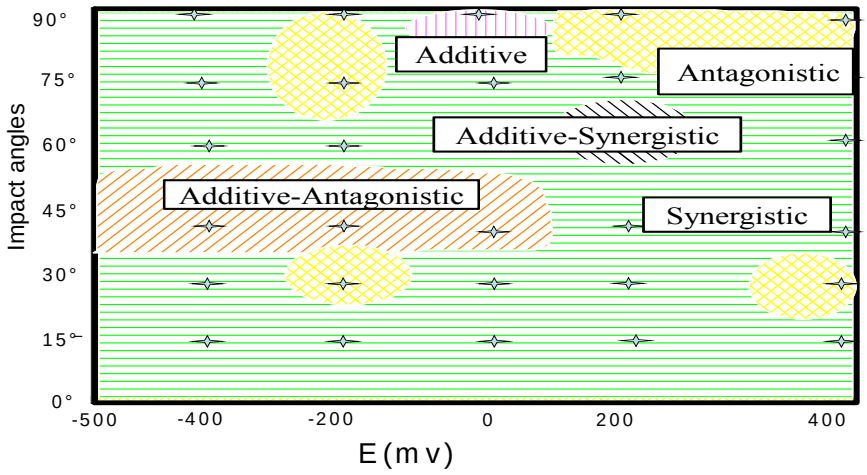

(a)

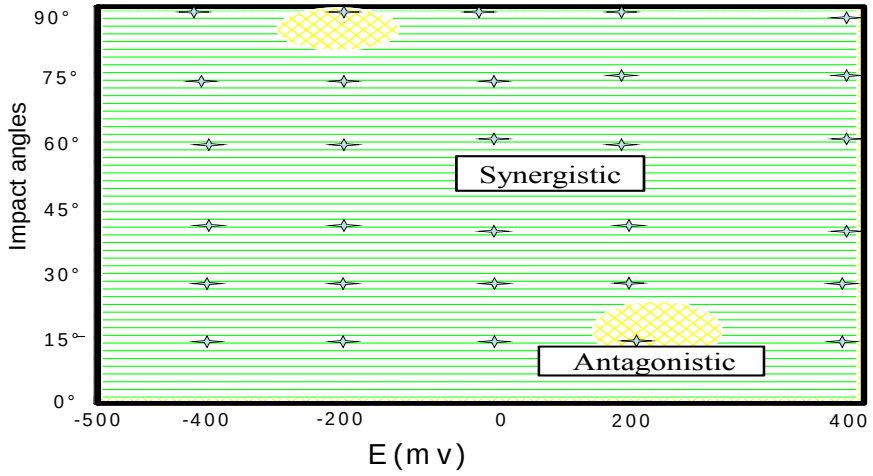

(b)

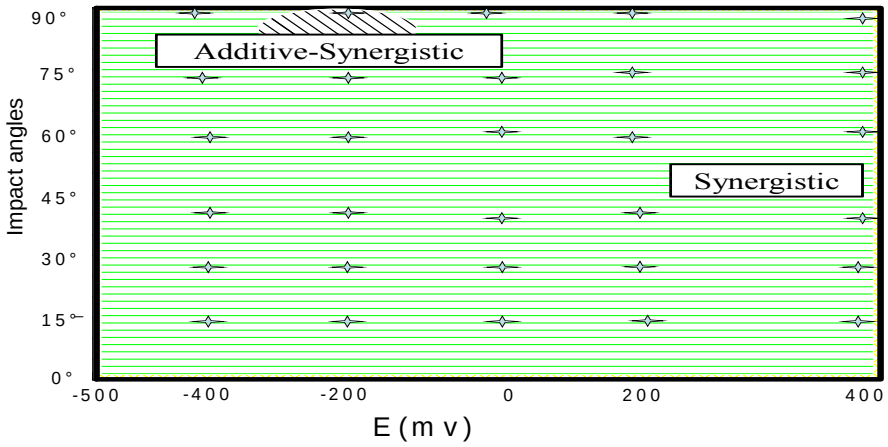

(c)

Fig.4.45: Erosion-corrosion additive-synergism maps for carbon steel at 2.5 m s^{-1} and particle size 600-710µm in(a) water (b) crude oil (c) oil /20% water.

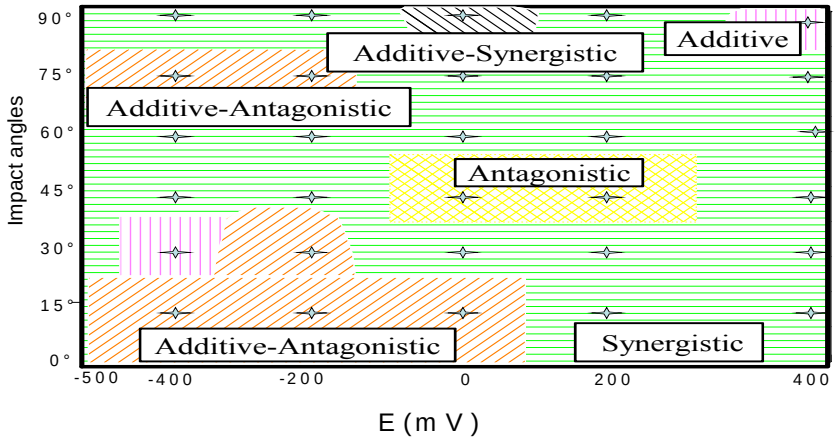

(a)

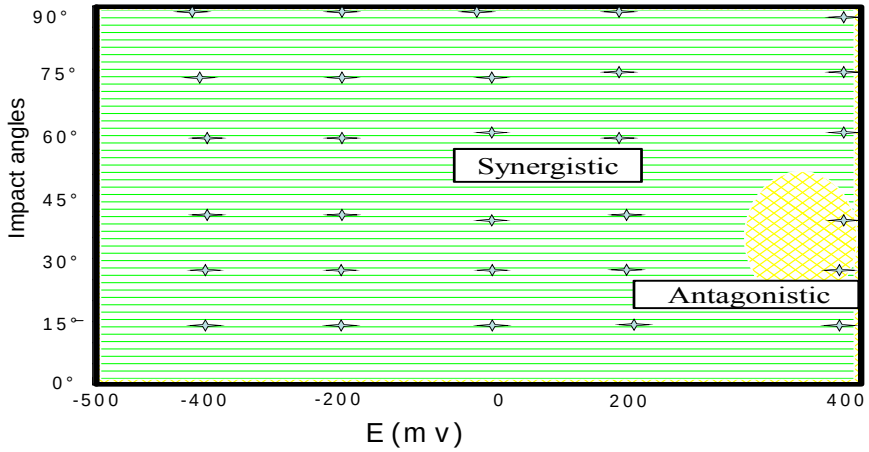

(b)

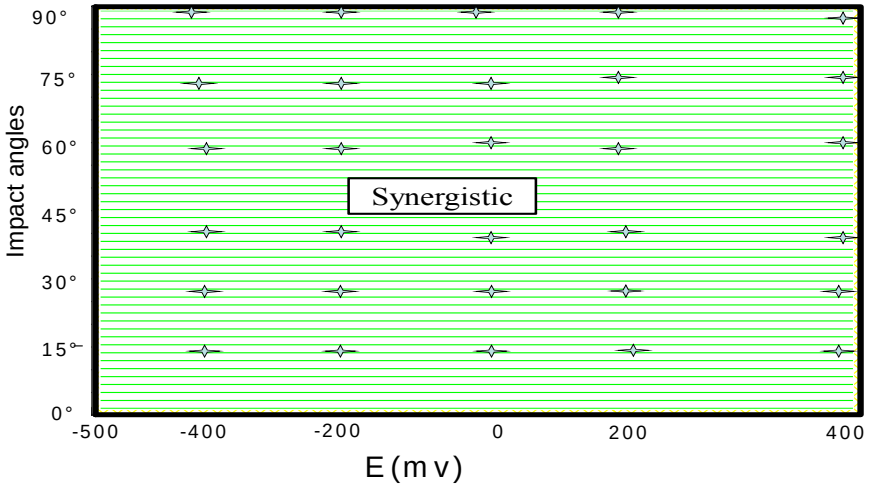

(c)

Fig.4.46: Erosion-corrosion additive-synergism maps for carbon steel at 3.5 m s^{-1} and particle size 600-710µm in(a) water (b) crude oil (c) oil /20% water.

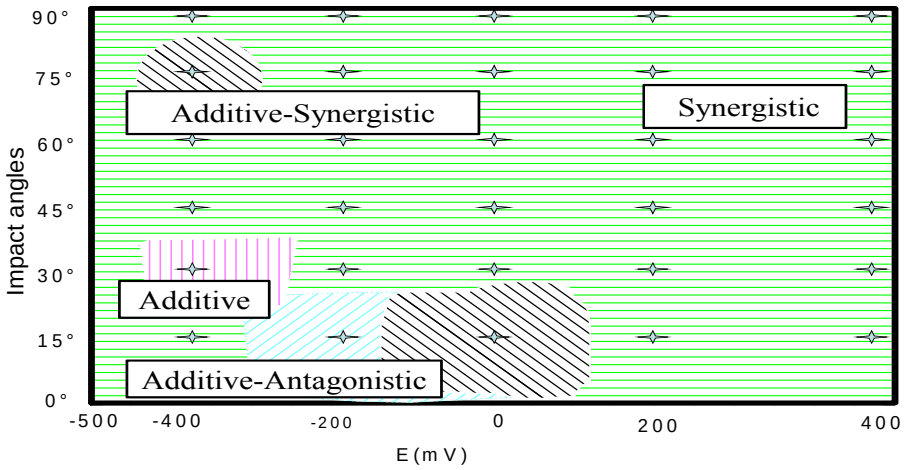

(a)

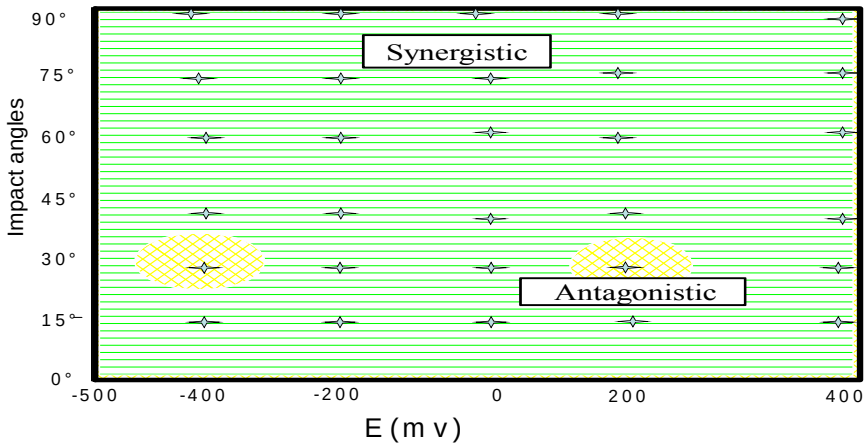

(b)

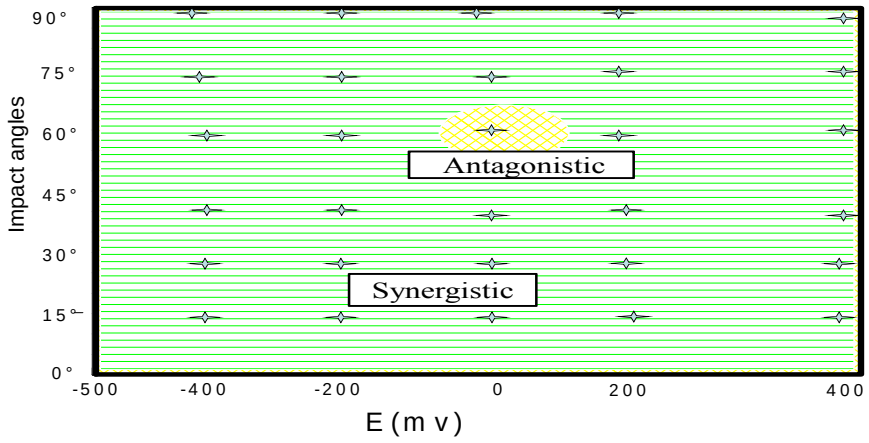

(c)

Fig.4.47: Erosion-corrosion additive-synergism maps for carbon steel at 4.5 m s^{-1} and particle size 600-710µm in(a) water (b) crude oil (c) oil /20% water.

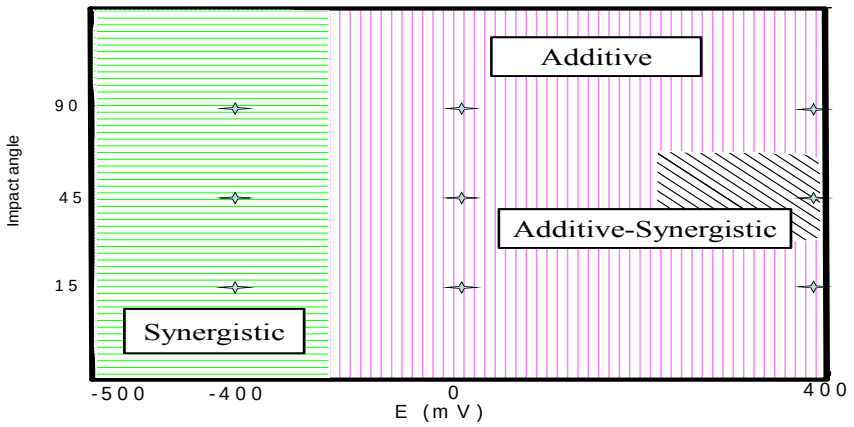

(a)

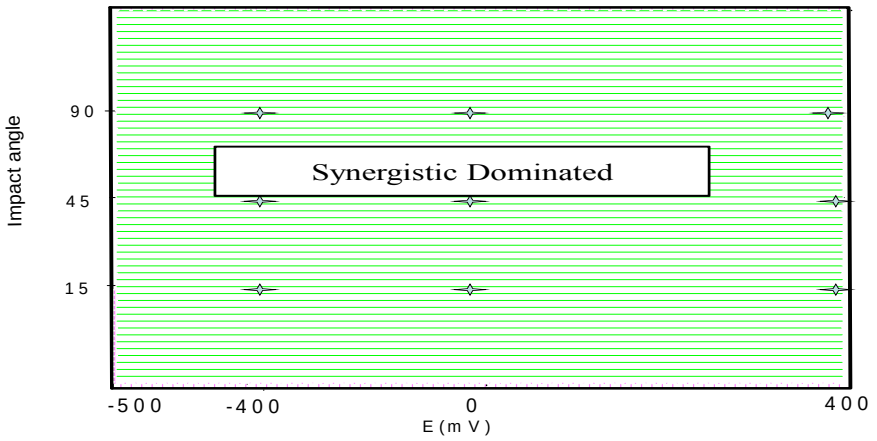

(b)

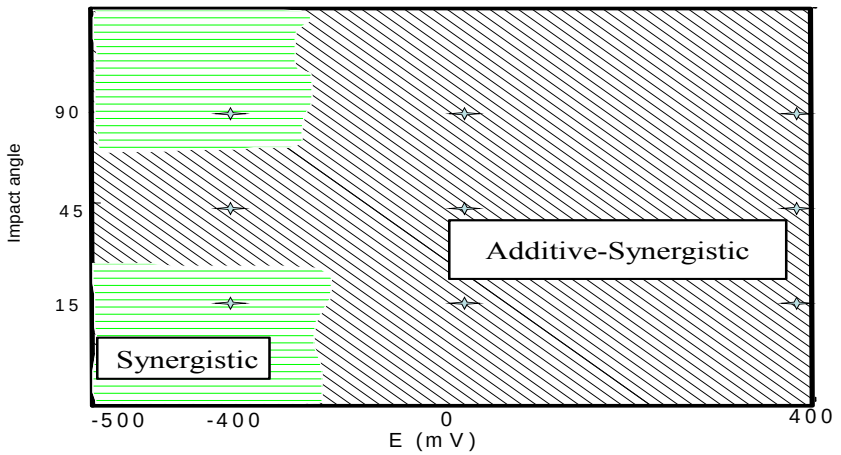

(c)

Fig.4.48: Erosion-corrosion additive-synergism maps for carbon steel at 2.5m $s^{-1}$and particle size 150-300µm in (a) water (b) crude oil (c) oil /20% water.

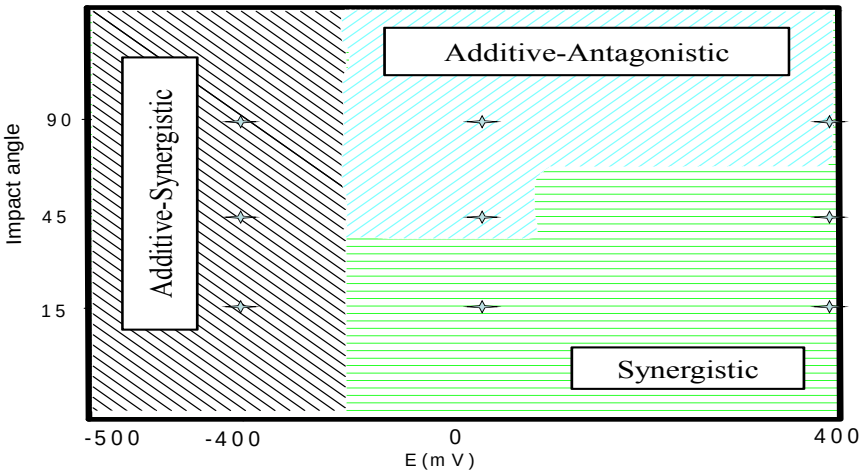

(a)

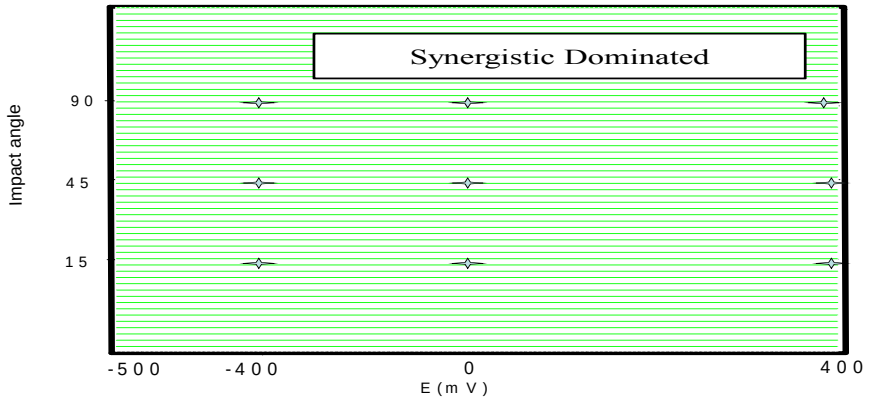

(b)

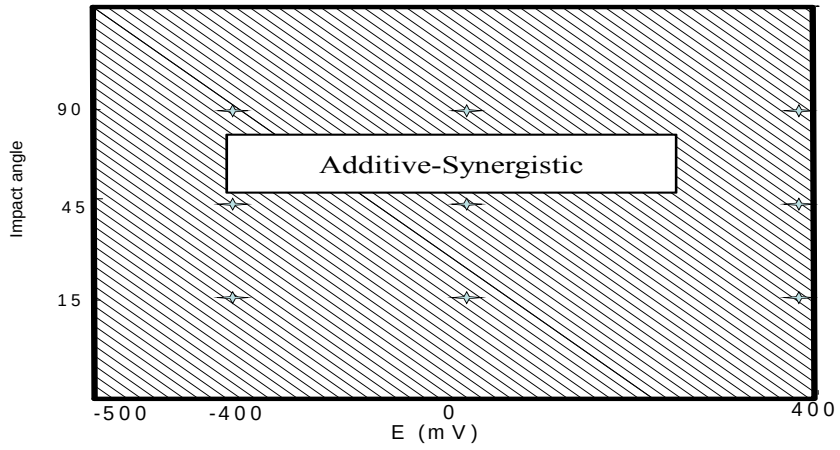

(c)

Fig.4.49: Erosion-corrosion additive-synergism maps for carbon steel at 3.5m $s^{-1}$and particle size 150-300µm in (a) water (b) crude oil (c) oil /20% water.

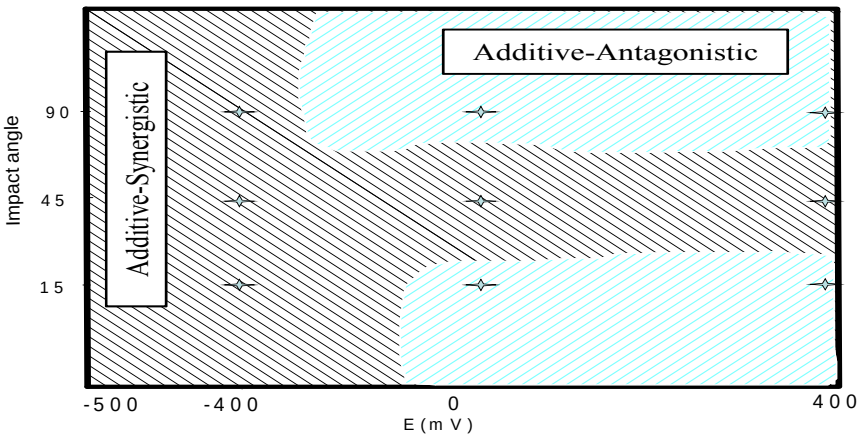

(a)

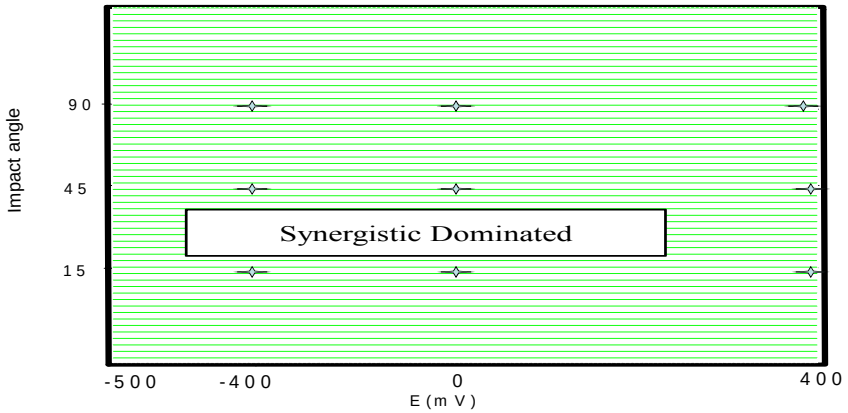

(b)

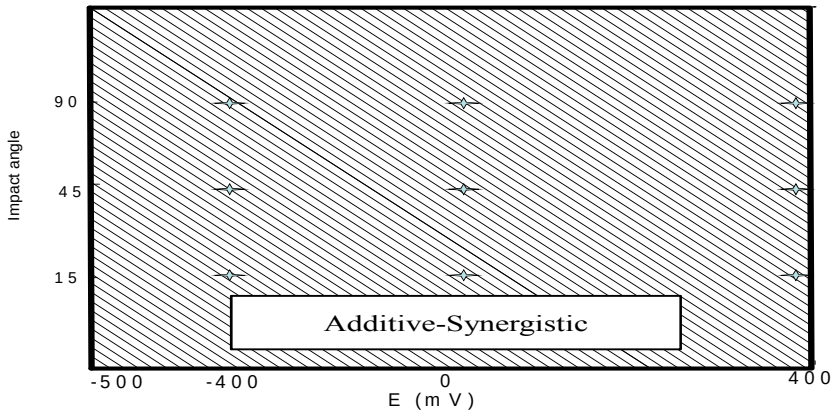

(c)

Fig.4.50: Erosion-corrosion additive-synergism maps for carbon steel at 4.5m $s^{-1}$and particle size 150-300µm in (a) water (b) crude oil (c) oil /20% water.

Tables.4.19: Erosion-corrosion mechanism maps for carbon steel in water at 2.5 m s^{-1} and particle size 600-710µm (a) -400mV (b) -200mV (c) 0mV (d) 200mV (e) 400mV

(a)

Impact angle	Ke(mg cm^{-2} h^{-1})	Kc(mg cm^{-2} h^{-1})	Ke/Kc
15°	2.59	1.72	1.51
30°	2.5	1.5	1.67
45°	2.39	2.21	1.08
60°	2.16	2.04	1.06
75°	1.96	1.93	1.02
90°	2.5	1.71	1.46

(b)

Impact angle	Ke(mg cm^{-2} h^{-1})	Kc(mg cm^{-2} h^{-1})	Ke/Kc
15°	2.45	1.78	1.38
30°	2.59	1.72	1.51
45°	2.17	2.43	0.89
60°	1.89	2.12	0.89
75°	1.57	2.24	0.701
90°	1.9	2.21	0.86

(c)

Impact angle	Ke(mg cm^{-2} h^{-1})	Kc(mg cm^{-2} h^{-1})	Ke/Kc
15°	2.58	1.82	1.42
30°	2.38	1.83	1.30
45°	1.7	2.71	0.63
60°	1.25	2.25	0.56
75°	2.16	2.46	0.88
90°	1.57	2.73	0.58

(d)

Impact angle	Ke(mg cm^{-2} h^{-1})	Kc(mg cm^{-2} h^{-1})	Ke/Kc
15°	2.43	1.95	1.25
30°	2.56	1.94	1.32
45°	2.58	2.03	1.27
60°	1.5	2.71	0.55
75°	2.26	1.34	1.69
90°	1.22	2.78	0.44

(e)

Impact angle	Ke(mg cm^{-2} h^{-1})	Kc(mg cm^{-2} h^{-1})	Ke/Kc
15°	2.44	1.97	1.24
30°	2.16	2.07	1.04
45°	3.16	2.16	1.46
60°	2.57	1.93	1.33
75°	0.71	2.74	0.26
90°	1.48	2.53	0.59

Tables.4.20: Erosion-corrosion mechanism maps for carbon steel in crude oil at 2.5 m s^{-1} and particle size 600-710 μm (a) -400mV (b) -200mV (c) 0mV (d) 200mV (e) 400mV

(a)

Impact angle	Ke(mg cm^{-2} h^{-1})	Kc(mg cm^{-2} h^{-1})	Ke/Kc
15°	2.48	2.11E-02	117.5
30°	1.99	1.22E-02	162.9
45°	2	1.02E-02	196.06
60°	2.08	1.85E-02	112.51
75°	2.1	2.02E-02	103.95
90°	2.09	1.81E-02	115.57

(b)

Impact angle	Ke(mg cm^{-2} h^{-1})	Kc(mg cm^{-2} h^{-1})	Ke/Kc
15°	2.58	1.63E-02	158.51
30°	2.38	1.65E-02	144.45
45°	2.69	1.47E-02	182.67
60°	2.78	1.93E-02	144.08
75°	3.14	2.12E-02	148.06
90°	3.13	1.97E-02	158.90

(c)

Impact angle	Ke(mg cm^{-2} h^{-1})	Kc(mg cm^{-2} h^{-1})	Ke/Kc
15°	3.38	1.85E-02	182.84
30°	3.10	1.71E-02	181.46
45°	3.13	1.39E-02	224.90
60°	3.38	1.90E-02	177.95
75°	3.24	1.98E-02	163.65
90°	3.38	2.00E-02	169

(d)

Impact angle	Ke(mg cm^{-2} h^{-1})	Kc(mg cm^{-2} h^{-1})	Ke/Kc
15°	3.76	1.94E-02	193.85
30°	3.49	1.49E-02	233.90
45°	3.55	1.51E-02	234.76
60°	3.1	2.00E-02	155
75°	3.58	2.33E-02	153.51
90°	3.98	2.42E-02	164.29

(e)

Impact angle	Ke(mg cm^{-2} h^{-1})	Kc(mg cm^{-2} h^{-1})	Ke/Kc
15°	4.289	2.14E-02	200.40
30°	3.52	1.52E-02	231.24
45°	4.19	1.48E-02	282.78
60°	3.98	2.31E-02	172.16
75°	3.69	2.40E-02	153.58
90°	4.08	2.65E-02	154.09

Tables.4.21: Erosion-corrosion mechanism maps for carbon steel in oil /20% water at 2.5 m s−1 and particle size 600-710 μ m(a) -400mV (b) -200mV (c) 0mV(d) 200mV (e) 400mV

(a)

Impact angle	Ke(mg cm $^{-2}$ h^{-1})	Kc(mg cm $^{-2}$ h^{-1})	Ke/Kc
15°	2.31	0.8	2.9
30°	1.92	0.78	2.5
45°	2.16	0.8	2.6
60°	2.42	0.8	3.1
75°	1.96	1	1.96
90°	2.18	0.9	2.4

(b)

Impact angle	Ke(mg cm $^{-2}$ h^{-1})	Kc(mg cm $^{-2}$ h^{-1})	Ke/Kc
15°	2.34	0.81	2.879
30°	2.41	0.79	3.046
45°	2.5	0.71	3.496
60°	2.44	0.80	3.045
75°	2.61	0.89	2.933
90°	1.87	0.91	2.055

(c)

Impact angle	Ke(mg cm $^{-2}$ h^{-1})	Kc(mg cm $^{-2}$ h^{-1})	Ke/Kc
15°	2.06	0.78	2.641
30°	2.71	0.8	3.388
45°	2.84	0.76	3.737
60°	2.68	0.82	3.268
75°	2.1	0.9	2.333
90°	2.13	0.78	2.731

(d)

Impact angle	Ke(mg cm $^{-2}$ h^{-1})	Kc(mg cm $^{-2}$ h^{-1})	Ke/Kc
15°	2.1	0.68	3.088
30°	2.35	0.9	2.611
45°	2.89	0.81	3.568
60°	2.64	0.96	2.75
75°	2.42	0.45	5.378
90°	2.27	0.73	3.11

(e)

Impact angle	Ke(mg cm $^{-2}$ h^{-1})	Kc(mg cm $^{-2}$ h^{-1})	Ke/Kc
15°	1.89	0.71	2.662
30°	2.68	0.72	3.722
45°	2.1	0.9	2.333
60°	2.02	0.78	2.59
75°	2.23	0.67	3.328
90°	2.4	0.8	3

Tables.4.22: Erosion-corrosion mechanism maps for carbon steel in water at 3.5 m s−1 and particle size 600-710 μ m (a) -400mV (b) -200mV (c) 0mV (d) 200mV (e) 400mV

(a)

Impact angle	Ke(mg cm $^{-2}$ h^{-1})	Kc(mg cm $^{-2}$ h^{-1})	Ke/Kc
15°	1.4	4.12	0.34
30°	1.81	4.21	0.43
45°	2.43	4.02	0.6
60°	2.39	3.91	0.61
75°	0.53	5.32	0.1
90°	1.9	4.31	0.44

(b)

Impact angle	Ke(mg cm $^{-2}$ h^{-1})	Kc(mg cm $^{-2}$ h^{-1})	Ke/Kc
15°	1.77	4.21	0.42
30°	2.11	3.91	0.54
45°	1.89	5	0.38
60°	2.2	4.25	0.52
75°	1.59	4.61	0.35
90°	1.97	4.38	0.45

(c)

Impact angle	Ke(mg cm $^{-2}$ h^{-1})	Kc(mg cm $^{-2}$ h^{-1})	Ke/Kc
15°	1.65	4.38	0.38
30°	2.42	3.78	0.64
45°	1.99	5.04	0.4
60°	2.7	4.51	0.6
75°	2.8	4.07	0.68
90°	2.48	5	0.49

(d)

Impact angle	Ke(mg cm $^{-2}$ h^{-1})	Kc(mg cm $^{-2}$ h^{-1})	Ke/Kc
15°	1.73	4.48	0.386
30°	3.4	4.1	0.829
45°	3.88	4.12	0.942
60°	2.83	5.01	0.565
75°	2.8	4.5	0.622
90°	2.5	5.52	0.453

(e)

Impact angle	Ke(mg cm $^{-2}$ h^{-1})	Kc(mg cm $^{-2}$ h^{-1})	Ke/Kc
15°	3.49	4.51	0.774
30°	3.57	4.23	0.844
45°	3.89	4.32	0.9
60°	2.79	5.21	0.536
75°	2.99	4.85	0.616
90°	2.11	5.81	0.363

Tables.4.23: Erosion-corrosion mechanism maps for carbon steel in crude oil at 3.5 m s−1 and particle size 600-710 μ m(a) -400mV (b) -200mV (c) 0mV (d) 200mV (e) 400mV

(a)

Impact angle	Ke(mg cm^{-2} h^{-1})	Kc(mg cm^{-2} h^{-1})	Ke/Kc
15°	4.56	1.89E-02	241.33
30°	3.97	2.62E-02	151.67
45°	4.48	2.00E-02	224
60°	4.19	2.43E-02	172.25
75°	4.69	1.92E-02	244.31
90°	4.75	2.62E-02	181.44

(b)

Impact angle	Ke(mg cm^{-2} h^{-1})	Kc(mg cm^{-2} h^{-1})	Ke/Kc
15°	5.099	2.09E-02	243.98
30°	4.17	3.02E-02	138.07
45°	4.58	2.21E-02	207.14
60°	4.68	2.53E-02	184.77
75°	4.83	2.02E-02	239.09
90°	4.97	2.74E-02	181.48

(c)

Impact angle	Ke(mg cm^{-2} h^{-1})	Kc(mg cm^{-2} h^{-1})	Ke/Kc
15°	5.07	2.59E-02	195.91
30°	4.47	2.70E-02	165.67
45°	4.98	1.81E-02	275.24
60°	4.87	2.61E-02	186.74
75°	4.84	2.76E-02	175.45
90°	5.18	2.91E-02	178.04

(d)

Impact angle	Ke(mg cm^{-2} h^{-1})	Kc(mg cm^{-2} h^{-1})	Ke/Kc
15°	5.57	2.61E-02	213.56
30°	5.17	2.78E-02	186.05
45°	5.85	1.92E-02	304.73
60°	4.98	1.99E-02	250.26
75°	5.09	3.76E-02	135.44
90°	5.75	3.01E-02	191.03

(e)

Impact angle	Ke(mg cm^{-2} h^{-1})	Kc(mg cm^{-2} h^{-1})	Ke/Kc
15°	6.97	2.58E-02	270.32
30°	6.37	3.08E-02	206.79
45°	6.18	2.02E-02	305.93
60°	8	2.19E-02	227.31
75°	5.97	2.96E-02	201.70
90°	6.47	3.21E-02	201.49

Tables.4.24: Erosion-corrosion mechanism maps for carbon steel in oil /20% water at 3.5 m s^{-1} and particle size 600-710 μ m (a) -400mV (b) -200mV (c) 0mV(d) 200mV (e) 400mV

(a)

Impact angle	Ke(mg cm^{-2} h^{-1})	Kc(mg cm^{-2} h^{-1})	Ke/Kc
15°	4.16	0.84	4.95
30°	3.71	0.89	4.17
45°	5.2	0.9	5.78
60°	4.42	0.98	4.51
75°	4.2	1	4.2
90°	5	1.1	4.545

(b)

Impact angle	Ke(mg cm^{-2} h^{-1})	Kc(mg cm^{-2} h^{-1})	Ke/Kc
15°	5.02	0.98	5.122
30°	4.56	1	4.56
45°	5.3	0.9	5.89
60°	4.98	1.12	4.45
75°	4.81	0.89	5.404
90°	5.2	1	5.2

(c)

Impact angle	Ke(mg cm^{-2} h^{-1})	Kc(mg cm^{-2} h^{-1})	Ke/Kc
15°	5.11	0.89	5.74
30°	3.9	1.2	3.25
45°	5.2	1	5.2
60°	4.89	1.23	3.976
75°	4.53	1	4.53
90°	5.32	0.98	5.43

(d)

Impact angle	Ke(mg cm^{-2} h^{-1})	Kc(mg cm^{-2} h^{-1})	Ke/Kc
15°	5.47	0.93	5.88
30°	5.32	0.98	5.43
45°	5.3	1.2	4.42
60°	5.22	0.78	6.69
75°	4.75	1.12	4.241
90°	5.18	1.23	4.211

(e)

Impact angle	Ke(mg cm^{-2} h^{-1})	Kc(mg cm^{-2} h^{-1})	Ke/Kc
15°	6.01	1.2	5.008
30°	5.51	1	5.51
45°	5.4	1.3	4.154
60°	6.2	0.8	7.75
75°	5.87	0.98	5.99
90°	5.8	1.2	4.833

Tables.4.25: Erosion-corrosion mechanism maps for carbon steel in water at 4.5 m s^{-1} and particle size 600-710 μ m (a) -400mV (b) -200mV (c) 0mV(d) 200mV (e) 400mV

(a)

Impact angle	Ke(mg cm^{-2} h^{-1})	Kc(mg cm^{-2} h^{-1})	Ke/Kc
15°	2.99	5.72	0.52
30°	2.87	5.93	0.48
45°	4.48	4.72	0.95
60°	3.3	5.4	0.61
75°	3	5.94	0.51
90°	4.69	4.78	0.98

(b)

Impact angle	Ke(mg cm^{-2} h^{-1})	Kc(mg cm^{-2} h^{-1})	Ke/Kc
15°	2.39	5.84	0.41
30°	4.88	4.12	1.15
45°	4.17	5.85	0.713
60°	4.65	5.67	0.82
75°	3.45	5.89	0.586
90°	5.48	4.83	1.135

(c)

Impact angle	Ke(mg cm^{-2} h^{-1})	Kc(mg cm^{-2} h^{-1})	Ke/Kc
15°	3.82	5.91	0.646
30°	5.76	4.45	1.294
45°	5.44	5.01	1.086
60°	4.71	5.56	0.847
75°	4.11	6.21	0.662
90°	3.47	6.03	0.575

(d)

Impact angle	Ke(mg cm^{-2} h^{-1})	Kc(mg cm^{-2} h^{-1})	Ke/Kc
15°	4.76	5.24	0.908
30°	5.51	4.81	1.146
45°	5.74	5.32	1.079
60°	4.88	5.87	0.831
75°	4.52	6	0.753
90°	4.19	6.13	0.684

(e)

Impact angle	Ke(mg cm^{-2} h^{-1})	Kc(mg cm^{-2} h^{-1})	Ke/Kc
15°	5.25	5.2	1.01
30°	5.62	4.9	1.147
45°	6.11	5.73	1.066
60°	6.05	5.07	1.193
75°	3.16	6.84	0.462
90°	4.29	6.73	0.637

Tables.4.26: Erosion-corrosion mechanism maps for carbon steel in crude oil at 4.5 m s^{-1} and particle size 600-710 μ m (a) -400mV (b) -200mV (c) 0mV(d) 200mV (e) 400mV

(a)

Impact angle	Ke(mg cm^{-2} h^{-1})	Kc(mg cm^{-2} h^{-1})	Ke/Kc
15°	7.47	2.88E-02	259.42
30°	6.18	3.28E-02	188.33
45°	7.095	2.52E-02	281.54
60°	6.67	3.19E-02	209.03
75°	6.97	3.03E-02	230.02
90°	7.14	4.12E-02	173.27

(b)

Impact angle	Ke(mg cm^{-2} h^{-1})	Kc(mg cm^{-2} h^{-1})	Ke/Kc
15°	7.24	3.78E-02	191.59
30°	6.97	3.41E-02	204.28
45°	6.99	2.98E-02	234.57
60°	6.83	4.19E-02	162.96
75°	7.015	3.48E-02	201.59
90°	7.76	3.99E-02	194.49

(c)

Impact angle	Ke(mg cm^{-2} h^{-1})	Kc(mg cm^{-2} h^{-1})	Ke/Kc
15°	7.96	4.28E-02	185.92
30°	7.44	4.01E-02	185.53
45°	7.42	3.08E-02	240.88
60°	6.96	3.89E-02	178.95
75°	6.66	3.88E-02	171.68
90°	7.40	4.56E-02	162.38

(d)

Impact angle	Ke(mg cm^{-2} h^{-1})	Kc(mg cm^{-2} h^{-1})	Ke/Kc
15°	8.43	4.50E-02	187.22
30°	7.94	3.91E-02	203.09
45°	7.74	3.58E-02	216.32
60°	7.1	4.09E-02	173.57
75°	6.96	3.78E-02	184.19
90°	7.95	4.78E-02	166.36

(e)

Impact angle	Ke(mg cm^{-2} h^{-1})	Kc(mg cm^{-2} h^{-1})	Ke/Kc
15°	8.07	4.78E-02	168.87
30°	7.96	4.51E-02	176.38
45°	8.41	4.00E-02	210.25
60°	8.05	5.19E-02	155.07
75°	7.85	4.18E-02	187.76
90°	8.18	5.18E-02	157.88

Tables.4.27: Erosion-corrosion mechanism maps for carbon steel in oil /20% water at 4.5 m s−1 and particle size 600-710 μ m (a) -400mV (b) -200mV (c) 0mV(d) 200mV (e) 400mV

(a)

Impact angle	Ke(mg cm $^{-2}$ h^{-1})	Kc(mg cm $^{-2}$ h^{-1})	Ke/Kc
15°	6.45	1.35	4.78
30°	6.07	1.21	5.017
45°	6.66	1.34	4.97
60°	5.82	1.2	4.85
75°	6.6	1.4	4.71
90°	6.75	1.45	4.66

(b)

Impact angle	Ke(mg cm $^{-2}$ h^{-1})	Kc(mg cm $^{-2}$ h^{-1})	Ke/Kc
15°	6.7	1.3	5.15
30°	6.98	1.32	5.29
45°	6.7	1.5	4.47
60°	6.51	1.1	5.92
75°	6.76	1.3	5.2
90°	7.1	1.5	4.73

(c)

Impact angle	Ke(mg cm $^{-2}$ h^{-1})	Kc(mg cm $^{-2}$ h^{-1})	Ke/Kc
15°	7.28	1.5	4.85
30°	7.08	1.32	5.36
45°	7.54	1.4	5.39
60°	6.79	1.21	5.61
75°	6.6	1.3	5.08
90°	7.12	1.6	4.45

(d)

Impact angle	Ke(mg cm $^{-2}$ h^{-1})	Kc(mg cm $^{-2}$ h^{-1})	Ke/Kc
15°	7.34	1.68	4.369
30°	7.4	1.6	4.625
45°	7.76	1.54	5.039
60°	8.68	1.32	6.576
75°	7.57	1.4	5.407
90°	7.9	1.7	4.647

(e)

Impact angle	Ke(mg cm $^{-2}$ h^{-1})	Kc(mg cm $^{-2}$ h^{-1})	Ke/Kc
15°	7.61	1.9	4.01
30°	7.67	1.85	4.15
45°	7.42	1.7	4.37
60°	7.32	1.68	4.36
75°	7.12	1.76	4.05
90°	7.98	1.89	4.22

Tables.4.28: Erosion-corrosion mechanism maps for carbon steel in water at 2.5 m s^{-1} and particle size 150-300µm (a) - 400mV (b) 0mV (c) 400mV

(a)

Impact angle	Ke(mg cm^{-2} h^{-1})	Kc(mg cm^{-2} h^{-1})	Ke/Kc
15°	1.5	2.5	0.6
45°	1.59	2.6	0.612
90°	1.14	2.4	0.475

(b)

Impact angle	Ke(mg cm^{-2} h^{-1})	Kc(mg cm^{-2} h^{-1})	Ke/Kc
15°	0.47	3.74	0.126
45°	0.7	3.8	0.184
90°	0.46	3.84	0.12

(c)

Impact angle	Ke(mg cm^{-2} h^{-1})	Kc(mg cm^{-2} h^{-1})	Ke/Kc
15°	0.46	3.84	0.12
45°	1.51	3.9	0.387
90°	0.5	3.9	0.128

Tables.4.29: Erosion-corrosion mechanism maps for carbon steel in crude oil at 2.5 m s^{-1} and particle size 150-300µm (a) - 400mV (b) 0mV (c) 400mV

(a)

Impact angle	Ke(mg cm^{-2} h^{-1})	Kc(mg cm^{-2} h^{-1})	Ke/Kc
15°	1.43	3.21E-01	4.45
45°	1.66	3.42E-01	4.85
90°	1.1	5.91E-01	1.79

(b)

Impact angle	Ke(mg cm^{-2} h^{-1})	Kc(mg cm^{-2} h^{-1})	Ke/Kc
15°	1.455	3.95E-01	3.68
45°	1.77	3.40E-01	5.21
90°	1.44	4.10E-01	3.51

(c)

Impact angle	Ke(mg cm^{-2} h^{-1})	Kc(mg cm^{-2} h^{-1})	Ke/Kc
15°	1.56	4.24E-01	3.67
45°	1.95	3.57E-01	5.45
90°	1.73	4.70E-01	3.68

Tables.4.30: Erosion-corrosion mechanism maps for carbon steel in oil /20% water at 2.5 m s−1 and particle size 150-300µm (a) - 400mV (b) 0mV (c) 400mV

(a)

Impact angle	Ke(mg cm $^{-2}$ h^{-1})	Kc(mg cm $^{-2}$ h^{-1})	Ke/Kc
15°	1.19	1.11E+00	1.07
45°	1.29	1.21E+00	1.06
90°	1.4	1.03E+00	1.36

(b)

Impact angle	Ke(mg cm $^{-2}$ h^{-1})	Kc(mg cm $^{-2}$ h^{-1})	Ke/Kc
15°	1.1	1.51E+00	0.72
45°	0.95	1.75E+00	0.54
90°	0.85	1.65E+00	0.51

(c)

Impact angle	Ke(mg cm $^{-2}$ h^{-1})	Kc(mg cm $^{-2}$ h^{-1})	Ke/Kc
15°	0.98	1.77E+00	0.55
45°	1.55	1.85E+00	0.84
90°	0.82	1.83E+00	0.45

Tables.4.31: Erosion-corrosion mechanism maps for carbon steel in water at 3.5 m s^{-1} and particle size 150-300µm (a) - 400mV (b) 0mV (c) 400mV

(a)

Impact angle	Ke(mg cm $^{-2}$ h^{-1})	Kc(mg cm $^{-2}$ h^{-1})	Ke/Kc
15°	1.22	3.98	0.31
45°	1.51	4.2	0.36
90°	1.1	4.5	0.24

(b)

Impact angle	Ke(mg cm $^{-2}$ h^{-1})	Kc(mg cm $^{-2}$ h^{-1})	Ke/Kc
15°	1.5	4	0.38
45°	1.05	5	0.21
90°	0.6	4.81	0.125

(c)

Impact angle	Ke(mg cm $^{-2}$ h^{-1})	Kc(mg cm $^{-2}$ h^{-1})	Ke/Kc
15°	2	4.2	0.476
45°	2	5	0.4
90°	0.6	5.4	0.11

Tables.4.32:Erosion-corrosion mechanism maps for carbon steel in crude oil at 3.5 m s^{-1} and particle size 150-300µm (a) - 400mV (b) 0mV (c) 400mV

(a)

Impact angle	Ke(mg cm^{-2} h^{-1})	Kc(mg cm^{-2} h^{-1})	Ke/Kc
15°	3.05	4.00E-01	7.63
45°	3.4	5.00E-01	6.8
90°	2.71	5.41E-01	5.01

(b)

Impact angle	Ke(mg cm^{-2} h^{-1})	Kc(mg cm^{-2} h^{-1})	Ke/Kc
15°	3.22	5.32E-01	6.05
45°	3.41	4.40E-01	7.75
90°	2.9	6.00E-01	4.83

(c)

Impact angle	Ke(mg cm^{-2} h^{-1})	Kc(mg cm^{-2} h^{-1})	Ke/Kc
15°	3.23	6.12E-01	5.27
45°	3.43	5.70E-01	6.02
90°	3.17	6.30E-01	5.03

Tables.4.33: Erosion-corrosion mechanism maps for carbon steel in oil /20% water at 3.5 m s−1 and particle size 150-300µm (a) - 400mV (b) 0mV (c) 400mV

(a)

Impact angle	Ke(mg cm^{-2} h^{-1})	Kc(mg cm^{-2} h^{-1})	Ke/Kc
15°	1.55	2.46E+00	0.63
45°	1.26	2.95E+00	0.43
90°	1.73	2.26E+00	0.76

(b)

Impact angle	Ke(mg cm^{-2} h^{-1})	Kc(mg cm^{-2} h^{-1})	Ke/Kc
15°	1.33	2.97E+00	0.45
45°	1.46	3.00E+00	0.49
90°	1.15	2.85E+00	0.40

(c)

Impact angle	Ke(mg cm^{-2} h^{-1})	Kc(mg cm^{-2} h^{-1})	Ke/Kc
15°	1.73	3.02E+00	0.57
45°	1.48	3.32E+00	0.45
90°	1.57	2.94E+00	0.53

Tables.4.34: Erosion-corrosion mechanism maps for carbon steel in water at 4.5 m s^{-1} and particle size 150-300µm (a) - 400mV (b) 0mV (c) 400mV

(a)

Impact angle	Ke(mg cm^{-2} h^{-1})	Kc(mg cm^{-2} h^{-1})	Ke/Kc
15°	2	5.5	0.36
45°	2.3	5.5	0.42
90°	1.6	5.7	0.28

(b)

Impact angle	Ke(mg cm^{-2} h^{-1})	Kc(mg cm^{-2} h^{-1})	Ke/Kc
15°	1.01	6.2	0.16
45°	2.11	5.89	0.36
90°	0.65	6.4	0.10

(c)

Impact angle	Ke(mg cm^{-2} h^{-1})	Kc(mg cm^{-2} h^{-1})	Ke/Kc
15°	0.95	6.5	0.15
45°	2.48	6.3	0.39
90°	1	7	0.14

Tables.4.35:Erosion-corrosion mechanism maps for carbon steel in crude oil at 4.5 m s^{-1} and particle size 150-300µm (a) - 400mV (b) 0mV (c) 400mV

(a)

Impact angle	Ke(mg cm^{-2} h^{-1})	Kc(mg cm^{-2} h^{-1})	Ke/Kc
15°	4.25	7.50E-01	5.67
45°	4.62	8.00E-01	5.78
90°	3.83	8.23E-01	4.65

(b)

Impact angle	Ke(mg cm^{-2} h^{-1})	Kc(mg cm^{-2} h^{-1})	Ke/Kc
15°	4.647	8.53E-01	5.45
45°	4.859	8.91E-01	5.45
90°	4.33	8.68E-01	4.99

(c)

Impact angle	Ke(mg cm^{-2} h^{-1})	Kc(mg cm^{-2} h^{-1})	Ke/Kc
15°	4.55	9.00E-01	5.06
45°	4.9	1.00E+00	4.9
90°	4.2	1.20E+00	3.5

Tables.4.36: Erosion-corrosion mechanism maps for carbon steel in oil /20% water at 4.5 m s−1 and particle size 150-300µm (a) - 400mV (b) 0mV (c) 400mV

(a)

Impact angle	Ke(mg cm $^{-2}$ h^{-1})	Kc(mg cm $^{-2}$ h^{-1})	Ke/Kc
15°	2.53	3.37E+00	0.75
45°	2.4	3.60E+00	0.67
90°	1.98	3.52E+00	0.562

(b)

Impact angle	Ke(mg cm $^{-2}$ h^{-1})	Kc(mg cm $^{-2}$ h^{-1})	Ke/Kc
15°	2.4	4.00E+00	0.6
45°	2.05	4.45E+00	0.46
90°	1.9	4.30E+00	0.44

(c)

Impact angle	Ke(mg cm $^{-2}$ h^{-1})	Kc(mg cm $^{-2}$ h^{-1})	Ke/Kc
15°	2.42	4.23E+00	0.57
45°	2.23	4.55E+00	0.49
90°	2.08	4.42E+00	0.47

Tables.4.37: Erosion-corrosion additive -synergism maps for carbon steel in water at 2.5 m $s^{-1}$and particle size 600-710µm (a) -400mV (b) -200mV (c) 0mV (d) 200mV (e) 400mV

(a)

Impact angle	Δke(mg cm^{-2} h^{-1})	Δkc(mg cm^{-2} h^{-1})	Δke/Δkc
15°	0.89	-0.21	-4.16
30°	0.9	-0.37	-2.43
45°	-0.11	0.16	-0.69
60°	0.76	0.03	25.33
75°	0.86	-0.22	-3.91
90°	0.9	-0.2	-4.5

(b)

Impact angle	Δke(mg cm^{-2} h^{-1})	Δkc(mg cm^{-2} h^{-1})	Δke/Δkc
15°	0.75	-0.14	-5.36
30°	0.99	0.04	24.75
45°	-0.33	0.53	-0.62
60°	0.49	-0.18	-2.72
75°	0.47	0.09	5.22
90°	0.3	0.28	1.071

(c)

Impact angle	Δke(mg cm^{-2} h^{-1})	Δkc(mg cm^{-2} h^{-1})	Δke/Δkc
15°	0.88	-0.16	-5.5
30°	0.78	-0.18	-4.33
45°	-0.8	1.47	-0.54
60°	-0.15	0.08	-1.88
75°	1.06	-0.24	-4.42
90°	-0.03	0.48	-0.06

(d)

Impact angle	Δke(mg cm^{-2} h^{-1})	Δkc(mg cm^{-2} h^{-1})	Δke/Δkc
15°	0.73	-0.05	-14.6
30°	0.96	-0.16	-6
45°	0.08	0.08	1
60°	0.1	0.63	0.16
75°	1.16	-0.96	-1.21
90°	-0.38	0.5	-0.76

(e)

Impact angle	Δke(mg cm^{-2} h^{-1})	Δkc(mg cm^{-2} h^{-1})	Δke/Δkc
15°	0.74	-0.1	-10.57
30°	0.56	0.04	14
45°	1.54	0.31	4.97
60°	1.17	-0.5	-2.49
75°	-0.39	0.32	-1.22
90°	-0.12	0.1	-1.2

Tables.4.38: Erosion-corrosion additive -synergism maps for carbon steel in crude oil at 2.5 m $s^{-1}$and particle size 600-710µm (a) -400mV (b) -200mV (c) 0mV (d) 200mV (e) 400mV

(a)

Impact angle	Δke(mg cm^{-2} h^{-1})	Δkc(mg cm^{-2} h^{-1})	Δke/Δkc
15°	0.5	1.10E-02	45.35
30°	0.79	1.00E-03	787.8
45°	0.1	-4.00E-03	-24.95
60°	1.08	4.30E-03	251.51
75°	1.08	4.00E-03	269.95
90°	0.39	-1.70E-03	-230.53

(b)

Impact angle	Δke(mg cm^{-2} h^{-1})	Δkc(mg cm^{-2} h^{-1})	Δke/Δkc
15°	0.60	2.20E-03	274
30°	1.18	2.40E-03	493
45°	0.79	-5.00E-04	-1570
60°	1.78	5.20E-03	342
75°	2.12	5.20E-03	407
90°	1.43	7.00E-04	2043

(c)

Impact angle	Δke(mg cm^{-2} h^{-1})	Δkc(mg cm^{-2} h^{-1})	Δke/Δkc
15°	1.40	-6.00E-04	-2337
30°	1.90	2.00E-03	951
45°	1.23	-6.00E-04	-2043
60°	2.38	4.60E-03	517
75°	2.22	4.60E-03	482
90°	1.68	5.00E-04	3360

(d)

Impact angle	Δke(mg cm^{-2} h^{-1})	Δkc(mg cm^{-2} h^{-1})	Δke/Δkc
15°	1.781	5.00E-04	3561
30°	2.29	-1.20E-03	-1904
45°	1.65	-4.00E-04	-4112
60°	2.1	5.80E-03	362
75°	2.56	7.10E-03	360
90°	2.28	5.20E-03	437

(e)

Impact angle	Δke(mg cm^{-2} h^{-1})	Δkc(mg cm^{-2} h^{-1})	Δke/Δkc
15°	1.78	2.90E-03	613
30°	2.29	-1.90E-03	-1202
45°	1.65	-1.30E-03	-1265
60°	2.1	-1.10E-03	-1906
75°	2.56	6.80E-03	375
90°	2.27	7.00E-03	324

Tables.4.39: Erosion-corrosion additive -synergism maps for carbon steel in oil /20% water at 2.5 m $s^{-1}$and particle size 600-710µm (a) -400mV (b) -200mV (c) 0mV (d) 200mV (e) 400mV

(a)

Impact angle	Δke(mg cm^{-2} h^{-1})	Δkc(mg cm^{-2} h^{-1})	Δke/Δkc
15°	0.33	-0.12	-2.75
30°	0.72	0.22	3.27
45°	0.26	0.22	1.18
60°	1.42	-0.13	-10.92
75°	0.94	0.43	2.19
90°	0.48	0.23	2.097

(b)

Impact angle	Δke(mg cm^{-2} h^{-1})	Δkc(mg cm^{-2} h^{-1})	Δke/Δkc
15°	0.36	-0.04	-9.42
30°	1.21	0.2	7.07
45°	0.6	-0.03	-22.92
60°	1.44	-0.1	-20.86
75°	1.59	0.2	8.37
90°	0.17	0.3	0.57

(c)

Impact angle	Δke(mg cm^{-2} h^{-1})	Δkc(mg cm^{-2} h^{-1})	Δke/Δkc
15°	0.08	-0.1	-1
30°	1.51	0.1	30.2
45°	0.94	-0.04	-23.5
60°	1.68	0.1	24
75°	1.08	0.1	12
90°	0.43	-0.02	-21.5

(d)

Impact angle	Δke(mg cm^{-2} h^{-1})	Δkc(mg cm^{-2} h^{-1})	Δke/Δkc
15°	0.12	-0.03	-4
30°	1.15	0.14	8.21
45°	0.99	-0.09	-11
60°	1.64	0.16	10.25
75°	1.4	-0.23	-6.09
90°	0.57	-0.06	-9.5

(e)

Impact angle	Δke(mg cm^{-2} h^{-1})	Δkc(mg cm^{-2} h^{-1})	Δke/Δkc
15°	-0.1	-0.1	1
30°	1.5	0.04	37
45°	0.2	0.15	1.33
60°	1.02	0.13	7.85
75°	1.21	-0.03	-40.3
90°	0.7	0.02	35

Tables.4.40: Erosion-corrosion additive -synergism maps for carbon steel in water at 3.5 m $s^{-1}$and particle size 600-710µm (a) -400mV (b) -200mV (c) 0mV (d) 200mV (e) 400mV

(a)

Impact angle	Δke(mg cm^{-2} h^{-1})	Δkc(mg cm^{-2} h^{-1})	Δke/Δkc
15°	-0.6	1.1	-0.55
30°	-0.06	0.8	-0.08
45°	-0.8	0.22	-3.5
60°	0.59	0.5	1.18
75°	-1.17	1.32	-0.89
90°	-0.3	0.21	-1.43

(b)

Impact angle	Δke(mg cm^{-2} h^{-1})	Δkc(mg cm^{-2} h^{-1})	Δke/Δkc
15°	-0.23	0.73	-0.32
30°	0.24	-0.29	-0.83
45°	-1.31	-0.07	-1.32
60°	0.4	0.75	0.53
75°	-0.11	0.51	-0.22
90°	-0.23	0.48	-0.48

(c)

Impact angle	Δke(mg cm^{-2} h^{-1})	Δkc(mg cm^{-2} h^{-1})	Δke/Δkc
15°	-0.35	0.86	-0.41
30°	0.55	0.17	3.24
45°	-1.21	0.23	-5.26
60°	0.9	0.82	1.09
75°	1.1	-0.6	-1.83
90°	0.28	0.99	0.28

(d)

Impact angle	Δke(mg cm^{-2} h^{-1})	Δkc(mg cm^{-2} h^{-1})	Δke/Δkc
15°	-0.27	0.87	-0.31
30°	1.53	0.6	2.55
45°	0.68	0.02	34
60°	1.03	0.41	2.51
75°	1.1	0.7	1.57
90°	0.3	1.61	0.19

(e)

Impact angle	Δke(mg cm^{-2} h^{-1})	Δkc(mg cm^{-2} h^{-1})	Δke/Δkc
15°	1.49	0.51	2.92
30°	1.7	0.75	2.27
45°	0.69	-0.49	-1.41
60°	0.99	0.91	1.09
75°	1.29	0.05	25.8
90°	-0.09	1.49	-0.06

Tables.4.41: Erosion-corrosion additive -synergism maps for carbon steel in crude oil at 3.5 m $s^{-1}$and particle size 600-710µm (a) -400mV (b) -200mV (c) 0mV (d) 200mV (e) 400mV

(a)

Impact angle	Δke(mg cm^{-2} h^{-1})	Δkc(mg cm^{-2} h^{-1})	Δke/Δkc
15°	2.26	-2.60E-03	-869
30°	2.17	5.10E-03	426
45°	2.08	2.00E-04	10400
60°	2.19	-1.20E-03	-1821
75°	2.84	-1.00E-03	-2840
90°	2.70	4.70E-03	575

(b)

Impact angle	Δke(mg cm^{-2} h^{-1})	Δkc(mg cm^{-2} h^{-1})	Δke/Δkc
15°	2.78	-2.20E-03	-1272
30°	2.37	4.10E-03	578
45°	2.18	3.40E-03	640
60°	2.68	5.00E-04	5349
75°	2.98	-5.80E-03	-513
90°	2.92	4.90E-03	596

(c)

Impact angle	Δke(mg cm^{-2} h^{-1})	Δkc(mg cm^{-2} h^{-1})	Δke/Δkc
15°	2.77	5.80E-03	478
30°	2.67	-2.00E-04	-13365
45°	2.58	-1.10E-03	-2347
60°	2.87	1.00E-04	28739
75°	2.99	8.00E-04	3741
90°	3.13	6.90E-03	454

(d)

Impact angle	Δke(mg cm^{-2} h^{-1})	Δkc(mg cm^{-2} h^{-1})	Δke/Δkc
15°	3.27	2.00E-03	1637
30°	3.37	-3.00E-04	-11241
45°	3.45	-4.00E-04	-8627
60°	2.98	-5.90E-03	-505
75°	3.24	1.06E-02	306
90°	3.7	7.10E-03	521

(e)

Impact angle	Δke(mg cm^{-2} h^{-1})	Δkc(mg cm^{-2} h^{-1})	Δke/Δkc
15°	4.67	5.00E-04	9348
30°	4.57	1.60E-03	2856
45°	3.78	5.00E-04	7560
60°	2.98	-4.30E-03	-6930
75°	4.12	1.80E-03	2289
90°	4.42	7.80E-03	566

Tables.4.42: Erosion-corrosion additive -synergism maps for carbon steel in oil /20% water at 3.5 m $s^{-1}$and particle size 600-710µm (a) -400mV (b) -200mV (c) 0mV (d) 200mV (e) 400mV

(a)

Impact angle	Δke(mg cm^{-2} h^{-1})	Δkc(mg cm^{-2} h^{-1})	Δke/Δkc
15°	1.86	-0.1	-26.57
30°	1.91	0.2	9.095
45°	2.8	0.2	18.66
60°	2.42	0.3	7.33
75°	2.35	0.3	7.83
90°	2.95	0.3	9.22

(b)

Impact angle	Δke(mg cm^{-2} h^{-1})	Δkc(mg cm^{-2} h^{-1})	Δke/Δkc
15°	2.7	0.1	24.73
30°	2.76	0.3	9.52
45°	2.9	0.12	24.17
60°	2.98	0.41	7.27
75°	2.96	0.1	32.89
90°	3.15	0.02	157.5

(c)

Impact angle	Δke(mg cm^{-2} h^{-1})	Δkc(mg cm^{-2} h^{-1})	Δke/Δkc
15°	2.8	-0.03	-93.67
30°	2.1	0.4	5.83
45°	2.8	0.1	28
60°	2.9	0.4	6.57
75°	2.68	-0.2	-11.65
90°	3.27	0.2	16.35

(d)

Impact angle	Δke(mg cm^{-2} h^{-1})	Δkc(mg cm^{-2} h^{-1})	Δke/Δkc
15°	3.17	0.13	24.38
30°	3.52	-0.22	-16
45°	2.9	0.2	14.5
60°	3.22	-0.11	-29.27
75°	2.9	-0.1	-36.25
90°	3.13	0.43	7.28

(e)

Impact angle	Δke(mg cm^{-2} h^{-1})	Δkc(mg cm^{-2} h^{-1})	Δke/Δkc
15°	3.7	0.2	18.55
30°	3.7	0.1	37.1
45°	3	0.5	6.52
60°	4.2	-0.1	-42
75°	4.0	-0.2	-25.13
90°	3.8	0.4	10.42

Tables.4.43:Erosion-corrosion additive -synergism maps for carbon steel in water at 4.5 m $s^{-1}$and particle size 600-710µm (a) -400mV (b) -200mV (c) 0mV(d) 200mV (e) 400mV

(a)

Impact angle	Δke(mg cm^{-2} h^{-1})	Δkc(mg cm^{-2} h^{-1})	Δke/Δkc
15°	-0.01	1.22	-0.01
30°	-0.11	1.11	-0.099
45°	0.58	-0.29	-2
60°	0.2	0.59	0.34
75°	0.7	0.71	0.99
90°	1.79	-0.07	-25.57

(b)

Impact angle	Δke(mg cm^{-2} h^{-1})	Δkc(mg cm^{-2} h^{-1})	Δke/Δkc
15°	-0.61	1.23	-0.50
30°	1.9	-0.81	-2.35
45°	0.27	0.12	2.25
60°	1.55	1.09	1.42
75°	1.15	0.99	1.16
90°	2.58	-0.54	-4.78

(c)

Impact angle	Δke(mg cm^{-2} h^{-1})	Δkc(mg cm^{-2} h^{-1})	Δke/Δkc
15°	0.82	1.1	0.75
30°	2.78	-0.22	-12.64
45°	1.54	-0.38	-4.05
60°	1.61	0.25	6.44
75°	1.81	1.24	1.46
90°	0.57	0.83	0.69

(d)

Impact angle	Δke(mg cm^{-2} h^{-1})	Δkc(mg cm^{-2} h^{-1})	Δke/Δkc
15°	1.76	0.26	6.77
30°	2.53	-0.2	-12.65
45°	1.84	0.28	6.57
60°	1.78	0.39	4.56
75°	2.22	1.04	2.13
90°	1.29	0.63	2.05

(e)

Impact angle	Δke(mg cm^{-2} h^{-1})	Δkc(mg cm^{-2} h^{-1})	Δke/Δkc
15°	2.25	0.12	18.75
30°	2.64	-0.12	-22
45°	2.21	0.84	2.63
60°	2.95	0.11	26.82
75°	0.86	1.74	0.49
90°	1.39	1.03	1.35

Tables .4.44: Erosion-corrosion additive -synergism maps for carbon steel in crude oil at 4.5 m $s^{-1}$and particle size 600-710µm (a) -400mV (b) -200mV (c) 0mV(d) 200mV (e) 400mV

(a)

Impact angle	Δke(mg cm^{-2} h^{-1})	Δkc(mg cm^{-2} h^{-1})	Δke/Δkc
15°	3.87	1.00E-03	3871
30°	3.18	2.60E-03	1222
45°	3.9	-4.60E-03	-847
60°	3.77	-1.30E-03	-2899
75°	4.67	-1.50E-03	-3113
90°	3.94	6.90E-03	571

(b)

Impact angle	Δke(mg cm^{-2} h^{-1})	Δkc(mg cm^{-2} h^{-1})	Δke/Δkc
15°	3.64	5.00E-03	728
30°	3.97	-5.00E-04	-7932
45°	3.79	-5.00E-04	-7580
60°	3.93	6.00E-04	6547
75°	4.72	2.00E-04	23576
90°	4.56	7.40E-03	616

(c)

Impact angle	Δke(mg cm^{-2} h^{-1})	Δkc(mg cm^{-2} h^{-1})	Δke/Δkc
15°	4.36	1.80E-03	2421
30°	4.44	5.00E-03	888
45°	4.22	-4.60E-03	-917
60°	4.06	-3.20E-03	-1269
75°	4.36	3.80E-03	1148
90°	4.20	1.04E-02	404

(d)

Impact angle	Δke(mg cm^{-2} h^{-1})	Δkc(mg cm^{-2} h^{-1})	Δke/Δkc
15°	4.83	7.00E-03	689
30°	4.94	-1.00E-03	-4941
45°	4.54	-1.60E-03	-2840
60°	4.2	-2.00E-04	-20996
75°	4.66	-3.20E-03	-1456
90°	4.75	9.10E-03	522

(e)

Impact angle	Δke(mg cm^{-2} h^{-1})	Δkc(mg cm^{-2} h^{-1})	Δke/Δkc
15°	4.47	-2.00E-04	-22361
30°	4.96	4.00E-03	1239
45°	5.21	8.00E-04	6513
60°	5.15	1.21E-02	425
75°	5.55	-2.00E-04	-27741
90°	4.98	1.01E-02	493

Tables.4.45: Erosion-corrosion additive -synergism maps for carbon steel in oil /20% water at 4.5 m $s^{-1}$and particle size 600-710µm (a) -400mV (b) -200mV (c) 0mV (d) 200mV (e) 400mV

(a)

Impact angle	Δke(mg cm^{-2} h^{-1})	Δkc(mg cm^{-2} h^{-1})	Δke/Δkc
15°	2.85	-0.05	-57
30°	3.07	-0.11	-28
45°	3.46	0.14	25
60°	2.92	-0.1	-29
75°	4.3	-0.1	-54
90°	3.55	0.3	14

(b)

Impact angle	Δke(mg cm^{-2} h^{-1})	Δkc(mg cm^{-2} h^{-1})	Δke/Δkc
15°	3.1	0.2	16
30°	3.98	0.2	20
45°	3.5	0.3	12
60°	3.61	-0.2	-16
75°	4.46	0.3	15
90°	3.9	0.3	14

(c)

Impact angle	Δke(mg cm^{-2} h^{-1})	Δkc(mg cm^{-2} h^{-1})	Δke/Δkc
15°	3.68	0.2	18.4
30°	4.08	0.2	20.71
45°	4.34	0.2	21.7
60°	3.89	-0.11	-35.36
75°	4.3	0.1	43
90°	3.92	0.3	13.07

(d)

Impact angle	Δke(mg cm^{-2} h^{-1})	Δkc(mg cm^{-2} h^{-1})	Δke/Δkc
15°	3.74	-0.02	-187
30°	4.4	-0.1	-44
45°	4.56	-0.14	-32.57
60°	5.78	-0.4	-15.21
75°	5.27	-0.1	-52.7
90°	4.7	0.3	15.67

(e)

Impact angle	Δke(mg cm^{-2} h^{-1})	Δkc(mg cm^{-2} h^{-1})	Δke/Δkc
15°	4.01	-0.1	-40.1
30°	4.67	-0.13	-35.92
45°	4.22	-0.1	-52.75
60°	4.42	0.2	22.1
75°	4.82	0.16	30.13
90°	4.78	-0.11	-43.45

Tables.4.46: Erosion-corrosion additive -synergism maps for carbon steel in water at 2.5 m s^{-1} and particle size 150-300µm (a) - 400mV (b) 0mV (c) 400mV

(a)

Impact angle	Δke(mg cm^{-2} h^{-1})	Δkc(mg cm^{-2} h^{-1})	Δke/Δkc
15°	0.9	0.57	1.59
45°	0.69	0.55	1.25
90°	0.61	0.49	1.24

(b)

Impact angle	Δke(mg cm^{-2} h^{-1})	Δkc(mg cm^{-2} h^{-1})	Δke/Δkc
15°	-0.13	1.76	-0.07
45°	-0.2	2.56	-0.08
90°	-0.07	1.59	-0.04

(c)

Impact angle	Δke(mg cm^{-2} h^{-1})	Δkc(mg cm^{-2} h^{-1})	Δke/Δkc
15°	-0.14	1.8	-0.08
45°	0.61	2.05	0.297
90°	-0.03	1.47	-0.02

Tables.4.47: Erosion-corrosion additive -synergism maps for carbon steel in crude oil at 2.5 m s^{-1} and particle size 150-300µm (a) - 400mV (b) 0mV (c) 400mV

(a)

Impact angle	Δke(mg cm^{-2} h^{-1})	Δkc(mg cm^{-2} h^{-1})	Δke/Δkc
15°	0.92	0.22	4.18
45°	0.91	0.2	4.54
90°	0.66	0.4	1.68

(b)

Impact angle	Δke(mg cm^{-2} h^{-1})	Δkc(mg cm^{-2} h^{-1})	Δke/Δkc
15°	0.95	0.2	4.63
45°	1.02	0.2	5.23
90°	1.04	0.22	4.84

(c)

Impact angle	Δke(mg cm^{-2} h^{-1})	Δkc(mg cm^{-2} h^{-1})	Δke/Δkc
15°	1.05	0.24	4.38
45°	1.2	0.2	6.11
90°	1.3	0.28	4.84

Tables.4.48: Erosion-corrosion additive -synergism maps for carbon steel in oil /20% water at 2.5 m s^{-1} and particle size 150-300µm (a) - 400mV (b) 0mV (c) 400mV

(a)

Impact angle	Δke(mg cm^{-2} h^{-1})	Δkc(mg cm^{-2} h^{-1})	Δke/Δkc
15°	0.68	0.2	3.55
45°	0.54	0.6	0.91
90°	1	0.4	2.77

(b)

Impact angle	Δke(mg cm^{-2} h^{-1})	Δkc(mg cm^{-2} h^{-1})	Δke/Δkc
15°	0.58	0.7	0.89
45°	0.2	1	0.21
90°	0.45	1	0.53

(c)

Impact angle	Δke(mg cm^{-2} h^{-1})	Δkc(mg cm^{-2} h^{-1})	Δke/Δkc
15°	0.47	0.97	0.48
45°	0.8	1.1	0.73
90°	0.42	1.1	0.4

Tables.4.49: Erosion-corrosion additive -synergism maps for carbon steel in water at 3.5 m s^{-1} and particle size 150-300µm (a) - 400mV (b) 0mV (c) 400mV

(a)

Impact angle	Δke(mg cm^{-2} h^{-1})	Δkc(mg cm^{-2} h^{-1})	Δke/Δkc
15°	0.28	0.96	0.29
45°	0.19	0.4	0.48
90°	0.18	0.4	0.45

(b)

Impact angle	Δke(mg cm^{-2} h^{-1})	Δkc(mg cm^{-2} h^{-1})	Δke/Δkc
15°	0.56	0.48	1.17
45°	-0.27	0.19	-1.42
90°	-0.32	0.8	-0.4

(c)

Impact angle	Δke(mg cm^{-2} h^{-1})	Δkc(mg cm^{-2} h^{-1})	Δke/Δkc
15°	1.06	0.2	5.3
45°	0.68	0.19	3.58
90°	-0.32	1.08	-0.3

Tables.4.50: Erosion-corrosion additive -synergism maps for carbon steel in crude oil at 3.5 m s^{-1} and particle size 150-300µm (a) - 400mV (b) 0mV (c) 400mV

(a)

Impact angle	Δke(mg cm^{-2} h^{-1})	Δkc(mg cm^{-2} h^{-1})	Δke/Δkc
15°	2.27	0.19	12.27
45°	2.56	0.30	8.48
90°	1.95	0.33	5.98

(b)

Impact angle	Δke(mg cm^{-2} h^{-1})	Δkc(mg cm^{-2} h^{-1})	Δke/Δkc
15°	2.44	0.33	7.37
45°	2.57	0.25	10.36
90°	2.14	0.38	5.66

(c)

Impact angle	Δke(mg cm^{-2} h^{-1})	Δkc(mg cm^{-2} h^{-1})	Δke/Δkc
15°	2.45	0.36	6.82
45°	2.59	0.37	6.94
90°	2.41	0.39	6.23

Tables.4.51: Erosion-corrosion additive -synergism maps for carbon steel in oil /20% water at 3.5 m s^{-1} and particle size 150-300µm (a) - 400mV (b) 0mV (c) 400mV

(a)

Impact angle	Δke(mg cm^{-2} h^{-1})	Δkc(mg cm^{-2} h^{-1})	Δke/Δkc
15°	0.77	1.55	0.495
45°	0.42	2.20	0.19
90°	0.97	1.48	0.65

(b)

Impact angle	Δke(mg cm^{-2} h^{-1})	Δkc(mg cm^{-2} h^{-1})	Δke/Δkc
15°	0.55	2.05	0.27
45°	0.62	2.1	0.3
90°	0.39	2.07	0.19

(c)

Impact angle	Δke(mg cm^{-2} h^{-1})	Δkc(mg cm^{-2} h^{-1})	Δke/Δkc
15°	0.95	2.02	0.47
45°	0.64	2.48	0.26
90°	0.81	2.1	0.39

Tables.4.52: Erosion-corrosion additive -synergism maps for carbon steel in water at 4.5 m s^{-1} and particle size 150-300µm (a) - 400mV (b) 0mV (c) 400mV

(a)

Impact angle	Δke(mg cm^{-2} h^{-1})	Δkc(mg cm^{-2} h^{-1})	Δke/Δkc
15°	0.25	1	0.25
45°	0.3	0.49	0.61
90°	0.1	0.85	0.12

(b)

Impact angle	Δke(mg cm^{-2} h^{-1})	Δkc(mg cm^{-2} h^{-1})	Δke/Δkc
15°	-0.74	1.39	-0.53
45°	0.11	0.5	0.22
90°	-0.85	1.2	-0.71

(c)

Impact angle	Δke(mg cm^{-2} h^{-1})	Δkc(mg cm^{-2} h^{-1})	Δke/Δkc
15°	-0.8	1.42	-0.56
45°	0.48	1.41	0.34
90°	-0.5	1.3	-0.38

Tables.4.53:Erosion-corrosion additive -synergism maps for carbon steel in crude oil at 4.5 m s^{-1} and particle size 150-300µm (a) - 400mV (b) 0mV (c) 400mV

(a)

Impact angle	Δke(mg cm^{-2} h^{-1})	Δkc(mg cm^{-2} h^{-1})	Δke/Δkc
15°	2.85	0.5	6.04
45°	2.92	0.5	5.82
90°	2.83	0.5	5.89

(b)

Impact angle	Δke(mg cm^{-2} h^{-1})	Δkc(mg cm^{-2} h^{-1})	Δke/Δkc
15°	3.25	0.44	7.33
45°	3.16	0.54	5.89
90°	3.33	0.52	6.46

(c)

Impact angle	Δke(mg cm^{-2} h^{-1})	Δkc(mg cm^{-2} h^{-1})	Δke/Δkc
15°	3.15	0.4	7.5
45°	3.2	0.6	5.26
90°	3.2	0.8	4.09

Tables.4.54: Erosion-corrosion additive -synergism maps for carbon steel in oil /20% water at 4.5 m s^{-1} and particle size 150-300μm (a) - 400mV (b) 0mV (c) 400mV

(a)

Impact angle	Δke(mg cm^{-2} h^{-1})	Δkc(mg cm^{-2} h^{-1})	Δke/Δkc
15°	1.13	1.97	0.57
45°	0.7	2.4	0.29
90°	0.98	2.3	0.42

(b)

Impact angle	Δke(mg cm^{-2} h^{-1})	Δkc(mg cm^{-2} h^{-1})	Δke/Δkc
15°	1	2.7	0.37
45°	0.35	3.25	0.11
90°	0.9	3	0.3

(c)

Impact angle	Δke(mg cm^{-2} h^{-1})	Δkc(mg cm^{-2} h^{-1})	Δke/Δkc
15°	1.02	2.23	0.46
45°	0.53	2.77	0.19
90°	1.08	2.42	0.45

Chapter 5

Results and discussion

(Effect of impact velocities and applied potentials on erosion-corrosion maps for particle sizes 600-710μm and 150-300μm)

5.0. Introduction

In this study, the carbon steel have been investigated at various of impact velocities and applied potentials at range of constant an impact angles, in water, crude oil and combined environments with different particle sizes (600-710µm and 150-300µm) as erodent particles.The polarization curves have been investigated at constant of impact angle for carbon steel in three environment for large particle sizes 600-710µm and a small particle sizes 150-300µm.

The total mass loss rate have been plotted as function of applied potentials for large particle sizes 600-710µm and a small particle sizes 150-300µm. The results have been used to establish erosion-corrosion mechanism, wastages and additive –synergism maps as function of impact velocities and applied potentials at range of constant impact angles for particle sizes (600-710µm and 150-300µm).

5.1. Effect of applied potential, impact velocity for particle sizes 600-710µm on erosion-corrosion of carbon steel maps

5.1.1 General

The effect of erosion-corrosion on carbon steel in three environments containing particles sized 600-710µm has been investigated in a slurry erosion impingement test rig with various applied potentials and impact velocities. The results of mass loss have been plotted as a function of applied potentials at constant impact angles.

5.1.2. Materials and procedure of erosion-corrosion test

The dimensions of the specimens were 25mm × 10mm × 4 mm. The area exposed to the impingement jet was 0.19cm^2, whilst the remaining area was covered by a coating in order to ensure that all corrosion measurements were related to the erosion-corrosion process only. Mass change measurements were made of the samples by using Mettler college 150 balance with an accuracy ±0.1mg. The tests were carried out at five applied potentials, -400, -200, 0, 200 and 400mV, and three impact velocities, 2.5, 3.5 and 4.5 m s^{-1} , for 30 minutes at six impact angles, 15°, 30°, 45°, 60°,75° and 90°.

5.1.3. Polarization curves for particle sizes 600-710µm

5.1.3.1. At impact angles of 15°, 90° and impact velocity 2.5 m s^{-1}

The corrosion testing was conducted under potentiodynamic conditions. Samples were in different environments to observe the corrosion behavior of carbon steel. For carbon steel in the water environment at an impact angles 15° and 90° Fig. 5.1(a) and (b), it is interesting to see that, the current density was increased with an increase in impact angle, from 15° to 90° at impact velocity of 2.5 m s^{-1}. However, for carbon steel in the crude oil environment Fig. 5.1(a), the average free corrosion potential (Ecorr) was higher value compared to the average free corrosion potential in the water environment. The average current density was about 0.0075 m A c m^{-2} at an impact angle of 15°. In addition, in the crude oil environment the value of cathodic current was greater than the anodic current consistent with [2,10and10].

5.1.3.2. At impact angles of 15°, 90° and impact velocity 3.5 m s^{-1}

In the water environment at impacts angle of 15° and 90° (Fig. 5.2 (a) and (b)), it was observed that the current density increased at a range between 0.8 to 1.0 m A cm^{-2}. However, for carbon steel in crude oil and oil/20% water environment (Fig. 5.2 (a) and (b))at impact angles of 15° and 90°the corrosion contribution was very small compared to corrosion contribution (Kc) in the water environment.

5.1.3.3. At impact angles of 15 °, 90° and impact velocity 4.5 m s^{-1}

For carbon steel in the water environment at impact angle of 15° and 90° the corrosion current density values were increased when impact velocity increased and the average value of current density was about 1.22 m A cm^{-2} Figs. 5.3 (a) and (b) . However, in the crude oil environment at impact angles 15° and 90° Figs. 5.3 (a) and (b), the corrosion current density was similar to all previous impact velocities. For carbon steel in oil/20% water environment Figs. 5.3 (a) and (b), it is clear that the current density was increased with an increase in impact velocity compared to corrosion contribution (Kc) in the crude oil environment.

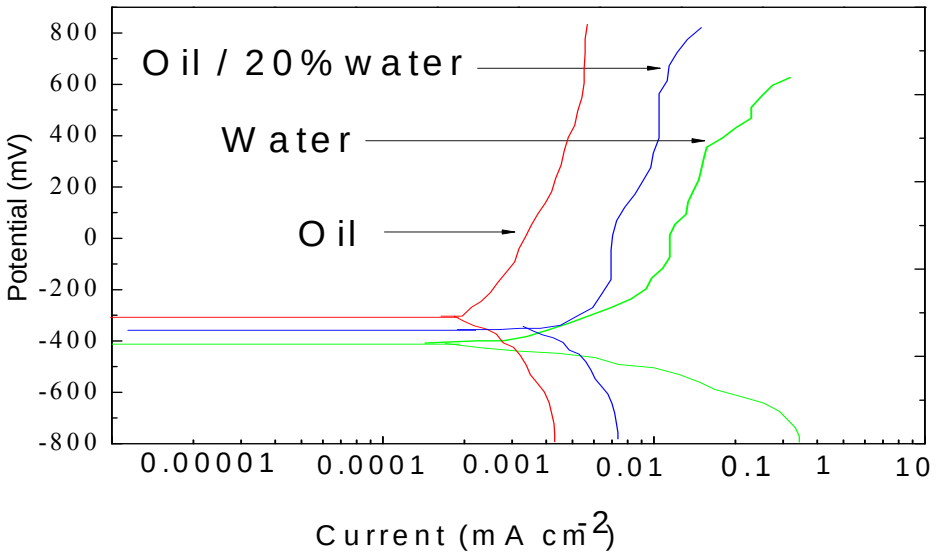

(a)

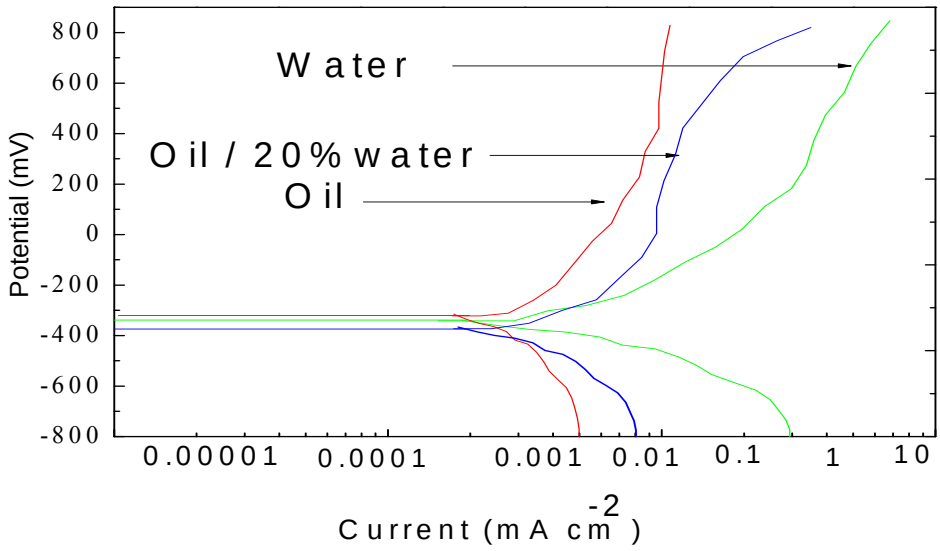

(b)

Fig.5.1: Polarization curves for carbon steel in three environments contain particle size 600-710µm and at 2.5 m s^{-1}: (a) 15° (b) 90°

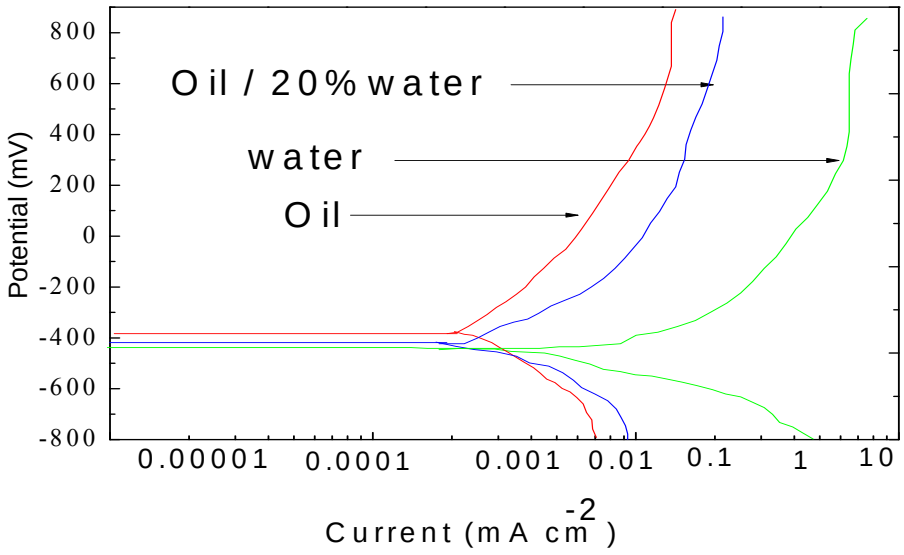

(a)

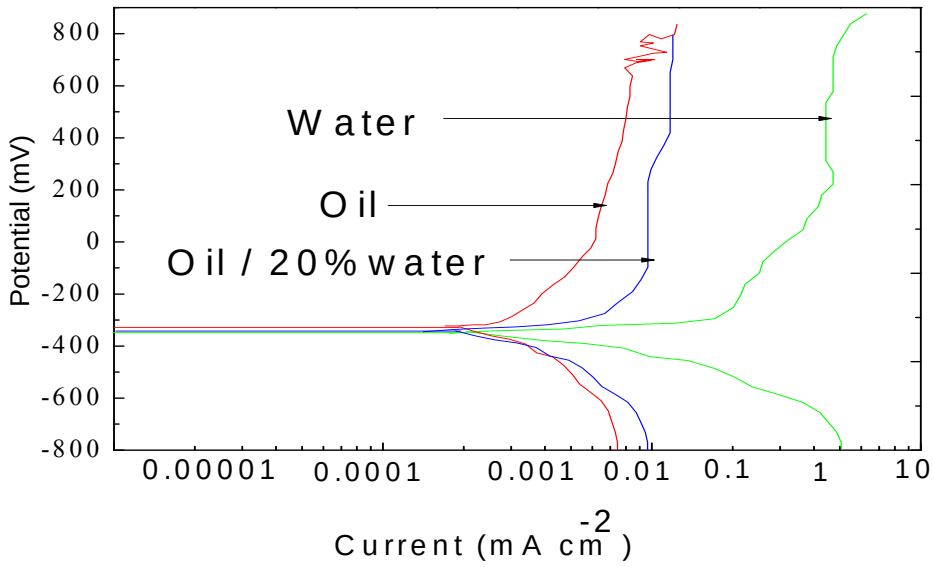

(b)

Fig.5.2: Polarization curves for carbon steel in three environments contain particle size 600-710µm and at 3.5 m s^{-1}: (a) 15° (b) 90°

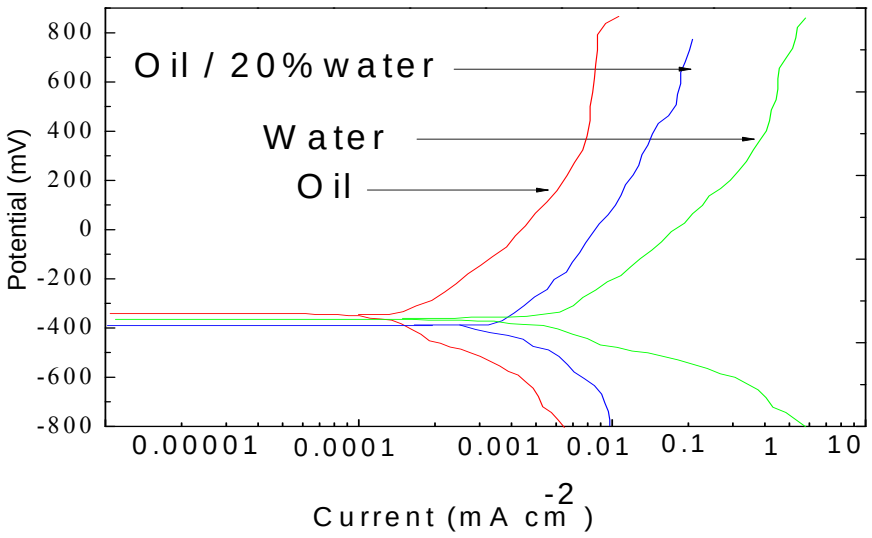

(a)

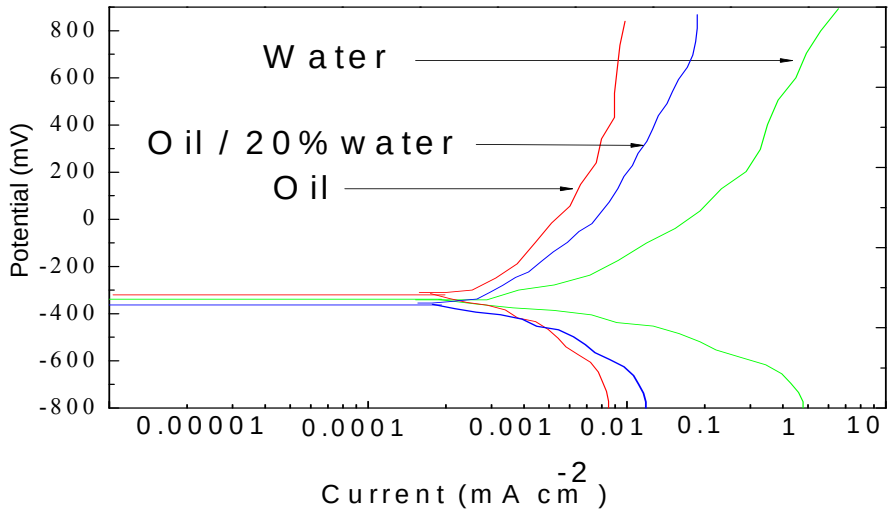

(b)

Fig.5.3: Polarization curves for carbon steel in three environments contain particle size 600-710µm and at 4.5 m s^{-1}: (a) 15° (b) 90°

5.1.4. Volume loss for particle sizes 600-710µm

The volume losses of carbon steel in the three environments contain particle sizes 600-710µm demonstrate that when the impact velocity was increased from a low velocity to a high impact velocity, the total volume losses (Kec) were increased in the three environments. However, the value of the mass losses in the reservoir water environment was highest, while the value of the volume losses in crude oil was less than in the mixed environment. Tables 5.1-5.18 show the results of the calculations of volume loss for Ke, Kc and Kec for difference environments contain particle sizes 600-710µm.

5.1.4.1. Mass loss in water reservoir

In the water environment the value of the value of erosion contribution (Ke) in water was increased less than the value of corrosion contribution (Kc) (Figures 5.7-5.10). In addition, for carbon steel in the water environment Figs. 5.4 (a-f) at an impact velocity of 2.5 m s^{-1}, high values of corrosion were recorded at positive applied potential (200 mV) was 2.78 mg cm^{-2} h^{-1} at an impact angle of 90°, while the low value of corrosion contribution was 1.5 mg cm^{-2} h^{-1} at impact angle of 30° and applied potential -400mV (Figures 5.4(a)). It is interesting to see that the value of erosion contribution (Ke) was also affected by an increase in the potential [6]. The greatest value of erosion contribution was 3.16 mg cm^{-2} h^{-1} at constant impact angle of 45° and applied potential of 400mV at an impact velocity of 2.5 m s^{-1} (Fig. 5.4(c)), while the lowest value of erosion contribution was 0.71 mg cm^{-2} h^{-1} at constant impact angle of 75° and at 400mV (Fig. 5.4(e)).

For carbon steel in the water environment at an impact velocity of 3.5 m s^{-1} Fig. 5.7, it can be seen that the total volume of mass loss rate (Kec) generally increased with an increase in impact velocity from 2.5 m s^{-1} to 3.5 m s^{-1}, and the highest total mass loss (Kec) was about 8.2 mg cm^{-2} h^{-1} at applied potential 400 mV and at constant impact angle of 45° (Fig. 5.7(c)). Furthermore, in the water environment the percentage of corrosion (Kc) was greater than the percentage of erosion (Ke) at the majority of impact angles and applied potentials.

With an increase in impact velocity from 3.5 to 4.5 m s^{-1} for carbon steel in water environment, the peak value of erosion-corrosion (Kec) was 11.84 mg cm^{-2} h^{-1} at impact angle of 45° and potential of 400mV(Fig. 5.10(c)). The lowest value of erosion contribution was at impact angle of 15° and at applied potential -200mV.

5.1.4.2. Mass loss in crude oil environment

For carbon steel in the crude oil environment at an impact velocity of 2.5 m s^{-1}, Figures.5.5 (a-f), there was a general decrease in the value of corrosion contribution (Kc) compared with that in the reservoir water environment. In addition, it can be observed that the value of corrosion contribution (Kc) was very low compared to erosion contribution at all impact angles and all applied potentials (Figures 5.5(a-f)). In actual fact, the percentage of total erosion-corrosion rate (Kec) pointed to the percentage of erosion contribution rate (Ke). The total volume loss rate (Kec) generally increased with an increase in impact velocity from 2.5 m s^{-1} to 3.5 m s^{-1}, and the peak volume loss was 7 mg cm^{-2} h^{-1} at impact angle of 15°and at applied potential 400mV,as demonstrated in (Fig.5.8(a)). The corrosion contribution had a very small increase compared to the previous impact velocity 2.5 m s^{-1} .On the other hand, the values of erosion contribution increased with an increase in impact velocity, and the highest value recorded was 8.42mg cm^{-2} h^{-1} at an impact angle of 15° at an impact velocity of 4.5 m s^{-1} (Fig. 5.11(a)).

5.1.4.3. Mass loss in oil/20% water

The percentage of erosion in oil/20% water contain large particle sizes 600-710µm Figures 5.6(a-f), was greater than the percentage of corrosion at the majority of test condition which dissimilar for carbon steel in oil/water contain a small particle sizes 150-300µm. The peak value of erosion at impact velocity 2.5 m s^{-1} was at impact angle 45°, about 2.89 mg .cm^{-2} h^{-1} at 200 mV, which is consistent with the findings of previous research [2, 10,11 and 6]. The value of corrosion usually has a greater value at the anodic regime, at potential 200mV and at an impact angle of 60°, at about 0.96 mg cm^{-2} h^{-1} (Fig. 5.6(d)).

In addition the total volume loss reached a maximum at about 10 mg cm^{-2} h^{-1} at impact angle of 60° and applied potential 200mV at impact velocity of 4.5 m s^{-1} and the minimum value was about 7 mg cm^{-2} h^{-1} at an impact angle of 60° and applied potential -400mV(Fig. 5.12(d)). The highest value of erosion contribution was 8.68 mg cm^{-2} h^{-1} at an impact angle 60°and applied potential 200mV (Fig. 5.12(d)).

Tables.5.1 Volume loss as function of potentials for carbon steel in water at 2.5 m $s^{-1}$and particle size 600-710µm (a) 15° (b) 30° (c) 45°

(a)

Applied potential mV	Ke(mg cm^{-2} h^{-1})	Kc(mg cm^{-2} h^{-1})	Kec(mg cm^{-2} h^{-1})
-400	2.59	1.72	4.31
-200	2.45	1.78	4.23
0	2.58	1.82	4.4
200	2.43	1.95	4.38
400	2.44	1.97	4.41

(b)

Applied potential mV	Ke(mg cm^{-2} h^{-1})	Kc(mg cm^{-2} h^{-1})	Kec(mg cm^{-2} h^{-1})
-400	2.5	1.5	4
-200	2.59	1.72	4.3
0	2.38	1.83	4.2
200	2.56	1.94	4.5
400	2.16	2.07	4.2

(c)

Applied potential mV	Ke(mg cm^{-2} h^{-1})	Kc(mg cm^{-2} h^{-1})	Kec(mg cm^{-2} h^{-1})
-400	2.39	2.21	4.6
-200	2.17	2.43	4.6
0	1.7	2.71	4.4
200	2.58	2.03	4.6
400	3.16	2.16	5.3

Tables.5.2: Volume loss as function of potentials for carbon steel in water at 2.5 m $s^{-1}$and particle size 600-710µm (a) 60° (b) 75° (c) 90°

(a)

Applied potential mV	Ke(mg cm^{-2} h^{-1})	Kc(mg cm^{-2} h^{-1})	Kec(mg cm^{-2} h^{-1})
-400	2.16	2.04	4.2
-200	1.89	2.12	4
0	1.25	2.25	3.5
200	1.5	2.71	4.2
400	2.57	1.93	4.5

(b)

Applied potential mV	Ke(mg cm^{-2} h^{-1})	Kc(mg cm^{-2} h^{-1})	Kec(mg cm^{-2} h^{-1})
-400	1.96	1.93	3.89
-200	1.57	2.24	3.8
0	2.16	2.46	4.6
200	2.26	1.34	3.6
400	0.71	2.74	3.5

(c)

Applied potential mV	Ke(mg cm^{-2} h^{-1})	Kc(mg cm^{-2} h^{-1})	Kec(mg cm^{-2} h^{-1})
-400	2.5	1.71	4.21
-200	1.9	2.21	4.1
0	1.57	2.73	4.3
200	1.22	2.78	4
400	1.48	2.53	4

Tables.5.3: Volume loss as function of potentials for carbon steel in crude oil at 2.5 m $s^{-1}$and particle size 600-710µm (a) 15° (b) 30° (c) 45°

(a)

Applied potential mV	Ke(mg cm^{-2} h^{-1})	Kc(mg cm^{-2} h^{-1})	Kec(mg cm^{-2} h^{-1})
-400	2.48	2.11E-02	2.5
-200	2.58	1.63E-02	2.6
0	3.38	1.85E-02	3.401
200	3.76	1.94E-02	3.78
400	4.29	2.14E-02	4.31

(b)

Applied potential mV	Ke(mg cm^{-2} h^{-1})	Kc(mg cm^{-2} h^{-1})	Kec(mg cm^{-2} h^{-1})
-400	1.99	1.22E-02	2
-200	2.38	1.65E-02	2.4
0	3.10	1.71E-02	3.12
200	3.49	1.49E-02	3.5
400	3.52	1.52E-02	3.53

(c)

Applied potential mV	Ke(mg cm^{-2} h^{-1})	Kc(mg cm^{-2} h^{-1})	Kec(mg cm^{-2} h^{-1})
-400	2	1.02E-02	2.01
-200	2.69	1.47E-02	2.7
0	3.13	1.39E-02	3.14
200	3.55	1.51E-02	3.56
400	4.19	1.48E-02	4.2

Tables.5.4: Volume loss as function of potentials for carbon steel in crude oil at 2.5 m $s^{-1}$and particle size 600-710µm (a) 60° (b) 75° (c) 90°

(a)

Applied potential mV	Ke(mg cm^{-2} h^{-1})	Kc(mg cm^{-2} h^{-1})	Kec(mg cm^{-2} h^{-1})
-400	2.08	1.85E-02	2.1
-200	2.78	1.93E-02	2.8
0	3.38	1.90E-02	3.4
200	3.1	2.00E-02	3.12
400	3.98	2.31E-02	4

(b)

Applied potential mV	Ke(mg cm^{-2} h^{-1})	Kc(mg cm^{-2} h^{-1})	Kec(mg cm^{-2} h^{-1})
-400	2.1	2.02E-02	2.12
-200	3.14	2.12E-02	3.16
0	3.24	1.98E-02	3.26
200	3.577	2.33E-02	3.6
400	3.69	2.40E-02	3.71

(c)

Applied potential mV	Ke(mg cm^{-2} h^{-1})	Kc(mg cm^{-2} h^{-1})	Kec(mg cm^{-2} h^{-1})
-400	2.1	1.81E-02	2.11
-200	3.13	1.97E-02	3.15
0	3.38	2.00E-02	3.4
200	3.98	2.42E-02	4
400	4.1	2.65E-02	4.11

Tables.5.5: Volume loss as function of potentials for carbon steel in oil /20% water at 2.5 m $s^{-1}$and particle size 600-710µm (a) 15° (b) 30° (c) 45°

(a)

Applied potential mV	Ke(mg cm^{-2} h^{-1})	Kc(mg cm^{-2} h^{-1})	Kec(mg cm^{-2} h^{-1})
-400	2.31	0.8	3.11
-200	2.34	0.81	3.15
0	2.06	0.8	2.84
200	2.1	0.68	2.78
400	1.89	0.71	2.6

(b)

Applied potential mV	Ke(mg cm^{-2} h^{-1})	Kc(mg cm^{-2} h^{-1})	Kec(mg cm^{-2} h^{-1})
-400	1.92	0.78	2.7
-200	2.41	0.79	3.2
0	2.71	0.8	3.51
200	2.35	0.9	3.25
400	2.68	0.72	3.4

(c)

Applied potential mV	Ke(mg cm^{-2} h^{-1})	Kc(mg cm^{-2} h^{-1})	Kec(mg cm^{-2} h^{-1})
-400	2.16	0.84	3
-200	2.5	0.71	3.2
0	2.84	0.76	3.6
200	2.89	0.81	3.7
400	2.1	0.9	3

Tables.5.6: Volume loss as function of potentials for carbon steel in oil /20% water at 2.5 m $s^{-1}$and particle size 600-710µm (a) 60° (b) 75° (c) 90°

(a)

Applied potential mV	Ke(mg cm^{-2} h^{-1})	Kc(mg cm^{-2} h^{-1})	Kec(mg cm^{-2} h^{-1})
-400	2.42	0.78	3.2
-200	2.44	0.80	3.24
0	2.68	0.82	3.5
200	2.64	0.96	3.6
400	2.02	0.78	2.8

(b)

Applied potential mV	Ke(mg cm^{-2} h^{-1})	Kc(mg cm^{-2} h^{-1})	Kec(mg cm^{-2} h^{-1})
-400	1.96	1	2.96
-200	2.61	0.89	3.5
0	2.1	0.9	3
200	2.42	0.45	2.87
400	2.23	0.67	2.9

(c)

Applied potential mV	Ke(mg cm^{-2} h^{-1})	Kc(mg cm^{-2} h^{-1})	Kec(mg cm^{-2} h^{-1})
-400	2.18	0.9	3.08
-200	1.87	0.91	2.78
0	2.13	0.78	2.91
200	2.27	0.73	3
400	2.4	0.8	3.2

Tables.5.7: Volume loss as function of potentials for carbon steel in water at 3.5 m $s^{-1}$and particle size 600-710µm (a) 15° (b) 30° (c) 45°

(a)

Applied potential mV	Ke(mg cm^{-2} h^{-1})	Kc(mg cm^{-2} h^{-1})	Kec(mg cm^{-2} h^{-1})
-400	1.4	4.12	5.52
-200	1.77	4.21	5.98
0	1.65	4.38	6.03
200	1.73	4.48	6.21
400	3.49	4.51	8

(b)

Applied potential	Ke(mg cm^{-2} h^{-1})	Kc(mg cm^{-2} h^{-1})	Kec(mg cm^{-2} h^{-1})
-400	1.81	4.21	6.02
-200	2.11	3.91	6.02
0	2.42	3.78	6.2
200	3.4	4.1	7.5
400	3.57	4.23	7.8

(c)

Applied potential mV	Ke(mg cm^{-2} h^{-1})	Kc(mg cm^{-2} h^{-1})	Kec(mg cm^{-2} h^{-1})
-400	2.43	4.02	6.45
-200	1.89	5	6.89
0	1.99	5.04	7.03
200	3.88	4.12	8
400	3.89	4.32	8.21

Tables.5.8: Volume loss as function of potentials for carbon steel in water at 3.5 m $s^{-1}$and particle size 600-710µm (a) 60° (b) 75° (c) 90°

(a)

Applied potential mV	Ke(mg cm^{-2} h^{-1})	Kc(mg cm^{-2} h^{-1})	Kec(mg cm^{-2} h^{-1})
-400	2.39	3.91	6.3
-200	2.2	4.25	6.45
0	2.7	4.51	7.21
200	2.83	5.01	7.84
400	2.79	5.21	8

(b)

Applied potential mV	Ke(mg cm^{-2} h^{-1})	Kc(mg cm^{-2} h^{-1})	Kec(mg cm^{-2} h^{-1})
-400	0.53	5.32	5.85
-200	1.59	4.61	6.2
0	2.8	4.07	6.87
200	2.8	4.5	7.3
400	2.99	4.85	7.84

(c)

Applied potential mV	Ke(mg cm^{-2} h^{-1})	Kc(mg cm^{-2} h^{-1})	Kec(mg cm^{-2} h^{-1})
-400	1.9	4.31	6.21
-200	1.97	4.38	6.35
0	2.48	5	7.48
200	2.5	5.52	8.02
400	2.11	5.81	7.92

Tables.5.9: Volume loss as function of potentials for carbon steel in crude oil at 3.5 m $s^{-1}$and particle size 600-710µm (a) 15° (b) 30° (c) 45°

(a)

Applied potential mV	Ke(mg cm^{-2} h^{-1})	Kc(mg cm^{-2} h^{-1})	Kec(mg cm^{-2} h^{-1})
-400	4.56	1.89E-02	4.58
-200	5.1	2.09E-02	5.12
0m	5.1	2.59E-02	5.1
200	5.57	2.61E-02	5.6
400	6.97	2.58E-02	7

(b)

Applied potential mV	Ke(mg cm^{-2} h^{-1})	Kc(mg cm^{-2} h^{-1})	Kec(mg cm^{-2} h^{-1})
-400	3.97	2.62E-02	4
-200	4.17	3.02E-02	4.2
0	4.47	2.70E-02	4.5
200	5.17	2.78E-02	5.2
400	6.37	3.08E-02	6.4

(c)

Applied potential mV	Ke(mg cm^{-2} h^{-1})	Kc(mg cm^{-2} h^{-1})	Kec(mg cm^{-2} h^{-1})
-400	4.48	2.00E-02	4.5
-200	4.58	2.21E-02	4.6
0	4.98	1.81E-02	5
200	5.85	1.92E-02	5.87
400	6.18	2.02E-02	6.2

Tables.5.10:Volume loss as function of potentials for carbon steel in crude oil at 3.5 m $s^{-1}$and particle size 600-710µm (a) 60° (b) 75° (c) 90°

(a)

Applied potential mV	Ke(mg cm^{-2} h^{-1})	Kc(mg cm^{-2} h^{-1})	Kec(mg cm^{-2} h^{-1})
-400	4.19	2.43E-02	4.21
-200	4.68	2.53E-02	4.7
0	4.87	2.61E-02	4.9
200	4.98	1.99E-02	5
400	4.98	2.19E-02	5

(b)

Applied potential mV	Ke(mg cm^{-2} h^{-1})	Kc(mg cm^{-2} h^{-1})	Kec(mg cm^{-2} h^{-1})
-400	4.69	1.92E-02	4.71
-200	4.83	2.02E-02	4.85
0	4.84	2.76E-02	4.87
200	5.09	3.76E-02	5.13
400	5.97	2.96E-02	6

(c)

Applied potential mV	Ke(mg cm^{-2} h^{-1})	Kc(mg cm^{-2} h^{-1})	Kec(mg cm^{-2} h^{-1})
-400	4.75	2.62E-02	4.78
-200	4.97	2.74E-02	5
0	5.18	2.91E-02	5.21
200	5.75	3.01E-02	5.78
400	6.47	3.21E-02	6.5

Tables.5.11: Volume loss as function of potentials for carbon steel in oil /20% water at 3.5 m $s^{-1}$and particle size 600-710µm (a) 15° (b) 30° (c) 45°

(a)

Applied potential mV	Ke(mg cm^{-2} h^{-1})	Kc(mg cm^{-2} h^{-1})	Kec(mg cm^{-2} h^{-1})
-400	4.16	0.84	5
-200	5.02	0.98	6
0	5.11	0.89	6
200	5.47	0.93	6.4
400	6.01	1.2	7.21

(b)

Applied potential mV	Ke(mg cm^{-2} h^{-1})	Kc(mg cm^{-2} h^{-1})	Kec(mg cm^{-2} h^{-1})
-400	3.71	0.89	4.6
-200	4.56	1	5.56
0	3.9	1.2	5.1
200	5.32	0.98	6.3
400	5.51	1	6.51

(c)

Applied potential mV	Ke(mg cm^{-2} h^{-1})	Kc(mg cm^{-2} h^{-1})	Kec(mg cm^{-2} h^{-1})
-400	5.2	0.9	6.1
-200	5.3	0.9	6.2
0	5.2	1	6.2
200	5.3	1.2	6.5
400	5.4	1.3	6.7

Tables.5.12: Volume loss as function of potentials for carbon steel in oil /20% water at 3.5 m $s^{-1}$and particle size 600-710µm (a) 60° (b) 75° (c) 90°

(a)

Applied potential mV	Ke(mg cm^{-2} h^{-1})	Kc(mg cm^{-2} h^{-1})	Kec(mg cm^{-2} h^{-1})
-400	4.42	0.98	5.4
-200	4.98	1.12	6.1
0	4.89	1.23	6.12
200	5.22	0.78	6
400	6.2	0.8	7

(b)

Applied potential mV	Ke(mg cm^{-2} h^{-1})	Kc(mg cm^{-2} h^{-1})	Kec(mg cm^{-2} h^{-1})
-400	4.2	1	5.2
-200	4.81	0.89	5.7
0	4.53	1	5.53
200	4.75	1.12	5.87
400	5.87	0.98	6.85

(c)

Applied potential mV	Ke(mg cm^{-2} h^{-1})	Kc(mg cm^{-2} h^{-1})	Kec(mg cm^{-2} h^{-1})
-400	5	1.1	6.1
-200	5.2	1	6.2
0	5.32	0.98	6.3
200	5.18	1.23	6.41
400	5.8	1.2	7

Tables.5.13: Volume loss as function of potentials for carbon steel in water at 4.5 m $s^{-1}$and particle size 600-710µm (a) 15° (b) 30° (c) 45°

(a)

Applied potential mV	Ke(mg cm^{-2} h^{-1})	Kc(mg cm^{-2} h^{-1})	Kec(mg cm^{-2} h^{-1})
-400	2.99	5.72	8.71
-200	2.39	5.84	8.23
0	3.82	5.91	9.73
200	4.76	5.24	10
400	5.25	5.2	10.45

(b)

Applied potential mV	Ke(mg cm^{-2} h^{-1})	Kc(mg cm^{-2} h^{-1})	Kec(mg cm^{-2} h^{-1})
-400	2.87	5.93	8.8
-200	4.88	4.12	9
0	5.76	4.45	10.21
200	5.51	4.81	10.32
400	5.62	4.9	10.52

(c)

Applied potential mV	Ke(mg cm^{-2} h^{-1})	Kc(mg cm^{-2} h^{-1})	Kec(mg cm^{-2} h^{-1})
-400	4.48	4.72	9.2
-200	4.17	5.85	10.02
0	5.44	5.01	10.45
200	5.74	5.32	11.06
400	6.11	5.73	11.84

Tables.5.14: Volume loss as function of potentials for carbon steel in water at 4.5 m $s^{-1}$and particle size 600-710µm (a) 60° (b) 75° (c) 90°

(a)

Applied potential mV	Ke(mg cm^{-2} h^{-1})	Kc(mg cm^{-2} h^{-1})	Kec(mg cm^{-2} h^{-1})
-400	3.3	5.4	8.7
-200	4.65	5.67	10.32
0	4.71	5.56	10.27
200	4.88	5.87	10.75
400	6.05	5.07	11.12

(b)

Applied potential mV	Ke(mg cm^{-2} h^{-1})	Kc(mg cm^{-2} h^{-1})	Kec(mg cm^{-2} h^{-1})
-400	3	5.94	8.94
-200	3.45	5.89	9.34
0	4.11	6.21	10.32
200	4.52	6	10.52
400	3.16	6.84	10

(c)

Applied potential mV	Ke(mg cm^{-2} h^{-1})	Kc(mg cm^{-2} h^{-1})	Kec(mg cm^{-2} h^{-1})
-400	4.69	4.78	9.47
-200	5.48	4.83	10.31
0	3.47	6.03	9.5
200	4.19	6.13	10.32
400	4.29	6.73	11.02

Tables.5.15: Volume loss as function of potentials for carbon steel in crude oil at 4.5 m $s^{-1}$and particle size 600-710μm (a) 15° (b) 30° (c) 45°

(a)

Applied potential mV	Ke(mg cm^{-2} h^{-1})	Kc(mg cm^{-2} h^{-1})	Kec(mg cm^{-2} h^{-1})
-400	7.47	2.88E-02	7.5
-200	7.24	3.78E-02	7.28
0	7.96	4.28E-02	8
200	8.43	4.50E-02	8.47
400	8.07	4.78E-02	8.12

(b)

Applied potential mV	Ke(mg cm^{-2} h^{-1})	Kc(mg cm^{-2} h^{-1})	Kec(mg cm^{-2} h^{-1})
-400	6.18	3.28E-02	6.21
-200	6.97	3.41E-02	7
0	7.44	4.01E-02	7.48
200	7.94	3.91E-02	7.98
400	7.96	4.51E-02	8

(c)

Applied potential mV	Ke(mg cm^{-2} h^{-1})	Kc(mg cm^{-2} h^{-1})	Kec(mg cm^{-2} h^{-1})
-400	7.1	2.52E-02	7.12
-200	6.9	2.98E-02	7.02
0	7.42	3.08E-02	7.45
200	7.74	3.58E-02	7.78
400	8.41	4.00E-02	8.45

Tables.5.16: Volume loss as function of potentials for carbon steel in crude oil at 4.5 m $s^{-1}$and particle size 600-710µm (a) 60° (b) 75° (c) 90°

(a)

Applied potential mV	Ke(mg cm^{-2} h^{-1})	Kc(mg cm^{-2} h^{-1})	Kec(mg cm^{-2} h^{-1})
-400	6.67	3.19E-02	6.7
-200	6.83	4.19E-02	6.87
0	6.96	3.89E-02	7
200	7.1	4.09E-02	7.14
400	8.1	5.19E-02	8.1

(b)

Applied potential mV	Ke(mg cm^{-2} h^{-1})	Kc(mg cm^{-2} h^{-1})	Kec(mg cm^{-2} h^{-1})
-400	6.97	3.03E-02	7
-200	7.015	3.48E-02	7.05
0	6.66	3.88E-02	6.7
200	6.96	3.78E-02	7
400	7.848	4.18E-02	7.89

(c)

Applied potential mV	Ke(mg cm^{-2} h^{-1})	Kc(mg cm^{-2} h^{-1})	Kec(mg cm^{-2} h^{-1})
-400	7.14	4.12E-02	7.18
-200	7.76	3.99E-02	7.8
0	7.404	4.56E-02	7.45
200	7.95	4.78E-02	8
400	8.178	5.18E-02	8.23

Tables.5.17: Volume loss as function of potentials for carbon steel in oil /20% water at 4.5 m $s^{-1}$and particle size 600-710µm (a) 15° (b) 30° (c) 45°

(a)

Applied potential mV	Ke(mg cm^{-2} h^{-1})	Kc(mg cm^{-2} h^{-1})	Kec(mg cm^{-2} h^{-1})
-400	6.45	1.35	7.8
-200	6.7	1.3	8
0	7.28	1.5	8.78
200	7.34	1.68	9.02
400	7.61	1.9	9.51

(b)

Applied potential mV	Ke(mg cm^{-2} h^{-1})	Kc(mg cm^{-2} h^{-1})	Kec(mg cm^{-2} h^{-1})
-400	6.07	1.21	7.28
-200	6.98	1.32	8.3
0	7.08	1.32	8.4
200	7.4	1.6	9
400	7.67	1.85	9.52

(c)

Applied potential mV	Ke(mg cm^{-2} h^{-1})	Kc(mg cm^{-2} h^{-1})	Kec(mg cm^{-2} h^{-1})
-400	6.66	1.34	8
-200	6.7	1.5	8.2
0	7.54	1.4	8.94
200	7.76	1.54	9.3
400	7.42	1.7	9.12

Tables.5.18: Volume loss as function of potentials for carbon steel in oil /20% water at 4.5 m $s^{-1}$and particle size 600-710µm (a) 60° (b) 75° (c) 90°

(a)

Applied potential mV	Ke(mg cm^{-2} h^{-1})	Kc(mg cm^{-2} h^{-1})	Kec(mg cm^{-2} h^{-1})
-400	5.82	1.2	7.02
-200	6.51	1.1	7.61
0	6.79	1.21	8
200	8.68	1.32	10
400	7.32	1.68	9

(b)

Applied potential mV	Ke(mg cm^{-2} h^{-1})	Kc(mg cm^{-2} h^{-1})	Kec(mg cm^{-2} h^{-1})
-400	6.6	1.4	8
-200	6.76	1.3	8.06
0	6.6	1.3	7.9
200	7.57	1.4	8.97
400	7.12	1.76	8.88

(c)

Applied potential mV	Ke(mg cm^{-2} h^{-1})	Kc(mg cm^{-2} h^{-1})	Kec(mg cm^{-2} h^{-1})
-400	6.75	1.45	8.2
-200	7.1	1.5	8.6
0	7.12	1.6	8.72
200	7.9	1.7	9.6
400	7.98	1.89	9.87

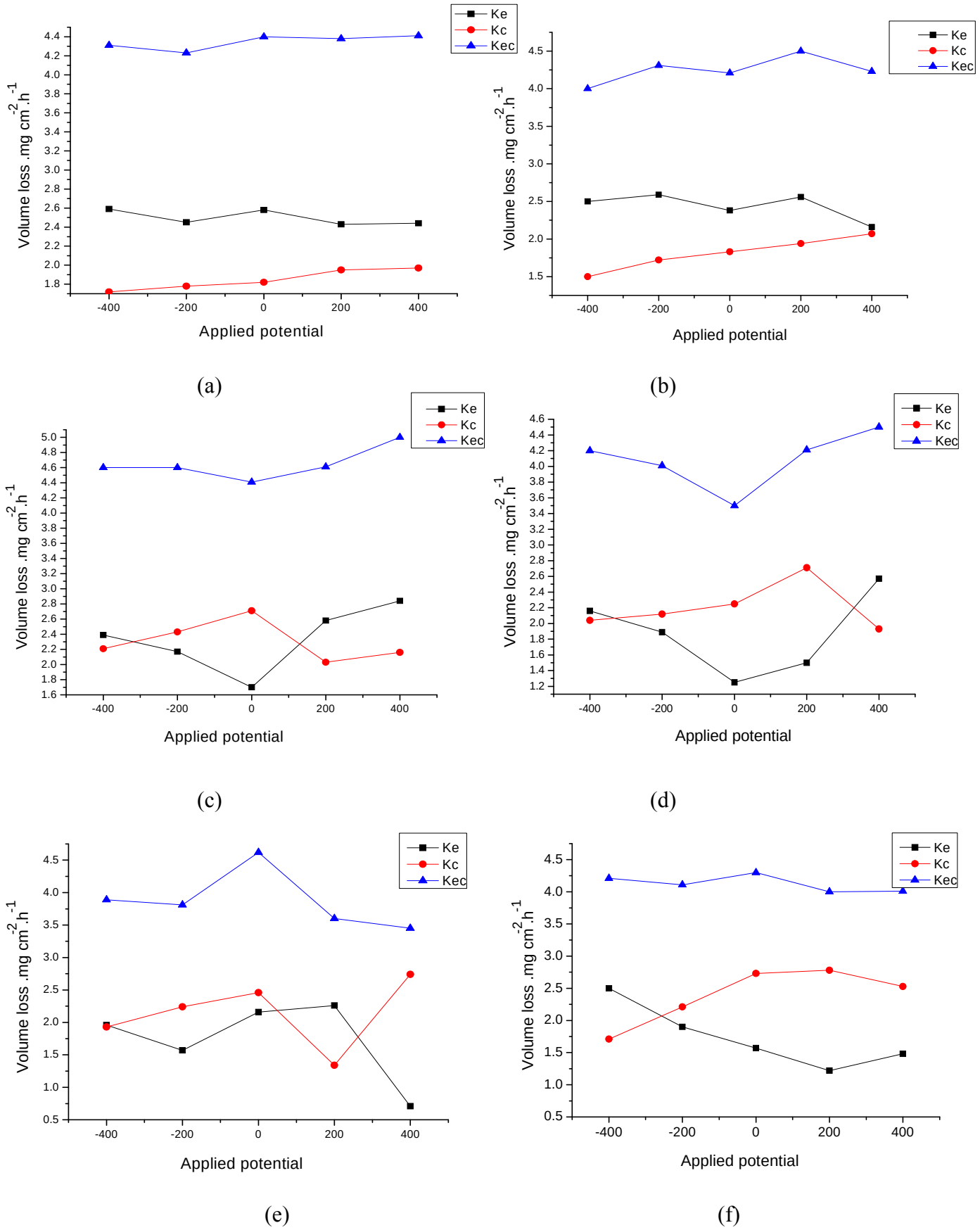

Fig.5.4: Volume loss as function of potentials for carbon steel in water at 2.5 m $s^{-1}$and particle size 600-710µm (a) 15° (b) 30° (c) 45°(d) 60° (e) 75° (f) 90°.

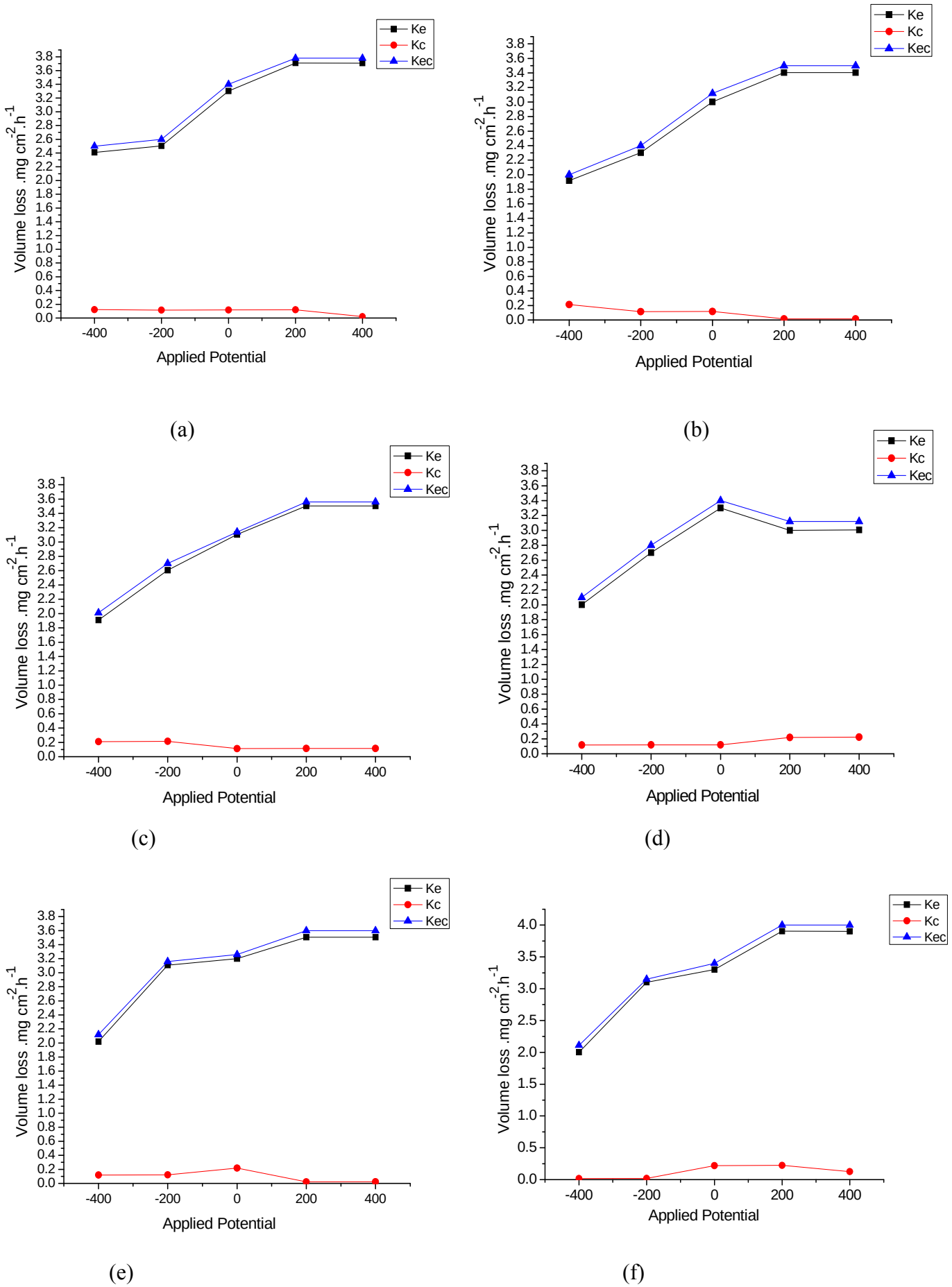

Fig.5.5: Volume loss as function of potentials for carbon steel in crude oil at 2.5 m $s^{-1}$and particle size 600-710µm (a) 15° (b) 30° (c) 45°(d) 60° (e) 75° (f) 90° .

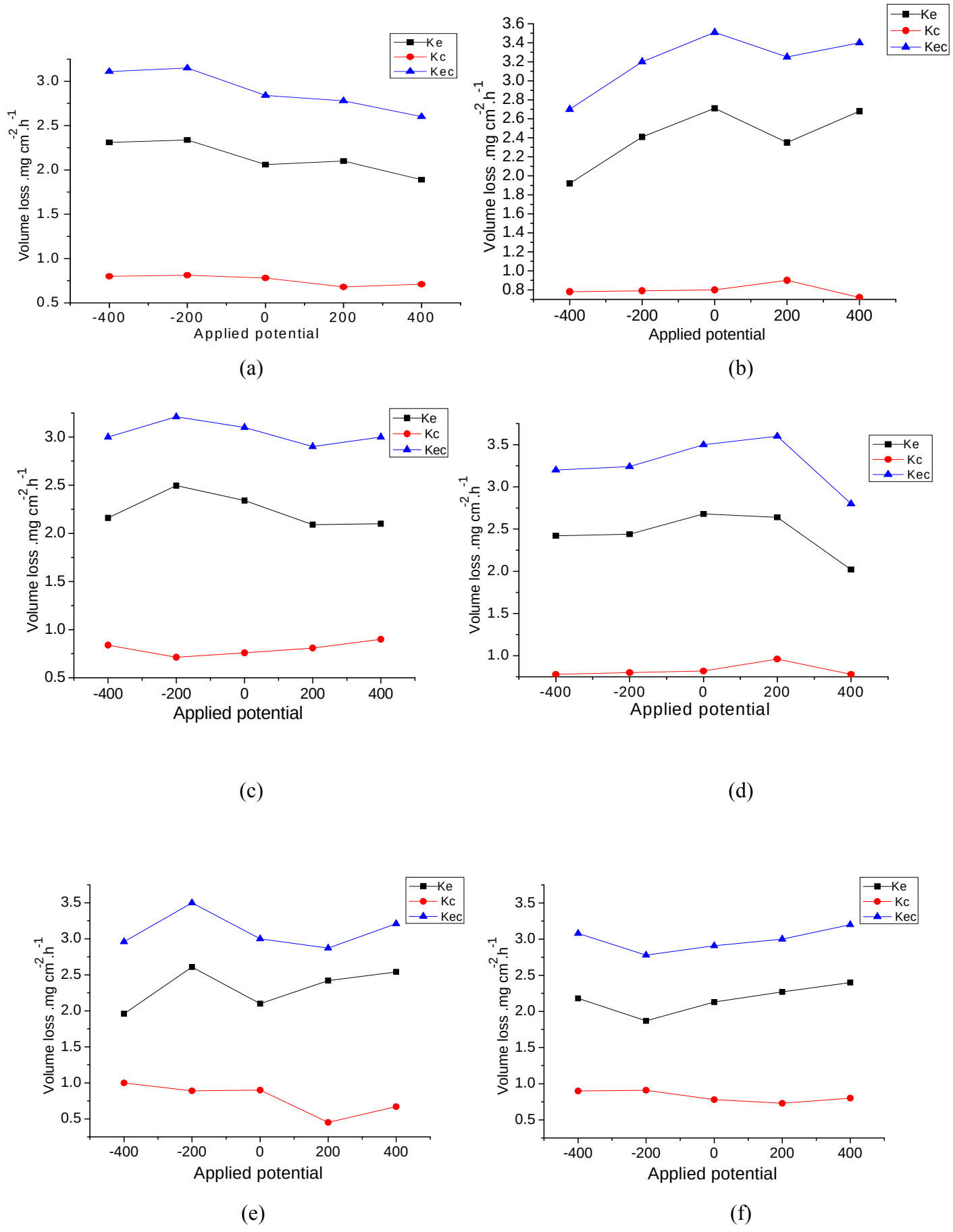

Fig.5.6: Volume loss as function of potentials for carbon steel in oil /20% water at 2.5 m $s^{-1}$and particle size 600-710µm (a) 15° (b) 30° (c) 45°(d) 60° (e) 75° (f) 90° .

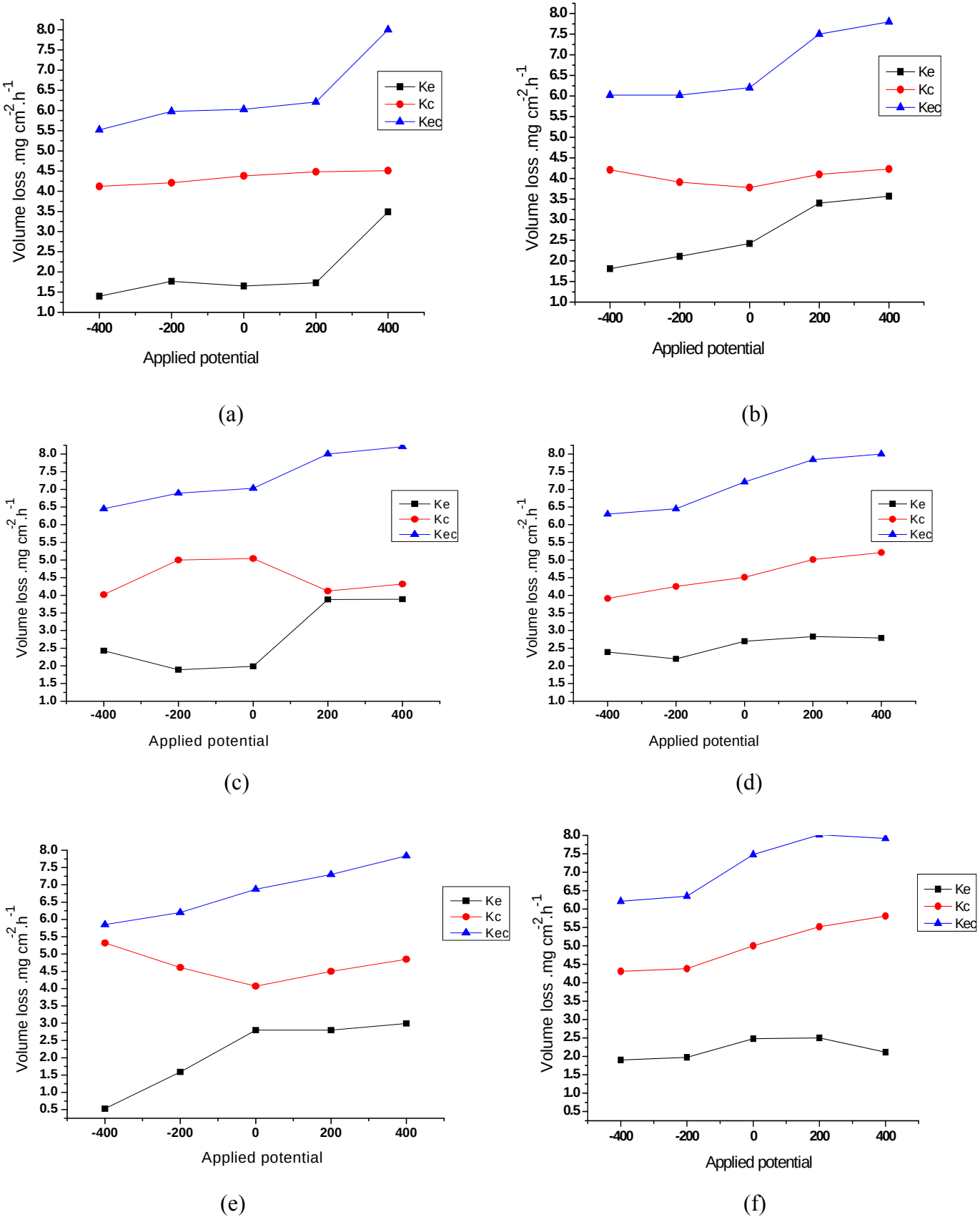

Fig.5.7: Volume loss as function of potentials for carbon steel in water at 3.5 m $s^{-1}$and particle size 600-710µm (a) 15° (b) 30° (c) 45°(d) 60° (e) 75° (f) 90° .

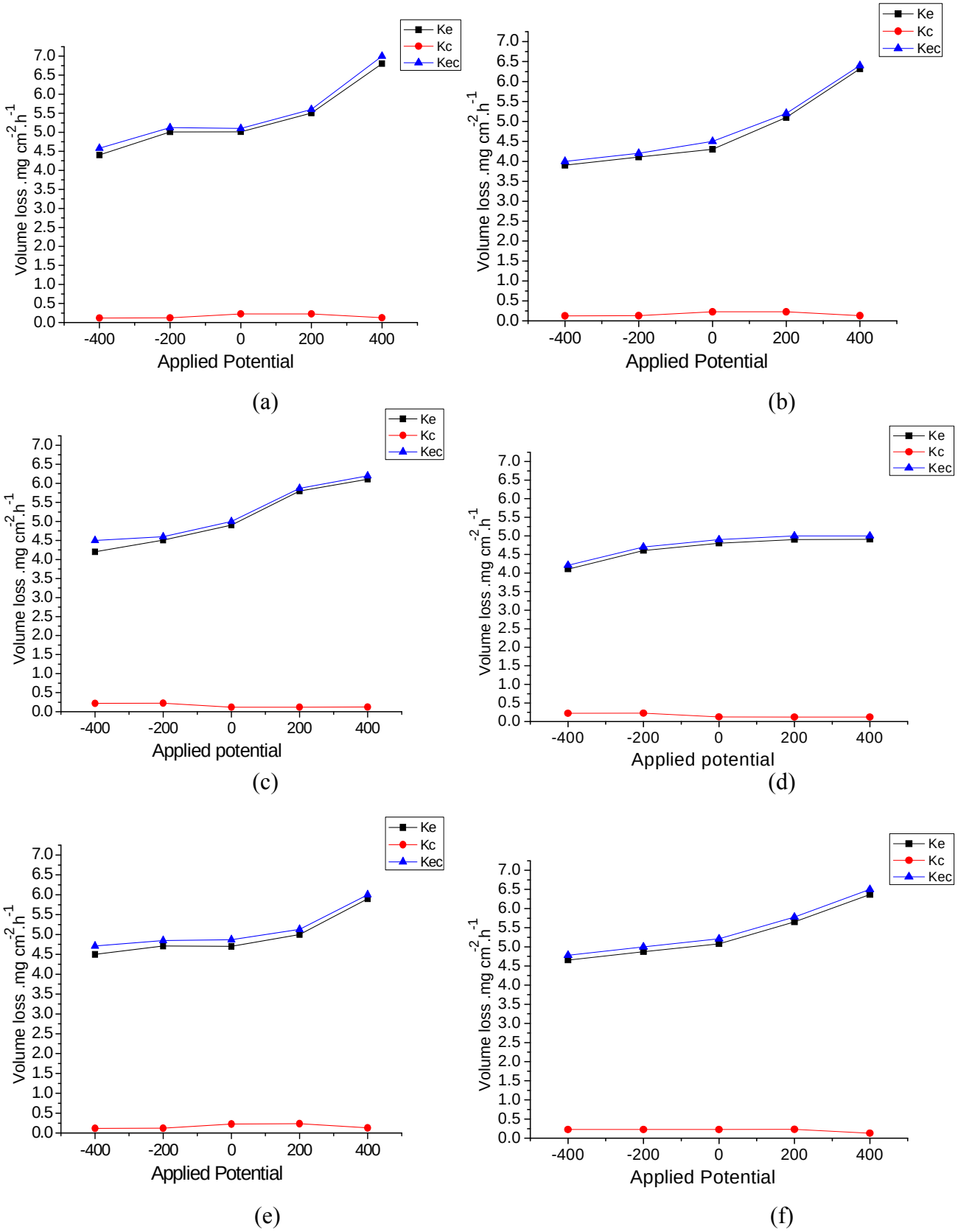

Fig.5.8: Volume loss as function of potentials for carbon steel in crude oil at 3.5 m $s^{-1}$and particle size 600-710µm (a) 15° (b) 30° (c) 45°(d) 60° (e) 75° (f) 90° .

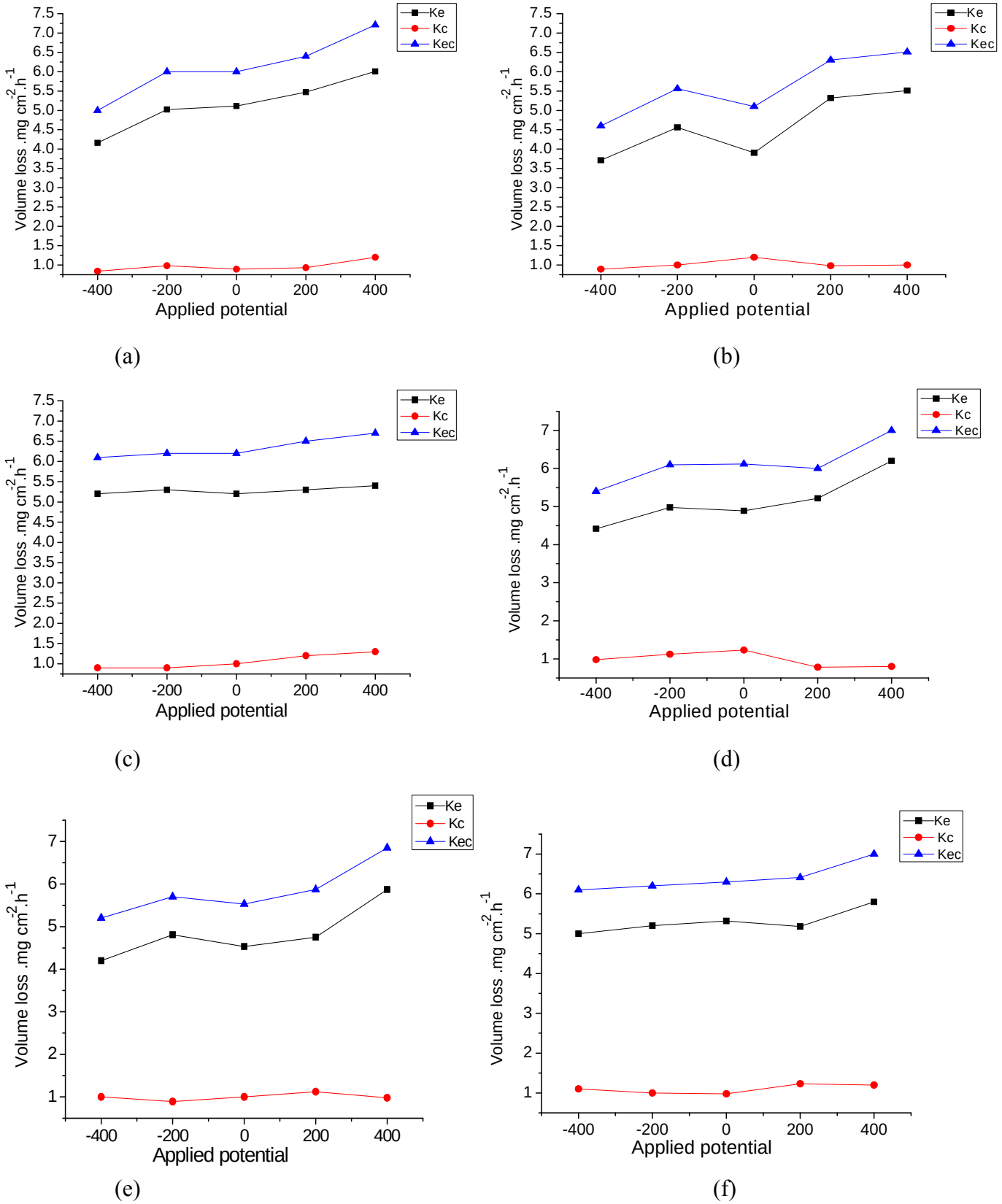

Fig.5.9: Volume loss as function of potentials for carbon steel in oil /20% water , 3.5 m $s^{-1}$and particle size 600-710µm (a) 15° (b) 30° (c) 45°(d) 60° (e) 75° (f) 90°.

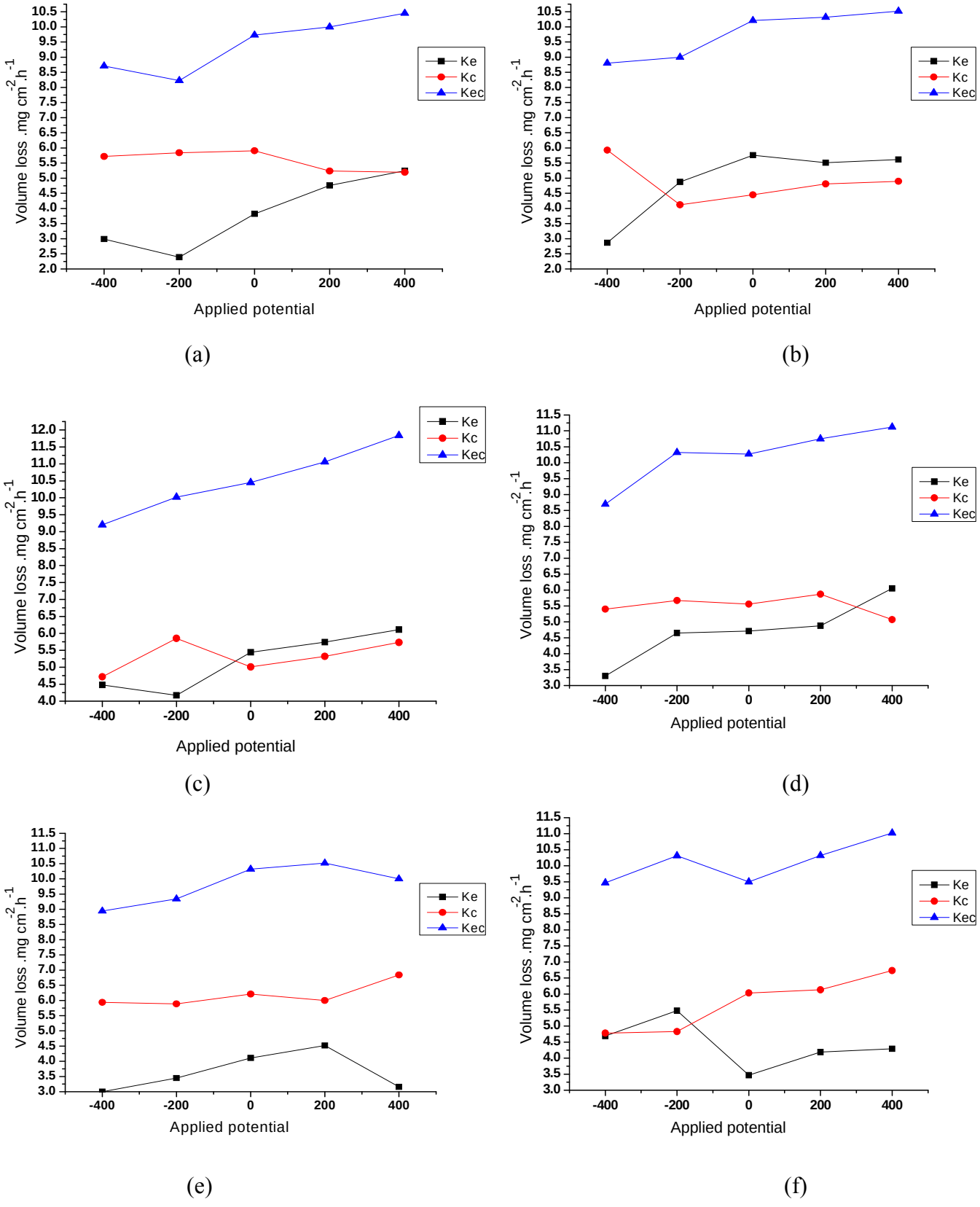

Fig.5.10: Volume loss as function of potentials for carbon steel in water at 4.5 m $s^{-1}$and particle size 600-710µm (a) 15° (b) 30° (c) 45°(d) 60° (e) 75° (f) 90° .

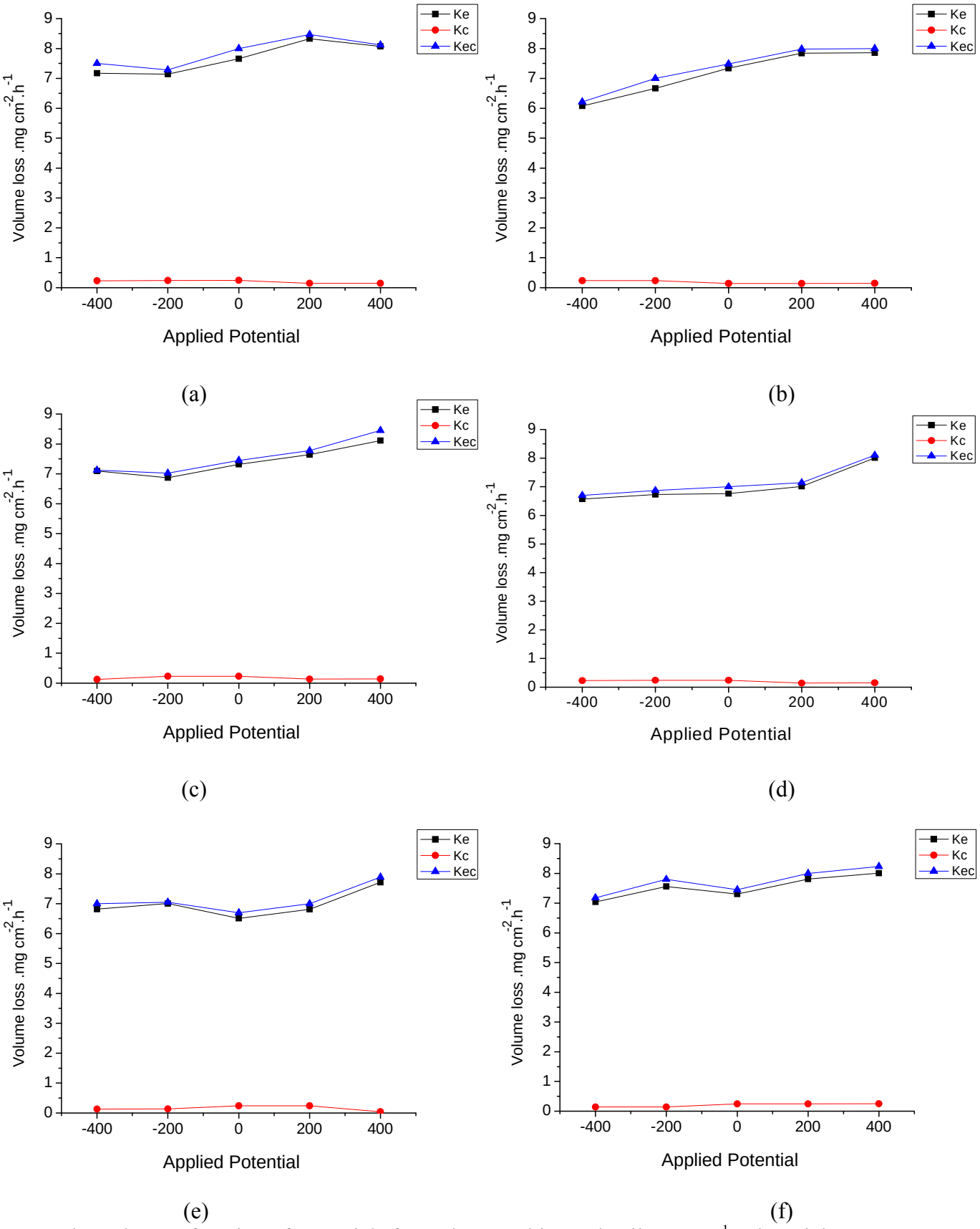

Fig.5.11: Volume loss as function of potentials for carbon steel in crude oil 4.5 m $s^{-1}$and particle size 600-710µm (a) 15° (b) 30° (c) 45°(d) 60° (e) 75° (f) 90° .

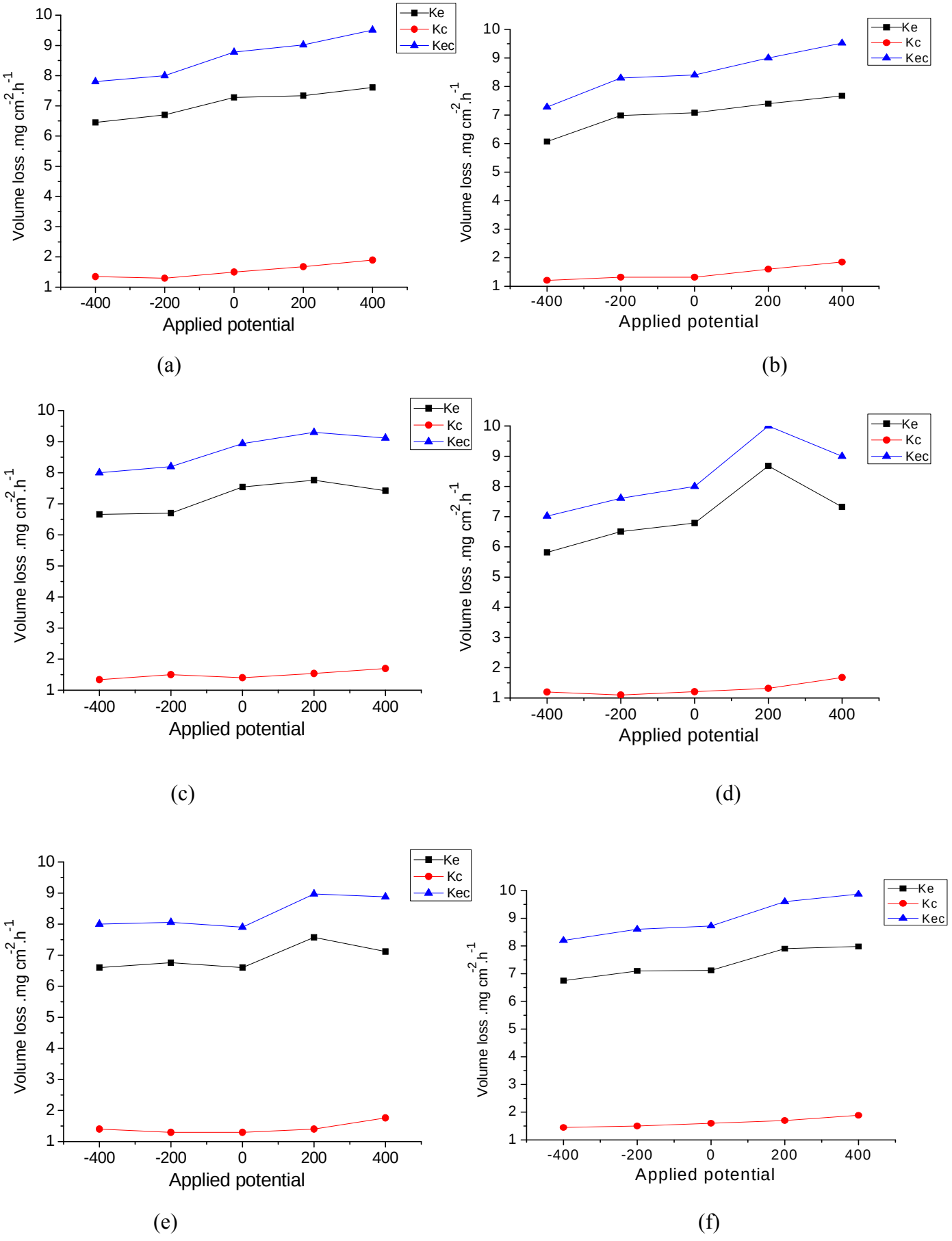

Fig.5.12: Volume loss as function of potentials for carbon steel in oil /20% water 4.5 m $s^{-1}$and particle size 600-710µm (a) 15° (b) 30° (c) 45°(d) 60° (e) 75° (f) 90° .

5.2. Effect of applied potential, impact velocity for particle size 150-30µm on erosion-corrosion maps

5.2.1. Conditions of the test

The dimensions of the specimens were 25mm× 10mm × 4 mm in the three environments containing particles sized 150-300µm. The area exposed to the impingement jet was 0.19cm^2, whilst the remaining area was covered by a coating in order to ensure that all corrosion measurements related to the erosion-corrosion process only. The tests were carried out at three potentials -400, 0 and 400mV, and three velocities, 2.5, 3.5 and 4.5 m s^{-1}, for 30 minutes at three impact angles, 15°, 45° and 90°.

5.2.2. Polarization curves for particle size 150-30µm

5.2.2.1. At impact angles of 15°, 90° and velocity 2.5 m s^{-1}

For carbon steel in the water environment containing particles sized 150-300µm at constant impact angle of 15° and impact velocity of 2.5 m s^{-1} Fig. 5.13(a) , it is interesting to see that the current density was increased with a decrease in particle size from 600-710µm to 150-300µm. In the crude oil environment containing particles sized 150-300µm Fig. 5.13(a), the current density was increase compared to that observed in the crude oil environment containing large particles sized 600-710µm, was 0.065 m A c m^{-2} at an impact angle of 15°, and an impact velocity of 2.5 m s^{-1}. In 20% water with crude oil at an impact angle of 15° and an impact velocity of 2.5 m s^{-1} (Fig. 5.13(a)), there was an increased in the corrosion current density compared with in the crude oil containing particles sized 150-300µm, was 0.25 m A c m^{-2}.

At an impact angle of 90° and an impact velocity of 2.5 m s^{-1} for carbon steel in the water environment containing particles sized 150-300µm Fig. 5.13(b), it is clear that the current density was quite dissimilar to current density at the previous impact angle of 15° was 0.79 mA cm^{-2}. In the crude oil environment containing particles sized 150-300µm (Fig. 5.13(b)) at constant impact angle of 90° and an impact velocity of 2.5 m s^{-1}, the corrosion current density was approximately 0.081 m A cm^{-2}. It can be seen that the value of the corrosion contribution remained small compared with that in the water and crude oil/20%water environment containing particles sized 150-300µm.

5.2.2.2. At impact angles of 15°, 90° and velocity 3.5 m s^{-1}

For carbon steel in the water environment containing particles sized 150-300µm (Fig. 5.14(a) and (b) at impact angles 15° , 90° and at an impact velocity of 3.5 m s^{-1}, it can be observed that the corrosion potential (Ecorr) was lesser compared with in crude oil environment containing particles sized 150-300µm. The current density for carbon steel in water environment at impact velocity of 3.5 m s^{-1} was greater than at impact velocity of 2.5 m s^{-1}. This is consistent with the findings of some other research, which found that an increase in velocity indicates an increase in corrosion value [20, 34 and 36].

For carbon steel in the crude oil environment at impacts angle 15°, 90° and at an impact velocity of 3.5 m s^{-1}Fig. 5.14(a) and (b), the corrosion contribution was very small compared to the corrosion contribution (Kc) in the water environment. However, in oil /20% water containing particles sized 150-300µm at impact angles 15, 90° and at an impact velocity of 3.5 m s^{-1} Fig. 5.14(a) and (b) , there was a small increase in the corrosion current density compared with water environment.

5.2.2.4. At impact angles of 15°, 90° and velocity 4.5 m s^{-1}

The value of current density in water environment was increased with an increase in impact angles and velocities Figs 5.15 (a) and (b). The value of current density of two impact angles 15°, 90° was 1.1 and 1.4 m A cm^{-2}. For carbon steel in the crude oil environment at impact angles 15°, 90° and at an impact velocity of 4.5ms^{-1} Fig. 5.15(a) and (b), the current was similar to all previous impact velocities and impact angles. In oil/20% water environment at impact angles of 15°, 90° and an impact velocity of 4.5ms^{-1} Fig. 5.15(a) and (b),it can be noticed that the current density was increased with an increase in impact velocity and decrease in particle size from 600-710µm to150-300µm.

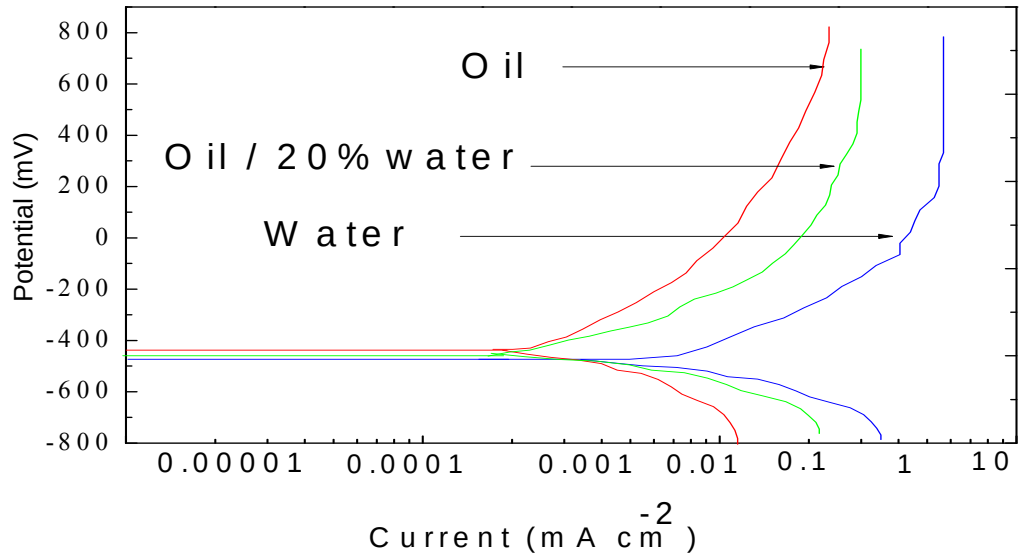

(a)

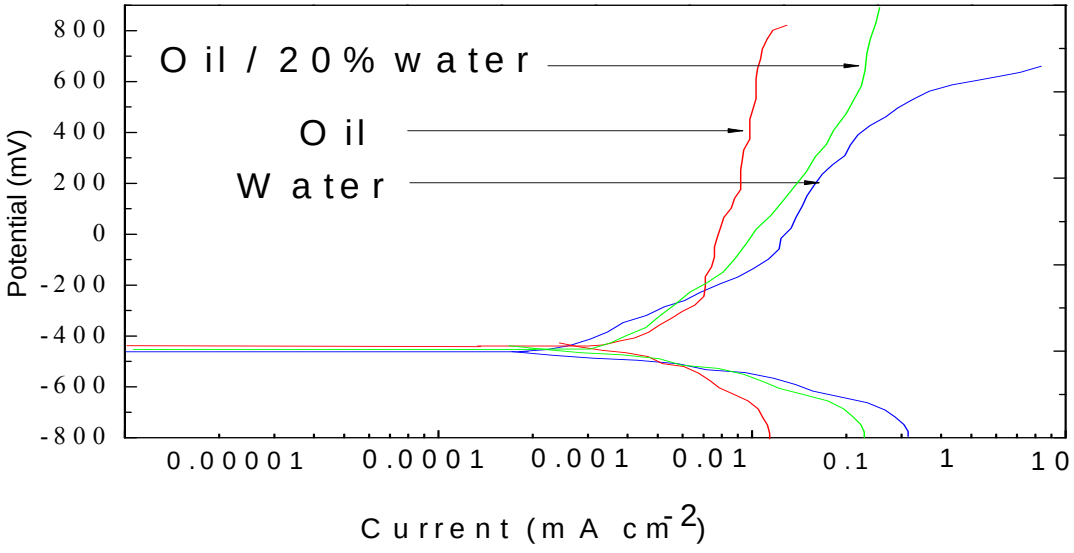

(b)

Fig.5.13: Polarization curves for carbon steel in three environments contain particle size 150-300µm and at 2.5 m s^{-1}: (a) 15° (b) 90°

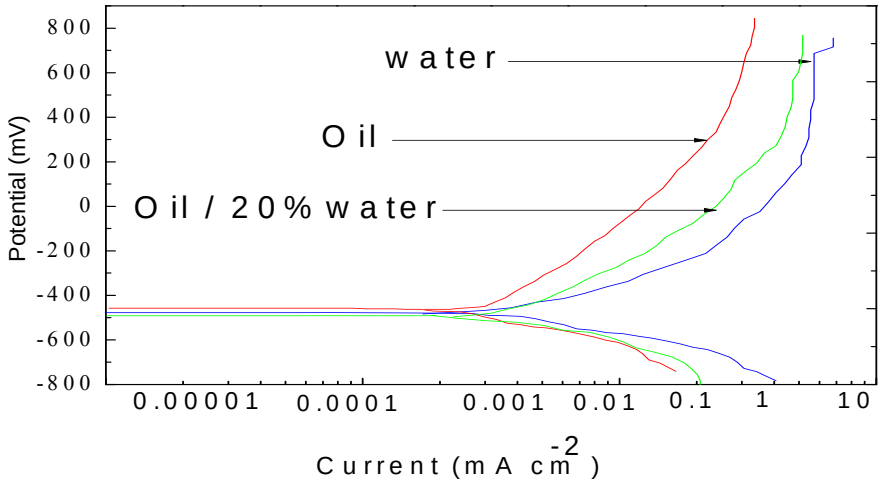

(a)

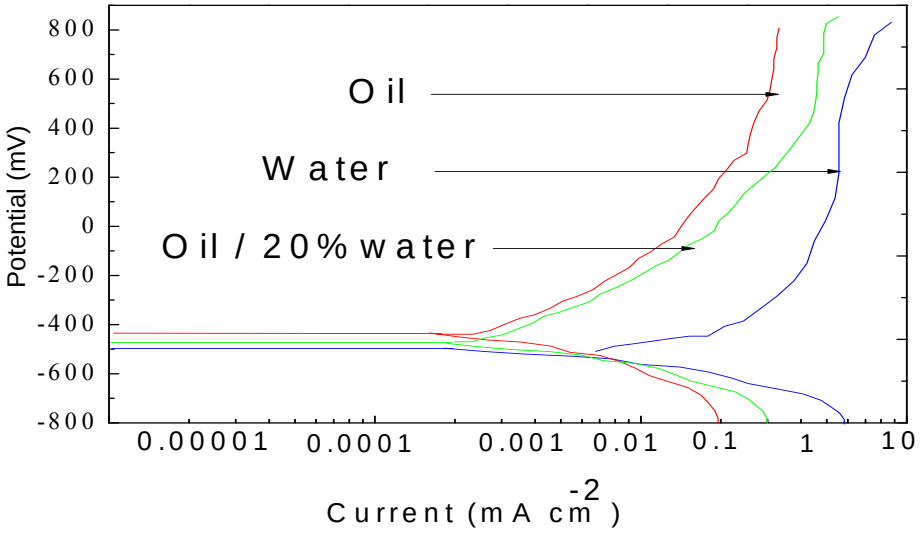

(b)

Fig.5.14: Polarization curves for carbon steel in three environments contain particle size 150-300µm and at 3.5 m s^{-1}: (a) 15° (b) 90°

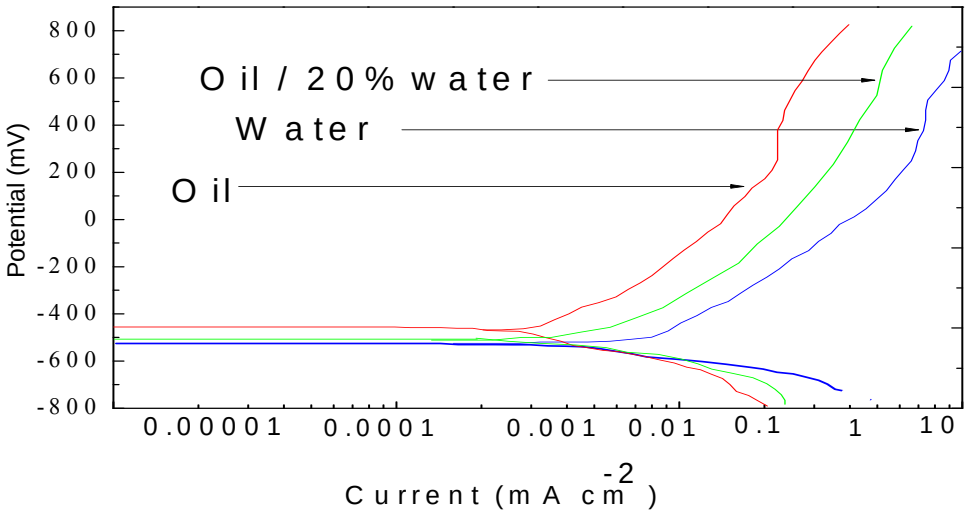

(a)

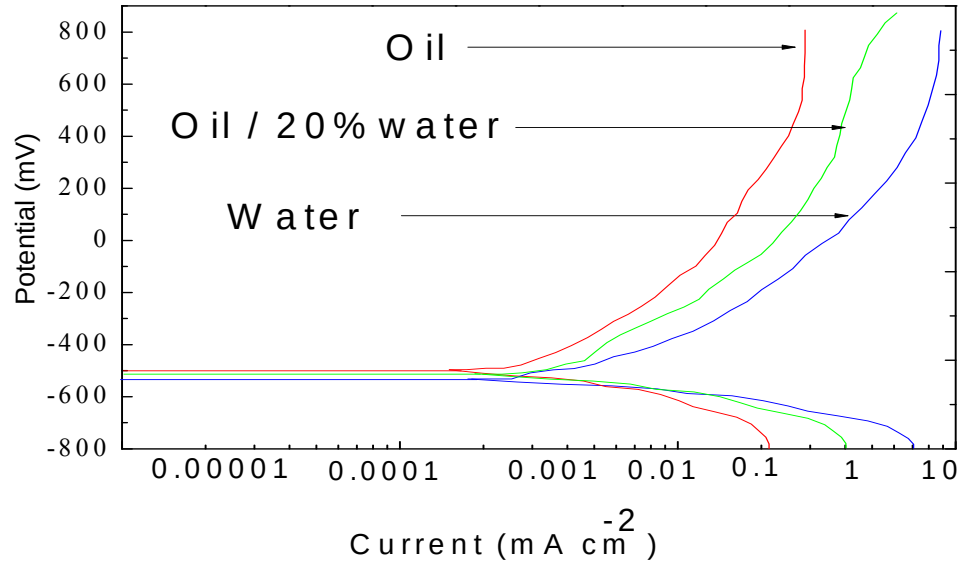

(b)

Fig.5.15: Polarization curves for carbon steel in three environments contain particle size 150-300µm and at 4.5 m s^{-1}: (a) 15° (b) 90°

5.2.3. Volume loss for particle sizes 150-300µm

The volume losses of carbon steel in the three environments containing particles sized 150-300µm demonstrate that when the particle size was changed from a large particle size (600-710µm) to a small particle size (150-300µm), the total volume losses decreased in the three environments. However, the value of the corrosion contribution (Kc) was increased for carbon steel in the reservoir water environment, being the highest, while the value of the corrosion contribution (Kc) in crude oil was less than in the mixed environments contain particle sizes 150-300µmFigs5.16-24. Tables 5.19-5.27: show the results of the calculations of volume loss for Ke, Kc and Kec for difference environments contain particle sizes 150-300µm.

5.2.3.1. Mass loss in water reservoir

For carbon steel in the water environment containing particles sized 150-300µm and at an impact velocity of 2.5 m s^{-1}, Fig. 5.16, it is clear that the total mass loss (Kec) and erosion (Ke) were decreased compared with the value of mass loss of carbon steel in water containing particles sized 600-710µm. However, the value of corrosion (Kc) with a small particle size 150-300µm was increased compared with the value of corrosion (Kc) of carbon steel in water containing particles sized 600-710µm (Fig. 5.4-12). The peak value of erosion-corrosion at an impact velocity of 2.5 m s^{-1} was 5.41mg cm^{-2} h^{-1} at constant impact angle of 45° and at a high potential of 400mV Fig.5.16 (b). The greatest value of erosion was 1.59 mg cm^{-2} h^{-1} at an impact angle of 45° at the low potential of -400mV Fig.5.16 (b), while the lowest value of erosion was 0.46 mg cm^{-2} h^{-1} at potential of 0 mV and at an impact angle of 90° Fig.5.16 (c).

The total mass loss (Kec) was generally increased with decrease in impact angle from 90° to 45° and the peak value of mass loss was 7 mg cm^{-2} h^{-1} at an applied potential of 400 mV and at an impact angle of 45° Fig. 5.19(b). Moreover, the percentage of corrosion (Kc) was greater than the percentage of erosion (Ke) at the majority of test conditions.

With an increase in velocity from 3.5 to 4.5 m s^{-1}, the peak value of erosion-corrosion was 8.78 mg cm^{-2} h^{-1} at constant impact angle of 45° and potential of 400mV Fig.5.22-(b). The peak value of corrosion was 7 mg cm^{-2} h^{-1} at an impact angle of 90° and a potential of 400mV Fig. 5.22(c), and the highest value of erosion was smaller than the percentage of corrosion was an approximately 2.48 mg cm^{-2} h^{-1} at constant impact angle of 45° and a potential of 400mV Fig. 5.22(b).

5.2.3.2. Mass loss in crude oil environment

For carbon steel in the crude oil environment containing particles sized 150-300µm at an impact velocity of 2.5 m s^{-1} Fig. 5.17, there was small increase in the corrosion (Kc) compared with that observed for the large particles sized 600-710µm Fig.5.5-11. However, in the crude oil environment containing particles sized 150-300µm at an impact velocity of 2.5 m s^{-1}, the values of corrosion (Kc) were very low compared to the values of erosion (Ke) Fig. 5.17.

At an impact velocity of 3.5 m s^{-1} in crude oil environment containing particles sized 150-300µm Fig. 5.20, the total volume loss (Kec) was increased compared with at the previous impact velocity of 2.5 m s^{-1}. Moreover, the values of erosion were increased. On the other hand, the value of corrosion saw a small increase compared to the value of erosion. The highest volume of total volume loss rate (kec) was 4 mg cm^{-2} h^{-1} at an impact angle of 45°and at applied potential 400mV, as shown in Fig. 5.20(b).

The total volume loss rate (Kec) was at its highest value at an impact velocity of 4.5 m s^{-1}. In addition, the values of erosion increased with an increase in impact angle from 15° to 45° and the peak value of erosion was recorded as 2.53 mg cm^{-2} h^{-1} at constant impact angle of 15° and an applied potential of 400mV Fig. 5.23(a).

5.2.3.3. Mass loss in oil/ 20% water

In the 20% water with crude oil environment containing particles sized 150-300µm at an impact velocity of 2.5 m s^{-1} Fig. 5.18-24, it is clear that the total volume loss rate (Kec) was generally decreased with a decrease in particle size from 600-710µm to150-300µm. It is interesting to see from Fig. 5.18(a-c) that there was crossover between Ke and Kc at potentials -400mV. Then the values of corrosion contribution became higher than the values of erosion contribution at all potentials at an impact velocitiesof 2.5- 4.5 m s^{-1} Fig. 5.18-24.

Tables.5.19: Volume loss as function of potentials for carbon steel in water at 2.5 m s^{-1} and particle size 150-300µm (a) 15° (b) 45° (c) 90°

(a)

Applied potential mV	Ke(mg cm^{-2} h^{-1})	Kc(mg cm^{-2} h^{-1})	Kec(mg cm^{-2} h^{-1})
-400	1.5	2.5	4
0	0.47	3.74	4.21
400	0.46	3.84	4.3

(b)

Applied potential mV	Ke(mg cm^{-2} h^{-1})	Kc(mg cm^{-2} h^{-1})	Kec(mg cm^{-2} h^{-1})
-400	1.6	2.6	4.19
0	0.7	3.8	4.5
400	1.51	3.9	5.41

(c)

Applied potential mV	Ke(mg cm^{-2} h^{-1})	Kc(mg cm^{-2} h^{-1})	Kec(mg cm^{-2} h^{-1})
-400	1.14	2.4	3.54
0	0.46	3.84	4.3
400	0.5	3.9	4.4

Tables.5.20: Volume loss as function of potentials for carbon steel in water at 3.5 m s^{-1} and particle size 150-300µm (a) 15° (b) 45° (c) 90°

(a)

Applied potential mV	Ke(mg cm^{-2} h^{-1})	Kc(mg cm^{-2} h^{-1})	Kec(mg cm^{-2} h^{-1})
-400	1.22	3.98	5.2
0	1.5	4	5.5
400	2	4.2	6.2

(b)

Applied potential mV	Ke(mg cm^{-2} h^{-1})	Kc(mg cm^{-2} h^{-1})	Kec(mg cm^{-2} h^{-1})
-400	1.51	4.2	5.71
0	1.05	5	6.05
400	2	5	7

(c)

Applied potential mV	Ke(mg cm^{-2} h^{-1})	Kc(mg cm^{-2} h^{-1})	Kec(mg cm^{-2} h^{-1})
-400	1.1	4.5	5.6
0	0.6	4.81	5.41
400	0.6	5.4	6

Tables.5.21: Volume loss as function of potentials for carbon steel in water at 4.5 m s^{-1} and particle size 150-300µm (a) 15° (b) 45° (c) 90°

(a)

Applied potential mV	Ke(mg cm^{-2} h^{-1})	Kc(mg cm^{-2} h^{-1})	Kec(mg cm^{-2} h^{-1})
-400	2	5.5	7.5
0	1.01	6.2	7.21
400	0.95	6.5	7.45

(b)

Applied potential mV	Ke(mg cm^{-2} h^{-1})	Kc(mg cm^{-2} h^{-1})	Kec(mg cm^{-2} h^{-1})
-400	2.3	5.5	7.8
0	2.11	5.89	8
400	2.48	6.3	8.78

(c)

Applied potential mV	Ke(mg cm^{-2} h^{-1})	Kc(mg cm^{-2} h^{-1})	Kec(mg cm^{-2} h^{-1})
-400	1.6	5.7	7.3
0	0.65	6.4	7.05
400	1	7	8

Tables.5.22: Volume loss as function of potentials for carbon steel in crude oil at 2.5 m s^{-1} and particle size 150-300µm (a) 15° (b) 45° (c) 90°

(a)

Applied potential mV	Ke(mg cm^{-2} h^{-1})	Kc(mg cm^{-2} h^{-1})	Kec(mg cm^{-2} h^{-1})
-400	1.43	3.21E-01	1.75
0	1.46	3.95E-01	1.85
400	1.56	4.24E-01	1.98

(b)

Applied potential mV	Ke(mg cm^{-2} h^{-1})	Kc(mg cm^{-2} h^{-1})	Kec(mg cm^{-2} h^{-1})
-400	1.66	3.42E-01	2
0	1.77	3.40E-01	2.11
400	1.95	3.57E-01	2.304

(c)

Applied potential mV	Ke(mg cm^{-2} h^{-1})	Kc(mg cm^{-2} h^{-1})	Kec(mg cm^{-2} h^{-1})
-400	1.1	5.91E-01	1.65
0	1.44	4.10E-01	1.85
400	1.73	4.70E-01	2.2

Tables.5.23: Volume loss as function of potentials for carbon steel in crude oil at 3.5 m s^{-1} and particle size 150-300µm (a) 15° (b) 45° (c) 90°

(a)

Applied potential mV	Ke(mg cm^{-2} h^{-1})	Kc(mg cm^{-2} h^{-1})	Kec(mg cm^{-2} h^{-1})
-400	3.05	4.00E-01	3.45
0m	3.22	5.32E-01	3.75
400	3.23	6.12E-01	3.84

(b)

Applied potential mV	Ke(mg cm^{-2} h^{-1})	Kc(mg cm^{-2} h^{-1})	Kec(mg cm^{-2} h^{-1})
-400	3.4	5.00E-01	3.9
0	3.41	4.40E-01	3.85
400	3.43	5.70E-01	4

(c)

Applied potential mV	Ke(mg cm^{-2} h^{-1})	Kc(mg cm^{-2} h^{-1})	Kec(mg cm^{-2} h^{-1})
-400	2.71	5.41E-01	3.25
0	2.9	6.00E-01	3.5
400	3.17	6.30E-01	3.8

Tables.5.24: Volume loss as function of potentials for carbon steel in crude oil at 4.5 m s^{-1} and particle size 150-300µm (a) 15° (b) 45° (c) 90°

(a)

Applied potential mV	Ke(mg cm^{-2} h^{-1})	Kc(mg cm^{-2} h^{-1})	Kec(mg cm^{-2} h^{-1})
-400	4.25	7.50E-01	5
0	4.65	8.53E-01	5.5
400	4.55	9.00E-01	5.45

(b)

Applied potential mV	Ke(mg cm^{-2} h^{-1})	Kc(mg cm^{-2} h^{-1})	Kec(mg cm^{-2} h^{-1})
-400	4.62	8.00E-01	5.42
0	4.86	8.91E-01	5.75
400	4.9	1.00E+00	5.9

(c)

Applied potential mV	Ke(mg cm^{-2} h^{-1})	Kc(mg cm^{-2} h^{-1})	Kec(mg cm^{-2} h^{-1})
-400	3.83	8.23E-01	4.65
0	4.33	8.68E-01	5.2
400	4.2	1.20E+00	5.4

Tables.5.25: Volume loss as function of potentials for carbon steel in oil /20% water at 2.5 m s^{-1} and particle size 150-300µm (a) 15° (b) 45° (c) 90°

(a)

Applied potential mV	Ke(mg cm^{-2} h^{-1})	Kc(mg cm^{-2} h^{-1})	Kec(mg cm^{-2} h^{-1})
-400	1.19	1.11E+00	2.3
0	1.09	1.51E+00	2.6
400	0.98	1.77E+00	2.75

(b)

Applied potential mV	Ke(mg cm^{-2} h^{-1})	Kc(mg cm^{-2} h^{-1})	Kec(mg cm^{-2} h^{-1})
-400	1.29	1.21E+00	2.5
0	0.95	1.75E+00	2.7
400	1.55	1.85E+00	3.4

(c)

Applied potential mV	Ke(mg cm^{-2} h^{-1})	Kc(mg cm^{-2} h^{-1})	Kec(mg cm^{-2} h^{-1})
-400	1.4	1.03E+00	2.43
0	0.85	1.65E+00	2.5
400	0.82	1.83E+00	2.65

Tables.5.26: Volume loss as function of potentials for carbon steel in oil /20% water at 3.5 m s^{-1} and particle size 150-300µm (a) 15° (b) 45° (c) 90°

(a)

Applied potential mV	Ke(mg cm^{-2} h^{-1})	Kc(mg cm^{-2} h^{-1})	Kec(mg cm^{-2} h^{-1})
-400	1.55	2.46E+00	4
0	1.33	2.97E+00	4.3
400	1.73	3.02E+00	4.75

(b)

Applied potential mV	Ke(mg cm^{-2} h^{-1})	Kc(mg cm^{-2} h^{-1})	Kec(mg cm^{-2} h^{-1})
-400	1.26	2.95E+00	4.21
0	1.46	3.00E+00	4.46
400	1.48	3.32E+00	4.8

(c)

Applied potential mV	Ke(mg cm^{-2} h^{-1})	Kc(mg cm^{-2} h^{-1})	Kec(mg cm^{-2} h^{-1})
-400	1.73	2.26E+00	3.98
0	1.15	2.85E+00	4
400	1.57	2.94E+00	4.51

Tables.5.27: Volume loss as function of potentials for carbon steel in oil /20% water 4.5 m s^{-1} and particle size 150-300µm (a) 15° (b) 45° (c) 90°

(a)

Applied potential mV	Ke(mg cm^{-2} h^{-1})	Kc(mg cm^{-2} h^{-1})	Kec(mg cm^{-2} h^{-1})
-400	2.53	3.37E+00	5.9
0	2.4	4.00E+00	6.4
400	2.42	4.23E+00	6.65

(b)

Applied potential mV	Ke(mg cm^{-2} h^{-1})	Kc(mg cm^{-2} h^{-1})	Kec(mg cm^{-2} h^{-1})
-400	2.4	3.60E+00	6
0	2.05	4.45E+00	6.5
400	2.23	4.55E+00	6.78

(c)

Applied potential mV	Ke(mg cm^{-2} h^{-1})	Kc(mg cm^{-2} h^{-1})	Kec(mg cm^{-2} h^{-1})
-400	1.98	3.52E+00	5.5
0	1.9	4.30E+00	6.2
400	2.08	4.42E+00	6.5

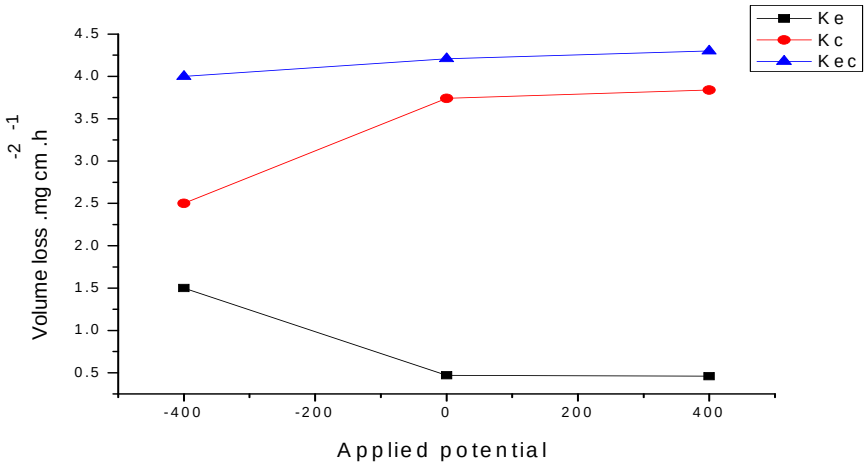

(a)

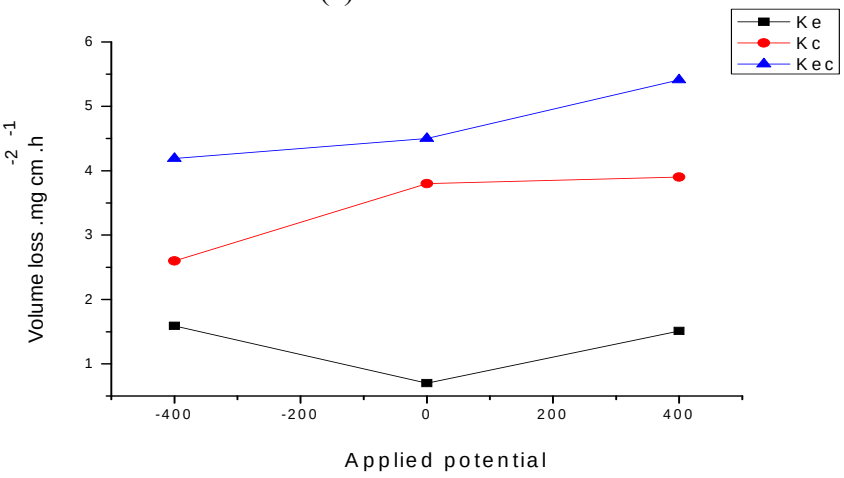

(b)

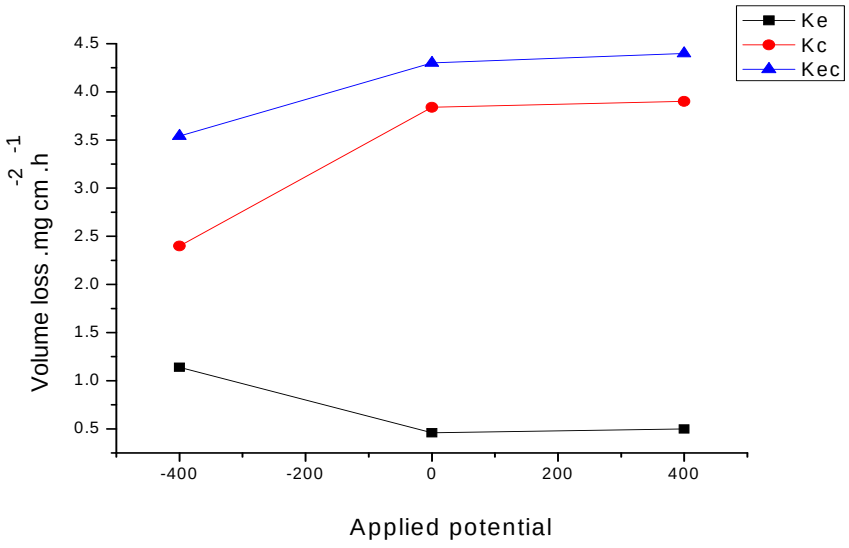

(c)

Fig.5.16: Volume loss as function of potentials for carbon steel in water at 2.5 m s^{-1} and particle size 150-300µm (a) 15° (b) 45° (c) 90°

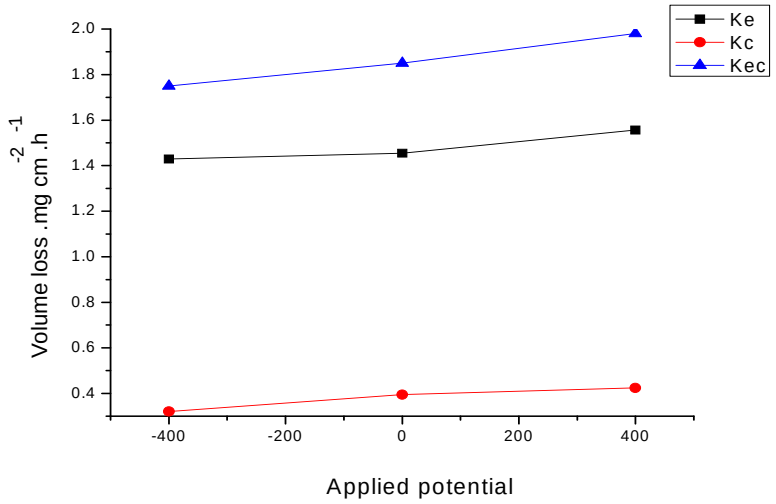

(a)

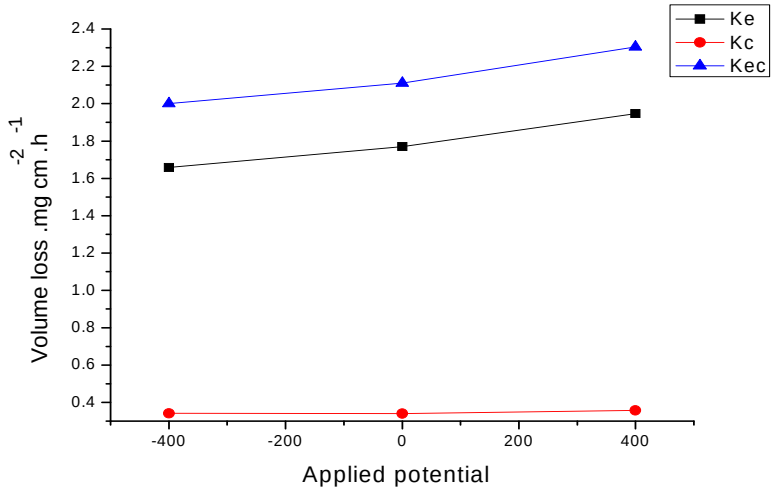

(b)

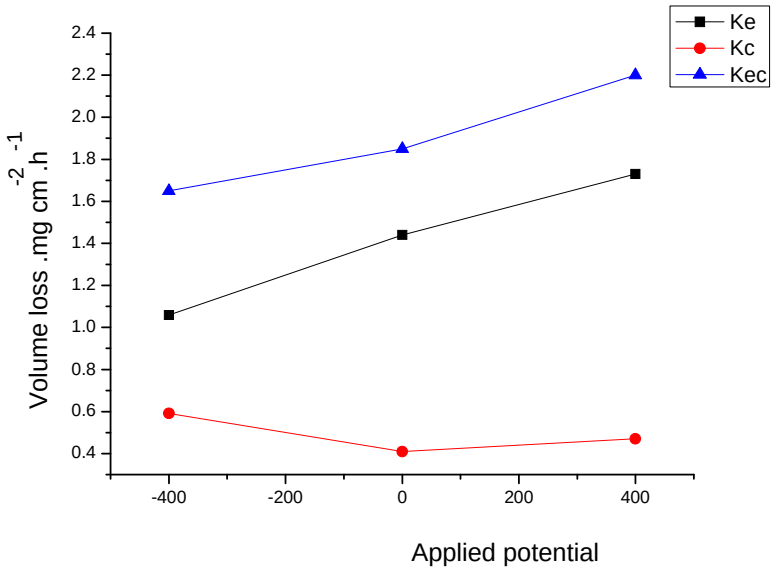

(c)

Fig.5.17: Volume loss as function of potentials for carbon steel in crude oil at 2.5 m s^{-1} and particle size 150-300µm (a) 15° (b) 45° (c) 90°.

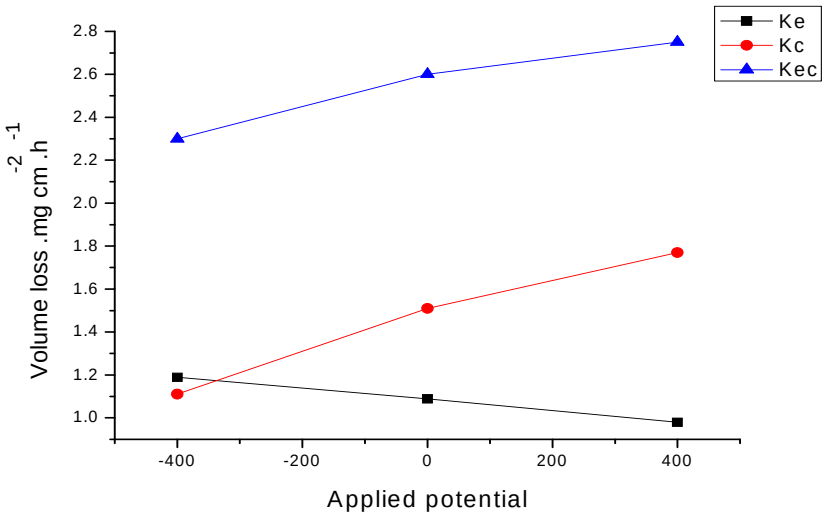

(a)

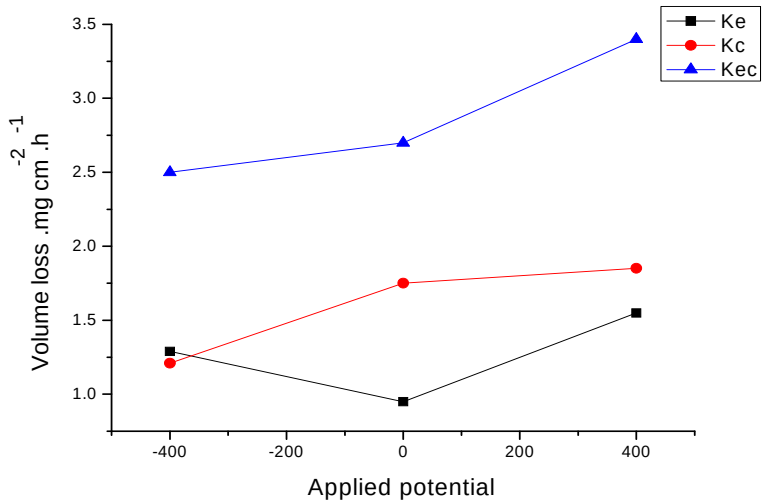

(b)

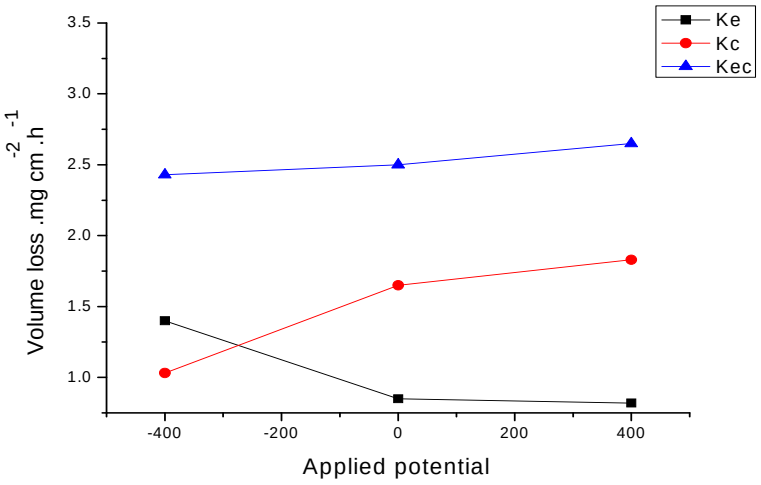

(c)

Fig.5.18: Volume loss as function of potentials for carbon steel in oil /20% water at 2.5 m s^{-1} and particle size 150-300µm (a) 15° (b) 45° (c) 90°

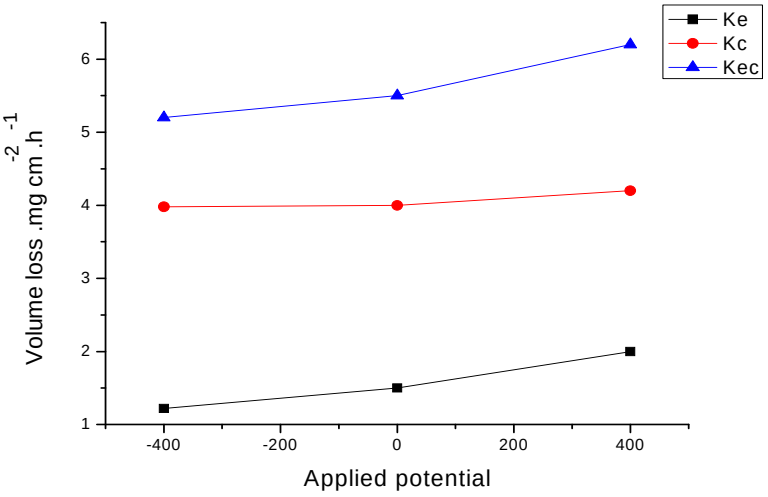

(a)

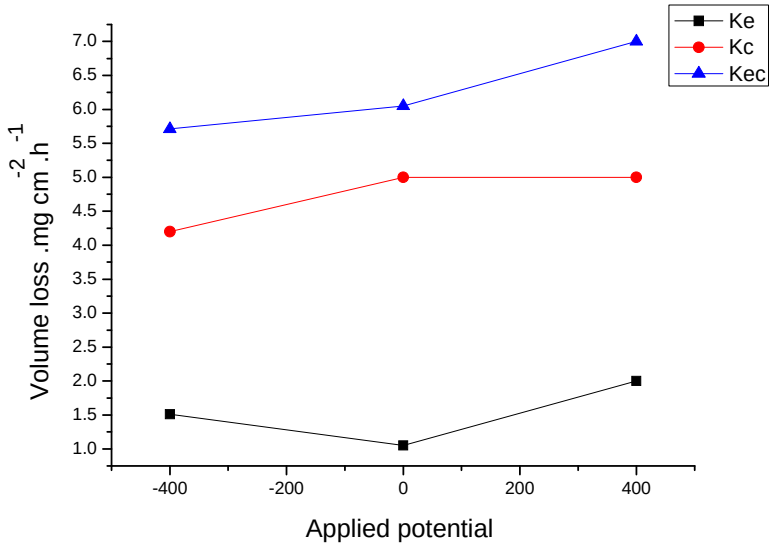

(b)

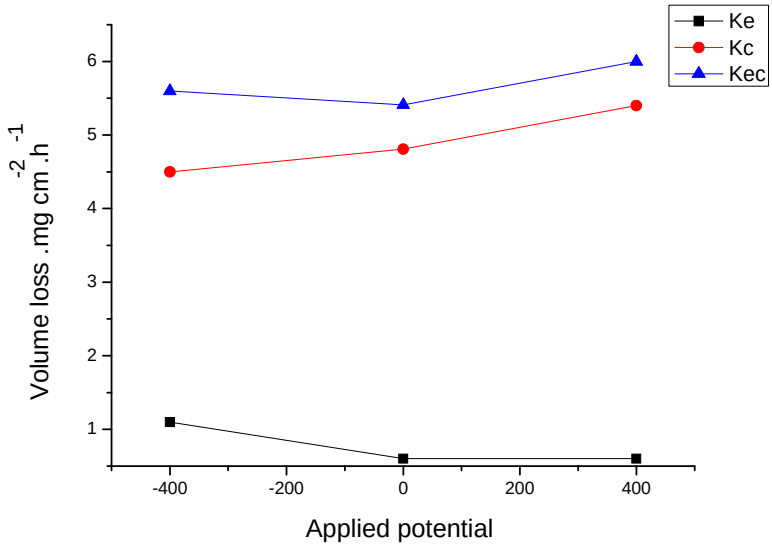

(c)

Fig.5.19: Volume loss as function of potentials for carbon steel in water at 3.5 m s^{-1} and particle size 150-300µm (a) 15° (b) 45° (c) 90° .

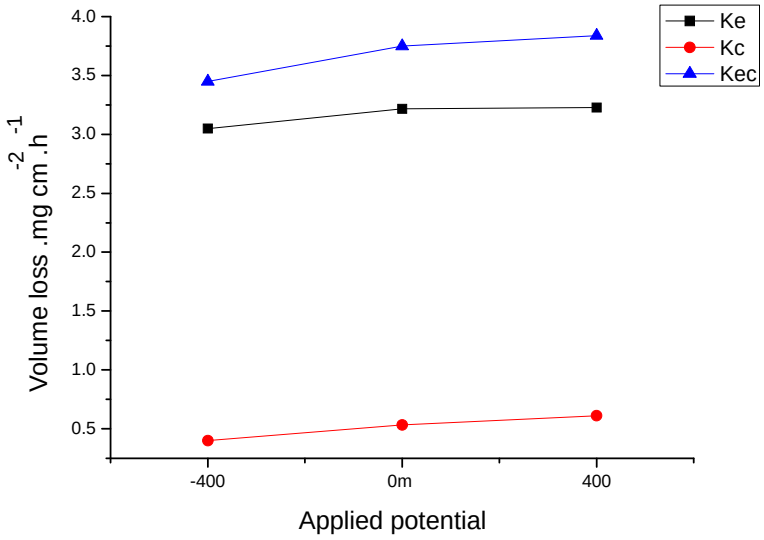

(a)

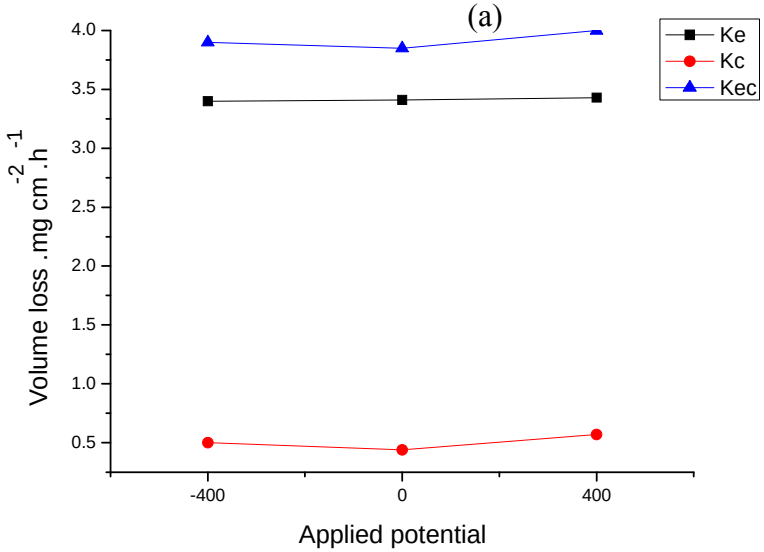

(b)

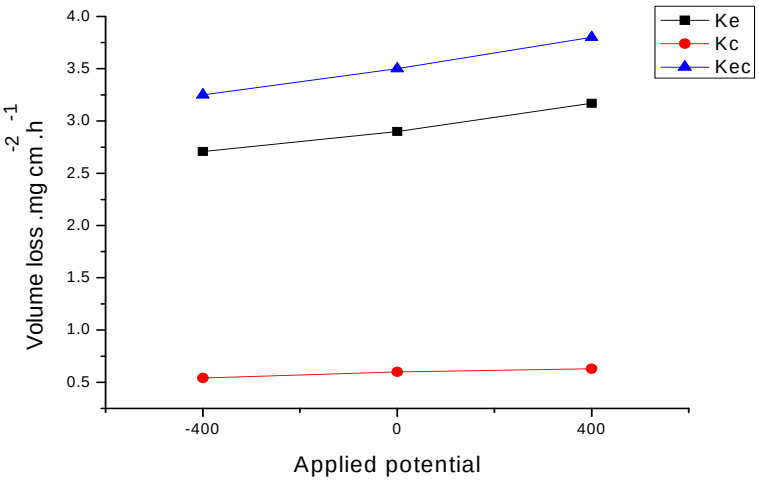

(c)

Fig.5.20: Volume loss as function of potentials for carbon steel in crude oil at 3.5 m s^{-1} and particle size 150-300µm (a) 15° (b) 45° (c) 90° .

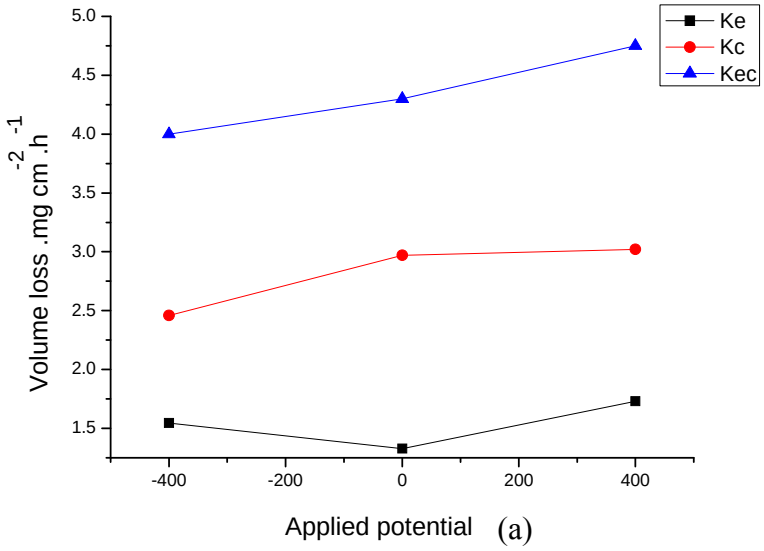

(a)

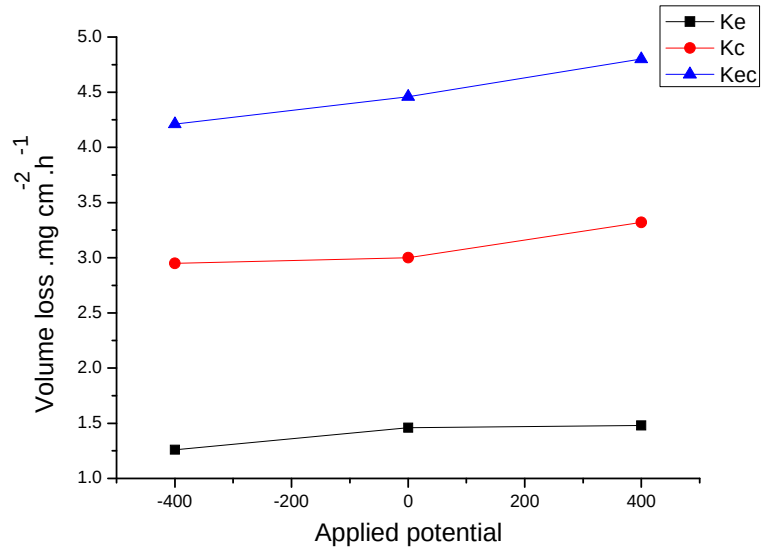

(b)

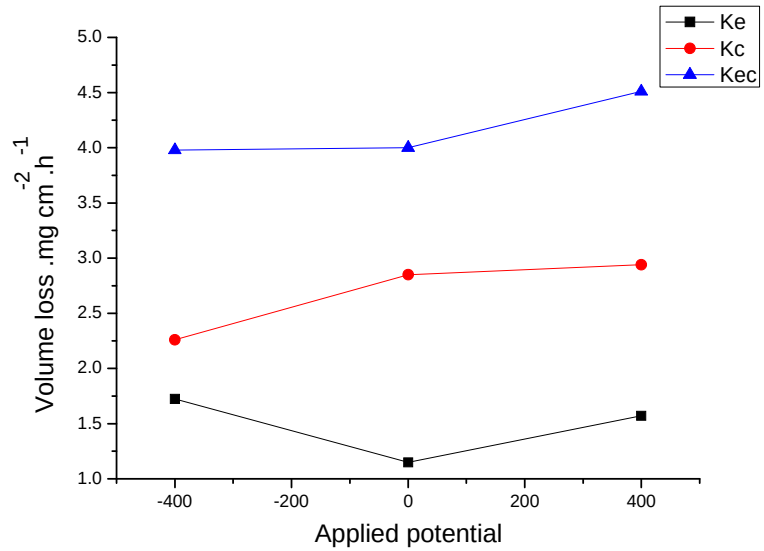

(c)

Fig.5.21: Volume loss as function of potentials for carbon steel in oil /20% water at 3.5 m s^{-1} and particle size 150-300µm (a) 15° (b) 45° (c) 90° .

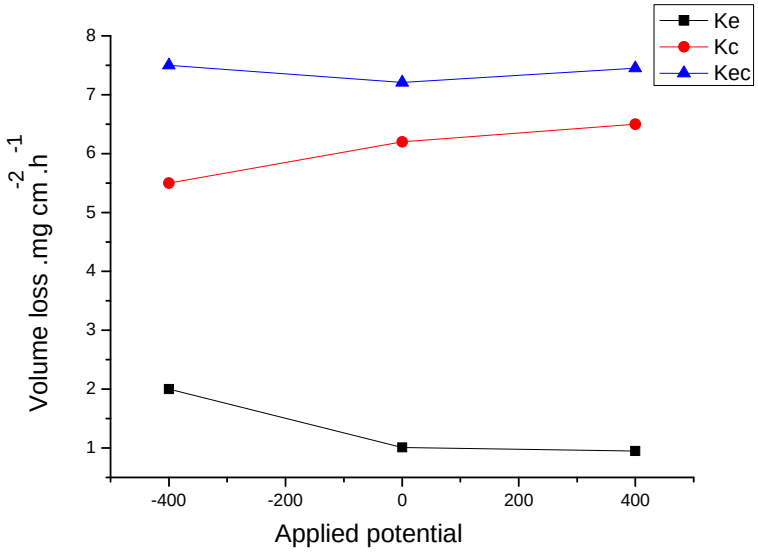

(a)

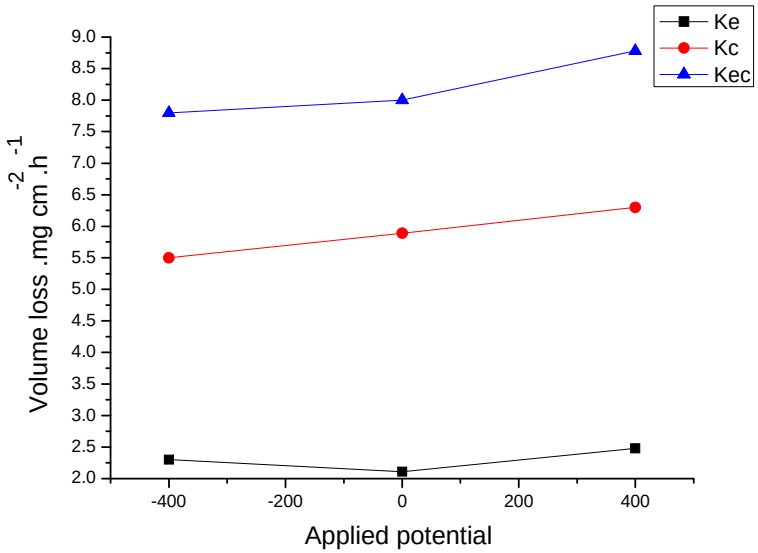

(b)

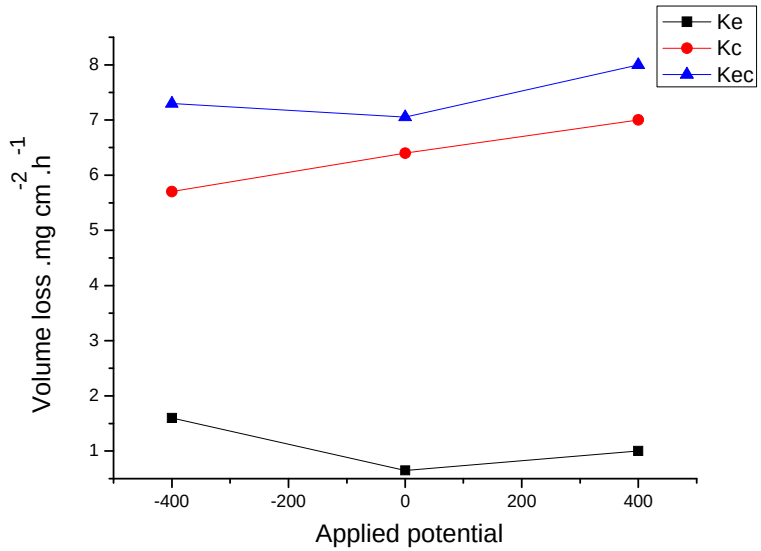

(c)

Fig.5.22: Volume loss as function of potentials for carbon steel in water at 4.5 m s^{-1} and particle size 150-300µm (a) 15° (b) 45° (c) 90° .

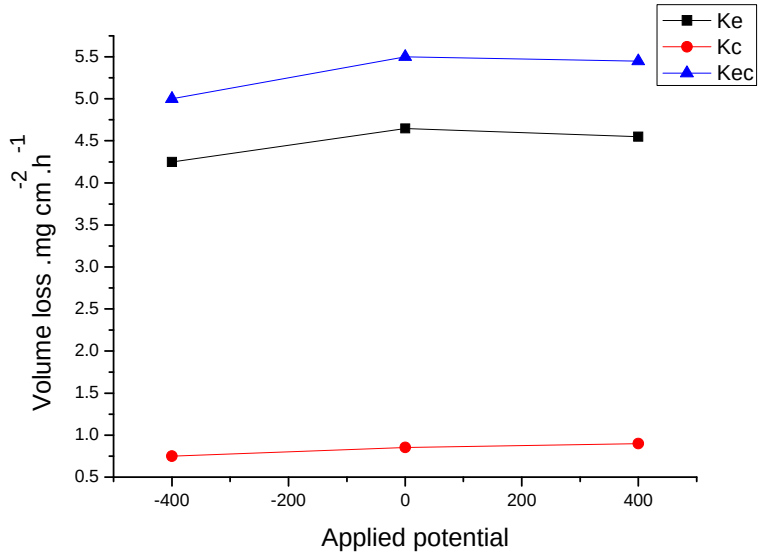

(a)

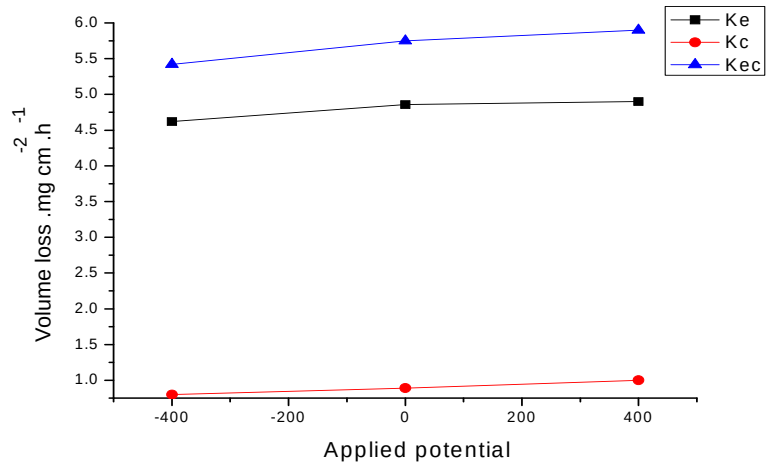

(b)

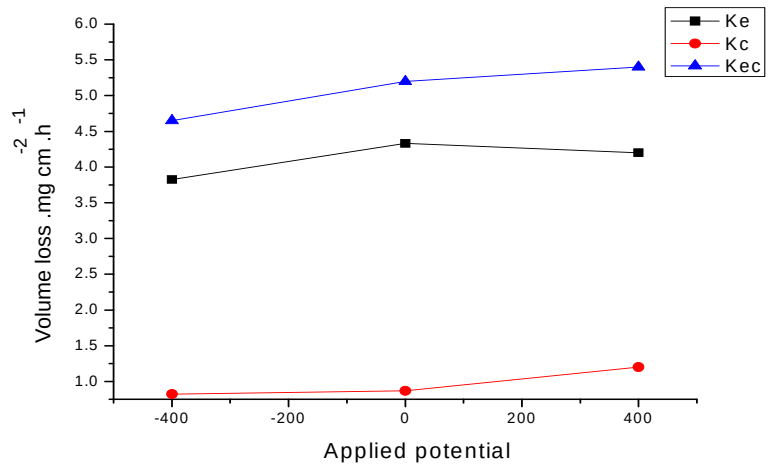

(c)

Fig.5.23: Volume loss as function of potentials for carbon steel in crude oil at 4.5 m s^{-1} and particle size 150-300µm (a) 15° (b) 45° (c) 90° .

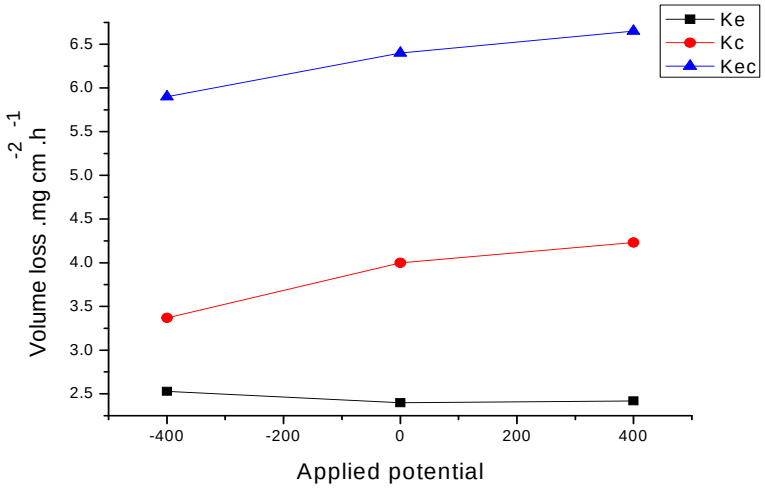

(a)

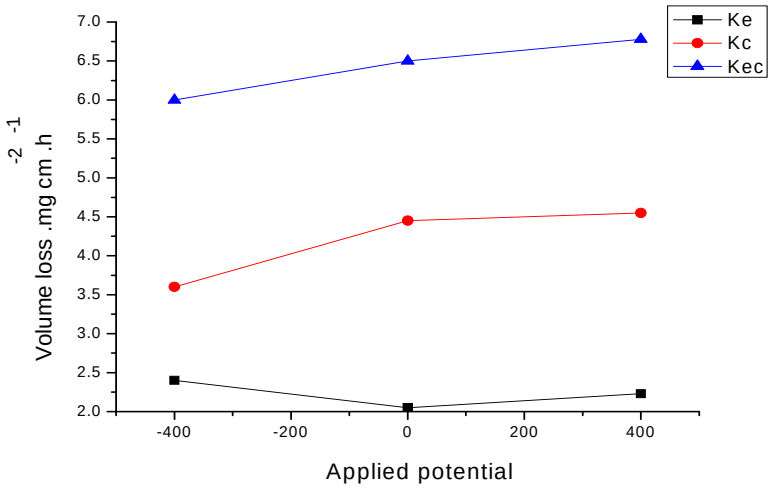

(b)

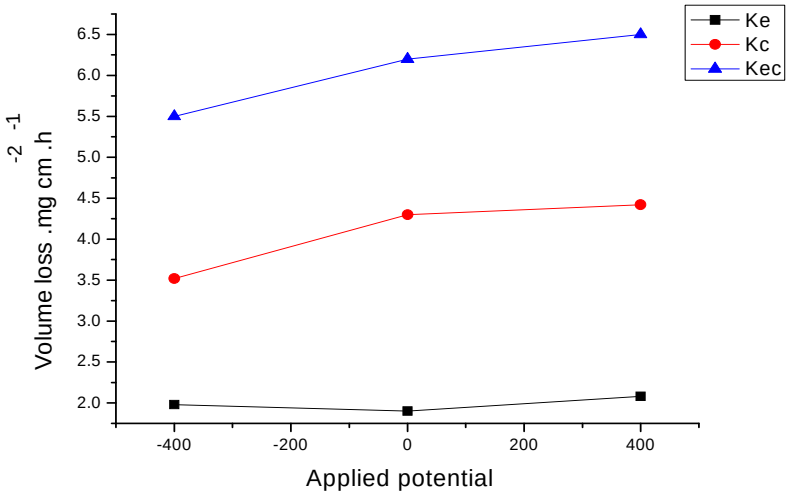

(c)

Fig.5.24: Volume loss as function of potentials for carbon steel in oil /20% water at 4.5 m s^{-1} and particle size 150-300µm (a) 15° (b) 45° (c) 90° .

5.3. Discussion

5.3.1. Polarization curves

For the carbon steel in the reservoir water containing particles sized 150-300μm and 600-710μm, the general trend is for the corrosion current densities to increase with an increase in impact velocity and impact angle from 15° to 90° (Figures 5.1-5.3 and Figures 5.13-5.15) [10]. This means that in these impact angles with increase in impact velocity decreases the corrosion resistance of the carbon steel. This could possibly be due to the effects of deformation on the surface at higher velocities leading to an increase in the exposure area (due to enhanced surface roughening) for exposure to the corrosive environment [2, 16 and 17].

For the carbon steel in the crude oil and oil/20%water environments, a similar pattern of increasing corrosion current density is observed, with an increase in impact velocity resulting in a small increase in the current densities recorded (Figures 5.1-5.3 and Figures 5.13-5.15 (a-b)). However, the extent of such increases is not as high compared to those for carbon steel in the reservoir water environment, probably due to the higher corrosion resistance in the oil.

5.3.2. Erosion-corrosion mass loss

It is interesting to see that the mass loss due to corrosion contribution (Kc) in the reservoir water and oil/20% water environments containing small particles sized 150-300µm is higher than in the reservoir water and oil/20% water environments containing large particles sized 600-710µm (tables5.1-5.18 and tables 5.19-5.27). As shown in the results, the effect of increasing mass loss rate is dependent on the test conditions such as impact angle, potential and velocity. For the carbon steel in reservoir water, there is a general increase in Kec value with increasing potential and decrease in impact angle from 60° to 30°.

The incidence of the particles impacting on the surface will increase as the impact velocity increases, causing a change in the rate of repassivation and passivation, and then leading to corrosion currents increasing [10-11]. This is consistent with the observed of corrosion currents density of carbon steel in the reservoir water and mixed environments, Figures 5.1-5.3 and Figures 5.13-5.15.

It can be concluded from the results that the current density in both crude oil and oil/20%water environments is lower than in the reservoir water which suggests better corrosion resistance of carbon steel in crude oil and oil/20% water environments containing particles sized 600-710µm than in reservoir water containing particles sized 600-710µm.

Moreover, the value of Kec in the three environments containing particles sized 600-710µm is greater than the value of Kec for carbon steel in the three environments containing small particles sized 150-300µm, because for carbon steel in the three environments containing small particles(150-300µm) the value of corrosion contribution is increased more than with large particles(600-710µm), which indicates the creation of a passive film and oil film on the surface of the specimen and that film decreases the value of erosion contribution (Ke)[10-11].

5.3.3. Erosion-corrosion maps

5.3.3.1. Erosion-corrosion mechanism maps

The corrosion process can either be dissolution, passivation, or transpassivation [34]. The erosion–corrosion mechanism maps (Figures 5.25-5.33) show where there is transition between the regimes as a function of the impact velocity and applied potential at constant impact angle. These maps are based on the ratio of the erosion to corrosion rate ratio Ke/Kc for carbon steel in the three environments containing particles sized 150-300μm and 600-710μm. The maps indicate that the boundaries for carbon steel in the crude oil and 20%water/oil environments are unlike those in the reservoir water environment due to presence of crude oil.

At constant impact angle of 15°, an erosion–dissolution regime is observed in reservoir water containing particles sized 600-710μm at lower potentials (Fig.5.25 (a)). This may be due to the effect of erosion on the specimen being higher than corrosion. On the other hand, at higher impact velocities and potentials there are a transition from erosion-passivation and erosion–dissolution regime to passivation-erosion regime for carbon steel in the reservoir water Fig.5.25(a), which may be the result of the formation of films on the surface of the specimen at the positive potentials (in anodic condition).

For the carbon steel in reservoir water containing particles sized 600-710μm (Fig.5.25 -5.30(a)) it is clear that there is a general tendency for the extent of corrosion to increase at higher potentials and impact velocities. It is possible that with increases in impact velocity, the amount of oxygen transferring to the surface increases, leading to an enhancement in the corrosion rate (passivation-repassivation) [10 and 11]. For the carbon steel in oil/20%water environments containing particles sized 600-710μm (Figs.5.25 -5.30(c)) it has been found that there is a transition between erosion–corrosion regimes with increases in impact angles from 15° to 90°. However, the erosion–dissolution regime dominates below -200 mV and the erosion–passivation regime dominates in anodic condition. This may be due to a change in corrosion mechanism at higher potentials.

On the other hand, in the crude oil environment containing particles sized 600-710μm (Figs.5.25 -5.30(b)) erosion is dominant at all impact velocities and applied potentials, that should be attributed to the role of the oil layer limiting the mass loss due to erosion-corrosion[2,6 and 11].

For carbon steel in reservoir water and combined environments containing particles sized150-300μm (Figures.5.31 -5.33(a) and(c)) the passivation-erosion regime is dominant across all maps and there is no change on the map with an increase in impact angle at all impact velocities and potentials, which could be attributed to corrosion products on the surface of the specimen creating a passive film that plays the main role in decreasing the effect of particle on the surface of specimen [17]. It is clear from Figures.5.31 -5.33(b) that for carbon steel in crude oil containing small particles sizes 150-300μm, the erosion-passivation is dominant, which could be due to presence of the oil film on the surface of specimen.

5.3.3.2. Erosion–corrosion wastage maps

From the results of erosion–corrosion wastage maps of carbon steel in the crude oil environments containing particles sized 600-710μm at impact angle of 15° -90° Figs.5.34-39(a), it is interesting that to see that the the medium wastage regime predominates only at highe impact velocity 4.5 ms^{-1}, on the other hand,the low wastage regime becomes dominate all the maps with changing in the particle sizes to 150-300μm and there is no evidence of presence of medium wastage regimes (Figs. 5.40-5.42(b)).This is attributed to the oil film on the surface of material.

However, in the reservoir water and combined environment containing particles sized 600-710μm at constant impact angle of 15°-90° the medium wastage regime dominates at high impact velocties 3.5-4.5 ms^{-1} and applied potentials between 0mV and 400mV, due to removal of the passive and oil film by particles impact, indicating an increase in the value of Kec (Figures 5.34-5.42(a-c)).

The low wastage regime predominated in all the maps in the reservoir water, combined environment containing particles sized 150-300μm at constant impact angle of 15°-90 at impact velocities between 2.5-3.5 ms^{-1} and that can be attributed to decrease in mass loss due to the passive film and oil film Figures 5.42(a)and(-c).

5.3.3.3. Erosion–corrosion additive-synergistic maps

Erosion-corrosion additive-synergism maps show the transition in the material degradation with change in the impact velocity and applied potentials. Tables 5.55-81 show the values of ΔKe/ΔKc ratio for the carbon steel in three different environments. From the results, at impact angles of 15°- 90°, it is clear that indicate that the additive-synergistic regime is highest in water environment containing small particles sized 150-300μm, Fig. 5.49-51(a).

On the other hand, the synergistic regime is dominate in the water environment containing large particles sized 600-710μm,could be attributed to increase the value of erosion (Ke). Also, the antagonistic regimes occupy the area at intermediate potentials possibly due to the protective effect of corrosion products on the surface of specimen Figs.5.45-46 (a).

The greater predominace of antagonistic regimes in the crude oil and oil /water environment containing large particles sized 600-710μm at impact angle of 60°, is attributed to the presence of the oil film protecting the surface of specimen from corrosion, Figs.5.46 (b-c). But, at higher impact angles, Fig. 5.48 (b-c), the level of antagonism is disappeared in the crude oil and combined environments consistent with the observation that the erosion rate is higher at 90° compared to 15° impact angles [10-11].

The synergistic regimes is dominate in the crude oil environment containing small particles sized 150-300μm at impact angle of 15°-90° and have been addressed in previous chapters (3) and (4). For carbon steel in the oil/20% water environment containing small particles sized 150-300μm (Figures 5.49-51(c)), the additive-synergistic regime is dominant, could due to the presence of water.

5.4 Summary

I. Polarization curves for erosion-corrosion of carbon steel in the three environments containing particles sized 600-710μm and 150-300μm have been produced at constant impact angle.

II. Volume loss of carbon steel in the three environments containing particles sized 600-710μm and 150-300μm has been investigated.

III. Erosion-corrosion maps for carbon steel in the three environments containing particles sized 600-710μm and 150-300μm have been produced at constant impact angles.

IV. The volume losses of carbon steel X52 in the three environments and five applied potentials, -400,-200, 0, 200 and 400mV, demonstrate that when the impact velocity is increased from a low impact velocity to a high impact velocity, the volume losses increases in the three environments. However, the value of mass losses from the reservoir water environment is highest, while the value of the volume losses in crude oil is less than in the mixed environment.

V. It can be concluded from the maps that the impact angles and impact velocities have significantly effect on determining the boundary of erosion–corrosion, as demonstrated in this chapter, and it can be also noted that the areas of erosion–corrosion are changed with a change in impact angles and impact velocities.

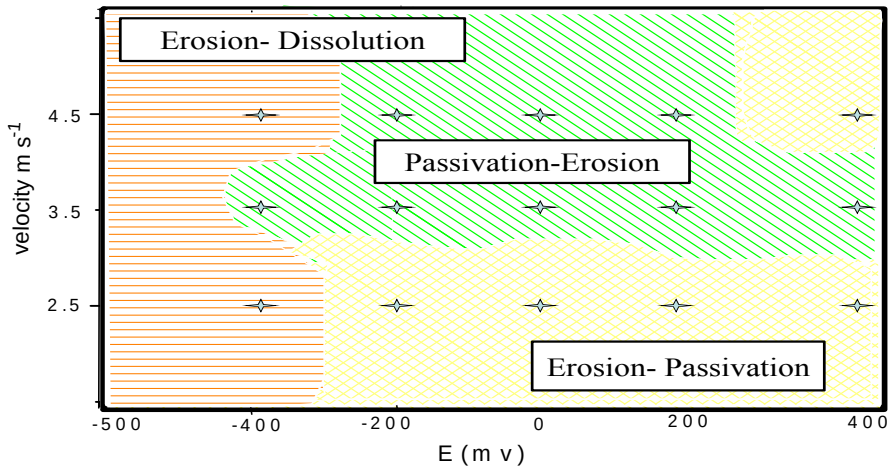

(a)

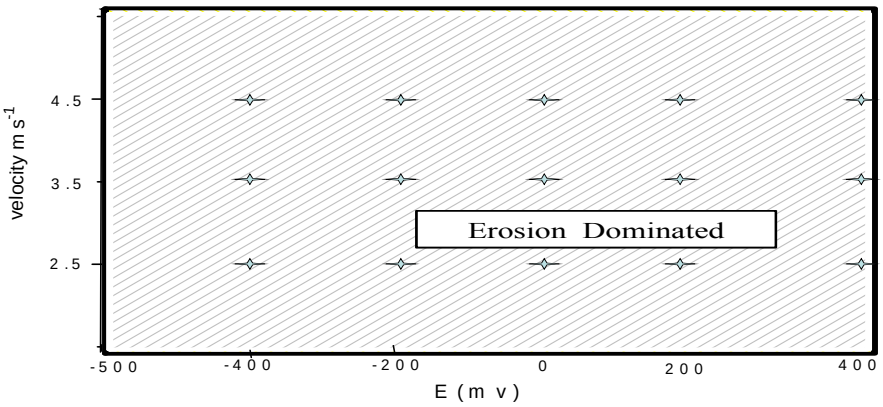

(b)

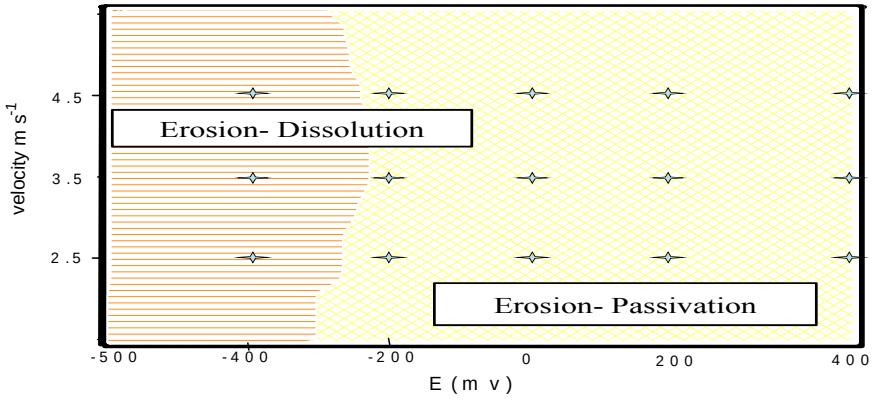

(c)

Fig.5.25: Erosion-corrosion mechanism maps for carbon steel at constant impact angle 15° and particle size 600-710µm in (a) water (b) crude oil (c) oil /20% water.

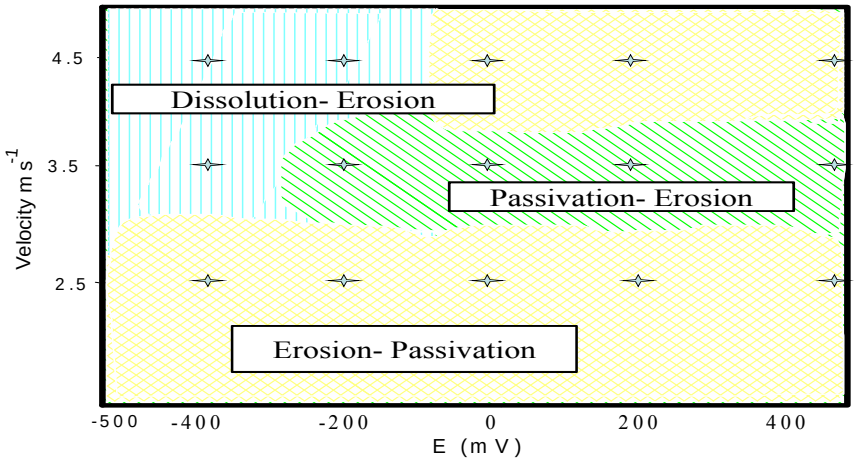

(a)

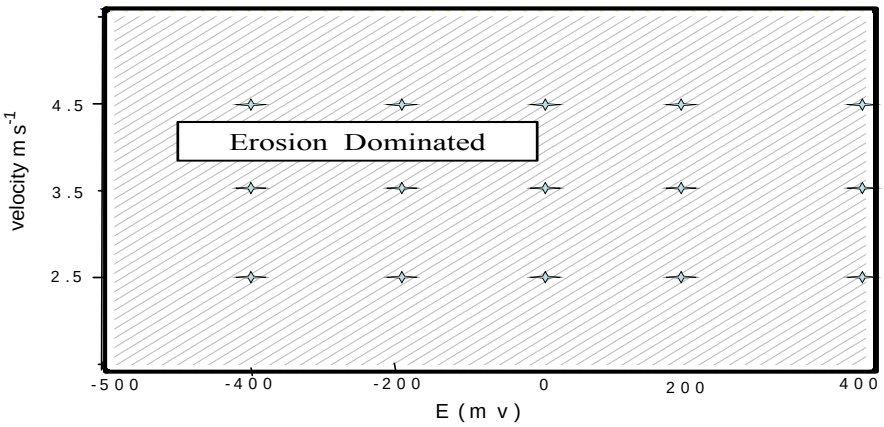

(b)

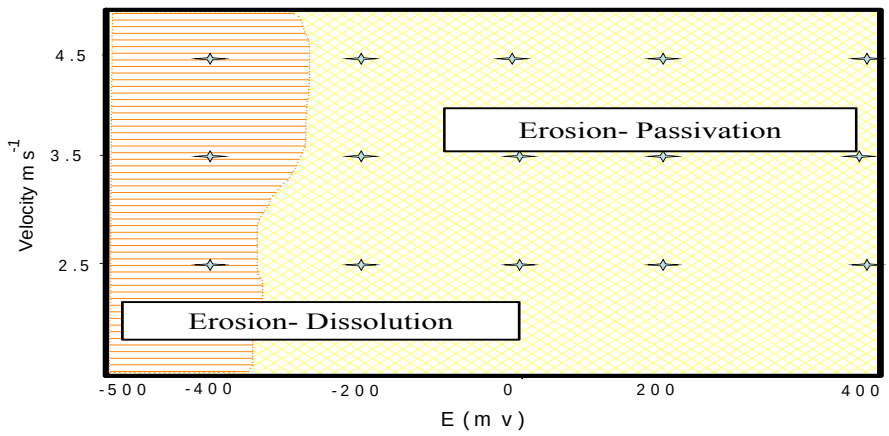

(c)

Fig.5.26: Erosion-corrosion mechanism maps for carbon steel at constant impact angle 30° and particle size 600-710µm in (a) water (b) crude oil (c) oil /20% water.

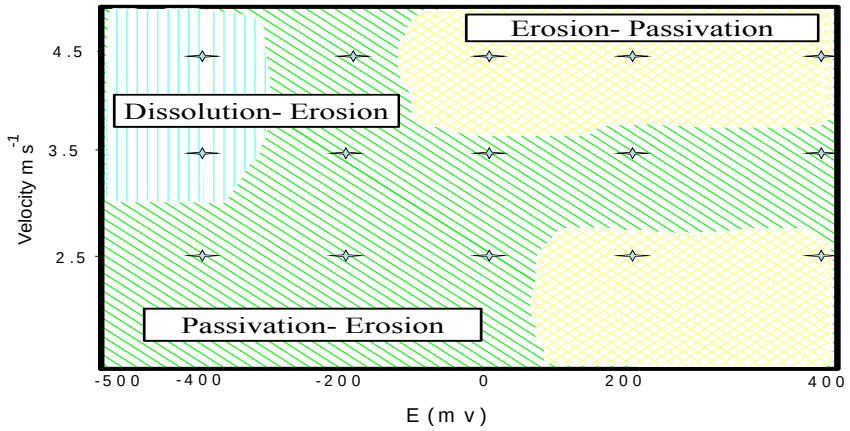

(a)

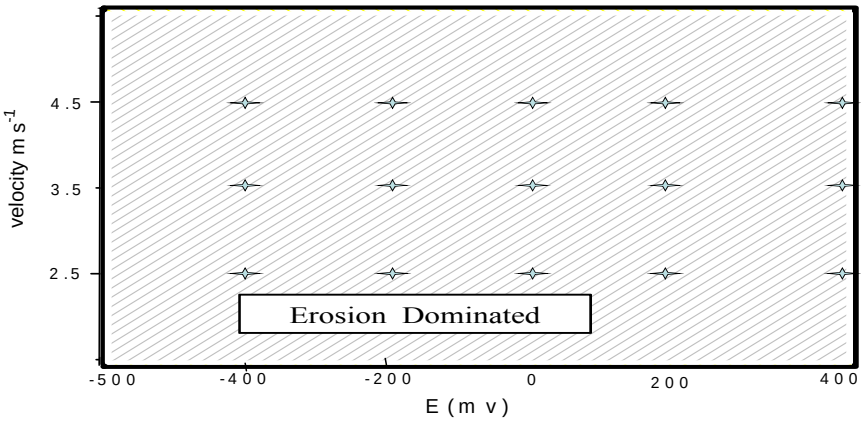

(b)

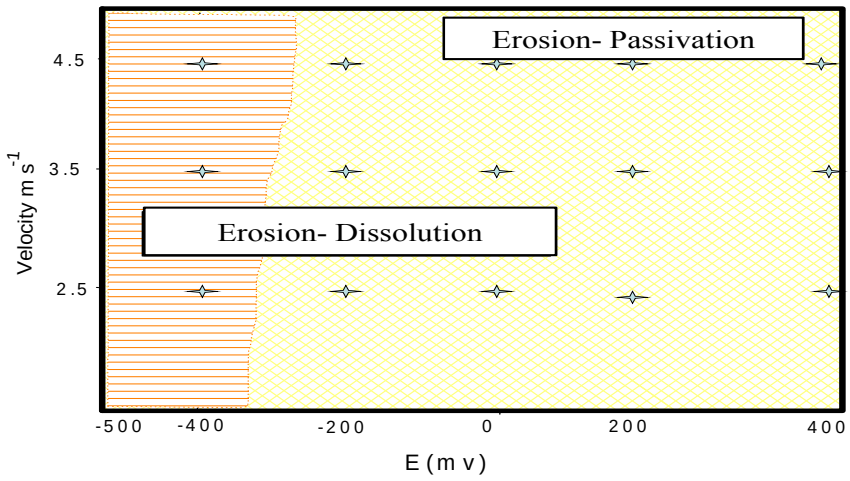

(c)

Fig.5.27: Erosion-corrosion mechanism maps for carbon steel at constant impact angle 45° and particle size 600-710µm in (a) water (b) crude oil (c) oil /20% water.

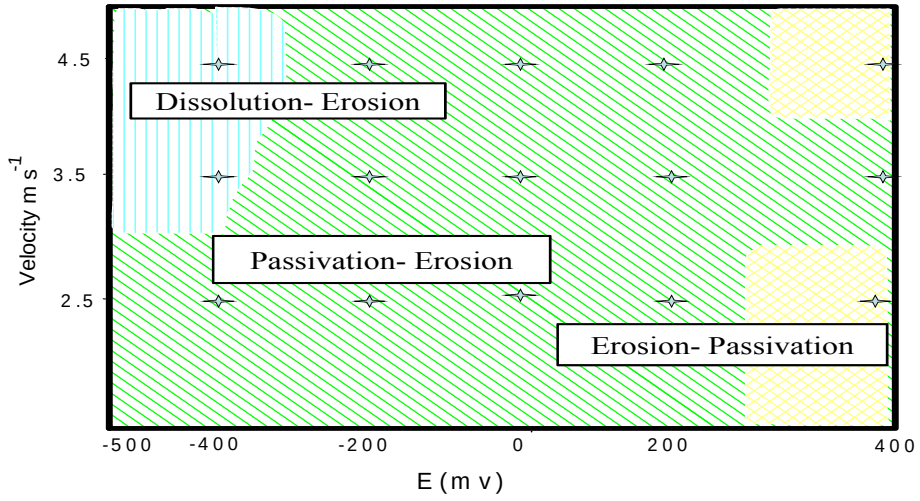

(a)

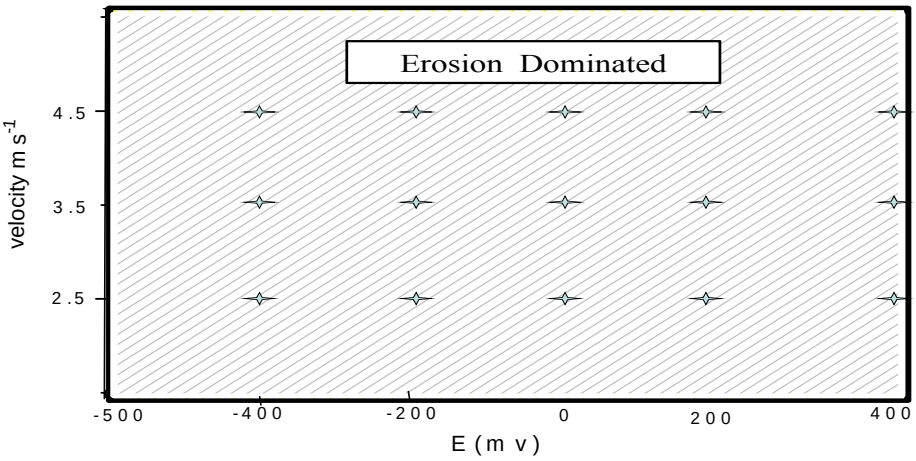

(b)

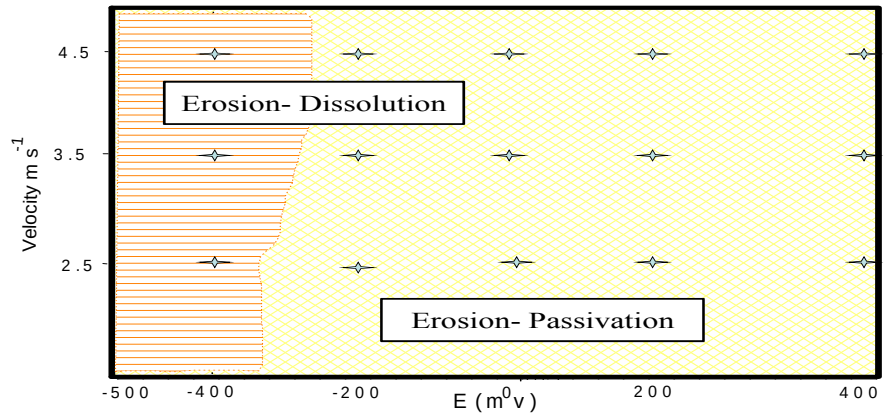

(c)

Fig.5.28: Erosion-corrosion mechanism maps for carbon steel at impact angle 60°and particle size 600-710µm in (a) water (b) crude oil (c) oil /20% water.

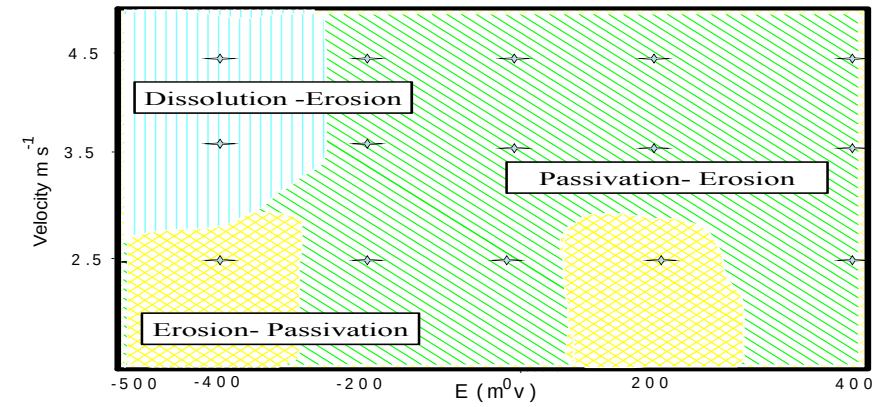

(a)

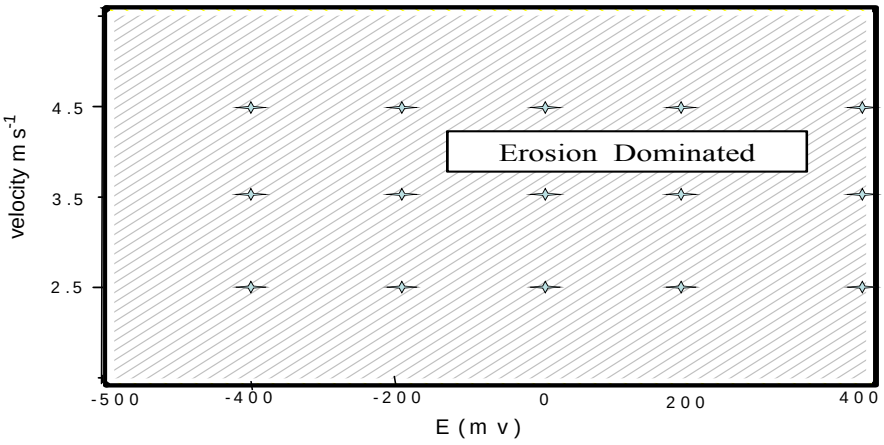

(b)

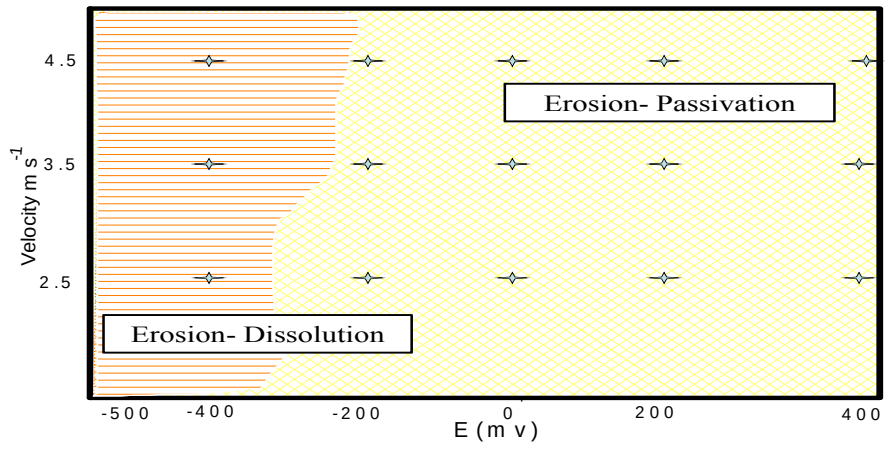

(c)

Fig.5.29: Erosion-corrosion mechanism maps for carbon steel at constant impact angle 75° and particle size 600-710µm in (a) water (b) crude oil (c) oil /20% water.

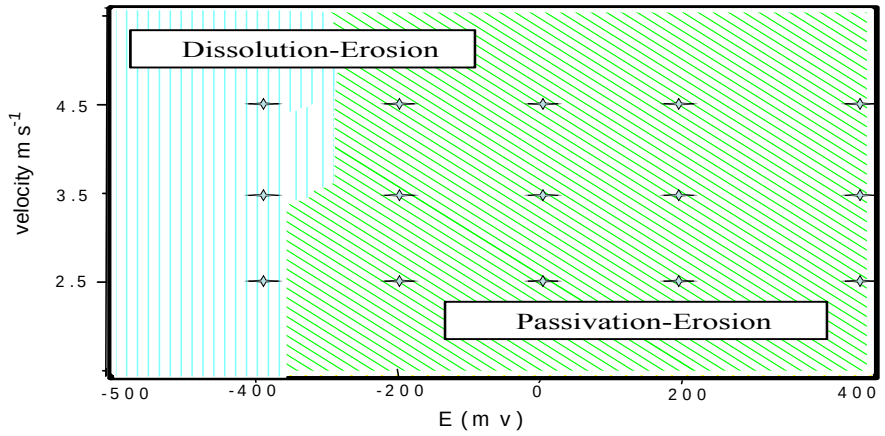

(a)

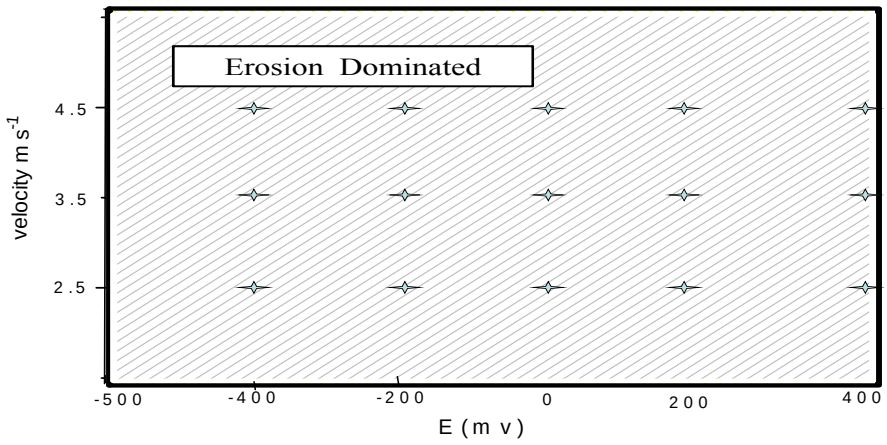

(b)

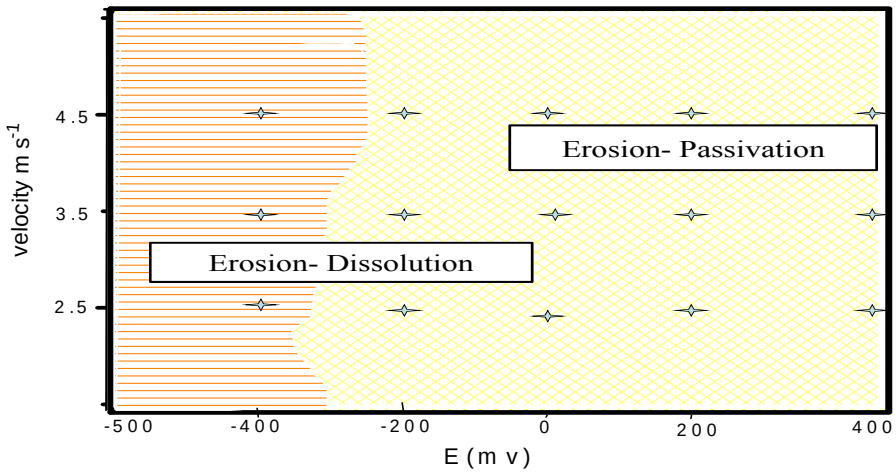

(c)

Fig.5.30: Erosion-corrosion mechanism maps for carbon steel at impact angle 90° and particle size 600-710µm in (a) water (b) crude oil (c) oil /20% water.

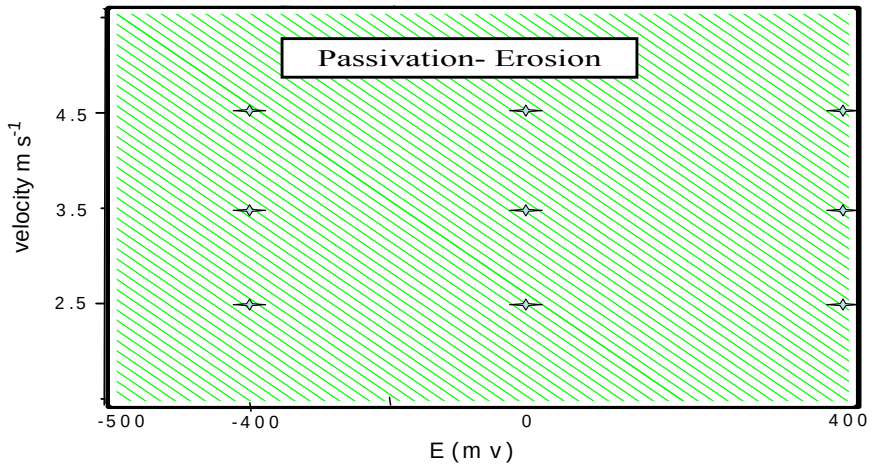

(a)

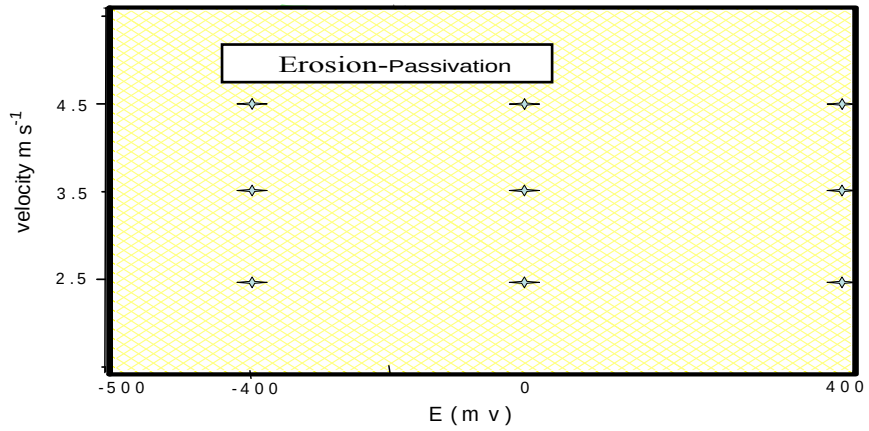

(b)

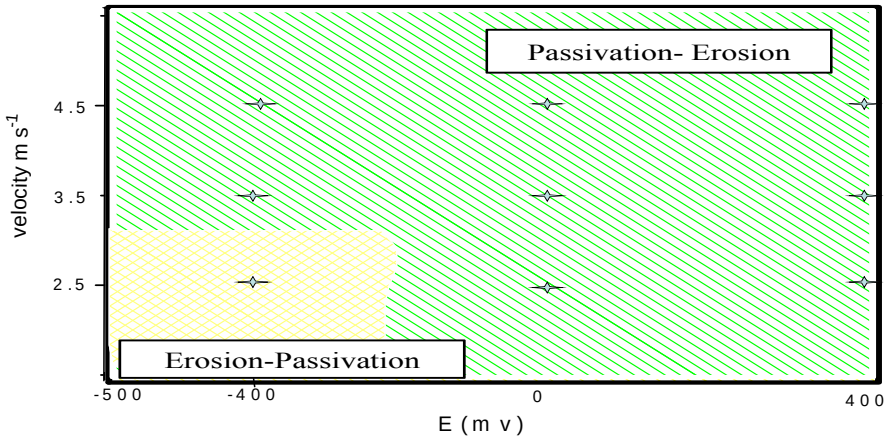

(c)

Fig.5.31: Erosion-corrosion mechanism maps for carbon steel at constant impact angle 15° and particle size 150-300µm in (a) water (b) crude oil (c) oil /20% water.

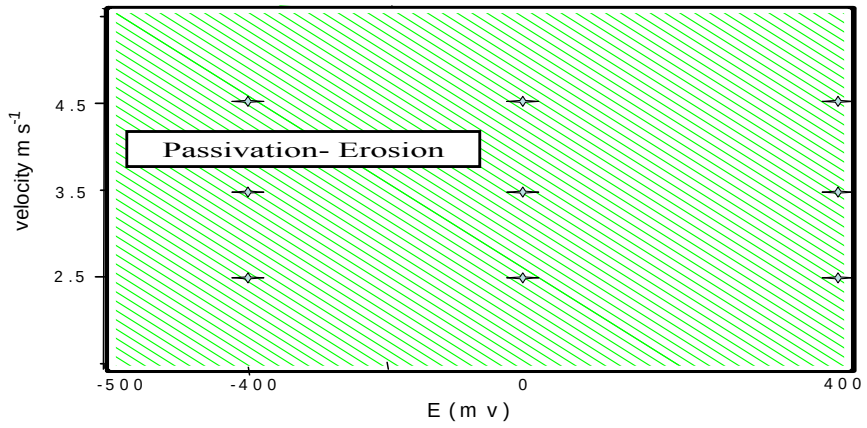

(a)

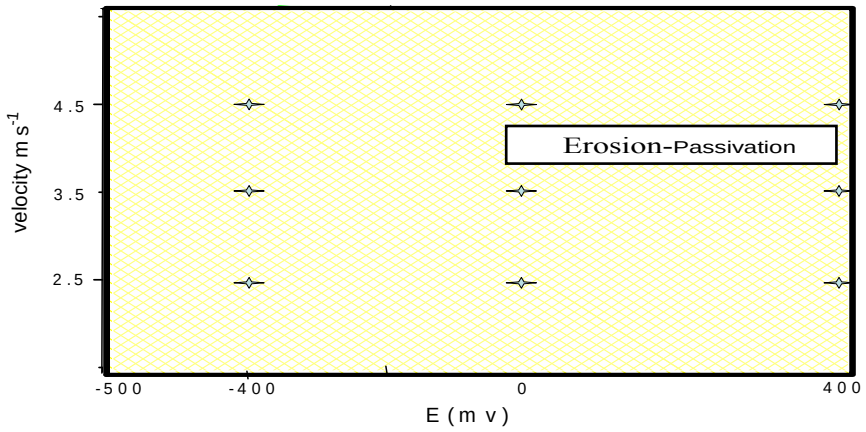

(b)

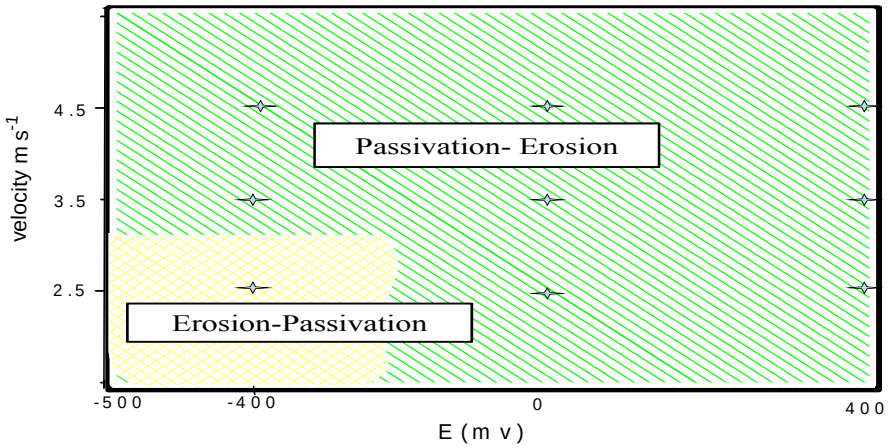

(c)

Fig.5.32: Erosion-corrosion mechanism maps for carbon steel at constant impact angle 45° and particle size 150-300µm in (a) water (b) crude oil (c) oil /20% water.

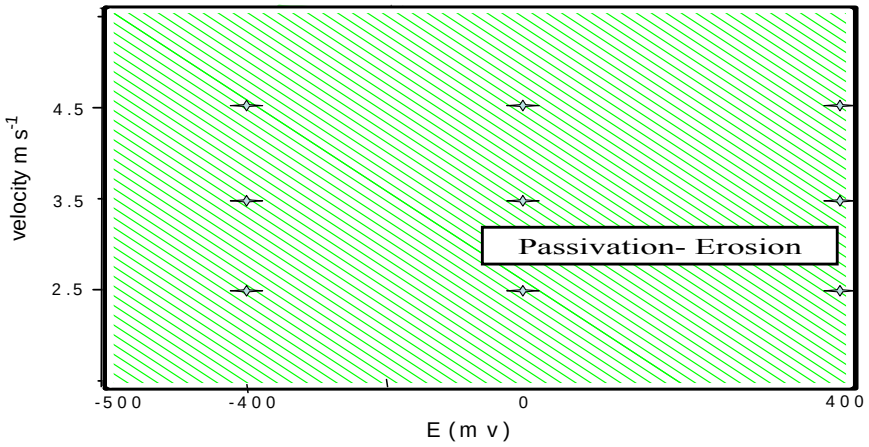

(a)

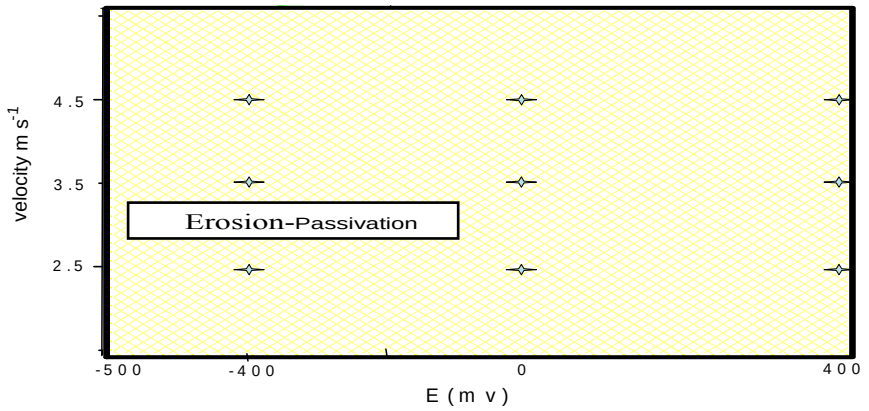

(b)

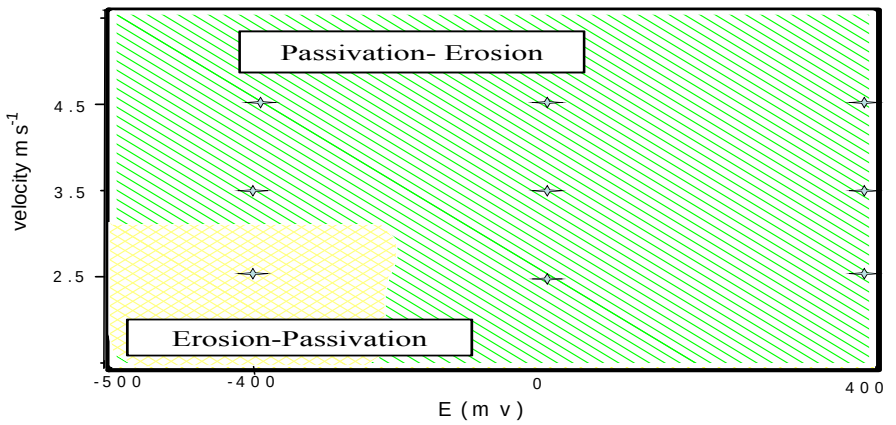

(c)

Fig.5.33: Erosion-corrosion mechanism maps for carbon steel at constant impact angle 90° and particle size 150-300µm in (a) water (b) crude oil (c) oil /20% water.

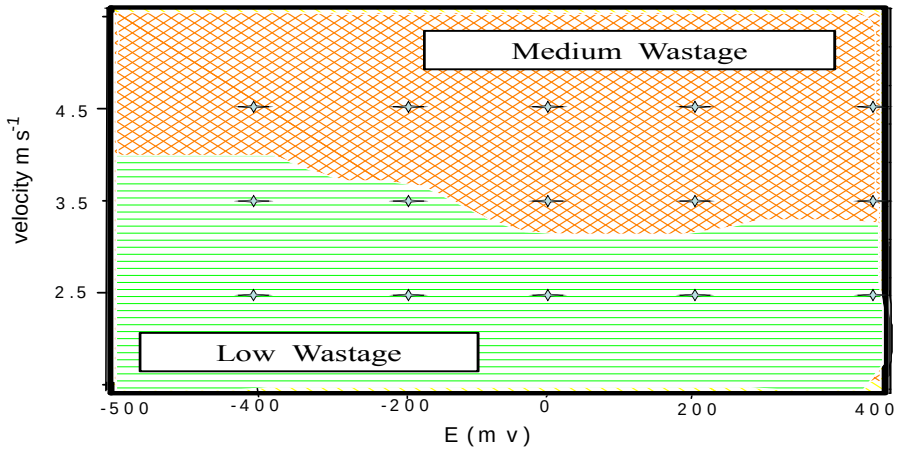

(a)

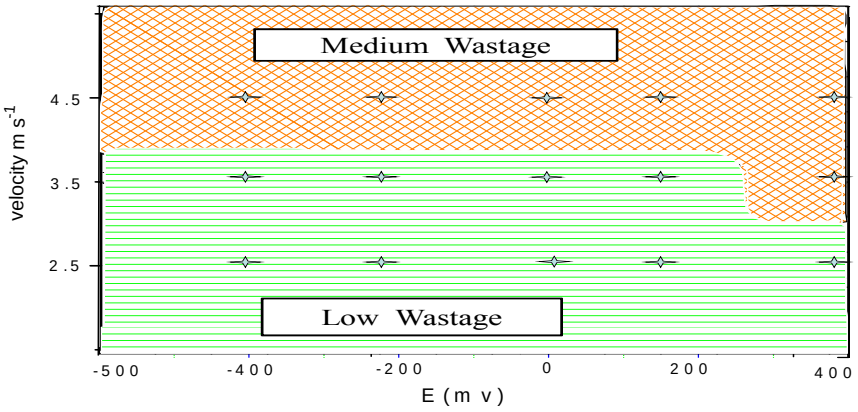

(b)

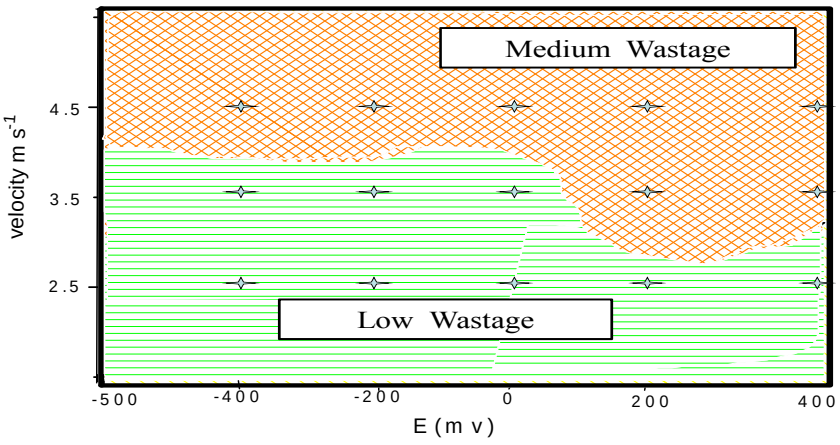

(c)

Fig.5.34: Erosion-corrosion wastage maps for carbon steel at constant impact angle 15° and particle size600-710µm in (a) water (b) crude oil (c) oil /20% water.

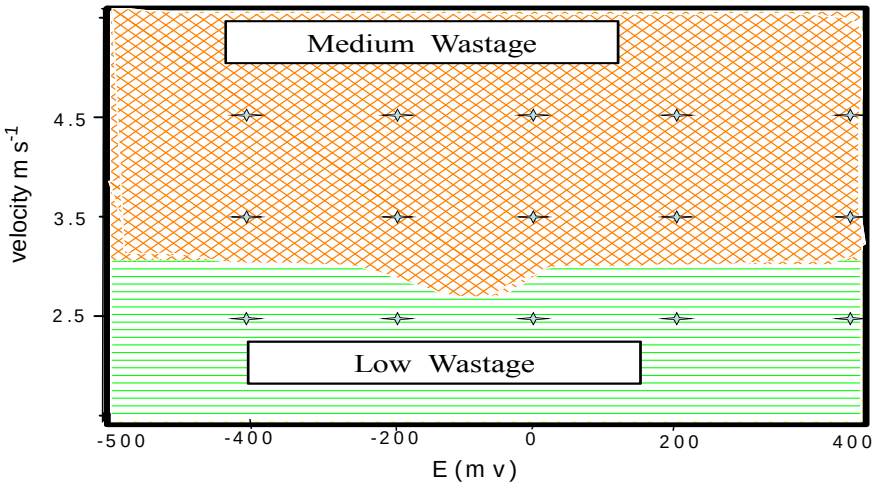

(a)

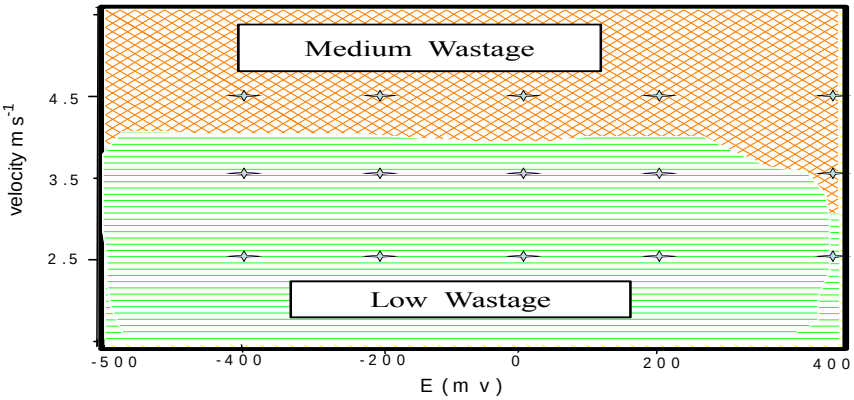

(b)

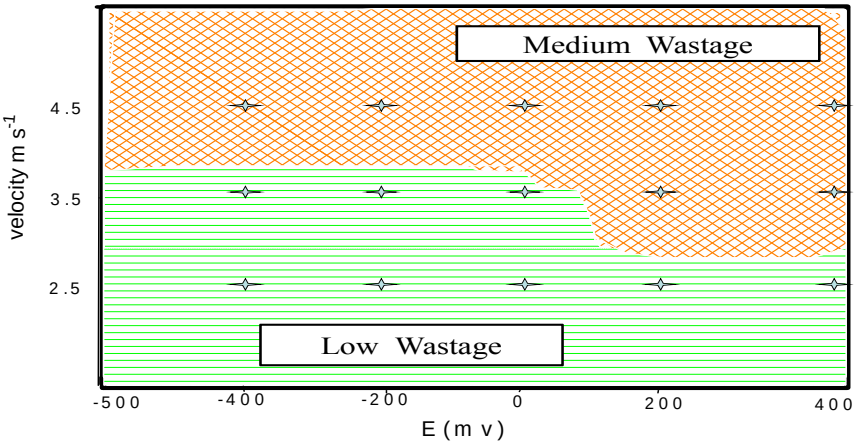

(c)

Fig.5.35: Erosion-corrosion wastage maps for carbon steel at constant impact angle 30° and particle size600-710µm in (a) water (b) crude oil (c) oil /20% water.

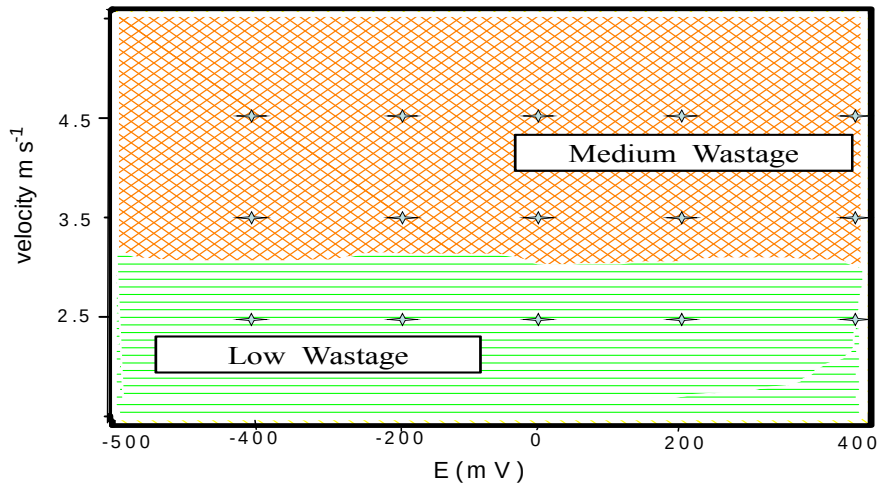

(a)

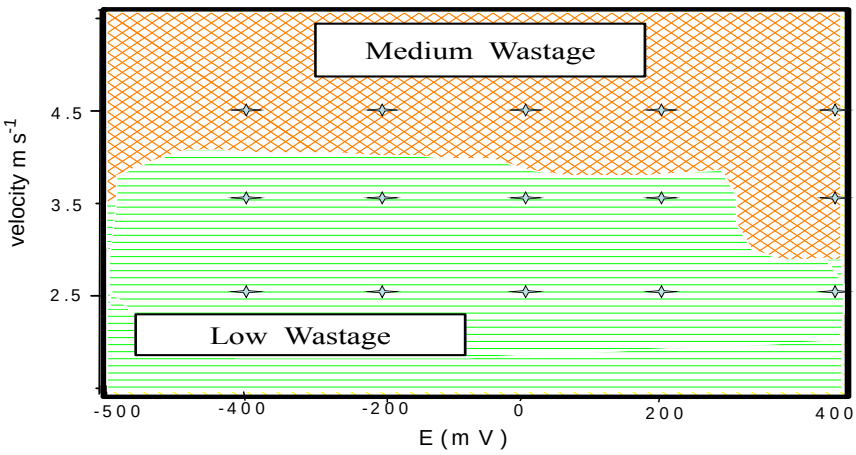

(b)

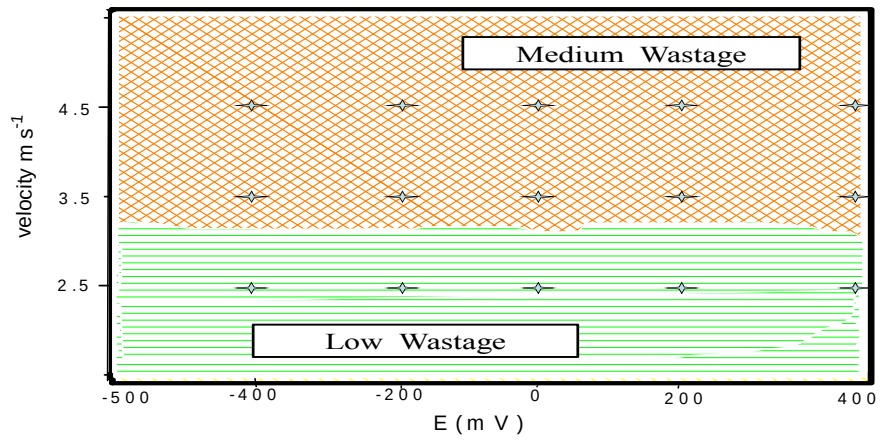

(c)

Fig.5.36: Erosion-corrosion wastage maps for carbon steel at constant impact angle 45° and particle size600-710µm in (a) water (b) crude oil (c) oil /20% water.

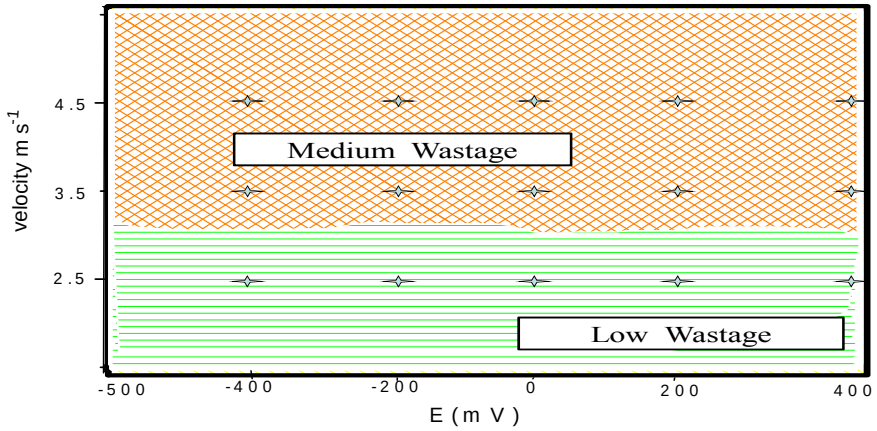

(a)

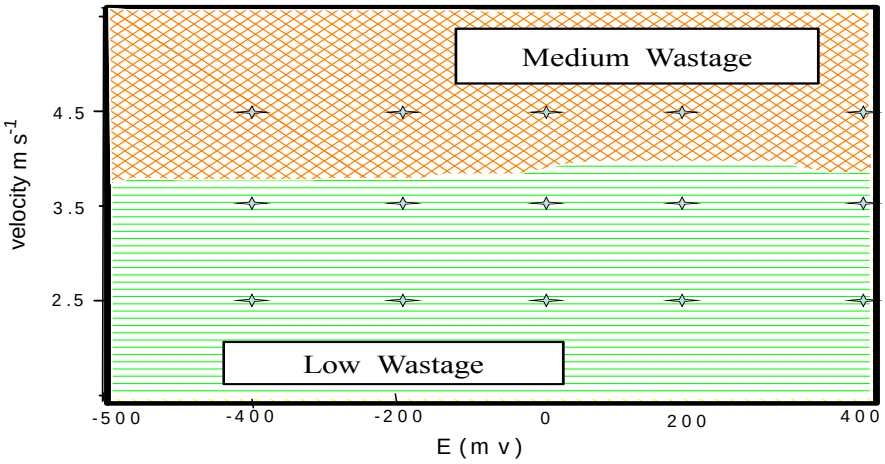

(b)

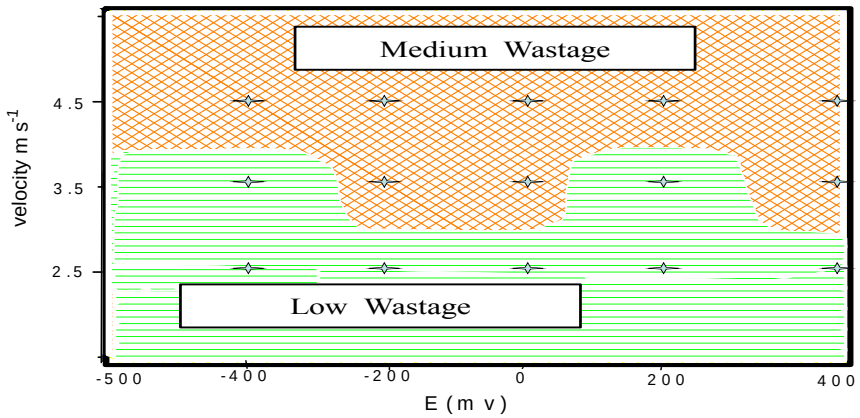

(c)

Fig.5.37: Erosion-corrosion wastage maps for carbon steel at constant impact angle 60° and particle size600-710µm in (a) water (b) crude oil (c) oil /20% water.

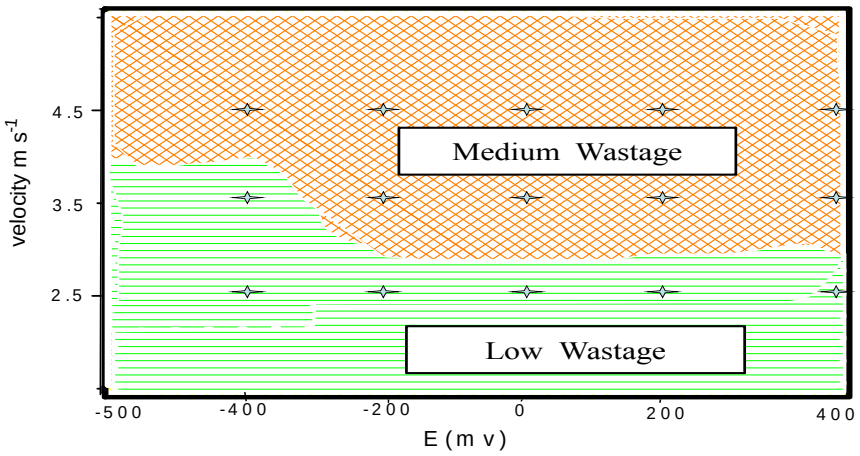

(a)

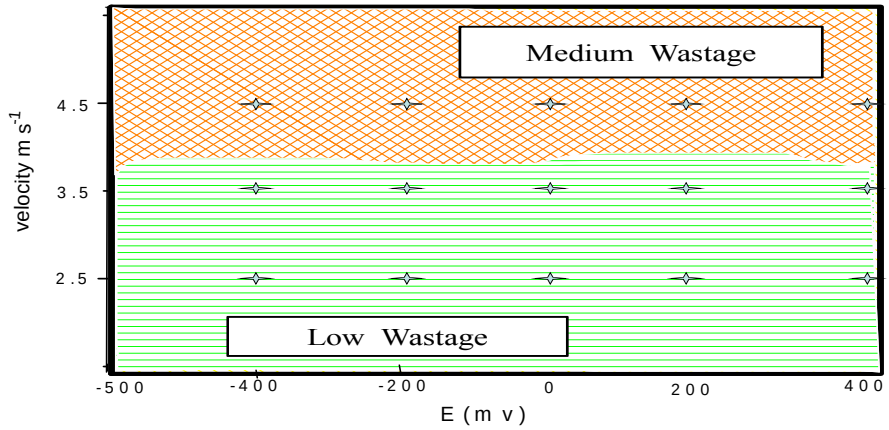

(a)

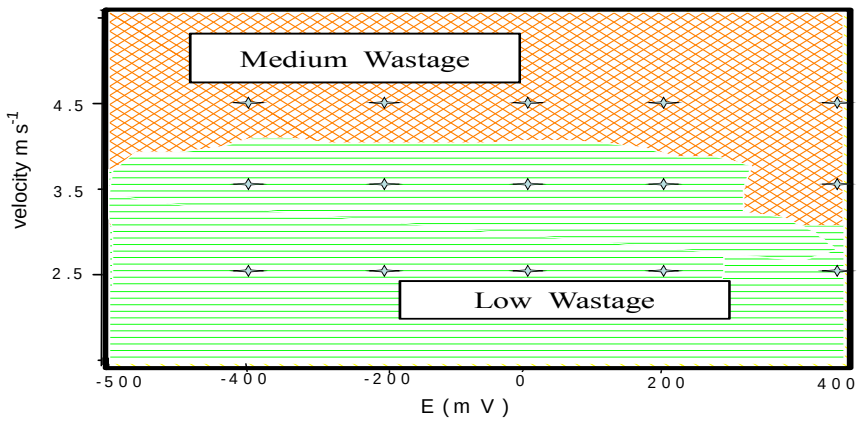

(c)

Fig.5.38: Erosion-corrosion wastage maps for carbon steel at constant impact angle75° and particle size600-710µm in (a) water (b) crude oil (c) oil /20% water.

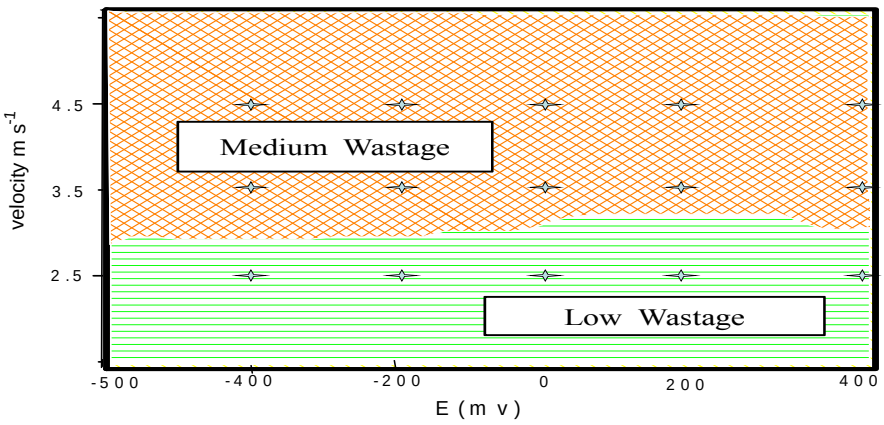

(a)

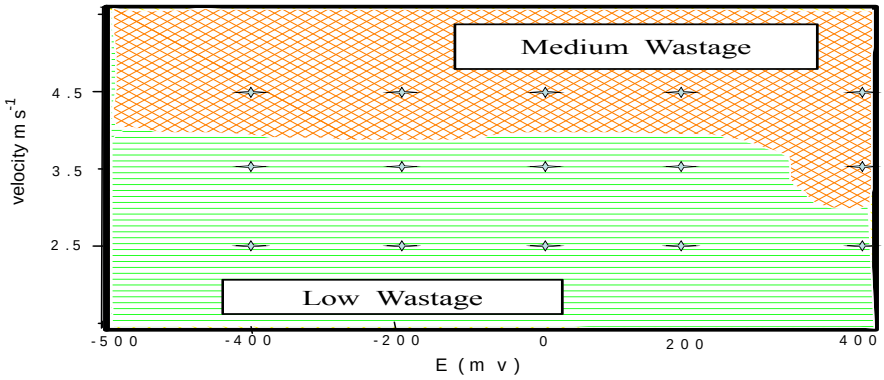

(b)

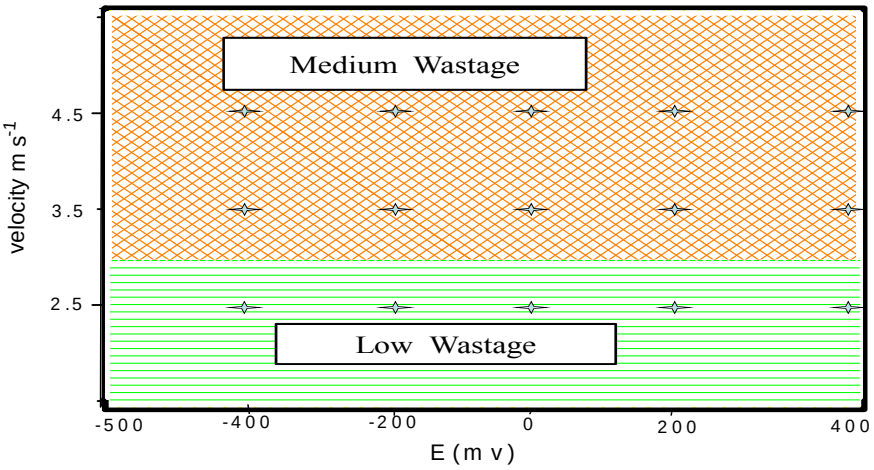

(c)

Fig.5.39: Erosion-corrosion wastage maps for carbon steel at constant impact angle 90° and particle size600-710µm in (a) water (b) crude oil (c) oil /20% water.

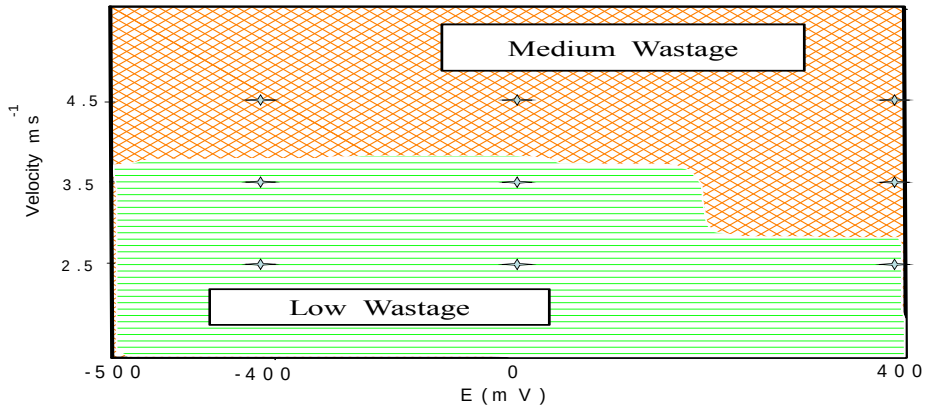

(a)

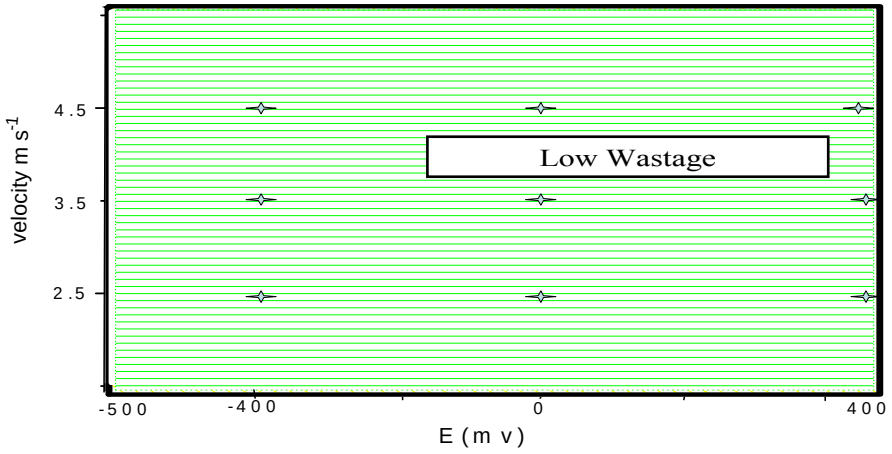

(b)

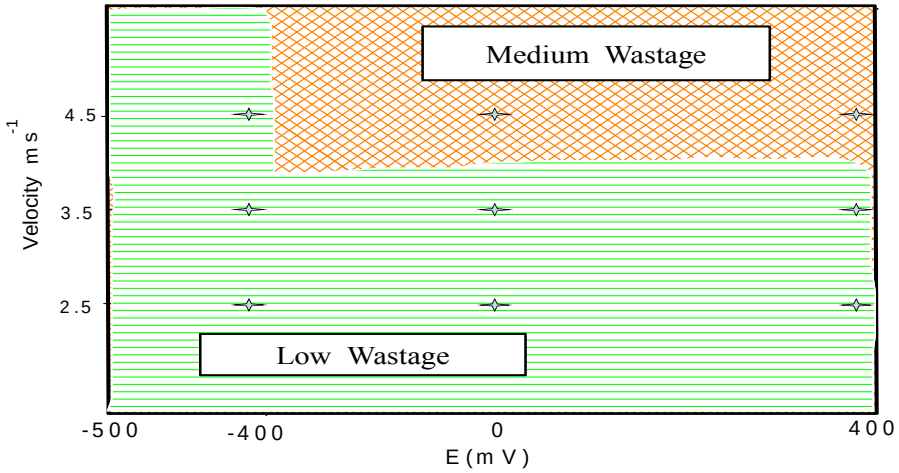

(c)

Fig.5.40: Erosion-corrosion wastage maps for carbon steel at impact angle 15° and particle size 150-300µm in (a) water (b) crude oil (c) oil /20% water.

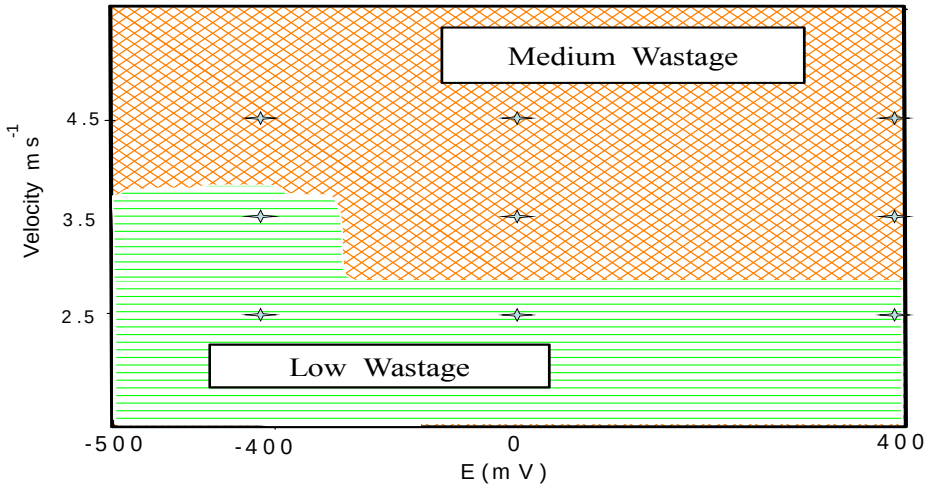

(a)

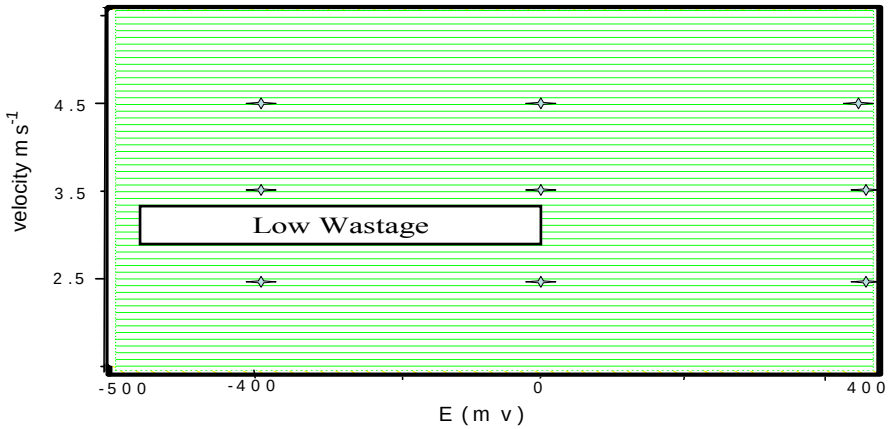

(b)

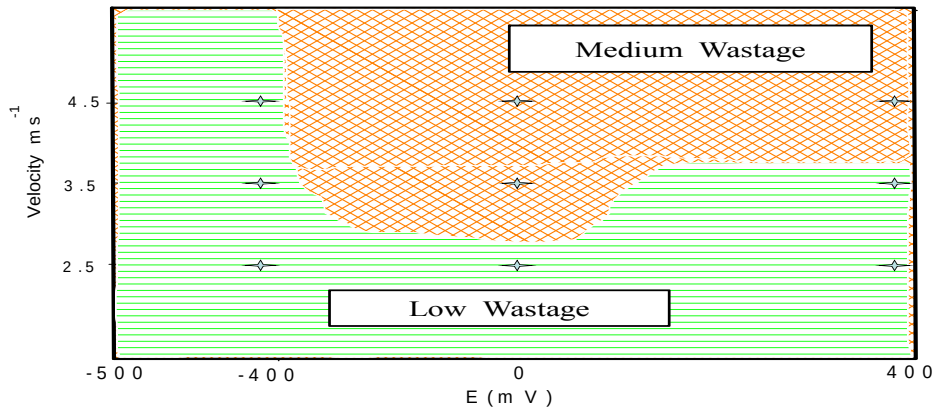

(c)

Fig.5.41: Erosion-corrosion wastage maps for carbon steel at impact angle 45° and particle size 150-300µm in (a) water (b) crude oil (c) oil /20% water.

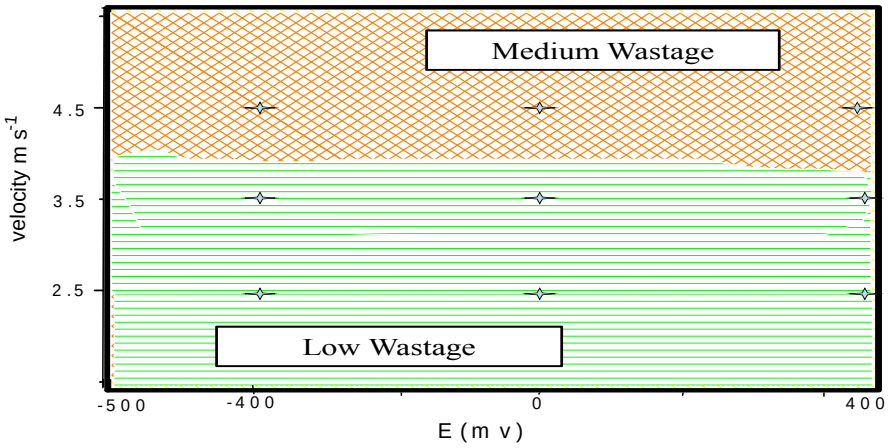

(a)

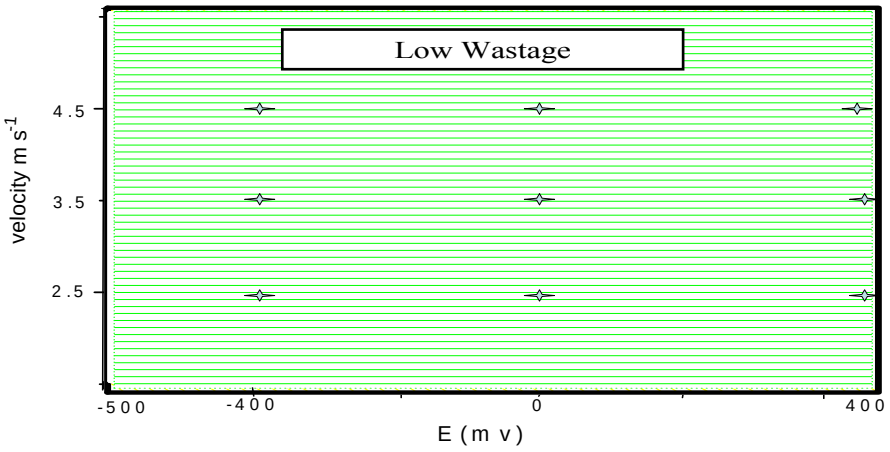

(b)

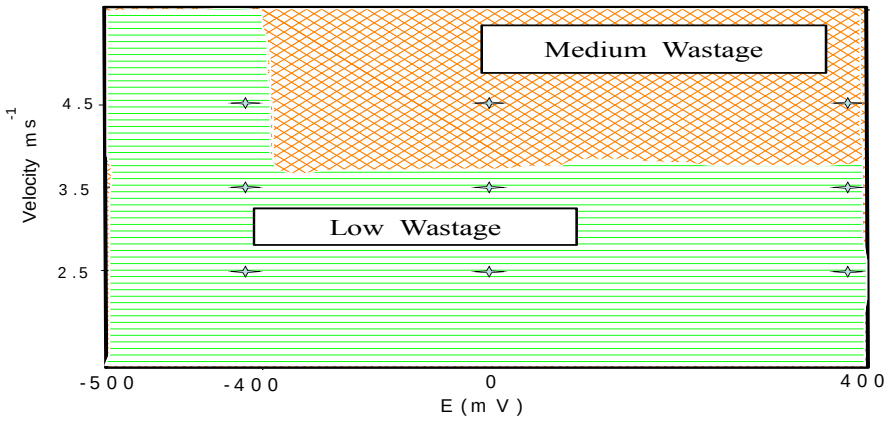

(c)

Fig.5.42: Erosion-corrosion wastage maps for carbon steel at impact angle 90° and particle size 150-300µm in (a) water (b) crude oil (c) oil /20% water.

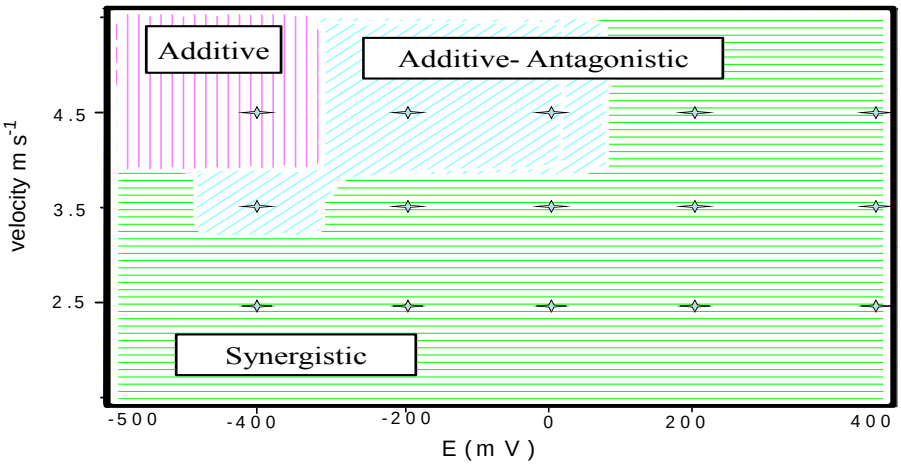

(a)

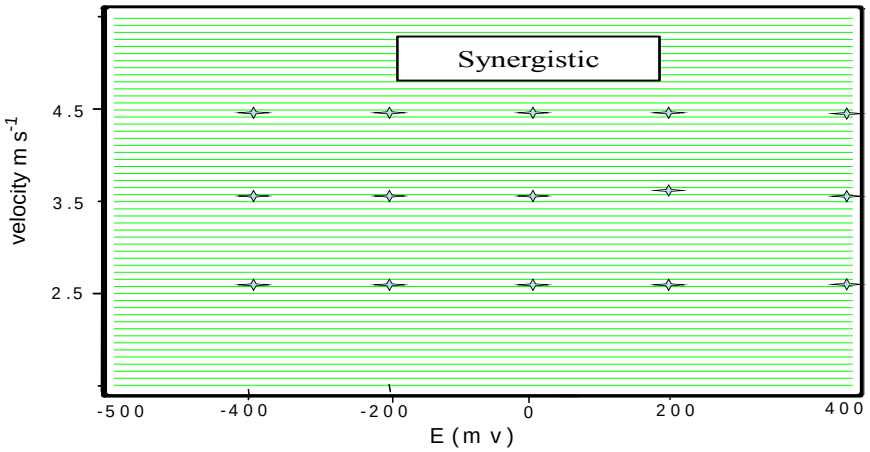

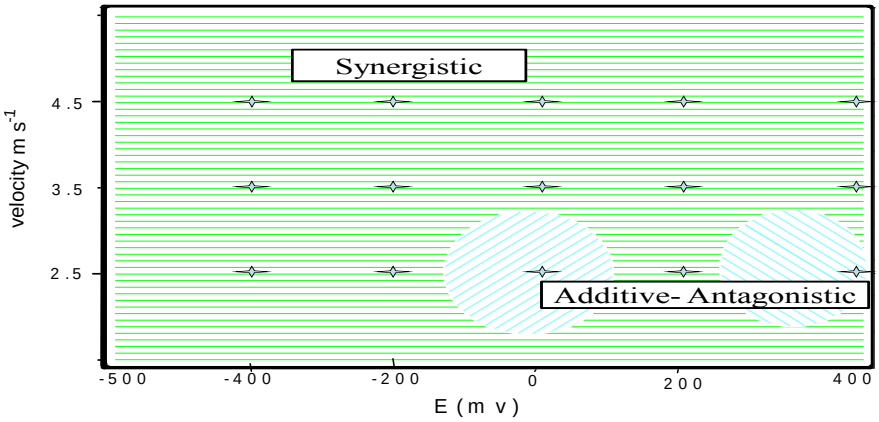

(c)

Fig.5.43: Erosion-corrosion additive-synergism maps for carbon steel at constant impact angle 15° and particle size 600-710µm in (a) water (b) crude oil (c) oil /20% water.

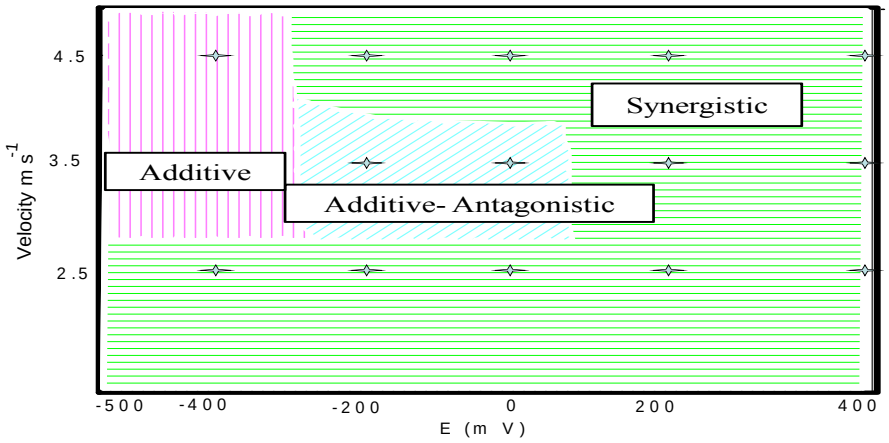

(a)

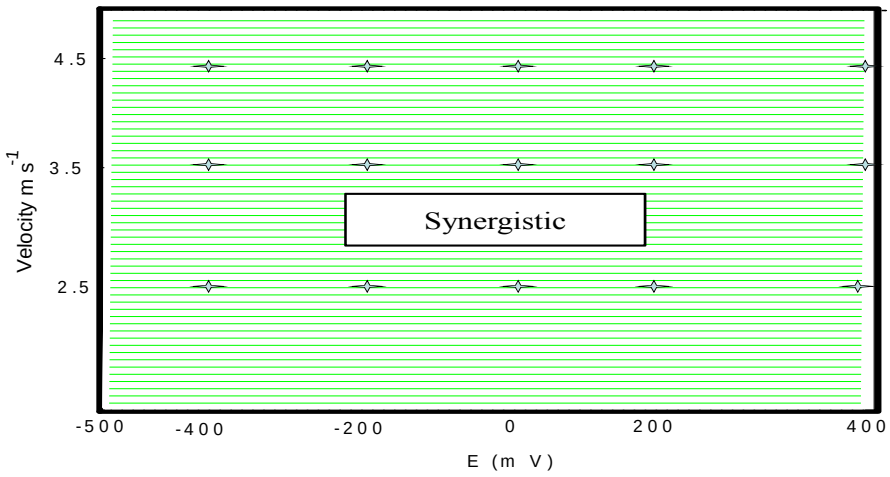

(b)

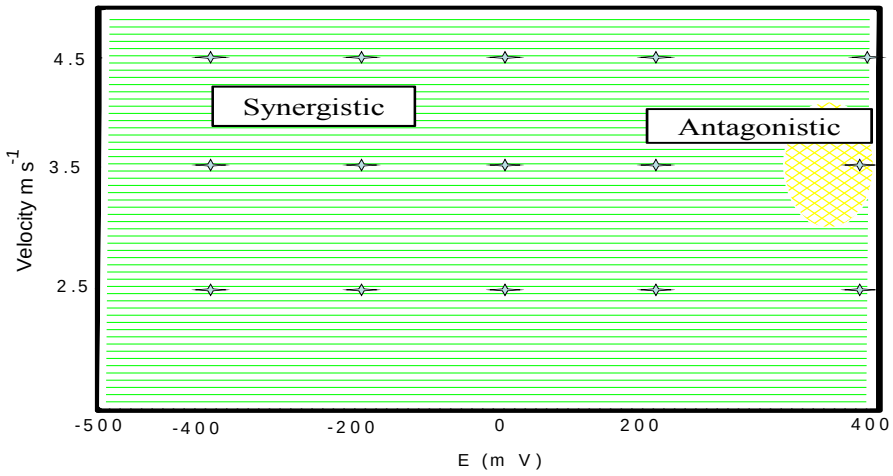

(c)

Fig.5.44: Erosion-corrosion additive-synergism maps for carbon steel at constant impact angle 30° and particle size 600-710µm in (a) water (b) crude oil (c) oil /20% water.

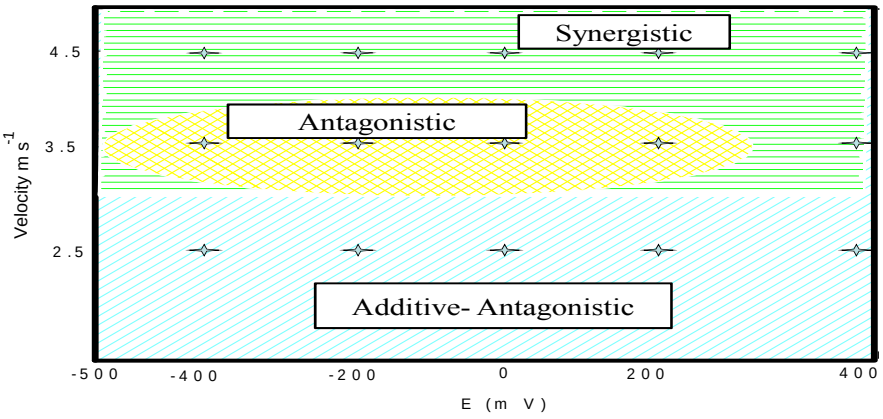

(a)

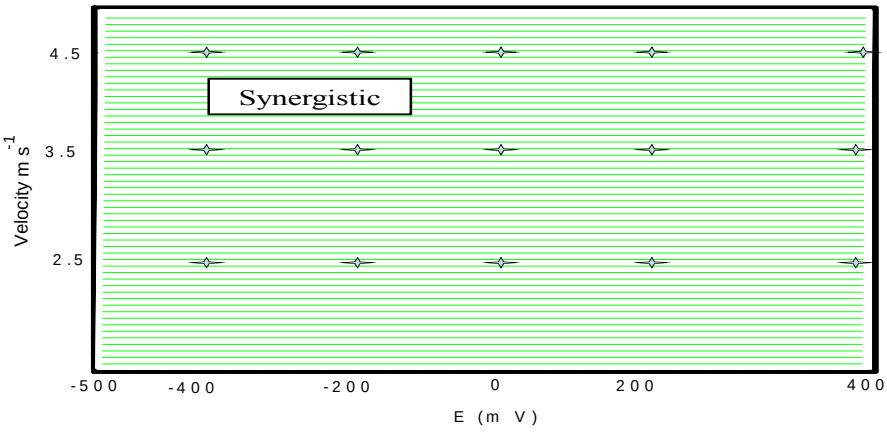

(b)

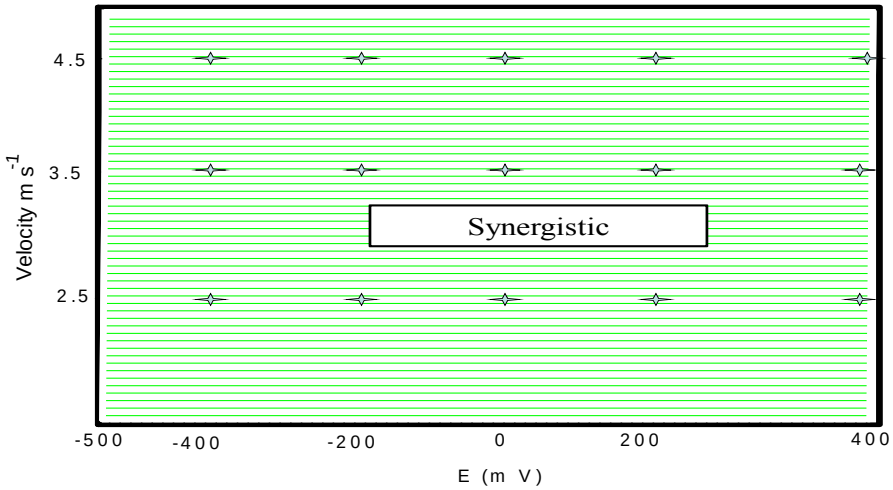

(c)

Fig.5.45: Erosion-corrosion additive-synergism maps for carbon steel at constant impact angle 45° and particle size600-710µm in (a) water (b) crude oil (c) oil /20% water.

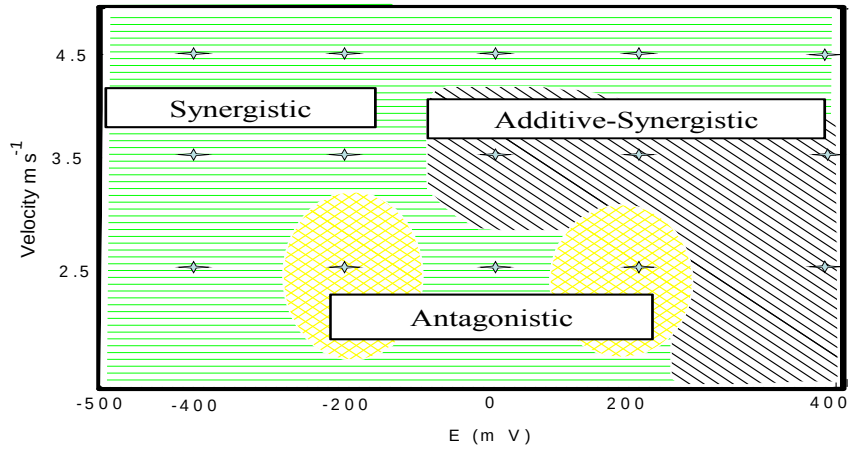

(a)

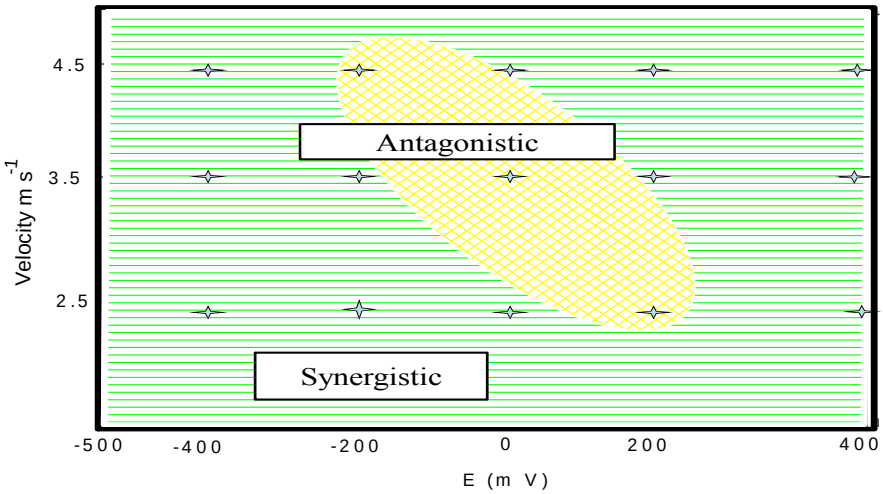

(b)

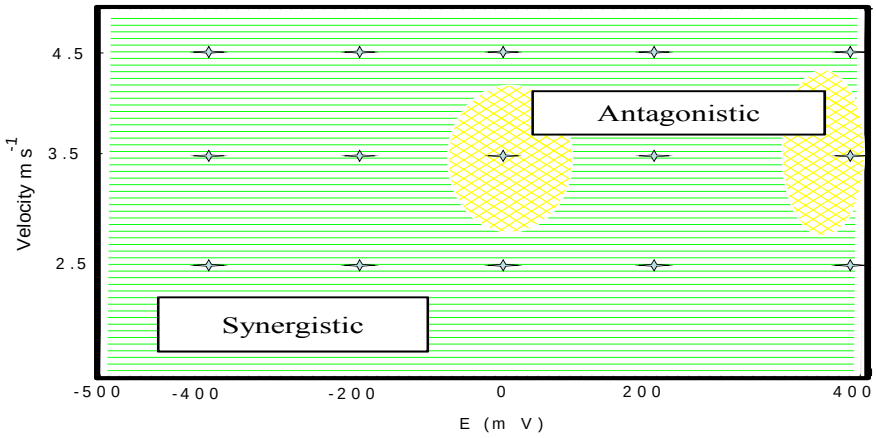

(c)

Fig.5.46: Erosion-corrosion additive-synergism maps for carbon steel at constant impact angle 60° and particle size600-710µm in (a) water (b) crude oil (c) oil /20% water.

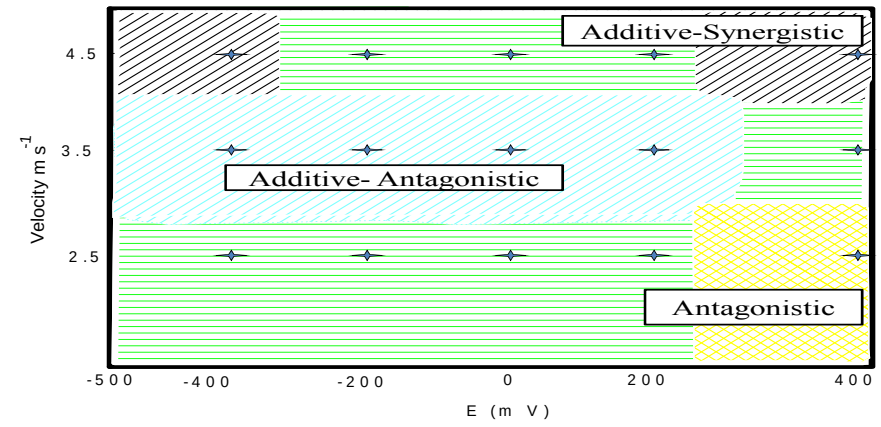

(a)

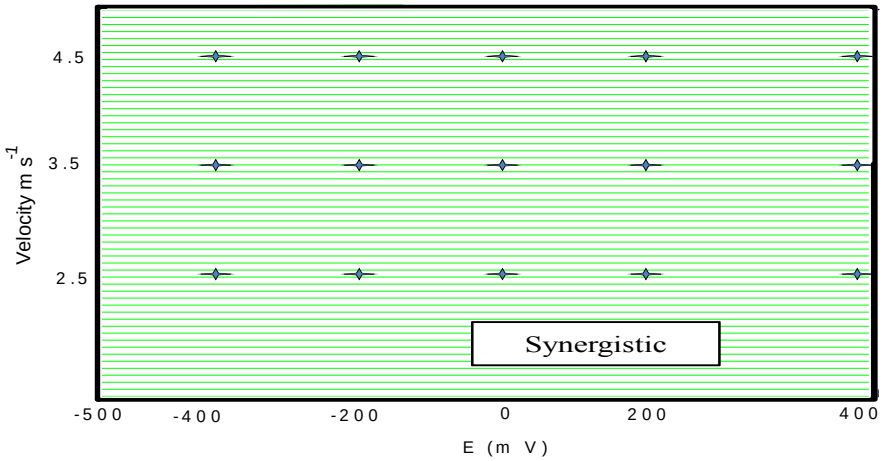

(b)

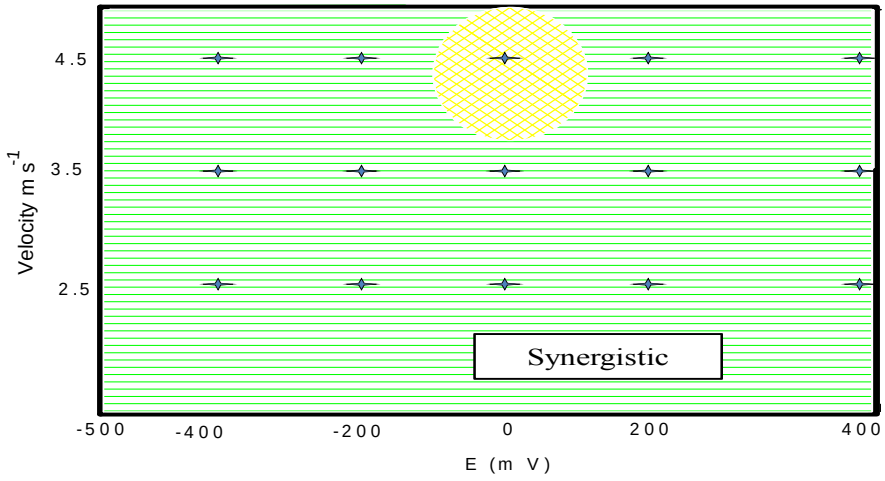

(c)

Fig.5.47: Erosion-corrosion additive-synergism maps for carbon steel at constant impact angle 75° and particle size600-710µm in (a) water (b) crude oil (c) oil /20% water.

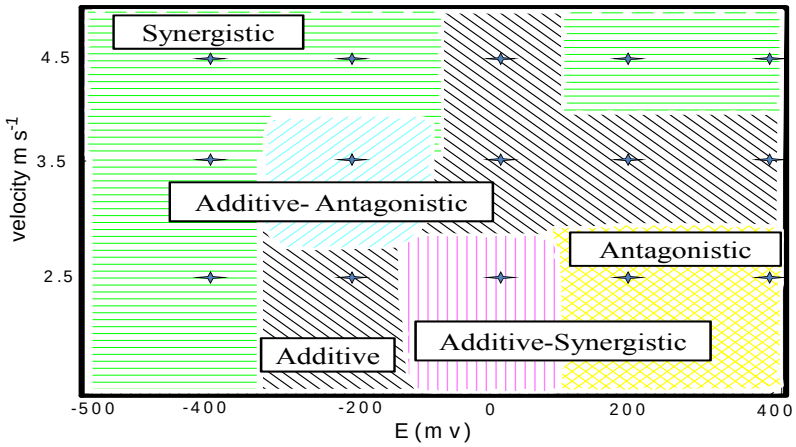

(a)

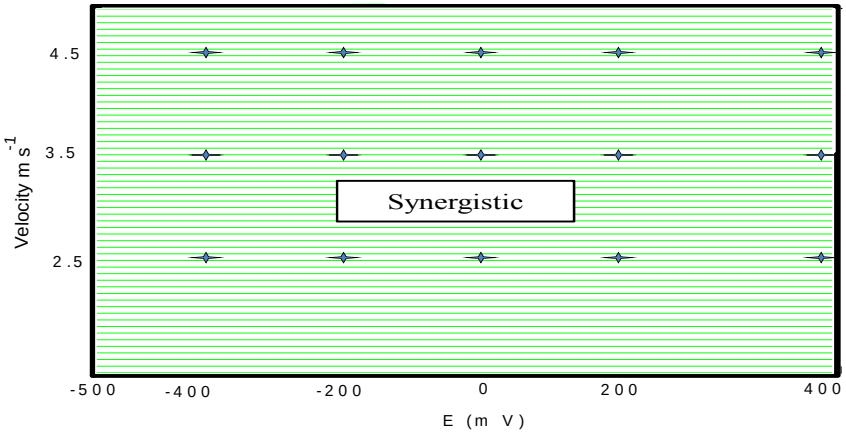

(b)

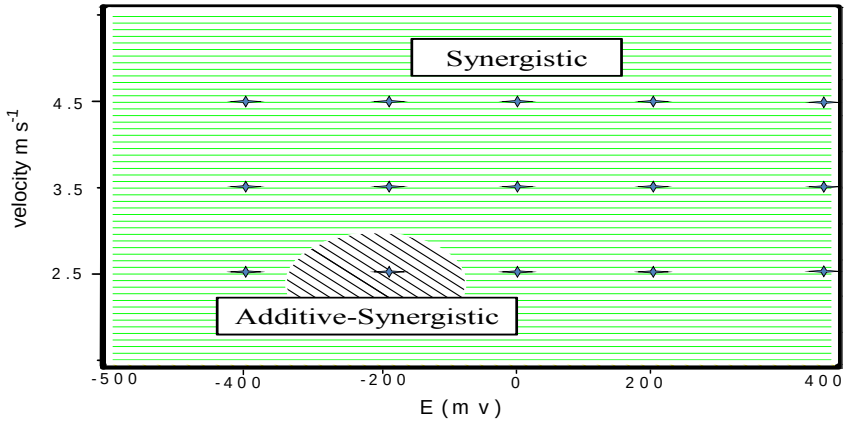

(c)

Fig.5.48: Erosion-corrosion additive-synergism maps for carbon steel at constant impact angle 90° and particle size600-710µm in (a) water (b) crude oil (c) oil /20% water.

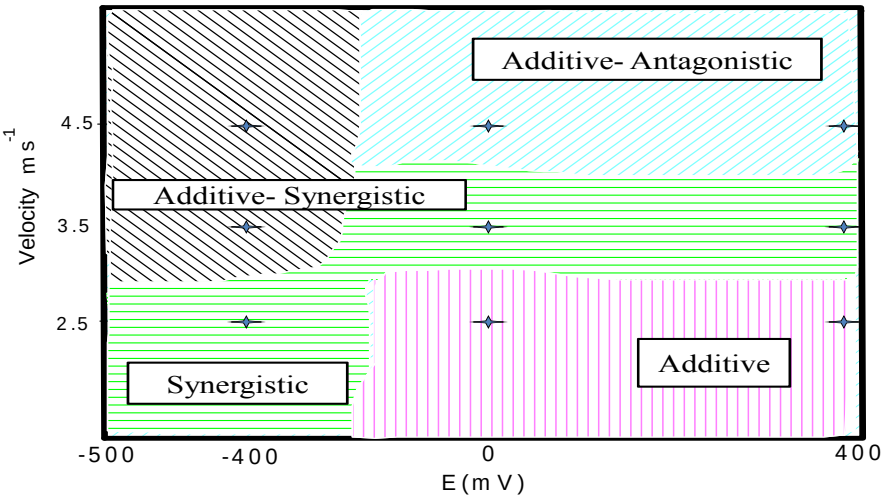

(a)

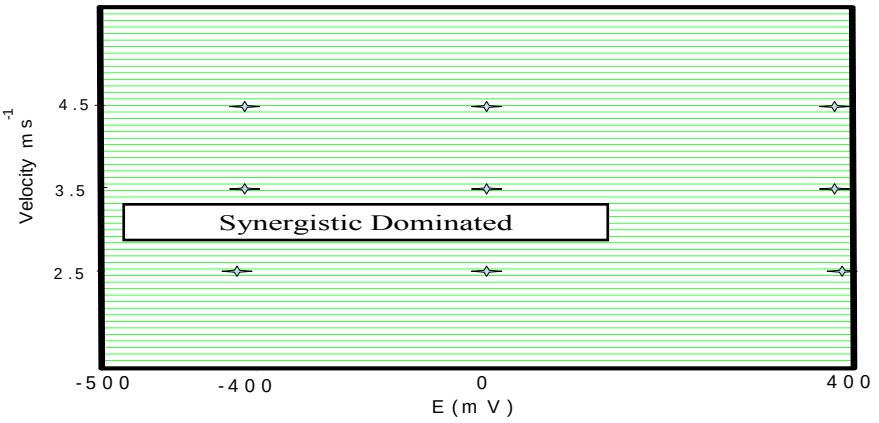

(b)

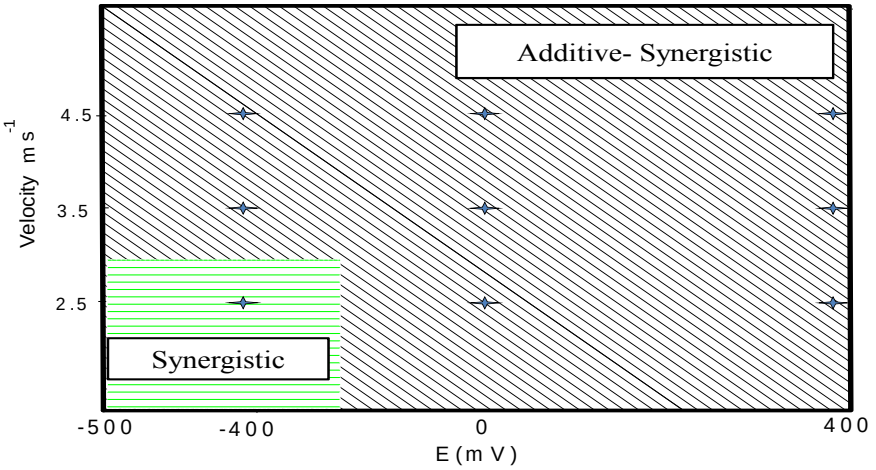

(c)

Fig.5.49: Erosion-corrosion additive-synergism maps for carbon steel at constant impact angle 15° and particle size 150-300µm in (a) water (b) crude oil (c) oil /20% water.

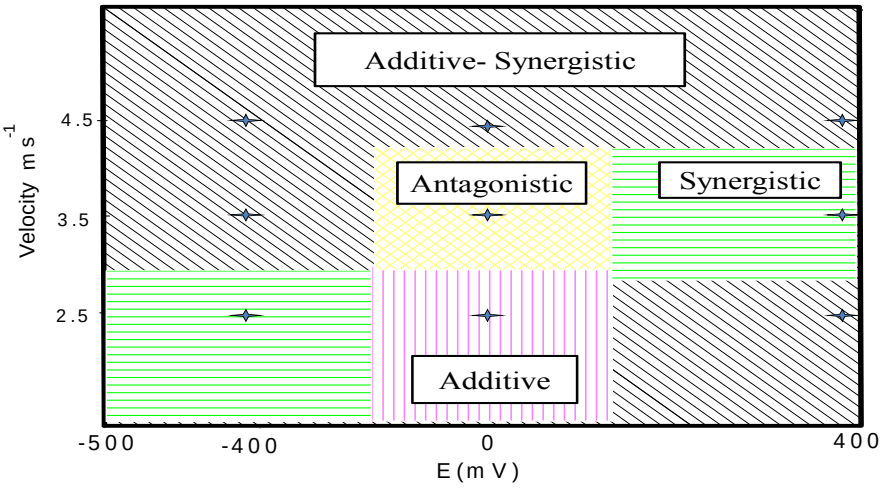

(a)

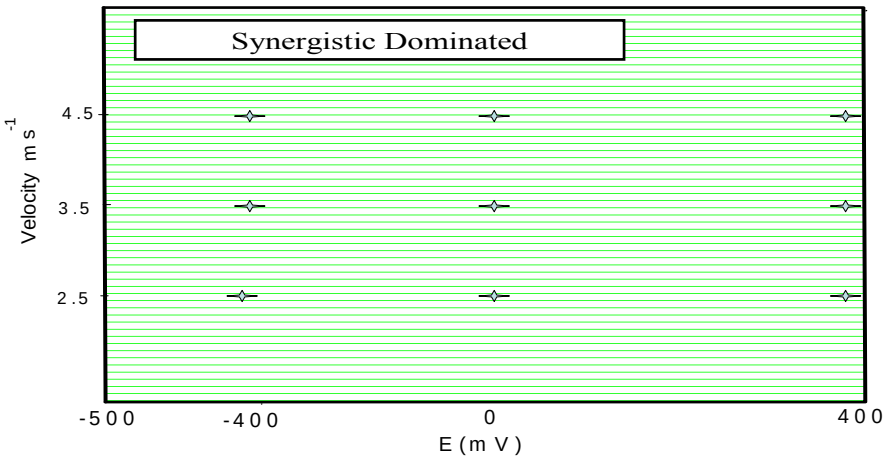

(b)

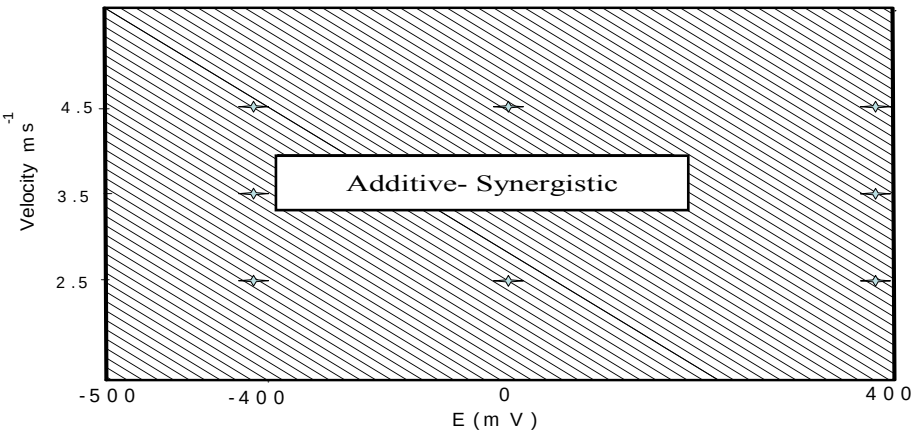

(c)

Fig.5.50: Erosion-corrosion additive-synergism maps for carbon steel at impact angle 45° and particle size 150-300µm in (a) water (b) crude oil (c) oil /20% water.

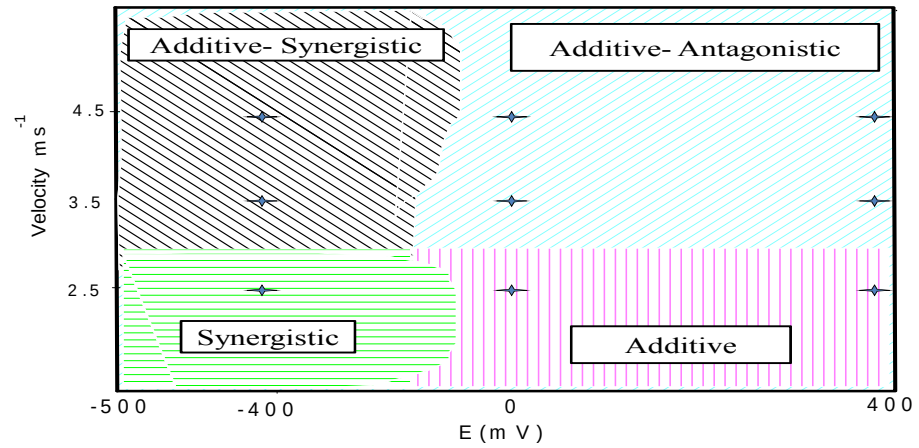

(a)

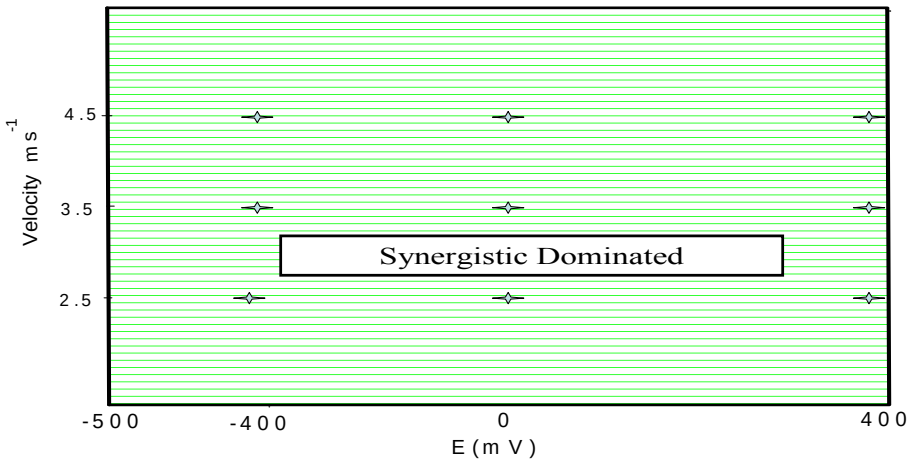

(b)

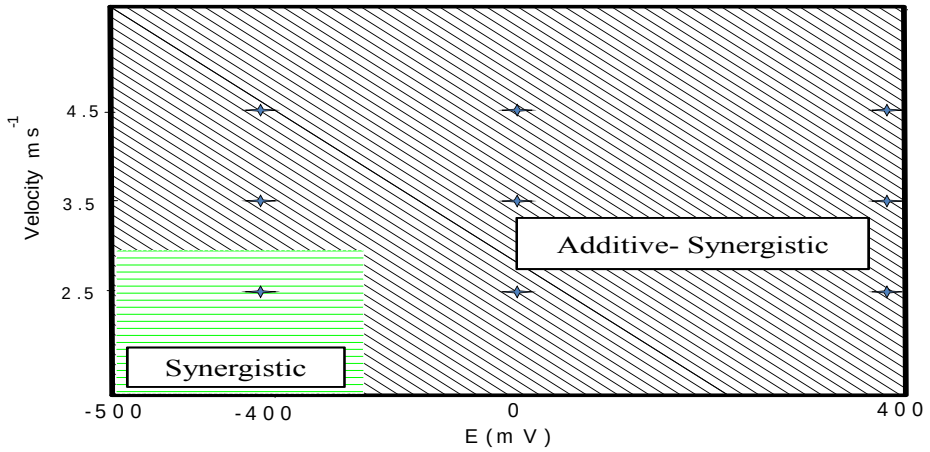

(c)

Fig.5.51: Erosion-corrosion additive-synergism maps for carbon steel at impact angle 90° and particle size 150-300µm in (a) water (b) crude oil (c) oil /20% water

Tables.5.28: Erosion-corrosion mechanism maps for carbon steel in water at 2.5 m s^{-1} and particle size 600-710μm (a) 15° (b) 30° (c) 45°

(a)

Applied potential mV	Ke(mg cm^{-2} h^{-1})	Kc(mg cm^{-2} h^{-1})	Ke/Kc
-400	2.59	1.72	1.506
-200	2.45	1.78	1.376
0	2.58	1.82	1.418
200	2.43	1.95	1.246
400	2.44	1.97	1.239

(b)

Applied potential mV	Ke(mg cm^{-2} h^{-1})	Kc(mg cm^{-2} h^{-1})	Ke/Kc
-400	2.5	1.5	1.667
-200	2.59	1.72	1.506
0	2.38	1.83	1.301
200	2.56	1.94	1.32
400	2.16	2.07	1.043

(c)

Applied potential mV	Ke(mg cm^{-2} h^{-1})	Kc(mg cm^{-2} h^{-1})	Ke/Kc
-400	2.39	2.21	1.08
-200	2.17	2.43	0.89
0	1.7	2.71	0.63
200	2.58	2.03	1.27
400	3.16	2.16	1.46

Tables.5. 29: Erosion-corrosion mechanism maps for carbon steel in water at 2.5 m s^{-1} and particle size 600-710µm (a) 60° (b) 75° (c) 90°

(a)

Applied potential mV	Ke(mg cm^{-2} h^{-1})	Kc(mg cm^{-2} h^{-1})	Ke/Kc
-400	2.16	2.04	1.059
-200	1.89	2.12	0.892
0	1.25	2.25	0.556
200	1.5	2.71	0.554
400	2.57	1.93	1.332

(b)

Applied potential mV	Ke(mg cm^{-2} h^{-1})	Kc(mg cm^{-2} h^{-1})	Ke/Kc
-400	1.96	1.93	1.02
-200	1.57	2.24	0.70
0	2.16	2.46	0.88
200	2.26	1.34	1.69
400	0.71	2.74	0.26

(c)

Applied potential mV	Ke(mg cm^{-2} h^{-1})	Kc(mg cm^{-2} h^{-1})	Ke/Kc
-400	2.5	1.71	1.46
-200	1.9	2.21	0.86
0	1.57	2.73	0.58
200	1.22	2.78	0.44
400	1.48	2.53	0.59

Tables.5. 30: Erosion-corrosion mechanism maps for carbon steel in crude oil at 2.5 m s^{-1} and particle size 600-710µm (a) 15° (b) 30° (c) 45°

(a)

Applied potential mV	Ke(mg cm^{-2} h^{-1})	Kc(mg cm^{-2} h^{-1})	Ke/Kc
-400	2.48	2.11E-02	117.48
-200	2.58	1.63E-02	158.51
0	3.38	1.85E-02	182.84
200	3.76	1.94E-02	193.845
400	4.29	2.14E-02	200.40

(b)

Applied potential mV	Ke(mg cm^{-2} h^{-1})	Kc(mg cm^{-2} h^{-1})	Ke/Kc
-400	1.99	1.22E-02	162.93
-200	2.38	1.65E-02	144.45
0	3.10	1.71E-02	181.46
200	3.49	1.49E-02	233.9
400	3.52	1.52E-02	231.24

(c)

Applied potential mV	Ke(mg cm^{-2} h^{-1})	Kc(mg cm^{-2} h^{-1})	Ke/Kc
-400	2	1.02E-02	196.06
-200	2.69	1.47E-02	182.67
0	3.13	1.39E-02	224.9
200	3.55	1.51E-02	234.76
400	4.19	1.48E-02	282.78

Tables.5. 31: Erosion-corrosion mechanism maps for carbon steel in crude oil at 2.5 m s^{-1} and particle size 600-710µm (a) 60° (b) 75° (c) 90°

(a)

Applied potential mV	Ke(mg cm^{-2} h^{-1})	Kc(mg cm^{-2} h^{-1})	Ke/Kc
-400	2.08	1.85E-02	112.51
-200	2.78	1.93E-02	144.08
0	3.38	1.90E-02	177.95
200	3.1	2.00E-02	155
400	3.98	2.31E-02	172.16

(b)

Applied potential mV	Ke(mg cm^{-2} h^{-1})	Kc(mg cm^{-2} h^{-1})	Ke/Kc
-400	2.1	2.02E-02	103.95
-200	3.14	2.12E-02	148.06
0	3.24	1.98E-02	163.65
200	3.58	2.33E-02	153.51
400	3.69	2.40E-02	153.58

(c)

Applied potential mV	Ke(mg cm^{-2} h^{-1})	Kc(mg cm^{-2} h^{-1})	Ke/Kc
-400	2.092	1.81E-02	115.57
-200	3.13	1.97E-02	158.9
0	3.38	2.00E-02	169
200	3.98	2.42E-02	164.29
400	4.08	2.65E-02	154.09

Tables.5.32: Erosion-corrosion mechanism maps for carbon steel in in oil /20% water at 2.5 m s^{-1} and particle size 600-710µm (a) 15° (b) 30° (c) 45°

(a)

Applied potential mV	Ke(mg cm^{-2} h^{-1})	Kc(mg cm^{-2} h^{-1})	Ke/Kc
-400	2.31	0.8	2.9
-200	2.34	0.8	2.9
0	2.06	0.8	2.64
200	2.1	0.68	3.1
400	1.89	0.71	2.66

(b)

Applied potential mV	Ke(mg cm^{-2} h^{-1})	Kc(mg cm^{-2} h^{-1})	Ke/Kc
-400	1.92	0.78	2.46
-200	2.41	0.791	3.1
0	2.71	0.8	3.39
200	2.35	0.9	2.611
400	2.68	0.72	3.72

(c)

Applied potential mV	Ke(mg cm^{-2} h^{-1})	Kc(mg cm^{-2} h^{-1})	Ke/Kc
-400	2.16	0.84	2.57
-200	2.496	0.714	3.496
0	2.84	0.76	3.737
200	2.89	0.81	3.568
400	2.1	0.9	2.333

Tables.5.33:Erosion-corrosion mechanism maps for carbon steel in oil /20% water at 2.5 m s^{-1} and particle size 600-710µm (a) 60° (b) 75° (c) 90°

(a)

Applied potential mV	Ke(mg cm^{-2} h^{-1})	Kc(mg cm^{-2} h^{-1})	Ke/Kc
-400	2.42	0.78	3.103
-200	2.439	0.801	3.045
0	2.68	0.82	3.268
200	2.64	0.96	2.75
400	2.02	0.78	2.59

(b)

Applied potential mV	Ke(mg cm^{-2} h^{-1})	Kc(mg cm^{-2} h^{-1})	Ke/Kc
-400	1.96	1	1.96
-200	2.61	0.89	2.933
0	2.1	0.9	2.333
200	2.42	0.45	5.378
400	2.23	0.67	3.328

(c)

Applied potential mV	Ke(mg cm^{-2} h^{-1})	Kc(mg cm^{-2} h^{-1})	Ke/Kc
-400	2.18	0.9	2.422
-200	1.87	0.91	2.055
0	2.13	0.78	2.731
200	2.27	0.73	3.11
400	2.4	0.8	3

Tables.5. 34: Erosion-corrosion mechanism maps for carbon steel in water at 3.5 m s^{-1} and particle size 600-710µm (a) 15° (b) 30° (c) 45°

(a)

Applied potential mV	Ke(mg cm^{-2} h^{-1})	Kc(mg cm^{-2} h^{-1})	Ke/Kc
-400	1.4	4.12	1.506
-200	1.77	4.21	0.42
0	1.65	4.38	0.377
200	1.73	4.48	0.386
400	3.49	4.51	0.774

(b)

Applied potential mV	Ke(mg cm^{-2} h^{-1})	Kc(mg cm^{-2} h^{-1})	Ke/Kc
-400	1.81	4.21	0.43
-200	2.11	3.91	0.54
0	2.42	3.78	0.64
200	3.4	4.1	0.829
400	3.57	4.23	0.844

(c)

Applied potential mV	Ke(mg cm^{-2} h^{-1})	Kc(mg cm^{-2} h^{-1})	Ke/Kc
-400	2.43	4.02	0.604
-200	1.89	5	0.378
0	1.99	5.04	0.395
200	3.88	4.12	0.942
400	3.89	4.32	0.9

Tables.5. 35: Erosion-corrosion mechanism maps for carbon steel in water at 3.5 m s^{-1} and particle size 600-710µm (a) 60° (b) 75° (c) 90°

(a)

Applied potential mV	Ke(mg cm^{-2} h^{-1})	Kc(mg cm^{-2} h^{-1})	Ke/Kc
-400	2.39	3.91	0.61
-200	2.2	4.25	0.52
0	2.7	4.51	0.6
200	2.83	5.01	0.57
400	2.79	5.21	0.54

(b)

Applied potential mV	Ke(mg cm^{-2} h^{-1})	Kc(mg cm^{-2} h^{-1})	Ke/Kc
-400	0.53	5.32	0.1
-200	1.59	4.61	0.35
0	2.8	4.07	0.69
200	2.8	4.5	0.62
400	2.99	4.85	0.62

(c)

Applied potential mV	Ke(mg cm^{-2} h^{-1})	Kc(mg cm^{-2} h^{-1})	Ke/Kc
-400	1.9	4.31	0.44
-200	1.97	4.38	0.45
0	2.48	5	0.5
200	2.5	5.52	0.45
400	2.11	5.81	0.36

Tables.5. 36: Erosion-corrosion mechanism maps for carbon steel crude oil at 3.5 m s^{-1} and particle size 600-710µm (a) 15° (b) 30° (c) 45°

(a)

Applied potential mV	Ke(mg cm^{-2} h^{-1})	Kc(mg cm^{-2} h^{-1})	Ke/Kc
-400	4.56	1.89E-02	241.33
-200	5.1	2.09E-02	243.98
0	5.07	2.59E-02	195.91
200	5.57	2.61E-02	213.56
400	6.97	2.58E-02	270.32

(b)

Applied potential mV	Ke(mg cm^{-2} h^{-1})	Kc(mg cm^{-2} h^{-1})	Ke/Kc
-400	3.97	2.62E-02	151.67
-200	4.17	3.02E-02	138.07
0	4.47	2.70E-02	165.67
200	5.17	2.78E-02	186.05
400	6.37	3.08E-02	206.79

(c)

Applied potential mV	Ke(mg cm^{-2} h^{-1})	Kc(mg cm^{-2} h^{-1})	Ke/Kc
-400	4.48	2.00E-02	224
-200	4.58	2.21E-02	207.14
0	4.98	1.81E-02	275.24
200	5.85	1.92E-02	304.73
400	6.18	2.02E-02	305.93

Tables.5.37: Erosion-corrosion mechanism maps for carbon steel in crude oil at 3.5 m s^{-1} and particle size 600-710µm (a)60° (b) 75° (c) 90°

(a)

Applied potential mV	Ke(mg cm^{-2} h^{-1})	Kc(mg cm^{-2} h^{-1})	Ke/Kc
-400	4.19	2.43E-02	172.25
-200	4.68	2.53E-02	184.77
0	4.87	2.61E-02	186.74
200	4.98	1.99E-02	250.26
400	4.978	2.19E-02	227.31

(b)

Applied potential mV	Ke(mg cm^{-2} h^{-1})	Kc(mg cm^{-2} h^{-1})	Ke/Kc
-400	4.69	1.92E-02	244.31
-200	4.83	2.02E-02	239.1
0	4.84	2.76E-02	175.45
200	5.09	3.76E-02	135.44
400	5.97	2.96E-02	201.70

(c)

Applied potential mV	Ke(mg cm^{-2} h^{-1})	Kc(mg cm^{-2} h^{-1})	Ke/Kc
-400	4.75	2.62E-02	181.44 1
-200	4.97	2.74E-02	181.48
0	5.18	2.91E-02	178.04
200	5.75	3.01E-02	191.03
400	6.47	3.21E-02	201.49

Tables.5. 38: Erosion-corrosion mechanism maps for carbon steel in oil /20% water at 3.5 m s^{-1} and particle size 600-710µm (a) 15° (b) 30° (c) 45°

(a)

Applied potential mV	Ke(mg cm^{-2} h^{-1})	Kc(mg cm^{-2} h^{-1})	Ke/Kc
-400	4.16	0.84	4.95
-200	5.02	0.98	5.12
0	5.11	0.89	5.74
200	5.47	0.93	5.88
400	6.01	1.2	5

(b)

Applied potential mV	Ke(mg cm^{-2} h^{-1})	Kc(mg cm^{-2} h^{-1})	Ke/Kc
-400	3.71	0.89	4.169
-200	4.56	1	4.56
0	3.9	1.2	3.25
200	5.32	0.98	5.429
400	5.51	1	5.51

(c)

Applied potential mV	Ke(mg cm^{-2} h^{-1})	Kc(mg cm^{-2} h^{-1})	Ke/Kc
-400	5.2	0.9	5.78
-200	5.3	0.9	5.9
0	5.2	1	5.2
200	5.3	1.2	4.4
400	5.4	1.3	4.15

Tables.5. 39: Erosion-corrosion mechanism maps for carbon steel in oil /20% water at 3.5 m s^{-1} and particle size 600-710µm (a) 60° (b) 75° (c) 90°

(a)

Applied potential mV	Ke(mg cm^{-2} h^{-1})	Kc(mg cm^{-2} h^{-1})	Ke/Kc
-400	4.42	0.98	4.51
-200	4.98	1.12	4.45
0	4.89	1.23	3.98
200	5.22	0.78	6.69
400	6.2	0.8	7.75

(b)

Applied potential mV	Ke(mg cm^{-2} h^{-1})	Kc(mg cm^{-2} h^{-1})	Ke/Kc
-400	4.2	1	4.2
-200	4.81	0.89	5.40
0	4.53	1	4.53
200	4.75	1.12	4.24
400	5.87	0.98	5.99

(c)

Applied potential mV	Ke(mg cm^{-2} h^{-1})	Kc(mg cm^{-2} h^{-1})	Ke/Kc
-400	5	1.1	4.55
-200	5.2	1	5.2
0	5.32	0.98	5.43
200	5.18	1.23	4.21
400	5.8	1.2	4.83

Tables.5. 40: Erosion-corrosion mechanism maps for carbon steel in water at 4.5 m s^{-1} and particle size 600-710µm (a) 15° (b) 30° (c) 45°

(a)

Applied potential mV	Ke(mg cm^{-2} h^{-1})	Kc(mg cm^{-2} h^{-1})	Ke/Kc
-400	2.99	5.72	0.523
-200	2.39	5.84	0.409
0	3.82	5.91	0.646
200	4.76	5.24	0.908
400	5.25	5.2	1.01

(b)

Applied potential mV	Ke(mg cm^{-2} h^{-1})	Kc(mg cm^{-2} h^{-1})	Ke/Kc
-400	2.87	5.93	0.48
-200	4.88	4.12	1.18
0	5.76	4.45	1.29
200	5.51	4.81	1.15
400	5.62	4.9	1.15

(c)

Applied potential mV	Ke(mg cm^{-2} h^{-1})	Kc(mg cm^{-2} h^{-1})	Ke/Kc
-400	4.48	4.72	0.95
-200	4.17	5.85	0.71
0	5.44	5.01	1.09
200	5.74	5.32	1.1
400	6.11	5.73	1.1

Tables.5. 41: Erosion-corrosion mechanism maps for carbon steel in water at 4.5 m s^{-1} and particle size 600-710µm (a) 60° (b) 75° (c) 90°

(a)

Applied potential mV	Ke(mg cm^{-2} h^{-1})	Kc(mg cm^{-2} h^{-1})	Ke/Kc
-400	3.3	5.4	0.61
-200	4.65	5.67	0.82
0	4.71	5.56	0.85
200	4.88	5.87	0.83
400	6.05	5.07	1.19

(b)

Applied potential mV	Ke(mg cm^{-2} h^{-1})	Kc(mg cm^{-2} h^{-1})	Ke/Kc
-400	3	5.94	0.51
-200	3.45	5.89	0.586
0	4.11	6.21	0.66
200	4.52	6	0.75
400	3.16	6.84	0.46

(c)

Applied potential mV	Ke(mg cm^{-2} h^{-1})	Kc(mg cm^{-2} h^{-1})	Ke/Kc
-400	4.69	4.78	0.98
-200	5.48	4.83	1.14
0	3.47	6.03	0.58
200	4.19	6.13	0.68
400	4.29	6.73	0.64

Tables.5. 42: Erosion-corrosion mechanism maps for carbon steel in crude oil at 4.5 m s^{-1} and particle size 600-710µm (a) 15° (b) 30° (c) 45°

(a)

Applied potential mV	Ke(mg cm^{-2} h^{-1})	Kc(mg cm^{-2} h^{-1})	Ke/Kc
-400	7.47	2.88E-02	259
-200	7.24	3.78E-02	192
0	7.96	4.28E-02	186
200	8.43	4.50E-02	187
400	8.07	4.78E-02	169

(b)

Applied potential mV	Ke(mg cm^{-2} h^{-1})	Kc(mg cm^{-2} h^{-1})	Ke/Kc
-400	6.177	3.28E-02	188
-200	6.966	3.41E-02	204
0	7.44	4.01E-02	186
200	7.941	3.91E-02	203
400	7.955	4.51E-02	176

(c)

Applied potential mV	Ke(mg cm^{-2} h^{-1})	Kc(mg cm^{-2} h^{-1})	Ke/Kc
-400	7.1	2.52E-02	282
-200	7	2.98E-02	235
0	7.42	3.08E-02	241
200	7.74	3.58E-02	216
400	8.41	4.00E-02	210

Tables.5. 43: Erosion-corrosion mechanism maps for carbon steel in crude oil at 4.5 m s^{-1} and particle size 600-710µm (a) 60° (b) 75° (c) 90°

(a)

Applied potential mV	Ke(mg cm^{-2} h^{-1})	Kc(mg cm^{-2} h^{-1})	Ke/Kc
-400	6.7	3.19E-02	209
-200	6.83	4.19E-02	163
0	6.96	3.89E-02	179
200	7.1	4.09E-02	174
400	8.1	5.19E-02	155

(b)

Applied potential mV	Ke(mg cm^{-2} h^{-1})	Kc(mg cm^{-2} h^{-1})	Ke/Kc
-400	6.97	3.03E-02	230
-200	7.02	3.48E-02	202
0	6.66	3.88E-02	172
200	6.962	3.78E-02	184
400	7.848	4.18E-02	188

(c)

Applied potential mV	Ke(mg cm^{-2} h^{-1})	Kc(mg cm^{-2} h^{-1})	Ke/Kc
-400	7.14	4.12E-02	173
-200	7.76	3.99E-02	194
0	7.40	4.56E-02	162
200	7.95	4.78E-02	166
400	8.18	5.18E-02	158

Tables.5. 44: Erosion-corrosion mechanism maps for carbon steel in oil /20% water at 4.5 m s^{-1} and particle size 600-710µm (a) 15° (b) 30° (c) 45°

(a)

Applied potential mV	Ke(mg cm^{-2} h^{-1})	Kc(mg cm^{-2} h^{-1})	Ke/Kc
-400	6.45	1.35	4.8
-200	6.7	1.3	5.15
0	7.28	1.5	4.85
200	7.34	1.68	4.37
400	7.61	1.9	4

(b)

Applied potential mV	Ke(mg cm^{-2} h^{-1})	Kc(mg cm^{-2} h^{-1})	Ke/Kc
-400	6.07	1.21	5.
-200	6.98	1.32	5.3
0	7.08	1.32	5.4
200	7.4	1.6	4.7
400	7.67	1.85	4.15

(c)

Applied potential mV	Ke(mg cm^{-2} h^{-1})	Kc(mg cm^{-2} h^{-1})	Ke/Kc
-400	6.66	1.34	4.97
-200	6.7	1.5	4.47
0	7.54	1.4	5.39
200	7.76	1.54	5.04
400	7.42	1.7	4.37

Tables.5. 45: Erosion-corrosion mechanism maps for carbon steel in oil /20% water at 4.5 m s^{-1} and particle size 600-710µm (a) 60° (b) 75° (c) 90°

(a)

Applied potential mV	Ke(mg cm^{-2} h^{-1})	Kc(mg cm^{-2} h^{-1})	Ke/Kc
-400	5.82	1.2	4.85
-200	6.51	1.1	5.92
0	6.79	1.21	5.61
200	8.68	1.32	6.58
400	7.32	1.68	4.36

(b)

Applied potential mV	Ke(mg cm^{-2} h^{-1})	Kc(mg cm^{-2} h^{-1})	Ke/Kc
-400	6.6	1.4	4.72
-200	6.76	1.3	5.2
0	6.6	1.3	5.08
200	7.57	1.4	5.41
400	7.12	1.76	4.05

(c)

Applied potential mV	Ke(mg cm^{-2} h^{-1})	Kc(mg cm^{-2} h^{-1})	Ke/Kc
-400	6.75	1.45	4.66
-200	7.1	1.5	4.73
0	7.12	1.6	4.45
200	7.9	1.7	4.65
400	7.98	1.89	4.22

Tables.5. 46:Erosion-corrosion mechanism maps for carbon steel in water at 2.5 m s^{-1} and particle size 150-300μm (a) 15° (b) 45° (c) 90°.

(a)

Applied potential mV	Ke(mg cm^{-2} h^{-1})	Kc(mg cm^{-2} h^{-1})	Ke/Kc
-400	1.5	2.5	0.6
0	0.47	3.74	0.126
400	0.46	3.84	0.12

(b)

Applied potential mV	Ke(mg cm^{-2} h^{-1})	Kc(mg cm^{-2} h^{-1})	Ke/Kc
-400	1.59	2.6	0.61
0	0.7	3.8	0.18
400	0.61	3.9	0.39

(c)

Applied potential mV	Ke(mg cm^{-2} h^{-1})	Kc(mg cm^{-2} h^{-1})	Ke/Kc
-400	1.14	2.4	0.48
0	0.46	3.84	0.12
400	0.5	3.9	0.13

Tables.5. 47: Erosion-corrosion mechanism maps for carbon steel in water at 3.5 m s^{-1} and particle size 150-300µm (a) 15° (b) 45° (c) 90°.

(a)

Applied potential mV	Ke(mg cm^{-2} h^{-1})	Kc(mg cm^{-2} h^{-1})	Ke/Kc
-400	1.22	3.98	0.31
0	1.5	4	0.38
400	2	4.2	0.48

(b)

Applied potential mV	Ke(mg cm^{-2} h^{-1})	Kc(mg cm^{-2} h^{-1})	Ke/Kc
-400	1.51	4.2	0.36
0	1.05	5	0.21
400	2	5	0.4

(c)

Applied potential mV	Ke(mg cm^{-2} h^{-1})	Kc(mg cm^{-2} h^{-1})	Ke/Kc
-400	1.1	4.5	0.24
0	0.6	4.81	0.13
400	0.6	5.4	0.11

Tables.5. 48: Erosion-corrosion mechanism maps for carbon steel in water at 4.5 m s^{-1} and particle size 150-300µm (a) 15° (b) 45° (c) 90°.

(a)

Applied potential mV	Ke(mg cm^{-2} h^{-1})	Kc(mg cm^{-2} h^{-1})	Ke/Kc
-400	2	5.5	0.36
0	1.01	6.2	0.16
400	0.95	6.5	0.15

(b)

Applied potential mV	Ke(mg cm^{-2} h^{-1})	Kc(mg cm^{-2} h^{-1})	Ke/Kc
-400	2.3	5.5	0.42
0	2.11	5.89	0.36
400	2.48	6.3	0.39

(c)

Applied potential mV	Ke(mg cm^{-2} h^{-1})	Kc(mg cm^{-2} h^{-1})	Ke/Kc
-400mv	1.6	5.7	0.28
0mv	0.65	6.4	0.10
400mv	1	7	0.14

Tables.5. 49: Erosion-corrosion mechanism maps for carbon steel in crude oil at 2.5 m s^{-1} and particle size 150-300µm (a) 15° (b) 45° (c) 90°.

(a)

Applied potential mV	Ke(mg cm^{-2} h^{-1})	Kc(mg cm^{-2} h^{-1})	Ke/Kc
-400	1.43	3.21E-01	4.5
0	1.46	3.95E-01	3.68
400	1.56	4.24E-01	3.66

(b)

Applied potential mV	Ke(mg cm^{-2} h^{-1})	Kc(mg cm^{-2} h^{-1})	Ke/Kc
-400	1.66	3.42E-01	4.85
0	1.77	3.40E-01	5.20
400	1.95	3.57E-01	5.45

(c)

Applied potential mV	Ke(mg cm^{-2} h^{-1})	Kc(mg cm^{-2} h^{-1})	Ke/Kc
-400	1.06	5.91E-01	1.79
0	1.44	4.10E-01	3.51
400	1.73	4.70E-01	3.68

Tables.5. 50: Erosion-corrosion mechanism maps for carbon steel in crude oil at 3.5 m s^{-1} and particle size 150-300µm (a) 15° (b) 45° (c) 90°.

(a)

Applied potential mV	Ke(mg cm^{-2} h^{-1})	Kc(mg cm^{-2} h^{-1})	Ke/Kc
-400	3.05	4.00E-01	7.63
0m	3.22	5.32E-01	6.1
400	3.23	6.12E-01	5.27

(b)

Applied potential mV	Ke(mg cm^{-2} h^{-1})	Kc(mg cm^{-2} h^{-1})	Ke/Kc
-400	3.4	5.00E-01	6.8
0	3.41	4.40E-01	7.75
400	3.43	5.70E-01	6.018

(c)

Applied potential mV	Ke(mg cm^{-2} h^{-1})	Kc(mg cm^{-2} h^{-1})	Ke/Kc
-400	2.71	5.41E-01	5
0	2.9	6.00E-01	4.83
400	3.17	6.30E-01	5

Tables.5. 51: Erosion-corrosion mechanism maps for carbon steel in crude oil at 4.5 m s^{-1} and particle size 150-300µm (a) 15° (b) 45° (c) 90°.

(a)

Applied potential mV	Ke(mg cm^{-2} h^{-1})	Kc(mg cm^{-2} h^{-1})	Ke/Kc
-400	4.25	7.50E-01	5.67
0	4.65	8.53E-01	5.44
400	4.55	9.00E-01	5.1

(b)

Applied potential mV	Ke(mg cm^{-2} h^{-1})	Kc(mg cm^{-2} h^{-1})	Ke/Kc
-400	4.62	8.00E-01	5.78
0	4.859	8.91E-01	5.45
400	4.9	1.00E+00	4.9

(c)

Applied potential mV	Ke(mg cm^{-2} h^{-1})	Kc(mg cm^{-2} h^{-1})	Ke/Kc
-400	3.83	8.23E-01	4.65
0	4.33	8.68E-01	4.99
400	4.2	1.20E+00	3.5

Tables.5.52: Erosion-corrosion mechanism maps for carbon steel in oil /20% water at 2.5 m s^{-1} and particle size 150-300µm (a) 15° (b) 45° (c) 90°.

(a)

Applied potential mV	Ke(mg cm^{-2} h^{-1})	Kc(mg cm^{-2} h^{-1})	Ke/Kc
-400	1.19	1.11E+00	1.07
0	1.1	1.51E+00	0.72
400	0.98	1.77E+00	0.55

(b)

Applied potential mV	Ke(mg cm^{-2} h^{-1})	Kc(mg cm^{-2} h^{-1})	Ke/Kc
-400	1.29	1.21E+00	1.06
0	0.95	1.75E+00	0.54
400	1.55	1.85E+00	0.84

(c)

Applied potential mV	Ke(mg cm^{-2} h^{-1})	Kc(mg cm^{-2} h^{-1})	Ke/Kc
-400	1.4	1.03E+00	1.36
0	0.85	1.65E+00	0.51
400	0.82	1.83E+00	0.45

Tables.5. 53: Erosion-corrosion mechanism maps for carbon steel in oil /20% water at 3.5 m s^{-1} and particle size 150-300µm (a) 15° (b) 45° (c) 90°.

(a)

Applied potential mV	Ke(mg cm^{-2} h^{-1})	Kc(mg cm^{-2} h^{-1})	Ke/Kc
-400	1.55	2.46E+00	0.63
0	1.33	2.97E+00	0.45
400	1.73	3.02E+00	0.57

(b)

Applied potential mV	Ke(mg cm^{-2} h^{-1})	Kc(mg cm^{-2} h^{-1})	Ke/Kc
-400	1.26	2.95E+00	0.43
0	1.46	3.00E+00	0.49
400	1.48	3.32E+00	0.45

(c)

Applied potential mV	Ke(mg cm^{-2} h^{-1})	Kc(mg cm^{-2} h^{-1})	Ke/Kc
-400	1.73	2.26E+00	0.76
0	1.15	2.85E+00	0.40
400	1.57	2.94E+00	0.53

Tables.5. 54: Erosion-corrosion mechanism maps for carbon steel in oil /20% water at 4.5 m s^{-1} and particle size 150-300µm (a) 15° (b) 45° (c) 90°.

(a)

Applied potential mV	Ke(mg cm^{-2} h^{-1})	Kc(mg cm^{-2} h^{-1})	Ke/Kc
-400	2.53	3.37E+00	0.75
0	2.4	4.00E+00	0.6
400	2.42	4.23E+00	0.57

(b)

Applied potential mV	Ke(mg cm^{-2} h^{-1})	Kc(mg cm^{-2} h^{-1})	Ke/Kc
-400	2.4	3.60E+00	0.67
0	2.05	4.45E+00	0.46
400	2.23	4.55E+00	0.49

(c)

Applied potential mV	Ke(mg cm^{-2} h^{-1})	Kc(mg cm^{-2} h^{-1})	Ke/Kc
-400	1.98	3.52E+00	0.56
0	1.9	4.30E+00	0.44
400	2.08	4.42E+00	0.47

Tables.5. 55: Erosion-corrosion additive -synergism maps for carbon steel in water at 2.5 m s^{-1} and particle size 600-710µm (a) 15° (b) 30° (c) 45°

(a)

Applied potential mV	Δke(mg cm^{-2} h^{-1})	Δkc(mg cm^{-2} h^{-1})	Δke/Δkc
-400	0.89	-0.21	-4.16
-200	0.75	-0.14	-5.36
0	0.88	-0.16	-5.5
200	0.73	-0.05	-14.6
400	0.74	-0.07	-10.57

(b)

Applied potential mV	Δke(mg cm^{-2} h^{-1})	Δkc(mg cm^{-2} h^{-1})	Δke/Δkc
-400	0.9	-0.37	-2.43
-200	0.99	0.04	24.75
0	0.78	-0.18	-4.33
200	0.96	-0.16	-6
400	0.56	0.04	14

(c)

Applied potential mV	Δke(mg cm^{-2} h^{-1})	Δkc(mg cm^{-2} h^{-1})	Δke/Δkc
-400	-0.11	0.16	-0.69
-200	-0.33	0.53	-0.62
0	-0.8	1.47	-0.54
200	0.08	0.08	1
400	1.54	0.31	4.97

Tables.5. 56: Erosion-corrosion additive -synergism maps for carbon steel in water at 2.5 m s^{-1} and particle size 600-710µm (a) 60° (b) 75° (c) 90°

(a)

Applied potential mV	Δke(mg cm^{-2} h^{-1})	Δkc(mg cm^{-2} h^{-1})	Δke/Δkc
-400	0.76	0.03	25.33
-200	0.49	-0.18	-2.72
0	-0.15	0.08	-1.88
200	0.1	0.63	0.16
400	1.17	-0.47	-2.49

(b)

Applied potential mV	Δke(mg cm^{-2} h^{-1})	Δkc(mg cm^{-2} h^{-1})	Δke/Δkc
-400	0.86	-0.22	-3.91
-200	0.47	0.09	5.22
0	1.06	-0.24	-4.42
200	1.16	-0.96	-1.21
400	-0.39	0.32	-1.22

(c)

Applied potential mV	Δke(mg cm^{-2} h^{-1})	Δkc(mg cm^{-2} h^{-1})	Δke/Δkc
-400	0.9	-0.2	-4.5
-200	0.3	0.28	1.07
0	-0.03	0.48	-0.06
200	-0.38	0.5	-0.76
400	-0.12	0.1	-1.2

Tables.5. 57: Erosion-corrosion additive -Synergism maps for carbon steel in water at 3.5 m s^{-1} and particle size 600-710µm (a) 15° (b) 30° (c) 45°

(a)

Applied potential	Δke(mg cm^{-2} h^{-1})	Δkc(mg cm^{-2} h^{-1})	Δke/Δkc
-400	-0.6	1.1	-0.55
-200	-0.23	0.73	-0.32
0	-0.35	0.86	-0.41
200	-0.27	0.87	-0.31
400	1.49	0.51	2.92

(b)

Applied potential	Δke(mg cm^{-2} h^{-1})	Δkc(mg cm^{-2} h^{-1})	Δke/Δkc
-400	-0.06	0.8	-0.075
-200	0.24	-0.29	-0.83
0	0.55	0.17	3.24
200	1.53	0.6	2.55
400	1.7	0.75	2.27

(c)

Applied potential	Δke(mg cm^{-2} h^{-1})	Δkc(mg cm^{-2} h^{-1})	Δke/Δkc
-400	-0.77	0.22	-3.5
-200	-1.31	-0.07	-1.32
0	-1.21	0.23	-5.26
200	0.68	0.02	34
400	0.69	-0.49	-1.41

Tables.5. 58: Erosion-corrosion additive -synergism maps for carbon steel in water at 3.5 m s^{-1} and particle size 600-710µm (a) 60° (b) 75° (c) 90°

(a)

Applied potential	Δke(mg cm^{-2} h^{-1})	Δkc(mg cm^{-2} h^{-1})	Δke/Δkc
-400	0.59	0.5	1.18
-200	0.4	0.75	0.53
0	0.9	0.82	1.097
200	1.03	0.41	2.51
400	0.99	0.91	1.09

(b)

Applied potential	Δke(mg cm^{-2} h^{-1})	Δkc(mg cm^{-2} h^{-1})	Δke/Δkc
-400	-1.17	1.32	-0.89
-200	-0.11	0.51	-0.22
0	1.1	-0.6	-1.83
200	1.1	0.7	1.57
400	1.29	0.05	25.8

(c)

Applied potential	Δke(mg cm^{-2} h^{-1})	Δkc(mg cm^{-2} h^{-1})	Δke/Δkc
-400	-0.3	0.21	-1.43
-200	-0.23	0.48	-0.48
0	0.28	0.99	0.28
200	0.3	1.61	0.19
400	-0.09	1.49	-0.06

Tables.5. 59: Erosion-corrosion additive -synergism maps for carbon steel in water at 4.5 m s^{-1} and particle size 600-710µm (a) 15° (b) 30° (c) 45°

(a)

Applied potential	Δke(mg cm^{-2} h^{-1})	Δkc(mg cm^{-2} h^{-1})	Δke/Δkc
-400	-0.01	1.22	-0.0082
-200	-0.61	1.23	-0.496
0	0.82	1.1	0.75
200	1.76	0.26	6.771
400	2.25	0.12	18.75

(b)

Applied potential	Δke(mg cm^{-2} h^{-1})	Δkc(mg cm^{-2} h^{-1})	Δke/Δkc
-400	-0.11	1.11	-0.099
-200	1.9	-0.81	-2.35
0	2.78	-0.22	-12.64
200	2.53	-0.2	-12.65
400	2.64	-0.12	-22

(c)

Applied potential	Δke(mg cm^{-2} h^{-1})	Δkc(mg cm^{-2} h^{-1})	Δke/Δkc
-400	0.58	-0.29	-2
-200	0.27	0.12	2.25
0	1.54	-0.38	-4.05
200	1.84	0.28	6.57
400	2.21	0.84	2.63

Tables.5. 60: Erosion-corrosion additive -synergism maps for carbon steel in water at 4.5 m s^{-1} and particle size 600-710µm (a) 60° (b) 75° (c) 90°

(a)

Applied potential mV	Δke(mg cm^{-2} h^{-1})	Δkc(mg cm^{-2} h^{-1})	Δke/Δkc
-400	0.2	0.59	0.34
-200	1.55	1.09	1.42
0	1.61	0.25	6.44
200	1.78	0.39	4.56
400	2.95	0.11	26.82

(b)

Applied potential mV	Δke(mg cm^{-2} h^{-1})	Δkc(mg cm^{-2} h^{-1})	Δke/Δkc
-400	0.7	0.71	0.986
-200	1.15	0.99	1.16
0	1.81	1.24	1.46
200	2.22	1.04	2.13
400	0.86	1.74	0.49

(c)

Applied potential mV	Δke(mg cm^{-2} h^{-1})	Δkc(mg cm^{-2} h^{-1})	Δke/Δkc
-400	1.79	-0.07	-25.57
-200	2.58	-0.54	-4.78
0	0.57	0.83	0.689
200	1.29	0.63	2.05
400	1.39	1.03	1.35

Tables.5. 61: Erosion-corrosion additive -Synergism maps for carbon steel in crude oil at 2.5 m s^{-1} and particle size 600-710µm (a) 15° (b) 30° (c) 45°

(a)

Applied potential mV	Δke(mg cm^{-2} h^{-1})	Δkc(mg cm^{-2} h^{-1})	Δke/Δkc
-400	0.5	1.10E-03	45
-200	0.60	2.20E-03	274
0	1.40	-6.00E-04	-2338
200	1.78	5.00E-04	3561
400	1.78	2.90E-03	613

(b)

Applied potential mV	Δke(mg cm^{-2} h^{-1})	Δkc(mg cm^{-2} h^{-1})	Δke/Δkc
-400	0.79	1.00E-03	788
-200	1.18	2.40E-03	493
0	1.90	2.00E-03	952
200	2.29	-1.20E-03	-1904
400	2.29	-1.90E-03	-1202

(c)

Applied potential mV	Δke(mg cm^{-2} h^{-1})	Δkc(mg cm^{-2} h^{-1})	Δke/Δkc
-400	0.1	-4.00E-03	-24.95
-200	0.785	-5.00E-04	-1570.6
0	1.226	-6.00E-04	-2045
200	1.645	-4.00E-04	-4112
400	1.645	-1.30E-03	-1266

Tables.5. 62: Erosion-corrosion additive -Synergism maps for carbon steel in crude oil at 2.5 m s^{-1} and particle size 600-710µm (a) 60° (b) 75° (c) 90°

(a)

Applied potential mV	Δke(mg cm^{-2} h^{-1})	Δkc(mg cm^{-2} h^{-1})	Δke/Δkc
-400	1.08	4.30E-03	251.51
-200	1.78	5.20E-03	342.44
0	2.38	4.60E-03	517.61
200	2.1	5.80E-03	362.07
400	2.1	-1.10E-03	-1906.27

(b)

Applied potential mV	Δke(mg cm^{-2} h^{-1})	Δkc(mg cm^{-2} h^{-1})	Δke/Δkc
-400	1.08	4.00E-03	269.95
-200	2.119	5.20E-03	407.46
0	2.22	4.60E-03	482.65
200	2.557	7.10E-03	360.098
400	2.556	6.80E-03	375.88

(c)

Applied potential	Δke(mg cm^{-2} h^{-1})	Δkc(mg cm^{-2} h^{-1})	Δke/Δkc
-400	0.392	-1.70E-03	-230.53
-200	1.43	7.00E-04	2043.29
0	1.68	5.00E-04	3360
200	2.276	5.20E-03	437.65
400	2.274	7.00E-03	324.79

Tables.5. 63: Erosion-corrosion additive -Synergism maps for carbon steel in crude oil at 3.5 m s^{-1} and particle size 600-710µm (a) 15° (b) 30° (c) 45°

(a)

Applied potential	Δke(mg cm^{-2} h^{-1})	Δkc(mg cm^{-2} h^{-1})	Δke/Δkc
-400	2.26	-2.60E-03	-869.65
-200	2.8	-2.20E-03	-1272
0	2.77	5.80E-03	478
200	3.27	2.00E-03	1637
400	4.67	5.00E-04	9348

(b)

Applied potential	Δke(mg cm^{-2} h^{-1})	Δkc(mg cm^{-2} h^{-1})	Δke/Δkc
-400	2.17	5.10E-03	426
-200	2.37	4.10E-03	578
0	2.67	-2.00E-04	-13365
200	3.37	-3.00E-04	-11241
400	4.57	1.60E-03	2856

(c)

Applied potential	Δke(mg cm^{-2} h^{-1})	Δkc(mg cm^{-2} h^{-1})	Δke/Δkc
-400	2.08	2.00E-04	10400
-200	2.18	3.40E-03	641
0	2.58	-1.10E-03	-2347
200	3.45	-4.00E-04	-8627
400	3.78	5.00E-04	7560

Tables.5. 64: Erosion-corrosion additive -Synergism maps for carbon steel in crude oil at 3.5 m s^{-1} and particle size 600-710µm (a) 60° (b) 75° (c) 90°

(a)

Applied potential	Δke(mg cm^{-2} h^{-1})	Δkc(mg cm^{-2} h^{-1})	Δke/Δkc
-400	2.19	-1.20E-03	-1821
-200	2.68	5.00E-04	5349
0	2.87	1.00E-04	28739
200	2.98	-5.90E-03	-505
400	2.98	-4.30E-03	-693

(b)

Applied potential	Δke(mg cm^{-2} h^{-1})	Δkc(mg cm^{-2} h^{-1})	Δke/Δkc
-400	2.84	-1.00E-03	-2841
-200	2.98	-5.80E-03	-514
0	2.99	8.00E-04	3741
200	3.24	1.06E-02	306
400	4.12	1.80E-03	2289

(c)

Applied potential	Δke(mg cm^{-2} h^{-1})	Δkc(mg cm^{-2} h^{-1})	Δke/Δkc
-400	2.70	4.70E-03	575
-200	2.92	4.90E-03	597
0	3.13	6.90E-03	454
200	3.7	7.10E-03	521
400	4.42	7.80E-03	566

Tables.5. 65: Erosion-corrosion additive -Synergism maps for carbon steel in crude oil at 4.5 m s^{-1} and particle size 600-710µm (a) 15° (b) 30° (c) 45°

(a)

Applied potential	Δke(mg cm^{-2} h^{-1})	Δkc(mg cm^{-2} h^{-1})	Δke/Δkc
-400	3.87	1.00E-03	3871
-200	3.64	5.00E-03	728
0	4.36	1.80E-03	2421
200	4.83	7.00E-03	689
400	4.47	-2.00E-04	-22361

(b)

Applied potential	Δke(mg cm^{-2} h^{-1})	Δkc(mg cm^{-2} h^{-1})	Δke/Δkc
-400	3.18	2.60E-03	1222
-200	3.97	-5.00E-04	-7932
0	4.44	5.00E-03	888
200	4.94	-1.00E-03	-4941
400	4.96	4.00E-03	1239

(c)

Applied potential	Δke(mg cm^{-2} h^{-1})	Δkc(mg cm^{-2} h^{-1})	Δke/Δkc
-400	3.9	-4.60E-03	-847
-200	3.79	-5.00E-04	-7580
0	4.22	-4.60E-03	-917
200	4.54	-1.60E-03	-2840
400	5.21	8.00E-04	6513

Tables.5. 66:Erosion-corrosion additive -Synergism maps for carbon steel in crude oil at 4.5 m s^{-1} and particle size 600-710µm (a) 60° (b) 75° (c) 90°

(a)

Applied potential	Δke(mg cm^{-2} h^{-1})	Δkc(mg cm^{-2} h^{-1})	Δke/Δkc
-400	3.77	-1.30E-03	-2899
-200	3.93	6.00E-04	6547
0	4.06	-3.20E-03	-1269
200	4.2	-2.00E-04	-20996
400	5.15	1.21E-02	425

(b)

Applied potential	Δke(mg cm^{-2} h^{-1})	Δkc(mg cm^{-2} h^{-1})	Δke/Δkc
-400	4.67	-1.50E-03	-3113
-200	4.72	2.00E-04	23576
0	4.36	3.80E-03	1148
200	4.66	-3.20E-03	-1457
400	5.55	-2.00E-04	-27741

(c)

Applied potential	Δke(mg cm^{-2} h^{-1})	Δkc(mg cm^{-2} h^{-1})	Δke/Δkc
-400	3.94	6.90E-03	571
-200	4.56	7.40E-03	616
0	4.20	1.04E-02	404
200	4.75	9.10E-03	522
400	4.98	1.01E-02	493

Tables.5. 67: Erosion-corrosion additive -synergism maps for carbon steel in oil /20% water at 2.5 m s^{-1} and particle size600-710µm (a) 15° (b) 30° (c) 45°

(a)

Applied potential	Δke(mg cm^{-2} h^{-1})	Δkc(mg cm^{-2} h^{-1})	Δke/Δkc
-400	0.33	-0.12	-2.75
-200	0.36	-0.04	-9.42
0	0.08	-0.08	-1
200	0.12	-0.03	-4
400	-0.09	-0.09	1

(b)

Applied potential	Δke(mg cm^{-2} h^{-1})	Δkc(mg cm^{-2} h^{-1})	Δke/Δkc
-400	0.72	0.22	3.27
-200	1.209	0.171	7.07
0	1.51	0.05	30.2
200	1.15	0.14	8.21
400	1.48	0.04	37

(c)

Applied potential	Δke(mg cm^{-2} h^{-1})	Δkc(mg cm^{-2} h^{-1})	Δke/Δkc
-400	0.26	0.22	1.18
-200	0.59	-0.03	-22.9
0	0.94	-0.04	-23.5
200	0.99	-0.09	-11
400	0.2	0.15	1.33

Tables.5. 68: Erosion-corrosion additive -synergism maps for carbon steel in oil /20% water at 2.5 m s^{-1} and particle size600-710µm (a)60° (b) 75° (c) 90°

(a)

Applied potential	Δke(mg cm^{-2} h^{-1})	Δkc(mg cm^{-2} h^{-1})	Δke/Δkc
-400	1.42	-0.13	-10.92
-200	1.44	-0.1	-20.86
0	1.68	0.1	24
200	1.64	0.16	10.25
400	1.02	0.13	7.85

(b)

Applied potential	Δke(mg cm^{-2} h^{-1})	Δkc(mg cm^{-2} h^{-1})	Δke/Δkc
-400	0.94	0.43	2.186
-200	1.59	0.19	8.368
0	1.08	0.1	12
200	1.4	-0.23	-6.087
400	1.21	-0.03	-40.33

(c)

Applied potential	Δke(mg cm^{-2} h^{-1})	Δkc(mg cm^{-2} h^{-1})	Δke/Δkc
-400	0.48	0.23	2.1
-200	0.17	0.3	0.57
0	0.43	-0.02	-22
200	0.57	-0.1	-10
400	0.7	0.02	35

Tables.5. 69: Erosion-corrosion additive -synergism maps for carbon steel in oil /20% water at 3.5 m s^{-1} and particle size600-710µm (a) 15° (b) 30° (c) 45°

(a)

Applied potential	Δke(mg cm^{-2} h^{-1})	Δkc(mg cm^{-2} h^{-1})	Δke/Δkc
-400	1.86	-0.07	-26.57
-200	2.72	0.11	24.727
0	2.81	-0.03	-93.67
200	3.17	0.13	24.38
400	3.71	0.2	18.55

(b)

Applied potential	Δke(mg cm^{-2} h^{-1})	Δkc(mg cm^{-2} h^{-1})	Δke/Δkc
-400	1.91	0.21	9.1
-200	2.76	0.29	9.52
0	2.1	0.36	5.83
200	3.52	-0.22	-16
400	3.71	0.1	37.1

(c)

Applied potential	Δke(mg cm^{-2} h^{-1})	Δkc(mg cm^{-2} h^{-1})	Δke/Δkc
-400	2.8	0.15	18.67
-200	2.9	0.12	24.17
0	2.8	0.1	28
200	2.9	0.2	14.5
400	3	0.46	6.52

Tables.5.70: Erosion-corrosion additive -synergism maps for carbon steel in oil /20% water at 3.5 m s^{-1} and particle size 600-710μm (a) 60° (b) 75° (c) 90°

(a)

Applied potential	Δke(mg cm^{-2} h^{-1})	Δkc(mg cm^{-2} h^{-1})	Δke/Δkc
-400	2.42	0.33	7.33
-200	2.98	0.41	7.27
0	2.89	0.44	6.57
200	3.22	-0.11	-29.27
400	4.2	-0.1	-42

(b)

Applied potential	Δke(mg cm^{-2} h^{-1})	Δkc(mg cm^{-2} h^{-1})	Δke/Δkc
-400	2.35	0.3	7.83
-200	2.96	0.09	32.89
0	2.68	-0.23	-11.65
200	2.9	-0.08	-36.25
400	4.02	-0.16	-25.13

(c)

Applied potential	Δke(mg cm^{-2} h^{-1})	Δkc(mg cm^{-2} h^{-1})	Δke/Δkc
-400	2.95	0.32	9.22
-200	3.15	0.02	157.5
0	3.27	0.2	16.35
200	3.13	0.43	7.28
400	3.75	0.36	10.42

Tables.5. 71:Erosion-corrosion additive -synergism maps for carbon steel in oil /20% water at 4.5 m s^{-1} and particle size 600-710µm (a) 15° (b) 30° (c) 45°

(a)

Applied potential	Δke(mg cm^{-2} h^{-1})	Δkc(mg cm^{-2} h^{-1})	Δke/Δkc
-400	2.85	-0.05	-57
-200	3.1	0.2	15.5
0	3.68	0.2	18.4
200	3.74	-0.02	-187
400	4.01	-0.1	-40.1

(b)

Applied potential	Δke(mg cm^{-2} h^{-1})	Δkc(mg cm^{-2} h^{-1})	Δke/Δkc
-400	3.07	-0.11	-28
-200	3.98	0.2	20.2
0	4.08	0.2	20.7
200	4.4	-0.1	-44
400	4.67	-0.13	-36

(c)

Applied potential	Δke(mg cm^{-2} h^{-1})	Δkc(mg cm^{-2} h^{-1})	Δke/Δkc
-400	3.46	0.14	24.7
-200	3.5	0.3	12
0	4.34	0.2	22
200	4.56	-0.14	-32.6
400	4.22	-0.08	-52.6

Tables.5. 72: Erosion-corrosion additive -synergism maps for carbon steel in oil /20% water at 4.5 m s^{-1} and particle size 600-710µm (a) 60° (b) 75° (c) 90°

(a)

Applied potential	Δke(mg cm^{-2} h^{-1})	Δkc(mg cm^{-2} h^{-1})	Δke/Δkc
-400	2.92	-0.1	-29.2
-200	3.61	-0.22	-16.41
0	3.89	-0.11	-35.36
200	5.78	-0.38	-15.21
400	4.42	0.2	22.1

(b)

Applied potential	Δke(mg cm^{-2} h^{-1})	Δkc(mg cm^{-2} h^{-1})	Δke/Δkc
-400	4.3	-0.08	-53.75
-200	4.46	0.3	14.87
0	4.3	0.1	43
200	5.27	-0.1	-52.7
400	4.82	0.16	30.13

(c)

Applied potential	Δke(mg cm^{-2} h^{-1})	Δkc(mg cm^{-2} h^{-1})	Δke/Δkc
-400	3.55	0.25	14.2
-200	3.9	0.29	13.45
0	3.92	0.3	13.07
200	4.7	0.3	15.67
400	4.78	-0.11	-43.45

Tables.5.73: Erosion-corrosion additive -synergism maps for carbon steel in water at 2.5 m s^{-1} and particle size 150-300μm (a) 15° (b) 45° (c) 90°.

(a)

Applied potential mV	Δke(mg cm^{-2} h^{-1})	Δkc(mg cm^{-2} h^{-1})	Δke/Δkc
-400	0.9	0.57	1.59
0	-0.13	1.76	-0.07
400	-0.14	1.8	-0.08

(b)

Applied potential mV	Δke(mg cm^{-2} h^{-1})	Δkc(mg cm^{-2} h^{-1})	Δke/Δkc
-400	0.69	0.55	1.25
0	-0.2	2.56	-0.08
400	0.61	2.05	0.3

(c)

Applied potential mV	Δke(mg cm^{-2} h^{-1})	Δkc(mg cm^{-2} h^{-1})	Δke/Δkc
-400	0.61	0.49	1.24
0	-0.07	1.59	-0.04
400	-0.03	1.47	-0.02

Tables.5. 74: Erosion-corrosion additive -Synergism maps for carbon steel in water at 3.5 m s^{-1} and particle size 150-300µm (a) 15° (b) 45° (c) 90°.

(a)

Applied potential mV	Δke(mg cm^{-2} h^{-1})	Δkc(mg cm^{-2} h^{-1})	Δke/Δkc
-400	0.28	0.96	0.29
0	0.56	0.48	1.17
400	1.06	0.2	5.3

(b)

Applied potential mV	Δke(mg cm^{-2} h^{-1})	Δkc(mg cm^{-2} h^{-1})	Δke/Δkc
-400	0.19	0.4	0.475
0	-0.27	0.19	-1.42
400	0.68	0.19	3.58

(c)

Applied potential mV	Δke(mg cm^{-2} h^{-1})	Δkc(mg cm^{-2} h^{-1})	Δke/Δkc
-400	0.18	0.4	0.45
0	-0.32	0.8	-0.4
400	-0.32	1.08	-0.296

Tables.5. 75: Erosion-corrosion additive -synergism maps for carbon steel in water at 4.5 m s^{-1} and particle size 150-300µm (a) 15° (b) 45° (c) 90°.

(a)

Applied potential mV	Δke(mg cm^{-2} h^{-1})	Δkc(mg cm^{-2} h^{-1})	Δke/Δkc
-400	0.25	1	0.25
0	-0.74	1.39	-0.53
400	-0.8	1.42	-0.56

(b)

Applied potential mV	Δke(mg cm^{-2} h^{-1})	Δkc(mg cm^{-2} h^{-1})	Δke/Δkc
-400	0.3	0.49	0.61
0	0.11	0.5	0.22
400	0.48	1.41	0.34

(c)

Applied potential mV	Δke(mg cm^{-2} h^{-1})	Δkc(mg cm^{-2} h^{-1})	Δke/Δkc
-400	0.1	0.85	0.12
0	-0.85	1.2	-0.71
400	-0.5	1.3	-0.38

Tables.5. 76: Erosion-corrosion additive -synergism maps for carbon steel in crude oil at 2.5 m s^{-1} and particle size 150-300μm (a) 15° (b) 45° (c) 90°.

(a)

Applied potential mV	Δke(mg cm^{-2} h^{-1})	Δkc(mg cm^{-2} h^{-1})	Δke/Δkc
-400	0.92	0.22	4.2
0	0.95	0.20	4.63
400	1.05	0.24	4.385

(b)

Applied potential mV	Δke(mg cm^{-2} h^{-1})	Δkc(mg cm^{-2} h^{-1})	Δke/Δkc
-400	0.908	0.2	4.54
0	1.02	0.12	5.23
400	1.2	0.2	6.11

(c)

Applied potential mV	Δke(mg cm^{-2} h^{-1})	Δkc(mg cm^{-2} h^{-1})	Δke/Δkc
-400	0.66	0.4	1.68
0	1.04	0.215	4.84
400	1.33	0.28	4.84

Tables.5. 77: Erosion-corrosion additive -Synergism maps for carbon steel in crude oil at 3.5 m s^{-1} and particle size 150-300μm (a) 15° (b) 45° (c) 90°.

(a)

Applied potential mV	Δke(mg cm^{-2} h^{-1})	Δkc(mg cm^{-2} h^{-1})	Δke/Δkc
-400	2.27	0.185	12.27
0	2.44	0.331	7.37
400	2.45	0.359	6.82

(b)

Applied potential mV	Δke(mg cm^{-2} h^{-1})	Δkc(mg cm^{-2} h^{-1})	Δke/Δkc
-400	2.56	0.30	8.48
0	2.57	0.25	10.36
400	2.59	0.37	6.94

(c)

Applied potential mV	Δke(mg cm^{-2} h^{-1})	Δkc(mg cm^{-2} h^{-1})	Δke/Δkc
-400	1.95	0.33	5.98
0	2.14	0.38	5.66
400	2.41	0.39	6.22

Tables.5.78:Erosion-corrosion additive -Synergism maps for carbon steel in crude oil at 4.5 m s^{-1} and particle size 150-300µm (a) 15° (b) 45° (c) 90°.

(a)

Applied potential mV	Δke(mg cm^{-2} h^{-1})	Δkc(mg cm^{-2} h^{-1})	Δke/Δkc
-400	2.85	0.472	6.04
0	3.247	0.4428	7.33
400	3.15	0.42	7.5

(b)

Applied potential mV	Δke(mg cm^{-2} h^{-1})	Δkc(mg cm^{-2} h^{-1})	Δke/Δkc
-400	2.9	0.50	5.82
0	3.16	0.54	5.89
400	3.2	0.61	5.26

(c)

Applied potential mV	Δke(mg cm^{-2} h^{-1})	Δkc(mg cm^{-2} h^{-1})	Δke/Δkc
-400	2.83	0.48	5.89
0	3.33	0.52	6.46
400	3.2	0.78	4.09

Tables.5. 79: Erosion-corrosion additive -synergism maps for carbon steel in oil /20% water at 2.5 m s^{-1} and particle size 150-300µm (a) 15° (b) 45° (c) 90°.

(a)

Applied potential mV	Δke(mg cm^{-2} h^{-1})	Δkc(mg cm^{-2} h^{-1})	Δke/Δkc
-400	0.68	0.19	3.55
0	0.58	0.65	0.89
400	0.47	0.97	0.48

(b)

Applied potential mV	Δke(mg cm^{-2} h^{-1})	Δkc(mg cm^{-2} h^{-1})	Δke/Δkc
-400	0.54	0.59	0.91
0	0.2	0.95	0.21
400	0.8	1.1	0.73

(c)

Applied potential mV	Δke(mg cm^{-2} h^{-1})	Δkc(mg cm^{-2} h^{-1})	Δke/Δkc
-400	0.9	0.36	2.77
0	0.45	0.85	0.53
400	0.42	1.05	0.398

Tables.5. 80: Erosion-corrosion additive -Synergism maps for carbon steel in oil /20% water at 3.5 m s^{-1} and particle size 150-300µm (a) 15° (b) 45° (c) 90°.

(a)

Applied potential mV	Δke(mg cm^{-2} h^{-1})	Δkc(mg cm^{-2} h^{-1})	Δke/Δkc
-400	0.77	1.55	0.5
0	0.55	2.05	0.3
400	0.95	2.02	0.47

(b)

Applied potential mV	Δke(mg cm^{-2} h^{-1})	Δkc(mg cm^{-2} h^{-1})	Δke/Δkc
-400	0.42	2.20	0.19
0	0.62	2.1	0.29
400	0.64	2.48	0.26

(c)

Applied potential mV	Δke(mg cm^{-2} h^{-1})	Δkc(mg cm^{-2} h^{-1})	Δke/Δkc
-400	0.97	1.48	0.65
0	0.39	2.07	0.19
400	0.81	2.1	0.39

Tables.5. 81: Erosion-corrosion additive -synergism maps for carbon steel in oil /20% water at 4.5 m s^{-1} and particle size 150-300µm (a) 15° (b) 45° (c) 90°.

(a)

Applied potential mV	Δke(mg cm^{-2} h^{-1})	Δkc(mg cm^{-2} h^{-1})	Δke/Δkc
-400	1.13	1.97	0.57
0	1	2.7	0.37
400	1.02	2.23	0.457

(b)

Applied potential mV	Δke(mg cm^{-2} h^{-1})	Δkc(mg cm^{-2} h^{-1})	Δke/Δkc
-400	0.7	2.4	0.291
0	0.35	3.25	0.11
400	0.53	2.77	0.19

(c)

Applied potential mV	Δke(mg cm^{-2} h^{-1})	Δkc(mg cm^{-2} h^{-1})	Δke/Δkc
-400	0.98	2.32	0.422
0	0.9	3	0.3
400	1.08	2.42	0.45

Chapter 6

General discussion and Conclusion

6.1. General discussion

6.1.1. Polarization curves

This part of the thesis, covering polarization curves, is an extension of the previous work on carbon steel carried out by Tian and Tang [10-11]. They found that the passive film on the surface cannot be maintained in flowing fluid. This implies that the current density increases with an increase in impact velocity due to removal of the passive film, which is similar to the results of this thesis regarding carbon steel in oil/water environments, which indicate that the value of current density increases with an increase in impact velocity (Fig. 3-1-6 and Fig. 3.22-24(b-c)).

Stack et al. [56] claimed that the highest value of current density was at an impact angle between 15°-45°, and the highest value of current density at an applied potential of 400mV. These results are similar to the results of this thesis regarding carbon steel in a water environment containing large particles sized 600-710μm (Fig. 4.1-3(a), as discussed in chapter 3-5). It can be observed that there are no surprises, because the erosion-corrosion parameters (such as impact angles and velocities) that are used in this thesis to investigate the carbon steel in the water environment are similar to those used to investigate mild steel by Stack et al. [56].

On the other hand, in the crude oil and combined environments the value of current density decreases compared to reservoir water containing particles sized 600-710μm and 150-300μm (Fig. 3.1-6(a-c) and Fig. 3.22-24 (a-c)) due to the lower solubility of the iron ions species in the crude oil, which is consistent with the findings of Tian and Tang [10-11]. Moreover, it can be observed from the results of the polarization curves in this thesis that an increase in the oil content indicates an increase in the cathodic polarization current and a decrease in the anodic polarization current, which cannot be pronounced in the water environment and is consistent with the previous study of Tian et al. [10].

Finally, it can be observed from the results of the polarization curves in chapter 5 of this thesis that the value of corrosion potentials (Ecorr) of carbon steel in the crude oil is higher than that of carbon steel in the water environment, and finally the corrosion potential of carbon steel in the reservoir water is lower than in the combined environments, as can be seen in Fig. 5.1-5.3 and Fig. 5.13-15.

6.1.2. Erosion-corrosion mass loss

The results of this thesis show that the erosion-corrosion mass loss depends on many parameters, such as impact velocity, impact angle, applied potentials and the size of the particles. Some researchers [10-11] found that in an oil/water slurries environment containing particles sized 600 μm (silicon), the value of erosion (Ke) was significantly higher than the value of corrosion Kc, and the percentage of erosion and corrosion to erosion–corrosion was approximately 70% and 30% respectively. However, the results of carbon steel in the crude oil/water environment containing particles sized 600-710μm in this thesis show that the percentage of erosion and corrosion to erosion–corrosion was approximately 80% and 20% respectively (Figs. 3.7-21). By comparing the results of Ke and Kc in this thesis to the results of Tian and Tang [10-11], it is very interesting to see that the value of erosion Ke in this thesis is increased and the value of corrosion contribution Kc decreased compared to that observed by Tian and Tang [10-11]. This may be attributed to the fact that they used silica sand as an erodent particle rather than Al_2O_3. The second reason may be the difference in the chemical and mechanical properties between the crude oil and simulated oil/water (which could be attributed to the mobility (viscosity)).

It should also be noticed from the results of mass loss in this thesis of carbon steel in the crude oil environment containing particles sized 600-710μm that the percentage of erosion and corrosion to erosion–corrosion was approximately 90% and 10% respectively (Figs. 3.7-21).

On the other hand, Stack et al. [36] found that the value of corrosion contribution (Kc) was significantly higher than the value of erosion contribution (Ke) in a sea water environment containing particles sized 50–250μm (silica). Also, in this thesis, regarding carbon steel in the reservoir water environment containing small particles sized 150-300μm it can be observed that the value of corrosion contribution Kc is higher than the value of Ke. By comparing these results to the results of this thesis (Figs. 5.16-22) it can be seen that the value of corrosion contribution Kc in this thesis is significantly lower than the value of Kc in the previous work of Stack et al [36]. This may be because they used silica and mild steel rather than aluminium oxide Al_2O_3 and carbon steel.

From the results in this thesis, it is not surprising that the value of Kec in the three environments containing particles sized 600-710µm (Fig. 3.7-3.21 and Fig .4.4-4.12) is greater than the value of Kec for carbon steel in the three environments containing small particles sized 150-300µm (Fig. 3.25-3.33 and Fig. 4.19- 4.27). This is because for carbon steel in the three environments containing small particles (150-300µm), the value of the corrosion product is increased more than with large particles (600-710µm), which indicates creation of a passive film on the surface of the specimen, and that the film decreases the effect of impact particles on the surface of the specimen [16-17].

It can be observed from the results of this thesis that the magnitude of the corrosion contribution (Kc) for carbon steel in the three environments indicates that at applied potentials −400 mV and -200mV there is a minimum mass loss compared to that recorded at higher applied potential values (higher than 0mV) (Fig. 3.7-3.21 and Fig. 3.25-3.33) [20, 34, and 36].

It can also be noticed from the results in chapters 3-5 that the value of corrosion contribution Kc for carbon steel in both crude oil and oil/20% water environments containing particles sized 600-710µm and 150-300µm is lower than that recorded in the water environment, which suggests better corrosion resistance of carbon steel in crude oil and combined environments compared to the reservoir water in all test conditions (Fig. 3.7-3.21 and Fig. 3.25-3.33).

Finally, it is clear that with a decrease in particle size from 600-710mm to 150-300mm, the value of corrosion contribution Kc increases with a decrease in the value of erosion contribution Ke in the water and combined environments, but in the crude oil environment the value of erosion contribution Ke remains greater than the corrosion contribution Kc (Fig. 3.7-3.21 and Fig. 3.25-3.33).

6.1.3. Erosion–corrosion maps

This part (erosion-corrosion maps) of the thesis is an extension of the previous work carried out by Stack et al. [18, 20, 34 and 36]. In their work, erosion–corrosion maps were constructed for material in an aqueous environment. However, the results in this thesis have been used to construct erosion-corrosion maps in oil/water slurries.

6.1.3.1. E**rosion-corrosion mechanism maps**

The methodology and boundaries for construction of erosion-corrosion mechanism maps have been addressed in chapter 3. Stack et al. [56] found that the erosion-passivation regime dominated between applied potentials 0 mV and 500mV. Also, the erosion–dissolution regime occupied the area between 0mV and 750mV and there was no change in the erosion-corrosion mechanism regimes with an increase in impact velocity from 3 $m\,s^{-1}$ to 4 $m\,s^{-1}$ in a sea water environment containing particles sized 500–710μm (Al_2O_3). These results are similar to the results of this thesis, as for carbon steel in the reservoir water containing particles sized 600-710 μm it can be observed that at an impact velocity of 3.5 $m\,s^{-1}$ the passivation-erosion regime dominated between applied potentials -400mV and 400mV. Also, the dissolution-erosion regime dominated at the low applied potential of -400mV (Fig. 4.34 (a)).

At an impact velocity of 4.5 $m\,s^{-1}$ with carbon steel in the reservoir water environment containing particles sized 600–710μm (Al_2O_3) it is clear that the passivation-erosion regime predominates and shifts to a high impact angle, which may be attributed to the passivation-repassivation phenomenon. The erosion-passivation regime is dominant at a low impact angle between 15°-50° (Fig.4.35 (a)), which could be due to destruction of the passive film at low impact angles. This implies that the results of this thesis regarding carbon steel in the reservoir water environment are similar to the results of the previous work carried out by Stack et al. [56].

Stack et al. [38] also developed an erosion–corrosion map of material in an aqueous environment and found that at a low impact velocity of 2 $m\,s^{-1}$ the particles had no effect on the passive film, which indicates that the passive film was not destroyed. Moreover, when the impact velocity was increased to 4 $m\,s^{-1}$ the current increased,

indicating that the passive film was being destroyed and repaired continuously. By comparing these results with the results of this thesis, it can be noticed that the results were similar to those of this thesis as the passivation–erosion regime dominates at a low impact velocity in the water containing large particles sized 600-710mm (Fig. 4.33-34(a)), which can be attributed to the hardness of corrosion products on the surface of the specimen, indicating a decrease in the effect of the impact particles on the surface.

From the results of the erosion-corrosion mechanism maps of this thesis, it can be observed that the passivation- erosion regime dominates in anodic conditions in the reservoir water and combined environments containing small particles sized 150-300μm (Fig. 3.36-41(a) and (c)), which may be due to the impact of particles on the passive film being a small and the effect of erodent not being sufficient to remove the passive film.

On the other hand, from the results of the erosion-corrosion maps in the crude oil environment containing large particles sized 600-710mm (Fig. 4.33-35(b)) it can be seen that the erosion regime dominates at low and high impact velocities. This can be attributed to the oil film on the surface of the specimen, indicating a decrease in the value of the corrosion.

6.1.3.2. **Erosion-corrosion wastage maps**

Erosion–corrosion wastage maps can be used to demonstrate the differences between levels of wastage as a function of velocity and electrochemical potential and impact angle. The methodology for constructing erosion-corrosion wastage maps has been addressed in chapter 3. Stack et al. [56] found that the high wastage regime was dominant at a high applied potential of 400mV and an impact angle lower than 30°, and a small area at an applied potential of -400mV at an impact angle of 90.In addition, the low and medium wastage regimes occupied areas at intermediate impact angles between 30° -60° and between -100mV and 400mV.

By comparing these results with the results of this thesis regarding carbon steel in the reservoir water environment containing particles sized 600–710μm it can be seen that there is no evidence of the presence of high wastage regimes on the wastage maps. In addition, from the results of this thesis regarding carbon steel in the reservoir water and combined environments, it can be observed that the medium wastage regime dominates and there is no presence of low wastage regime at the impact velocity 4.5 m s^{-1} (Fig. 4.41 (a) and (c)). This may be attributed to the use of mild steel rather than carbon steel.

On the other hand, from the results of the erosion-corrosion wastage maps of this thesis regarding the crude oil environment containing particles sized 150-300μm (Fig. 3.47-3.49 (b)) it can be seen that the low wastage regime covers the entire map in all test conditions. This can be attributed to the oil film having good corrosion resistance [6, 10 and 11]. However, at a high impact velocity of 4.5 m s^{-1} in the crude oil environment with large particles sized 600-710μm (Fig. 4.41 (b)), the medium wastage regime dominates due to an increase in the value of erosion contribution.

6.1.3.3. Erosion-corrosion additive-synergism maps

Corrosion may enhance erosion and this interaction is defined as synergistic behaviour (ΔKe) [36]. On the other hand, corrosion may also reduce erosion, i.e. by corrosion of the product on the surface of the specimen; this mechanism is defined as 'antagonistic' (-ΔKe) [20, 34 and 36]. The additive behaviour defines the situation where enhancement of corrosion is due to erosion ΔKc. Both synergistic and antagonistic behaviours are characteristics of erosion-corrosion processes [34].

Stack et al. [36] found that the additive–synergistic regime dominated the area between -100mV and -35mV for mild steel in a sea water environment containing particles sized 50–250μm (silica) at a constant impact velocity of 3 m s^{-1}. These results are similar to the results of this thesis for carbon steel in the reservoir water environment containing particles sized 150–300μm (Al_2O_3). The results of this thesis regarding carbon steel in the reservoir water environment containing particles sized 150–300μm show that the additive–synergistic and additive–antagonistic regimes predominate and there is good evidence of the presence of the 'antagonistic' regime on the map (Fig. 3.54 (a)).This is possibly due to the increased oxygen concentration at higher impact velovity3.5 m s^{-1} [2].

By comparing between the results of this thesis regarding carbon steel in the reservoir water environment containing particles sized 150–300μm and 600–710μm it can be observed that the synergistic regime occupies a significant area on the map in the reservoir water containing particles sized 600–710μm (Fig. 3.51 (a) Fig. 3.56 (a)) . This may be attributed to an increase in the value of erosion contribution (Ke).

On the other hand, from the erosion-corrosion additive-synergism maps of this thesis for carbon steel in crude oil containing small particles sized 150-300μm it can be observed that the synergistic regime dominates and there is no evidence of the predominance of the antagonistic regime in all test conditions (Fig. 3.55-57 (b)). Also, for carbon steel in the crude oil and combined environments with an increase in particle size from 150-300 μm to 600-710μm it can be noticed that the synergistic regime is decreased at some impact angles and replaced by the antagonistic regime (Fig. 3.50 (b-c)). These reasons have been addressed in chapters 3 and 4.

6.1.3. **Mechanism description of test material**

The analysis of the volume loss results, as function of impact angle, Fig6.1-2(a-c), indicates that the peak value of Kec at lower impact angles with increases in water content in the slurry mixture. Fig. 6.3-8 shows schematically the change in mechanism of erosion and corrosion on the surface with working parameters as follows:

a- Clearly, at exposure to low impact velocity 2.5 m s^{-1} and low angle 15° for carbon steel in water and oil/20% water environments, a small part of the specimen, small parts of the passive film formed due to corrosion product are removed by the impact of particles, with Figs. 6.3 (a) and (c) showing evidence of erosion-corrosion interaction. Figs. 6.3(b), for carbon steel in crude oil at a low impact velocity of 2.5 m s^{-1} and a low angle of 15°, segments of the specimen are removed and there is no evidence of a passive film on the surface of the specimen compared with in water and combined environments due to lower solubility of Fe ions in the crude oil [10-11].

It can be observed from the results that, the value of erosion contribution Ke in crude oil is significantly higher than in water and combined environment which confirm that there is no oxide film on the surface of specimen in crude oil.

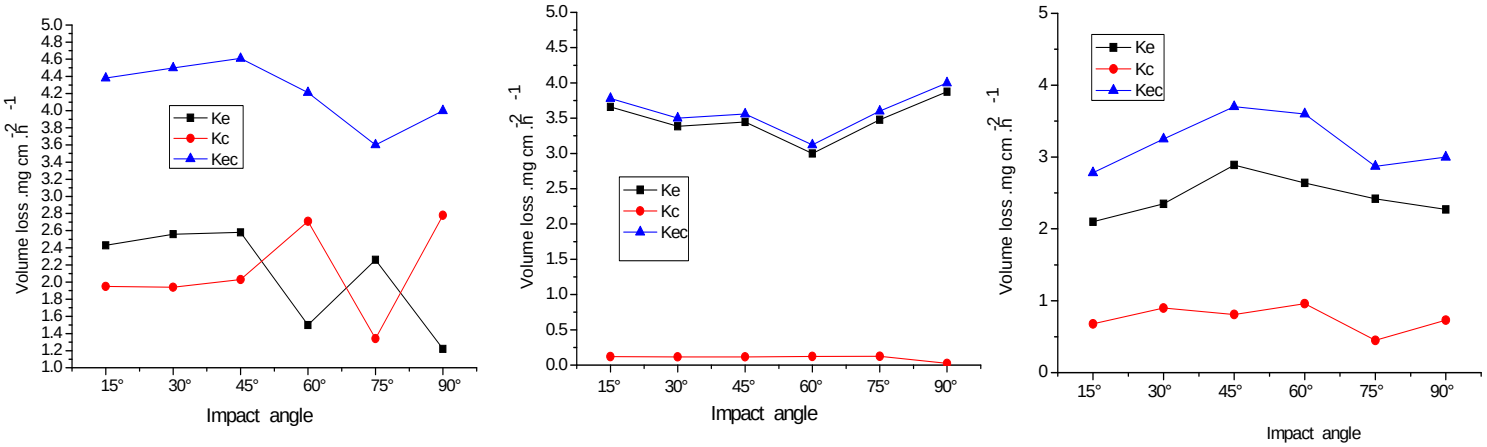

(a) (b) (c)

Fig.6.1: Volume loss as function of impact angles for carbon steel with large particles sized 600-710µm at 200 mV and 2.5 m s^{-1} impact velocity in (a) water(b) crude oil (c) oil/ 20% water

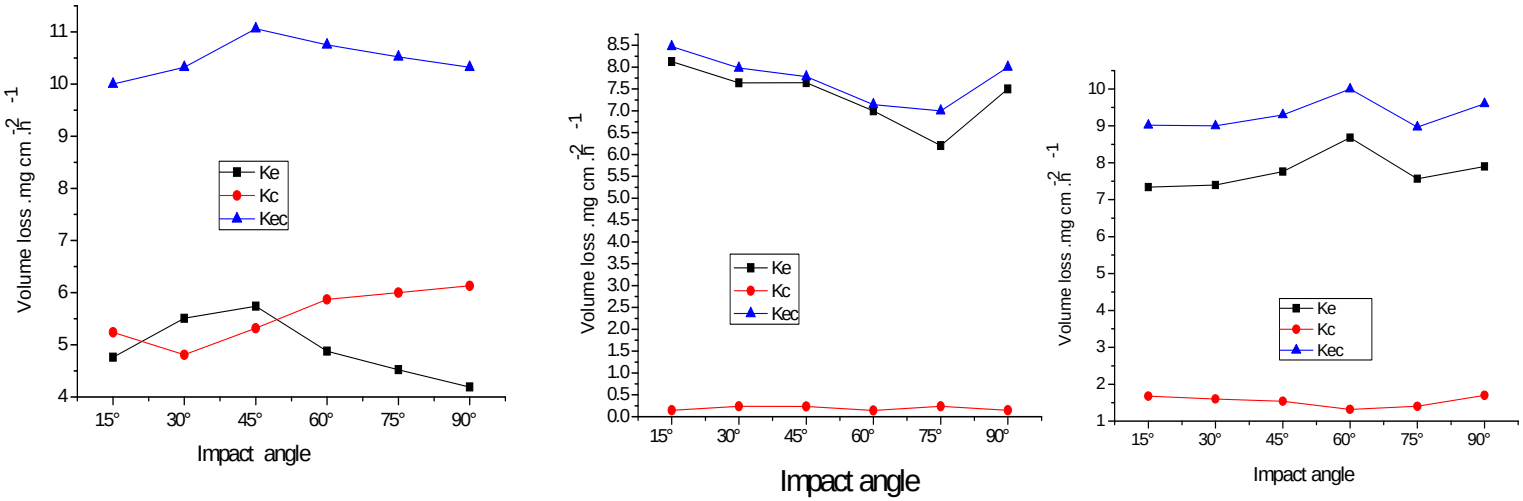

(a) (b) (c)

Fig.6.2: Volume loss as function of impact angles for carbon steel with large particles sized 600-710µm at 200 mV and 4.5 m s^{-1} impact velocity in (a) water(b) crude oil (c) oil/ 20% water

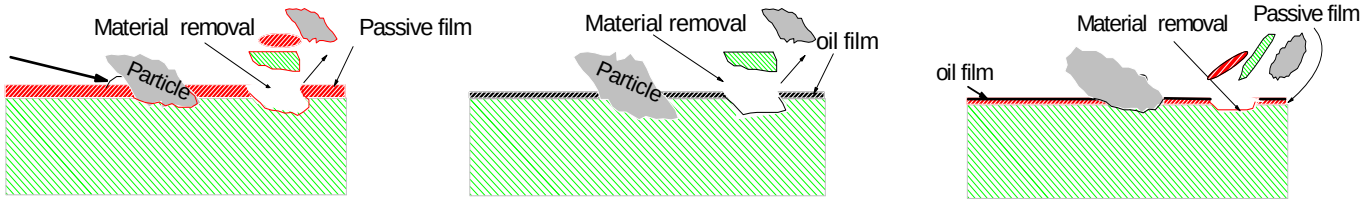

(a) (b) (c)

Fig.6. 3: Schematic diagram showing changing in mechanism of erosion-corrosion for carbon steel with large particles sized 600-710µm at impact angle 15° and 2.5 m s^{-1} impact velocity in (a) water (b) crude oil (c) oil/20% water.

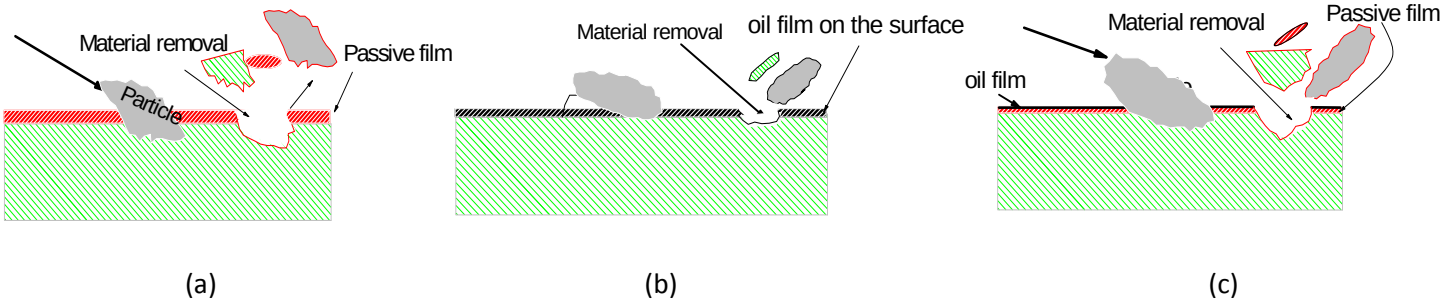

Fig. 6.4: Schematic diagram showing changing in mechanism of erosion-corrosion for carbon steel with large particles sized 600-710µm at impact angle 45° and 2.5 m s^{-1} impact velocity in (a) water (b) crude oil (c) oil/20% water.

b- For carbon steel in reservoir water and combined environments at an impact velocity of 2.5 m s^{-1} and intermediate impact angle of 45°, the value of (Kec) increased compared with previous an impact angle of 15°, exhibited higher wastage at shallow impact angles (Figs. 6.4 (a) and (c)), and the reverse occurring in the crude oil conditions Figs.6.4 (b).

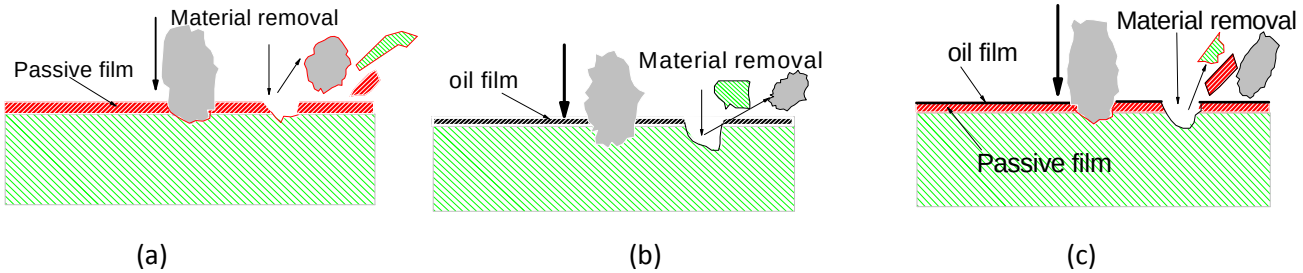

Fig. 6.5: Schematic diagram showing changing in mechanism of erosion-corrosion for carbon steel with large particles sized 600-710µm at impact angle 90° and 2.5 m s^{-1} impact velocity in (a) water (b) crude oil (c) oil/20% water.

c- At a low impact velocity of 2.5 m s^{-1} and a high impact angle of 90° for carbon steel in water and oil/20% water environments(Figs. 6.5 (a) and (c)), it can be seen that , the erosion-corrosion reduced compared to at lower impact angles which attributed to the passive film on the surface of the specimen (-Δke). However, in the crude oil environment Fig. 6.5 (b), it can be seen that, there is an increase in the value of Ke compared with at an impact angle of 45°.

d- The performance for carbon steel in three environments at high impact velocity of 4.5 m s^{-1} and at impact angles of 15°, 45°and 90° Fig. 6.6- Fig. 6.8, was similar to that observed at the low impact velocity of 2.5 m s^{-1}.

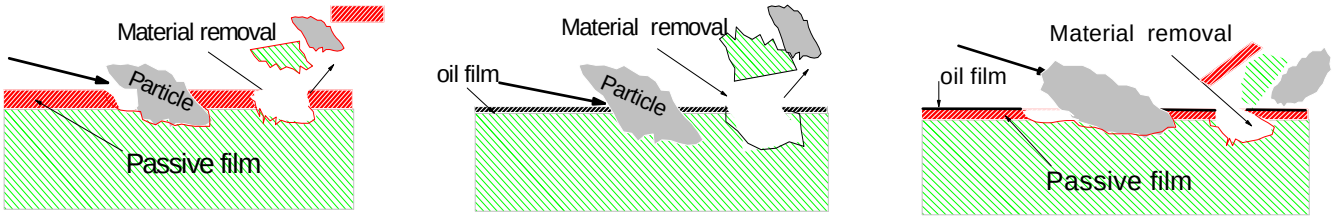

(b) (b) (c)

Fig. 6.6: Schematic diagram showing changing in mechanism of erosion-corrosion for carbon steel with large particles sized 600-710µm at impact angle 15° and 4.5 m s^{-1} impact velocity in (a) water (b) crude oil (c) oil/20% water.

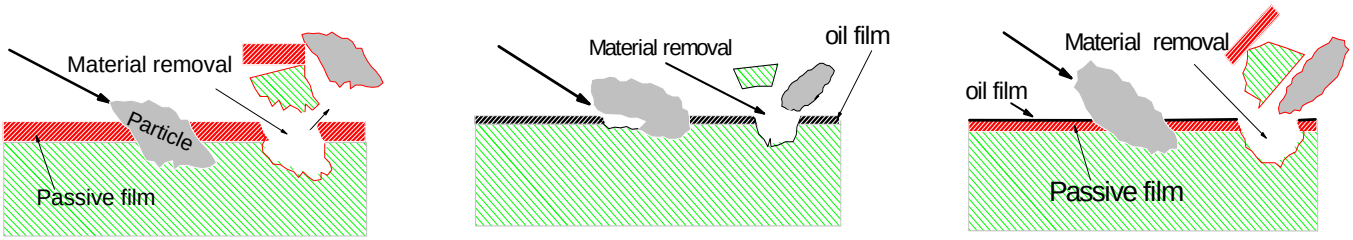

(b) (b) (c)

Fig. 6.7: Schematic diagram showing changing in mechanism of erosion-corrosion for carbon steel with large particles sized 600-710µm at impact angle 45° and 4.5 m s^{-1} impact velocity in (a) water (b) crude oil (c) oil/20% water.

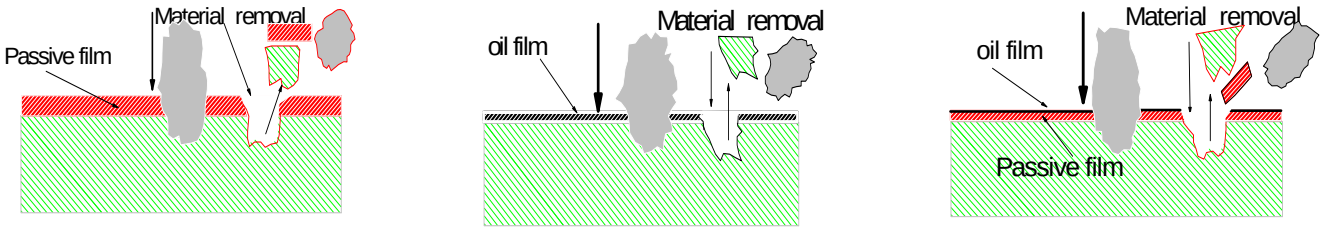

(b) (b) (c)

Fig. 6.8: Schematic diagram showing changing in mechanism of erosion-corrosion for carbon steel with large particles sized 600-710µm at impact angle 90° and4.5 m s^{-1} impact velocity in (a) water (b) crude oil (c) oil/20% water.

6.2. Conclusion

From the investigation of erosion-corrosion of carbon steel in three environments containing different particle sizes, the following points can be concluded:

- It can be concluded from the previous studies of erosion-corrosion were in the oil environments that this work was the first erosion-corrosion mapping study in oil /water slurries.

- From the values of the mass loss of carbon steel in the three environments containing particles sized 600-710µm and 150-300µm it can be concluded that the value of total erosion-corrosion (kec) of carbon steel in water environments was higher than the value of total erosion-corrosion (kec) of carbon steel in oil / 20% water environments, while the value of total erosion-corrosion (kec) of carbon steel in crude oil environments was the lowest.

- The volumes of corrosion contribution (kc) of carbon steel were similar to the volumes of erosion contribution (ke) in water environments containing particles sized 600-710µm. However, the volumes of erosion contribution (ke) of carbon steel were greater than the volumes of corrosion contribution (kc) in a crude oil and oil / 20% water environments containing particles sized 600-710µm.

- The results show that when particle size was changed from 600-710µm to 150-300µm, the values of corrosion contribution (kc) of carbon steel were increased compared to the volumes of erosion contribution (ke) in water and combined environments containing particles sized 150-300µm, but the values of corrosion contribution (kc) of carbon steel remained small compared to the volumes of erosion contribution (ke) in crude oil environments containing particles sized 150-300µm.

-The volume of corrosion contribution (kc) was increased with an increase in the potentials, which were attributed to an increase in the value of current density.

- The cathodic polarization current density increased and the anodic current density decreased with increase in oil content in the solution.

- Crude oil accelerated the cathodic reduction of oxygen and inhibited dissolution of ions of the steel.

-The increase of sand size from 150-300µm to 600-710µm decreased the anodic polarization curve density.

- The erosion contribution (ke) was also affected by an increase in the applied potential through the interaction between erosion and corrosion by corrosion enhanced erosion, as corrosion increases with an increase in potentials.

- The volume of erosion contribution (ke) of carbon steel in the three environments containing large particles sized 600-710µm was increased from 30° to 60°, while the peak value of erosion contribution (ke) was at an impact angle of 45° for carbon steel in the three environments containing small particles sized 150-300µm.

- The wastage maps of carbon steel in crude oil environments containing small particles sized 150-300µm showed that the low wastage regime was dominated during all impact velocities and there was no evidence of the presence of medium wastage regime on the maps, which was attributed to the creation of the oil film on the surface of the specimen which protected against the impact of particles. On the other hand, the medium wastage regime dominated the maps for carbon steel in the three environments containing large particles 600-710µm at high impact velocities 4.5 $m\ s^{-1}$. From the results of the wastage maps there was no evidence of the presence of high wastage effect on the specimen at these parameters.

- The erosion-corrosion additive-synergism maps showed that the synergistic regimes dominated the maps of carbon steel in crude oil containing small particles sized 150-300µm, while antagonistic and synergistic behaviour dominated the maps of carbon steel in crude oil containing large particles sized 600-710µm.

- The erosion-corrosion mechanism maps for carbon steel in the crude oil environment containing small particles sized 150-300µm showed that the erosion-passive regimes dominated the entire maps, while the erosion regime dominated for carbon steel in the crude oil environment containing large particles sized 600-710µm.

- The erosion-corrosion mechanism maps for carbon steel in reservoir water and the combined environments containing small particles sized 150-300µm showed that the passive-erosion regime dominated, which was attributed to a decrease in the volume of erosion contribution due to the thickness of the passive film on the surface of the specimen.

- The crude oil environment exhibited a higher corrosion resistance compared to the reservoir water and combined environments due to inhibiting dissolution of ions of the steel which indicated to decrease the current density.

- The erosion-corrosion tests of carbon steel showed dependency on test parameters studied, such as mechanical and electrochemical conditions.

- It can be concluded from the erosion-corrosion results that the contribution of erosion to erosion-corrosion for carbon steel in the crude oil environment containing large particles sized 600-710µm was about 90%, and the contribution of corrosion to erosion-corrosion for carbon steel in the crude oil environment was approximately 10%.

-In addition, the contribution of erosion to erosion-corrosion of carbon steel in 20% water in the crude oil environment containing large particles sized 600-710µm was about 80%, and the contribution of corrosion to erosion-corrosion of carbon steel in the combined environments was approximately 20%.

- Finally, the contribution of erosion to erosion-corrosion for carbon steel in the crude oil environment containing small particles sized 150-300µm was about 85%, and the contribution of erosion to erosion-corrosion for carbon steel in the reservoir water environment containing small particles sized 150-300µm was approximately 25%.

6.3. Future work

Based on this study of erosion-corrosion of carbon steel in three environments, the following future work will help with the understanding of complex mechanisms of erosion-corrosion of materials in different environments and parameters:

1- Study of a wider range of operating conditions, such as increased impact velocities and temperatures.
2- Study of a wider range of concentrations and pH.
3- Study of the effect of particle shape on materials is needed because erosion-corrosion can be changed as a function of size and shape, such as angular and rounded erodent particles.
4- Investigation of the effect of crude oil at low and high API gravity on materials as this may have an effect on the erosion contribution.
5- Working with different types of particles, such as silica sand, because the mass loss by aluminium oxide (Al_2O_3) may be different.
6- Study of different materials in combined environments with low percentages of water (lower than 5%) and with crude oil, and at higher values of water (about 40%) with crude oil in order to study the effect of erosion-corrosion on the materials.

Bibliography

[1] R .Hamzah, D.J Stephenson and J.E. Strutt, Erosion of material used in petroleum production, Wear 186 (187) (1995) 493-496.

[2] M. Stack, G. Abdulrahman, Mapping erosion-corrosion of carbon steel in oil exploration conditions: Some new approaches to characterizing mechanisms and Synergies, Tribology International, 43 (7) (2010) 1268-1277.

[3] I. Finnie, Erosion of surface by solid particles, Wear 3 (1960)87–103.

[4] NACE, Corrosion control in petroleum production, (1979).

[5] G. Fontana, Corrosion Engineering, Third edition, 1986.

[6] G.H. Abdulrahman and M.M. Stack, Erosion-corrosion maps for carbon steel in crude oil/water slurries: impact angle and applied potential effects , 11th Mediterannean Petroleum Conference and Exhibition, Tripoli, Libya, 23-25 February 2010 pp1-10

[7] M. Pourbaix , Atlas of electrochemical equilibrium in aqueous solutions, Section 2. , NACE, Houston (1974).

[8] Z.D. Cui, S. L. Wu, S. L. Zhu and X.J. Yang, study on corrosion properties of pipelines in simulated produced water saturated with supercritical CO2, Applied surface science, 252(2006)2368-2374

[9] Kewei. Gao, Fang Yu and Xiaolu. Pang, Mechanical of CO2 corrosion product scales and their relationship to corrosion rate, corrosion science 50 (2008)2796-2803

[10] B.R Tian and Y.F. Cheng electrochemical corrosion behaviour of X-65 steel in the simulated oil sand slurry. I. Effects of hydrodynamic condition, Corrosion Science 50 (2008) 773-779.

[11] X .Tang, L.Y. Xu and Y.F. Cheng, Electrochemical corrosion behavior of X-65 steel in the simulated oil–sand slurry. II: Synergism of erosion and corrosion, Corrosion Science, 50 (2008) 1469–1474.

[12] DU Cui-wei, LI Xiao-gang, Zhang Liang, Effect of Environmental Factors On Electrochemical Behavior of X70 Pipeline Steel in Simulated Soil Solution, Journal of Iron and steel research, international 2009, 16(6): 52-57

[13] G.A. Zhang a, b, Y.F. Cheng a, Electrochemical corrosion of X65 pipe steel in Oil/water emulsion, Corrosion Science 51 (2009) 901–907

[14] M. M Stack, F. H. Stott and G. C. Wood, modelling the transitions between erosion- corrosion regimes at elevated temperatures using computer graphics, 8th. International conference on erosion by liquid and solid impact, Cambridge England, Paper No. 92A, Sept. 1994.

[15] A. Levy, Solid Particle Erosion and Erosion-Corrosion of Materials, second Edition, ASM International, 1997

[16] S.S. Rajah Ram, T.J. Harvey, R. J. K. Wood, Erosion–corrosion resistance of engineering materials in various test conditions, Wear 267 (2009) 244–254

[17] S.S. Rajah Ram, T.J. Harvey, R. J. K. Electrochemical investigation of erosion- corrosion using a slurry pot erosion tester, Tribology International, 44 (3) (2011) 232-240.

[18] Y.P. Purandare, A.P.Ehiasarian and M.M .Stack, CrN/NbN coatings deposited by HIPIMS: A preliminary study of erosion– corrosion performance, Surface and Coatings Technology, 204, 8, (2010)1158- 1162.

[19] M. M. Stack, S. Zhou and R.C. Newman, Characterization of synergistic effects between erosion and corrosion in an aqueous environment using electrochemical techniques. Corrosion Science, 52 (1996) 934-946.

[20] M.M. Stack, T. M. A. AbdEl-Badia, Some comments on mapping the combined effects of slurry concentration, impact velocity and electrochemical potential on the erosion–corrosion of WC/Co–Cr coatings, Wear 264 (9-10) (2008) 826–837.

[21] A. Levy, J. Yan, J. Patterson, Elevated temperature erosion of steels, Wear 108(1986)43–60.

[22] I.M. Hutchings and R.E. Winter, Particle erosion of ductile metals: a mechanism of material removal, Wear 27(1974) 121–128.

[23] H. Mcl. Clark, Particle velocity and size effect in laboratory slurry erosion measurements or... do you know what your particles are doing?, Tribology International 35 (2002)617–624.

[24] M.M .Stack and Pungwiwat N, Erosion–corrosion mapping of Fe in aqueous slurries: some views on a new rationale for defining the erosion–corrosion interaction, Wear 256 (5) (2004) 565-576.

[25] M.M. Stack, N. Corlett and S. Zhou, Impact angle effects on the transition boundaries of the aqueous erosion–corrosion map. Wear225 (1999)190–198.

[26] G.T. Burstein and K. Sasaki, Effect of impact angle on the slurry erosion-corrosion of 304L stainless steel,Wear.240(2000) 80-94.

[27] M.M. Stack and D. Pena, Solid particle erosion of Ni-Cr/WC metal matrix composites at elevated temperatures: construction of erosion mechanism and process control maps, Wear 203 (1997) 489-497.

[28] Nahum Gat and Widen Tabakoff, Some effect of temperature on the erosion of Metals, wear 50 (1977) 85-94.

[29] I. Finnie, some observation on the erosion of ductile metals, Wear 19 (1972) 81- 90.

[30] J.B. Zu, G.T. Burstein and I. M. Hutchings, Comparative study of the slurry erosion and free-fall particle erosion of aluminium, Wear 149(1991) 73-84.

[31] J. Zu, G.T. Burstein and I. M. Hutchings, Velocity effects on erosion – corrosion of CrN/NbN " super lattice " PVD coatings, Surface & Coatings Technology201 (2006) 361 – 370

[32] S. Randall, K. Kien and Clark, on the particle size effect in slurry erosion,wear,149(1991)55-71

[33] Y. Li, G. T. Burstein and I. M. Hutchings, Influence of environmental composition and electrochemical potential on the slurry erosion-corrosion of aluminium, Wear 181–183(1995) 70–79.

[34] M.M. Stack, T. M. Abd El Badia, Mapping erosion–corrosion of WC/Co–Cr based composite coatings: particle velocity and applied potential Effects, Surface& Coatings Technology 201(3-4) (2006)1335–1347.

[35] G.T .Burstein, Y. Li and I.M. Hutchings, The influence of corrosion on the erosion of aluminium by aqueous silica slurries, Wear 186-187 (Part 2) (1995) 515 – 522.

[36] M. M. Stack, T. M. Abd El Badia, on the construction of erosion-corrosion maps for wc/co-cr-based coatings in aqueous conditions, Wear 261 (11-12) (2006)1181–1190.

[37] I. Finnie, J .Wolak and Y .Kabil, Erosion of metals by solid particles, Journal of Materials 2(1967) 682- 700.

[38] M.M. Stack, S. Zhou and R.C. Newman, Identification of transitions in erosion corrosion regimes in aqueous environments, Wear, 186-187, (1995) 523-532.

[39] R. A. Saravanan, M.K .Surappa and B.N .Pramila Bai, Erosion of A356 Al---SiC_{μ} composites due to multiple particle impact, Wear, 202 (1997) 154-164.

[40] I. Finnie, D. H. McFadden, on the velocity dependence of erosion of ductile Metals by solid particles at low angles of incidence, Wear, 48 (1) (1978)181–190.

[41] G.W. Stachowiak and A. W. Batchelor, Engineering Tribology, 3rd edition, pub. Butterworth Heinemann, 2005.

[42] M.V. Swain and J.T Hagan, Indentation plasticity and the ensuing fracture of glass, Journal of Physics (1976) 9 2201.

[43] A. K. Cousens and I. M. Hutchings, A critical study of the erosion of an aluminium alloy by solid spherical particles at normal impingement, Wear 88 (1983) 335- 358

[44] H. Matsumura and Y Oka, H Hiura, M Yano, The role of passivating film in preventing slurry erosion-corrosion of austenitic stainless steel, ISIJ International 31(2) (1991)168–176

[45] H. Clark and L.C. Burmeister, the influence of the squeeze film on particle impact velocities in erosion, International Journal of Impact Engineering, volume, (1992) pp. 415-426

[46] I. M. Hutchings and A.J. Sparks, Effects of erodent recycling in solid particle erosion testing, Wear 162-164(1993) 139-147.

[47] S. Raghuvir Singh and B.Narendra, Corrosion degradation and prevention by surface modification of biometallic materials, J Mater Sci: Mater Med 18 (2007) 725–751.

[48] M.M .Stack, F.H Stott and G.C Wood, The effect of pre-oxidation of chromia and alumina forming alloys on erosion in laboratory simulated fluidized-bed conditions, Corrosion Science 33(1992) 965-983.

[49] F. H .Stott, M. P. Jordan, S Lekatos, M. M .Stack and G. C.Wood, The erosion-corrosion of alloys under oxidizing-sulphidizing conditions at high temperature, Wear 186-187. (1995) 291-298.

[50] J. Postlethwaite and R.A Brierley, Electrochemical flow cell for elevated temperature/ pressure aqueous corrosion studies, Corrosion science 10 (12) (1970) 885-890.

[51] J. Postlethwaite and J. Sephton, Effects of mass-transport and oxide films on the cathodic reduction of O_2 on Ni, Corrosion science 10 (11) (1970) 775-784.

[52] S. Zhou, M.M. Stack, R. C. Newman, Electrochemical studies of anodic dissolution of mild steel in a carbonate-bicarbonate buffer under erosion-corrosion conditions , CorrosionScience38 (7) (1996)1071–1084.

[53] T. Hodgkiess and A. Neville, Electrochemical and mechanical interactions during erosion–corrosion of a high-velocity oxy-fuel coating and a stainless steel, wear, 233-235(1999) 623-634

[54] D.B. Wei, J.X. Huang, A.W. Zhang, Z.Y. Jiang, A.K. Tieu, X. Shi, S.H. Jiao, X.Y. Qu, Study on the oxidation of stainless steels 304 and 304L in humid air and the friction during hot rolling, Wear 267 (2009) 1741-1745.

[55] R. Malka, S. Nesic, D. A. Gulino, Erosion-corrosion and synergistic effect in disturbed liquid-particle flow, Wear262 (7-8) (2007)791–799.

[56] M. M. Stack, Y. Purandare, P. Hovsepian, Velocity effects on erosion corrosion of CrN/NbN "superlattice" PVD coatings , Surface & Coatings Technology 201 (2006) 361–370.

[57] M. Roy, K. K. Ray, G. Sundararajan, An analysis of the transition from metal erosion to oxide erosion,Wear217(2)(1998)312–320.

[58] M. M. Stack, Y. Purandare, P. Hovsepian, Impact angle effects on the erosion-corrosion of superlattice crn/nbn pvd coatings, Surface & Coatings Technology 188(2004)556–565.

[59] S.A. Morsi, A. J. Alexander, An investigation of particle trajectories in two phase flow systems, Journal of Fluid Mechanics Digital Archive55(02) 193–208(2006)

[60] M. M. Stack, N. Corlett, S. Zhou, Some thoughts on the effect of elastic rebounds on the boundaries of the aqueous erosion-corrosion map,Wear214(2) (1998) 175–185

[61] G. Sundararajan, Y. Tirupataiah, The localization of plastic flow under dynamic indentation conditions: I. experimental results, Acta Materialia 54(3) (2006)565– 575

[62] M.J. Graham, J.A. Bardwell, G.I. Sproule, D.F. Mitchell, B.R. MacDougall, The growth and stability of passive films, Corrosion Science35 (1993)13–18

[63] Y. I. Oka, H. Ohnogi, T. Hosokawa, M. Matsumura, The impact angle dependence of erosion damage caused by solid particle impact,Wear203(1997) 573–579

[64] M. M. Stack, N. Corlett, S. Turgoose, Some recent advances in the development of theoretical approaches for the construction of erosion-corrosion maps in aqueous conditions,Wear233(1999)535–541.

[65] P. Kritzer, Corrosion in high-temperature and supercritical water and aqueous solutions: a review, The Journal of Supercritical Fluids 29 (1-2) (2004)1–29.

[66] B. Poulson, Complexities in predicting erosion-corrosion, Wear, 233-235(1999) 497–504

[67] G.R. Desale, B. K. Gandhi, S. Jain, Improvement in the design of a pot tester to simulate erosion wear due to solid-liquid mixture,Wear259(1-6)(2005) 196 –202

[68] H. M. Clark, R. B. Hartwich, A re-examination of the particle size effect in slurry erosion, Wear248 (1-2) (2001)147–161.

[69] H.Meng, X.Hu, A. Neville, A systematic erosion-corrosion study of two stainless steels in marine conditions via experimental design, Wear, 263 (2007)355-362.

[70] X. Tang, C. Li, F. Ayello, J. Cai, S. Nesic, C. I. T. Cruz and J. N. Al-Khamis Effect of oil type on phase wetting transition and corrosion in oil-Water Flow, NACE corrosion, 2007 conference, paper, 170, Houston, USA, 2007

[71] P. Doron, D.Barnea, Flow pattern maps for solid-liquid flow in pipes, International Journal of Multiphase Flow 22(2) (1996)273–283.

[72] R. J. Llewellyn, S. K. Yick, K. F. Dolman, Scouring erosion resistance of metallic materials used in slurry pump service,Wear256(6)(2004)592–599.

[73] W. Tsai, J.A.C. Humphrey, I. Cornet, A.V. Levy, Experimental measurement of accelerated erosion in a slurry pot tester,Wear68(3)(1981)289–303.

[74] M.M. Stack, N. Pungwiwat, A note on the construction of materials performance maps for resistance to erosion in aqueous slurries, Wear 215(1- 2) (1998) 67–76.

[75] H. W. Wang, M. M. Stack, Corrosion of pvd in coatings under simultaneous erosion in sodium carbonate bicarbonate buffered slurries, Surface and coatingsTechnology105 (1-2) (1998)141–146

[76] R. E. Melchers, R. Jeffrey, Early corrosion of mild steel in sea water, Corrosion Science47 (7) (2005)1678–1693.

[77] B. Lawn and R. Wilshaw, Review indentation fracture: principles and applications, Journal of Material science, 10 (1975) 1049-1081

[78] H. Guo, B. Lu, J.Luo, Interaction of mechanical and electrochemical factors in erosion-corrosion of carbon steel, Electrochemical Acta 51 (2) (2005) 315 – 323.

[79] M.M. Stack, F. H. Stott and G. C. Wood, Review of mechanisms of erosion-corrosion of alloys at elevated temperatures, Wear 162–164 (1993) 706–712.

[80] K.M. Nho, Experimental investigation of heat flow rate and directional effect on contact conductance of anisotropic ground/lapped interfaces, Ph.d thesis, University of Waterloo, Canada (1990).

[81] C. Davis, P. Frawley, modelling of erosion-corrosion in practical geometries, Corrosion Science 51 (2009)769–775.

[82] R.J.K. Wood, T. F. Jones, Investigations of sand-water induced erosive wear of AISI304L stainless steel pipes by pilot-scale and laboratory-scale testing, Wear 255(1)(2003)206–218.

[83] R. J. K. Wood, T. F. Jones, J. Ganeshalingam, N. J. Miles, Comparison of predicted and experimental erosion estimates in slurry ducts,Wear256(9-10) (2004)937–947.

[84] J. G. Mbabazi, T. J. Sheer, R. Shandu, A model to predict erosion on mild steel surfaces impacted by boiler fly ash particles, Wear 257(5-6)(2004)612 –624.

[85] M.M. Stack, Q. Songroehrle, F.H. Stott, G. C. Wood, Computer simulation of erosion-corrosion interaction at elevated temperature,Wear181(1995)516– 523.

[86] M.M. Stack and S.M.Abdelrahman, Some reflections on a model to predict the erosion of the passive film on pure metals , Proc. ASAT 2009, 1-5, Cairo, Egypt, May 26-28 2009.

[87] M. M. Stack, M. M. Antonov, I. Hussainova, Some views on the erosion-corrosion response of bulk chromium carbide based cermets, Journal of Physics D- Applied Physics39 (15) (2006)3165–3174

[88] M.M. Stack, S. Zhou, R. C. Newman, Effects of particle velocity and applied Potential on erosion of mild steel in carbonate/bicarbonate slurry, Materials Science and Technology12 (3) (1996)261–268.

[89] M. M. Stack, N. Pungwiwat, Slurry erosion of metallic, polymers, and ceramics: particle size effects, Materials Science and Technology 15 (3) (1999) 337–344

[90] I. Finnie, The mechanism of erosion of ductile metals, in: Proceedings of the Third US National Congress of Applied Mechanics, American Society of Mechanical Engineers, 1958, pp.527–532

[91] T.E. Howes, P. M. Rogers, J. A. Little, I. M. Hutchings, Erosion-corrosion of mild steel in a temperature gradient,Wear186-187(Part1)(1995)316–324.

[92] J.G.A. Bitter, A study of erosion phenomena part-1 Wear6 (1) (1963)5–21

[93] G. Sundararajan and P.G. Shewmon, Anew model for the erosion of metals at normal incidence, Wear84(2)(1983)237–258.

[94] D. Chen, M. Sarumi, S. T. S. Al-Hassani, Su. Gan, Z. Yin, A model for erosion at normal impact,Wear205(1-2)(1997)32–39.

[95] M. M. Stack, C. Lakatos, F. H. Stott, Erosion-corrosion regimes: Number, nomenclature and justification, Tribology International 28 (7) (1995) 445–451

[96] M.M. Stack, F. H. Stott, An approach to modelling erosion-corrosion of alloys using erosion-corrosion maps, CorrosionScience35 (5-8)(1993)1027–1034.

[97] M.M. Stack, NR. Corlett, S. Zhou, Construction of erosion-corrosion maps for erosion in aqueous slurries, Materials Science and Technology 12 (8) (1996) 662–672

[98] S. Lim, MF. Ashby, Overview no.55wear-mechanism maps, Acta Metallurgica 35(1) (1987)1–24.

[99] J.B. Zu, I.M. Hutchings and G.T. Burstein, Design of a slurry erosion test rig, Wear140 (2) (1990)331–344.

[100] M.T. Mathew, M.M .Stack, B. Matijevic, L.A.Rocha and E.Ariza, Micro-abrasion resistance of thermo chemically treated steels in aqueous solutions: Mechanisms, maps, materials selection, Tribology International, 41 (2) (2008) 141-149.

[101] G.L. Sheldon, A. Kanhere, An investigation of impingement erosion using single particle,Wear21(1)(1972)195–209.

[102] J. X. Bouillard, R. W. Lyczkowski, on the erosion of heat exchanger tube banks in fluidized-bed combustors, Powder Technology 68 (1)(1991)37–51.

[103] G. L. Sheldon, I. Finnie, The mechanism of material removal in the erosive cutting of brittle materials, Journal of Engineering for Industry, Trans ASME 88(1966)393–400.

[104] L. Niu and Y.F. Cheng, Corrosion behaviour of X-70 pipe steel in near-neutral pH solution, Applied Surface Science, 253 (2007) 8626-8631.

[105] R. J. K. Wood, Erosion-corrosion interactions and their effect on marine and offshore materials, Wear261 (9) (2006)1012–1023.

[106] H. Guo, B.T. Lu and J. Luo, Study on passivation and erosion-enhanced corrosion resistance by mott-schottky analysis, Electrochemical Acta52 (3)(2006) 1108 –1116

[107] J. J. Liu, Y. Z. Lin, X. Y. Li, Numerical simulation for carbon steel flow induced corrosion in high- velocity flow seawater, Anti-Corrosion method. Materials55 (2) (2008)66–72.

[108] L. Niu, Y. Cheng, Synergistic effects of fluid flow and sand particles on erosion corrosion of aluminium in ethylene glycol-water solutions,Wear265(3-4)(2008) 367–374

[109] J. Postlethwaite, Effect of chromate inhibitor on the mechanical and electrochemical components of erosion-corrosion in aqueous slurries of sand,Corrosion 37(1)(1981)1–5.

[110] K. Nandakumar, H. Cunkui, S. Chiovelli, P.Minev, L.Jingli, A comprehensive phenomenological model for erosion of materials in jet flow, Powder Technology 187(2008)273–279.

[111] M. M. Stack, L. Bray, Interpretation of wastage mechanisms of materials exposed to elevated temperature erosion-, corrosion using erosion-corrosion maps andcomputergraphics,Wear186(1)(1995)273–283

[112] Y.F. Cheng, M. Wilmot and J.L. Luo, The role of chloride ions in pitting of carbon steel studied by statistical analysis of electrochemical noise, Applied Surface Science, 152 (1999) 161

[113] B.R. Tian and Y.F. Cheng, Erosion-corrosion of hydro transport pipes in oil sand slurries, Bulletin of Electrochemistry, 22 (2006) 329-335.

[114] J. C. Walton, G. Cragnolino, S. K. Kalandros, A numerical model of crevice corrosion for passive and active metals, Corrosion Science38(1)(1996)1–18.

[115] C. Zhong, X. Tang, Y.F. Cheng, Corrosion of steel under the defected coating studied by localized electrochemical impedance spectroscopy, Electrochemical Acta53 (2008) 4740-4747.

[116] J.I. Achebo, Computational analysis of erosion wear rate in a pipeline using the drift flux models based on eulerian continuum equations, in: Proceedings of the World Congress on Engineering, WCE-2009, Vol. I, London, UK, 2009

[117] I. Hutchings, A model for the erosion of metals by spherical particles at normal incidence, Wear70 (3)(1981)269–281.

[118] R. M. Brach, Impact dynamics with applications to solid particle erosion, International Journal of ImpactEngineering7 (1) (1988)37–53.

[119] Y. Tirupataiah, B. Venkataraman, G. Sundararajan, The nature of the elastic rebound of a hard ball impacting on ductile metallic target materials, Materials Science and Engineering a-Structural Materials Properties Microstructure and Processing1 24(2) (1990)133–140.

[120] M. M. Stack, S. Zhou, A methodology for the construction oft he erosion- corrosion map in aqueous environments, Wear203 (1997)474–488. solution, Applied Numerical Mathematics 55(3)(2005) 253–263.

[121] B. T. Lu, J. L. Lou, Synergism of electrochemical and mechanical factors in erosion- corrosion, Journal of Physical Chemistry B110(9)(2006)4217–4231.

[122] J. F. Addis, Erosion-corrosion in disturbed liquid/particle flow, Master's thesis, Russ College of Engineering and Technology, Ohio University (2008)

[123] J. Burwell, Survey of possible wear mechanisms, Wear1 (2) (1957)119–141

[124] M.M. Stack, N. Corlett, S.Turgoose, Some thoughts on modelling the effects of oxygen and particle concentration on the erosion-corrosion of steels in aqueous slurries, Wear 255(1-6)(2003)225–236.

[125] B. Lu, J. Luo, F. Mohammadi, K. Wang, X. Wan, Correlation between repassivation kinetics and corrosion rate over a passive surface in flowing slurry, Electrochemical Acta53 (23) (2008)7022–7031.

[126] J.H. Neilson, A. Gilchrist, Erosion by a stream of solid particles, Wear 11 (2) (1968)111–122.

[127] A. Forder, A numerical investigation of solid particle erosion experienced within oilfield control valves, Wear216 (2)(1998)184–193.

[128] I. Hutchings, Some comments on the theoretical treatment of erosive particle Impacts the 5th International conference on erosion by solid and liquid impact,5th, Cambridge , UK, 1979, pp.1–6

[129] G.T. Burstein, K. Sasaki, The birth of corrosion pits as stimulated by slurry erosion, Corrosion Science 42 (2000) 841-860

[130] J. Challen, P. Oxley, An explanation of the different regimes of friction and wear using asperity deformation models,Wear53(2)(1979)229–243.

[131] M. M. Stack, N. Pungwiwat, Particulate erosion-corrosion of al in aqueous conditions: some perspectives on ph effects on the erosion-corrosion map,Tribology International35(2002)651–660.

[132] P. Marcus (Eds.), Corrosion Mechanisms in Theory and Practice, 2nd Edited, New York, USA, 2002

[133] J. Jiang, M. M. Stack, A. Neville, Modelling the tribo-corrosion interaction in aqueous sliding conditions,TribologyInternational35(10)(2002)669–679.

[134] N. Crawford, G. Cunningham, S. Spence, An experimental investigation into the pressure drop for turbulent flow in 90° elbow bends, Journal of Process Mechanical Engineering221 (2) (2007)77–88.

[135] M. M. Stack, F. H. Stott, G. C. Wood, Review of mechanisms of erosion-corrosion of alloys at elevated temperature,Wear162(1993)706–712.

[136] M. Suckling, C. Allen, Critical variables in high temperature erosive wear, Wear203-204(1997)528–536.

[137] G. T. Burstein, K. Sasaki, Detecting electrochemical transients generated by erosion- corrosion, Electrochimica Acta 46(24-25)(2001)3675–3683.

[138] M. Reyes, A. Neville, Mechanisms of erosion-corrosion on a cobalt-base alloy and stainless-steel UNS S17400 in aggressive slurries, Journal of Materials Engineering and Performance10 (6) (2001)723–730.

[139] P.R. Roberge, Corrosion Engineering: Principles and Practice, McGraw-Hill, New York, USA, (2008)

[140] T.J. Harvey, J. A. Wharton, R. J.K. Wood, Development of a synergy model for erosion- corrosion of carbon steel in a slurry pot, Tribology - Materials, Surfaces & Interfaces1 (1) (2007)33–47.

[141] M. M. Stack, Some issues relating to the construction of materials selection maps for resistance to elevated temperature erosion, Tribology International 30(6)(1997)435–444.

[142] H. Guo, B. Lu, J. Luo, Response of surface mechanical properties to electrochemical dissolution determined by in situ nano-indentation technique, Electrochemistry Communications, 8 (7) (2006)1092–1098.

[143] I. Finnie, Some reflections on the past and future of erosion, wear 186–187 (1995), pp. 1–10

[144] Yu .Fang and Guoan Zhang, Mechanical properties of CO_2 corrosion product scales and their relationship to corrosion rates, Corrosion Science 50 (2008) 2796–2803.

[145] J.G.A. Bitter, A study of erosion phenomena, Part 2, Wear 6(1963) 169–190

[146] B.W. Madsen, Methods of Measuring wear-corrosion synergism, Wear 181-183(1995) 476–484

[147] M. M. Stack, J. S. James, Q. Lu, Erosion-corrosion of chromium steel in a rotating cylinder electrode system: some comments on particle size effects, Wear 256(5) (2004)557–564.

[148] M.M. Stack, S.M. Abdelrahman and B.D. Jana, A new methodology for modelling erosion-corrosion regimes of real surfaces: gliding down the galvanic series for a range of metal corrosion systems, Wear, 268, 3-4, 533-542, 2010

[149] I.M. Hutchings, Prediction of the resistance of metals to erosion by solid particles, Wear 35 (1975) 371–374

[150] C. Retamoso, H. Quiroga Becerra, D. Macdonald, The corrosion of carbon steel in oil-in-water emulsions under controlled hydrodynamic conditions, Corrosion Science 42 (2000) 561-575.

.